



ISSW 2017

Proceedings of the 16th
**International
Ship Stability Workshop**
Belgrade · Serbia · 5-7 June 2017

Editor: Igor Bačkalov

**The 16th International Ship Stability Workshop is organized by the
Department of Naval Architecture, Faculty of Mechanical Engineering
University of Belgrade
under the auspices of the STAB International Standing Committee.**



The 16th International Ship Stability Workshop is supported by



The Royal Institution of
Naval Architects



**BUREAU
VERITAS**



VAHALI
QUALITY SHIPS SINCE 1923

ELOMATIC
CONSULTING & ENGINEERING

*Maritime Bureau of Shipping
MBS Project doo – Tivat*

Proceedings of the 16th International Ship Stability Workshop (ISSW 2017)

Belgrade, Serbia, 5-7 June, 2017

Editor: Igor Bačkalov

ISBN: 978-86-7083-935-9

STAB International Standing Committee

Chairman:

Prof. Konstantinos Spyrou

National Technical University of Athens

Members:

Dr. Vadim L. Belenky

David Taylor Model Basin

Mr. Hendrik Bruhns

Herbert Software Solutions

Dr. Gabriele Bulian

University of Trieste

Prof. Alexander B. Degtyarev

St. Petersburg State University

Prof. Alberto Francescutto

University of Trieste

Dr. Jan Otto de Kat

American Bureau of Shipping

Dr. Toru Katayama

Osaka Prefecture University

Prof. Luis Perez-Rojas

Universidad Politécnica de Madrid

Mr. William S. Peters

U.S. Coast Guard

Prof. Marcelo Santos Neves

Universidade Federal do Rio de Janeiro

Prof. Naoya Umeda

Osaka University

Prof. Dracos Vassalos

University of Strathclyde

Dr. Frans van Walree

Maritime Research Institute Netherlands

Role of the International Standing Committee

- I. To be responsible for deciding the location and frequency of STAB Conferences and of the International Ship Stability Workshops (ISSW).
- II. To offer suggestions and agree the makeup of the National Committee and appoint the Chair of that Committee.
- III. To set out the terms of reference for the National Committee, in discussion with that Committee, including the broad technical content of the event.
- IV. To assist the National Committee with the selection of papers.
- V. To provide support to the National Committee, by way of suggesting speakers/exhibitors.
- VI. To have a consultative role in setting of fees for the conference.
- VII. To interact with and provide guidance to the Stability R&D Committee as appropriate.

Local Organizing Committee of ISSW 2017

Dr. Igor Bačkalov

Dr. Nikola Momčilović

Dr. Milan Kalajdžić

Stefan Rudaković, M.Sc.

Prof. Milorad Motok

All Local Organizing Committee members come from Department of Naval Architecture, Faculty of Mechanical Engineering, University of Belgrade.

Acknowledgements

Cover photo by Özen Güney. The assistance of Aleksandar Kostić, Damir Vlajnić, Aleksandar Bačkalov and Stefan Rudaković in prepress is acknowledged. Lidija Bačkalov is acknowledged for the bibliographic record of the Proceedings.

About International Ship Stability Workshop

International Ship Stability Workshop (ISSW) is a part of a longstanding series of international technical meetings in the field of ship stability, dynamics and safety, consisting of the STAB conferences, which are held every third year, and the ISSW workshops, which are held in the years between the conferences. These conferences and workshops are initiated and supervised by an International Standing Committee (ISC) and arranged and hosted by a Local Organizing Committee, each time in different corners of the world. General information about ISSW, STAB, ISC, SRDC (Stability Research and Development Committee), proceedings from past events, and other information concerning ship stability, dynamics and safety, can be found at www.shipstab.org.

Previous International Ship Stability Workshops

1995, Glasgow, UK	2007, Hamburg, Germany
1996, Osaka, Japan	2008, Daejeon, Korea
1997, Hersonissos, Crete, Greece	2010, Wageningen, The Netherlands
1998, St. John's, Newfoundland, Canada	2011, Washington, USA
2001, Trieste, Italy	2013, Brest, Brittany, France
2002, New York, USA	2014, Kuala Lumpur, Malaysia
2004, Shanghai, China	2016, Stockholm, Sweden
2005, Istanbul, Turkey	

Disclaimer

The opinions expressed in the papers included in the Proceedings are those of the authors and not necessarily those of any organization with which the authors have been associated.

Contents

Session 1: Challenges in the development of Second Generation Intact Stability Criteria

Session Chairs: William Peters, Jan Otto de Kat and Konstantinos Spyrou

- On the consistency of the level 1 and 2 vulnerability criteria in the Second Generation Intact Stability 3
by Markus Tompuri, Pekka Ruponen and Daniel Lindroth
- Sample applications of the Second Generation Intact Stability Criteria – robustness and consistency analysis 9
by Carsten Schrøter, Marie Lützen, Henrik Erichsen, Jørgen Juncher Jensen, Hans Otto Kristensen, Preben Hagelskjær Lauridsen, Onur Tunccan and Jens Peter Baltsersen
- Challenges of Dead Ship condition vulnerability criteria development 15
by William S. Peters and Vadim Belenky
- Model experiment on pure loss of stability for a ship in astern waves and its relationship with the Second Generation Intact Stability Criteria 21
by Naoya Umeda, Mizuki Osugi, Masahiro Sakai, Akihiko Matsuda and Daisuke Terada
- Possible simplifications of direct stability assessment 27
by Vladimir Shigunov

Session 2: Onboard intact stability management using advanced technologies

Session Chairs: Naoya Umeda and Hirotada Hashimoto

- A case study on operational limitations by means of navigation simulation 41
by Hirotada Hashimoto, Yuuki Taniguchi and Michio Fujii
- Acquisition and prediction of wave surface by marine radar for the safety of small ships 49
by Hironori Susaki, Yoshiaki Hirakawa, Takehiko Takayama and Tsugukiyo Hirayama
- On safe navigation support system using GPS compass 57
by Daisuke Terada, Masahiro Tamashima, Ikuo Nakao and Akihiko Matsuda

Session 3: Operational aspects of damage stability

Session Chairs: Teemu Manderbacka and Hendrik Bruhns

- How to buy time following a flooding incident – intelligent quantification of emergency response measures 67
by Kristian Bertheussen Karoliuss and Dracos Vassalos
- Impact assessment of wave statistics on ship survivability 73
by Donald Paterson, Georgios Atzamos, Dracos Vassalos and Evangelos Boulougouris
- Implications of different alternatives for damage stability analysis in decision support 81
by Petri Pennanen, Teemu Manderbacka and Pekka Ruponen

Session 4: Stability of naval vessels

Session Chairs: Jean-François Leguen and Timothy C. Smith

- An integration of present navy ships intact stability criteria in the perspective of ship performance assessment in a seaway 89
by Nicola Petacco, Paola Gualeni, Jean-Yves Billard and François Grinnaert
- Iced maritime routes, impact on stability for naval ships 97
by Paul Creismas, Guillaume Lannel and Jean-François Leguen
- Adverse health effects and reduced work ability due to vertical accelerations in high-performance marine craft personnel 103
by Manudul Pahansen de Alwis and Karl Garme

Session 5: Probabilistic computation in stability assessment

Session Chairs: Vadim Belenky and Arthur M. Reed

- Linear seakeeping high sea state applicability 111
by Timothy C. Smith and Kevin M. Silva
- Including diffraction and radiation into probabilistic description of capsizing 117
by Kenneth Weems and Vadim Belenky
- Modeling broaching-to and capsizing with extreme value theory 125
by Vadim Belenky, Kenneth Weems, Kostas Spyrou, Vlas Pipiras and Themistocles Sapsis
- Evaluation of the critical wave groups method for calculating the probability of extreme ship responses in beam seas 131
by Panayiotis A. Anastopoulos, Kostas J. Spyrou

Session 6: Stability and safety of inland and river-sea ships

Session Chairs: Gabriele Bulian and Igor Bačkalov

- Practicalities of loading instruments for inland waterway tankers 141
by Herbert Koelman and Egbert van IJken
- Stability and seakeeping of river-sea vessels: Classification rules 149
by Jean-Michel Chatelier, Wa Nzengu Nzengu and Raffaele Cocito
- On application of standard methods for roll damping prediction to inland vessels 159
by Stefan Rudaković and Igor Bačkalov

Session 7: Issues of stability modeling

Session Chairs: Vladimir Shigunov

- Verification and validation aspects of development and implementation of the Second Generation Intact Stability Criteria 169
by Arthur M. Reed

Study on vulnerability criteria for surf riding / broaching with a model experiment <i>by Min Gu, Jilong Chu, Yang Han and Jiang Lu</i>	175
Study on standard mathematical model of pure loss of stability in stern-quartering waves <i>by Jiang Lu and Min Gu</i>	181

Session 8: Stability of fishing vessels

Session Chairs: Luis Pérez Rojas and Marcos Míguez González

A new era of fishing vessel safety emerges <i>by Georgios Atzamos, Dracos Vassalos, Evangelos Boulougouris and Donald Paterson</i>	193
The Characteristics of Capsizing Phenomena of Japanese Fishing Vessels <i>by Akihiko Matsuda, Daisuke Terada and Hirotada Hashimoto</i>	199
Contributions on Roll Damping Coefficient for Fishing Vessels <i>by Adriana Oliva Remola and Luis Pérez Rojas</i>	207
Use of the Wolfson stability guidance for appraising the operational stability of small fishing vessels <i>by Matteo Scarponi</i>	213
Towards real-time identification of initial stability from ship roll motion analysis <i>by Marcos Míguez González, Gabriele Bulian, Lucía Santiago Caamaño and Vicente Díaz Casás</i>	221

Session 9: Stability of high-speed craft

Session Chairs: Frans van Walree, Anders Rosén and Toru Katayama

A motion estimation method of high speed craft in irregular sea by using onboard monitoring motion time series data for motion control <i>by Daisuke Terada, Ryosuke Amano and Toru Katayama</i>	233
High-speed craft dynamics in waves: challenges and opportunities related to the current safety philosophy <i>by Anders Rosén, Ermina Begovic, Mikael Razola and Karl Garne</i>	239
Validation of simulation tools for a RHIB operating in heavy seas <i>by Frans van Walree and William L. Thomas</i>	249

Session 1

**Challenges in the development of
Second Generation Intact Stability Criteria**

Session Chairs

William Peters

Jan Otto de Kat

Konstantinos Spyrou

On the consistency of the level 1 and 2 vulnerability criteria in the Second Generation Intact Stability

Markus Tompuri, *NAPA*, markus.tompuri@napa.fi

Pekka Ruponen, *NAPA*, pekka.ruponen@napa.fi

Daniel Lindroth, *NAPA*, daniel.lindroth@napa.fi

ABSTRACT

The development of the draft regulations and explanatory notes for the second generation intact stability criteria is ongoing at IMO. For levels 1 and 2, the drafts are already nearly finalized. However, previous sample ship calculations have revealed potential inconsistency in some cases. This paper studies three failure modes: parametric roll, pure loss of stability and excessive accelerations. Additional sample ship results are provided, and the potential sources of inconsistency between level 1 and level 2 are discussed. Also some alternative approaches to resolve the inconsistencies are presented.

Keywords: *Second Generation Intact Stability Criteria, Parametric roll, Pure loss of stability, Excessive accelerations.*

1. BACKGROUND

The development of the so-called second generation intact stability criteria is ongoing at IMO. After several years of hard work (Umeda and Francescutto, 2016), the draft regulations and explanatory notes are nearly ready for level 1 and 2. A vast amount of sample ship results have been submitted, and some inconsistencies between level 1 and level 2 have been observed. An inconsistency here means that the level 1 check is passed while the level 2 check for the same failure mode is not.

In this paper potential sources for inconsistency between level 1 and level 2 for the different failure modes are discussed, supported by sample calculation results. For each failure mode a characteristic sample vessel that is potentially vulnerable is used. Finally, some ways to solve the inconsistencies by adjusting the draft regulations are suggested.

The study is limited to three failure modes: parametric roll, pure loss of stability and excessive accelerations. All calculations have been done with the NAPA software, based on the latest draft regulations IMO (2014 and 2015). Surf-riding/broaching has been excluded since the level 2 calculations would require a lot of data on resistance and propulsion, which is not easily available. Also dead ship condition has been excluded due to the yet unresolved conflict with the mandatory weather criterion. In addition, updates to

dead ship calculations procedures have been recently proposed.

2. PARAMETRIC ROLL

Parametric roll has been identified as a possible failure mode, especially for container ships. Therefore, the C11 container ship has been selected as a representative sample vessel for this study. Several different loading conditions are calculated. The natural roll period is approximated based on GM value by using the simplified formula in the weather criterion of IS Code 2008. Level 1 is calculated both with the direct method, using the real GM variation in a longitudinal wave, and with the extremely simplified alternative. Level 2 check 2 is calculated with a time-domain 1-DOF simulation, using GZ curves in waves. The results are presented in Table 1, showing consistency.

Table 1 Sample results for parametric roll with C11 container ship. Red color is indicating that ship fails to meet the standard for the level.

Draft (m)	GM (m)	level 1 simple	level 1	level 2 check 1	level 2 check 2
8.00	2.50	1.290	0.731	0.000	0.000
9.00	2.10	1.331	0.932	0.425	0.001
10.00	1.90	1.307	1.035	0.216	0.006
11.00	1.80	1.216	0.988	0.216	0.011
12.00	1.70	1.106	0.890	0.216	0.012

Level 1

The extremely simplified alternative for level 1 check does not provide any additional value.

Hydrostatic calculations in a wave are trivial, and available in all advanced naval architectural software. The results of the simplified method are much more conservative, and thus a different threshold value could be considered.

Level 2

The standard for level 2 check 2 has remained unchanged since SDC1 (IMO, 2013, Annex 1), and the early sample ship calculation results were done using the averaging method (IMO, 2014). However, recently most of the sample ship calculations have been done using the time-domain method (IMO, 2016). In general, using the more realistic time-domain method, with GZ evaluated in waves, results in smaller index values.

The time-domain method for level 2 check 2 recognizes also lower resonance frequencies of parametric roll, whereas the level 1 and level 2 check 1 are based only on the main resonance. This is a potential source for inconsistency, but such a case has not been identified.

It should also be noted that the current draft regulation is based on a fixed set of forward speeds in both head and following seas. In many cases, the main resonance frequency for parametric roll can occur between these calculation speeds.

3. PURE LOSS OF STABILITY

The pure loss of stability failure mode may be relevant to relative fast and slender ships, such as RoRo or smaller passenger ships. From the sample calculations submitted to IMO (2016), it can be seen that there are multiple cases where large passenger ships are found vulnerable according to the level 2 calculations. There are however no known cases of pure loss of stability accidents for this type of ships. This paper tries to identify possible factors contributing to this. Therefore, the 300 m long FLOODSTAND cruise ship “A” is used for the sample calculations.

Results

Passenger ships have a more stringent limit for the second check of the pure loss of stability where the maximum permitted heel angle is 15 degrees, compared to 25 degrees for other ships.

For pure loss of stability to occur, the ship needs to spend a considerable time with the wave crest close to amidships. Therefore a Froude

number limitation was introduced to the criterion to exclude ships with a Froude number below 0.24 outright.

Due to the abovementioned reason the sample ship used for this study was selected to be a large passenger ship with a design Froude number of 0.24.

Table 2 Sample results for pure loss of stability for a large passenger ship. Red color is indicating that ship fails to meet the standard for the level.

Draft (m)	GM (m)	level 1 simple	level 1	level 2 CR1	level 2 CR2
8.1	1.9	-3.543	-0.715	0.088	0.155
8.4	2.1	-2.983	-0.44	0.017	0.087
8.8	2.4	-2.29	-0.06	0.001	0.035

The extremely simplified alternative for level 1 gives results that are in an order of magnitude more conservative compared to the more accurate direct GM calculation in waves. Thus a different threshold value could be considered for the different methods in level 1.

From the level 2 calculation results we can determine that the second check CR2 is the dominating one. In this check the static heeling angle under the heeling lever R_{PL3} is calculated. This heeling lever is intended to replicate the centrifugal force due to large yaw angular velocity, possibly caused by the wave. The heeling lever is defined as:

$$R_{PL3} = 8(H_i/\lambda)dF_n^2 \tag{1}$$

where H_i is wave height, λ is wave length and d is draft amidships. Background information on this equation can be found from (IMO, 2012), where the standard has been based on model tests of three ships. In equation (1), it is assumed that the vertical distance between the center of gravity and the acting point of the hydrodynamic force z_H is equal to the draft of the ship. If this assumption is ignored and z_H is used instead of d , the results become:

Table 3 Sample results studying assumption made on the R_{PL3} heeling lever.

Draft (m)	GM (m)	z_H (m)	level 2 CR2, z_H	level 2 CR2, $z_H = d$
8.1	1.9	15.24	0.174	0.155
8.4	2.1	14.60	0.127	0.087
8.8	2.4	13.76	0.046	0.035

Based on the results shown in Table 2 and Table 3, it seems the heeling lever may be overly conservative and not reflecting the heeling moment experienced by the ship in waves, especially if considering the inertia of the ship.

Another cause for inconsistencies, especially for passenger ships, is the far more stringent maximum heel angle requirement compared other vessels for CR2. These in combination with the level 1 threshold set for the simple method is a likely culprit of the inconsistencies found in the sample calculations at IMO (2016).

The Froude number limitation may also be problematic, as can be seen in the sample calculation above. The selected sample ship currently fails pure loss of stability level 2, but if the design Froude number would be $F_n = 0.239$, the ship would have passed without need for any further analysis, and currently it even fails the level 2 analysis.

4. EXCESSIVE ACCELERATIONS

The excessive accelerations failure mode concerns vulnerability to excessive lateral accelerations caused by the ships response to waves. Some serious accidents have occurred e.g. to large container ships in ballast condition, but also other ship types where persons can be high above the sea level and that may operate with a higher GM are potentially vulnerable.

In the regulation draft (IMO, 2015) there are several standards proposed both for level 1 and level 2 which makes consistency analysis more difficult. The draft regulation also contain a criteria to allow a loading condition to pass the vulnerability checks without investigation. This criterion consists of two parts that both must be met:

- GM is below 8% of the breadth of the ship, and
- the highest location where persons are present is lower than 70% of the breadth of the ship.

In this two-part criterion three main parameters are found and thus selected for further analysis. Exploratory calculations, while varying the GM, breadth and height, were carried out using a general container ship hull form with a length of 195 m. While GM and height easily can be changed in the calculations, the breadth variation was done by transforming the hull shape. Two different x locations, at midship and at the bow, were used for the location where the accelerations were estimated. The vertical position, where the accelerations need to be calculated, is the highest location where crew or passengers may be present. For cargo ships this is usually the bridge, but for passengers ships multiple locations may need to be addressed (Tompuri et al, 2016).

The damping was calculated both with bilge keels and without them, using the semi-empirical Ikeda's method (Kawahara et. al., 2009).

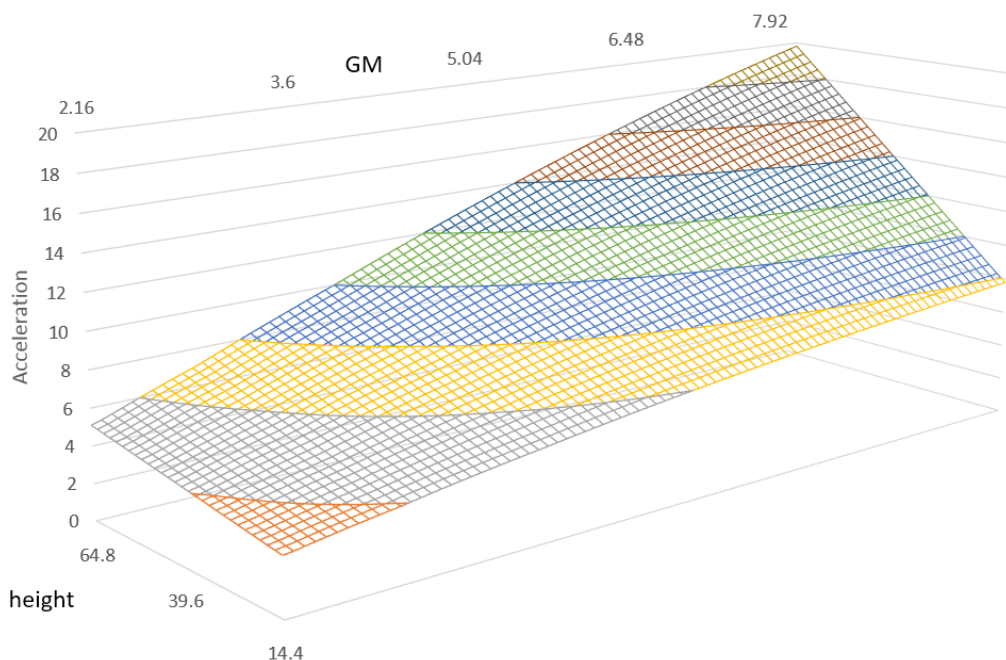


Figure 1: Level 1 as a function of GM and height (midship, B=36).

Level 1

Results shows that an increase in height and GM amplifies the level 1 results. This effect appears to be common for different breadths, and both with or without bilge keels.

Level 2

Level 2 results on the other hand behaves quite different depending on if bilge keels are used or not. No bilge keels seems to induce a GM resonance, as can be seen from figure 2 below, resulting in a differently shaped level 2 results field, while breadth and x location mainly influences the amplitude.

Looking at the standards proposed for both levels, and superimposing the pass/fail boundaries from the level 2 results on the level 1 results reveals more. The level 2 standards 0.043 and 0.0281

results in allowed level 1 accelerations in the bow of up to over 20m/s². A level 2 standard of 0.001 results in level 1 accelerations of up to 12m/s², and level 2 standard 0.00011 in level 1 accelerations up to 10m/s². These values all naturally depend on the ship, x location, breadth, height and GM. It should be noted that for certain values the varied parameters, both the level 1 and level 2 criteria, can fail when the most conservative standard is used. However these cases would automatically be excluded from the calculation based on the height/breadth and GM/breadth ratios.

The standards applied in the reports for sample ships submitted to IMO (2016) have been different. The standards chosen is one possible source for inconsistency and it is therefore important to look at the actual values calculated instead of only the judgement pass or fail.

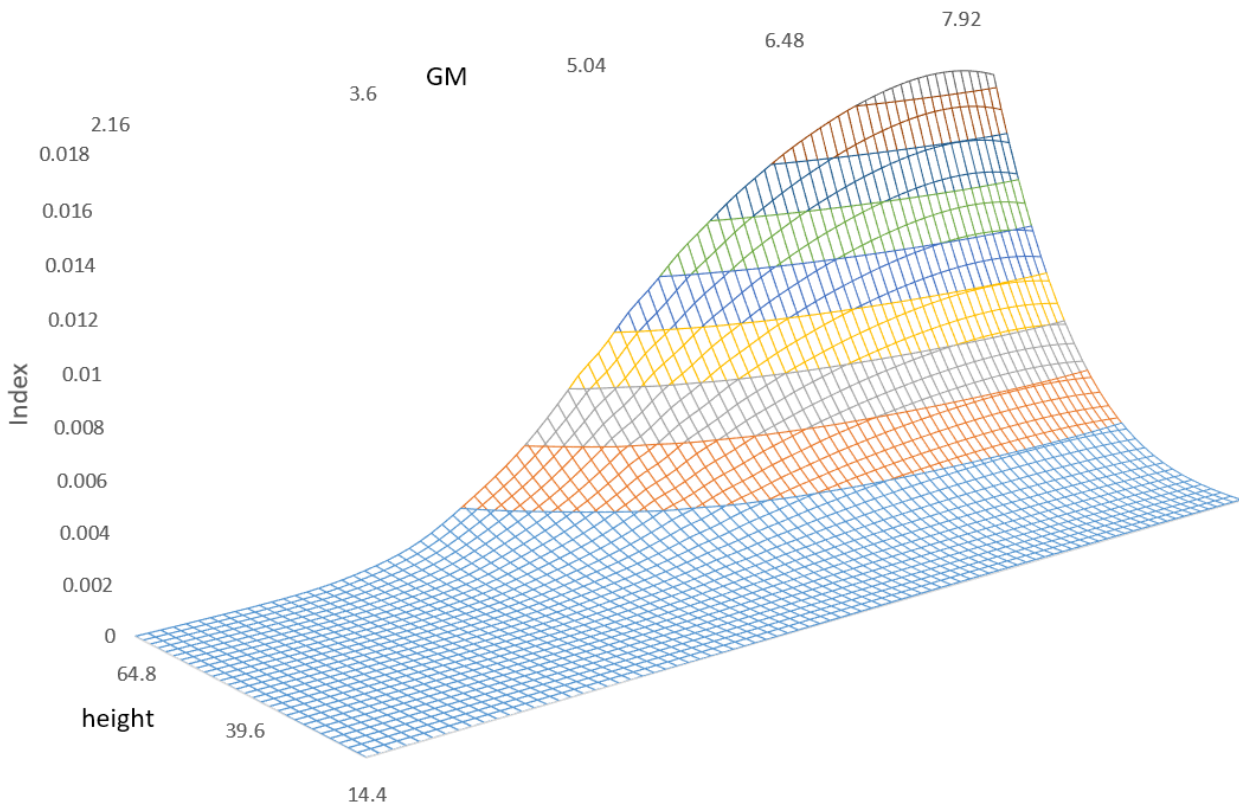


Figure 2: Level 2 with bilge keels (midship, B=36).

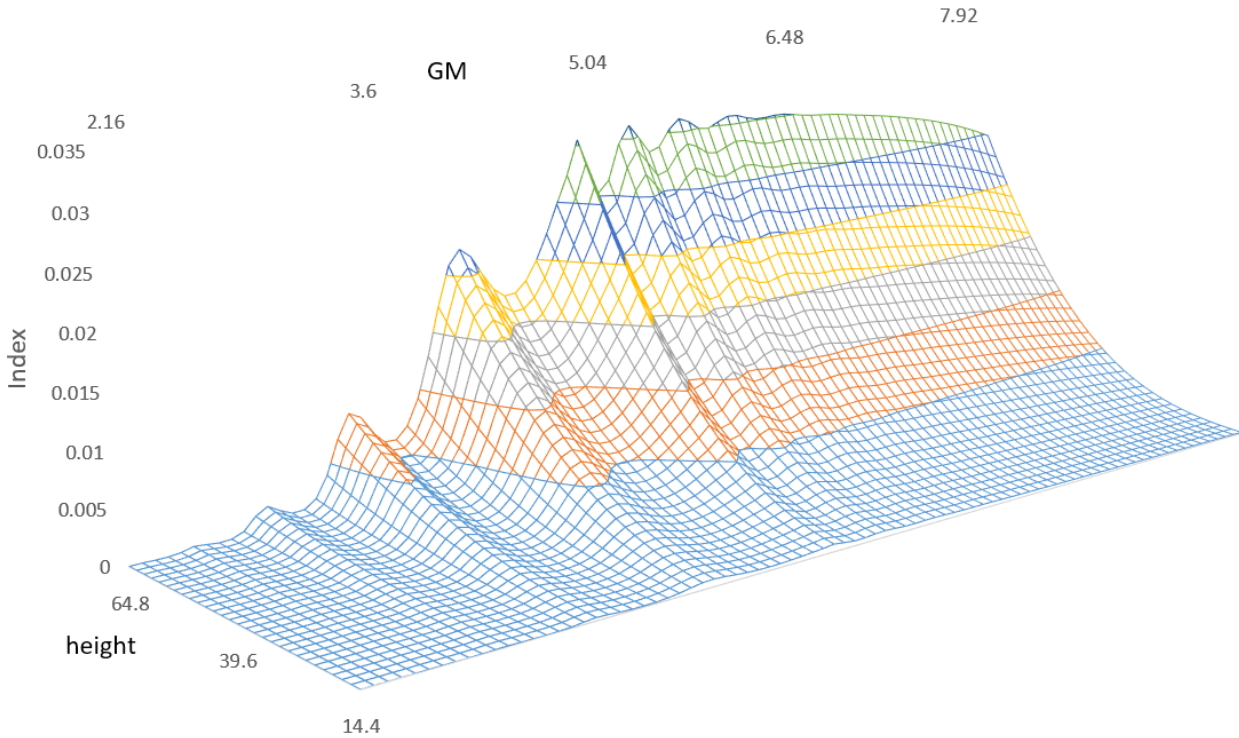


Figure 3: Level 2 without bilge keels (midship, B=36).

5. DISCUSSION

When developing criteria that will be applicable for decades to come, it is important that the regulations are well formulated and works for all the intended ships. The selected methods should be based on physics, well tested and without restrictions or assumptions on ship particulars.

From the results in this paper and from the calculations submitted to IMO (2016) it is clear that the level 1 threshold for parametric roll and pure loss of stability are based on the simplified method. As the direct calculation of GM in waves is an alternative it should also have a different threshold value to avoid inconsistencies. It is also important that level 1 and level 2 thresholds are considered as a whole to avoid inconsistencies.

Currently the bilge keels are the only roll damping devices that can be taken into account when assessing roll damping coefficients. This may be problem for example for ice going vessels that typically do not have bilge keels, but often incorporate other roll damping measures such as antiroll tanks. Inconsistencies for ice-going ships has also been reported to IMO (2016, Annex 3).

Level 1 should work as a conservative check and quickly filter out the ships that should not experience a certain stability failure mode. Level 2

on the other hand introduces sea states and also considerations on the likelihood for the events to occur. Level 3, or direct assessment, is the most accurate analysis, but unfortunately results based on level 3 have not yet been submitted and the calculation is still under development. By widening the calculation spread and applying the results from a higher criteria level to a lower one could help in refining the standards and methods used.

From experience it is known that these stability failures fortunately are rare events. Good seamanship and possible counter measures performed by the crew are likely also contributing factors to keep the number of accidents for these failure modes low.

The Second Generation Stability Criteria are intended for all ships, and thus the methods chosen need to be general in nature and their limitations must be solved. More research into the subject is still needed and inconsistencies should be solved.

REFERENCES

- Umeda, N., Francescutto, A., 2016 "Current state of the second generation intact stability criteria - achievements and remaining issues" Proceedings of the 15th International Ship Stability Workshop, 13-15 June 2016, Sweden.
- IMO, 2012, SLF 55 INF-15 Annex 10
- IMO, 2013, SDC 1, INF-8 Annex 1

IMO, 2014, SDC 2 WP.4 Annex 1 and Annex 2

IMO, 2015, SDC 3 WP. 5 Annex 2

IMO, 2016, SDC 4- INF-4

Kawahara, Y., Maekawa, K., Ikeda, Y., 2009, "A Simple Prediction Formula of Roll Damping of Conventional Cargo Ships on the Basis of Ikeda's Method and Its Limitation", Proceedings of the 10th International Conference on Stability of Ships and Ocean Vehicles, (STAB2009), St. Petersburg, Russia, pp. 387-398.

Tompuri, M., Ruponen, P., Forss, M., Lindroth, D. 2015, "Application of the Second Generation Intact Stability Criteria in Initial Ship Design", *SNAME Transactions*, Vol. 122, pp. 20-45.

Tompuri, M., Ruponen, P., Lindroth, D. 2016, "Second generation intact stability criteria and operational limitations in initial ship design", Proceedings of PRADS2016, 4-8 September 2016, Copenhagen, Denmark.

Sample Applications of the Second Generation Intact Stability Criteria – Robustness and Consistency Analysis

Carsten Schrøter, *Knud E. Hansen A/S*, cas@knudehansen.com

Marie Lützen, *University of Southern Denmark*, mlut@iti.sdu.dk

Henrik Erichsen, *Lloyds Register Marine*, henrik.erichsen@lr.org

Jørgen Juncher Jensen, *Technical University of Denmark*, jjj@mek.dtu.dk

Hans Otto Kristensen, *HOK Marineconsult ApS*, hokmarine@mail.dk

Preben Hagelskjær Lauridsen, *OSK-ShipTech A/S*, pl@osk-shiptech.com

Onur Tunccan, *Odense Maritime Technology A/S*, otu@odensemaritime.com

Jens Peter Baltersen, *DFDS A/S*, Jens.Baltersen@dfds.com

ABSTRACT

A new Intact Stability Code, the so-called Second Generation of Intact Stability Criteria, is currently under development and validation by the International Maritime Organization (IMO). The criteria are separated into five failure modes, each of which is analyzed by two vulnerability levels and, if needed, a direct numerical simulation. The present paper summarizes results testing the vulnerability levels in these new stability criteria. The calculations are carried out for 17 ships using the full matrix of operational draughts, trims and GM values. Each failure mode criterion is examined individually regarding construction of a GM limit curve for the full range of operational draughts. The consistency of the outcomes has been analyzed, and finally examined whether the new criteria tend to be more or less conservative compared to the present rules by evaluating approved loading conditions.

Keywords: *IMO, Second generation intact stability criteria, Sample calculations, GM limit curves*

1. INTRODUCTION

New intact stability criteria are currently being developed and validated at IMO. The new criteria, which differ very much from the formulations in the current IS Code 2008 (IMO 2008), is based on first principles with the stability examined for the ship sailing in waves. The new intact stability criteria are separated into five failure modes: pure loss of stability, parametric roll, dead ship condition, excessive acceleration and surf-riding/broaching. Each of these failure modes is divided into three levels – two vulnerability levels and a third level, which consists of numerical simulations of the ship's behavior in waves.

Several papers have already presented results for specific vessels. Tompuri et al. (2015) discuss in details computational methods to be used in the Second Generation Intact Stability Criteria, focusing on level 1 and level 2 procedures for parametric roll, pure loss of stability and surf-riding/broaching. They also provide detailed calculations and sensitivity analyses for a specific RoPax Vessel and stress the need for software able

to do the extensive calculations. The detailed discussions attached to Tompuri et al. (2015) give a very valuable insight in the current status of development of the new criteria.

The present paper summarizes results performed for testing the Second Generation of Intact Stability Criteria. The paper deals with all five failure modes, with the first four modes evaluated for level 1 and 2 whereas the last criterion, surf-riding/ broaching, is evaluated for the first level only. The calculations are carried out for 17 ships for the full matrix of operational draughts (light service condition to summer draught), trims (even keel and two extreme trims forward and aft) and GM values. The results are presented as GM limit curves from the two levels and compared with the approved GM limit curve from the stability book.

The criteria used in the present calculations are based on Second Generation Intact Stability Criteria as amended in February 2015 and January 2016 by the Sub-Committee on Ship Design and

Construction of IMO. Furthermore, the explanatory notes from SDC 3/ WP.5. Annex 3-7 are consulted.

- Pure loss of stability (SDC 2/WP.4 Annex 1 (2.10.2.1 + 2.10.2.3))
- Parametric roll (SDC 2/WP.4 Annex 2 (2.11.2.1 + 2.11.2.3))
- Surf-riding /Broaching (SDC 2/WP.4 Annex 3)
- Dead ship condition (SDC 3/WP.5 Annex 1)
- Excessive acceleration (SDC 3/WP.5 Annex 2)

Three types of analysis have been performed:

1. Each criterion has been examined individually for the possibility of obtaining usable results for construction of a GM limit curve for the full range of operational draughts.
2. The relationship between level 1 and level 2 – the requirement that level 1 is more restrictive in GM limits than level 2 has been examined.
3. Will the new regulation be more or less conservative? The analysis has been performed for approved loading conditions.

All calculations have been carried out using NAPA stability software XNAPA Release B137 2016.0 sgis, VARDEF*SGIS.MATRIX. This is the same software as used in Tompuri et al. (2015). A more detailed description of the analysis can be seen in a information paper submitted to SDC 4 (IMO, 20016) A more detailed description of the analysis can be seen in a information paper submitted to SDC 4 (IMO, 20016)

2. SAMPLE SHIPS

The sample ships used for the calculation comprise 17 existing vessels. They include eight RoRo ships (six passenger and two cargo vessels); two installation vessels (jack-up vessels); three supply vessels – one standby vessel, one cable layer and one anchor handler; one bulk carrier and three container vessels. Detailed information of the ships and their loading conditions are available. The sample ship particulars can be seen in Table 1.

3. ANALYSIS

The analysis is performed for the full matrix of operational draughts from light ship to summer draught and for three trims – even and two extreme trims forward and aft. The calculations are carried out for the five modes of stability failure:

- Pure loss of stability
- Parametric roll
- Dead ship
- Excessive acceleration
- Surf-riding / Broaching

All modes are evaluated for criteria levels 1 and 2, except the last failure mode, where only level 1 is carried out. This last criterion, surf-riding/ broaching is a function of length and speed of the vessel and does not depend on GM of the vessel. The criterion pure loss of stability applies only to ships for which the Froude number exceeds 0.24.

In the mode ‘Pure loss of stability’ in criteria level 2, ships with low weather deck / low buoyant hull can give some unexpected results. The problem is caused when the regulatory wave crest results in water accumulated on the weather deck making the vessel much more vulnerable than it in fact is, see Figure 1. How to deal with this is not yet defined in the explanatory notes.



Figure 1: Illustration of “pure loss of stability” problem.

However, as the whole idea with the criteria is to understand the ships behavior to certain stability failure modes in waves, the hull form is some cases slightly modified, resulting in a more ‘appropriate’ hull form including all parts that provides buoyancy, even though they are not fully watertight due to freeing ports, mooring holes etc..

Table 1: Principal particulars of the sample ships.

Id	Type	L [m]	Fn	Built
1	RoRo Passenger	159.3	0.303	2016
2	RoRo Passenger	135.0	0.262	1997
3	RoRo Passenger	183.6	0.298	2009
4	RoRo Passenger	92.3	0.246	2010
5	RoRo Passenger	88.8	0.298	2013
6	RoRo Passenger	39.6	0.287	2011
7	Ro-Ro Cargo	180.5	0.261	2009
8	Ro-Ro Cargo	185.9	0.241	2014
9	Installation Vessel	155.6	0.170	2009
10	Installation Vessel	79.3	0.169	2011
11	Supply Standby	39.2	0.315	2011
12	Supply Cable Layer	120.4	0.175	2016
13	Supply Anchor Handler	81.6	0.310	2000
14	Bulk Carrier	174.6	0.173	2012
15	Container Ship	382.6	0.208	2006
16	Container Ship	324.6	0.222	1997
17	Feeder Vessel	154.1	0.250	1991

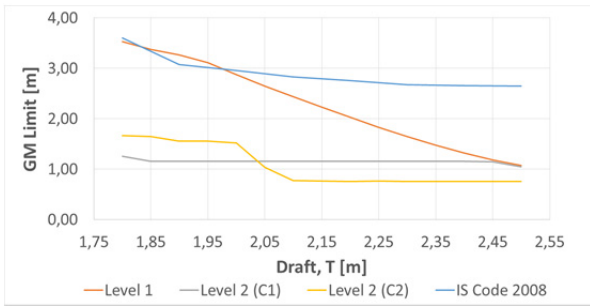


Figure 2: GM limit (T), Ship no. 6. Parametric roll – Trim Aft.

T [m] ->	1,80	1,85	1,90	1,95	2,00	2,05	2,10	2,15	2,20	2,25	2,30	2,35	2,40	2,45	2,50
0,50	0,999723	0,999829	0,999723	0,999723	0,999784	0,99967	0,999776	0,981413	0,944723	0,908274	0,867975	0,826277	0,783628	0,740228	0,697123
0,60	0,401473	0,364894	0,361204	0,328152	0,300658	0,283079	0,273306	0,255042	0,213733	0,195643	0,154949	0,136595	0,106229	0,104251	0,104251
0,70	0,215928	0,165096	0,175206	0,175206	0,175206	0,146461	0,151115	0,150762	0,118891	0,149063	0,136287	0,145849	0,136399	0,147018	0,136315
0,80	0,067038	0,067038	0,067038	0,030251	0,030251	0,030177	0,030171	0,007609	0,005674	0,005674	0,005674	0,005688	0,001864	0,002227	0,002245
0,90	0,000534	0,012973	8,94E-05	2,39E-05	2,39E-05	0	0	0	0,000006	0	0,000006	2,39E-05	0,000006	0,000101	0,000101
1,00	0,197812	0,194187	0,095044	0,098178	0,098851	0,081899	0,03876	0,011907	0,004161	0,000817	0,000117	2,39E-05	0,000006	0,000006	0,000006
1,10	0,148781	0,096632	0,025496	0,050534	0,050101	0,020118	0,007909	0,001346	0,001991	0,000639	0,001336	0,004117	0,01848	0	0
1,20	0,043295	0,034114	0,012728	0,021842	0,019676	0,019084	0,015468	0,014887	0,001047	0,012974	0,013976	0,012394	0,004137	0,002932	0,000028
1,30	0,019541	0,044388	0,044399	0,015102	0,023469	0,030474	0,043853	0,043446	0,004041	0,014422	0,005021	0,001367	0,001358	0,000349	0,231E-05
1,40	0,048124	0,076644	0,076118	0,054319	0,054279	0,054277	0,015917	0,030382	0,013203	0,004226	0,001367	0,000303	9,34E-05	2,43E-05	2,61E-05
1,50	0,064533	0,079934	0,078108	0,07688	0,06791	0,017428	0,015817	0,003355	0,001438	0,004029	8,91E-05	0,000006	0,000006	0	0
1,60	0,064153	0,080295	0,048896	0,046692	0,011957	0,015002	0,005364	0,001527	9,51E-05	2,39E-05	0	0	0	0	0
1,70	0,048589	0,017025	0,015895	0,015086	0,005983	0,00222	0,000532	8,91E-05	0,000006	0	0	0	0	0	0
1,80	0,015895	0,000983	0,004396	0,002213	0,000797	0,000162	2,39E-05	0	0	0	0	0	0	0	0
1,90	0,001028	0,000791	0,000241	8,91E-05	2,39E-05	0	0	0	0	0	0	0	0	0	0
2,00	0,000156	0,000096	0	0	0	0	0	0	0	0	0	0	0	0	0

Figure 3: Matrix (T, GM), Ship no. 6. Parametric roll, Level 2 (C2) – Trim Aft.

Inconsistency between Level 1 and Level 2

When analyzing the results from level 1 and level 2, it is expected that level 1 is more restrictive in GM limits than level 2. As the failure mode surf-riding/broaching is not based on a GM evaluation, it is not included in this analysis. For vessels having inconsistent GM results, the highest GM value is chosen.

The results from the analysis are shown in Table 3. The green color indicates that there is a proper relationship between the levels i.e. level 1 is more conservative than level 2 for all operational draughts. The red color indicates the opposite – if the whole or a part of the GM limit curve for level 2 is more restrictive than level 1, the cell is marked red. When it was not possible to obtain results for one of the levels, the consistency between the levels could not be evaluated; this is indicated with white or blue cells in the table.

Table 3 shows that in nearly half of the cases, level 2 results are more conservative than level 1; for the criterion pure loss of stability, it is the case for all vessels!

Loading Condition – Will the new regulation be more or less conservative?

The analysis is performed for approved operational loading conditions taken from the ship stability book. The results are summarized in Table 4.

4. CONCLUSIONS

A series of 17 existing vessels have been evaluated against the current version of Second Generation Intact Stability Criteria (SGISC). These criteria comprise five failure modes: Pure loss of stability, parametric roll, dead ship, excessive acceleration and surf-riding/ broaching. Results have been analyzed for different loading and trim conditions in terms of limiting GM curves. This study resulted in the following conclusions.

Construction of limiting GM curves (Table 2): With one or two exceptions for the vessels considered, it is not possible to derive a limiting GM curve. This is so especially for the parametric roll and dead ship failure modes, i.e. at a given draught multiple permissible GM values would be obtained for most of the vessels.

Inconsistency between level 1 and level 2 evaluation (Table 3): None of the vessels shows a consistent result when applying level 2 versus level 1 analysis for all failure modes. For more than half of the cases the limiting GM required by level 2 would be higher (more restrictive) than for level 1 analysis, which is not the intention.

Currently allowable loading conditions (Table 4): When evaluated at realistic operational GM (or KG) conditions allowed according to the current intact and damage stability criteria, none of the vessels satisfies all of the SGISC failure modes. The majority of vessels satisfy some of the failure modes under certain loading conditions. Some of the vessels satisfy the parametric roll criteria for all loading conditions considered. Very few vessels satisfy the excessive acceleration criterion in any loading condition.

In summary, it is concluded that the newly proposed intact stability criteria deliver inconsistent results for all vessels considered.

Table 3: Evaluation of the failure mode criteria – inconsistency between level 1 and level 2.

Green OK - GM limit for L1 > GM for L2 (except for excessive acceleration, where it is opposite)
 Red Not OK - GM limit for L1 < GM for L2 (except for excessive acceleration, where it is opposite)
 Blue No results - Computational problems for one or both levels
 Grey No results – no GM limit curve available due to inconsistency in results
 White No results – criterion does not apply to ship (Froude number lower than 0.24)

	Pure loss of stability			Parametric roll C1			Parametric roll C2			Dead ship			Excessive acc.		
	Aft	Even	Fwd	Aft	Even	Fwd	Aft	Even	Fwd	Aft	Even	Fwd	Aft	Even	Fwd
1	Red	Red	Red	Green	Green	Green	Green	Green	Green	Green	Green	Green	Green	Green	Green
2	Red	Red	Red	Red	Red	Red	Green	Green	Green	Green	Green	Green	Green	Green	Green
3	Red	Red	Red	Green	Green	Green	Green	Green	Green	Green	Green	Green	Green	Green	Green
4	White	White	White	Red	Red	Red	Green	Green	Green	Green	Green	Green	Green	Green	Green
5	Blue	Red	Red	Green	Green	Red	Blue	Red	Red	Red	Red	Red	Red	Red	Red
6	Red	Red	Red	Green	Green	Green	Red	Red	Red	Red	Red	Red	Red	Red	Red
7	Red	Red	Red	Green	Green	Green	Blue	Blue	Blue	Blue	Blue	Blue	Blue	Blue	Blue
8	Red	Red	Red	Red	Red	Red	Green	Green	Green	Green	Green	Green	Green	Green	Green
9	White	White	White	Red	Red	Red	Green	Green	Green	Green	Green	Green	Green	Green	Green
10	White	White	White	Blue	Blue	Blue	Red	Red	Red	Red	Red	Red	Red	Red	Red
11	Red	Red	Red	Blue	Blue	Blue	Red	Red	Red	Red	Red	Red	Red	Red	Red
12	White	White	White	Red	Red	Red	Green	Green	Green	Green	Green	Green	Green	Green	Green
13	Red	Red	Red	Red	Red	Red	Green	Green	Green	Green	Green	Green	Green	Green	Green
14	White	White	White	Green	Green	Green	Blue	Blue	Blue	Blue	Blue	Blue	Blue	Blue	Blue
15	White	White	White	Green	Green	Green	Blue	Blue	Blue	Blue	Blue	Blue	Blue	Blue	Blue
16	White	White	White	Green	Green	Green	Blue	Blue	Blue	Blue	Blue	Blue	Blue	Blue	Blue
17	Red	Red	Red	Green	Green	Green	Green	Green	Green	Green	Green	Green	Green	Green	Green

ACKNOWLEDGEMENTS

The work described in this paper has been financed by The Danish Maritime Fund.

The work was carried out by a consortium consisting of: Project group: IDA Maritime, The Society of Engineers, OSK-ShipTech A/S, Knud E. Hansen A/S, Odense Maritime Technology A/S, Maersk Maritime Technology, Lloyds Register Marine, Technical University of Denmark and University of Southern Denmark.

The work has been assisted by and advisory board consisting of: American Bureau of Shipping, ABS, Maersk Maritime Technology, MMT, Baltic and International Maritime Council, BIMCO, DFDS, and Danish Maritime Authority.

Table 4: Evaluation of loading conditions.

Green All loading conditions comply with the criteria
 Red One or more loading conditions do not comply with the new criteria. The number in the cell indicates the percentage of loading conditions not complying.
 Blue No useful results for GM limit (whole or part of curve).
 White Not calculated – criterion does not apply to ship (Froude number lower than 0.24)

	Pure loss of stability		Parametric roll			Dead ship		Excessive acc.	
	L1	L2	L1	L2 C1	L2 C2	L1	L2	L1	L2
1	Green	37	Green	Green	Green	Green	Green	Green	Blue
2	Green	Green	Green	Green	Green	Green	Green	100	Green
3	Green	Green	100	100	Green	Green	Green	100	100
4	Green	Green	Green	Green	Green	Green	100	100	100
5	Green	Green	Green	Green	Green	Green	100	33	Green
6	Green	Green	Green	Green	Green	Green	100	100	100
7	77	77	100	92	77	Blue	Blue	23	23
8	Green	Green	Green	Green	Green	Green	Green	13	Green
9	Green	Green	Green	Green	Green	Green	100	100	100
10	Green	Green	Green	Blue	Green	100	Green	Green	Green
11	100	100	Green	Blue	Green	33	100	100	100
12	Green	Green	Green	Green	Blue	Green	25	55	18
13	Green	55	Green	Green	Green	9	72	Green	27
14	Green	Green	Green	Blue	Blue	Blue	Green	74	52
15	Green	Green	50	12	Blue	Blue	Blue	25	Blue
16	Green	Green	100	100	Blue	Blue	Blue	Green	Blue
17	50	67	Green	Green	Green	Green	Green	82	33

REFERENCES

Ikeda Y., Himeno Y., Tanaka N., 1978, “A Prediction Method for Ship Roll Damping”, Report of Department of Naval Architecture, University of Osaka Prefecture, Report no. 00405
 IMO, 2008, “The international code on intact stability” (IS Code 2008)
 IMO, 2015, SDC 2/WP.4, Development of Second Generation Intact Stability Criteria. Report of the Working Group, London, UK.
 IMO, 2016, SDC 3/WP.5, Development of Second Generation Intact Stability Criteria. Report of the Working Group, London, UK.
 IMO, 2016, SDC 4/INF.9, Sample Ship Calculation Results, Submitted by Denmark, London, UK.
 Tompuri, M, Ruponen, P, Forss M, Lindroth, D (2015). “Application of the Second Generation Intact Stability Criteria in Initial Ship Design”, Transactions - Society of Naval Architects and Marine Engineers, Vol 122, pp 20-45

This page is intentionally left blank

Challenges of Dead Ship condition Vulnerability Criteria Development

William S. Peters, *U.S. Coast Guard (CG-ENG-2)*, william.s.peters@uscg.mil

Vadim Belenky, Ph.D., *Naval Surface Warfare Center Carderock Division*, vadim.belenky@navy.mil

ABSTRACT

The dead-ship condition is one of five stability failure modes for which second generation intact stability criteria (SGISC) is being developed by the International Maritime Organization (IMO). SGISC consists of three levels of successive assessment that are of increasing complexity: Levels 1 and 2 vulnerability criteria are intended to identify loading conditions that are not vulnerable to the given failure mode. The third level – a Direct Stability Assessment (DSA) -- is envisioned to involve the application of sophisticated, proprietary computer software that meet IMO agreed specifications. These assessment levels should be consistent: an assessment outcome of “not vulnerable” for a loading condition in Level 1 or 2, respectively, should not have an opposite outcome for Level 2 or DSA, respectively.

However, the dead-ship condition failure mode is different from the other failure modes since it is the only one that includes existing mandatory criteria (first generation) at the Level 1 assessment (the severe wind and rolling criterion – Weather Criterion, 2008 IS Code, part A, 2.3). Hence, consistency between Levels 1 and 2 in the dead-ship condition assessments is important to maintain the integrity of the 2008 IS Code. Otherwise, the potential exists for an unsafe situation if the SGISC vulnerability criteria are significantly less restrictive than the Weather Criterion because then motivation would exist to design for loading conditions beyond the applicability ranges of the Weather Criterion. This paper addresses these challenges.

Keywords: *dead-ship condition, second generation intact stability criteria (SGISC), vulnerability criteria, Weather Criterion, 2008 IS Code.*

1. INTRODUCTION

The second generation intact stability criteria (SGISC) under development by the International Maritime Organization (IMO), consists of three levels of successive assessment. Level 1 vulnerability criteria is intended as a simple assessment to identify loading conditions that are not vulnerable to the given failure mode. Level 2 is intended as a more complex analytical assessment applied to those loading conditions that do not satisfy the Level 1 standard. Loading conditions that do not satisfy the Level 2 standard may be subject to the third level – a Direct Stability Assessment (DSA), which is envisioned to involve the application of sophisticated, proprietary computer software that meet IMO agreed specifications. These assessment levels should be consistent: an assessment outcome of “not vulnerable” for a loading condition in Level 1

should not have an opposite outcome for Level 2. Likewise, a “not vulnerable” Level 2 outcome should not have an opposite outcome for DSA.

The dead-ship condition failure mode, however, is different since it includes existing mandatory criteria (first generation) as the Level 1 assessment (the severe wind and rolling criterion – Weather Criterion, 2008 IS Code, part A, 2.3). As a result, consistency between Levels 1 and 2 in the dead-ship condition assessments is important to maintain the integrity of the 2008 IS Code. In the case where the SGISC vulnerability criteria are significantly less restrictive than the Weather Criterion, the potential exists for an unsafe situation because motivation would exist for designers to choose loading conditions that are beyond the applicability ranges of the Weather Criterion.

Internal consistency is the first challenge of the dead-ship condition vulnerability criteria in Levels

1 and 2. The Weather Criterion is used as the Level 1 criteria and has the following characteristics:

1. it uses a deterministic model for the wind gust as 1.5 times the mean wind speed.
2. it uses a semi-empirical method to determine the roll-back angle.
3. it defines failure as a physical possibility of exceedance of an unacceptable level resulting from a single wind gust.

The Weather Criterion was developed based on ships with loading conditions with certain characteristics ($B/d < 3.5$ and $-0.3 < (KG/d-1) < 0.5$ and $T < 20s$) and when the loading condition is beyond those ranges. Model tests can be used to assess the wind heeling and the roll-back angle. Otherwise, for Level 1 vulnerability criteria, the Weather Criterion model is extended up to $T < 30s$.

On the other hand, the Level 2 vulnerability criteria has been developed using a probabilistic model for the wind gust based on the spectrum of wind velocity in which the roll-back angle is assessed from ship motion calculations, and stability failure is defined as a probability of exceeding an unacceptable level within one hour's duration. Because the Level 2 model is expected to be more advanced and detailed than the Level 1/Weather Criterion model, some degree of inconsistency can be expected. However, partly because the Weather Criterion is mandatory, there is no information about an accident involving the dead ship condition to assist with setting the standard for the Level 2.

To address these challenges, three objectives can be established:

- Ensure that the calculation methods used for the vulnerability criteria Level 2 are robust and are used within their applicability range.
- Choose the standard to ensure the integrity of the 2008 IS Code and consistency between the Levels 1 and 2 vulnerability criteria.
- Accept a certain probability of inconsistency and treat this probability as a safety level to then be used to set the standard.

The inconsistency of the analysis procedure and some preliminary results are described below.

2. ASSESSMENT OF INCONSISTENCY

How can the consistency between the Weather Criterion and the Level 2 vulnerability criteria be assessed?

Consider a ship in a critical condition on the Weather Criterion, such that any increase of the KG will mean the criterion is not satisfied. This critical condition means that either area a exactly equals area b , or the angle of heel under steady action of wind exactly equals its limit value (16 degrees or 80% of deck edge immersion, whichever is less).

The Level 2 vulnerability criterion is formulated probabilistically. The result of the calculation for Level 2 is a probability of at least one exceedance of the prescribed roll angle within an hour. The Level 2 vulnerability criterion can be applied to loading conditions of several ships where the Weather Criterion is fully applicable and are in a critical condition. If the Weather Criterion and Level 2 vulnerability criterion are absolutely consistent, the calculated probabilities should be exactly the same.

However, as a result of using different mathematical models for ship rolling under wind and wave action, those probabilities cannot be the same. Variation of these probabilistic values can be used to assess the inherent level of inconsistency between Levels 1 and 2.

Applicability of the Weather Criterion

The first step in this procedure is to ensure that $B/d < 3.5$, which can be achieved by selecting a draft. A ship where no operational draft corresponds to the condition $B/d < 3.5$ should be excluded from the sample.

Initial KG value is computed as:

$$KG_0 = BM + KB - GM_{\min} \quad (1)$$

Here, the lowest $GM_{\min} = 0.15$ m is taken from the requirements in the paragraph 2.2.4 of part A of the 2008 IS code.

Using accepted draft, KG_0 and assuming zero trim, one can compute the GZ curve. However, it is not guaranteed this KG_0 is realistic as it may not satisfy the other requirements of the 2008 IS code, part A/2.2. Nevertheless, there is sufficient information to compute the maximum KG based on the requirements of the 2008 IS code, A/2.2. This maximum KG is subsequently referred to as KG_1 .

There are limiting values of the KG based on the draft that can be easily derived from satisfying the inequality $-0.3 < (KG/d-1) < 0.5$:

$$KG_2 = 1.5d \quad (2)$$

$$KG_3 = 0.7d \quad (3)$$

Finally, there is the roll period condition $T < 20s$. Having in mind that the roll period is computed as described in paragraph A/2.3.4, 2008 IS Code:

$$T = \frac{2 \cdot C \cdot B}{\sqrt{GM}} \quad (4)$$

Where B is the moulded breadth and C is computed as:

$$C = 0.373 + 0.023 \frac{B}{d} - 0.043 \frac{L_{wl}}{100} \quad (5)$$

Where L_{wl} is the waterline length of the ship (m).

Thus, the KG meeting the requirement $T = 20s$ can be computed as:

$$KG_4 = BM + KB - \frac{C^2 \cdot B^2}{100} \quad (6)$$

The KG value for further computation can be chosen as:

$$KG = \min(KG_1, KG_2, KG_4) \quad (7)$$

However if the chosen KG is less than KG_3 , the ship should be excluded from the sample as the applicability ranges of the Weather Criterion cannot be achieved. The result of formula (7) also has to be checked for practicality – if such a KG value can be actually encountered on the ship.

Because the KG -value is defined by the conditions of applicability of the Weather Criterion, it may be used to achieve the critical condition of the Weather Criterion. Those critical conditions are frequently achieved by artificially increasing the windage area and height of its center until either area a exactly equals area b , or the angle of heel under steady action of wind exactly equals 16 degrees or 80% of deck edge immersion, whichever is less.

Calculation Process

The choice of the draft and KG value together with the assumption of zero trim defines all the input data needed for the calculation of the Level 2 vulnerability criteria. The calculation flow follows the description provided in Annex 4 of IMO document SDC 4/5/1 with the exception of two elements:

1. Instead of using the “standard” methodology for the estimation of the effective wave slope, a

direct pressure integration method is used, as described in Annex 10 to IMO document SDC 4/INF.

2. Instead of using the relative response amplitude operator (RAO), H_{rel} , the absolute RAO, H , is used in the formula 3.3.2.7-2 from Annex 4 of IMO document SDC 4/5/1.

The Level 2 vulnerability criteria value, C , is computed as described in paragraph 2.13.3.2.1 of Annex 1 of IMO document SDC 3/WP.5. Each criterion value, C , represents one point in a further statistical assessment.

3. INITIAL RESULTS

To check the feasibility of the procedure described in section 2. above, it was applied to 15 sample ship loading conditions; the characteristics of these ship’s loading conditions, as well as the calculation results are given in Table 1. If the Weather Criterion and Level 2 vulnerability were totally consistent, all the C values would be the same. The fact they are not indicates the inconsistency between the Weather Criterion and Level 2 vulnerability criterion. The question then becomes how much inconsistency can be tolerated? The remainder of this section provides the quantification of the probability of inconsistency.

To facilitate setting the Level 2 probability criterion, a normal distribution is assumed for the results. Q-Q plot of the centered and standardized criteria value is shown in Figure 1. While agreement is not perfect, the assumption of a normal distribution still can be accepted in the first expansion. If further collection of data rejects the normal distribution assumption, the next candidate would be a log-normal distribution. Setting the standard based on a direct estimate of the quantiles is also possible, if sufficient sample size is available.

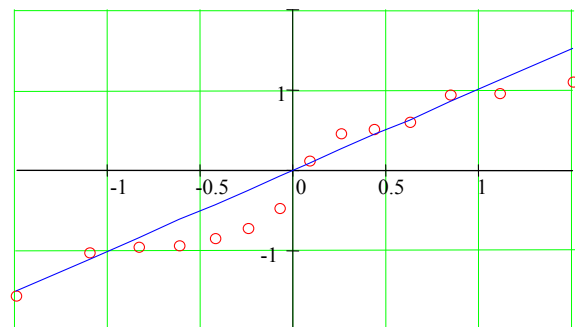


Figure 1: Q-Q Plot of the Criterion Values.

Estimations of the mean and standard deviation of these data points are, respectively:

$$\hat{E} = \frac{1}{n} \sum_{i=1}^n x_i = 0.219 \quad (8)$$

$$\hat{\sigma} = \sqrt{\frac{1}{n-1} \sum_{i=1}^n (x_i - \hat{E})^2} = 0.0107 \quad (9)$$

As the distribution of the data is assumed to be normal, the distribution of the estimate of the mean value follows the Student-t distribution, while the variance estimate distribution is related to the chi-square, χ^2 , distribution. The boundaries of the estimates (8) and (9) with the confidence probability $\beta = 0.95$ are:

$$\hat{E}_{low,up} = \hat{E} \mp \frac{\sigma}{\sqrt{n}} Q_t = [0.0159, 0.278] \quad (10)$$

Where $Q_t = 2.145$ is a quantile of Student-t distribution, computed for the probability $0.5(1 + \beta)$ and $n - 1 = 14$ degrees of freedom.

$$\hat{E}_{low,up} = \hat{\sigma} \sqrt{\frac{n-1}{\chi_{n-1}^2(0.5(1 \pm \beta))}} = [0.00785, 0.0169] \quad (11)$$

Where $\chi_{n-1}^2(0.5(1 \pm \beta))$ is a quantile of the χ^2 , distribution, computed for the probabilities $0.5(1 \pm \beta)$ and $n - 1 = 14$ degrees of freedom.

To show how the standard can be set with this data, a suggestion to accept a probability of inconsistency as $p = 0.05$ is studied. Then, the standard can be proposed as:

$$R_{DS0} = \hat{E} + \hat{\sigma} \cdot Q_N(1 - p) = 0.0395 \quad (12)$$

Where Q_N is a quantile of a standard normal distribution computed for the probability $1 - p$.

The confidence interval computed in equation (10) and (11) can be propagated further to evaluate how uncertain the results of these calculations are:

$$S_{low,up} = \hat{E}_{low,up} + \hat{\sigma}_{low,up} \cdot Q_N(1 - p) = [0.0289, 0.0557] \quad (13)$$

Indeed, as more ships are added as data points to these calculations, the confidence interval decreases. A decreasing p will increase the proposed standard. A noteworthy point is that this analysis (even performed on so few ships) produced a value close to what was proposed in the paragraph

2.13.3.1 at Annex 1 of IMO document SDC 3/WP.5.

CONCLUSIONS

This paper considered one of the main challenges of the vulnerability assessment in the dead ship condition, the consistency between the mandatory requirements in Part A of the 2008 IS Code/ Level 1 and the IMO Level 2 second generation intact stability criteria for the dead-ship condition. The particular difficulty for the dead-ship condition is that the process of ship rolling under the action of irregular waves and gusty wind is described with different mathematical models in the Weather Criterion and the Level 2 vulnerability criteria.

The proposed idea is to accept a certain probability of inconsistency and from this probability find the standard for the Level 2 vulnerability criteria. This approach uses statistics generated with a number of ships that are in a critical condition on the Weather Criterion and for which the Weather Criterion is fully applicable.

ACKNOWLEDGEMENTS

The work described in this paper has been funded by the Office of Design and Engineering Standards of the US Coast Guard (CG-ENG) under the guidance of Mr. Jaideep Sirkar. The authors are grateful to Mr. K. Weems (NSWCCD) for his help with calculations and to Prof. K. Spyrou for fruitful discussions on the methodology of calculations.

REFERENCES

- IMO 2016, "SDC 4/5/1 – Finalization of Second Generation Intact Stability Criteria, Report of the Correspondence Group", Submitted by Japan, 11 November 2016.
- IMO 2016a "SDC 4/INF4 - Finalization of Second Generation Intact Stability Criteria, Information, Collected by the Correspondence Group on Intact Stability", Submitted by Japan, 9 December 2016.
- IMO 2016b "SDC 3/WP.5- Finalization of Second Generation Intact Stability Criteria, Amendments to Part B of the 2008 IS Code on Towing, Lifting and Anchor Handling Operations" Report of the Working Group (Part 1) 21 January 2017.

Table 1: Summary of Calculations

Type	<i>L</i> (m)	<i>D</i> (m)	<i>L/B</i>	<i>B/d</i>	<i>KG/d-1</i>	<i>T</i> (s)	<i>C_B</i>	<i>C_M</i>	<i>C_W</i>	<i>GM</i> (m)	ϕ_{max} (deg)	<i>GZ_{max}</i> (m)	ϕ_v (deg)	Criterion, <i>C</i>
Cargo ship	159	9.8	6.95	2.34	-0.12	16.21	0.59	0.99	0.72	1.02	26	0.42	56	0.017
Containership	274	10.6	8.53	3.04	0.19	20.00	0.54	0.92	0.67	1.09	46	1.35	79	0.042
RoPax	140	5.8	6.93	3.49	0.50	12.64	0.59	0.93	0.80	1.59	73	2.01	129	0.032
Bulk Carrier	149	10.8	6.47	2.13	-0.16	20.00	0.80	0.99	0.87	0.68	42	0.67	65	0.012
Containership	262	11.5	6.55	3.48	0.50	15.56	0.56	0.96	0.77	3.06	44	2.23	76	0.013
LNG carrier	257	12.0	6.17	3.47	0.36	20.00	0.78	0.98	0.83	2.04	38	2.11	63	0.032
Passenger	248	10.3	6.90	3.50	0.50	16.14	0.72	0.98	0.87	2.39	36	1.40	74	0.005
Cargo ship	122	7.0	7.01	2.50	-0.05	20.00	0.70	0.99	0.79	0.43	56	1.21	111	0.014
Bulk Carrier	280	17.6	5.96	2.67	-0.14	14.21	0.82	1.00	0.89	4.31	26	1.63	59	0.027
Containership	283	12.1	8.80	2.66	0.14	20.00	0.64	0.95	0.83	1.01	39	1.22	60	0.034
Containership	330	15.1	7.24	3.01	0.31	20.00	0.65	0.98	0.84	1.88	38	1.84	59	0.023
Tanker	320	21.1	5.52	2.75	-0.01	20.00	0.80	1.00	0.88	3.00	28	1.54	48	0.012
Containership	327	13.2	7.17	3.47	0.50	17.90	0.58	0.90	0.77	2.53	34	1.68	54	0.011
Containership	376	16.5	6.53	3.49	0.46	20.00	0.61	0.95	0.80	2.82	49	3.15	78	0.027
Containership	198	10.4	6.66	2.86	0.20	20.00	0.60	0.98	0.78	1.11	51	1.88	89	0.028

This page is intentionally left blank

Model Experiment on Pure Loss of Stability for a Ship in Astern Waves and Its Relationship with the Second Generation Intact Stability Criteria

Naoya Umeda, *Osaka University*, umeda@naoe.eng.osaka-u.ac.jp

Mizuki Osugi, Masahiro Sakai, *Osaka University*,

Akihiko Matsuda, Daisuke Terada, *National Research Institute of Fisheries Engineering*

ABSTRACT

For examining the applicability of direct stability assessment for pure loss of stability in astern waves to the accident due to the relevant failure mode, a model experiment for an ocean research vessel which has a hull form similar to the accident vessel was executed and then its results are compared with the numerical simulation using a coupled surge-sway-roll-yaw model. As a result, it was confirmed that the numerical simulation to be used for direct assessment qualitatively and quantitatively explains the experimental results. This good agreement suggests that the applicable speed limit for the draft criteria is reasonable and the deck space surrounded bulwark should be regarded as water-tight for the numerical simulation.

Keywords: *direct stability assessment, bulwark, ocean research vessel.*

1. INTRODUCTION

The second generation intact stability criteria, which are now under development at the International Maritime Organization (IMO), will include explicit design requirements for preventing stability failures due to restoring variation in waves for the first time at the IMO. This could be useful for designers to avoid possible capsizing accident. To demonstrate such benefit for ship designers, at least it should be examined whether the new requirement could prevent major capsizing accidents in the past.

In 1980's an ocean research vessel was lost off Fukushima in Japan when she ran in heavy astern seas. This accident was widely reported in media with the term "broaching". The accident investigation finally suggests that this accident was triggered with loss of restoring moment in stern quartering waves (The Japan Association of Marine Safety, 1990). Thus it is important whether the draft stability criteria for pure loss of stability in following waves to be included in the second generation intact stability criteria can explain this accident or not.

It is known that the restoring moment is likely to change when the wavelength is nearly equal to the ship length. When the midship of a ship is

located at a wave crest, the roll restoring moment could reduce or nearly become zero and as a result, capsizing could be occurred sometimes. Paulling (Oakley et al., 1974) named this kind of capsizing mode as "pure loss of stability" and defined as "A ship encounters one or more very steep high waves, with little or no preliminary rolling motion, simply loses all stability when a crest moves into the amidships position and 'flops' over".

The new intact stability criteria of pure loss of stability are composed of the two-layered vulnerability criteria and the direct stability assessment procedure. Here the direct stability assessment procedure is most accurate and normally relies on numerical simulation in the time domain, which should be validated with model experiment. Once this direct stability assessment procedure is established, the vulnerability criteria can be easily developed as a simplified version of the direct assessment.

As one of the numerical simulation tools to be used for the direct assessment for pure loss of stability, a surge-sway-yaw-roll (4DoF) simulation model was proposed by Kubo et al. (2012) and validated with free running model experiment of the C11 class containership. However, the containership accidents due to pure

loss of stability are not so well known so that we conducted free running experiment using the model of a ship which is similar to the lost ocean research vessel and then compared the results with the numerical simulation of the 4DoF model. This comparison could facilitate our discussion on the criteria for pure loss of stability.

2. ACCIDENT IN ASTERN SEAS

In June 1986, a research ship sunk off Fukushima in Japan on its maiden voyage without any emergency call. The maritime court concluded that the height of centre of gravity was increased due to several changes of design during construction and then during her maiden voyage the ship heeled significantly when she ran in severe stern quartering waves. The principal particulars of the ship at the initial design stage and the estimated condition at the accident are shown in Tables 1 and 2, respectively.

Table 1: Principal particular of the accident ship in the initial design phase.

Items	Ship
Length(PP)	22.00m
Breadth	5.00m
Depth	2.20m
Mean draught	1.75m
GM	0.56m

Table 2: Condition when the accident occurred

Ship speed	10[kts]
Wave height	3.0[m]
Wave period	5~6[s]
Encounter angle	-45[degrees]
GM	0.41[m]

In this study, we used a ship having a relatively similar hull form in the literature (Small Ship R&D committee, 1988) for the model experiment. The standard condition for the experiment was the Froude number, F_n , of 0.35, the wave steepness, H/λ , of 1/13, the wavelength to ship length ratio, λ/L_{pp} , were 1.75, and the encounter heading angle, χ , were -30 degrees from the wave direction. These are selected to be close to the accident condition except for the heading angle, which is slightly smaller because of the width of the used model basin.

3. MODEL EXPERIMENT

The free running model experiment was carried out at a seakeeping and manoeuvring basin of the National Reserch Institute of Fisheries Engineering, which is 60 m long, 25 m wide and 3.2 m deep. A 1/10 scaled model was used; its principal dimensions and model photo are shown in Table 3 and Figure 1, respectively. In this experiment, two different metacentric heights, GMs, were used: GM of 0.041 m simulates the accident, and that of 0.056m was based on the initial design. The model has a extended low weather deck which are surrounded by bulwark with freeing ports.

Table 3: Principal particulars of the ship model

Items	Ship	Model
Length(PP)	22.00m	2.20m
Breadth	4.90m	0.49m
Depth	2.20m	0.22m
Mean draught	1.75m	0.175m
Block coefficient	0.61	0.61
Metacentric height	0.41m 0.56m	0.041m 0.056m



Figure 1: Photo of the ship model

Table 4: Experimental condition

Froude number	0.15,0.20,0.25,0.30,0.35,0.385,0.40
Wave steepness	0.025,0.04,0.05,0.06,1/13,0.1
The wave length to ship length ratio	0.80,1.0,1.25,1.5,1.75,2.0
Encounter angle	-5,-15,-30,-45
Rudder gain	0.5,1,2,3

The ship model ran in regular stern quartering waves with a proportional autopilot for keeping a mean heading angle from the wave direction and with a constant propeller revolution. The roll, pitch and yaw angle were measured by an optical fibre gyroscope inside the ship model,

and the ship position was detected by a total station system, which consists of a theodolite and a prism. The experimental conditions are shown in Table 4, and were based on the standard one and those for identifying sensitivities of the operational parameters.

The experimental procedure was based on the ITTC recommended procedures for intact stability model tests, 7.5-02-07-04.1. First the model was situated near the wave maker. After the wave train propagates enough in the model basin, the model propeller revolution was increased to the specified value to achieve the required speed and the steering system activated.

4. RESULT OF MODEL EXPERIMENT

Examples of time histories measured in the experiment with the accident and designed GM are shown in Figure 2 and Figure 3, respectively. Here the term “wave height” in these graph represents the wave displacement at midship, which is defined downward positive. The roll and yaw angles are defined starboard positive. The examples indicate that the ship significantly rolls to the starboard direction whenever the ship centre meets a wave crest. This can be regarded as typical pure loss of stability mode. Larger roll angle can be found in case of the accident GM.

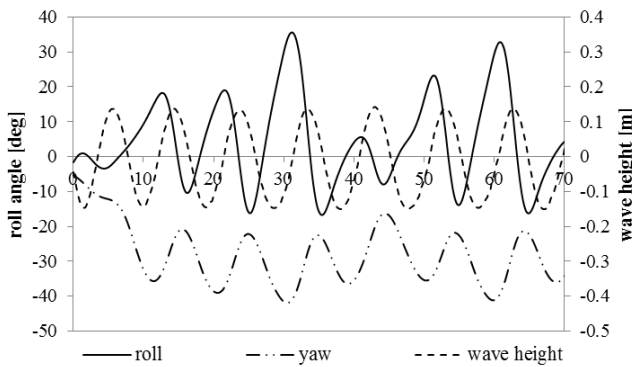


Figure 2: An example of time history of regular wave in GM=0.41m ($F_n=0.35$, $H/\lambda=1/13$, $\lambda/L=1.75$, $K_p=1.0$, $\chi=-30$ [deg])

The effects of several parameters on the maximum roll angle, based on the free running model experiment, are shown in Figures. 4-8. The maximum roll angle increases with the ship forward speed and the wave steepness, as shown in Figures 4-5. In particular, the significant increase of the roll angle can be found when the Froude number is above 0.3. This measured tendency supports the draft vulnerability criteria,

which are designed to be applied only the Froude number of 0.24 or over. It is also noteworthy the roll angle is not proportional to the wave steepness so that the phenomenon is nonlinear. The maximum roll angle has a peak at the wavelength to ship length ratio of 1.25 or 1.5 and at the heading angle of -30 degrees. The effect of the rudder gain is not significant so that the operational effect could be limited for this mode.

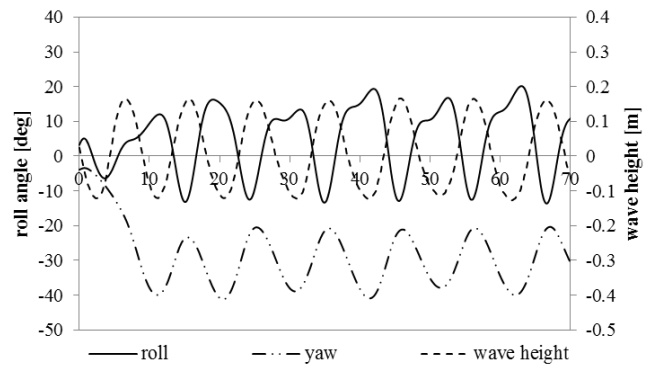


Figure 3: An example of time history of regular wave in GM=0.56m ($F_n=0.35$, $H/\lambda=1/13$, $\lambda/L=1.75$, $K_p=1.0$, $\chi=-30$ [deg])

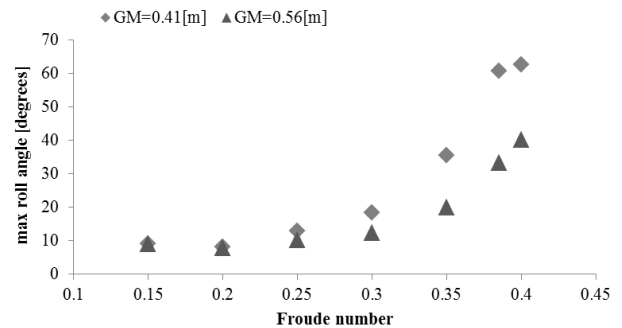


Figure 4: Effect of the Froude number on the maximum roll angle with $H/\lambda=1/13$, $\lambda/L=1.75$, $K_p=1.0$, $\chi=-30$ [degrees]

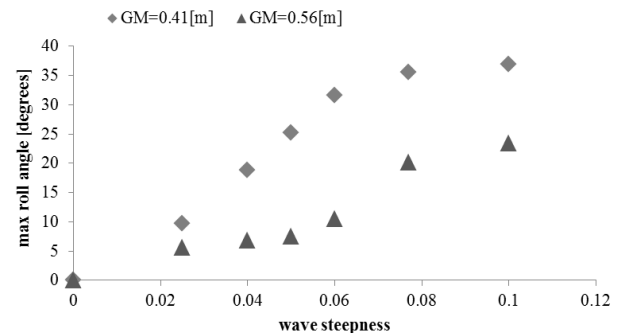


Figure 5: Effect of the wave steepness on the maximum roll angle with $F_n=0.35$, $\lambda/L=1.75$, $K_p=1.0$ and $\chi=-30$ [degrees]

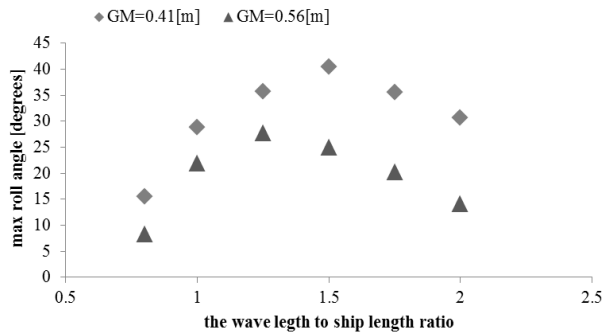


Figure 6: Effect of the wavelength on the maximum roll angle with $F_n=0.35$, $H/\lambda=1/13$, $K_p=1.0$ and $\chi=-30$ [degrees]

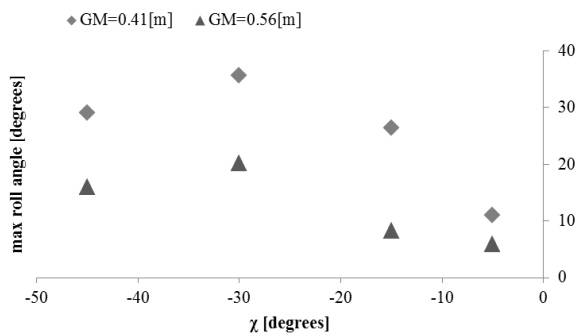


Figure 7: Effect of the heading angle on the maximum roll angle with $F_n=0.35$, $H/\lambda=1/13$, $\lambda/L=1.75$ and $K_p=1.0$

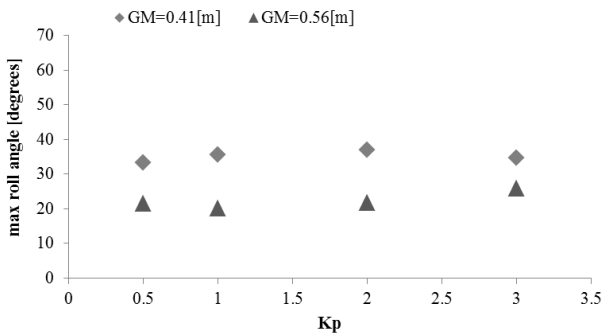


Figure 8: Effect of the rudder gain on the maximum roll angle with $F_n=0.35$, $H/\lambda=1/13$, $\lambda/L=1.75$ and $\chi=-30$ [degrees]

5. COMPARISON WITH NUMERICAL SIMULATION

As a next step, the numerical simulation using a coupled surge-sway-yaw-roll model developed by Kubo et al. were executed and compare its results with the model experiment mentioned above. This model is based on a manoeuvring simulation model with wave-induced forces and moments estimated with a slender body theory

under the low encounter frequency assumption (Umeda et al., 1995) as well as the restoring variation under the Froude-Krylov assumption. For calculating the restoring moment, the hull is water-tight up to the level of bulwark top. The calculated righting arms are shown in Figure 9. The roll damping moment was estimated with the roll decay test data as shown in Figure 10. The hull manoeuvring coefficients used here are from the measured ones for the offshore supply vessel model and the rudder parameters are estimated empirically.

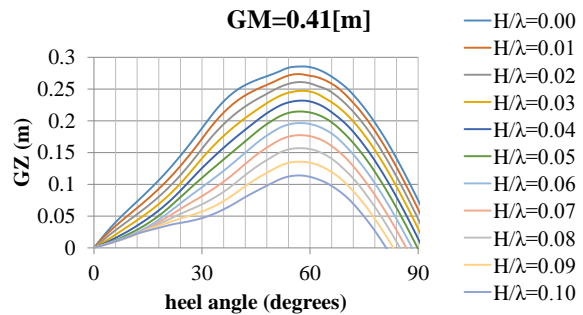


Figure 9: GZ curves used for numerical simulation in longitudinal waves with the wave steepness ranging 0 to 0.1 and the wavelength to ship length ratio of 1 at the wave crest amidship.

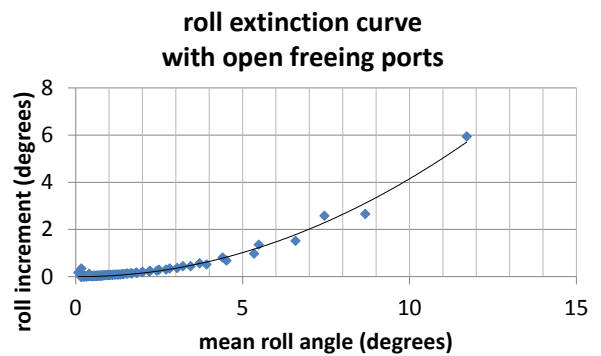


Figure 10: Roll extinction curve of roll decay tests with open freeing port.

As shown in Figures 11-12, the numerical simulation well explains the qualitative difference between two different GMs. In case of the design GM the roll motion includes superharmonics but in the accident GM does not so. For the maximum and minimum values of the roll angle, quantitative agreement between the numerical simulation and the model experiment can be found. However, if we calculated the restoring moment up to the weather deck, the ship in the numerical simulation frequently results in capsizing. This

suggests that the bulwark is effective to prevent water ingress above the weather deck at least for short duration when the water level exceeds the weather deck but is still below the bulwark. This could be a clue for developing reasonable vulnerability criteria.

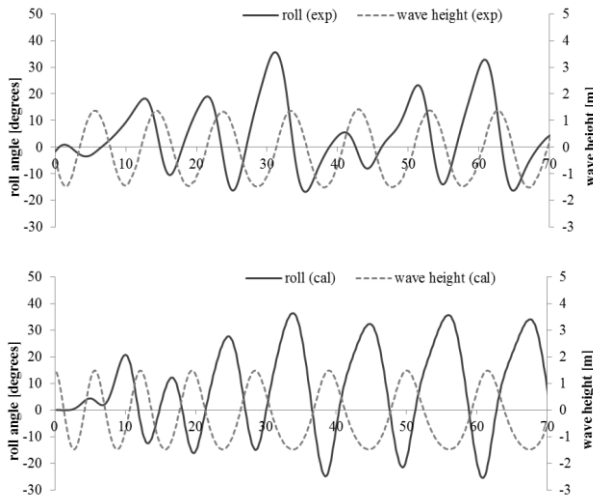


Figure 11: Comparison of ship motions between the experiment and the simulation in GM=0.41m with $F_n=0.35$, $H/\lambda = 1/13$, $\lambda/L=1.75$, $K_p=1.0$ and $\chi = -30$ [degrees]

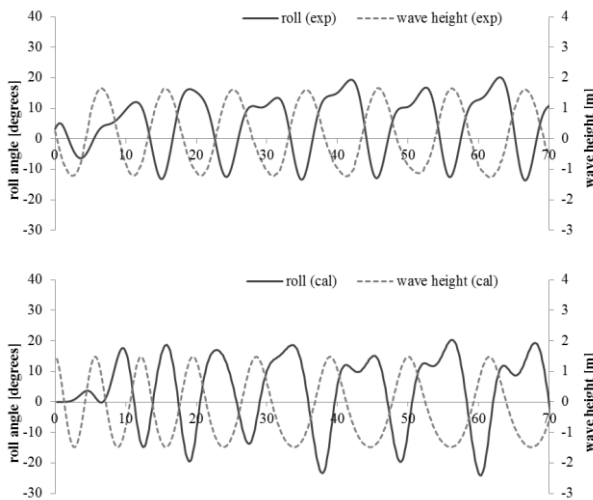


Figure 12: Comparison of ship motions between the experiment and the simulation in GM=0.56m with $F_n=0.35$, $H/\lambda = 1/13$, $\lambda/L=1.75$, $K_p=1.0$ and $\chi = -30$ [degrees]

Wider comparisons between the numerical simulation and the model experiment for several operational parameters are shown in Figures 13-18. The agreement between the two is generally satisfactory except for the low speed cases and extremely high wave steepness cases. Since low speed case results in relatively high encounter frequency, the wave making and inertia effects

could not be neglected so that the simulation model based on high frequency assumption should be applied as well in future.

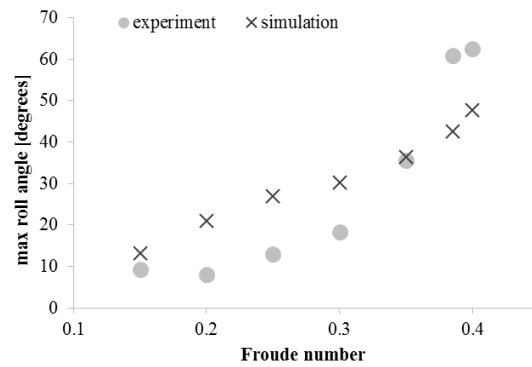


Figure 13: Comparison of the roll angle as a function of the Froude number between the experiment and the simulation with GM=0.41m, $F_n=0.15-0.4$, $H/\lambda = 1/13$, $\lambda/L=1.75$, $K_p=1.0$ and $\chi = -30$ [degrees]

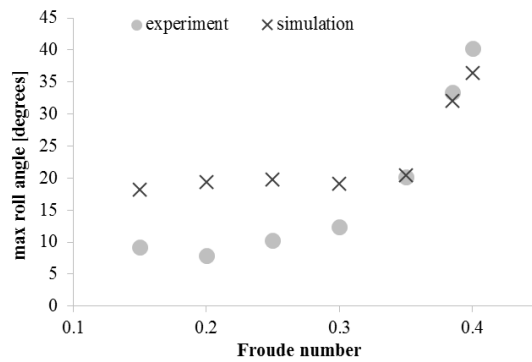


Figure 14: Comparison of the roll angle as a function of the Froude number between the experiment and the simulation with GM=0.56m, $F_n=0.15-0.4$, $H/\lambda = 1/13$, $\lambda/L=1.75$, $K_p=1.0$ and $\chi = -30$ [degrees]

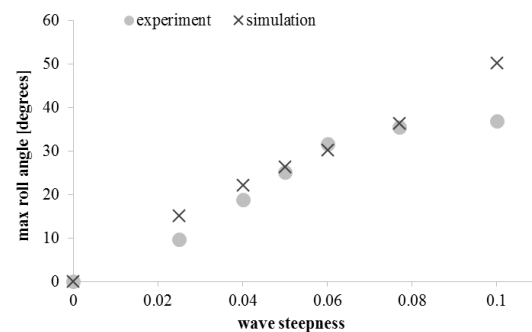


Figure 15: Comparison of the roll angle as a function of the wave steepness between the experiment and the simulation with GM=0.41m, $F_n=0.35$, $H/\lambda = 0.025-0.1$, $\lambda/L=1.75$, $K_p=1.0$ and $\chi = -30$ [degrees]

6. CONCLUSIONS

The manoeuvring-based surge-sway-yaw-roll simulation model shows qualitative and

quantitative agreements with the free-running model experiment in which significant roll were observed whenever the centre of the ocean research vessel model running in stern quartering waves meets a wave crest.

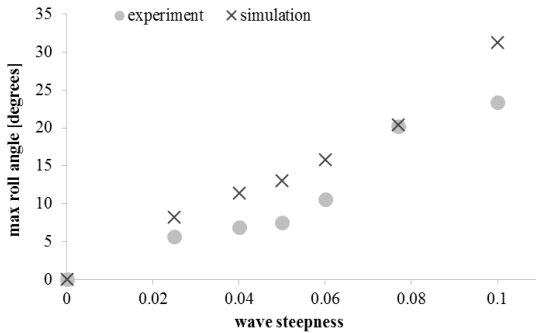


Figure 16: Comparison of roll angle as a function of the wave steepness between the experiment and the simulation with $GM=0.56m$, $F_n=0.35$, $H/\lambda =0.025\sim0.1$, $\lambda /L=1.75$, $K_p=1.0$ and $\chi =-30$ [degrees]

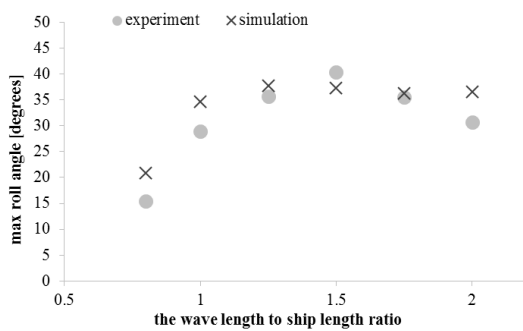


Figure 17: Comparison of roll angle as a function of the wavelength between the experiment and the simulation with $GM=0.41m$, $F_n=0.35$, $H/\lambda =1/13$, $\lambda /L=0.8\sim2.0$, $K_p=1.0$ and $\chi =-30$ [degrees]

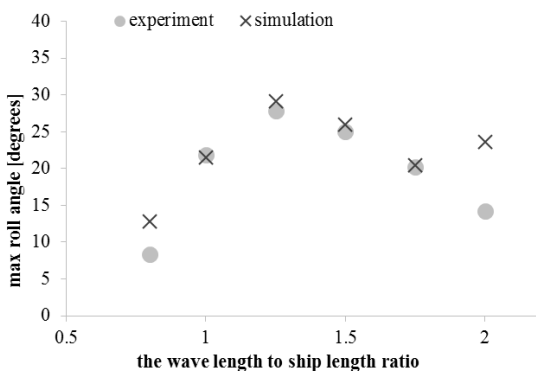


Figure 18: Comparison of roll angle as a function of the wavelength between the experiment and the simulation with $GM=0.56m$, $F_n=0.35$, $H/\lambda =1/13$, $\lambda /L=0.8\sim2.0$, $K_p=1.0$ and $\chi =-30$ [degrees]

This suggests that :

1. such numerical tool as a possible direct stability assessment procedure tool well explains the known accident due to pure loss of stability in stern quartering waves;
2. danger of pure loss of stability drastically increases when the Froude number is 0.3 or over.
3. the volume surrounded with the bulwark could be regarded as water-tight because of limited time duration.

Acknowledgements This work was supported by a Grant-in Aid for Scientific Research from the Japan Society for Promotion of Science (JSPS KAKENHI Grant Number 15H02327). It was partly carried out as a research activity of Goal-based Stability Criteria Project of Japan Ship Technology Research Association in the fiscal years of 2016 funded by the Nippon Foundation. The authors appreciate Messrs. Thet Zaw Htet, Shusuke Ohiwa and Taiki Murakami from Osaka University for their effective assistance in the experiment.

REFERENCES

Kubo H., Umeda N., Yamane K. and Matsuda A., 2012: “Pure Loss of Stability in Astern Seas -Is It Really Pure?-, Proc. of the 6th Asia-Pacific Workshop on Marine Hydrodynamics, Johor, pp.307-312.

Oakley O.H., J.R. Paulling and P.D. Wood, 1974: “Ship Motions and Capsizing in Astern Seas”, Proceedings of the 22nd Symposium on Naval Hydrodynamics, Cambridge, pp.1-51.

Small Ship R&D committee, 1988: “Report of R&D for Improving Safety and Profitability of Small Craft”, Report of Tsukuba Research Institute, Japan Shipbuilding Promotion Foundation, pp. 10-70, in Japanese.

The Japan Association of Marine Safety, 1990: “Diaster of the submarine support vessel Herios”, Sea and Safety, No. 375, pp. 2-11, in Japanese.

Umeda N., Yamakoshi Y. and Suzuki S.1995: “Experimental Study for Wave Forces on a Ship Running in Quartering Seas with Very Low Encounter Frequency”, Proc. of the International Symposium on Ship Safety in a Seaway, Kaliningrad, Vol.1, No.14, pp.1-18, Vol.1, No.14, pp.1-18.

Umeda N., Aqmil A., Sakai S., Matsuda A., Terada D., 2016: “Model Experiment of an Offshore Supply Vessel Running in Astern Waves”, Proc. of the 15th ISSW, Stockholme, 11-16.

Possible Simplifications of Direct Stability Assessment

Vladimir Shigunov, *DNV GL SE, Hamburg, Germany*, vladimir.shigunov@dnvgl.com

ABSTRACT

The second generation intact stability criteria, presently developed at IMO, are based on three alternative assessment procedures: level 1, level 2 and a direct stability assessment (DSA). DSA is the most accurate assessment available in SGISC, however, it requires significant computational effort. To reduce it, three simplifications are considered to enable using DSA in practical design approval: extrapolation of the average time to stability failure over wave height, reduction of the assessment to few selected design situations and use of deterministic safety criteria in design situations.

Keywords: *Second-Generation Intact Stability Criteria, Direct Stability Assessment, Probabilistic Assessment.*

1. INTRODUCTION

The framework of the second generation intact stability criteria (SGISC) [1] relies on three alternative assessment procedures: level 1 (L1), level 2 (L2) and direct stability assessment (DSA). Compliance with any of these assessments is sufficient to fulfil SGISC. Alternatively, ship-specific operational limitations (OL) or operational guidance (OG) can be developed for loading conditions failing to fulfil the criteria.

Assessment of a loading condition is done by comparing a *criterion* (measure that quantifies ship safety in seaway) with a *standard* (threshold value that separates safe and unsafe values of the criterion). In a *probabilistic DSA*, the probability of stability failure (or a similar measure, such as rate of stability failures per time) is used as a criterion, thus a probabilistic DSA requires some form of counting of stability failure events per given time, which means that such events need to be encountered in the simulations. This leads to the *problem of rarity*, because for the cases where DSA will be relevant in practice, stability failure events are very rare. Moreover, a reliable estimate of stability failure probability requires simulation of a sufficiently large number of stability failure events, which further increases required simulation time.

On the other hand, DSA is intended to be the most accurate procedure available in SGISC, which considers all relevant physics in the most accurate way. Thus, simulation tools employed in DSA are rather slow and require much more computational time than those in L1 and L2, i.e. simplifications

are required in *probabilistic procedures* to enable the use of DSA in practical design approval. Several probabilistic procedures have been proposed so far reducing the required simulation time or number of simulations or both. Here, two of such probabilistic procedures are studied: extrapolation of the average time to stability failure over wave height and reduction of the number of cases considered in the assessment to few selected *design situations* defined by the specified ship speed and wave height, direction and period.

The advantage of the extrapolation of time to stability failure over wave height is that it provides, in feasible computational time, probability of stability failure for all combinations of wave height, period and direction encountered during a design life of a ship, and the results of such DSA can be directly used as an OG.

In the *design situations* method, the assessment is performed for few selected combinations of ship speed and wave height, direction and period, referred to as design situations, which significantly reduces the number of required simulations. The drawback of this approach is that the results of DSA cannot be directly used as OG, thus OG will have to be developed for loading conditions failing to fulfil DSA. On the other hand, such a quick DSA procedure will efficiently reduce the number of loading conditions requiring OG. Paper [2] shows that this method reduces the required computational time by an order of magnitude compared to the extrapolation method. On the other hand, significant scatter of the dependencies of the stability failure probability computed over all sea

states and all wave headings on the results of the procedure based on design situations was found between various ships and loading conditions. This paper tests the idea of using different design situations for different stability failure modes and considers, as the first step, dead ship stability failure in beam seaway.

The drawback of a probabilistic DSA is the need to directly simulate rare stability failure events, which requires long simulation times even when design situations are used; besides, probabilistic DSA is very difficult to do using model tests instead of numerical simulations. Therefore, another idea tested here to further simplify and accelerate DSA combines design situations with *non-probabilistic (deterministic) safety criteria*, such as the expected maximum roll amplitude during a specified time, mean roll amplitude etc. Evaluation of such criteria requires much less simulation time and is much easier to implement in model tests than evaluation of stability failure probability. Therefore, it appears worthwhile to check whether such simplified criteria are sufficiently accurate for practical use.

2. PROBABILISTIC ASSESSMENT

In a probabilistic DSA procedure, the probability of stability failure is used directly as a safety measure (criterion). Therefore, such DSA requires some form of counting of stability failure events. The probability of stability failure of a ship in a given loading condition during a given exposure time can be found by performing a sufficiently big number of simulations of a given duration, covering all relevant sea states, wave directions and ship speeds, and dividing the number of simulations in which a stability failure occurred by the total number of simulations. An alternative approach, based on the assumption of stability failure events as a Poisson process, can be used *if stability failure events are independent of each other*. This independence is obvious for the stability failure events in the reality; in numerical simulations, independence of stability failure events should be provided by the procedure. Here, each numerical simulation was performed (in a given sea state) only until the first stability failure event (here, exceedance of 40° roll angle). After that, the simulation was stopped and restarted, in the same sea state, with a different set of random phases,

frequencies and directions of the wave components composing sea state.

For a Poisson process, the time to stability failure T is a random *exponentially distributed variable* with a constant *rate parameter* r and the following well-known characteristics:

1. Probability density function

$$f(T) = re^{-rT}, T \geq 0, 0 \text{ otherwise} \quad (1)$$

2. Cumulative distribution function

$$f(T) = 1 - e^{-rT} \text{ for } T \geq 0, 0 \text{ otherwise} \quad (2)$$

3. Expected time until stability failure

$$E\{T\} \equiv \bar{T} = 1/r \quad (3)$$

4. Standard deviation of time until failure

$$\sigma\{T\} = 1/r = \bar{T} \quad (4)$$

5. Variance of time until stability failure

$$Var\{T\} = 1/r^2 = \bar{T}^2 \quad (5)$$

6. Probability of at least one failure during time t

$$p = 1 - e^{-rt} = 1 - e^{-t/\bar{T}} \quad (6)$$

7. Maximum likelihood estimate of rate r

$$\tilde{r} = N / \sum_{i=1}^N T_i \quad (7)$$

where T_i are time intervals until stability failure from each of N realisations;

8. Maximum likelihood estimate of the expected time until stability failure

$$\tilde{T} = \frac{1}{N} \sum_{i=1}^N T_i \quad (8)$$

9. If T_1, \dots, T_L are independent exponentially distributed variables, m in $\{T_1, \dots, T_L\}$ is also exponentially distributed with rate $r = r_1 + \dots + r_L$; this is very convenient for combining stability failure modes.

Relation (4) allows estimating other statistical characteristics of an exponential distribution knowing only the estimated expected value \tilde{T} . To check this relation for exceedance of a given roll amplitude, Fig. 1 shows the ratio of the estimate of standard deviation of time to failure to the estimate of the expected time to failure as a function of the number of simulated stability failure events, whereas Fig. 2 shows the estimate of standard deviation $\sigma\{T\}$ vs. the expected value estimate \tilde{T} after $N=200$ simulated stability failure events; the results confirm that equations (4) and (5) can be used to estimate the standard deviation and variance of the time until stability failure event (for a given loading condition, forward speed and course, and wave height, direction and period).

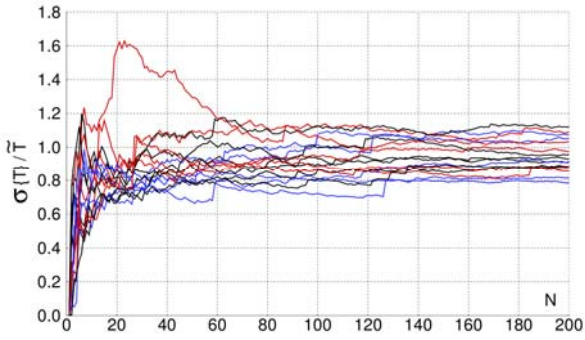


Fig. 1. Ratio of estimate of time to failure standard deviation to estimate of expected time to failure depending on number of simulated failures

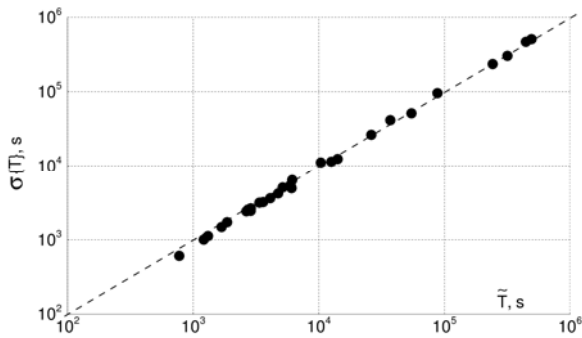


Fig. 2. Estimate of time to failure standard deviation vs. estimate of expected failure time for 200 simulated failure events

According to the central limit theorem, for a sufficiently large sample size N the expected time to failure can be assumed normally distributed with the standard deviation $\sigma\{\bar{T}\} = \sigma\{T\}/N^{0.5}$, where $\sigma\{T\}$ is the standard deviation of the time to stability failure and N is the sample size. Then, for example a 95%-confidence interval for the expected time to stability failure, $\bar{T} \pm 1.96 \cdot \sigma\{\bar{T}\}$, can be estimated as $\tilde{T} \pm 1.96 \cdot \tilde{T}/N^{0.5}$, or $\tilde{T}(1 \pm 0.14)$ for $N=200$. This can be used to estimate the required number of simulated stability failures to estimate the expected time to stability failure with a given accuracy $\Delta\tilde{T}/\tilde{T}$,

$$N = 1.96^2 / \left(\frac{\Delta\tilde{T}}{\tilde{T}} \right)^2 \quad (9)$$

where $\Delta\tilde{T}$ is a 95%-confidence interval for the estimate of the expected time to failure. Figure 3 shows the estimate of the expected time to failure depending on the number N of simulated failure events from simulations together with the boundary of $\Delta\tilde{T}/\tilde{T}$ according to (9) and $\pm 5\%$ boundaries. The figure shows that 5%-accuracy requires about $N=200$ simulated failure events.

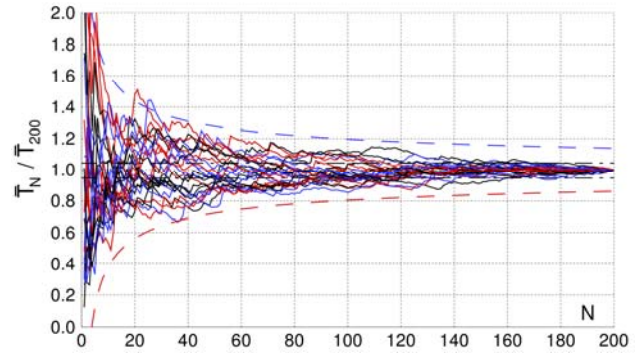


Fig. 3. Estimate of expected time to failure depending on the number of simulated failure events (solid lines) vs. estimate (9) (dashed lines) and 5%-tolerance boundaries (dash-dotted lines)

3. EXTRAPOLATION OVER H_s

The problem of rarity together with the problem of large number of stability failure events that need to be simulated need probabilistic procedures which can reduce required simulation time. This study considers the method of extrapolation of the expected time to stability failure \bar{T} over significant wave height h_s (at a given wave period, wave direction and ship forward speed). The extrapolation method proposed in [3] is applied here in the following form:

$$\ln T = A + B/h_s^2 \quad (10)$$

where T means in this section the expected time to stability failure, h_s is the significant wave height and A and B are constant coefficients, independent from the significant wave height but dependent on the ship, loading condition, ship forward speed, wave period and wave direction.

This procedure efficiently calculates the rate of failure events for all sea states encountered during the design life of a ship, thus the results can be directly used as OG. In [2] it was shown that the procedure can provide accurate results; here the uncertainties of this procedure are quantified by comparison with direct simulations. The main particulars of ships and load cases used in testing are summarised in Table 1 (length between perpendiculars L_{pp} , waterline breadth B_{wl} , draught midships d and metacentric height GM).

In [2] it was recommended to use extrapolation (10) only for $\ln T > 6$ (i.e. for $T > 400$ s) to avoid possible concave portions of the dependencies of $\ln T$ on $1/h_s^2$, which would lead to non-conservative extrapolation (over-estimation of the expected time

Table 1. Main particulars of ships and loading conditions

Ship	L_{pp} , m	B_{wl} , m	d , m (GM , m)
Cruise vessel	230	32	6.9 (1.5, 2.0, 2.5, 3.25, 3.75, 4.0)
1700 TEU container ship	160	28	9.5 (0.5, 1.2, 1.9), 5.5 (5.75, 6.75, 7.75)
8400 TEU container ship	317	43	13.93 (0.89), 14.44 (1.26), 14.48 (2.01), 11.36 (5.0, 6.93, 9.0)
14000 TEU container ship	350	51	8.5 (1.0, 2.0, 3.0), 14.5 (9.0, 12.0, 15.0)
RoPax	175	30	5.5 (3.7, 4.5, 5.2, 5.9 and 6.6)

to stability failure). Figure 4 shows all identified concave dependencies of $\ln T$ on $1/h_s^2$ and dependencies which are concave when $\ln T > 6$. Obviously, excluding portions with $\ln T < 6$ drastically reduces the possibility of non-conservative extrapolation, and even for the remaining curves, accurate extrapolation can be done using their portions at large $1/h_s^2$.

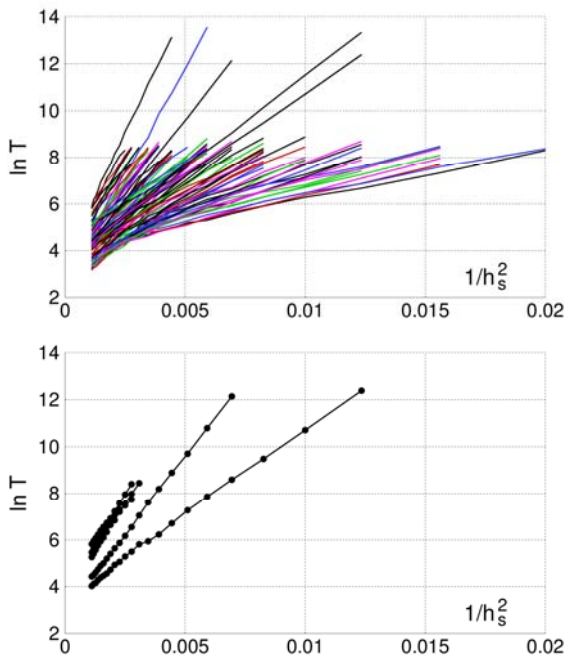


Fig. 4. Cases with concave dependency of $\ln T$ on $1/h_s^2$ taking (top) and not taking (bottom) into account results with $\ln T < 6$

To quantify the accuracy of extrapolation (10), 4, 5 and 6 points were selected starting from the minimum wave height for which the results were available from direct simulations. Correspondingly, extrapolation (10) was performed using 3, 4 or 5 points, respectively, and the deviation was defined

between the extrapolated and directly computed expected time to failure at the minimum significant wave height for which direct simulation results were available. The percentage was calculated of the extrapolated values lying within the 95%-confidence interval of the directly computed estimate of the expected time to stability failure, which was defined as $\tilde{T}(1 \pm 0.14)$ using $N=200$.

In [2] it was suggested that if extrapolation (10) of time to failure over wave height is used, the required number of simulated failure events can be reduced due to the smoothing action of the linear fit with regard to the random oscillations of \tilde{T} estimates. Therefore, the procedure was repeated using $N=20$ simulated stability failure events.

Figure 5 shows the results as a histogram of the ratio of the extrapolated to directly computed estimate of the expected time to failure; the y-axis corresponds to the number of cases (normed on 1) and the x-axis corresponds to the ratio of the extrapolated expected time to failure \tilde{T}_{extr} to the directly estimated one \tilde{T} . The top and bottom plots correspond to $N=200$ and 20 simulated stability failure events, respectively.

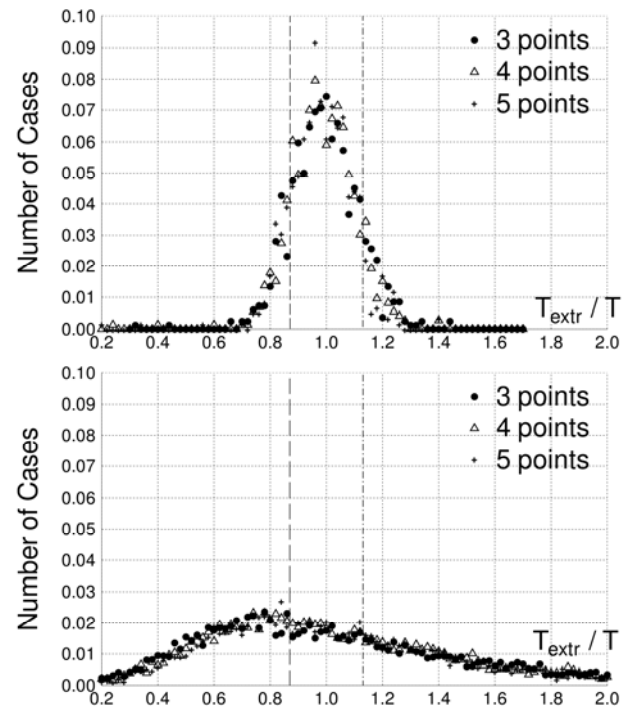


Fig. 5. Histogram (number of cases normed on 1) of ratio $\tilde{T}_{extr} / \tilde{T}$ and 95%-confidence interval of directly computed \tilde{T} (vertical lines) for $N=200$ (left) and 20 (right) simulated stability failure events

The results indicate that $N=20$ simulated failure events is not enough, whereas 200 simulated stability failure events lead to sufficiently accurate results. In particular, when 200 failure events are simulated and 3 points are used for extrapolation, over 77% of the extrapolated values of time to failure are within the 95% confidence interval of the directly computed estimate of the expected time to failure. This means a loss of accuracy due to extrapolation of about 20% (if 95% of extrapolated values were within the 95% confidence interval of the directly computed ones, the extrapolation would have been exact in a statistical sense). When 4 or 5 points are used for extrapolation, over 80% of the extrapolated values of time to failure lie within the 95% confidence interval of the directly computed estimate, which means a loss of accuracy due to extrapolation of about 16%. However, the results demonstrate presence of some outliers which require manual check (note that these outliers are not always related to extrapolation problems, but sometimes to directly computed estimates of time to failure). Figure 6 shows examples of non-conservative (over-estimation of the time to stability failure) and conservative (under-estimation of the time to stability failure) outliers, whereas Fig. 7 shows examples of accurate extrapolation.

Another series of comparisons of the extrapolated with directly computed time to failure used 3, 4, ..., 10 points for extrapolation starting with the maximum significant wave height for which $\ln T > 6$ and using all remaining available directly computed values of time to failure to estimate the ratio $\tilde{T}_{\text{extr}}/\tilde{T}$. Minimum and maximum (left- and right-hand plots, respectively, in Fig. 8) values were separately evaluated over all significant wave heights for the same wave period and direction. Figure 8 shows histograms of the ratio $\tilde{T}_{\text{extr}}/\tilde{T}$ for (from top to bottom) 3, 4, ..., 10 extrapolation points. The width of the band of the values $\tilde{T}_{\text{extr}}/\tilde{T}$ decreases with the increasing number of points used for extrapolation; however, even using 10 points still can lead to both conservative and non-conservative outliers which require manual corrections, Fig. 9.

Linear extrapolation (10) of $\ln T$ over $1/h_s^2$ is a useful practical tool to estimate the time to stability failure for cases where it cannot be estimated otherwise. The results of testing show that the

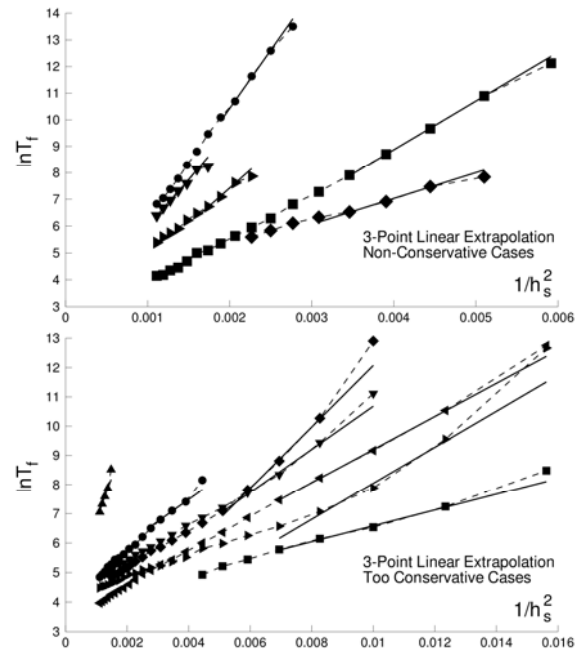


Fig. 6. Examples of non-conservative (top) and conservative (bottom) cases using 3 points for extrapolation

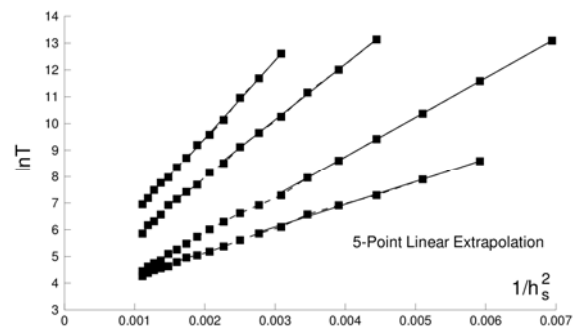


Fig. 7. Examples of accurate extrapolation cases using 5 points for extrapolation

method cannot be used fully automatically to compute time to stability failure for all sea states in a given wave climate and may require manual adjustment (i.e. removal of outliers) for some cases. On the other hand, the method can be efficiently used if the number of situations used in the DSA is not too large.

4. DESIGN SITUATIONS

A probabilistic DSA requires, in principle, summation of short-term stability failure probabilities over all contributing sea states of the relevant wave climate and all seaway directions.

For example, North-Atlantic scatter table [4] contains 197 sea states with non-zero probabilities; if DSA is done for every 10° seaway directions, the number of short-term conditions is 1970 for each forward speed and each assessed loading condition.

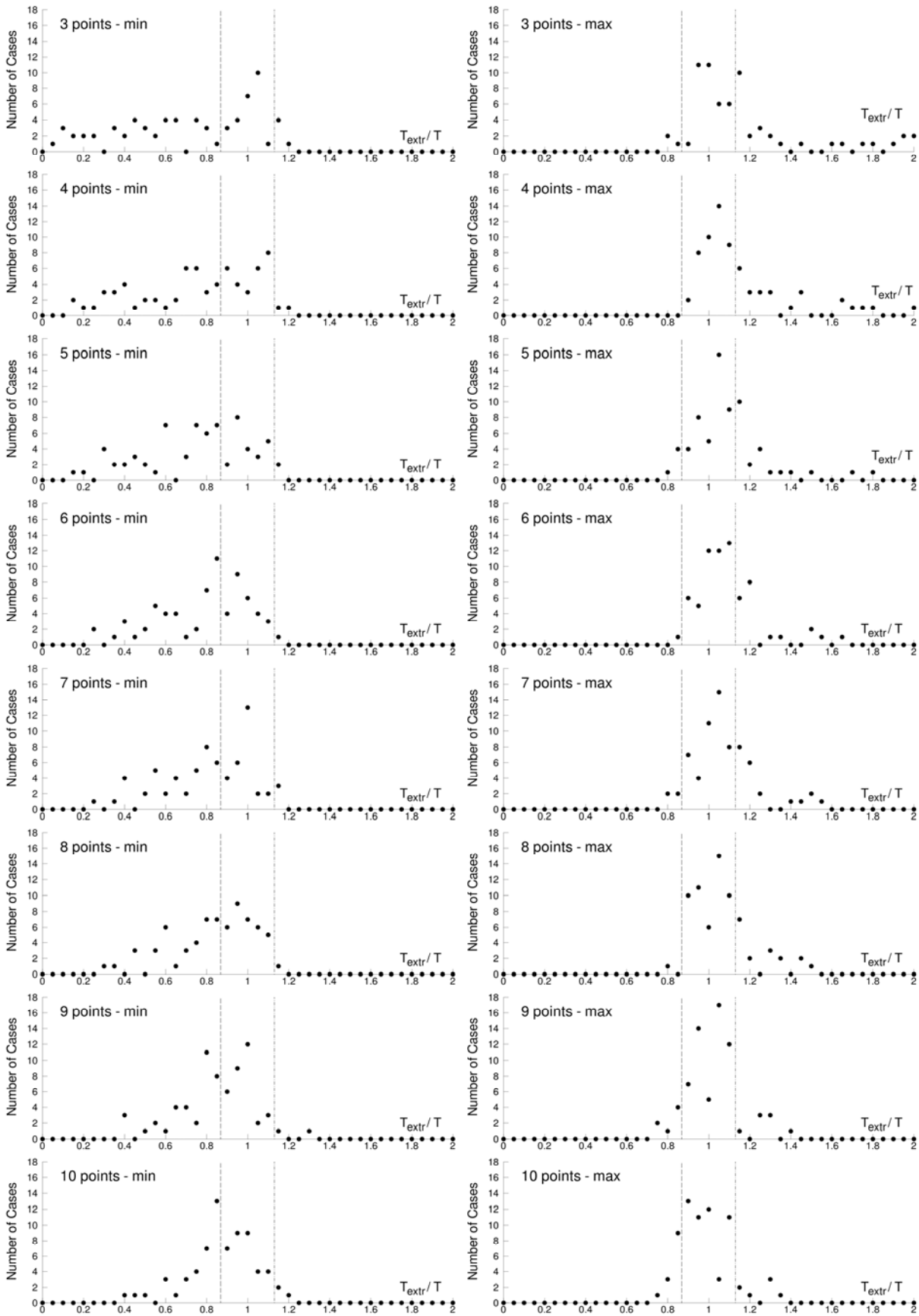


Fig. 8. Histograms of minimum (left) and maximum (right) ratio of $\tilde{T}_{extr}/\tilde{T}$ over all available results using (from top to bottom) 3, 4, ..., 10 points for extrapolation of $\ln \tilde{T}$ over wave height

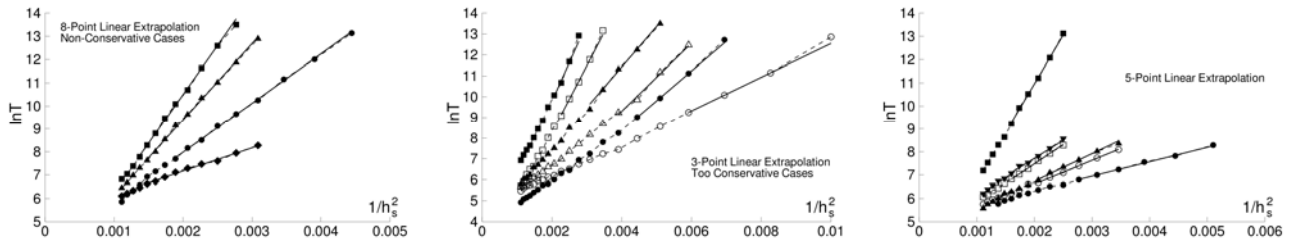


Fig. 9. Examples of non-conservative (left), conservative (middle) and accurate (right) extrapolations

This requires a robust and efficient procedure able to efficiently calculate failure probabilities in all relevant short-term conditions; besides, such assessment is impossible to do using model tests. Paper [2] discussed another possibility, based on reducing DSA to the assessment for few combinations of sea state parameters (wave height, period and direction) and ship forward speed, referred here as *design situations*.

The idea of this simplification is that a safety criterion S , based on the assessment in few selected conditions, can be used to norm stability if its relation to the “true” long-term probability of failure W is monotonous and does not show significant scatter between ships, loading conditions and forward speeds, Fig. 10; the standard for this simplified criterion can be defined using a sufficient number of representative case studies.

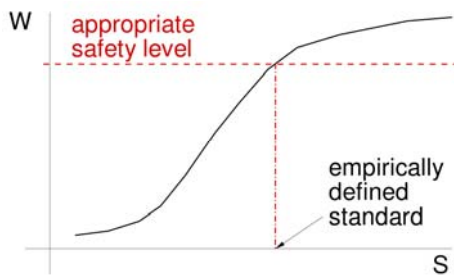


Fig. 10. Idea of simplified safety criterion S ; W is safety measure, e.g. long-term probability of stability failure

Note that the exact dependency $W(S)$ does not matter in the practical approval and is not required, as long as it is known that such dependency, in principle, exists, is monotonous and does not show significant scatter between different ships.

A drawback of this approach is that DSA is separated from OG: results of DSA cannot be directly used as OG. On the other hand, such simplified DSA procedure allows efficient identification of those loading conditions which require OG, thus reducing the number of cases requiring more time-consuming simulations. Paper [2] showed significant scatter of relation $W(S)$

between different ships, loading conditions and forward speeds. To improve this method, it is proposed to use different “dedicated” design situations (i.e. combinations of sea state, ship speed, wave direction and wave period) for different failure modes. Here, roll in beam sea is considered to address the dead ship condition stability failure mode, assuming exceedance of 40° roll angle as a stability failure event (in principle, the conclusions will also be valid for the excessive accelerations stability failure mode).

Ships and loading conditions listed in Table 1 were used. Different forward speeds were applied and evaluated separately: even though dead ship condition corresponds to zero forward speed, the influence of forward speed on roll motion in beam seas manifests itself mostly through roll damping, therefore, non-zero speeds were also used in this study to ensure that the dependency $W(S)$ does not show significant scatter between cases with different roll damping characteristics.

Several ways to select design sea states were used; in all cases, a range of mean wave periods T_1 was applied and only one significant wave height h_s per wave period, selected according to (Fig. 11)

1. Steepness table from [5]; simplified criteria: sum and maximum of the short-term weighted failure rate $p_s \cdot r$ over design sea states; p_s is the occurrence frequency of a sea state and $r=1/T$ is the stability failure rate in a sea state, Fig. 12.
2. Constant steepness $h_s = \text{const} \cdot 0.5gT_1^2/\pi$, with $\text{const}=0.02, 0.04, \dots, 0.1$; the same simplified criteria as in 1 were used.
3. Lines of constant density of seaway probability p_s , corresponding to sea state duration of one month, one week and one day per year, one day in ten years and one hour in ten years; simplified criteria: sum and maximum of the short-term failure rate over all design sea states.
4. Constant normed quantiles p_s^* , defined for each T_1 as cumulative p_s value from the maximum to current h_s , at levels 0.2, 0.02, ..., $2 \cdot 10^{-5}$, with the same simplified criteria as in 3.

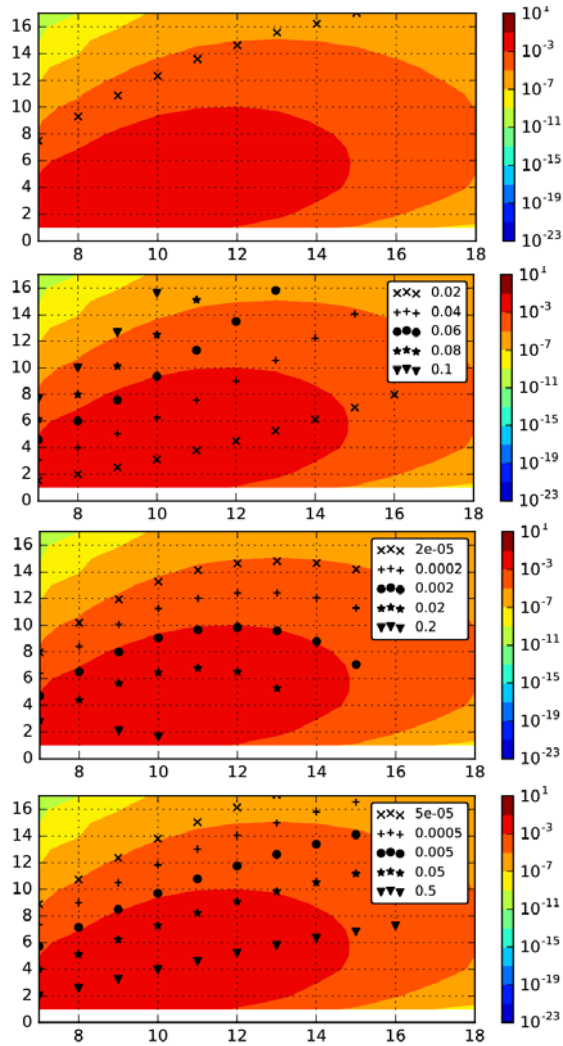


Fig. 11. Design sea states (symbols) vs. mean wave period T_1 , s, (x axis) – significant wave height h_s , m, (y axis) using (from top to bottom) steepness table from [5], constant steepness lines, normed and not normed quantiles; colours show constant density of seaway occurrence probability p_s

- Constant not normed quantiles p_s^{**} , defined as p_s^* values divided by the occurrence probability of each sea state wave period T_1 (i.e. quantiles not taking into account differences in the occurrence probability of different wave periods), at levels 0.5, 0.05, ..., $5 \cdot 10^{-5}$, with the same simplified criteria as in 3.

The long-term rate of stability failure $W = \sum_s p_s(h_s, T_1; \text{ship}, LC, \nu) r(h_s, T_1; \text{ship}, LC, \nu)$ was directly computed; here ν is the ship forward speed and $s=(h_s, T_1)$ denotes all sea states of the North Atlantic scatter table. Figures 13 to 17 plot the simplified criteria evaluated in the design sea states (y axis) vs. criterion W (x axis).

The best correlation of a simplified criterion with the long-term stability failure rate is achieved using lines of constant probability of occurrence of sea states, followed by the very similar lines of

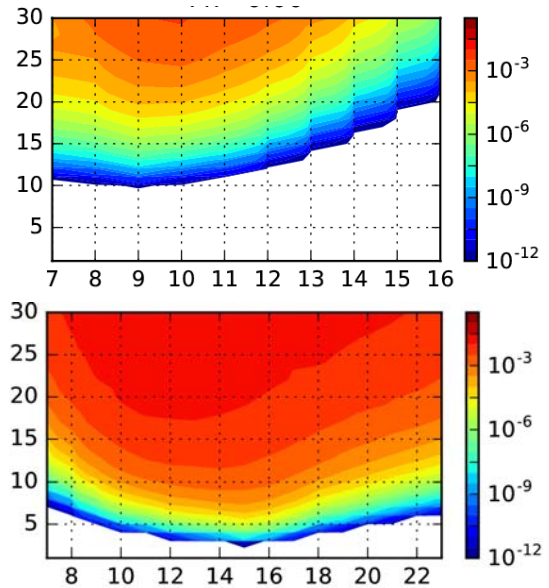


Fig. 12. Short-term stability failure rate $r=1/T$ of RoPax vessel, $GM=4.5$ (top) and 14000 TEU container vessel at $GM=1.0$ (bottom) at zero forward speed in beam seaway vs. mean wave period T_1 , s, (x axis) and significant wave height h_s , m, (y axis)

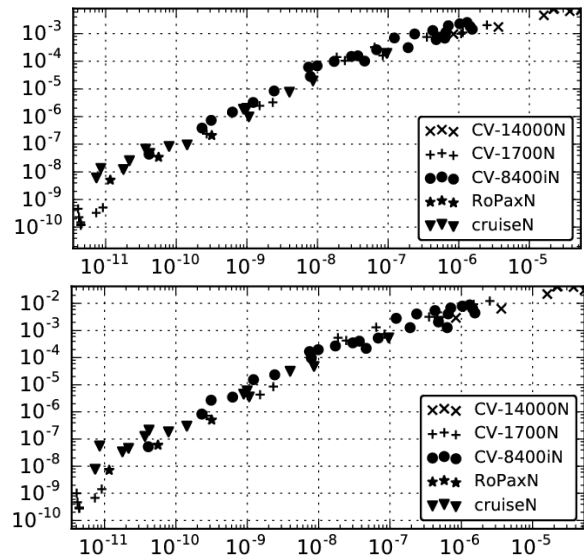


Fig. 13. Simplified criteria: maximum (top) and sum (bottom) of $p_s r$, 1/s, (y axis) vs. long-term stability failure rate W , 1/s, (x axis) for design sea states according to steepness table from [5]

constant normed quantiles and then by lines of constant quantiles. The next are criteria defined along the steepness line from [5]; worst suitable are the criteria defined along the lines of constant steepness. In all cases, criteria defined by the sum over all design sea states are very similar to criteria defined as the maximum value over all sea states. For the criteria defined along the lines of constant occurrence probability of sea states and constant quantiles, the performance of the criteria improves with increasing steepness.

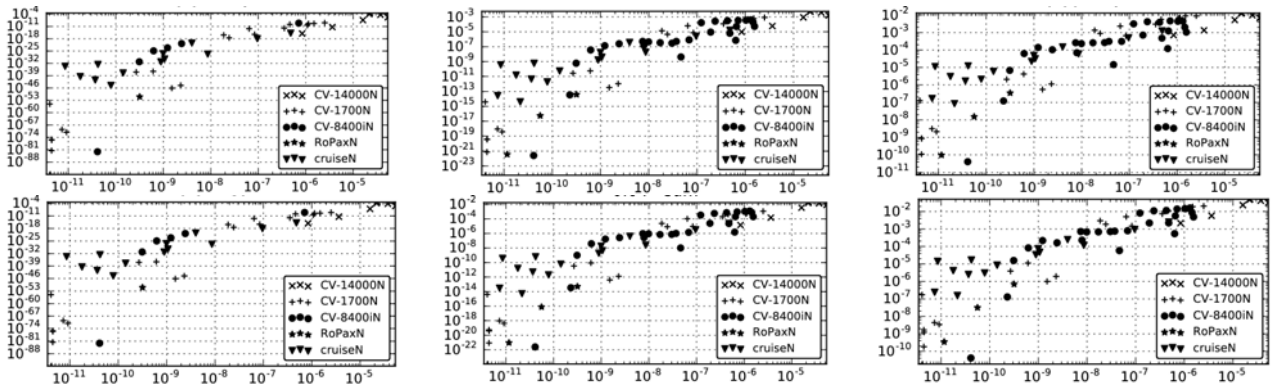


Fig. 14. Simplified criteria: maximum (top) and sum (bottom) of $p_s r$, 1/s, (y axis) vs. long-term stability failure rate W , 1/s, (x axis) in design sea states along lines of constant steepness $h_s = \text{const} \cdot 0.5gT_1^2/\pi$, $\text{const}=0.02, 0.04$ and 0.06 (from left to right)

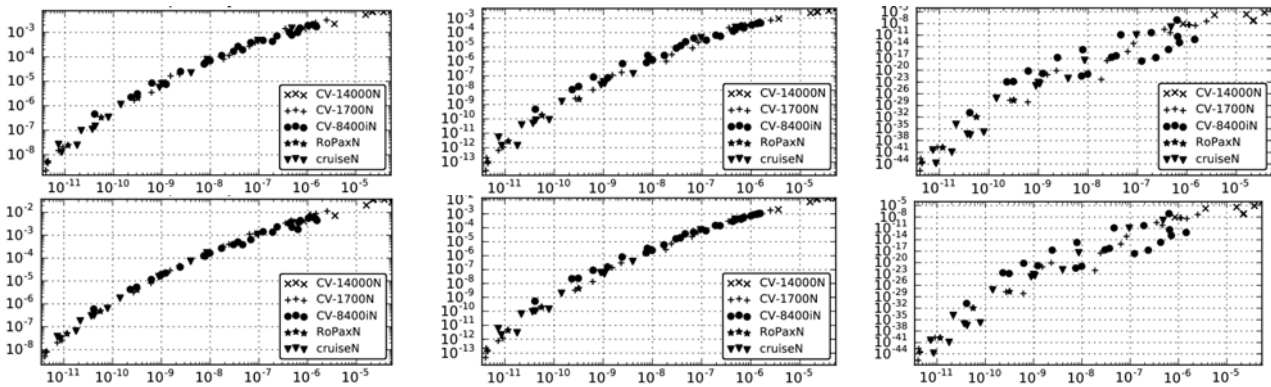


Fig. 15. Simplified criteria: maximum (top) and sum (bottom) of short-term failure rate r , 1/s, (y axis) vs. long-term stability failure rate W , 1/s, (x axis) in design sea states with constant seaway occurrence probability density of (from left to right) 1 hour per 10 years, 1 day per 10 years and 1 week per year

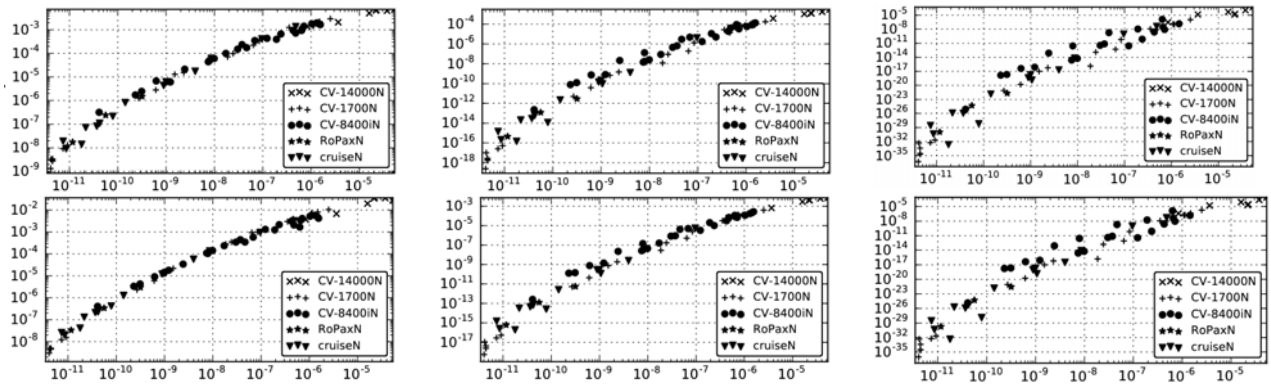


Fig. 16. Simplified criteria: maximum (top) and sum (bottom) of short-term failure rate r , 1/s, (y axis) vs. long-term stability failure rate W , 1/s, (x axis) in design sea states with constant normed quantiles of (from left to right) $2 \cdot 10^{-5}$, $2 \cdot 10^{-3}$ and 0.02

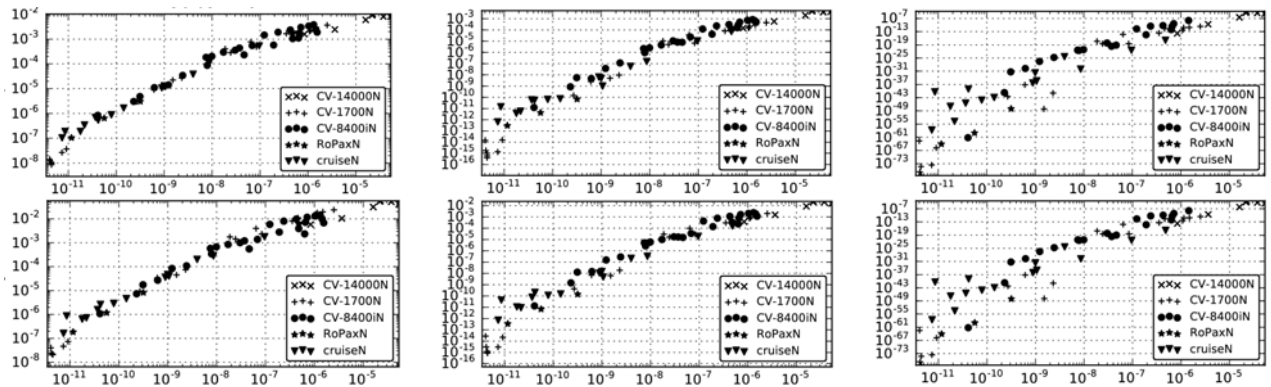


Fig. 17. Simplified criteria – maximum (top) and sum (bottom) – of short-term failure rate r , 1/s, (y axis) vs. long-term stability failure rate W , 1/s, (x axis) in design sea states with constant quantiles of (from left to right) $5 \cdot 10^{-5}$, $5 \cdot 10^{-3}$ and 0.5

5. NON-PROBABILISTIC DSA

A drawback of a probabilistic DSA is the need to encounter stability failure events in simulations (or in model tests), which requires long simulation times or big model test durations. This means, for example, that model tests can be used only for the validation of numerical simulations for few selected situations, and it is impossible to provide DSA based on only model tests. An appealing idea is to combine the design situations method with non-probabilistic (deterministic) criteria, e.g. expected maximum roll amplitude per given exposure time, mean roll amplitude etc. Such non-probabilistic measures require much less simulation or model testing time for their definition.

The idea is the same as shown in Fig. 10: if the selected non-probabilistic criterion is monotonously related to the true safety measure (e.g. long-term failure probability), and scatter between ships, loading conditions and forward speeds is small, the simplified criterion can be directly used for norming; its standard should be fine-tuned using a representative ship sample. Two simplified non-probabilistic short-term criteria, average and expected 3-hour maximum roll amplitude, defined in the same design sea states as described in the previous section, are compared between different ships, loading conditions and forward speeds in irregular beam seaways to assess their correlation with the long-term rate of stability failure W . Results in Fig. 18 to 20 show significant scatter of the dependencies $W(S)$ between different ships, loading conditions and forward speeds, as well as non-monotonous dependencies.

6. CONCLUSIONS

Probabilistic DSA uses directly stability failure probability as a safety measure (criterion), thus some form of counting of stability failure events is required. Because stability failure events are very rare for the cases practically relevant for DSA, very long simulations are necessary. Because simulation tools employed in a DSA are rather slow compared to methods used L1 and L2, some simplifications are needed in the probabilistic assessment methods to make DSA feasible in design and approval.

Several possibilities to simplify probabilistic assessment are studied: *extrapolation* of the time to stability failure over wave height, reduction of the number of considered situations to few selected

design situations (combinations of ship speed and wave height, direction and period) and use of *non-probabilistic (deterministic)* safety criteria.

The *extrapolation* of time to stability failure over wave height provides, in acceptable computational time, average time to stability failure for all combinations of wave height, period and direction encountered during a design life of a ship, i.e. results of such DSA can be directly used as OG. The procedure leads to sufficiently accurate results in most cases, however, some outliers are present, which require manual control; therefore, it is easy to use when the number of considered situations is not large. It is important to do such studies for other available statistical extrapolation methods to address their accuracy, robustness and feasibility with respect to practical design and approval.

In the *design situations* method, the assessment is performed for few selected situations, which significantly reduces required simulation time. A drawback of this approach is that DSA results cannot be used directly as OG, thus OG will have to be additionally developed for loading conditions failing to fulfil DSA requirements. Several ways for the selection of design sea states were tested: based on the wave steepness table from [5], constant wave steepness, constant occurrence frequency of the sea state, and constant quantiles of significant wave height exceedance. The results were compared with the long-term stability failure probability obtained by the direct summation over all sea states in the scatter table. The best simplified criterion is the sum of the short-term failure rate along the lines of constant occurrence probability of sea states; the performance of the simplified criteria improves with increasing steepness of the design sea states.

A further possibility to simplify and accelerate a DSA is to combine design situations with *non-probabilistic (deterministic)* safety criteria, such as the expected maximum roll amplitude per specified time, mean roll amplitude etc. Evaluation of such criteria requires much less simulation time and is much easier to implement in model tests compared to the evaluation of stability failure probability. The results show, however, significant scatter of the dependencies of the long-term failure rate on the non-probabilistic criteria between ships, loading cases and forward speeds and multiple instances of non-monotonous dependencies, thus the tested non-probabilistic criteria cannot be used in DSA.

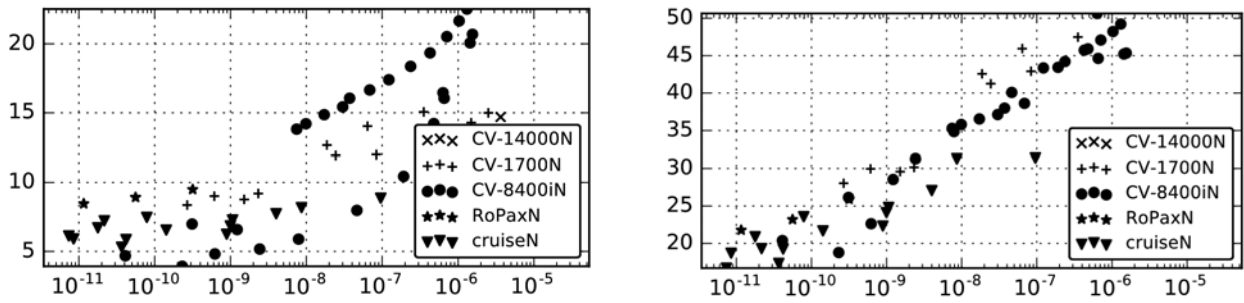


Fig. 18. Maximum short-term average roll amplitude (left) and expected 3-hour maximum roll amplitude (right) in degree, y-axis, vs. long-term stability failure rate W , 1/s, (x axis) over design sea states according to [5]

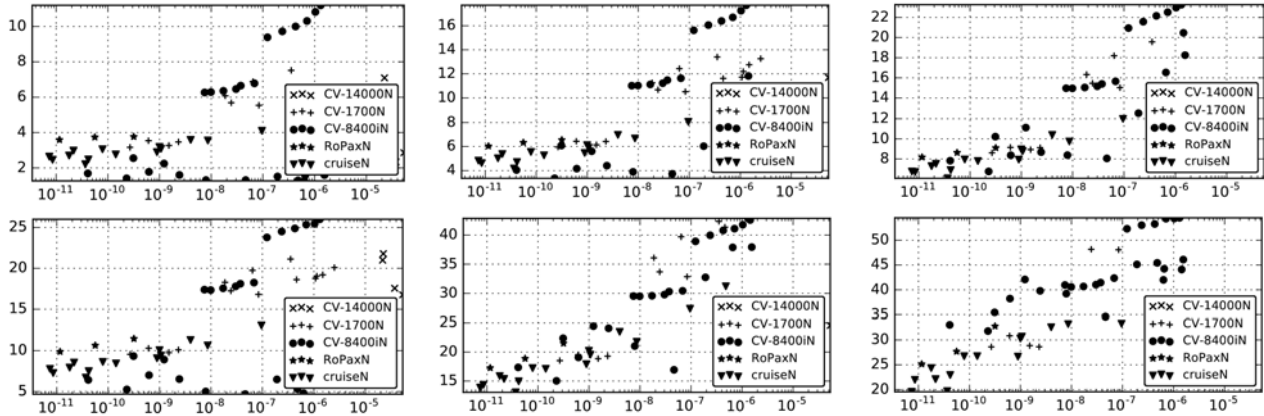


Fig. 19. Maximum short-term average (top) and expected 3 hour maximum (bottom) roll amplitude in degree over design sea states along lines of constant steepness (0.02, 0.04 and 0.06 from left to right) (y axis) vs. long-term stability failure rate W in 1/s, (x axis)

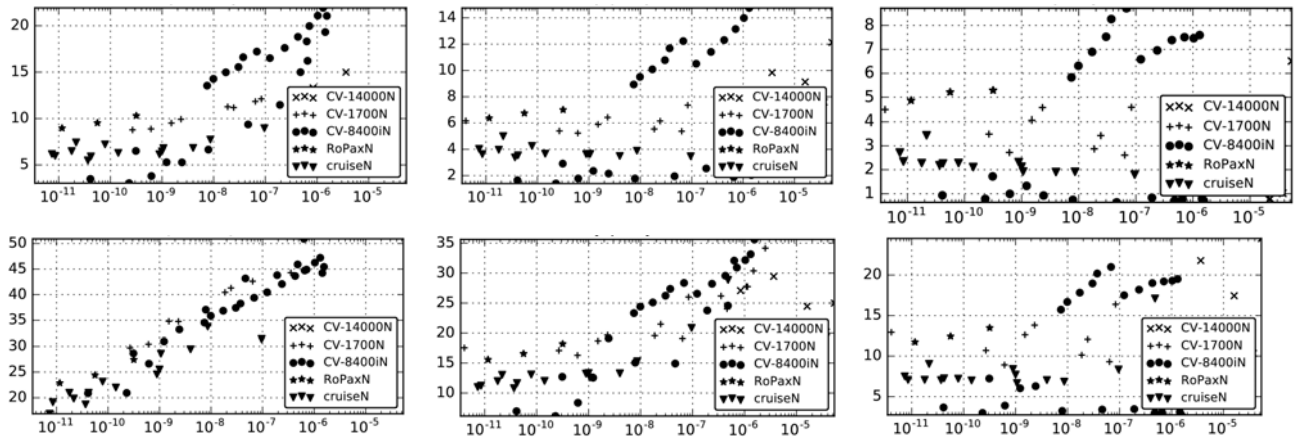


Fig. 20. Short-term average (top) and expected 3 hour maximum (bottom) roll amplitude, degree, (y-axis), maximum over design sea states with constant seaway occurrence probability density of (from left to right) 1 hour per 10 years, 1 day per year and 1 week per year vs. long-term stability failure rate W , 1/s, (x axis)

REFERENCES

[1] IMO-SLF (2011) Report of the working group at SLF 53 (part 2). SLF 54/3/1, Annex 1: Framework for the Second Generation Intact Stability Criteria.
 [2] IMO-SDC (2015) Probabilistic direct stability assessment and operational guidance, Paper SDC 3/INF.12 submitted by Germany.
 [3] Tongué, E. and Söding, H. (1986) Computing capsizing frequencies of ships in seaway, Proceedings, 3rd Int. Conf.

on Stability of Ships and Ocean Vehicles.

[4] International Association of Classification Societies (IACS) (2001) Standard Wave Data. - IACS Rec. 34.
 [5] IMO-MSA (2006) Interim guidelines for alternative assessment of the weather criterion, Circular MSC.1/Circ.1200.

This page is intentionally left blank

Session 2

**Onboard intact stability management
using advanced technologies**

Session Chairs

Naoya Umeda

Hirotsada Hashimoto

A case study on operational limitations by means of navigation simulation

Hirota Hashimoto, *Kobe University*, hashimoto@port.kobe-u.ac.jp

Yuuki Taniguchi, *Kobe University*, taniguchi_y@port.kobe-u.ac.jp

Michio Fujii, *Marine Technical College*, fujii-m4g6@jmets.ac.jp

ABSTRACT

In the second generation intact stability criterion, even a ship who fails to pass the level 2 vulnerability criteria, can be operated by imposing operational limitations. Since the introduction of operational limitations is a new attempt to guarantee the safety of ships at sea, which is out of the framework of the conventional safety standards, careful consideration and sufficient number of case studies are necessary. Therefore, a case study is performed to investigate the impact of operational limitations on actual ship navigation by means of navigation simulation. In this study, parametric roll is selected as a major stability failure mode and requirements for the implementation of operational limitations are discussed.

Keywords: *Second Generation Intact Stability Criteria, Operational Limitations, Navigation Simulation, Parametric Roll, Container Ship*

1. INTRODUCTION

Currently, a lot of intensive discussions and works are made toward the finalization of the Second Generation Intact Stability Criteria (SGISC) at International Maritime Organization (IMO) [IMO, 2017]. In SGISC, the risk of failure of a ship is evaluated in three levels for five stability failure modes, i.e. pure loss of stability, parametric roll, surf-riding/broaching, dead ship and excessive acceleration. The level 1 vulnerability criteria can be easily applied instead of setting the maximum safety level, and the evaluation complexity becomes higher while the safety margin does smaller in the level 2 vulnerability criteria. The third level is so called direct stability assessment (DSA) which requires complex calculations to evaluate the safety level of ships. Model experiments could be required in DSA but the safety margin becomes lowest. If a ship fails to pass the level 1 vulnerability criteria, the ship has to pass level 2 or DSA criteria to guarantee the safety at sea. However, ships can be operated even though they fail to pass level 2 or DSA, by imposing operational limitations (OL) or operational guidance (OG) as risk control option. In principle, the introduction of OL and OG into SGISC has

been agreed at IMO. However, there is almost no research on this topic whereas it is an important issue for the finalization of SGISC. Therefore, at this moment, it is not clear how to implement OL/OG and how much operational efforts are needed when they are imposed. It is a big challenge to guarantee the safety of ships by means of the combination of passive design criteria and active operational measures [Bačkalov et al., 2016]. In order to make the OL useful and practically executable as the risk control option, sufficient number of case studies is needed to reveal positive and negative impacts on actual operation and to propose how to avoid specified dangerous conditions during navigation. It is also important to involve shipping companies and ship masters who actually operate ships to formulate rational but executable OL.

In response to these situations, we conducted a numerical study using navigation simulation to provide information for the formulation of OL. Since a container ship is selected as the subject ship, parametric roll is a typical stability failure mode and hence OL for parametric roll is discussed in this paper. Based on the simulation results, we try to derive appropriate limiting parameters for OL from viewpoints of degree of achievement of safe

navigation and change of ship route, and delay time.

2. OPERATIONAL LIMITATIONS AND OPERATIONAL GUIDANCE

Operational limitations

The discussion on OL has just started at the Ship Design and Construction (SDC) sub-committee at IMO and specific requirements have not been decided, but it has been agreed that OL should be set based on calculation results of Level 2 criteria or DSA. Since it is hard to execute DSA because of its high calculation-complexity, OL would be set from the Level 2 results in most cases. Based on calculation results for each stability failure mode, dangerous conditions to be avoided are obtained depending on loading conditions as the combination of significant wave height, average zero-crossing wave period, and ship speed. Only measures for surf-riding are considered for the surf-riding/broaching failure mode as the level 2 criteria. In case one or more possible loading conditions from departure to arrival do not pass the level 2 vulnerability criteria, a captain needs to change the loading condition or to avoid specified dangerous conditions by following the OL procedure. In case applying OL, navigation guidance of MSC/Circ.1228 is superseded by OL. The reason why the avoidance of specified dangerous conditions is not mandatory is that SGISC will be in the non-mandatory part (Part B) of Intact Stability (IS) code for the time being. Because the dangerous conditions to be avoided are determined from numerical results of the Level 2 vulnerability criteria which are simpler and has larger safety margin than DSA, the specified dangerous conditions are wider and patterns of ship speed and wave relative direction are quite limited. In this sense, it is the rough estimation of dangerous condition, so OL has the aspect of route selection/change in navigation rather than detailed requests for ship handling. Although the wave data, such as significant wave height and wave period, is essential for the implementation of OL, it is hard to accurately predict/measure them on the ship especially in stormy weather. Therefore it is desirable to use navigation supporting systems combined with reliable weather forecast and on-board measurement.

Operational guidance

It has been already agreed that OG should be set based on calculation results of DSA. OG is guidance to avoid stability failure by operational countermeasures in ship navigation and ship handling. Even though a ship, who fails to pass DSA, can be operated if a ship master follows the OG procedure to avoid specified dangerous conditions at sea. Based on numerical results of DSA, dangerous conditions to be avoided are determined depending on loading conditions as the combination of significant wave height, average zero-crossing wave period, ship speed and wave relative direction, for each stability failure modes. Thanks to detailed calculations in DSA, broaching itself is considered in OG while surf-riding is done in OL. In case one or more possible loading conditions from departure to arrival do not pass DSA, a captain needs to change the loading condition or to avoid specified dangerous conditions by following the OG procedure. In this case, number of selections of ship speed is larger than that of OL and the influence of wave relative direction can be considered in OG. In order to take advantage of OG, advanced instruments to accurately measure sea state on-board, using like X-band wave radar, is important and real-time supporting systems for ship handling are desired in the future.

3. NAVIGATION SIMULATION

Simulation model

In this study, we use a ship navigation simulation to investigate the influence of introduction of OL on actual navigation. The navigation simulation is based on a simulation model developed for weather routing [Kobayashi et al., 2015]. In this model, a mathematical model for ship manoeuvre so-called MMG model, is used and solved to calculate ship horizontal motions at sea. And then the ship arrival point is calculated by Mercator's sailing from moving distance and course, which are obtained by solving the MMG model. Hydrodynamic forces by ocean currents and winds, and added resistance in waves are taken into account as external forces acting on the ship hull. The wind pressure is calculated by an empirical formula [Fujiwara et al., 1998] and the added resistance is done by Enhanced Unified Theory [Kashiwagi, 1992] provided by Osaka University.

With respect to ocean currents, 5-day average data with the longitude interval of 1.0° and the latitude interval of 1.0° are used, which are provided by NOAA (American Oceanic and Atmospheric Administration). With respect to winds and waves, every 6 hours data supplied by NCEP (American Environment Prediction Center) are used and are collected for number of days needed for simulation. Here the longitude interval is 1.25° and the latitude interval is 1.0° . The Powell method which is an unconstrained nonlinear optimization method [Powell, 1964] is used to search for the optimum route that minimizes an evaluation function such as amount of fuel consumption. Bezier curve is adopted as a mean for conveniently expressing complicated route curves with small number of control points. In the navigation simulation taking OL into account, an extraordinary large penalty fee is imposed according to the staying time in specified dangerous conditions, and the optimum route is selected to minimize the total operational cost (fuel cost + penalty fee). By this way, the most economical route can be obtained while complying with OL.

Simulation condition

In this study, a container ship is selected as the subject ship because container ships play a major role for international trading. Since container ships have relatively slender body, and exaggerated bow flare and transom stern, they prone to suffer parametric roll due to the significant variation of stability in waves. A case study is performed for a C11 container ship engaged in trans-Pacific services (Yokohama - San Francisco) in winter, by means of the navigation simulation mentioned above. We try to confirm whether the ship can avoid specified dangerous conditions by operational efforts and to reveal how navigation routes and navigation time are changed by imposing OL. Principal particulars of the subject C11 container ship in full load condition are shown in Table 1 [Levadou and van't Veer, 2006]. The hull form of this ship is similar to that of the accident ship who experienced parametric roll of about 40 degrees in the North Pacific in 1998.

Table 1: Principal particulars of the subject ship.

Length between perpendiculars : L_{pp}	262.0 m
Breadth : B	40.0 m
Draught : d	11.5 m
Depth : D	24.45 m
Total projected area of bilge keels : A_{BK}	30.6 m ²
Navigation speed in calm water : V	20.0 kt
Metacentric height : GM	1.965 m
Designed natural roll period : T_ϕ	25.1 s

The dangerous conditions for parametric roll exceeding 25 degrees used for OL are obtained by a calculation program developed by Osaka University [Maki, et al., 2011]. The subject ship in full load condition fails to pass neither the first nor second checks of the Level 2 vulnerability criteria. This result is reasonable because the required value is set to reject the accident ship. Since the dangerous conditions to be avoided are determined based on the results of Level 2 vulnerability criteria, the operational effort to avoid the danger discussed in this study is considered as OL not OG. The specific dangerous conditions for the subject ship are shown in Fig.1. Here $H_{1/3}$ denotes significant wave height and T_z does average zero-crossing wave period. The heading angle of 0 degrees means following waves and 180 degrees does head waves, and F_n represents the Froude number. Although calculation results in following waves are not presented, parametric roll exceeding 25 degrees does not occur in any conditions.

In case wave relative direction is used as a limiting parameter for OL, it is set to avoid the encounter angle of 90 to 270 degrees because parametric roll only happens in head sea condition for the subject ship. This means that the ship could be judged as dangerous when the major encounter angle is in 90 to 270 degrees. The ship speed in calm water is set as 20 knots. In the navigation simulation, a navigation route that minimizes the operational cost including the penalty fee is obtained as the optimal route while avoiding the specified dangerous conditions for parametric roll occurrence.

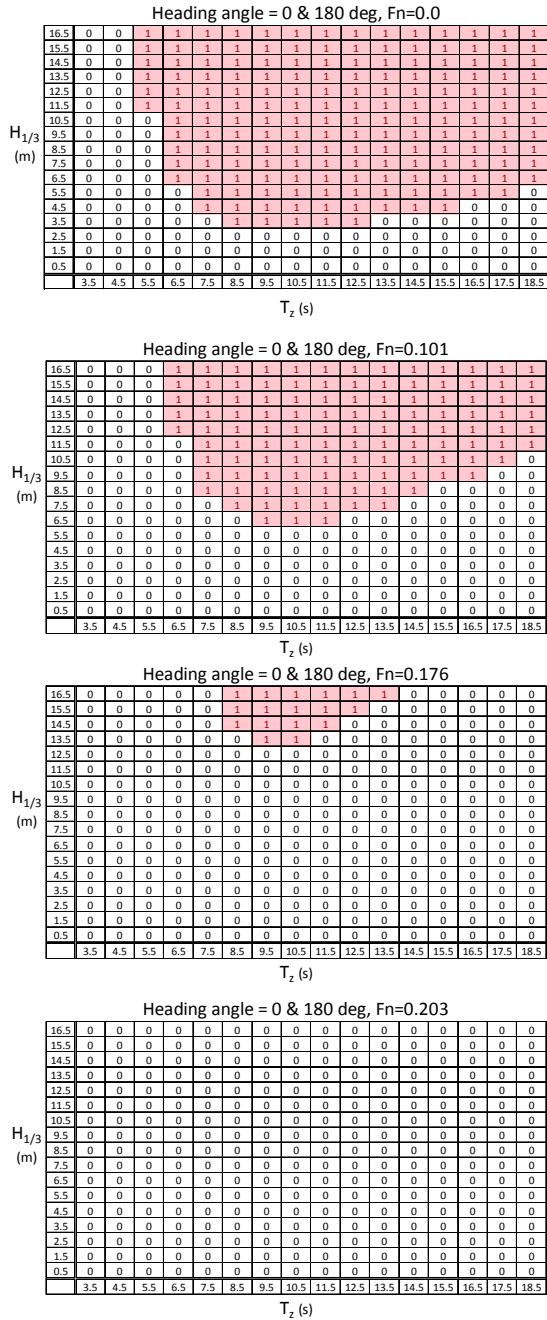


Figure 1: Tables of dangerous condition.

Validation of navigation simulation

Before the numerical investigation on OL, the validity of the navigation simulation should be demonstrated. Therefore actual navigation records are compared with simulation results. The actual navigation records are derived from AIS (Automatic Identification System) data collected by a satellite in 2015-2016. The ship length is obtained from the static data of AIS. Some required information for the navigation simulation, such as average navigation speed, is obtained from the dynamic data of AIS. To obtain numerical results to be compared with the actual navigation data, we

prepared the data of ocean currents, winds and waves for the corresponding period to the AIS data, and navigation simulations were performed by matching the departure time, the departure point and the destination. Figure 1 shows examples of the comparison result for a container ship engaged in the North Pacific routes in winter. Since the present simulation is seeking for a route that minimizes operational cost but the safety margin generally set by a ship master due to the uncertainty of weather forecast is not reflected, the navigation simulation avoided the harsh sea area at the minimum safety distance. Although this is one of points to be improved to realize more accurate navigation simulation, the present navigation simulation looks reproducing the actual navigation qualitatively. Therefore we use it for the discussion on OL in the following.

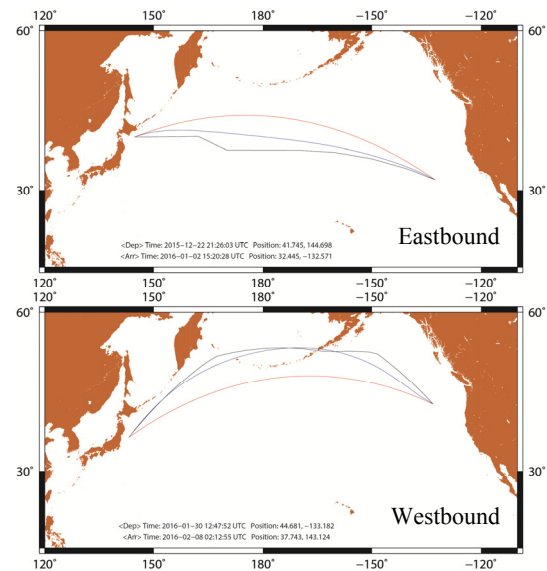


Figure 2: Comparison of navigation routes between AIS data and navigation simulation. (Red: great circle, Black: AIS data, Blue: simulation)

4. RESULTS AND DISCUSSION

Limiting parameters for operational limitations

Although it is needed to select limiting parameters used for OL, there would be significant influence on ship operation in terms of planning and changing of navigation routes, so careful discussion on the impact of OL on actual navigation is necessary. Of course it is desirable to keep the number of limiting parameters to minimum to suppress the complexity in implementation. The combination of limiting

parameters in the investigation is shown in Table 2. Here, significant wave height is the most important factor to assess the stability failure, so it is used as the limiting parameter in all cases. Ship speed is the most important control parameter in operation and the encounter wave period is determined according to the speed, so the priority of them is lower than that of significant wave height. Case 0 means normal operation without OL. As the Case number increases the number of limiting parameters used in OL increases, so the difficulty level of execution becomes higher. Although the dangerous range of wave direction is not determined in the Level 2 vulnerability criteria, parametric roll does not occur in following waves for the tested loading condition, according to Fig.1. Therefore it is judged as not dangerous if the major wave relative direction is in -90 to 90 degrees regardless of other conditions. This situation (Case 4-6) could be considered as an example of simplified OG.

Table 2: Combination of limiting parameters for OL.

Case	H _{1/3}	Ship speed	T _z	Wave encounter angle
0				
1	✓			
2	✓	✓		
3	✓	✓	✓	
4	✓			✓
5	✓	✓		✓
6	✓	✓	✓	✓

Influence of operational limitations on ship navigation

Figure 3-4 shows numerical results of navigation simulation imposing OL. As sample cases in the North Pacific in winter, three dates of departure, December 6, 2008, January 10 and 17, 2009, are selected. The maximum and average of significant wave height and mean wave period, encountered in the navigation along the great circle, are shown in Table 3. In case the departure date is January 10, the average significant wave height is 5.24 m in eastbound, which is a very severe condition of the top 3% of the North Pacific in winter. In the figures, GC shows the great circle giving minimum navigation distance. FOC shows the optimum navigation route in terms of fuel oil consumption without OL, which corresponds to Case 0, and

other six results are ship routes with consideration of OL according to the combinations of limiting parameters in Table 2. Figure 5-6 shows the percentage of time staying in the dangerous conditions and the total navigation time. GC means the simulation result navigating along the great circle, and OR means the result corresponding to Case 0 ~ 6.

Table 3: Sea state for navigation simulation.

Eastbound			
Day of departure	Max. H _{1/3}	Ave. H _{1/3}	Ave. T _z
6/12/2008	5.41 m	3.62 m	7.38 s
10/1/2009	9.60 m	5.24 m	10.10 s
17/1/2009	5.68 m	3.50 m	9.29 s
Westbound			
6/12/2008	7.41 m	3.54 m	8.91 s
10/1/2009	8.32 m	4.53 m	9.40 s
17/1/2009	6.15 m	3.66 m	9.42 s

In case of eastbound, Case 2 and 3 show the same navigation route while Case 1, using significant wave height alone, does much different result from them. In addition, the consideration of encounter wave direction has no influence on the results because ship runs in following seas in most situations. In case of westbound, the significant difference can be seen in the navigation routes and numerical results with OL are apart from the FOC result. The consideration of encounter wave direction helps to avoid the dangerous conditions for the case with the departure date of 6/12/2008. Figure 5-6 shows the numerical results of rate of stay in dangerous conditions and navigation time. The ship cannot avoid the dangerous conditions appropriately in Case 1 both in the eastbound and westbound results. On the other hand, numerical results of Case 2-6 can achieve the safe navigation with the reasonable navigation time. In the case with departure date of 10/1/2009 in westbound, the ship cannot avoid the specified dangerous conditions completely in Case 2-3 because the sea state is the top 3% of the North Pacific in winter. It is noteworthy that the ship can avoid all the dangerous conditions when the wave encounter

angle is added to the limiting parameters for OL even in such severe weather.

From the numerical investigation using the navigation simulation, it is demonstrated that the influence of OL on actual navigation is small in eastbound while it is significantly large in westbound. The reason is that the major wave encounter direction is following seas in eastbound and is head seas in westbound, in the North Pacific in winter. It is also demonstrated that OL using significant wave height alone cannot achieve the safe navigation even with the operational effort. According to Figure 1, the ship is not navigable in water area where significant wave height exceeds 2.5 m if the speed or other elements are not used as the limiting parameters. Therefore there is no route that the ship can avoid the dangerous conditions completely. Although OL using significant wave height alone as the limiting parameter is preferable to suppress the complexity in implementation, it cannot be recommended as an operational countermeasure for the stability failure due to parametric roll. On the other hand, it is mostly possible to avoid dangerous conditions if ship speed is added to the limiting parameters for OL. Since the speed control to ensure the stability, depending on the sea state encountered, is not easy on board, it is expected to develop navigation supporting systems to help making decision for ship masters.

5. CONCLUSIONS

The influence of operational limitations on ship navigation was numerically investigated by means of the navigation simulation for the C11 container ship in trans-Pacific in winter. Several combinations of limiting parameters were investigated for operational limitations on parametric roll. As a result, it is demonstrated that the operational limitations using significant wave height alone cannot achieve the safe navigation at all. On the other hand, it is mostly possible to avoid the specified dangerous conditions if the ship speed is added to the limiting parameters. In this case, the delay of arrival due to OL would be practically acceptable. In addition, the consideration of wave encounter angle helps to realize the safe navigation in some cases.

Further investigation for different type of ships, different water areas is desired and similar case studies on other stability failure modes are also important toward the finalization of second generation intact stability criteria. For actual uses of OL, wave radars or advanced technologies should be preferably implemented.

ACKNOWLEDGEMENTS

This work was carried out as a research activity of Goal-Based Stability Criteria Project of Japan Ship Technology Research Association in the fiscal year of 2016, funded by the Nippon Foundation, and was partially supported by JSPS KAKENHI Grant Number of 15H02327.

REFERENCES

- Bačkalov, I., Bulian G., Rosén, A., Shigunov, V., Themelis, N., 2016, "Improvement of ship stability and safety in intact condition through operational measures: challenges and opportunities", *Ocean Engineering*, 120, pp.353-361.
- Kobayashi, H., Hashimoto, H., Taniguchi, Y., Yoneda, S., 2015, "Advanced Optimized Weather Routing for an Ocean-Going Vessel", *Proceedings of the 2015 International Association of Institutes of Navigation World Congress*.
- Fujiwara, T., Ueno, M. and Nimura, T., 1998, "Estimation of Wind Forces and Moments acting on Ships", *Journal of The Society of Naval Architects of Japan*, 183, pp.77-90. (in Japanese).
- IMO, 2017, SDC 4/WP.4
- Kashiwagi, M., 1992, "Added Resistance, Wave-Induced Steady Sway Force and Yaw Moment on an Advancing Ship", *Ship Technology Res.*, 39(1).
- Levadou, M. and van't Veer, R., 2006, "Parametric Roll and Ship Design", *Proceedings of the 9th International Conference of Ships and Ocean Vehicles*, Hamburg, 1, pp.191-206.
- Powell, M. J. D., 1964, "An efficient method for finding the minimum of a function of several variables without calculating derivatives", *Computer Journal*, 7(2), pp.155-162.
- Maki, A., Umeda, N., Shiotani, S., Kobayashi, E., 2011, "Parametric rolling prediction in irregular seas using combination of deterministic ship dynamics and probabilistic wave theory", *Journal of Marine Science and Technology*, 16(3), pp.294-310.

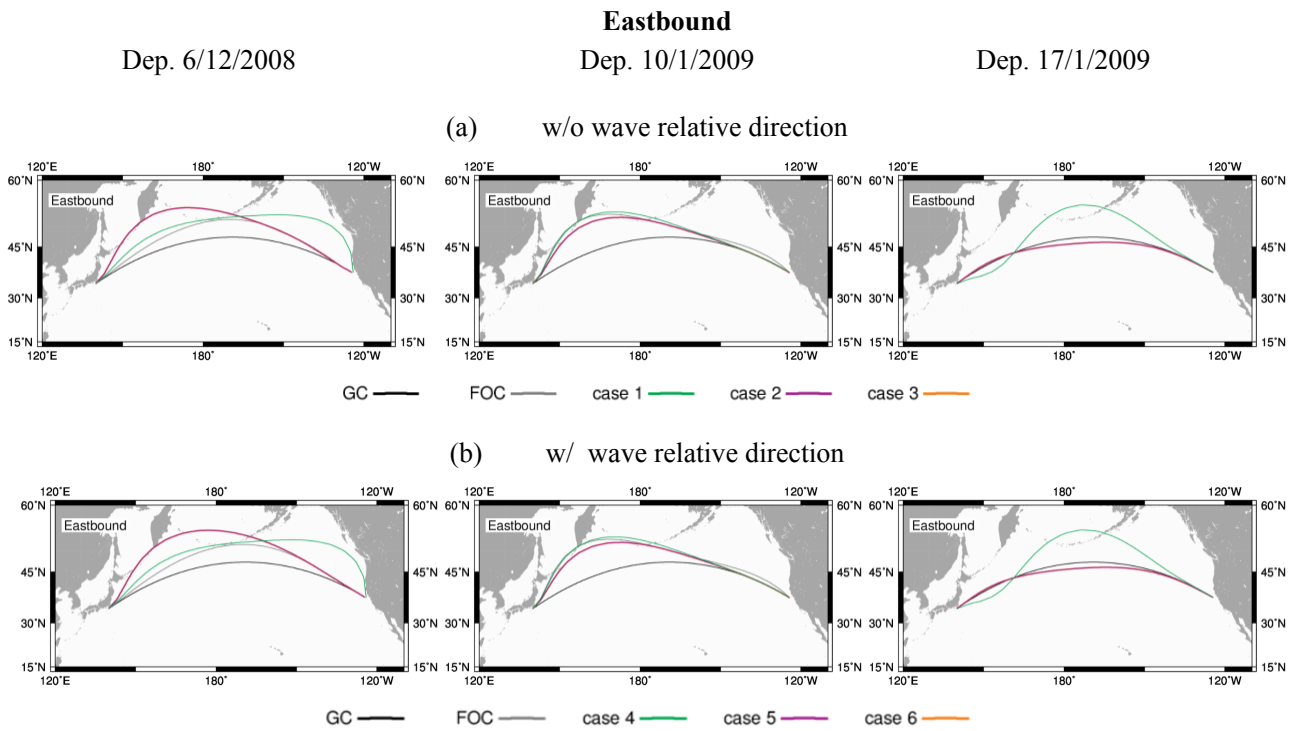


**Figure 3: Comparison of navigation routes imposing operational limitations.
(Eastbound)**

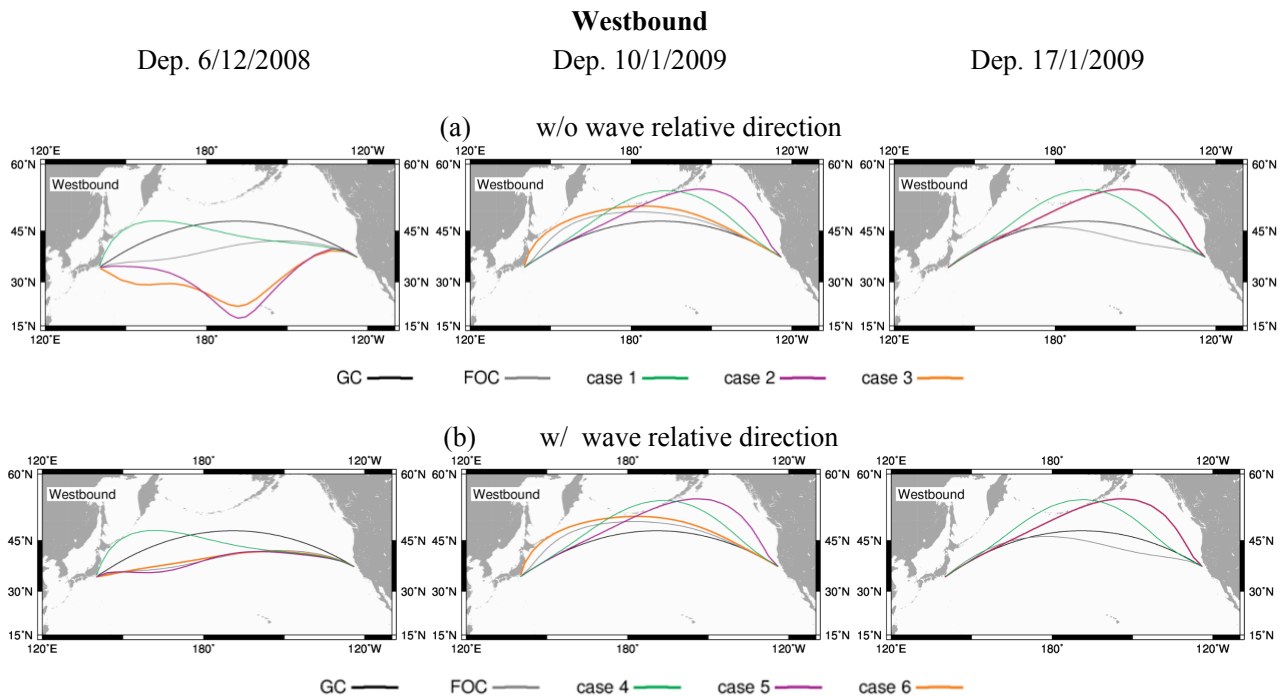


**Figure 4: Comparison of navigation trajectory imposing operational limitations.
(Westbound)**

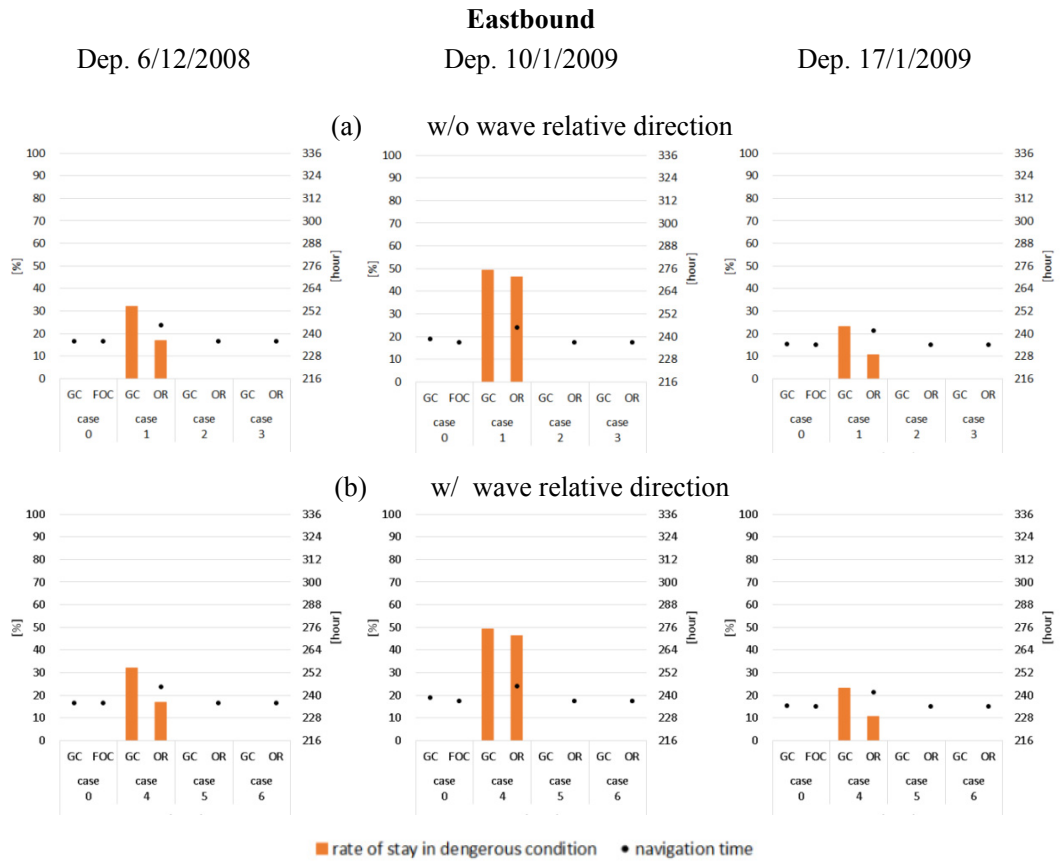


Figure 5: Comparison of achievement of safe navigation and navigation time.

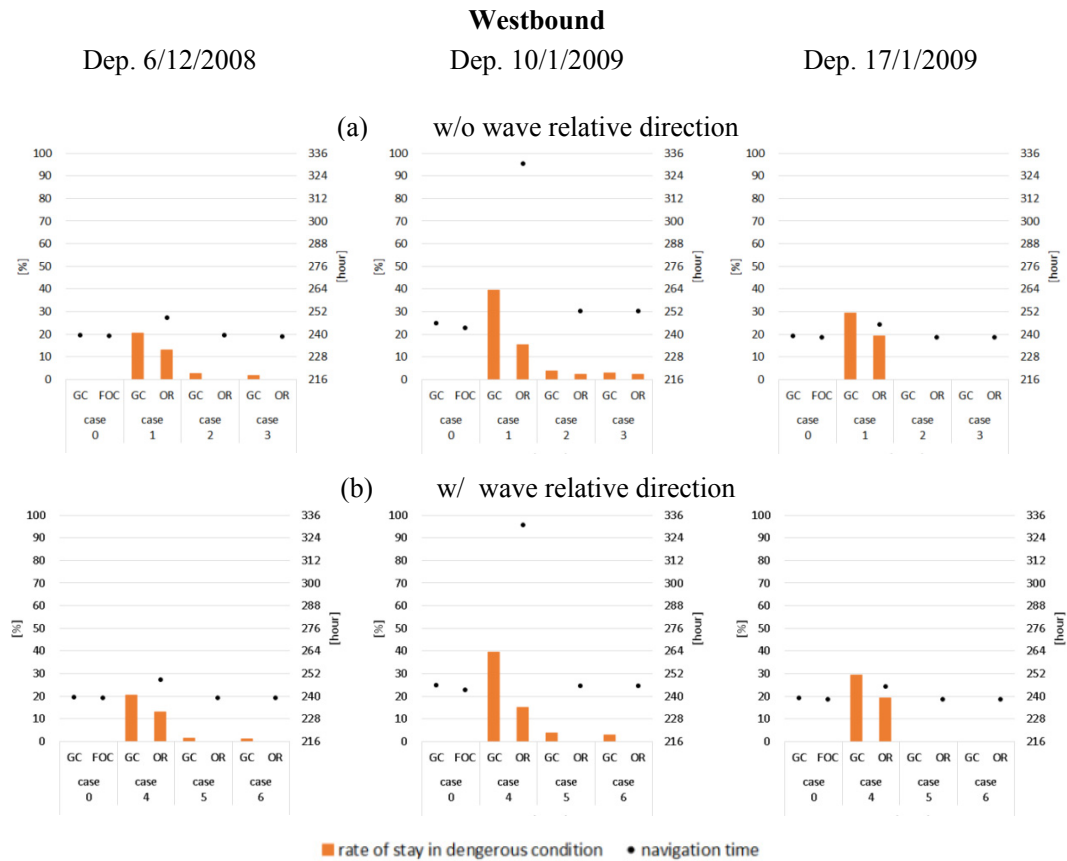


Figure 6: Comparison of achievement of safe navigation and navigation time

Acquisition and prediction of wave surface by marine radar for the safety of small ships

Hironori Susaki, *FURUNO ELECTRIC CO., LTD.*, hironori.susaki@furuno.co.jp

Yoshiaki Hirakawa, *Yokohama National University*, hirakawa-yoshiaki-jd@ynu.ac.jp

Takehiko Takayama, *Yokohama National University*, takayama-takehiko-yf@ynu.ac.jp

Tsugukiyo Hirayama, *Yokohama National University*, hirayama-tsugukiyo-nr@ynu.ac.jp

ABSTRACT

In recent years, wave observation by marine radar becomes increasing importance for the safety and the improvement of fuel efficiency of the ship. There are several wave radar systems for only wave observation and almost of wave radar systems for wave prediction are under development. The wave prediction is important especially for small ships, considering of stability by water on deck caused by a direct hits of wave. For avoiding direct hits of wave breaking, the authors attempts to predict encounter wave profile by utilizing a marine radar with a new algorithm based on the Fourier analysis and water wave dispersion relationship. Through the field experiments, the accuracy of wave observation verified by a wave buoy and the predicted wave surface shows good agreement with the actual wave surface.

Keywords: *Wave observation, Radar, Wavy buoy, Field experiments.*

1. INTRODUCTION

The research utilizing marine radars for wave observation started from 1975, it can be seen in the report by the Japan Ship Technology Research Association. It reported about the analysis to obtain the wave direction from PPI (Plan Position Indicator) images. After such a research, several wave radar systems were put to practical use, significant wave height, average period and directional distribution can be obtained by the wave radar systems.

YNU (Yokohama National University) group (Hirayama et.al.) started related research from 2000, and Nomiyama & Hirayama (2003) showed by numerical approach that individual waves can be obtained by PPI images and it opens the way for wave prediction in very short term (Nishimura & Hirayama et.al. (2004, 2005)). If incident waves can be predicted, ship motion also can be predicted. It leads to improvement of the ship safety and the energy saving navigation.

Especially for fishing vessels, smaller than cargo ships, prediction of incident waves will be very useful, for example, to avoid capsizing by waves. Table.1.1 shows an example of the distribution of the maximum rolling angle of a ship model by breaking wave hitting in the wave tank of

YNU (Fig.1.1) . From this it will be said that phase-difference information between the ship position and the wave is important. In this case, the height of the breaking wave is near the breadth of the ship. In this paper, the authors reported about the practical verification of wave observation and prediction utilizing marine radars by field experiments. Also, the theory of acquisition of ocean wave surface by a marine radar, verification by a wave buoy and examples of field experiments are reported.



Figure 1.1: The experiment for the breaking wave hitting

Table 1.1: Distribution of maximum rolling angle of fishing vessel by breaking wave hitting

		Heading Angle(deg)						
		45	60	75	90	105	120	135
Position from breaking point (mm)	800	32.66	43.76	48.09	45.43	43.06	44.78	28.09
	600	34.57	43.76	54.47	48.85	46.06	53.47	35.16
	400	32.76	42.03	51.11	50.29	48.00	45.86	29.81
	200	25.06	43.09	54.91	55.58	51.55	48.61	30.42
	0	24.64	29.18	40.90	51.11	45.96	40.22	26.66
	-200	22.88	23.08	25.54	41.45	27.87	29.54	23.37
	-400	20.40	19.33	25.49	24.86	21.19	26.15	20.06
-600	21.13	23.85	24.32	24.41	24.94	22.41	24.00	

2. THEORY

Strong intensity region of the image of a PPI is considered as the results of Bragg-Back-Scattering occurred in the ripples or white caps generated mainly by winds and these regions are also considered as existing around wave crests. But those intensities do not depend precisely on wave heights or wave slopes, so for the estimation of wave heights from PPI image we must develop other techniques.

First step is to obtain three dimensional Fourier spectrum (complex) for estimating power spectrum (real) of wave itself, eliminating noise part not relating to waves.

Here, $\zeta(x, y, t)$ is the density of PPI image and its three dimensional Fourier Spectrum $F(k_x, k_y, \omega)$ is obtained by equation (1). F is complex, then decomposed as formula (2) using real part and imaginary part. From this, phase part of F is defined as formula (3).

$$F(k_x, k_y, \omega) = \int_{-\infty}^{\infty} \int_{-\infty}^{\infty} \int_{-\infty}^{\infty} \zeta(x, y, t) \cdot e^{-i(k_x \cdot x + k_y \cdot y + \omega \cdot t)} dx dy dt \quad (1)$$

$$F(k_x, k_y) = F_{real}(k_x, k_y) + i \cdot F_{imag}(k_x, k_y) \quad (2)$$

$$\phi = \tan^{-1} \left(\frac{F_{imag}(k_x, k_y)}{F_{real}(k_x, k_y)} \right) \quad (3)$$

For eliminating the non-wave information in PPI-images, so called dispersion relation of gravity wave is introduced as a filter shown as equation (4).

Here vector U is ship speed, vector k is wave number, g is gravitational acceleration and ω is encounter frequency. ω -surface expressed by equation (4) is shown as Fig.2.1, and called as dispersion-shell (Borge et.al.(2000)).

$$\omega = \sqrt{g \times k + \bar{k} \cdot \vec{U}} \quad (4)$$

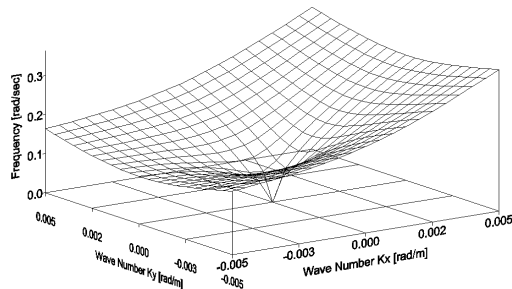


Fig.2.1 Example of the Dispersion Shell of surface wave (U=15knots)

Intensity of power spectrum of waves obtained by the product of F and F^* (* means complex conjugate) also appear on the surface expressed as Fig.2.1, so, non-wave power is easily eliminated. From the power spectrum of wave, conventional information as significant wave height and mean wave frequency are estimated easily, by the volume and moment of spectrum as equation (5)~(8).

Here L_x, L_y, T are the size of analysing area of PPI image in x-y plane and time domain, P is directional spectrum in wave number, S is point spectrum in circular frequency, m_n is n-th moment, and T_{01}, T_{02} are mean periods defined by spectral moments. Fig.2.2 is an example of actual power spectrum appeared on the dispersion shell. Some fluctuations can be seen.

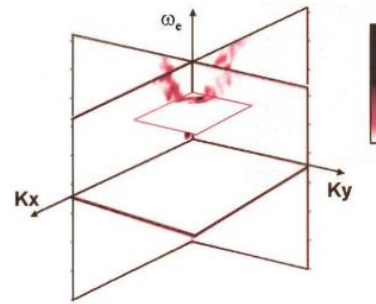


Fig.2.2 Example of power-spectrum-density over the dispersion shell.

$$P(k_x, k_y) = 2 \frac{\int_{\omega > 0} |F(k_x, k_y, \omega)|^2 d\omega}{L_x \cdot L_y \cdot T} \quad (5)$$

$$S(\omega) = \int_{-\pi}^{\pi} P(\omega, \theta) d\theta \quad (6)$$

$$m_n = \int_0^{\infty} \omega^n \cdot S(\omega) d\omega \quad (7)$$

$$H_{1/3} = 4.01 \cdot \sqrt{m_0}$$

$$T_{01} = 2\pi \cdot \frac{m_0}{m_1} \quad (8)$$

$$T_{02} = 2\pi \cdot \sqrt{\frac{m_0}{m_2}}$$

Area for analysis

The intensity of PPI image of marine radar, affected by the strength and direction of winds over the sea surface, it is better that the area of analysis is chosen in the direction of winds coming, because

PPI-intensity become strong in the direction that wind is blowing from and not blowing to.

Decision of wave height

As already described, the intensity of PPI images including bias are not proportional to wave height ,so, the scale of vertical axis of power spectrum has some ambiguity. For resolving this problem, we introduced a method (patented) utilizing the monitoring ship motion (mainly heaving motion) spectrum and theoretical response amplitude operator between wave and motion.

3. FIELD EXPERIMENTS

The research ship “Taka-maru” ($L_{OA}=29.5m$) belonging to the NRIFE (National Research Institute of Fisheries Engineering, Japan), the training ship “Fukae-maru” ($L_{OA}=49.95m$, Kobe University, Japan) and the training ship “Shinyo-maru” ($L_{OA}=60.0m$, Tokyo University of Marine Science and Technology) are utilized for the field experiments. Wave radars are installed on each ship. Fig.3.1-3.3 show “Taka-maru”, “Fukae-maru” and “Shinyo-maru”. The red dotted circle in Fig3.1-3.3 shows the additional radar(s) specially for wave measurement.

For large ships, the height of additional radars are set as low as possible in order to reproduce the height-condition of small ships.



Figure 3.1: The research ship “Taka-maru”



Figure 3.2: The training ship “Fukae-maru”



Figure 3.3: The training ship “Shinyo-maru”

Wave observation by small buoys

To verify the result from the wave radar system, small buoys are developed and utilized. Conventional wave buoys are large, expensive and for long-term measurement. To realize small size (light), not so expensive and for short-term measurement, the “Ultra-Small-Directional-Wave-buoy” (Small-buoy) was developed by Hirayama et.al. The Small-buoy is mainly used in the field experiment utilizing “Taka-maru”. After development of the Small-buoy the “Mini-buoy” was developed by Hirakawa et.al. (2003, 2016), because the field experiments utilizing “Fukae-maru” and Shinyo-maru” need smaller buoy.

Fig.3.4 shows the developed buoys for this research and principal dimensions of the buoys are shown in Table 3.1.



Figure 3.4: The Mini-buoy (Left) and the Ultra-Small-Directional-Wave-Buoy (Right)

Table 3.1: Principal Dimensions of the Mini-buoy and Ultra-small-directional-wave-buoy

	Mini-buoy	Small-buoy
Length of leg	0.3m	0.61m
Height from the bottom	0.3m	0.75m
Weight	4kg	13kg
Communication range	10m	600m
Time for recording	20hours	8hours

The motion of the buoy (height, period and direction) are measured and MLM (Maximum Likelihood Method) is utilized to calculate directional wave spectrum.

The measured vertical displacement using the sensors in Small-buoy was verified utilizing an image analysis method. As can be seen in Fig.3.5, markers for tracking is set on the buoy (2 points) and horizontal line (2 points). The time history of vertical displacement of the buoy shown in Fig.3.5 can be obtained. In Fig.3.6 the blue line shows the power spectrums of measured vertical displacement and the red line shows the power spectrum of wave calculated from the motion of image of the buoy.

The Mini-buoy was verified utilizing the experimental towing tank in YNU (Fig.3.7). The power spectrum of wave calculated from the motion of the buoy is compared with the power spectrum of wave measured by the wave probe in Fig.3.8.

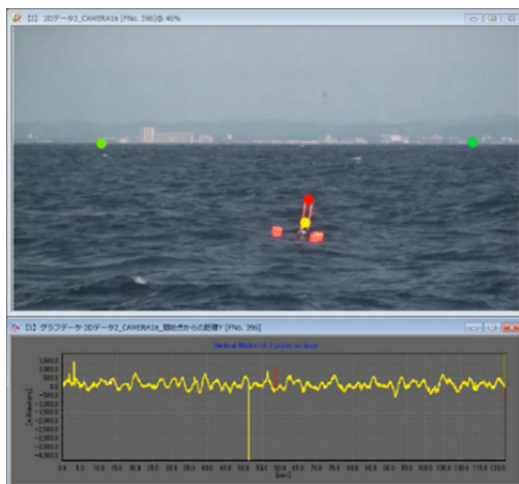


Figure 3.5: The image analysis of the buoy motion

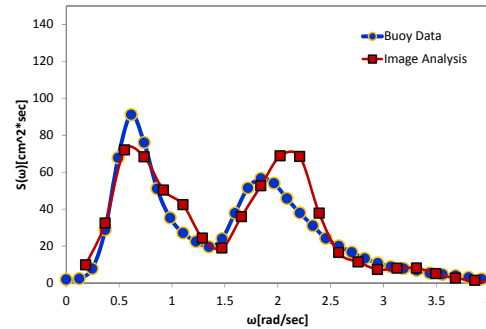


Figure 3.6: The power spectrum of measured vertical displacement of the buoy and analyzed data from the image of buoy motion.

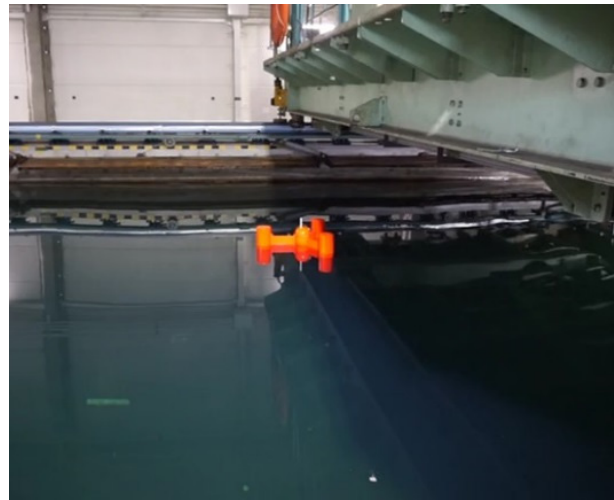


Figure 3.7: The verification experiment of the Mini-buoy in the experimental towing tank

Comparison between Wave probe and Mini-buoy

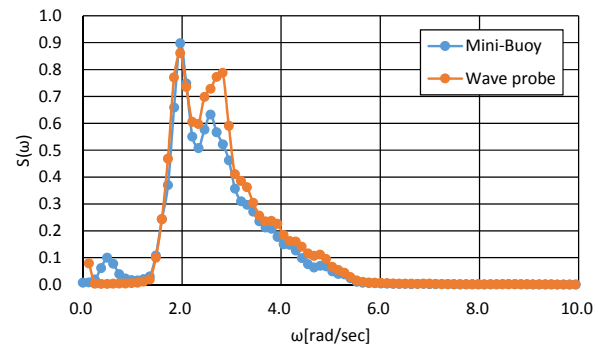


Figure 3.8: The power spectrum of wave by the Mini-buoy and the power spectrum of wave by the wave probe

Concrete example of wave observation by marine radar

We show an example of PPI image in Fig.3.9 (bow up drawing). This is obtained using commercial marine radar (DRS12A (4-feet antenna by Furuno). Rotation rate of antenna is 48rpm. Spectrum (Fig.3.10, north up drawing) is estimated using raw signal including back scatter from the sea surface and applying the method described in the

section 2. The observed date is Jun.14 2012 as shown in the Fig.3.9.

The range of PPI is 1500m, and the selected square area in this PPI for analysis is 1km by 1km. Wind coming direction is from the ship bow, so the selected area is also set in the direction of wind coming.

As can be seen from the spectrum, other than the main wave direction (wave 1), wave2 and wave3 seems exist as also shown in Fig.3.9.

In case of carrying out wave prediction (time history of surface elevation at the designated position and time), the phase part defined by the equation (3) is needed.

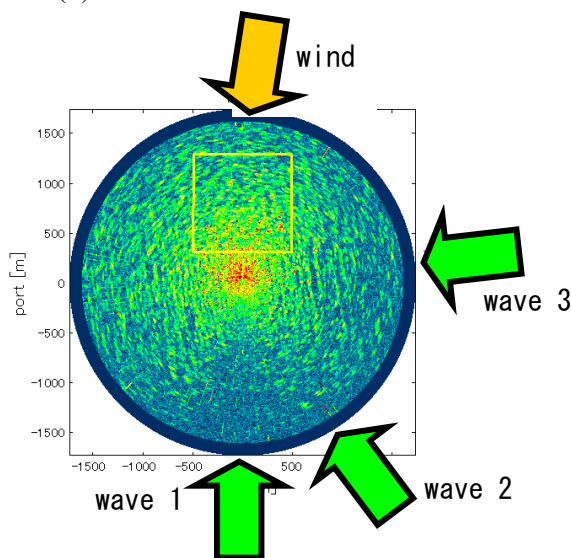


Figure 3.9: Example of PPI image of a radar (Jun.14 2012 12:46). Bow up expression.

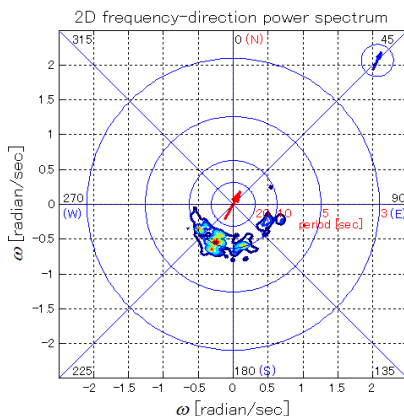


Figure 3.10: Example of obtained directional spectrum in frequency domain

Verification by wave buoy

The buoys are enough smaller than the wavelength and the motion of the buoys follow the slope and elevation of the wave surface. The

directional distribution can be estimated from the motion of the buoy based on ergodic property. On the other hand, the radar can catch the total information of wave surface directly without the assumption of ergodicity, inside its range. So, the accuracy of directional characteristics by the radar is better than the buoys. From these kinds of reasons, wave height and period by the radar are verified by that by the buoy. Fig. 3.11 and 3.12 show the comparison between the radar and the buoy about the significant wave height and the average wave period. As can be seen in Fig. 3.11 and 3.12, the errors by the radar based on the buoy are plus or minus 7.0% in wave height and plus or minus 6.6% in wave period.

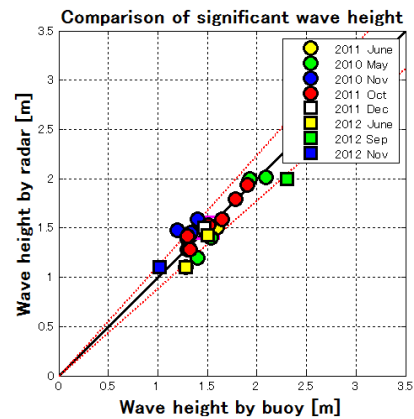


Figure 3.11 Comparison between radar and buoy from the past field experiments (Wave height)

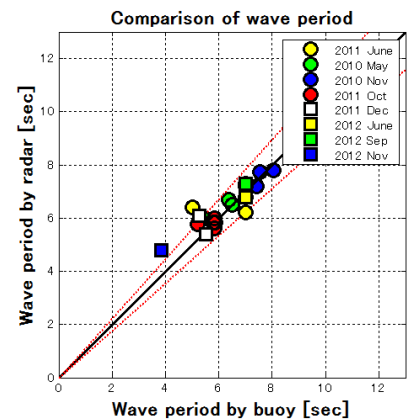


Figure 3.12 Comparison between radar and buoy from the past field experiments (Wave period)

Wave surface prediction

Watching the wave radar, we can know that the intensity of the surface back scatter moves with the wave speed. This means that the wave radar can detect the characteristics of surface wave. So, if we can obtain the accurate wave spectrum from PPI

image, then we can carry out the prediction of wave surface around the radar in relatively short time, 30sec, 60sec for example, and narrow area, 1km by 1km for example, according to the selected area by the wave radar. Prediction can be made changing the phase part of the spectrum according to the phase speed of component waves.

In case of predicting the wave surface (elevation map) by the Inverse Fast Fourier Transformation (IFFT), we need the following phase shift as equation (9) according to the time passing as Δt sec. The original phase $\phi(\omega(k),t)$ is given by equation (3).

By putting the wave buoy inside this map, then we can verify the accuracy of this prediction. Furthermore, by this method, we can predict the time-history of wave elevation at the desired point and time or that according to the trajectory of the moving ship.

$$\phi(\omega(k), t + \Delta t) = \phi(\omega(k), t) + \omega(k) \cdot \Delta t \quad (9)$$

Those predictions will contribute to avoiding the meeting with dangerous situation for ships, especially small ships like fishing boat.

Test at sea cannot always meet with such a dangerous condition, so the useful cases are not enough, we show an example as follows.

This is the case carried out using the ship named Taka-Maru, already described, on 14th June 2012, at around the point of 34.92-latitude and 139.61-longitude off Boso-peninsula near Tokyo. About this case, the ship is rested condition. Significant wave heights both from directional mini wave buoy and wave radar were about 1.8m.

Point wave spectrum from wave radar is shown in Fig.3.13. This is obtained integrating the Fig.3.10 in angular direction. Unit of abscissa is rad/s, and ordinate is relative power. Absolute power can be determined using monitored heaving motion of this ship as already described. From this determination, significant wave height is 2.03 m and mean wave period (T_{02}) is 8.47sec. So, it will be said that the swell is dominant.

Fig.3.14 show the time variant in 20-minutes of ship heading direction (\square) and wave coming directions (Δ show the primary or dominant wave, “O” show the secondary wave) estimated from the directional spectrum from wave radar. Ordinate range is 0-degree to 360-degrees. About wave direction, 0-dgree means wave coming from ship bow. 360-degrees fluctuations of ship heading occur from the 360 degrees-ambiguity of the definition of direction.

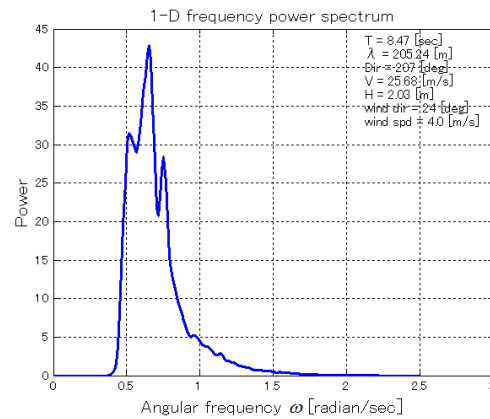


Figure 3.13: Example of point spectrum at 12:46 obtained from radar analysis. $H_{1/3}=1.83m$, $T_{02}=8.34sec$, Wind Speed=3.0m/s

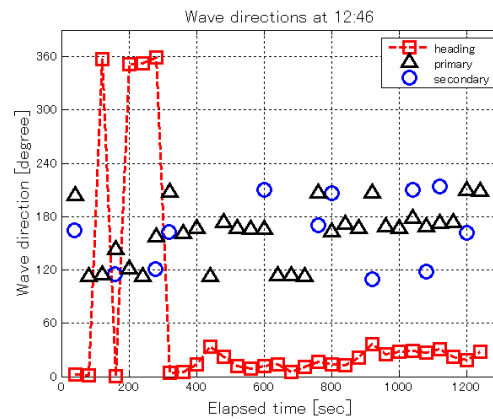


Figure 3.14: Change of the ship heading-angle(\square), primary(Δ) and secondary(\circ) direction obtained from directional wave spectrum by wave radar, according to the time.

Fig.3.15 shows the comparison of predicted (left) and actual (right) wave map expressing surface elevation. Prediction is executed after 30 seconds from the initial time. In equation (9), Δt is put as 30sec for this case. Actual ones are the wave map obtained through the process of wave filter (equation (4)), corresponding to the time of the left figure. In short time, deviation of spectrum is small, then difference of significant wave height between predicted and actual one is small.

Usually, wave field cannot be obtained at the center part of PPI, namely near-radar position, but the wave map can be obtained at this center, because this map is obtained by the superposition of infinitely continuing long crested regular waves. This point seems superior point of this predicting method.

The numerals under each figure in Fig.3.15 show the rotated number of rotating antenna of the radar. The needed time for one rotation of this wave radar is 1.25 sec. Then, for example, 44 of 44(30)

means a predicted wave map using PPI image at the 44th rotation time and (30) means the predicted map at 30 seconds after. So, the rotation number at the predicted time become 68 from the started time. Numeral 68 of actual wave map in the right corresponds to the observed wave map at the rotation number is 68.

In the Fig.3.15, continuous prediction maps are shown, and in case of practical wave radar system, similar continuous renewals are shown in a display.

In this example, as the predictions are made in very short time, so the predicted wave maps seem relatively coincide with those of actual ones.

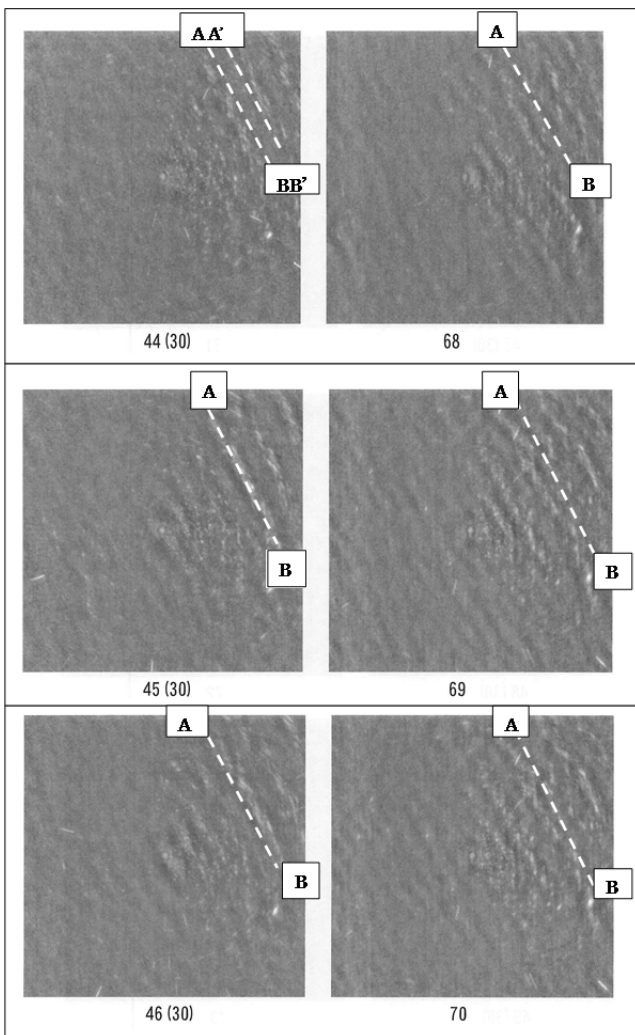


Figure 3.15: Comparison of the predicted wave fields after 30 seconds (left), and obtained wave fields by the radar after 30seconds (right). Numerals, 44 for example, means the number of the rotation of radar antenna. Inserted lines are reference line parallel to crest lines.

In order to evaluate more in details, we watch the movement of crest lines of waves. The period of dominant wave from wave spectrum is 8 seconds, the wavelength of this component wave is 99.8m, and the phase speed is 12.5m/s. This means that the

crest of this wave moves about 16m (1/6 of wavelength) within the time of one rotation of radar antenna.

The inclined dotted line A B in the upper figure of Fig.3.15 is drawn parallel to wave crest line, and A'B' line is drawn by the space of one wave length. From those auxiliary lines, it can be seen that the wave map express tones corresponding to the crest lines of dominant wave. The same lines as this AB are drawn also in the following figures.

It can also be seen that the wave main direction of left and right wave map coincide with each other. Furthermore comparing with the upper, middle, bottom wave maps of the left column each other, it can be seen that the dominant wave moves to upper diagonal direction. This result also be seen in the actual wave map of the right column.

This means that if the wave at AB line is dangerous one, then we can alarm a ship approaching to the position of AB line, in 30 seconds ahead. Of course this alarm can be given to the own ship. Those comparisons must be made more for validating the accuracy of predictions.

4. CONCLUSIONS

The accuracy of wave height and period estimated by the wave radar are shown, they are plus or minus 7.0% in wave height and plus or minus 6.6% in wave period compared to wave buoys.

The practical example of very short term wave prediction is shown utilizing the extracted information of individual wave from PPI images by marine radar.

The analysis method of wave surface prediction utilizes the information of the individual wave including the phase, so the wave surface all over the position in the range even at the antenna position (namely ship position) can be estimated.

The verification experiment is not enough in case of rough sea condition as over 3m wave height. So, additional field experiments are needed.

ACKNOWLEDGMENT

The authors would like to thank Japan Science and Technology Agency (JST), the crews of Takamaru, Fukae-maru and Shinyo-maru, the students of Kobe University, Tokyo University of Marine Science and Technology and Yokohama National

university and National Research Institute of Fisheries Engineering. We also express our appreciation to Mr. Reiji Nishikawa of YNU for his support to us. This work has been supported by JST.

REFERENCES

- MIROS, "SM-050 Wave and Current Radar Mk III", <http://www.miros.no/>.
- Chang-Kyu Rheem, 2007, "Water Surface Wave Observation by using Microwave Doppler Radar in Experimental Basin", *Journal of the Japan Society of Naval Architects and Ocean Engineers* 6, pp. 65-73.
- Chang-Kyu Rheem, 2008, "Sea Surface Wave Observation by using CW Doppler Radar and Effect of Radar irradiation Width", *Journal of the Japan Society of Naval Architects and Ocean Engineers* 8, pp. 61-69.
- Koji Nishimura, Tsugukiyo Hirayama, D.H. Nomiya, Yoshiaki Hirakawa, Takehiko Takayama, 2004, "Navigation System for Dangerous-Wave-Avoidance Maneuver as an Application of Marine Radar and Motion Simulation Technique" Conference proceedings the Society of Naval Architects of Japan (4), pp.91-92.
- Koji Nishimura, Tsugukiyo Hirayama, Takehiko Takayama, Yoshiaki Hirakawa, D.H. Nomiya, 2005, "Unsteady Rolling Due to Turning Manoeuvre in Waves-II : Motion Simulation Based on Encounter Wave Prediction by Wave Radar", *The Journal of Japan Institute of Navigation* 112, pp. 307-314.
- Tsugukiyo Hirayama, Yoshiaki Hirakawa, D.H. Nomiya, Koji Nishimura, Takehiko Takayama, 2005, "On the distinction and prediction of encountering individual waves by the ship radar", Conference proceedings the Society of Naval Architects of Japan (5), pp. 87-88.
- Nieto, Borge JC, Soares CG, 2000, "Analysis of directional wave field using X-band navigation radar", *Coastal Engineering* 40, pp. 375-391.
- Takase Fabio K., Tsugukiyo Hirayama, 2000, "Evaluation of Marine Wave Radar(Part I) : Fundamental Considerations and Numerical Generation of Radar Image", *Journal of the Society of Naval Architects of Japan* (187), pp. 85-92.
- Takase Fabio K., Tsugukiyo Hirayama, Park Seung Geun, 2000, "Evaluation of Marine Wave Radar (Part II) - Wave Parameters from Radar Images -", *Journal of the Society of Naval Architects of Japan* (188), pp. 225-237.
- Tsugukiyo Hirayama, Park Seung Geun, Takase Fabio K, Kiyoshi Miyakawa, Takehiko Takayama, 2001, "Estimating method of surrounding-wave-characteristics utilizing marine radar", Conference proceedings the Japanese Society of Fisheries Engineering (13), pp. 147-150.
- Tsugukiyo Hirayama, Park Seung Geun, Yoshiaki Hirakawa, , Takehiko Takayama, 2002, "Development of a Wave Field Detector using the Marine Radar and Measured Example", *Journal of the Society of Naval Architects of Japan* (191), pp. 51-56.
- D.H. Nomiya, Tsugukiyo Hirayama, 2003, "Numerical Simulation Applied to Real-time Ocean Wave Analysis : Wave radar", Conference proceedings the Society of Naval Architects of Japan (1), pp. 5-6.
- D.H. Nomiya, Tsugukiyo Hirayama, 2003, "Evaluation of marine radar as an ocean-wave-field detector through full numerical simulation", *Journal of marine science and technology* 8(2), pp.88-98.
- D.H. Nomiya, Tsugukiyo Hirayama, Takehiko Takayama, Yoshiaki Hirakawa, Koji Nishimura, Daigo Kabuto, 2003, "Wave-Field-Detection by the Marine Radar on a Small Ship", Conference proceedings the Society of Naval Architects of Japan, pp. 139-140.
- Yoshiaki Hirakawa, Takehiko Takayama, Tsugukiyo Hirayama, Koji Nishimura, 2003, "Improvement of Directional-Wave-Mini-Buoy and Field Experiments", Conference proceedings Joint Autumn Meeting of Three Societies of Naval Architects in Japan, pp. 63-66.
- Yoshiaki Hirakawa, Hironori Susaki, Seishi Sasaki, Takehiko Takayama, Akihiko Matsuda, Tsugukiyo Hirayama, 2015, "Acquisition of Ocean Wave Surface by X-band Ship Radar and Very-short-term Wave Surface Prediction", *Journal of the Japan Society of Naval Architects and Ocean Engineers* 22, pp. 235-242.
- Yoshiaki Hirakawa, Takehiko Takayama, Tsugukiyo Hirayama, Hironori Susaki, 2016, "Development of Mini-Buoy for short term measurement of ocean wave", OCEANS 2016 MTS/IEEE Monterey.

On Safe Navigation Support System using GPS Compass

Daisuke Terada, *National Defense Academy*, dterada@nda.ac.jp

Masahiro Tamashima, *FLUID TECHNO Co., Ltd.*, mtamashima@fluidtechno.com

Ikuo Nakao, *FLUID TECHNO Co., Ltd.*, inakao@fluidtechno.com

Akihiko Matsuda, *Japan Fisheries Research and Education Agency*, amatsuda@affrc.go.jp

ABSTRACT

For making the onboard use of operational guidance in the IMO second generation intact stability criteria feasible, it is proposed to use a GPS compass for estimating a directional wave spectrum onboard based on Wave Buoy Analogy. As a discussing in 1980s, if the directional wave spectrum can be estimated onboard, then ship motions, a bending stress and so on can be estimated and predicted without direct measurement of them based on the linear superposition theory. Since as the basic theory a Bayesian statistics, namely a general state space modeling procedure, is used, the proposed method can even use under navigation in the following seas. In order to verify the effectiveness of the proposed method, model experiments and onboard experiments are carried out. As the results, it is confirmed the effectiveness of the proposed method, although several future tasks exists.

Keywords: *General state space modelling procedure, Ensemble Kalman Filter, Nonlinear observation.*

1. INTRODUCTION

It goes without saying that it is most important task for a captain, officers and sailors to remain a safe navigation in rough seas. In order to realize this, firstly, under navigation they need to appropriately make the use of operational guidance in the IMO second generation intact stability criteria feasible. In this study, a novel navigation support system using a GPS compass is introduced to realize this purpose. A GPS compass, which was developed in recent years, is new nautical instruments to understand a ship course, position, speed and so on. Especially, the one with built-in a clinometer using acceleration sensor can also measure the ship motions such as pitch motion, roll motion and heave motion, simultaneously. In this paper GPS compass with this function is called the "GPS+M". We focused on this function. That is, by using this GPS compass, we can obtain various information to remain a safe navigation in rough seas.

As well known, in the research field of seakeeping quality, ship motions can evaluate statistically by multiplying response amplitude operators (RAO) based on the linear potential theory and given directional wave spectra. Therefore, if we can prepare the RAO of the ship and can give the encounter directional wave

spectrum, then we can evaluate statistical values of ship motions theoretically. In 1980s, this idea had been concretely realized by many ship builders. However, in these systems, officers and sailors had to input several information which are the ship speed, statistical values of encounter waves and so on. Moreover, a transverse metacentric height, namely GM, was also required to calculate the RAO of motions. Consequently, they were not popular. In order to solve one of disadvantages, in 1990s, as well as wave buoy system, an encounter directional wave spectrum under navigation can be evaluated by using the knowledge of statistical science that is especially Bayesian statistics as shown Iseki and Ohtsu [1994] firstly. In recent years, this procedure is called a 'Wave Buoy Analogy (WBA)'. In WBA, the directional wave spectrum can be evaluated by using a RAO concerning ship motions calculated theoretically and a cross spectrum obtained by calculating from measured time series of ship motions. Moreover, Iseki and Terada [2002] showed that ship motions and a longitudinal bending moment can be predicted by using the estimated directional wave spectrum. In this case, the measurement of ship motions can be done by an Inertial Measurement Unit (IMU). Therefore, even if we used the WBA, the ship speed had to input by officers and sailors. It should be noted that the IMU is not an equipment

designated by law, although there are the IMU which can take in a signal of GPS.

On the other hand, as mentioned before, the GPS+M can simultaneously measure both of the ship speed and motions. Therefore, disadvantages of the systems developed in 1980s can be solved by using the GPS+M. Moreover, in our recent research [Terada et al. (2016)], we had developed the estimation method of GM based on nonlinear state space modeling procedure which is a type of time series modeling procedure. It means that the estimation of the directional wave spectrum can be automatically achieved by the use of the GPS+M.

From this background, we considered that it can be developed the navigation support system in rough seas which has the function of the statistical prediction. The system contains the estimation of GM, the selection of RAO corresponding the ship speed and the displacement, the calculation of cross spectrum, the estimation of directional wave spectrum and the prediction of ship motions. In these items, especially, as to the estimation procedure of directional wave spectrum, a novel procedure using a general state space modeling is proposed. The feature of this is that at the same time the cross spectrum was calculated, the directional wave spectrum can be evaluated based on filtering process in state estimation of general state space modeling procedure. In this paper, we explain this in detail. The proposed system was verified based on model experiments and onboard experiments. The sample ship is a container ship of coastwise navigation.

2. OUTLINE OF PROPOSED SYSTEM

Figure 1 shows the basic concept of the proposed system. As mentioned above, the most important key technology is the GPS+M. As shown this figure, the information for the ship position, the speed and motions, namely the pitch, the roll and the heave, are simultaneously obtained by it. That is, by using the GPS+M, the time synchronization of each data can be realized naturally. In this system, as to the roll motion, the damping coefficient and the natural frequency are firstly estimated, after that the GM are estimated based on Terada et al. [2016]. As to the detail of this process, see the reference. In this case, if the GM can be estimated, then the RAO for motions with the ship speed and the GM as parameters can be calculated

or selected from the database, because the ship speed are given by the GPS+M. Moreover, the cross spectrum of motions can be done automatically by the vector autoregressive modeling procedure [Kitagawa, 2010] based on the minimum AIC (Akaike Information Criterion) [Akaike, 1974] estimation. Thus, the problem of the past research work is solved completely in meaning of the applying of WBA. As to the methodology of WBA, a general state space modeling based on an ensemble Kalman filter (EnKF) [Evensen, 2003] is proposed in after section. Therefore, if an accurate directional wave spectrum can be estimated, then the ship responses such as motions, moment and so on can be estimated without a direct measurement, and the prediction of them can be realized under an assumption of stationarity with respect to waves as well as the past research work.

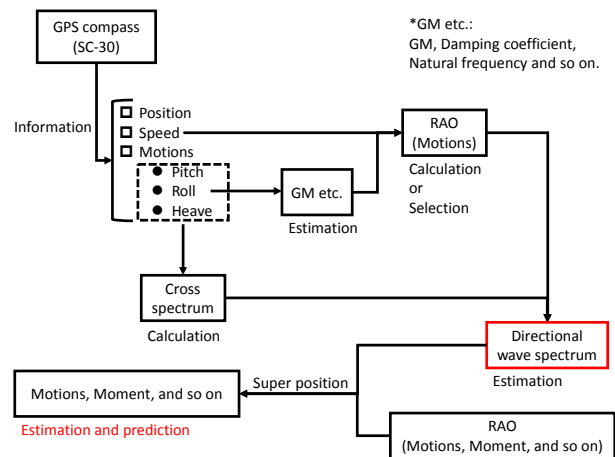


Figure 1: Basic concept of the proposed system.

3. ESTIMATION OF DIRECTIONAL WAVE SPECTRUM

3.1 Modeling

As mentioned before, if ship motions are considered to be linear responses to incident waves, then the cross spectrum of ship motions and the directional wave spectrum are related by the RAO as follows:

$$\Phi_{mn} = \int_{-\pi}^{\pi} H_m(f_e, \chi) H_n^*(f_e, \chi) E(f_e, \chi) d\chi \quad (1)$$

where f_e is an encounter frequency, $E(f_e, \chi)$ is the directional wave spectrum based on the encounter frequency, Φ_{mn} is the cross spectrum between the m -th and n -th components, $H_m(f_e, \chi)$ is the RAO of

the m -th component of the time series, and the notation "*" means the complex conjugate.

On the other hand, the directional wave spectrum expressed by absolute wave frequencies are convenience because of a statistical prediction of ship motions, bending stress and so on. However, in this equation, when the ship runs under the following seas, the relationship between the encounter wave frequency f_e and the absolute frequency f_0 becomes triple valued function problem as shown in Figure 2. According to Iseki and Ohtsu [1994], it can be dealt with this problem appropriately.

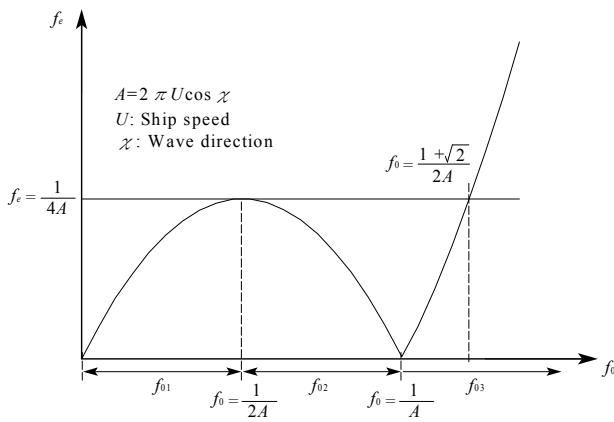


Figure 2: Relationship between encounter wave frequencies and absolute wave frequencies.

Considering this problem in the following seas, the discrete form of the equation (1) can be expressed by the following matrix expression:

$$\begin{aligned} \Phi(f_e) = & \mathbf{H}(f_{01})\mathbf{E}(f_{01})\mathbf{H}(f_{01})^{*\top} \\ & + \mathbf{H}(f_{02})\mathbf{E}(f_{02})\mathbf{H}(f_{02})^{*\top} \\ & + \mathbf{H}(f_{03})\mathbf{E}(f_{03})\mathbf{H}(f_{03})^{*\top} \end{aligned} \quad (2)$$

where f_{01} , f_{02} and f_{03} are the absolute wave frequencies that correspond to the encounter wave frequencies f_e , $\Phi(f_e)$ is the measured cross spectrum matrix, $\mathbf{H}(f_{0i})$ and $\mathbf{E}(f_{0i})$ ($i=1,2,3$) denote the matrices of the RAO of ship motions and the directional wave spectrum at the f_{01} , f_{02} and f_{03} , respectively. It should be noted that the number of elements with $i = 1$ is K , and the number of elements with $i = 2$ and 3 representing the contribution from the following seas is $K1 (< K/2)$. In this equation, since $\Phi(f_e)$ is a Hermitian matrix, this equation can be reduced to a multivariate

regressive model expression using only the upper triangular matrix:

$$\mathbf{y} = \mathbf{A}\mathbf{F}(\mathbf{x}) + \mathbf{w} \quad (3)$$

where, \mathbf{y} is the $(9 \times l)$ cross spectrum vector which is composed of real and imaginary parts of each element of $\Phi(f_e)$. Noted that l is the divided number of the spectrum. And \mathbf{A} is the $(9 \times l, k \times m)$ coefficient matrix which is composed of products of the RAO of ship motions. Note that k and m are the divided number of the encounter angle and the absolute wave frequency. Moreover, $\mathbf{w} \sim \mathcal{N}(0, \Sigma)$ is a $(9 \times l)$ Gaussian white noise sequence vector introduced for stochastic treatment and $\mathbf{F}(\mathbf{x})$ is the $(k \times m)$ unknown coefficient vector which is composed of the discretized directional wave spectrum. In the actual calculation, the unknown parameter vector should be expressed in the following form to avoid the estimation of a negative directional wave spectrum:

$$\begin{aligned} \mathbf{F}(\mathbf{x})^\top = & [\exp(x_1), \dots, \exp(x_j)] \\ (\exp(x_j) = & E_j(f_0), j = 1, \dots, k \times m) \end{aligned} \quad (4)$$

where, $E_j(f_0) = E(f_0, \chi_k)$, and χ_k denotes a discretized encounter angle.

In this case, if the cross spectrum can be obtained any time step recursively, then the idea of WBA can be extended into the estimation of changing directional wave spectrum with time. That is, equation (3) can be expressed by the following equation:

$$\mathbf{y}_t = \mathbf{A}_t \mathbf{F}(\mathbf{x}_t) + \mathbf{w}_t \quad (5)$$

where, in this equation the subscript t means any time step.

In this case, consider that equation (4) is a nonlinear observation model in a general state space model. Moreover, consider a smoothness prior with respect to the change of the directional wave spectrum as a system model of the general state space model. Then, the time varying directional wave spectrum can be dealt with as the

problem of the following general state space modelling:

$$\begin{cases} \mathbf{x}_t = \mathbf{x}_{t-1} + \mathbf{v}_t \\ \mathbf{y}_t = \mathbf{A}_t F(\mathbf{x}_t) + \mathbf{w}_t \end{cases} \quad (6)$$

here,

$$\mathbf{x}_t^T = [\ln(x_{1,t}), \dots, \ln(x_{J,t})]$$

$$F(\mathbf{x}_t)^T = \exp[\ln(x_{1,t}), \dots, \ln(x_{J,t})].$$

and, \mathbf{x}_t is a state vector, \mathbf{v}_t is a system noise vector, \mathbf{y}_t is an observation vector, \mathbf{A}_t is a state transition matrix and \mathbf{w}_t is an observation noise vector, respectively.

As shown in equation (6), since the observation model is nonlinear, it should be noted that an appropriate state estimation method must be used. As to a nonlinear filtering theory of the state estimation, there are the particle Monte Carlo filter [Kitagawa, 1993], the ensemble Kalman filter (EnKF) [Evensen, 2003] and so on. In this study, the EnKF is used from the viewpoint of the computational time. However, since the EnKF is a type of the Kalman filter, equation (6) including nonlinear observation model cannot be directly used. In order to solve this problem, consider the extended state vector \mathbf{z}_t , the extended state transition matrix and the extended observation vector as follows:

$$\mathbf{z}_t = \begin{pmatrix} \mathbf{x}_t \\ \mathbf{A}_t F(\mathbf{x}_t) \end{pmatrix} \quad (7)$$

$$\tilde{\mathbf{A}}_t = \begin{pmatrix} \mathbf{0}_{(9 \times l, m \times k)} & \mathbf{I}_{(9 \times l, 9 \times l)} \end{pmatrix} \quad (8)$$

$$f_t(\mathbf{z}_{t-1}, \mathbf{v}_t) = \begin{pmatrix} \mathbf{x}_{t-1} + \mathbf{v}_t \\ \mathbf{A}_t F(\mathbf{x}_{t-1} + \mathbf{v}_t) \end{pmatrix} \quad (9)$$

As the result, the equation (6) can be transformed into as follows:

$$\begin{cases} \mathbf{z}_t = f_t(\mathbf{z}_{t-1}, \mathbf{v}_t) \\ \mathbf{y}_t = \tilde{\mathbf{A}}_t \mathbf{z}_t + \mathbf{w}_t \end{cases}, \quad (10)$$

and since this equation is formally a linear state space representation, the EnKF can be used.

3.2 State estimation

In the EnKF, a state estimation can be done by using ensembles from the probability distribution as well as a particle Monte Carlo filter. Under given the general state space model, the EnKF concretely calculates a predictive distribution $p(\mathbf{z}_t | \mathbf{y}_{t-1})$ and a filter distribution $p(\mathbf{z}_t | \mathbf{y}_t)$ recursively using the M ensemble member $\{\mathbf{z}_{t|t}^{(i)}\}_{i=1}^M$. According to Evensen [2003], concrete algorithm can be written as follows:

[Step 1] Generate an initial ensemble $\{\mathbf{z}_{0|0}^{(i)}\}_{i=1}^M$.

[Step 2] Repeat the following steps for $n=1 \sim N$.

(1) One-step-ahead prediction

(a) Generate an ensemble $\{\mathbf{v}_t^{(i)}\}_{i=1}^M$ of the system noise.

(b) For $i=1, \dots, M$, compute the following equation:

$$\mathbf{z}_{t|t-1}^{(i)} = f_t(\mathbf{z}_{t-1|t-1}^{(i)}, \mathbf{v}_t^{(i)}) \quad (11)$$

(2) Filter

(a) Generate an ensemble $\{\mathbf{w}_t^{(i)}\}_{i=1}^M$ of the observation noise.

(b) For $i=1, \dots, M$, compute the following equations:

$$\tilde{\mathbf{z}}_{t|t-1}^{(i)} = \mathbf{z}_{t|t-1}^{(i)} - \frac{1}{M} \sum_{j=1}^M \mathbf{z}_{t|t-1}^{(j)} \quad (12)$$

$$\hat{\mathbf{V}}_{t|t-1} = \frac{1}{M} \sum_{j=1}^M \tilde{\mathbf{z}}_{t|t-1}^{(j)} \tilde{\mathbf{z}}_{t|t-1}^{(j)T} \quad (13)$$

$$\tilde{\mathbf{W}}_t^{(i)} = \mathbf{w}_t^{(i)} - \frac{1}{M} \sum_{j=1}^M \mathbf{w}_t^{(j)} \quad (14)$$

$$\hat{\Sigma}_t = \frac{1}{M-1} \sum_{j=1}^M \tilde{\mathbf{W}}_t^{(j)} \tilde{\mathbf{W}}_t^{(j)T} \quad (15)$$

$$\hat{\mathbf{K}}_t = \hat{\mathbf{V}}_{t|t-1} \tilde{\mathbf{A}}_t^T \left(\tilde{\mathbf{A}}_t \hat{\mathbf{V}}_{t|t-1} \tilde{\mathbf{A}}_t^T + \hat{\Sigma}_t \right)^{-1} \quad (16)$$

(c) For $i=1, \dots, M$, compute the following equation:

$$z_{t|t}^{(i)} = z_{t|t-1}^{(i)} + \hat{K}_t \left(\mathbf{y}_t + \tilde{\mathbf{W}}_t^{(i)} - \tilde{\mathbf{A}}_t z_{t|t-1}^{(i)} \right) \quad (17)$$

4. RESULTS AND DISCUSSIONS

4.1 Model experiments

In order to verify the proposed procedure, we firstly carried out the free running model experiments concerning a container ship at the marine dynamics basin belonging to Japan Fisheries Research and Education Agency. The principal particulars and the photo are shown in Table 1 and Figure 1, respectively.

Table 1: Principal particulars of the sample ship.

L_{pp}	85.0 m	GM	0.828 m
B	14.0 m	T_ϕ	13.3 sec
d_m	3.54 m	k'_{yy}	0.264
W	2993.21ton		

Note: Scale ratio = 1/33



Figure 2: Photo of the sample ship.

One of the results of the model experiments is shown in this subsection. The conditions in the model experiments are as follows:

- The model ship speed is corresponding to 10[knots] in actual ship.
- The encounter angle relationship between the ship course and the wave direction is 0[degrees], that is, the model ship ran under the following seas.
- The measurement device is the Fiber Optic Gyro (FOG) sensor made by Tamagawa seiki Co., Ltd., and its sampling rate is 20[Hz]. It should be noted that a vertical acceleration was used for the analysis, since in model experiments the heave can not be measured.

- The waves are the long-crested irregular waves, are reproduced by the conditions in which the significant wave height $H_{1/3}$ is 1[m] and the mean period T_{01} is 6[sec].
- Note that the results of the model scale have been transformed in to the value of the actual ship.

As preparation of the estimation of the directional wave spectrum, as shown in Figure 3 the 100 data set from one record of the measured time series data such that the number of analysis data always becomes 300 samples were made, because the measurement time in the model experiment has the constraint. It should be noted that to use 300 samples is decided by the viewpoint of the calculation time.

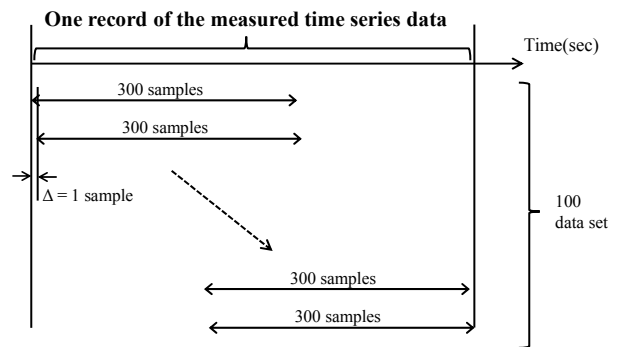


Figure 3: Schematic diagram concerning the contraction of the data set.

From Figure 4 to Figure 6 show the three kinds of characteristics, namely significant wave height, wave mean period and wave direction, obtained by the integral of the estimated directional wave spectrum, respectively. In these figures, the horizontal axis indicates the sample data number, and the vertical axis indicates the characteristics of the estimated directional wave spectrum. Figure 4 shows the significant wave height, Figure 5 shows the mean period, and Figure 6 shows the direction of the wave, respectively. From these figures, it can be confirmed that each characteristic of the estimated directional wave spectrum converges to the set values with time, even though the condition of the encounter angle with respect to waves is the following seas. Therefore, it can be considered that the proposed method for the estimation of the directional wave spectrum is effective.

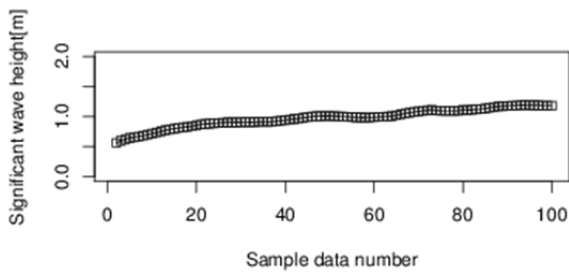


Figure 4: Estimated significant wave height.

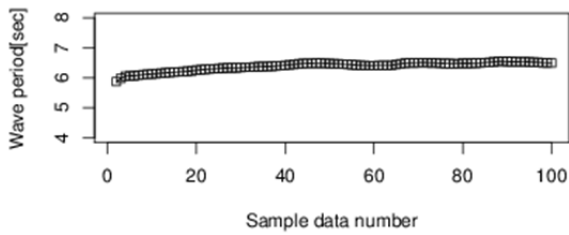


Figure 5: Estimated mean period.

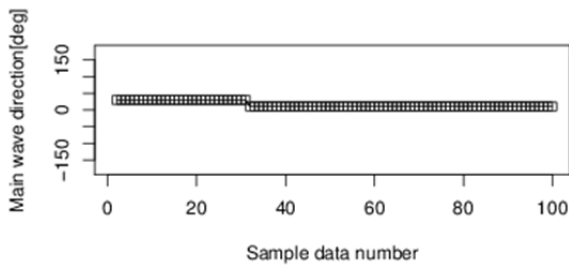


Figure 6: Estimated main wave direction.

4.2 Onboard experiments

One of the results of the onboard experiments is shown in this subsection. The sample ship is the same one used in the model experiments. In the onboard experiments, as the GPS compass, the “SC-30” made by FURUNO ELECTRIC CO., LTD. was used. The SC-30 was set as the Figure 7 at the upper of flying bridge of the sample ship. The data which was measured at 14 [UTC] o’clock on Feb. 8, 2014 is used in the analysis. In this case, the sampling time is the 1.0 [sec]. Figure 8 shows the ship’s position where data was measured.

Figures 9 (a) ~ (e) show the time series between 1,200 [sec] was measured by the SC-30. From top to bottom, the ship course, the speed, the pitch, the roll and the heave are shown, respectively. From these figures, it can be seen that the sample ship bounds for the east at the ship speed about 11 [knots]. And, it can be also seen that the motions

are large. Here, these data were analyzed every 300 samples (300 [sec]). It is called that the first 300 samples is ‘case01’, the second 300 samples is ‘case02’, the third 300 samples is ‘case03’ and the last one is ‘case04’, respectively.



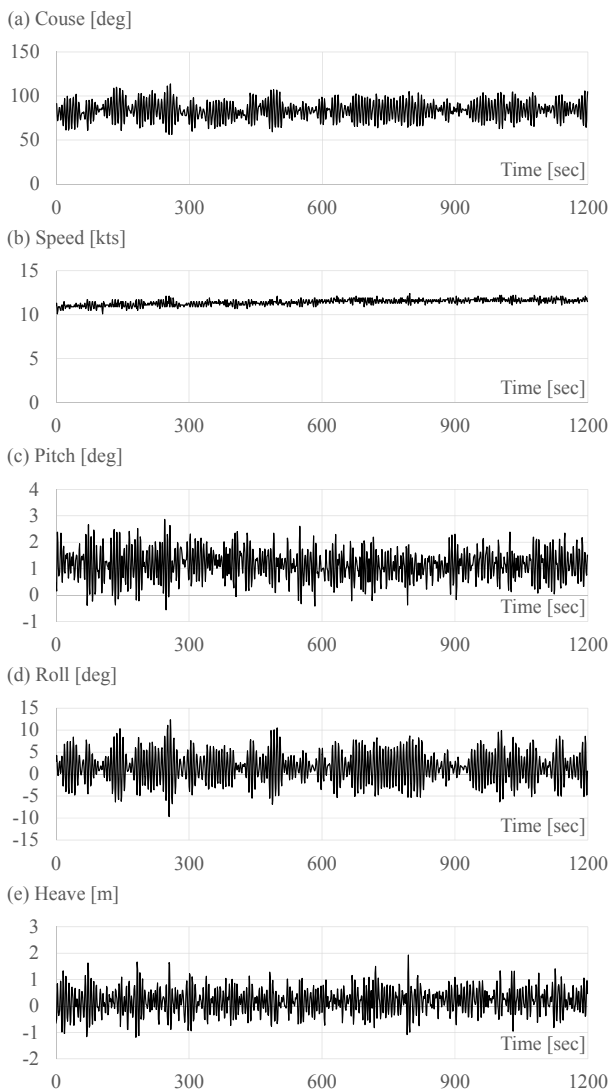
Figure 7: Photo of installation state of the SC-30.



Figure 8: Ship’s position where data for the analysis was measured.

Table 2 shows the results of the analysis and the results of the wave prediction in Japan Meteorological Agency (JMA) [JMA(A), 2017]. From this table, as to the significant wave height, it can be seen that the estimated values by the proposed method are good agreement with the wave prediction values in the JMA, though the target time is slight different. However, as to the wave mean period, both results are slight different, moreover as to the wave direction, both results are quite different. As one of this cause, it is considered that the wave prediction method in the JMA can not take multi-directionality into consideration as

shown Sasa et al. [2015], although our proposed method can deal with multi-directionality of waves. As the reference information, we investigated the wind information of the JMA observation point, which is Munakata city, Fukuoka Prefecture, closest to the ship's position [JMA(B), 2017]. According to this records, the direction varied from SSE to WSW, and the velocity varied from 1.5 [m/s] to 1.0[m/s], respectively. Therefore, at least, as to the wave direction, it can be considered that the accuracy of the wave prediction values in the JMA is low, because there is the fact in which the direction of the wind and wind waves is almost same. Note that as to this, it is necessary to verify more in detail.



Figures 9: Time series for the data analysis.

Table 2: Comparison with the estimated values by the proposed method and the wave prediction values in the JMA.

	$H_{1/3}$ [m]	T_{01} [sec]	Wave direction	
			Main	2 nd
case01	2.37	6.28	South	North
case02	2.37	6.28	South	NNW
case03	2.35	6.27	South	North
case04	2.33	6.25	South	NNW
JMA [UTC1200]	2.0	9.0	NNE	
[UTC2400]	1.6	4.0	NNW	

5. CONCLUSIONS

In this research, from the view point in which under navigation ship's crews appropriately make the use of operational guidance in the IMO second generation intact stability criteria feasible, the safe navigation support system using GPS compass is introduced. The system contains the estimation of GM, the selection of the response amplitude operator corresponding the ship speed and the displacement, the calculation of cross spectrum, the estimation of directional wave spectrum and the prediction of ship motions. In these items, especially, as to the estimation procedure of directional wave spectrum, a novel procedure using a general state space modeling was proposed. The feature of this is that at the same time the cross spectrum was calculated, the directional wave spectrum can be evaluated based on filtering process in state estimation of general state space modeling procedure. In order to verify the effectiveness of the proposed method for the estimation of directional wave spectrum, the model experiments and the onboard experiments are carried out. Obtained findings are summarized as follows:

- (1) From the results of the model experiments, under the condition in which the ship motions exist, it can be confirmed that the estimated directional wave spectrum based on the proposed method is good agreement with the set one, since the characteristics obtained by the integral of the estimated directional wave spectrum converge the set values with time.
- (2) From the onboard experiments, as to the significant wave height, it can be seen that the estimated values by the proposed method are good agreement with the wave prediction values in the Japan Meteorological Agency, though the target time is slight different. However, as to the wave mean period, both

results are slight different, moreover as to the wave direction, both results are quite different. Therefore, as a future task, it is necessary to verify this reason more in detail comparison with an onboard experiment using a wave buoy and a wave RADAR.

Terada, D., Tamashima, M., Nakao, I. and Matsuda, A, 2016, "Estimation of the metacentric height by using onboard monitoring roll data based on time series analysis", Proceedings of the 15th International Ship Stability Workshop, pp.209–215.

6. ACKNOWLEDGEMENT

This work was supported by the commissioned project for R&D of marine science and technology in Nagasaki Industrial Promotion Foundation. Authors would like to thank all affiliated parties.

REFERENCES

- Akaike, H., 1974, "A new look at the statistical model identification", IEEE Trans. Autom. Control vol. 19, pp. 716–723.
- Evensen, G., 2003, "The Ensemble Kalman Filter: theoretical formulation and practical implementation", Ocean Dynamics, 53, pp.343–367.
- Kitagawa, G., 1993, "Monte-Carlo filtering and smoothing for non-Gaussian nonlinear state space models", Proceedings of 2nd U.S.-Japan Joint Seminar on Statistical Time Series Analysis, pp.110–131.
- Kitagawa, G., 2010, "Introduction to time series modeling", CRC Press.
- Iseki, T. and Ohtsu, K., 1994, "Bayesian estimation of directional wave spectra based on ship motions (2nd report)"(In Japanese), Journal of the Society of Naval Architects of Japan, No. 176, pp.99–105.
- Iseki, T. and Terada, D., 2002, "Bayesian estimation of directional wave spectra for ship guidance system", International Journal of Offshore and Polar Engineering, Vol. 12, No. 1, pp.25–30.
- Japan Meteorological Agency, 2017/04/11(accessed), "http://www.data.jma.go.jp/kaiyou/db/wave/chart/wavepoint/wave_point.html?point=18&year=2014&month=2"(In Japanese)
- Japan Meteorological Agency, 2017/05/01(accessed), "http://www.data.jma.go.jp/obd/stats/etrn/view/hourly_a1.php?prec_no=82&block_no=0943&year=2014&month=2&day=8&view=" (In Japanese)
- Sasa, K., Terada, D., Shiotani, S., Wakabayashi, N., Ikebuchi, T., Chen, C., Takayama, A, Uchida, M, 2015, "Evaluation of ship performance in international transportation using an onboard measurement system – in case of a bulk carrier in international voyages", Ocean Engineering, Vol. 104, pp.294–309.

Session 3

Operational aspects of damage stability

Session Chairs

Hendrik Bruhns

Teemu Manderbacka

How to buy time following a flooding incident – intelligent quantification of emergency response measures

Kristian Bertheussen Karolius, *University of Strathclyde*, kristian.karolius@strath.ac.uk

Dracos Vassalos, *University of Strathclyde*, d.vassalos@strath.ac.uk

ABSTRACT

Increasing vessel size and complexity creates high uncertainty in flooding situations, and it is challenging for the crew to obtain a complete overview and make fully informed decisions. Time is of the essence, and to optimise decision making and ensure decisions are made on time, we propose adopting the concept of *Dynamic Barrier Management* through increased use of sensors and analytics. Focus will be placed on emergency responses as their impact on safety has not been quantified in terms of risk reduction to the same extent as for passive design barriers. Based on the idea of increased use of advanced analytics and sensors, particularly flooding sensors, this paper aims to present current research ideas and planned development of a method in which active mitigation measures such as emergency response actions can be quantified in terms of effective risk reduction based on real-time measurements and simulations during an accident, i.e. intelligent quantification of emergency response measures.

Keywords: *Dynamic Barrier Management, Emergency Response, Decision Support, Flooding, Mitigation*

1. INTRODUCTION

As the world is changing fast, so is the maritime industry. New megaships continue to outsize older designs as economies of scale continue to offer a competitive edge to ship-owners and operators in an ever-competitive market. The new giants of the sea and the increasing complexity of their on-board systems and their interactions are posing challenges to the maritime industry in terms of potential hidden risks. We continue to strive towards a safer industry, but are we able to keep up with today's immense pace of change?

An intensive search for better and more optimised design solutions has been seen in the last few decades, especially following the introduction of risk-based ship design methods (Papanikolaou et al., 2009) and the introduction of risk-based standards such as the probabilistic damage stability regulations outlined in Ch. II-1 of SOLAS (2009). Utilising these methods of risk reduction, numerous means for reaching more optimal and cost efficient designs have been developed through the introduction of risk control options or safety barriers aimed at either accident prevention, or mitigation post-accident.

With regards to hull breach and flooding, development of such measures has been focused primarily on survivability and mitigation rather than prevention. It seems now, however, that this is about to change as focus has shifted towards research and developments of preventative measures for avoiding hull damages altogether, a concept that has shown to be more cost efficient if successful. The various safety barriers introduced to reduce risk are many, and can roughly be classed as passive means built in to the design, i.e. inherent safety, or as active means which may relate to process, people, technology, environment, etc. Several of the built-in barriers need physical activation to be in their functioning state, e.g. sliding watertight doors, pumps/valves, cross/down-flooding, etc. and are therefore highly dependent on active means in terms of human response and actuation.

The way we handle and manage these barriers during the life-cycle of a vessel has lately been questioned. What happens to risk of a vessel when the barriers change and deteriorate and how can we ensure that this does not result in risk reaching unacceptable levels during the vessel operational-life? Trying to answer such questions, a new concept has emerged with roots in the offshore oil and gas industry, namely *Dynamic Barrier Management*.

The concept is aimed at continuous monitoring and management of safety critical barriers by utilising sensor measurements and analytics (Astrup et. al 2015). Despite the fact that focus has shifted from mitigation towards prevention, it is the authors’ belief that there is still room for great improvements in a vessel’s survivability through optimising active barriers such as emergency response actions and their interaction with available systems.

The impact of emergency response on safety has not yet been quantified in terms of risk reduction to the same extent as for purely passive design barriers. Based on the idea of increased use of advanced sensors and analytics, especially flooding sensors, this paper aims to present current research ideas and planned development of a method in which active mitigation measures such as emergency response actions can be quantified in terms of effective risk reduction based on real-time measurements and simulations during an accident, i.e. intelligent quantification of emergency response measures.

2. CURRENT CHALLENGES

The increase in vessel size and system complexity introduces new challenges in any emergency situation, hull breach and flooding situations being no exception. It is difficult for a human to grasp the immensity of such situations, the numerous possible damage conditions, water propagation and progressive flooding through pipes, doors and other internal openings. This also includes multiple free surface effects and motions induced by external forces.

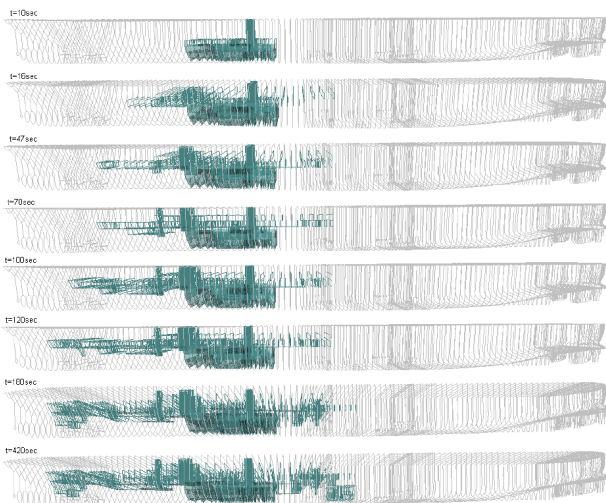


Figure 1: Progressive flooding of vessel during 7 min at Hs=4m. (Tsakalakis, 2009).

Figure 1 illustrates the complexity of a flooding incident, demonstrating the propagation of floodwater in a vessel during only a 7-minute time period. For the crew to have a complete overview of the situation, there are multiple variables that require consideration such as damage extent, flooding rate and taking inventory of available systems, including also all the external environmental variables. Before the crew manage to get hold of all this information and evaluate the situation, the situation can become unmanageable.

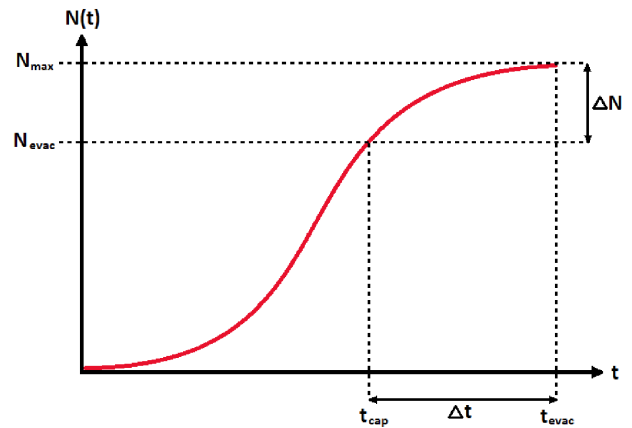


Figure 2: Interplay between time to capsizes and evacuation time. Adapted from Papanikolaou et al. (2009).

Even when information is available on the current status, the final outcome is still uncertain and information to take the correct and most optimal decisions is limited at best. The two most important variables in any flooding accident is the time to capsizes and the evacuation time, which are depicted in figures 1 and 2. If the time it takes to evacuate is longer than the time it takes for the vessel to capsizes and sink, we have to assume there will be losses in terms of human life. The magnitude of loss will be closely related to the difference between these times, but most importantly it can be seen as a measure of potential improvement. If we can implement any active measures to decrease Δt , we can save lives. In an ideal design, the time to capsizes should be ∞ for all expected damage scenarios, and as a minimum the following inequality should be true:

$$t_{cap} > t_{evac} \tag{1}$$

But a perfect design does not exist. We do however have the tools available, and it is befit on us to optimise these tools to the highest level possible. Optimised tools will waste less time following flooding incidents, increase Δt , and allow for more effective evacuation, thus saving more lives.

3. PROPOSED METHODOLOGY

As initially mentioned, innovative technologies present a challenge, but in addition to considering their risk contribution, it is important also to embrace the possibilities such innovation can bring. If implemented correctly, it is believed that such technology could be used to optimise the current emergency response and operational measures. Today, the physics that governs the flooding process is well understood, and several tools of replicating the phenomena through time domain simulations are available. By introducing sensors to relevant compartments and available safety critical systems, real-time data and status can be used in combination with flooding simulation software to assist crew in adopting the most optimal measures during emergencies.

In theory, such optimisation techniques can be used for other accident categories such as fire, but in this instance, focus is placed on flooding scenarios. Systematic application of sensors to relevant compartments and safety critical systems would result in a reduction in the high uncertainty following a flooding incident. Information regarding the damage extent and flooding rate would be provided with increased accuracy, i.e. current initial condition and its rate of change. Some uncertainty will still be present, but sensor-based inference could be utilised in order to determine/limit the number of initial damage cases to investigate further using simulations.

Relevant initial damage cases can be prepared using available statistics, and time-domain simulations. This data can be stored onboard in a database from which the system could infer the n^{th} most probable cases using all available evidence. As time progresses, continuous measurements from the sensors would then update this inference as more detailed evidence becomes available and the number of cases would reduce. Furthermore, having sensors on installed safety systems such as doors, valves, pumps, etc. their availability post damage is known. This information combined with knowledge of the initial condition, can be used in advanced flooding simulations to predict the most likely outcomes. Such information can then be used to facilitate the best risk-based decisions for containing or suppressing the flooding process, thus increasing the time available for evacuation, or even safe return to port.

Having real-time data on the initial situation limits the need for extensive simulations and we need only focus on the actual damage cases. This is particularly important if simulations are to be performed in real-time onboard the vessel. This derives from the fact that one of the sources of uncertainty originates from the complexity of the internal architecture in cruise ships, making flood progression a chaotic process. Chaotic processes introduce complexity and uncertainty that is time-consuming to address. The idea of utilising sensors is not a new one, and several developments on the topic have been published. A lot of work has been done during the project FLOODSTAND (2009) where sensors were implemented on watertight doors, including simulations to predict the impact of watertight doors in varying states on the vessels' survivability.

The problem encountered initially in this project was the long simulation time for conducting a global risk assessment, encompassing all damage scenarios. However, this should not be a problem when flooding sensors are used, as they provide an initial indication of the damage extent, thus localising the problem. They also provide information on the path of floodwater propagation, thus removing the uncertainty associated with the flooding process and rendering flooding progression predictable. Instead of thousands of combinations for the whole ship, only a small portion would be required, limiting the simulation time considerably. NAPA has also worked on similar approaches (Ruponen, et al. 2015) using flooding sensors and time-domain simulations but were limited to consider flood-level sensors, door status and loading condition only. Their time-domain simulations have

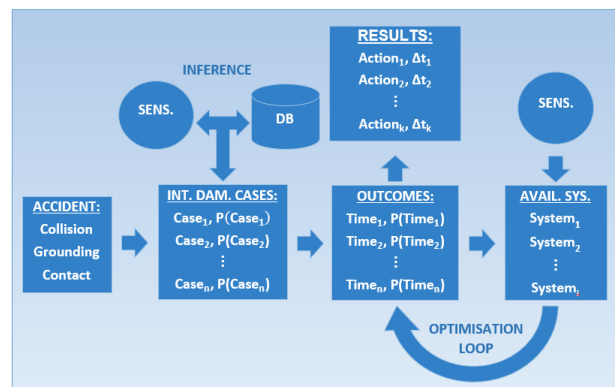


Figure 3: Initial outline of methodology.

further been limited to calm-water, i.e. no influences from waves considered. Their method uses color coding within the user interface for the vessels crew, providing simplistic and transparent representation of the situation and it's severity-potential. The applied color coding is in line with the proposed method for assessing and communicating the safety status of vessels in maritime distress situations, namely Vessel TRIAGE (Nordström et al. 2016).

Earlier developments on the topic comprise of Ölcer and Majunder (2006), where a case-based reasoning decision support method based on pre-calculated damage cases was suggested. Each of these damage cases have corresponding counter-flooding advice for maximising the residual freeboard and stability. This approach lacks the possibility to use real loading conditions, sensors, and status of safety critical systems. The method is highly dependent on the pre-calculated cases, and their sampling density as identifying the closest case necessarily do not mean the actual case.

The innovation behind the proposal presented in this paper is the combined utilisation of flooding sensors and sensors reflecting the availability of safety-critical control systems post-accident. It is an extension of the idea of *Dynamic Barrier Management* but with focus on optimisation of the relationship between procedural and design barriers in the post damaged conditions. Furthermore, decisions will be based on probabilities, meaning that the initial conditions selected for detailed simulation should be the n^{th} most probable cases that could occur considering available evidence from various sensors. An initial outline of the methodology is illustrated in figure 3. It is our intention to use the time domain flooding simulation software PROTEUS3 (Jasionowski, 2001) for the development of the method. The software accounts for transient-, cross-, & progressive-flooding, the impact of multifree surfaces as well as watertight and semi-watertight doors including any damage scenario (collision, grounding, raking, etc.) for a damaged ship in waves. A typical flooding model from Proteus is shown in figure 4.

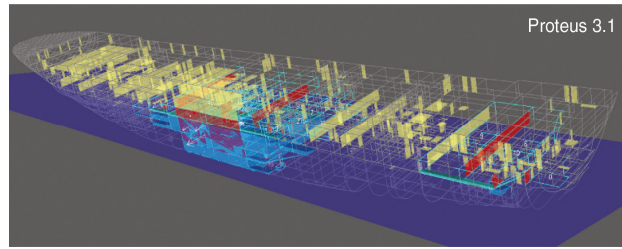


Figure 4: Typical Proteus model used for survivability analysis. (Papanikolaou et al., 2009).

4. INITIAL RESEARCH

The overall idea and concepts have been outlined in the previous sections, however at first, focus will be placed on developing the method of identifying the initial damage extent. One solution to this may be to utilize inference to get the n^{th} possible initial damage conditions based on the available sensor input used as evidence. This will cover the variability of the problem, but the remaining uncertainty in terms of sensor errors and other influences should be considered as well.

The next step is then to consider how to manage the simulations required. This can be done either by using real-time simulations onboard or by having detailed pre-calculated simulations stored in an onboard database. A major determining factor for deciding this will be the speed of the onboard simulations. If the simulation-time is too long, it will erode any safety benefits offered by the methodology. We need also to decide which active measures to assess initially. For a typical cruise vessel, the following main actions are available options for mitigating risk following a flooding incident and are deemed suitable for initial testing of the methodology:

Closing of external and internal openings such as doors, ventilation, damaged pipes, etc.

Counter-ballasting to alter the floating position of the vessel and centre of gravity.

Recovered buoyancy in the form of high expansion foam as suggested by Vassalos et al. (2016).

Any increase in time-to-capsize will result in a subsequent decrease in evacuation time as they share several common parameters such as heel, amount of floodwater obstruction and the availability of systems. There are, however, other pertinent parameters associated with evacuation time which will not be considered under the scope of this investigation.

Being able to find a detailed quantified measure of risk in terms of reduction in potential loss of life, or ΔN from figure 2, would require detailed information on evacuation time. For simplification purposes, it is possible to limit the scope of the research in the initial phases by assuming an overall constant mean evacuation time for quantification of the optimised time to capsize. Alternatively, the time to capsize is itself a measure of risk, so for further simplicity, it could be sufficient to consider optimisation in terms of this variable only.

Finally, an optimal application of the methodology would be to present real-time case-specific decision support. This could be in the form of a list of actions that could be taken by the crew based on the available systems, and rated on optimal added time to capsize. Optimisation techniques for identifying such decisions are currently being investigated, which is a continuation of the work outlined in Vassalos et al. (2015). In any case, developing a method in which uncertainty is reduced, and where an estimated time to capsize is presented to the crew in real-time, is of high value. This is the case even if the real-time decision support is not reached at the first instance. It is not only important to identify actions for increasing the available time, but also for making more efficient use of it in cases where time cannot be increased by any means. Knowing the time available before capsize would have an immense impact on the crew decisions on how to use the time available, and answer questions such as *if* and *when* to commence evacuation.

5. CONCLUSIONS

The concept of emergency response is not a new one and a number of measures are outlined in IMO's IMDG Code (2016), including also the requirement for having damage control plans and booklet for assistance in flooding situations as outlined in SOLAS (2009) Reg. II-1/19. Several class societies also provide emergency response expert services for ship-owners. It is well understood that time is one of the most critical variables in an emergency situation involving flooding. It is therefore important to identify new ways of optimising the time available before a vessel capsizes and we strongly believe there is room for improvement utilising new technologies.

Even if only the time to capsize can be estimated in real-time, it would be of great value in the decision-making process onboard. Our hope is to, in the future, to give decision support to the crew in terms of a case-specific list of actions rated by their added time to capsize. Further, the idea could be extended to other accident categories, and be part of a larger safety management system for the vessel. The method could also be possible to be used on autonomous vessels' for identifying the most optimised decisions for survival and safe return to port to avoid vessel loss. As there will be no crewmembers to initiate the damage response, this must be implemented by actuators which will also require a system enabling quantified decision making.

6. REFERENCES

- Papanikolaou et al., 2009, "Risk-Based Ship Design", Springer, Berlin.
- International Maritime Organization, 2009, "Ch. II-1 of SOLAS Consolidated Edition 2009", as adopted in IMO Res. MSC 216(82)), 2006.
- Astrup et al., 2015, "A framework Addressing Major Accident Risk in the Maritime Industry", Wmtc2015 – SNAME.
- Tsakalakis, 2009, "Performance-Based Damage Survivability of Passenger Ships and Design Implications", PhD Thesis, Glasgow, UK.
- Research project FLOODSTAND, 2009, "Integrated Flooding Control and Standard for Stability and Crises Management", Project number 218532.
- Ruponen, et al., 2015, "Prediction of Survivability for Decision Support in Ship Flooding Emergencies", STAB conference 2015, Glasgow, UK.
- Nordström et al. 2016, "Vessel TRIAGE: A method for assessing and communicating the safety status of vessels in maritime distress situations", Safety Science 85 (2016), p.117-129.
- Ölcer and Majunder, 2006, "A Case-Based Decision Support System for Flooding Crises Onboard Ships", Quality and Reliability Engineering International 22, p.59-78.
- Jasionowski, 2001, "An Integrated Approach to Damage Ship Survivability Assessment", PhD Thesis, Glasgow, UK.

Vassalos et al., 2016, "An alternative system for damage stability enhancement", Proceedings of the 15th International Ship Stability Workshop 2016, Stockholm, Sweden.

Vassalos, et. al., 2015, "Life-cycle risk (damage stability) management of passenger ships", STAB conference 2015, Glasgow, UK.

International Maritime Organization, 2016, "IMDG Code, Supplement: 'The EmS Guide – Emergency Response Procedures for Ships Carrying Dangerous Goods'"

International Maritime Organization, 2009, "Reg.II-1/19 of SOLAS Consolidated Edition 2009", supported by IMO MSC.1/Circ.1245.

Impact Assessment of Wave Statistics on Ship Survivability

Donald Paterson, *Maritime Safety Research Centre*, d.paterson@strath.ac.uk

Georgios Atzamos, *Maritime Safety Research Centre*, georgios.atzamos@strath.ac.uk

Dracos Vassalos, *Maritime Safety Research Centre*, d.vassalos@strath.ac.uk

Evangelos Boulougouris, *Maritime Safety Research Centre*, evangelos.boulougouris@strath.ac.uk

ABSTRACT

This paper presents a brief summary of the work conducted by the MSRC at Strathclyde University in which the effect of operational location on the estimation of a vessel's survival probability has been investigated and new s-factor formulations proposed. Further work is presented in which updated accident wave statistics have been used in order to assess the impact of vessel specific data on the predicted survivability. A test case on a large container ship has been conducted in order to gauge the effect of the new s-factor formula on the Attained Subdivision Index and thus the vessel safety level with regards to collision damage.

Keywords: *Survivability, Damage Stability, Probabilistic framework, s-factor.*

1. INTRODUCTION

Accurate estimation of survivability is of paramount importance when assessing ship damage stability performance. Survivability is influenced by a multifarious range of parameters all of which are situational dependant; however, at the highest level, survivability can be viewed as an outcome involving both the post-damage restoring properties of the vessel and the prevailing sea state.

The current IMO instrument for conducting damage stability assessment and thus estimating survivability is the probabilistic framework outlined in SOLAS 2009 [1]. At the heart of this approach is the so called s-factor which accounts for the probability of a vessel surviving a given damage scenario in waves. In this case, survivability in waves refers to a distribution of wave heights formed based on recorded accident sea states at the time of collisions. This assumption, therefore, fails to directly account for the influence of operational area on survivability and more alarmingly implies that a vessel's survivability is independent of its operational environment. Furthermore, as the accident data used in the creation of the distribution of wave heights behind the SOLAS s-factor comprised of accident data relating to all ship types, it fails to account for the influence of ship specific data.

This paper aims to shed some light on the influence such parameters have on survivability. A new distribution of wave heights is derived comprising specifically vessel accident data and a new s-factor formulation is proposed. The impact of operational location on survivability is also assessed by using trade region specific significant wave height distributions to create new s-factor formulations for four key ship trade regions. Finally, the influence of the newly proposed s-factor formulations on the Attained Subdivision Index is assessed through conducting a test case on a large container ship.

2. THE S-FACTOR

The "s-factor" is a core component of the probabilistic damage stability framework, known commonly as SOLAS 2009 [1], and is a measure of a damaged ships' survivability in waves.

With the assumption, as in SOLAS, that only H_s has bearing on the survivability and neglecting other environmental factors such as spectral shape, the probability of a ship surviving collision damage that has led to hull breach and flooding can be determined by application of total probability theorem as [2]:

$$s_i = \int_0^{\infty} dH_s \cdot f_{H_s|coll}(H_s) \cdot F_{surv}(H_s) \quad (1)$$

Where: $f_{H_s|coll}(H_s)$ is probability density distribution of sea states expected to be encountered

during collision and $F_{Surv}(H_S)$ is the survival probability when a vessel is subjected to a given damage case and exposed to a sea state characterised by significant wave height H_S .

The development of the s-factor was based largely on the findings of the EU research project HARDER [3] in which model tests were conducted with a limited exposure time of 30 minutes and thus the probability of survival, as it exists in SOLAS 2009, is in fact a conditional probability [4]:

$$F_{Surv}(H_S) \equiv F_{Surv}(t = 30min|H_S) \quad (2)$$

This leads to the following expression of the survival probability:

$$s_i(t = 30min) = \int_0^{\infty} dH_S \cdot f_{H_S|coll}(H_S) \cdot F_{Surv}(t = 30min|H_S) \quad (3)$$

One of the key underlying assumptions in SOLAS 2009 is that, for a given damage case, there exists a critical significant wave height H_{Scrit} such that a vessel damaged in a sea state relative to this parameter will always survive for lower H_S and always capsize for higher H_S . This theory has its roots in what is known as the capsize band [5] which represents the range of sea states in which the capsize probability transitions from unlikely to certain, often represented by a sigmoid curve as in Figure 1 [6].

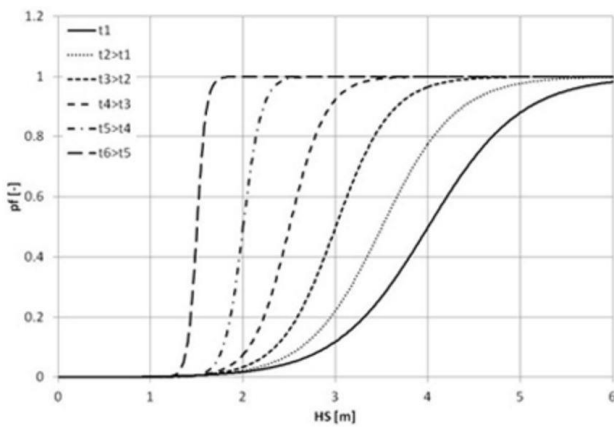


Figure 1: Example of capsize band represented by sigmoid curve and with varying observation time.

H_{Scrit} is defined as the sea state at which a ship in a given loading condition and a specified damage

case is exposed to the action of beam random waves for 30 minutes would have a 50% chance of survival [5]. Drawing on this, the survival probability for a specified loading condition and damage case when exposed to a given sea state for 30 minutes and could be approximated by a step function centred on the sea state H_{Scrit} [4].

$$F_{Surv}(H_S) = \begin{cases} 1 & \Leftrightarrow H_S \leq H_{Scrit} \\ 0 & \Leftrightarrow H_S > H_{Scrit} \end{cases} \quad (4)$$

This is essentially the limiting case of the capsize band concept and substituting 4 into 3 leads to:

$$s_i = \int_0^{H_{Scrit}} dH_S \cdot f_{H_S|coll}(H_S) = cd f_{H_S}(H_{Scrit,i}) \quad (5)$$

The distribution of wave heights utilised in the formation of the SOLAS s-factor, Figure 2, was produced during project HARDER following statistical analysis of sea states encountered during collision accidents and comprising 389 recorded incidents [2].

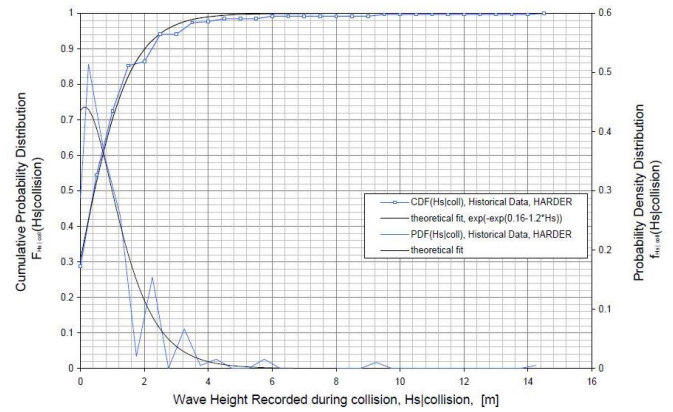


Figure 2: Accident wave statistics CDF

Following regression of the statistical distribution of sea states with respect to H_{Scrit} the s-factor could be expressed as:

$$s_i = \Pr\{H_S \leq H_{s,crit,i}\} = \exp^{-\exp(0.16-1.2H_{s,crit,i})} \quad (6)$$

Where $H_{s,crit,i}$ is given as:

$$H_{s,crit}|_{t=30min} = 4 \left(\frac{\min(GZmax, 0.12)}{TGZmax} \cdot \frac{\min(Range, 16)}{TRange} \right) \quad (7)$$

Based on the HARDER findings in which three dimensional regression was used to correlate the mean survival sea states experienced during model testing of specific damage scenarios (worst 2-compartment damage case) to GZmax and GZRange stability parameters and where TGZmax and TRange where defined as 0.12m and 16deg respectively, based on the best fit correlation [3].

The s-factor formula in its commonly known format and as expressed in SOLAS 2009 was also derived during project HARDER, where a combined formulation for predicting the survival probability was derived by using the individual model test survival sea states multiplied by the probability of sea state occurrence and then regressing a GZ-based formula to this data producing the following:

$$s = K \cdot \left(\frac{\min(GZmax, 0.12)}{0.12} \cdot \frac{\min(Range, 16)}{16} \right)^{0.25} \quad (8)$$

3. TRADE REGION SPECIFIC S-FACTOR

As was discussed in the previous section, within the probabilistic damage stability framework the s-factor is intended to represent the probability of surviving a given damage scenario in waves. It therefore combines:

- The restoring capabilities of the vessel and thus its ability to survive in waves.
- The assumed distribution of sea states.

Through using the “critical significant wave height” concept, which is a conditional parameter, survivability is measured based on both the post damage stability properties of the vessel in a given damage scenario, which define $H_{s,crit,i}$ for that scenario and the distribution of sea states, which allows the s-factor to be determined as the likelihood the survival sea state, $H_{s,crit,i}$, will not be exceeded at the time of collision (again for that specific scenario).

During project HARDER it was asserted that there exists a certain range of sea states in which

collision accidents occur and hence accident wave statistics were used in order to define the sea state distribution behind the SOLAS s-factor. However, such an assumption implies that a vessel’s survivability is independent of its area of operation, meaning that two identical vessels when subjected to the same damage scenario have the same probability of survival even if one is located in the North Atlantic ($0m \leq H_s \leq 9m$) and the other in the Mediterranean ($0m \leq H_s \leq 5m$). This cannot be the case.

In order to capture the influence of operational area on survivability it is proposed to use localised wave distributions as a basis for trade region specific s-factor formulations. As such, four key ship trade regions have been selected for assessment including the North Atlantic, Caribbean, Southeast Asia and the Mediterranean. For each location, average annual wave statistics [7] have been collated and the corresponding cumulative distribution of significant wave heights, $cdf_{H_s}(H_s)$ has been fitted to the data using the following function form:

$$cdf_{H_s}(H_s) = \exp(-\exp(\alpha - \beta \cdot H_s)) \quad (9)$$

Where α and β are regression coefficients based on trade region.

In addition, Global annual wave statistics have also been assessed for comparison purposes. The results of this process are summarised in table 1 and figure 3 below.

Table 1: Trade region specific regression coefficients

Trade Region	Regression Coefficients
Caribbean	Alpha=1.8880, beta=1.2035
Mediterranean	Alpha=1.1780, beta=1.1320
Southeast Asia	Alpha=1.2622, beta=1.2280
Global annual	Alpha=1.1717, beta=0.9042
North Atlantic	Alpha=1.9179, beta=0.7383

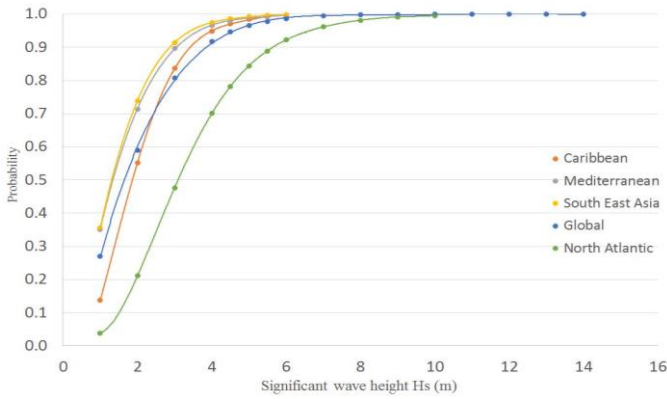


Figure 3: Accident wave statistics CDF

The survivability within each trade region can then calculated using the following formulation:

$$s_i = \Pr\{H_s \leq H_{s,crit,i}\} = \exp^{-\exp(\alpha-\beta H_{s,crit,i})} \quad (10)$$

Where α and β are the trade region-specific regression coefficients.

Estimating Critical Significant Wave Height

During project HARDER the regression formula for estimating $H_{s,crit}$ based on both GZmax and Range parameters was limited to $H_s=4m$ and for this reason it cannot be applied, in its current form, to the trade regions where the probable significant wave height exceeds this value, i.e. the North Atlantic where $H_s=9m$ has been recorded. Instead a formula in the same format as (7), has been produced for each trade region through three dimensional regression of the surface produced from the HARDER model test results which links Range and GZmax to the survival sea state, shown in Figure 4. In each case the regression has been limited to the H_s which constitutes the 99th percentile significant wave height within each trade region.

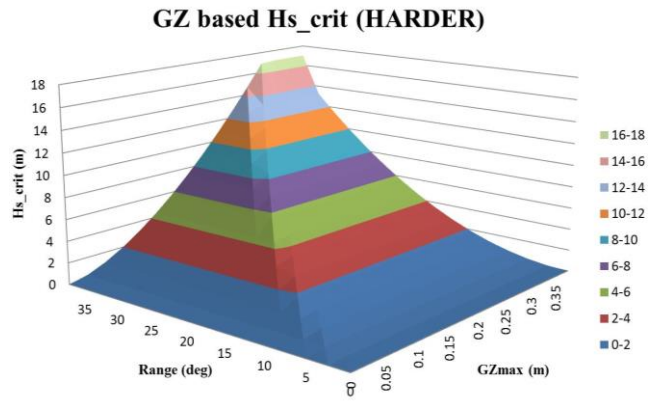


Figure 4: GZ-based $H_{s,crit}$

It should be noted that the prediction of the critical significant wave height, for a given damage case, is independent of trade region, however, regional specific $H_{s,crit,i}$ formulations have been derived in order to facilitate the creation of GZ-based trade region specific s-factor formulations. The results of this process are summarised below along with the regression accuracies:

Table 2: Summary of region specific $H_{s,crit}$ formulations

CAR	$H_{s,crit} = 6 * \left(\frac{\min(GZmax, TGZmax)}{0.19m} \cdot \frac{\min(Range, TRange)}{25deg} \right)$
MED	$H_{s,crit} = 5 * \left(\frac{\min(GZmax, TGZmax)}{0.16m} \cdot \frac{\min(Range, TRange)}{23deg} \right)$
SEA	$H_{s,crit} = 5 * \left(\frac{\min(GZmax, TGZmax)}{0.16m} \cdot \frac{\min(Range, TRange)}{23deg} \right)$
GLO	$H_{s,crit} = 6 * \left(\frac{\min(GZmax, TGZmax)}{0.19m} \cdot \frac{\min(Range, TRange)}{25deg} \right)$
NA	$H_{s,crit} = 9 * \left(\frac{\min(GZmax, TGZmax)}{0.21m} \cdot \frac{\min(Range, TRange)}{38deg} \right)$

Table 3: Summary of regression accuracy

Highest overestimate	Lowest Underestimate	Mean error	Sum of Squares
0.85	-1.03	0.1289	7.092
1.06	-1.18	0.10398	13.337
1.18	-0.955	-0.146	11.849
1.18	-0.955	-0.146	11.849
1.06	-1.18	0.10398	13.337
1.23	-1.553	0.0762	21.442

GZ-based combined s-factor formula

Combined s-factor formulations for each trade region in a similar format to that proposed in HARDER have also been derived. Assuming that the true survivability can be estimated using (10), a surface relating survivability to both GZmax and Range has been produced on a finely discretized grid of combinations ($GZ_{max}, Range$) as shown in Figure 5.

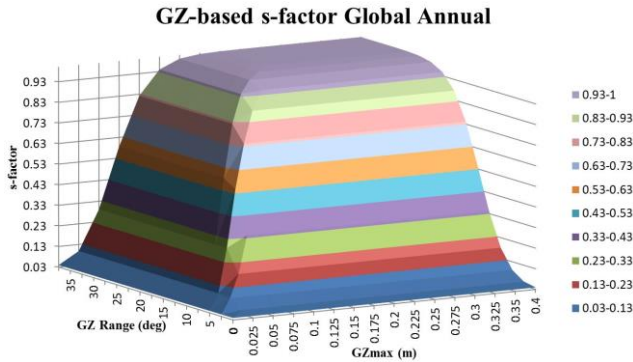


Figure 5: GZ-based s-factor

GZ-based s-factor formulations have then been created for each trade region through performing three dimensional regressions to the region specific surfaces linking survivability to stability parameters in the following format:

$$s = \left(\frac{H_{s,crit}}{H_{s,lim}} \right)^x = \left(\frac{\min(GZ_{max}, TGZ_{max})}{TGZ_{max}} \cdot \frac{\min(Range, TRange)}{TRange} \right)^x \quad (11)$$

Where $H_{s,lim}$ is the region specific 99th percentile H_s , TGZ_{max} and $TRange$ are the region-specific limiting stability parameters and x is an exponent based on the best fit correlation. The results of this process are provided below along with the regression accuracies:

Table 4: Region specific s-factor formulations

CAR	$s = \left(\frac{\min(GZ_{max}, TGZ_{max})}{0.19m} \cdot \frac{\min(Range, TRange)}{25deg} \right)^{0.7}$
MED	$s = \left(\frac{\min(GZ_{max}, TGZ_{max})}{0.16m} \cdot \frac{\min(Range, TRange)}{23deg} \right)^{0.6}$
SEA	$s = \left(\frac{\min(GZ_{max}, TGZ_{max})}{0.16m} \cdot \frac{\min(Range, TRange)}{23deg} \right)^{0.6}$
GLO	$s = \left(\frac{\min(GZ_{max}, TGZ_{max})}{0.19m} \cdot \frac{\min(Range, TRange)}{25deg} \right)^{0.6}$
NA	$s = \left(\frac{\min(GZ_{max}, TGZ_{max})}{0.21} \cdot \frac{\min(Range, TRange)}{38deg} \right)^{0.9}$

Table 5: Regression Accuracy

Highest overestimate	Lowest Underestimate	Mean error	Sum of Squares
0.164	-0.225	0.023	0.9
0.09	-0.167	-0.018	0.478
0.099	-0.194	-0.024	0.616
0.097	-0.15	-0.009	0.543
0.103	-0.25	-0.019	0.55

4. DERIVATION OF SHIP SPECIFIC ACCIDENT DATA BASES

The current SOLAS 2009 s-factor formulation utilises wave statistics based on the average significant wave height encountered during recorded accidents for all vessels and as such fails to distinguish between ship type. As an alternative, a new method is proposed in which ship specific accident data is utilised. In the following an example of this process is provided in which a new accident database is derived comprising of passenger vessel data only and using weather data in order to fill information gaps.

A total of 129 accidents have been collated into a comprehensive list comprising exact accident location, time, description of the accident, name of the vessel and their IMO number. As shown in Figure 6, two passenger ship types have been considered that have been involved in a total number of 50 groundings and 79 collisions. Most of the accidents took place at open sea with only 18% close to estuaries or coastal waters. The accidents have occurred in a period spanning from 2005 to 2016.

129 Accidents			
50 Groundings		79 Collisions	
16 Cruise ships	34 RoPax	24 Cruise ships	55 RoPax

Figure 6: Database summary

The information was, however, incomplete and as such the environmental conditions at the time of the accidents were inadequate. In order to fill this information gap, accident time and date information was used to identify the significant wave height and average periods experienced during each recorded accident. For this purpose, a number of wave databases [8] were utilised and the significant wave height at the exact time of the accident was obtained. The online data comprises wave height measurements for all days at increments of three hours taken over a 10-year period for each of the locations the accidents occurred. Knowing the date, time and location of each accident, the significant wave height could be found in each case. In cases where the time of the accident did not coincide with the time of a wave height reading, the value was estimated as the average between the two closest time points.

Using the same approach as in the previous section, a curve has been fitted to the data of the functional form as outlined in (9) producing the formula as shown in (12) and the CDF as presented in Figure 7.

$$CDF(H_s) = e^{-e^{(0.6887-1.1958 \times H_s)}} \quad (12)$$

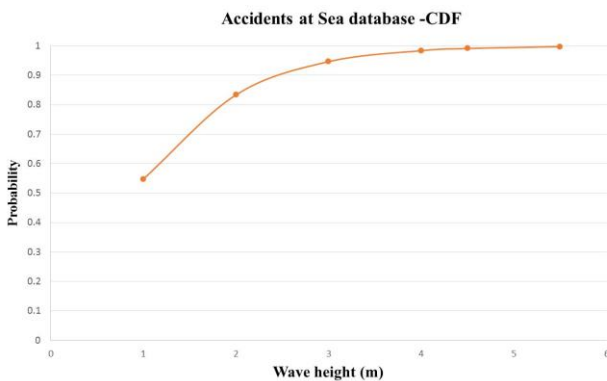


Figure 7: Accident Based Distribution of Wave Heights

Based on the wave height CDF the survivability according to the updated accident database can be expressed as:

$$s_i = \Pr\{H_s \leq H_{s,crit,i}\} = e^{-e^{(0.6887-1.1958H_s)}} \quad (13)$$

As previously, a formula for predicting the critical significant wave height can be derived through regression, this time limited to $H_s=4.5m$, that being the significant wave height which constitutes the 99th percentile within the distribution. The resultant expression for $H_{s,crit,i}$ is as follows:

$$H_{s,crit} = 4.5 * \left(\frac{\min(GZmax, TGZmax)}{0.16m} \cdot \frac{\min(Range, TRange)}{20deg} \right) \quad (14)$$

With the following regression accuracy:

Sum of squares:	7.092
Mean error	0.1289 m
Highest over estimate	0.85 m
Lowest underestimate	1.03 m

A combined formulation for predicting the survival probability can then be found through regression conducted according to the previously outlined methodology, producing the following s-factor formula:

$$s = \left(\frac{\min(GZmax, TGZmax)}{0.16m} \cdot \frac{\min(Range, TRange)}{20deg} \right)^{0.4} \quad (15)$$

5. IMPACT ON ATTAINED INDEX

The extent of the ultimate impact on the safety level has yet to be determined. To this end, a large container ship has been subjected to a probabilistic damage stability assessment, the results of which have been used in combination with the aforementioned survivability formulae to determine the Attained Index in each case. This provides the conditional probability of the ship surviving collision damage and as such is a measure of the ship's safety level in this respect.

The results of the assessment are summarised in figure 8 below:

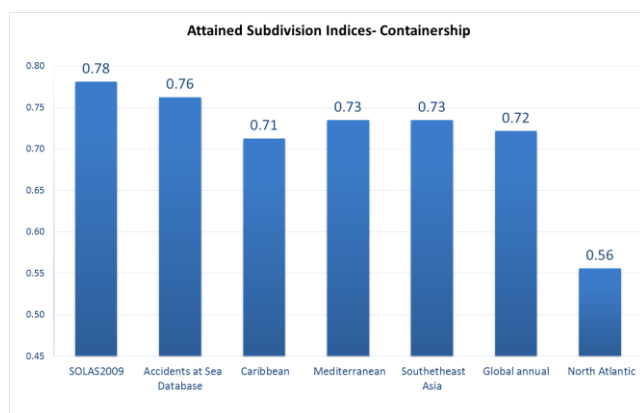


Figure 8: Trade Region Specific Attained Index Comparison

A decrease is marked in the Attained Index of each case when compared to SOLAS 2009. In the case in which North Atlantic wave statistics were used, the Attained Index decreased significantly by 28%. This highlights the stringency and impact of very high waves on vessels. Similarly, the use of Caribbean wave statistics yielded a reduction of 9%, whilst, the Accidents at Sea Database statistics almost a 2% decline. The Attained index obtained for the Accidents at Sea Database is 6% higher than the global annual statistics, which implies that the significant wave heights experienced during accidents are in fact less severe than the global statistical average.

In summary the results show that the wave statistics utilised in the determination of the survival probability hold a large influence over the magnitude of the final Attained indices. More significantly, A-Indices linked to specific operational areas could be derived to reflect survivability of the vessel linked to the operating environment.

6. CONCLUSIONS

In light of the findings of the work reported in this paper, the following conclusions can be drawn:

- It is possible to generate trade region specific s-factor formulations using local wave statistics.
- The current SOLAS s-factor through failing to account for area of operation appears to overestimate survivability.
- Weather data records can be used in order to fill information gaps for incidents in which the sea state at the time of accident was previously unknown.
- Using an updated ship specific accident database, the distribution of wave heights used in the formation of the SOLAS s-factor has been shown not to provide ample coverage of all wave heights experienced.
- As a result of the above, SOLAS overestimates the survivability in comparison to the updated database.

7. REFERENCES

- [1] IMO, "RESOLUTION MSC.216(82)," IMO, 2006.
- [2] A. Jasionowski, "Study of the specific damage stability parameters of Ro-Ro passenger vessels according to SOLAS 2009 including water on deck calculation," EMSA, 2009.
- [3] C. Tuzcu, "A Performance-Based Assessment of the survival of Damaged Ships: Final Outcome of the EU Research Project HARDER," *Marine Technology*, vol. 40, nr 4, pp. 288-295, 2003.
- [4] J. Cichowicz, "Damage Survivability of Passenger Ships - Re-Engineering the Safety Factor," *MDPI*, 2016.
- [5] N. Tsakalakis, "The Capsize Band Concept Revisited," i *the 11th International Ship Stability Workshop*, Wageningen, 2010.
- [6] D. Vassalos, "Damage Survivability of Cruise Ships- Evidence and Conjecture," i *International Conference on the Stability of Ships and Ocean Vehicles*, Glasgow, 2015.
- [7] N. Dacunha, *Global Wave Statistics*, London: British Maritime Technology Ltd., 1986.
- [8] BMT, "Waveclimate," 2016. [Online]. Available: <http://www.waveclimate.com/>. [Använd September 2016].

This page is intentionally left blank

Implications of different alternatives for damage stability analysis in decision support

Petri Pennanen, *Napa Ltd.*, petri.pennanen@napa.fi

Teemu Manderbacka *Napa Ltd.*, teemu.manderbacka@napa.fi

Pekka Ruponen *Napa Ltd.*, pekka.ruponen@napa.fi

ABSTRACT

A decision support system for passenger ships in flooding casualty has been recognized as an important tool on modern cruise ships. There are several applications already at the market and in the use, some of which have been developed during the years without a direct link to any compelling requirement set forth in the international rule framework. After the Costa Concordia accident, the rule requirements have been developed at the IMO. These requirements form the minimum solution for a decision support system, based on the extension of the existing loading or stability computer system. However, there are systems that have been developed purely from the end users' needs, and which have functionality exceeding the rule-based minimum requirements. This paper presents different alternatives for a decision support system for flooding emergencies. Technical background, accuracy, usability and usefulness of the two approaches are compared with, taking into account the important statutory approval point of view.

Keywords: *Damage stability, Decision support system, loading computer, passenger ship.*

1. INTRODUCTION

Ship flooding accident requires rapid and correct decisions onboard the ship. The situation may evolve fast, leaving the crew with a tight time-frame for organizing appropriate actions. A decision support system is thus an essential tool in a distressed accident situation. Jasionowski (2011) proposes a monitoring tool informing the crew about the current status of the ship, in this way improving the awareness of the crew and thus helping the decision making in case of a flooding accident. Varela et al. (2014) emphasize the need to provide the crew with prediction of the progression of flooding and present an initial on-board decision support system. A more elaborate system providing means of communicating the status of the situation is presented by Nordström et al. (2016).

The IMO has taken the decision that all passenger ships of certain size, built after 2014, need to be equipped with a stability computer capable of providing the master with operational information after a flooding casualty and/or shore based support proving the same. The requirement is included in the SOLAS text and more detailed guidelines are given as MSC Circulars 1400 and 1532 (IMO 2011, 2016).

In the recent SDC subcommittee working group, the relation of the guidelines was made clear, meaning that the Circular 1400 only affects ships built between 01 Jan 2014 and 13 May 2016, whereas the revised circular 1532 affects ships built after 13 May 2016. In its report to the parent committee MSC, the subcommittee also proposes this requirement to be applied on all existing passenger ship, built before 2014. For this purpose, a new guideline will be developed, taking into account the characteristics of older tonnage.

Passenger ships built before 2014 represent a vast amount of different ships, including pure passenger ships and ropax vessels, covered by many editions of SOLAS conventions in use at the time of their construction. Many of the ships have been designed to meet the deterministic damage stability requirements and majority of the ships do not have flooding sensors, which are mandatory on ships built after 2010.

Modern passenger ships built after 2016 all have flooding sensors in place. If an adequate number of well-placed flood level sensors are installed, it makes the calculation of time-domain flooding prediction possible, provided that some other conditions are met, as discussed in Takkinen et al.

(2017). These ships are also well documented in way of compartmentation details and usually have automation systems ready to provide all needed data for the damage stability computer directly through interfaces. On the contrary, the installation of the flood level sensors to older ships is complicated or nearly impossible in practice.

Taking into consideration these fundamental differences in equipment, it seems obvious that it is possible to develop more enhanced decision support for modern ships than for older ships. All systems, however, need to fulfill the rule requirements, as well as the end users' expectations.

2. ALTERNATIVES FOR DAMAGE STABILITY ANALYSIS

Conventionally, the damage stability information onboard is provided by calculating the final equilibrium of the damaged ship in the current loading condition. Loading computer software relying on static damage stability method is used for this purpose. International Association of Classification Societies defines three different types of stability software in the Unified Regulations regarding Onboard Computers for Stability Calculations (IACS, 2006) depending on the vessel's stability requirements. Type 1 is only for intact stability and Types 2 and 3 cover also the damage stability. More recent developments of the onboard software include time-domain damage stability prediction (Varela et al. 2014 and Ruponen et al. 2015 & 2016). Such solutions are installed on the newer passenger ships for better operational information of damage stability and to provide time perspective of the evolution of the stability for enhanced decision support.

Static damage stability

The method applied on some of the existing loading computer systems, widely installed on cruise ships, is to give the user possibility to manually define rooms and compartments damaged (open to sea). The system utilizes a 3-D model of the ship and calculates the final equilibrium position, usually with a few intermediate stages.

The calculation is based on the current loading condition, prepared using the loading computer. This

system differs from the direct damage analysis (IACS Type 3 loading computer), since the Type 3 calculates all rule-based, deterministic damage cases (for example SOLAS 1974/90) using the current loading condition. Type 3 is suitable for checking the design rule compliance before sailing but the same is achieved using the GM limiting curves (IACS Type 2 loading computer). In real life, the damages occurring naturally are deterministic but the extent of the damage may differ from those defined in the rules (for example two-compartment damages).

This fact also rules out the systems based on pre-calculated damage scenarios since the number of loading/damage condition permutations is infinite. It is important that the calculations always are based on the real, current loading condition, as stipulated in the rules.

It is understood that the IACS is preparing a definition for Type 4 loading computer, which would be able to calculate the results of any damage extent for a given loading condition and reflect the requirements presented in Circular 1532. The information of the damage definition would be based on sensor information about detected flooding extent and/or manual breach definition by the user. The definition of the Type 4 is, however, not yet available.

The result of damage stability calculations is traditionally presented as the GZ curve, possibly with deterministic criteria comparison (MET/NOT MET), as shown in Figure 1.

Based on the GZ curve and some knowledge of the specific ship in question, an experienced captain (on board) or naval architect (shore based support) can estimate the severity of the flooding case. This information still needs to be combined with the information of the prevailing weather and geographic conditions, when evaluating the need of evacuation compared to Safe Return to Port (SRtP). Furthermore, it is impossible to define the time frame until the equilibrium will be reached. It may also be difficult to judge how the situation will evolve, for example due to progressive flooding.

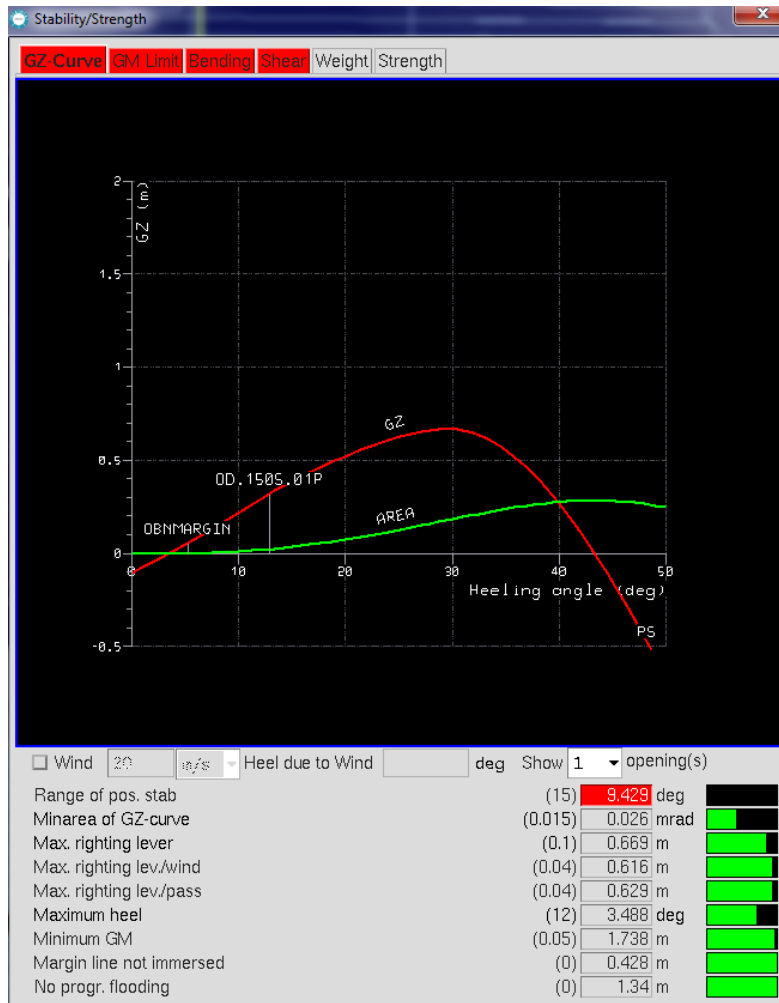


Figure 1: Example of typical damage stability output from a Type 4 Loading Computer

Time-domain damage stability prediction

An advanced approach to decision support is to use time-domain flooding simulation, combined with the measurement data from the automation system. The concept is introduced in Pennanen et al. (2015), and details of the applied calculation methods are presented in Ruponen et al. (2015, 2017). The Vessel TRIAGE system (Nordström et al. 2016) is used to present the severity of the situation, based on the latest measurement data and prediction of progressive flooding.

The time-domain prediction for progressive flooding and quasi-stationary ship motions is constantly updated, using the latest measurement data from the automation system. For practical reasons, each prediction is done for three hours, based on the Safe Return to Port requirements. Instead of informing the user on the stability at the intermediate stages of the flooding, the system communicates the severity of the situation to the user

and provides the predicted evolution of the situation, and the important time perspective of the consequences.

3. CASE STUDY

A potential, realistic damage case of a 125 000 Gross Tonnage passenger ship is presented here in order to demonstrate some of the differences of the alternative approaches of damage stability analysis of the decision support systems. It should be bore in mind that in some damage cases the differences might not be so pronounced, and that it is difficult, if not impossible, to make a fully comprehensive study of all the potential cases.

Damage scenario

In the presented case the breach is a long and narrow raking damage near the waterline, which could be caused by ice for instance, or in collision with another ship or even side grounding. The breach extends over seven WT compartments, including



Figure 2: Small breach extending to several compartments

both main engine rooms, Figure 2. In this damage case the ship will be eventually lost, but the flooding takes several hours.

Reference results for the progression of flooding and the evolution of the stability are calculated in calm water with time accurate simulation. The ship is equipped with flooding sensors, which are taken as fully operational in this case, thus providing the onboard system with the information on the current status of the flooding. The floodwater does not immediately reach the sensors in all damaged compartments. In this case, about 10 min after damage, the flood level sensors indicate that the total of 7 compartments are flooded.

Flooding prediction results

Examples of the results from time-domain flooding prediction are presented in Figure 3. About 10 min after damage, the level sensors have detected all breached WT compartments, and the second prediction provides information that the ship will remain stable afloat for 3 hours. About 3 h after the damage the updated predictions start to indicate that eventually the heeling will start to increase. Finally, the prediction started 5 h after damage provides a reasonable estimate that the ship will capsize.

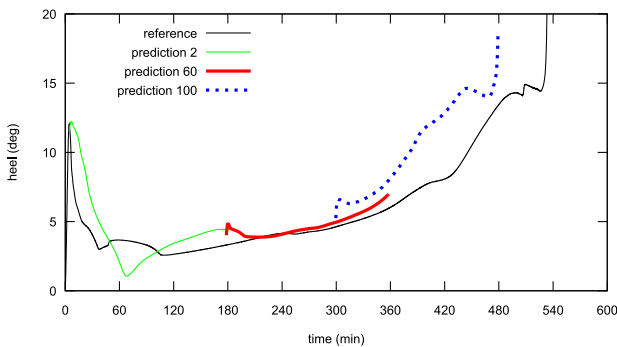


Figure 3: Time-domain flooding prediction results for the small but extensive breach

Loading computer results

The loading computer indicates the detected flooding, and the user can breach also additional compartments manually. The final equilibrium condition is calculated by considering the damaged compartments as lost buoyancy. In addition, typically 5 intermediate stages of flooding are calculated. In the studied damage scenario the ship capsizes during the intermediate flooding, and the last stable floating position for the 3rd stage is shown in Figure 4. The loading computer can only calculate the final condition and a number of intermediate stages, but the time-scale cannot be evaluated.



Figure 4: Example of damage stability results from a loading computer

Analysis of results

Both the loading computer and the time-domain flooding prediction indicate that the situation is extremely serious, and eventually the ship will sink or capsize. An experienced captain could tell this result also based on the fact that the flooding is detected in seven WT compartments.

The major benefit of the time-domain flooding prediction is the estimate of the time-to-sink. In this damage scenario there is plenty of time for orderly evacuation and abandonment. Also assistance from the nearby ships can be waited for. In addition, the flooding is very slow and active counteractions, such as pumping could be used to further increase the available time.

4. DISCUSSION

In the presented damage case the flooding and capsize of the ship took nearly 9 hours, leaving the crew with sufficient time for orderly evacuation. However, the results obtained from the static loading computer give an impression of a more severe case. The lack of information on the available time may lead to rushed evacuation actions, jeopardizing unnecessarily the safety of the people on board. In some other case the situation may evolve more rapidly, and fast decisions and actions are required. Also in such a case, the immediate results from the time-domain simulation are valuable.

IMO Circ. 1532 states that the “shore based support should be operational within one hour”. In practice the gathering of the information of the situation may take a substantial amount of time. After this, with a full awareness of the situation, the shore based support will be able to provide results on the evolution of the situation and possible recommended actions. For serious damage cases this may be too long a time for efficient decision making for orderly evacuation and abandonment. Taking all this into account, an onboard decision support system with automatically launched time-domain prediction of progressive flooding would appear useful in addition to the loading computer and shore based support.

Statutory approval

The approval of the onboard stability computer is in practice conducted by the classification societies, which need to implement the Type 4 (or Circular 1532) requirements in their rules. This will most likely restrict the scope of approval of the damage stability analysis to those provided by the loading computer.

At least one classification society has defined a more advanced system to be installed onboard, consisting of flood level sensors and a loading computer with appropriate damage stability functionality. This definition exceeds the Circular 1532 requirements, and there is an approval procedure in place. In the future, it should be discussed, if also time-domain prediction based systems could be checked and approved by the classes – at least at the algorithm level – in order to increase credibility and trust.

5. CONCLUSIONS

Taking into consideration the pace of involvement of the damage cases, like the Costa Concordia case, it is utmost important that there is a system onboard the ship, capable of giving immediate alert as well as rapid view of the severity and progress of the scenario.

A loading computer based system will provide an estimation of the situation at end of the flooding. The evaluation of the severity may require expert level interpretation of the results, but it can be done. This kind of system is also suitable for training and drills, as it provides the user with understanding of the extent and type of damages the ship eventually can or cannot survive.

Taking one step further in the user friendliness and usefulness of the system, is provision of time-domain prediction of the flooding scenario. Getting a view to the time scale of the damage scenario helps in the decision making. The severity of the case can also be based on the involvement of the events, and thus be dynamic and easily communicable. In order to keep the loading computer functional for its primary purpose for planning and checking the loading condition for rule compliance, the time-domain prediction should run as a separate, dedicated system. This separate system can be complemented with other safety-related functions, like vulnerability monitoring, without causing problems in the class approval of the loading computer.

Although shore based support seldom can respond rapidly in the early stages of flooding, it can provide valuable support for the master in course of a slowly progressing flooding case. Shore based support can concentrate on analyzing the case and calculate alternative scenarios to cope with it. According to the rules, shore based support is anyway required for the provision of post-damage residual strength information.

In order to increase maritime safety, all passenger ships should be equipped with a loading computer capable of performing damage stability analysis onboard. In addition to this, shore based support should be provided for increased safety and redundancy. Consequently, new ships equipped with properly located, good quality flood water level sensors will benefit of complementing the loading

computer with a time-domain prediction based decision support system installed onboard.

REFERENCES

- IACS 2006, "Requirements Concerning LOAD LINE"
International Association of Classification Societies, latest revisions of UR L: Subdivision, Stability and Load Line
<http://www.iacs.org.uk/publications/publications.aspx?pageid=4§ionid=3> accessed April 13, 2017.
- IMO 2011, "MSC.1/Circ.1400 - Guidelines on Operational Information for Masters of Passenger Ships for Safe Return to Port by Own Power or Under Tow", May 27, 2011.
- IMO 2016, "MSC.1/Circ.1532 - Revised Guidelines on Operational Information for Masters of Passenger Ships for Safe Return to Port", June 6, 2016.
- Jasionowski, A. 2011. "Decision Support for Ship Flooding Crisis Management", *Ocean Engineering*, Vol. 38, pp. 1568-1581.
- Nordström, J., Goerlandt, F., Sarsama, J., Leppänen, P., Nissilä, M., Ruponen, P., Lübcke, T., Sonninen, S. 2016. "Vessel TRIAGE: a method for assessing and communicating the safety status of vessels in maritime distress situations", *Safety Science*, 85:117-129.
- Pennanen, P., Ruponen, P., Ramm-Schmidt, H. 2015, "Integrated Decision Support System for Increased Passenger Ship Safety", *Damaged Ship III, Royal Institution of Naval Architects*, 25-26 March 2015, London, UK.
- Ruponen, P., Lindroth, D., Pennanen, P., 2015, "Prediction of Survivability for Decision Support in Ship flooding Emergency", *Proceedings of the 12th International Conference on the Stability of Ships and Ocean Vehicles STAB2015*, 14-19 June 2015, Glasgow, UK, pp. 987-997.
- Ruponen, P., Pulkkinen, A., Laaksonen, J. 2017, "A method for breach assessment onboard a damaged passenger ship", *Applied Ocean Research*, Vol. 64, pp. 236-248.
- Takkinen, E., Ruponen, P., Pennanen, P., 2017, "Required flooding sensor arrangement for reliable automatic damage detection", *RINA Smart Ship Technology*, 24-25 January 2017, London, UK.
- Varela, J.M., Rodrigues, J.M., Guedes Soares, C. 2014. "On-board Decision Support System for Ship Flooding Emergency Response", *Procedia Computer Science*, Vol. 29, pp. 1688-1700.

Session 4
Stability of naval vessels

Session Chairs
Jean-François Leguen
Timothy C. Smith

An integration of present navy ships intact stability criteria in the perspective of ship performance assessment in a seaway

Nicola Petacco, *University of Genoa*, nicola.petacco@edu.unige.it

Paola Gualeni, *University of Genoa*, paola.gualeni@unige.it

Jean-Yves Billard, *French Naval Academy Research Institute*, jean-yves.billard@ecole-navale.fr

François Grinnaert, *French Naval Academy Research Institute*, francois.grinnaert@ecole-navale.fr

ABSTRACT

In the paper a possible integration of the present intact stability criteria for navy ships is proposed with the aim to include ship stability performance assessment in a seaway. In this view, IMO Second Generation Intact Stability Criteria (SGISC) are considered, as an interesting source of inspiration. In the background, the innovative approach formulated within the Naval Ship Code is described, as a possible framework where the above mentioned integration can take place. In order to get practical feasibility test, applications are carried out on three navy ship typologies, characterized by different sizes and operational profiles in order to compare the level of severity of the present intact stability navy criteria with the one implied by the first vulnerability level criteria of the SGISC. As a further step, then the second vulnerability level criterion for the dead ship stability failure mode is applied to the same set of ships. The criterion in fact can be a possible supplement of investigation, beside the usual beam winds combined with rolling criterion, in order to better frame ship behavior in a seaway.

Keywords: *Intact Stability, Naval Ships, Wind and Waves.*

1. INTRODUCTION

The importance to assess stability performance of naval ships in extreme seas is well known, together with the implied challenges: for example the large amplitude motions reliable prediction and the identification of suitable performance-based criteria (Reed, 2009). Naval ships in principle share with merchant ships the same general issues relevant to stability failures but the safety rules framework to comply with is different, since Navies are not under IMO regulations. Another important difference is that naval vessel, due to their operational profile, often cannot avoid dangerous weather conditions when fulfilling their missions, while a commercial vessel often can choose an alternative route.

The attention to ship stability in waves is in parallel with an increasing interest in the development of risk based stability criteria. The trend is to frame the discussion about ship performance within a risk assessment procedure, dealing with the risk of capsizing (Peters, 2010; Tellet 2011).

At the beginning of the 21st century, NATO initiated an effort to develop the Naval Ship Code

i.e. a goal-based standard for naval vessels that could guide navies and classification societies in the development of rules for naval vessels. The intent was to develop regulations for naval vessels that paralleled the IMO regulations for commercial vessels. A brief overview about the Naval Ship Code is going to be developed in the following.

The present Navy stability standard, from one side are recognized as a valuable reference in order to design appropriately safe ships. On the other side it is doubtful that they are able to truly capture the dynamic behavior of ships in extreme conditions. (Perrault et al. 2010).

It is recognized that the hydrostatics-based standards have attempted to incorporate some consideration of dynamic issues through the so called “beam winds combined with rolling criterion” i.e. the effect of beam wind and seas on ship behavior that in the IMO context is named weather criterion.

Nevertheless, it is recognized as well that the a possible way to overcome the limitations of the present standard seems to be the calculation of the probability of capsize as directly related to the probability of exceeding a critical roll angle, due to the environmental conditions. The methodology

employed in determining the probability of exceeding a critical roll angle is described most of the times using time domain simulations combined with probabilistic input data for the wave conditions and heading and speed (Beaupuy et al. 2012).

In parallel with what above, the vulnerability criteria developed by IMO, in particular the second level vulnerability criteria, have been already indicated as reasonable tool, for example in an early design stage (Alman, 2010), in order to assess the ship behavior in waves.

Within the multilayered framework of the SGISC, the third and upper level of assessment is in line with the probability of capsizing prediction coupled with a suitable ship motion computational tool, which in principle, should be able to capture all the non-linear phenomena necessary for capsizing prediction. In the SGISC terminology this is named Direct Assessment (DA). With this in mind, the assessment tools developed as second level vulnerability criteria have been developed in order to be a good compromise between accuracy of results and computational engagement.

In this paper, in relation with the dead ship condition stability failure, the second vulnerability criteria is applied to a naval ship in order to investigate the applicability to this ship category and to compare results with the present intact stability standards for naval ships. In particular, the second vulnerability level performs a more extensive assessment, because of the wider scenario of environmental condition to be considered and the modelling of roll motion of the vessel by means of a one-degree of freedom (1-DOF).

Moreover, a wider comparison is made between such standards and the SGISC, in terms of all the first level vulnerability criteria for the whole set of stability failure modes addressed by IMO. Three different naval ship typologies have been considered i.e. and helicopter carrier, a destroyer and a patrol vessel.

2. PRESENT NAVY SHIPS INTACT CRITERIA

For the purpose of this paper, as brief overview of selected navy intact stability criteria has been carried out.

United States Navy (NAVSEA, 2016), United Kingdom MOD (2000), France MOD (1999) and Italy MOD (1980) rule texts have been considered and a very similar structure in terms of criteria and standard values have been identified as expected. In fact, at a different extent, all of them are related with approach and criteria developed by Sarching and Goldberg (1962).

Looking for a general outline among them, indeed it is possible to spot the attention paid to the righting arm standing alone and moreover under the effect of different inclining moments i.e. turning at speed, the crowding of people on one side and the lifting of heavy load on one side. The influence of ice is also to be taken into consideration. What above with reference to specified loading conditions

As far as sea-state effects, the assessment beam winds influence together with rolling (fixed angle of 25 degrees for all the investigated rule texts) is requested.

The wind speed is actually a differentiated value, varying from 40 kn to 100 kn, in relation with the Administration and the naval ship typology.

The action of environmental conditions is very relevant from the safety point of view and in order to possibly improve or better validate the criteria, some investigations about the wind modeling in the beam winds combined with ship rolling has been carried out, with the support also of experimental tests (Luquet et al. 2015, Ariffin et al. 2016).

As a general remark, as it is well known, the set of rules to be applied for naval ships is unquestionably more severe if compared with the IMO Intact Stability Code (IMO, 2008) and this is coherent with the more severe operational profile warships have to fulfill with. For the same reason usually a thorough investigation of the seakeeping performances are carried out for this ship category, both on short term and/or long term perspective, with attention to specific issues like for example accelerations, slamming events or to more comprehensive parameters like operational indexes.

As already mentioned, the stability assessment in a seaway at the more exhaustive extent in principle is a seakeeping problem, with the need to capture all the necessary dynamic phenomena up to capsizing, often characterized by challenging non-

linearities. This process, beside to be expensive and time consuming, requires the appropriate numerical tool for the ship dynamic behavior prediction.

In line with a more thorough assessment of ship performance in waves, but as an intermediate phase between the present intact stability criteria and a challenging seakeeping prediction at large angles, the application of SGISC are assumed to be interesting also for navy ships.

3. THE SECOND GENERATION IS CRITERIA

The Maritime Safety Committee (MSC of the International Maritime Organization (IMO) approved and issued the Intact stability code in 2008 (IS Code) (IMO, 2008). Within IS Code is pointed out that new approaches to assess ship stability are required, with specific reference to the ship behavior in a seaway.

Therefore, a working group was established by IMO to select and to develop the so called second generation intact stability criteria. The working group has identified different stability failure modes related to the following phenomena:

- Variation of righting arm in waves;
- Dead ship condition;
- Maneuvering-related failures.

For a more accurate description on the physics of the phenomena see (Belenky et al, 2008) and (Belenky et al, 2011).

The ship compliance is assessed by a multi-tiered approach structured in three levels, with increasing accuracy of formulation: in case the ship is not able to comply with the 1st level criterion (L1), she has to be assessed according to 2nd level criteria (L2). As already mentioned, a direct assessment (DA), for instance by means of a suitable numerical tool, should be carried out in case some vulnerability is evidenced also at the 2nd level criterion.. An Operational Guidance (OG) is to be adopted and approved by the Flag Administration, if the issue cannot be settled in the design phase. Along the years, an intense research and development activity for each mode of failure has been carried out by the IMO Working Group and by the international scientific community. An important and significant part of the literature to this regard is collected in the proceedings of the

International Conference on Stability of Ship Ocean Vehicles (STAB) and the International Ship Stability Workshop (ISSW) of the latest years.

In 2015, at the 2nd meeting of the SDC (it is the IMO Ship Design and Construction Subcommittee), the rule texts of criteria for Parametric Roll (PR), Pure Loss of Stability (PLS) and Surf-Riding/Broaching (SR) have been finalized (IMO, 2015). While the complete criteria of Dead Ship condition (DS) and Excessive Acceleration (EA) failures have been delivered at the end of the 3rd SDC session (IMO, 2016).

Dead Ship condition criteria – 2nd Level

This criterion analyses the ship vulnerability in the dead ship scenario. To do that, a long-term and a short-term probability indexes are evaluated. A ship is considered vulnerable to the dead ship condition failure mode when:

$$C < R_{DS0} \quad (1)$$

where R_{DS0} is the risk threshold, to be chosen among 0.04 and 0.06. C is the long-term probability index that measures the vulnerability of the ship. This index is based on the probability of occurrence of short-term environmental condition.

$$C = \sum_{i=1}^N W_i \cdot C_{S_i} \quad (2)$$

W_i is a short-term weighting factor for the specific environmental condition. The short-term dead ship stability failure index, C_{S_i} , for the relevant short-term environmental condition under consideration, is a measure of the probability that the ship will exceed specified heel angles at least once in the exposure time considered (1 hour), taking into account an effective relative angle between the vessel and the waves. To evaluate the short-term index, a heeling lever due to wind effects is calculated. The wind and beam seas are derived by means of the analysis of the sea and gust spectra. Waves are characterized, in the short-term, by a significant wave height H_S and a zero crossing period T_Z . The spectrum of wave elevation is of the Bretschneider/Two parameters Pierson-Moskowitz type. The mean wind speed U_w is determined solely from the significant wave height H_S . The wind is assumed to fluctuate around the mean wind velocity. The total wind speed is given by the sum of the mean wind speed and the gust fluctuation speed. The spectrum of the gust is of the Davenport

type, and it depends on the mean wind speed. The long-term characterization of the standard environmental conditions is given by means of a given wave scatter diagram. More details about the procedure are given in the Explanatory Notes (IMO, 2016-ANNEX 6).

4. THE NAVAL SHIP CODE

The concept of the formal risk assessment, or design for safety approach, is already implemented by IMO within its rulemaking activity.

NATO has followed a similar attitude in adopting Goal Based Standards (GBS) as a basis for the “Naval Ship Code” ANEP-77 (NATO, 2014). GBS are a powerful tool able to establish a framework for integrating stability into a risk based design process (Alman, 2011). Within a goal based standards, a goal or ‘safety objective’ is defined through a series of tiers or a framework for verification through design construction and operation.

In ANEP-77, the goal based standards approach is structured on five tiers as follows:

- Tier 0 - Aim (Philosophies and Principles)
- Tier 1 – Goal
- Tier 2 – Functional Areas
- Tier 3 – Performance Requirements
- Tier 4 – Verification Methods
- Tier 5 – Justification

Performance requirements are defined in relation with ship operational profile and verified using appropriate criteria. As already mentioned the basic principle of a goal based approach is that the goals should represent the top tiers of the framework, against which ship is verified both at design and construction stages, and during ship operation. This approach has several advantages over more traditional prescriptive standards even though the Naval Ship Code can become prescriptive if appropriate. Alternatively, it can remain at a high level applying other standards and relevant assurance processes. In this way GBS approach permits innovation by allowing alternative arrangements to be justified as complying with the higher level requirements.

The Naval Ship Code is recalled as significant in this paper because it can represent the

background framework where application of SGISC to naval ships can find a possible rational collocation.

Moreover, in the introduction chapter of the Naval Ship Code, it is stated that the overall aim of the Code is to provide a standard for naval surface ship safety based on and benchmarked against IMO conventions and resolutions.

In this sense a continuous attention to IMO safety rules and their development is considered as an appropriate attitude.

In chapter III Buoyancy, Stability and Controllability, the main goals for such safety issues are identified. The buoyancy, freeboard, main sub-division compartment and stability characteristics of the ship shall be designed, constructed and maintained to:

- Provide an adequate reserve of buoyancy in all foreseeable intact and damaged conditions, in the environment for which the ship is to operate;
- Provide adequate stability to avoid capsizing in all foreseeable intact and damaged conditions, in the environment for which the ship is to operate, under the precepts of good seamanship;
- Permit embarked persons to carry out their duties as safely as reasonably practical;
- Protect the embarked persons and essential safety functions in the event of foreseeable accidents and emergencies at least until the persons have reached a place of safety or the threat has receded including preventing the malfunction of the life-saving systems and equipment.

An important reference is made to environmental condition.

Verification that the ship complies with this high level aims shall be by the Naval Administration. Provision of evidence to support verification shall be by the owner.

5. THE APPLICATION CASES

In order to obtain an immediate flavor on the real feasibility about consistent integration between present navy intact stability rules and IMO SGISC, some investigations are carried out.

The application of such IMO criteria to navy ships has already been studied in the latest years with interesting results (Tomaszeck and Bassler, 2015; Grinnaert et al. 2016).

The selected ships are a destroyer unit, a helicopter carrier and a patrol vessel.

Main ships data are given in Table 1.

Table 1 – Main Data of investigated vessels

			Destroyer	Heli-Carrier	Patrol Vessel
Length BP	L_{BP}	(m)	142	172	80.6
Breadth	B	(m)	19.1	24	9.6
Draught	T	(m)	6.15	6.50	3.37
Displacement	Δ	(t)	8634	11768	1250
Froude number	F_n	-	0.413	0.338	0.457

Due to the importance of the areas exposed to wind, special attention is given to the shape and dimensions of ship’s windage areas that for each ship are appropriately designed on the basis of similar existing units.

First vulnerability level assessments –All stability failure modes

At first, the three ships are investigated calculating the max KG curves derived from the compliance with the SGISC first vulnerability level criteria for all the stability failure modes..

Results, for each vessel described above, are shown in Figure 1, 2 and 3. In the same figures, it is possible to put in evidence the max KG curves (indicated with “Navy”) that derive from the compliance with a set of criteria representative of the present intact stability requirements for navy ships.

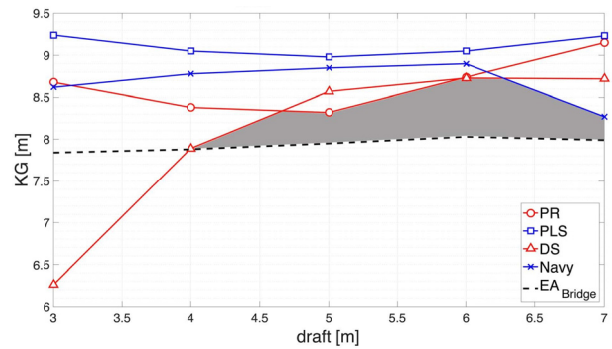


Figure 1 – KG_{max} curves for Destroyer

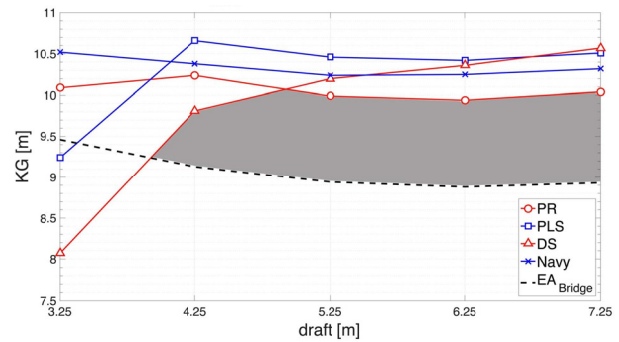


Figure 2 – KG_{max} curves for Helicopter carrier

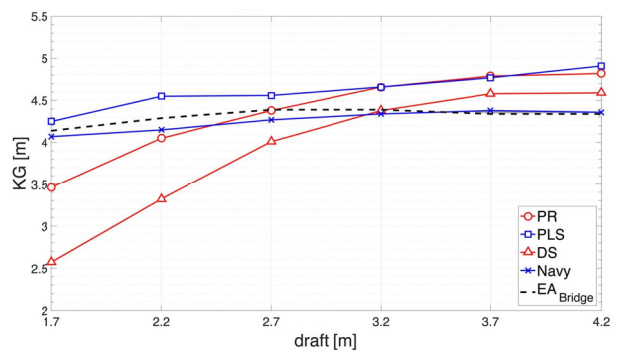


Figure 3 – KG_{max} curves for Patrol Vessel

In order to better understand the results, it is worthwhile to remind that for the case of Excessive Accelerations the curve should be named as the curve of the min KG i.e. it is required that the KG value is higher with reference to that curve. It is immediately evident how the “design space” (indicated with a grey area) is limited for the Helicopter carrier and the Destroyer; the same “design space” is totally non existing for the Patrol Vessel.

Since the set of criteria that have been applied are first level vulnerability criteria, it is definitely advisable to proceed to the second level in order to be able in case to design the ship.

It is interesting to point out that the present intact stability standard for navy ships are well positioned in between the other curves, denoting a comparable and equivalent level of safety with SGISC-first vulnerability level.

Second vulnerability level assessment - Dead ship condition

The further investigation, raising to the higher second vulnerability level, is specifically limited to the dead ship condition stability failure.

As already mentioned, the Naval Ship Code is based on goal based approach i.e. a performance assessment perspective. In this sense it is not so easy to find a suitable methodology to carry out the performance assessment. The second vulnerability level criteria developed by IMO can be considered as a possible option, worth to be investigated. The second level criteria are defined to be a wide-ranging tool able to better frame the ship behavior than first level ones and, even though not expressly meant, they are in principle suitable to be applied also to navy ship category. The beam winds combined with ship rolling criterion, as already described in its traditional present formulation within the Naval Ship Code, is applied for a wind speed of 100 kn. The derived max KG curves are shown in Figure 4, 5 and 6, where also results derived from the application of second vulnerability level criterion are reported.

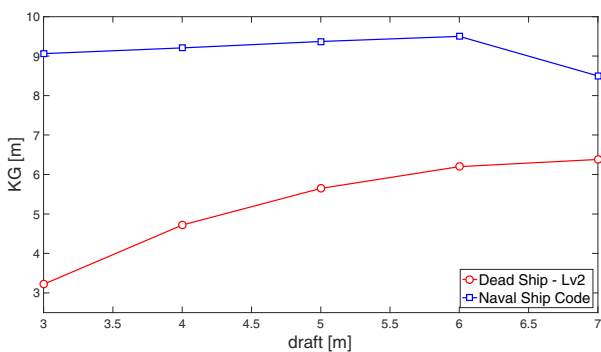


Figure 4 – KG_{max} curves for Destroyer

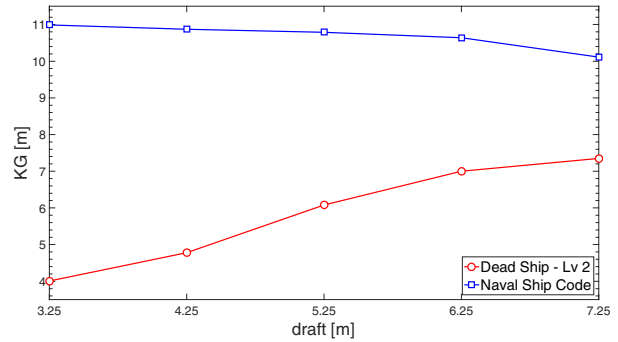


Figure 5 – KG_{max} curves for Helicopter carrier

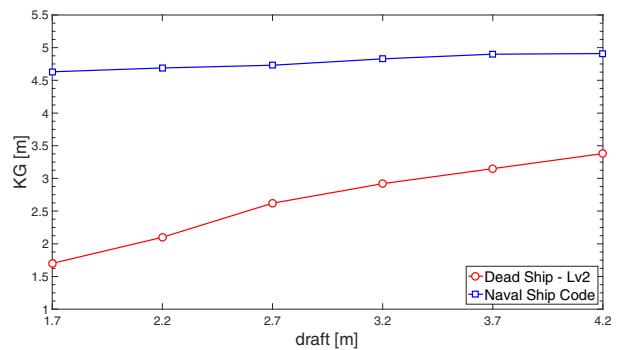


Figure 6 – KG_{max} curves for Patrol Vessel

The max KG curves derived from SGISC second vulnerability level are significantly more severe than the present wind+ship roll criterion, for all the three investigated ships.

Moreover, results are not in line with what expected: the beam winds combined with ship rolling criterion, applied with 100 kn wind speed, was expected to be in principle more severe than the second vulnerability level approach. This one in fact is more extensive in terms of sea state conditions investigated, including less severe environment conditions..

6. CONCLUSIONS

Due to the need to find efficient tools to investigate ship dynamic stability in waves, the SGISC are applied to a set of naval ship category i.e. a helicopter carrier, a destroyer and a patrol vessel. A special attention is paid to the ship performance assessment for beam winds combined with ship rolling, since naval ships cannot limit in principle their operational profile in case of weather and sea state adverse conditions.

The application of the first vulnerability level criteria, for all the stability failure modes, to the

three ships has evidenced the nearly equivalent level of safety of the present intact stability rules for naval ships when compared with the SGISC curves/first vulnerability level.

A critical issue is that the max KG curve for the excessive acceleration failure mode, when combined with other curves, practically limits the “design space” to a very narrow area, especially for the patrol vessel.

As regards the application of the second level vulnerability criterion for the dead ship condition stability failure, results give evidence about the higher severity of the criterion when compared with the one applied by the Naval Ship Code and practically equivalent to the beam winds combined with ship rolling already applied by Navies.

REFERENCES

- Alman P.R., 2010 “Approaches for Evaluating Dynamic Stability in Design” Proceedings of the 11th International Ship Stability Workshop, (ISSW2010), Wageningen, The Netherlands
- Alman P.R., 2011 “Thoughts on Integrating Stability into Risk Based Methods for Naval Ship Design” Proceedings of the 11th International Ship Stability Workshop, (ISSW2010), Wageningen, The Netherlands
- Ariffin A., Mansor S., Laurens J-M., 2016, “Conduction of a wind tunnel experiment to investigate the ship stability weather criterion” Proceedings of the 15th International Ship Stability Workshop, 13-15June 2016, Stockholm, Sweden
- Beaupuy B., Stachelhausen N., Billard J-Y., Mogenicato E., Vonier P., Leguen J-F., 2012, “Operability of French Naval Ships over 50 Years” Proceedings of the 11th International Conference on the Stability of Ships and Ocean Vehicles, Athens, Greece.
- Belenky V., Bassler C.C., Spyrou K.J., 2011 ‘Development of Second Generation Intact Stability Criteria’, Hydromechanics Department Report (Naval Warfare Center Carderock Division - USA)
- Belenky V., de Kat, J.O., Umeda N., 2008 ‘Toward Performance-Based Criteria for Intact Stability’, Marine Technology 45, 2008.
- FR-MOD 1999 “N° 6018 A – Stabilité des Batiments de Surface de La Marine Nationale”.
- Grinnaert F., Gualeni, P., Billard, J-Y., Laurens J-M., Petaccion., 2016, ”Application of 2nd Generation Intact Stability Criteria on Naval Ships” Proceedings of the 15th International Ship Stability Workshop, 13-15June 2016, Stockholm, Sweden
- IMO 2008, ‘Adoption of the International Code on Intact Stability’, MSC Resolution MSC.267(85).
- IMO 2015, ‘Development of Second Generation Intact Stability Criteria’, SDC 2 / WP.4.
- IMO 2016, ‘Finalization of Second Generation Intact Stability Criteria’, SDC 3 / WP.5.
- IT-MOD, 1980 “NAV-04-A013 - Norme per la stabilità e la riserva di galleggiabilità delle navi di superficie”.
- Luquet R., Vonier P., Prior A., Leguen J.F., 2015, “Aerodynamics Loads on a Heeled Ship” Proceedings of the 12th International Conference on the Stability of Ships and Ocean Vehicles, 14-19 June 2015, Glasgow, UK.
- NATO, 2014, “Nato Standard Anep-77 Naval Ship Sode” Edition E version 1, NATO Standardization Agency (NSA)
- Perrault D., 2013, “Examination of the Probability Results for Extreme Roll of Naval Vessels” Proceedings of the 13th International Ship Stability Workshop, Brest.
- Peters A., 2010, “Tolerable Capsize Risk of a Naval Vessel”, Proceedings of the 11th International Ship Stability Workshop, (ISSW2010), Wageningen, The Netherlands
- Reed A.M., 2009 “A Naval Perspective on Ship Stability”, Proceedings of the 10th International Conference on Stability of Ships and Ocean Vehicles, (STAB2009), St. Petersburg, Russia, pp. 21-43.
- Sarchin T.H., Goldberg L.L., 1962, “Stability and Buoyancy Criteria for U.S. Naval Surface Ships” Transactions SNAME, 1962
- NAVSEA, 2016, “T9070-AF-DPC-010/079-1 Design Practices and Criteria for U.S. Navy Surface Ship Stability and Reserve Buoyancy”.
- Tellet D., 2011, “Incorporating Risk into Naval Ship Weight and Stability Control” Proceedings of the 12th International Ship Stability Workshop, (ISSW2011), Washington, USA.
- UK-MOD, 2000, “ NES 109 - Stability Standards For Surface Ships - Part 1 - Conventional Ships”.
- Tomaszek, H.A., Bassler C.C, 2015, “Dynamic Stability Assessment of Naval Ships in Early-Stage Design” Proceedings of the 12th International Conference on the Stability of Ships and Ocean Vehicles, Glasgow, UK.

This page is intentionally left blank

Iced Maritime Routes, impact on Stability for Naval Ships

Paul CREISMEAS, *DGA Techniques hydrodynamiques, BP 510, Chaussée du Vexin, 27 105 Val de Reuil cedex, France, paul.creismeas@intradef.gouv.fr*

Guillaume LANNEL, *DGA Techniques hydrodynamiques, BP 510, Chaussée du Vexin, 27 105 Val de Reuil cedex, France, guillaume.lannel@intradef.gouv.fr*

Jean-François LEGUEN, *DGA Techniques hydrodynamiques, BP 510, Chaussée du Vexin, 27 105 Val de Reuil cedex, France, jean-francois.leguen@intradef.gouv.fr*

ABSTRACT

Three factors can be pointed out in order to explain the motivation for iced seas or partially iced seas sailing: Climate environment, shortening of commercial route, offshore oil and gas exploitation. It is necessary to prove the ability of a ship to break the ice and to resist to ice shock. A list of laboratory, which can perform those evaluations, is given. The stability is also sensitive to the increase of mass by ice accretion on superstructures, and taken into account by some rules.

Keywords: *Ice, Maritime routes, Rules, Laboratories.*

1. INTRODUCTION

Three factors can be pointed out to explain the motivations to sail on iced maritime routes:

- Climate conditions,
- Shortening of maritime route and
- Offshore oil and gas exploitation.

Climate conditions involve regions with maritime coast opened on iced sea during most part of the year or which are located around the polar circle. Countries such as Finland, Sweden, Federation of Russia whose coasts are around Baltic sea and Bothnie gulf are telling examples of the first case and countries such as Canada, Norway and the north coast of the Federation of Russia belong to the second one, figure 1.

Such countries must maintain both port and offshore traffic, such as ferry services and must guarantee the security in their own territorial waters with ice-worthy warships needed to patrol.

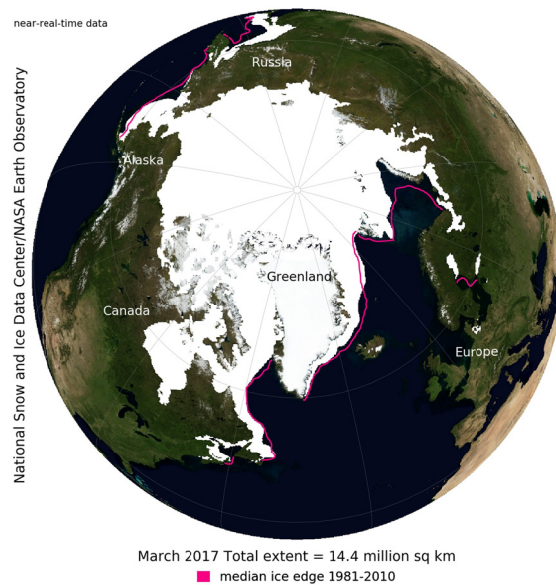


Figure 1: Extent of ice in Arctic region for March 2017 - Courtesy of the National Snow and Ice Data Center, University of Colorado, Boulder.

2. MARITIME ROUTES

There are two major maritime merchant routes. One route links European ports to those located along the East coast of the United-States, through the Canal of Panama and the other one links European ports to ports on Chinese and Japan coast, figure 2. Alternative maritime routes from Arctic make substantial shortening in term of distance travelled, respectively Northwest Passage and Northern Sea Route, as shown in Table 1.

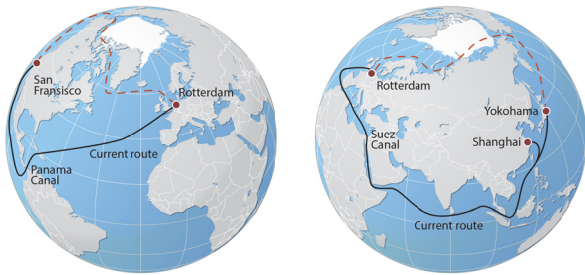


Figure 2: Current maritime routes and arctic maritime routes: left Northwest Passage, right: Northern Sea Route, from AMAP, 2012.

Table 1: Distance travelled for the major maritime route and their alternative

	Current route through The Panama Canal	Alternative route through Arctic, Northwest Passage
Maritime routes from Europe to East coast of the United-states	≈17000 km	≈14000 km
	Current route through Canal of Suez	Alternative route through Arctic, Northern Sea Route
Maritime routes from Europe to coasts of China or Japan	≈21000 km	≈14000 km

The ships which sail along the Arctic routes must be ice-breakers or vessels with the capability to follow ice-breakers, that is to say with a hull and propellers able to resist ice-cube shocks.

Oil resources are important in Arctic region, figure 3, and the exploitation of these resources are under important environmental constraints. The structure of offshore platforms must resist ice pressure and the OSV in charge to supply must be proved to be ice-cube shock resistant and moreover these units have to perform dynamic positioning in iced sea conditions.

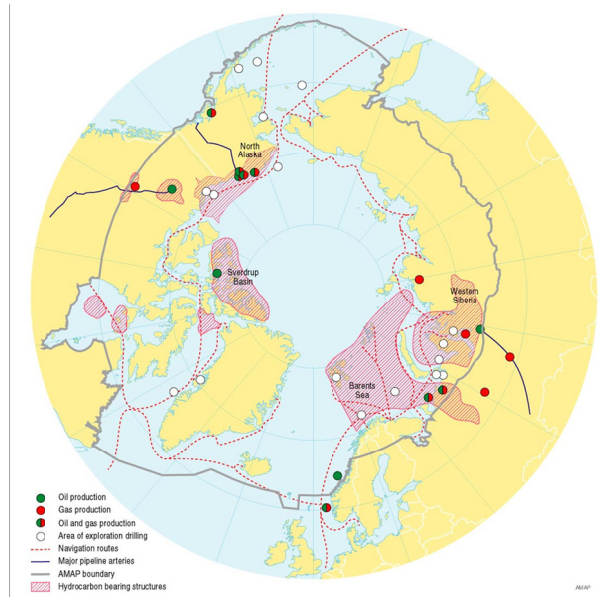


Figure 3: Major areas of oil and gas development and potential development in the arctic and major shipping routes and possible new routes through arctic waters (from AMAP, 2012).

3. EXPERIMENTS IN ICED TANKS

Many establishments are involved in iced sea tests. The main objective is to prove the ability of the future vessel to break the ice, for ice-breakers projects, or to resist ice cube shocks for the other iced-seas going vessels. The ability of the propulsors, propellers or azipod, to ingest iced block without any damage must be demonstrated too. A list of the major test sites which owns an ice model basin is given in Table 2.

To obtain ice layer with the right thickness in a basin and to maintain the right temperature inside the enclosure for the tests may be of high costs, in both energy and time. Establishments involved in iced sea tests, but without appropriate facilities, have developed alternative and innovative methodologies by using artificial ice to perform tests. According to this kind of method, pieces made of polystyrene stand for iced water to study the effects of ice cubes shocks and, more recently, paraffin-based blocks stand for floating ice block to study the ingestion of ice by the propulsors. The former method is used at the University of Pusan (Won-Joon Lee and Moon-Chan Kim, 2013) and the later by MARIN (G.Hagesteijn, 2015).

4. ICE ACCRETION

In above section we discussed only about iced sea, but icing phenomenon may occur on the hull and on the superstructure of a iced-sea-going vessel. This kind of icing may occur when sailing in ice free water, the causes of the icing phenomenon is a low temperature and a significant rate of humidity. We can cite as a telling example the frosty fog. Frosty fog is composed of non-frozen droplets in super cooled state. Such a state is a metastable one; the droplets froze as soon as they meet any element of the boat, hull or superstructure. The same phenomenon occurs on in land facilities, involving hot tension wire for example or air traffic when plane flies through an icing cloud. Hull and superstructure icing may be dangerous for the stability of the ship. On the one hand, ice accretion means significant additive weight for the ship, and on the other hand a non-symmetric accretion means the ship heels on her side and the heeling may lead to capsizing.

At sea the main reasons for ice accretion are;

- Freezing spray,
- Super-cooled fog
- Freezing rain or drizzle
- Failing wet snow.

The most probable reason (about 90%) is the freezing spray that is studied below. That can explain why most of the rules consider only ice accretion in the bow area of the ship (one over three front part).

5. PREDICTION OF ICE ACCRETION

Many theories exist to predict the ice accretion as Overland. The parameters of those theories are: the freezing point of salt water, the air and water temperature, wind speed and time of exposure in order to determine the risk of ice accretion, PR.

$$PR = V_a (T_f - T_a) / (1 + 0.3 (T_w - T_f))$$

With T_f freezing point of sea water (°C)

T_a air temperature (°C)

T_w sea temperature (°C)

V_a wind speed (m/s)

From this risk, PR, some propose to determine empirically the rate of ice accretion, IR, in centimeter increasing of thickness by hour.

Then, with a time exposure it is possible to estimate the thickness and the mass of ice.

Lozowski propose some more sophisticate theory than the one presented above.

Relying on those theories it is possible to make prediction from usual weather forecast given by most meteorological centres as NOAA.

6. RULES

Assumptions

The presence of icing degrades the already very rough environment to which a ship is subjected. The accumulation of ice in the topside harms the stability of the ship. Currently, some simple technologically solutions to effectively combat ice accumulation exist but usually note supposed to be effectiveness for the rules. Main icing abatement are: mechanicals methods (including electro expulsive deicing system, pneumatic or high pressure water jets), thermal methods or chemical methods freezing point depressants or ice-phobic coating.

This is why the French and some foreign navies have sought to determine coherent criteria in order to better understand this phenomenon. Each vessel that is subject to this environment must therefore comply with these criteria. To ensure this, the Navies must make calculations based on multiple assumptions. For IMO, only ships who have to sail in some particular zones (more or less northern than 60°N and southern than 60°S) have to follow specific checks: The ships have to follow intact criteria for extra loads.

As most of the occidental rules, French rules, came from the Sarchin and Golberg work. To propose their criteria for ice accretion they used the feedback of the “wind-class” US icebreakers. The performed an inverse calculation to determine the maximum thickness of ice is acceptable on these ships for usual intact stability criteria. It was this thickness that was proposed for the naval rules criteria. This value matches well with a 20 hours’ time exposure with a small rates of accretion as assumption. This time exposure was determined by 8 years of feedback from a “wind-class” US icebreaker.

Comparisons

In order to carry out the comparison, it is necessary to begin by agreeing on the same definition of hypotheses and criteria. The objective is to make the compared rules communicate better with each other. If the starting assumptions are different from the rules, then it is not possible to compare the results and the criteria. The most severe criterion cannot therefore be determined. Such a divergence in the definition of assumptions raises the question of how they were obtained.

An initial assessment can be made. In order to facilitate understanding, a table summarizing the main assumptions of some navies is given below. The navies appearing there have been selected because they have many differences between them. The values shown vary from one a navy to another, as does the definition of the starting assumptions. It is also observed that the input data (mass of the ice, center of gravity,...) and the output criteria are quasi-identical; which is an important first step towards standardizing assumptions and criteria.

There are almost as many starting assumptions as there are navies. Some prefer to calculate the mass of the ice by considering a certain distribution on the exposed surfaces of the ship, others prefer to consider that it is a function of its displacement. The divergences do not end there; they are also present in the definition of the position of the center of gravity of the ice or the wind speed to be taken into account.

Although the definition of the criteria is similar from one navy to another, the threshold is nevertheless different for some of them. For example, whereas the criterion on the GMt without wind imposes that it is higher than 0.15 m for the BVNR (France), The Royal Australian Navy imposes that it is greater than 0.6 m. The question of the severity of one regulation in relation to another must be raised.

7. ACKNOWLEDGMENTS

This study was based on CRNAV (Cooperative Research Navies) discussions. For the French part, the study is funded by the French Ministry of Defence to support DGA Hydrodynamics in its research activities.

REFERENCES

- AMAP, 2012, "Arctic Climate Issues 2011: Changes in Arctic Snow, Water, Ice and Permafrost, SWIPA 2011 Overview Report. Arctic Monitoring and Assessment Programme (AMAP)", Cartographer/designer : Hugo AhleniusOslo, updated 06/12/2013.
- Bureau Veritas, NR 483, November 2011, "Rules for the classification of Naval Ships".
- DDS 079-1 version 2.01, 2008, "Design Data Sheet Stability and Buoyancy of US Naval Surface Ships".
- Hagesteijn, G., J. B. 2015. "Ship Resistance Validation Using Artificial Ice". In *Proceedings of the ASME 2015 34th International Conference on Ocean Offshore and Arctic Engineering*, Saint Jean de terre-Neuve, Canada, OMAE41804.
- Hayes, P., "The Royal Australian Navy Stability Standard", STAB 2000.
- Lozowski, E. P., Szilder, K., Makkonen, L., „Computer Simulation of Marine Ice Accretion“, *Philosophical Transaction of the Royal Society*, 10.1098/rsta.2000.0687.
- MIL, 1993, "The Prevention / Removal of Ice Accretion Aboard Naval Surface Ships – A survey of Available Methods" MSEI Report N°1571-26-1.
- Overland, J. E., 1990, "Prediction of vessel Icing for Near-Freezing Sea Temperatures", *American Meteorological Society*.
- Ryerson, C., 2008 "Assessment of superstructure ice protection as applied to offshore oil operations safety", Cold regions research and engineering laboratory (USA)
- Sarchin, T. H. and Golberg, L. L., 1962, "Stability and Buoyancy Criteria for U. S. Naval Surface Ships, SNBAME volume 70.
- Thomas, W. L. III, 1991, "Bering sea topside icing probabilities for two naval combatants" DTRC report.
- Won-Joon Lee and Moon-Chan Kim, S.-K. L.-y., 2013, "Numerical and experimental investigation of the resistance performance of an icebreaking cargo vessel in pack ice conditions". *Int. J. Naval Archit. Ocean Eng.* 5 :116 131.

Table 2: Characteristics of the major ice model basin

Establishment	Length (m)	Width (m)	Depth (m)	Max velocity of the carriage (m/s)	Ice characteristics	Max ice temp. (°C)	Name of the facility
Krylov (Russia)	102	10	2 - 4	1.5	Thickness from 10 to 130 mm – Duration of producing: from 1 to 2 days		Ice basin
Aker Arctic Technology (AARC) (Finland)	75	12	2.1	Main carriage 3 Second carriage (lateral) 1.5			Ice Model Test Facility
NRC CNRC (Canada)	90	12	3	4	Thickness from 5 to 150 mm – rate of growth: 2.5 mm/hour	-30	Saint Jean de Terre Neuve Facility
NRC CNRC (Canada)	27	7	1.1			-20	Ottawa facility
KRISO (Korea)	42	32	2.5	Main carriage 3 Second carriage (lateral) 3		-30	Ice Basin
Aalto University (Finland)	40	40	2.8		Thickness from 20 cm to 30 cm – the ice layer is from a water spray	-12	Ice Basin
NMRI (Japan)	35	6	1.8		Thickness 30 cm – rate of growth:40 mm within 15 hours	-35	Ice Basin
ERDC CRRL (United-States)	37	9	2.4		Thickness: 15 cm	-24	Ice Engineering Basin
HSVA (Germany)	78	10	5	Main carriage: 3 Second carriage: 3	Saline ice	-20	Large Ice Model Basin
HSVA (Germany)	30	6	1.2	Recirculating water canal	Saline ice – rate of growth: 2 mm/hour	-16	AETB – Arctic Environment Test Basin
JMUC – Japan Maritime United Corporation (Japan)	20	6	1.8	Upper carriage: from 0.4 to 1.5 Underwater carriage: unknown	Rate of growth: 8 mm/hour	-22	Ice basin
University of Tianjin	20	5	1.5	0.5		-22	Ice basin
Arctic and Antarctic Research Institute (Russia)	35	5	1.8				Test Ice Tank

Table 3: Comparisons of some rules

		France (Bureau Veritas Naval Rules)	US Navy	Australia
APPLICATION	Navigation area	Only for ships sailing north of 65 ° and south of 60 ° or in winter frost zone.	No restrictions	No restrictions
	Class of ship	Presence of an additional class, more severe	Presence of an additional class "ICE"	Not applicable for "polar" vessels
PARAMETER(S)	Wind	70% of nominal wind: 100 knots for «unrestricted service» (80 knots for ships not employed in storms).	70 knots (unrestricted), 45 knots (restricted service)	70 knots (unrestricted), 60 knots (restricted service)
	Mass of ice (t)	- DL _{nato} <1000t, M=10% of full load condition -DL _{nato} >1000 t : 140 kg / m ² on the decks on the 1/3 front (Above the exposed deck) and 70 kg / m ² on the vertical or oblique walls of the 1/3 front (above the exposed deck), including the side walls but not the masts.	$\Delta^{2/3}$	15 cm (950 kg/m ³) exposed decks and walls
	XG of ice (m/PPAR)	DL _{nato} < 1000t : CoG of considered displacement DL _{nato} > 1000 t : , CoG of ice on the 1/3 front)	5/6 LOA / PPAR	CoG of ice
	KG of ice (m/OH)	DL _{nato} < 1000t : CoG of considered displacement DL _{nato} > 1000 t : , CoG of ice on the 1/3 front)	1.2 m / exposed deck	CoG of ice
	YG of ice (m)	DL _{nato} < 1000t : CoG of considered displacement DL _{nato} > 1000 t : , CoG of ice on the 1/3 front)	0 m	CoG of ice (0 m)
CRITERIA WITHOUT WIND	Area (0°-30°) (m.rad)	0,051	-	0,055
	Area (0°-40°) (m.rad)	0,085	-	0,09
	Area (30°-40°) (m.rad)	0,033	-	0,03
	Gzmax (m)	0,24	-	0,3
	GMt (m)	0,15	-	0,6
	Angle GZmax	25° >= théta >= 30°	-	30°
CRITERIA WITH WIND	Wind profil	variable	variable	variable
	HAwind	variable	variable	variable
	théta R	25°	25°	25°
	Area A1/A2	1,4	1,4	1,4
	théta C	30°	15°	30°
	GZ1/GZmax	0,6	0,6	0,6

Adverse health effects and reduced work ability due to vertical accelerations in high-performance marine craft personnel

Manudul Pahansen de Alwis, *Centre for Naval Architecture, Department of Aeronautical and Vehicle Engineering, School of Engineering Sciences, KTH Royal Institute of Technology, Stockholm, Sweden, pahansen@kth.se*

Karl Garne, *Centre for Naval Architecture, Department of Aeronautical and Vehicle Engineering, School of Engineering Sciences, KTH Royal Institute of Technology, Stockholm, Sweden, garne@kth.se*

ABSTRACT

Human factors engineering is a key parameter in High-Performance Marine Craft (HPMC) design since the human tolerance to working conditions aboard, in fact, decides the operational limits. So far, the deficiency of the knowledge on how the crew is influenced by the working conditions in terms of health risk and work performance has led the designing process to exit before incorporating the human element when determining these operational limits. Knowledge, on the relationship of the physical and perceived exposure conditions and on risk factors for health and work performance impairments, would open up possibilities for drawing the operational limits at the design stage and providing feedback to the crew during operations. This is investigated in a research program and the current study pilot test a set of High-Performance Marine Craft Personnel (HPMCP) in order to collect data on their work exposure, health and performance impairments. The study collects subjective and objective data and investigates their correlation and the potential risk factors. Although the amount of data collected is too limited to draw direct conclusions, the pilot test confirms the feasibility of the set-up and the method giving good inputs and experience to the research crew.

Keywords: *Whole-body vibration, Epidemiology, High-Speed Craft, Human Factors.*

1. INTRODUCTION

In attempts to incorporate human factors in the design of High-Performance Marine Craft (HPMC), it has become evident the deficiency of the knowledge on how the crew is influenced by the working conditions in terms of health risk and work performance. The latter is expected to jeopardize the system performance as well as safety at sea, where crews and passengers are demanded for physical fitness in order to successfully complete their missions. In the context of simulation-based design, the present study constitutes a pilot test of a longitudinal investigation of work exposure, health, and performance in High-Performance Marine Craft Personnel (HPMCP). The study has been started by KTH Royal Institute of Technology in collaboration with Karolinska Institutet, the Swedish Coast Guard and Institute of Aviation Medicine Norway, which is a part of an ongoing program investigating relationship between working conditions aboard HPMC and the

outcomes in terms of systems performance and occupants' health.

The pilot test is designed to correlate physical and perceived working conditions identifying performance and health related risk factors by collecting objective and subjective work-exposure data and subjective performance indicators and health data. In the event objective and subjective data correlate, either can be used to level the severity of the working conditions aboard. Moreover, if risk factors can be linked to condition severity it will be possible to depict risk related to the conditions perceived and measured onboard or predicted at the design stage. The latter can be used to adopt the speed reduction curve to human health and performance while the former to crew guidance during operation.

The paper attempts to identify the correlation between subjective and objective data while discussing the lessons learnt from the process.

2. METHODS

Study design

The set-up is designed as a field research on HPMC crew in operation, a sample of eight Norwegian Special Operations Command officers during an eight weeks exercise where HPMC are operated as a part of the program. Craft acceleration and GPS data is objectively recorded by vibration measurement systems installed onboard while work related exposure, performance and health data is subjectively collected via web-based questionnaires.

Instrumentation and data collection

Four HPMC, 11.25m rigid inflatable boats (RIBs), are instrumented as shown in Figure 1. Two craft are fitted with two measurement systems, one in the driver and navigator area and the other one in the passenger area. The remaining two craft are installed with one measurement system on each due to the limited availability of the instruments. The six measurement systems, Figure 2, specifically designed for the purpose, are prototypes consisting of one tri-axial accelerometer, two single-axis accelerometers, GPS antenna and a data acquisition unit with eleven input channels. The system records acceleration and GPS data at 600Hz and 1Hz respectively and stores on a local memory.

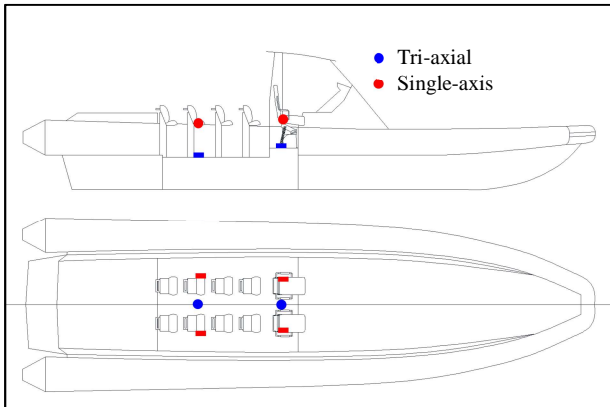


Figure 1: Instrumentation of craft.

Tri-axial accelerometers are fitted on the floor at the center-line, one in between coxswain and navigator seats and the other in the passenger area as shown in Figure 1. The two single-axis accelerometers, measuring vertical accelerations, are mounted each on the coxswain, navigator and passenger seat frames below the cushions. GPS antenna, logging longitudes, latitudes, speed, course over ground and coordinated universal time stamp,

is installed on the mast. The data acquisition unit is secured inside a water proof cover on the base of the mast. The accelerometers are calibrated before the installation and considered reliable.



Figure 2: Vibration measurement system.

Although the measurements are intended to be started as the craft ignition key is turned on, in this test, a separate switch is installed due to some technical confidentiality concerns.

Self-reported data is collected by two sets of web-based questionnaires, [de Alwis et al. 2016 and lo Martire et al. 2017], hereinafter referred to as Q1 and Q2 respectively. Q1 collecting demography, life-style, work-exposure and health data, is answered at the beginning of the study by every subject as a base-line questionnaire and considered as a reference data set. Q2 consists of two modules of which one module measuring work exposure and performance indicators is answered daily after each work shift and the other module for musculoskeletal pain is answered weekly during the exercise. The daily module of Q2 is answered regardless their activities, i.e. seaborne or not. All the questionnaires are completed on the subjects' personal smartphones. The data is collected for two months.

Analysis of data

The subjective health impairments are assessed in terms of prevalence and incidence of musculoskeletal pain. Prevalence, i.e. existence of pain, is determined under ten major body areas and expressed as the number of subjects having pain during the past six months and seven days. Incidence, i.e. occurrence of new pain events during a specific time period, is scrutinized weekly and then expressed as the number of subjects

incurred new pain events during the entire eight-week exercise program. Musculoskeletal pain data is collected using a high resolution pain areas scheme having 18 different pain areas and the results are merged and presented under ten major body areas.

The subjective performance impairments are evaluated using a fatigue symptoms based aggregated scoring system developed in de Alwis et al. 2016 and lo Martire et al. 2017, and presented as the number of fatigue symptoms. The fatigue symptoms based aggregated score system was developed considering the correlation of five fatigue symptoms: tiredness, concentration difficulties, decision making complications, headache and motion sickness with the perceived ride quality.

The subjective work exposure is mainly measured as perceived ride quality by 4-point ordinal Likert rating scale quantizing perceived ride quality as 1 = Very smooth (good comfort with no or very few bumps, 2 = Smooth, 3 = Rough, 4 = Very rough (considerable discomfort or strain as a result of sea state, vessel speed, or both).

The objective vibration exposure, measured as acceleration, is quantified by daily equivalent static compression dose (S_{ed}), [ISO 2631-5:2004]. This method considers adverse effects on the lumbar spine as the dominating health risks of exposure to vibration containing repeated shocks.

3. RESULTS

All eight subjects have answered Q1 and the daily part of Q2 where only six have answered the weekly part of Q2. The response sequence can be seen in Table 1.

Table 1: Response sequence of Q2.

Respondent ID	Number of Responses			
	Q2 – Daily			Q2 - Weekly
	At sea	Not at sea	%*	
P1	6	0	15.0	1
P2	1	0	2.50	2
P3	1	1	5.00	0
P4	6	0	15.0	3
P5	12	5	42.5	1
P6	2	1	7.50	0
P7	14	11	62.5	2
P8	11	9	50.0	6

* Calculated considering Norwegian occupational regulations demanding an average two-day rest per week.

Of 80 responses, 27 are related to non-seaborne activities.

General health status

According to the data collected by Q1, 7 out of 8 subjects got musculoskeletal pain in different body areas considering the past six months period whereas majority of them, 5 out of 7, having neck and lower back pain. Prevalence of musculoskeletal pain in different body areas considering past 6 months and 7 days is provided in Table 2.

Table 2: Prevalence of musculoskeletal pain in different body areas considering past 6 months and 7 days.

Pain Area	Number of Subjects	
	6 months	7 days
Neck	5	0
Lower back	5	0
Head	2	1
Knee	2	0
Lower leg	2	0
Shoulder	1	0
Upper back	1	0
Elbow	0	0
Forearm and wrist	0	0
Hip and thigh	0	0

It can be seen from the results that only one person was having head pain during the past 7 days period. The occurrence of new pain events during the eight-week exercise program are shown in Table 3.

Table 3: Occurrence of new pain events during eight-week exercise program

Pain Area	Number of Subjects
Neck	5
Lower back	4
Head	1
Knee	2
Lower leg	0
Shoulder	1
Upper back	4
Elbow	1
Forearm and wrist	2
Hip and thigh	0

Four subjects believed that the cause for their pain events was work at sea.

Table 4 shows the measured and perceived vibration exposure and the performance indicators during the first four weeks of the exercise. Subjective data is not available on certain days. Vibration levels on the craft floor indicates about the exposure without a shock mitigation seat.

Table 4: Measured and perceived vibration exposure and the performance indicators during the first four weeks.

Week and Day*	Craft ID	Analyzed Duration [Hours]	S _{ed} [MPa]		Respondent ID	Task	Ride Quality	Fatigue Score ⁺
			Craft Floor	On Seat				
W1-D1	C2	1.6	0.6	0.5	P7	D	VS	1
				0.5	-	N	-	-
W1-D1	C5	2.2	0.7	0.8	P5	D	S	1
				0.5	P8	N	VS	2
W1-D5	C2	0.6	2.1	1.9	P7	D	VS	0
				1.7	-	N	-	-
W1-D5	C5	0.5	2.2	1.8	P5	D	R	1
				1.9	-	N	-	-
W1-D6	C5	0.4	0.8	0.8	-	D	-	-
				0.9	-	N	-	-
W1-D7	C5	0.3	0.3	0.2	P7	D	VS	1
				0.3	-	N	-	-
W3-D3	C1	8.2	6.5	5.4	P5	D	VR	2
				6.9	P8	N	R	3
W3-D4	C1	5.3	5.4	4.2	P5	D	VR	2
				5.5	P8	N	R	3
W4-D2	C3	1.3	1.7	1.1	-	D	-	-
				1.2	-	N	-	-
W4-D5	C3	3.0	1.1	0.7	-	D	-	-
				0.7	-	N	-	-
W4-D6	C5	1.5	1.2	1.2	-	D	-	-
				1.2	-	N	-	-

★ W – Week, D – Day of the week
 + Fatigue score - Number of fatigue symptoms
 D – Driver, N – Navigator
 S – Smooth, VS – Very smooth, R – Rough, VR – Very rough
 – Data not available

Perceived ride quality shows a correlation with the measured acceleration exposure as can be seen in Figure 3.

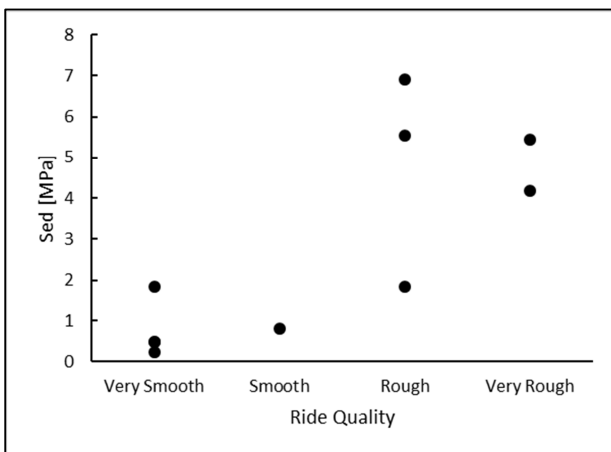


Figure 3: Acceleration exposure relative to self-reported ride quality.

Figure 4 shows that, although no subject has experienced more than three fatigue symptoms, there is a correlation between the fatigue score and the measured acceleration exposure.

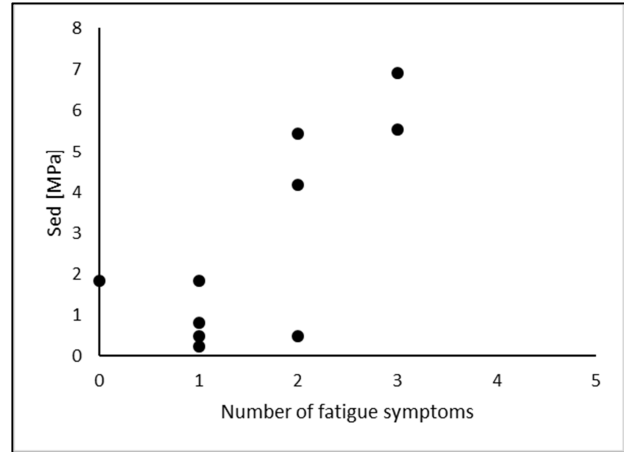


Figure 4: Acceleration exposure relative to fatigue score.

The response of the fatigue symptoms based aggregated scoring system to the perceived ride quality is shown in Figure 5.

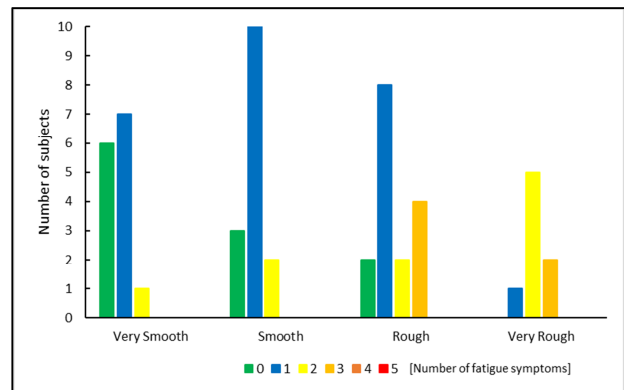


Figure 5: Response of the fatigue symptoms based aggregated scoring system to the perceived ride quality.

The results show that the number of subjects with 0-5 fatigue symptoms scores is proportional to the self-reported ride quality.

4. DISCUSSIONS

Eight Norwegian special operations command officers answered two web-based questionnaires providing data mainly on work exposure, musculoskeletal pain and performance indicators during a period of two months. Simultaneously acceleration data was also measured aboard the craft they operated.

Pain prevalence data during past 6 months shows that the body area based pain prevalence

distribution differs from the general population, [Brattberg G et al. 1989, Fejer R et al. 2006 and Hoy D et al. 2012]. Prevalence of neck and lower back pain is higher than that of the general population. Since in Q1, the subjects reported that they had not experienced any pain during the past 7 days, it was decided that they had no prevailing pain, except head pain, at the time of starting the exercise. Most of the subjects got neck pain during the exercise followed by upper and lower back pain.

Since Figure 3 and 4 indicates that the subjective ride quality and the performance indicators (fatigue score) correlate with the measured acceleration exposure, the perceived ride quality can be used to grade the exposure severity as well as performance degradation, in the absence of measured vibration data.

It is observed, in Table 4, that in most occasions, despite the fact that driver and navigator had used shock mitigation seats, their vibration exposure levels (S_{ed}) exceeded the upper limit for the lifetime exposure, i.e. 0.8 MPa, [ISO 2631-5:2004]. This tends one to think that there might be a relationship between vibration exposure and the health impairments in HPMCP, since the pain incidence is high. This relationship could further be investigated using a summary score of weekly vibration exposure with pain incidence or pain intensity data.

It is interesting to see, in Table 4, that perceived ride quality of the navigator is lower than that of the driver operating the craft. This might be due to individual perception differences or the navigator was concentrating on the navigation panel. A similar trend is observed in the other exposure categories such as sea conditions, wind conditions, noise level, temperature, sea spray and visibility. In certain cases S_{ed} levels on seat are higher than the levels on craft floor, a reason for which could be the varying body posture found by the daily part of Q2, i.e. mainly sitting, but standing in rough sea conditions. This problem could be addressed by introducing a sensor to the measurement system for indicating the occupant's posture, for instance, sitting or standing, which will provide information on another objective and subjective relationship, i.e. body posture.

It was found that the vibration measurement systems lack the requisite robustness to withstand the rugged environments. Some of the devices stopped recording data after experiencing large impacts and two systems completely broken during the first four weeks of operation. The objective data collection was affected by this issue since the craft installed with these defective instruments had been used for the exercises in many occasions. In certain cases self-reported data suggests that the duration of operation was about seven to ten hours per day where the measurement systems have recorded data for less than an hour. Moreover, GPS data confirmed that the subjective data is correct. Furthermore, it was identified that the objective vibration data was not available, in some occasions, as the crew had forgotten to switch-on the measurement system.

Another problem was the confidentiality of the population which hindered identifying the actual reasons for the missing data, for instance, the days when objective data is available but the subjective data is not and vice versa. It was also revealed that the subjects were not allowed to access their phones during several weeks due to which the study lost a large amount of subjective data. Availability of cellular network was also another critical issue with the data collection when the subjects spend multiple days out in the sea or forests.

During the eight-week exercise program, the study subjects had participated not only in HPMC operations, but also in other activities such as running, diving and parachute jumping, which could significantly affect their health and performance. It was difficult to account these effects in the analysis since their training schedules were confidential.

Even though the number of subjects was only eight, the results indicate correlations between the subjective and objective data which could be further improved by studying larger populations. Taking into consideration all the above aspects KTH in collaboration with Karolinska Institutet and the Swedish Coast Guard has now started the main study of investigating work exposure, health and performance of HPMCP and quantifying their association using measured vibration environments. Q1 and Q2 has now been updated based on the inputs received from this pilot study and more robust instruments have been occupied based on the

lessons learnt. As a study population coast guards are mainly involved with sea going activities and the other activities affecting their health and performance are comparatively less. The population is sufficiently large and the mission-confidentiality is relatively low. The data collection has already been started with the baseline data set, i.e. Q1.

5. CONCLUSION

Although the amount of data collected is not sufficient to draw direct conclusions on the relationships between subjective and objective data and identification of related risk factors, the pilot study suggests that the set-up and the method are feasible. The inputs received, experiences gathered and the lessons learnt strengthened the main study which has already been started.

Important aspects in need of consideration after the pilot test are;

- Selection of study population.
 - a) Size
 - b) Activities
 - c) Confidentiality
- Modifications to the vibration measurement system.
 - a) Robustness in rugged environments
 - b) User-friendliness, especially in data retrieval
 - c) Start data recoding with craft ignition key
 - d) Subject's posture identification method
 - e) Objective craft ID detection method
- Summary score method for the assessment of weekly vibration exposure in order to analyze the correlation between musculoskeletal pain and the vibration exposure levels.
- Mode of answering the questionnaires including the availability of cellular network signals.
- Further improvements to the questionnaires.
 - a) More mechanisms for the identification of missingness of data
 - b) Introduce memorizing features for one-time data, for instance, anthropometric and demographic data.
 - c) Fatigue score system
 - d) Resorting the items on priority basis
 - e) Rephrasing the pain questions
- Introduce objective performance indicators to the study program, such as cognition, bio-marker and electromyography (EMG) data.

6. ACKNOWLEDGEMENTS

Jan Ivar Kåsin of Institute of Aviation Medicine Norway is acknowledged for coordinating the pilot test with the subjects and calibrating the vibration measurement systems. Acknowledgements to Norwegian Special Operations Command officers for their participation in the pilot test as study subjects.

REFERENCES

- de Alwis M. P., Lo Martire R., Ang B. O., Garne K., "Development and validation of a web-based questionnaire for surveying the health and working conditions of high-performance marine craft populations", *BMJ Open* 2016;6(6):e011681.
- Lo Martire R, de Alwis M P, Ång B. O., Garne K., "A web-based questionnaire for longitudinal investigation of work exposure, musculoskeletal pain, and performance in high-performance marine craft populations", submitted for publication Jan 2017.
- ISO 2631-5:2004 Mechanical vibration and shock – evaluation of human exposure to whole-body vibration – Part 5: Method for Evaluation of Vibration Containing Multiple Shocks. International Organization for Standardization, Geneva 2004.
- Brattberg G., Thordslund M., Wikman A., "The prevalence of pain in a general population. The results of a postal survey in a county of Sweden", *Elsevier, Pain*, 37 (1989) 215-222.
- Fejer R., Kyvik K. O., Hartvigsen J., "The prevalence of neck pain in the world population: a systematic critical review of the literature", *Eur Spine J* (2006) 15: 834-848, DOI 10.1007/s00586-004-0864-4.
- Hoy D., Bain C., Williams G., March L., Brooks P., Blyth F., Woolf A., Vos T., Buchbinder R., "A Systematic Review of the Global Prevalence of Low Back Pain", *Arthritis & Rheumatism*, Vol. 64, No. 6, June 2012, pp 2028 –2037, DOI 10.1002/art.34347

Session 5

Probabilistic computation in stability assessment

Session Chairs

Vadim Belenky

Arthur M. Reed

Linear Seakeeping High Sea State Applicability

Timothy C. Smith, *Naval Surface Warfare Center Carderock Division*, timothy.c.smith1@navy.mil

Kevin M. Silva, *Naval Surface Warfare Center Carderock Division*, kevin.m.silva1@navy.mil

ABSTRACT

The small motion assumption of linear seakeeping codes is well known. The validity of this assumption is investigated by comparisons with a body exact non-linear seakeeping code over a range of significant wave height. A metric based on relative motion is proposed to quantify the validity of the assumption and indicate up to what point linear seakeeping is appropriate.

Keywords: *Linear Seakeeping; numerical simulations.*

1. INTRODUCTION

Despite the advent of relatively computationally fast non-linear time domain seakeeping programs, there is still some use for linear strip-theory seakeeping programs. Frequency domain programs can produce seakeeping predictions for many speeds, relative wave headings, and seaways in seconds of computation. This is especially useful for including seakeeping in early design analysis of alternatives and calculating mission operability. Time histories based on linear response amplitude operators (RAOs) are also fast to compute and provide representative motions for ship system design/evaluation.

The main assumptions of linear strip-theory seakeeping codes are well known. The first is that calculations are performed about the mean undisturbed waterline. Hydrostatics, radiation, diffraction, and incident wave forces are all calculated on the submerged portion of the hull at the mean undisturbed waterline. This is also stated as a “wall sided” and “small motion” assumptions. These descriptions explain in a physical sense what using the mean undisturbed waterline to define the submerged hull actually means. “Wall sided” indicates that the hydrostatic properties are not changing as the ship moves. “Small motion” indicates that the submerged geometry used for radiation, diffraction, and incident wave force calculations can be considered constant. O’Dea and Walden (1985) examined linear seakeeping with respect to bow flare and wave steepness.

The other main assumption of linear strip-theory seakeeping relates to the independence of the two dimensional strips. The strips are assumed to be independent but in actuality flow from one will influence flow from strips further aft. As a result low speed strip-theory is limited to Froude numbers less than 0.3-0.35. Higher speed strip-theories have been formulated. This paper does not address the validity of using low speed strip-theory above Froude numbers of 0.3-0.35.

Lastly, as a direct result of having a constant submerged volume, the equations of motion can be solved for a unit wave height and linearly scaled to higher wave heights. This is most obviously seen with heavily damped heave and pitch motion. However, roll has non-linear damping and most linear seakeeping programs have some iterative or computational scheme to account for this and do not scale roll linearly with wave height.

However, seakeeping predictions in very small waves, where linear seakeeping assumptions are valid, are not very useful. Fortunately, the assumptions can be stretched and produce useful results at wave heights of interest. This paper discusses a metric to identify when the linear seakeeping assumptions are more than stretched but broken.

2. COMPARISON APPROACH

The validity of linear scaling of results will be determined by comparing linear strip theory results with non-linear time domain results for the same hull form, loading condition, and seaways. Heave,

pitch, and roll root mean square (RMS) values will be compared for a range of wave heights. The comparison will be made as a ratio of the RMS motion value at a given wave height over the RMS motion value of the lowest wave height considered. For linear response, that ratio is a straight line when plotted against wave height. Non-linear response will deviate from that line.

Motions will be calculated at 15 knots ($Fr=0.2062$) for headings from head to following seas in 30 deg increments. While this is not a complete matrix, it avoids higher Froude numbers and provides enough headings for a preliminary evaluation. The wave heights considered range from 3.25m to 12m in 1.75m increment. This is from mid-Sea State 5 to mid-Sea State 8 following STANAG 4194 (NATO 1983). The wave heights corresponds to 0.5 to 1.84 times the draft. A 14 second modal period is used for all the wave heights, so the steepness increases with wave height. The waves are long-crested. The spectra shape is Bretschneider.

The hull form used for this study is a generic naval combatant that has been widely studied in the public domain (DTMB model 5415) (Longo and Stern, 2005). See Figure 1 for a view of geometry and Table 1 loading condition details at full scale.

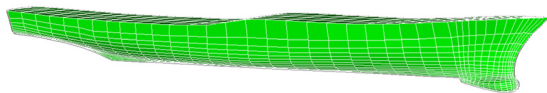


Figure 1: Geometry of model 5415

Table 1: Full scale principle dimensions of DTMB 5415.

Parameter	Units	
Length between Perpendiculars	m	142.0
Beam	m	18.87
Draft, baseline	m	6.51
Trim (+bow down)	m	0.00
Displacement	tonnes	9381.8
LCG (aft FP)	m	72.14
KG	m	7.86
GM	m	1.63
Roll Gyradius	m	7.05
Pitch Gyradius	m	35.5
Yaw Gyradius	m	35.5

This hull form is a traditional monohull with a small amount of flare forward. As most of the hull is “wall sided” the expectation is that linear strip theory should be appropriate at a much higher wave height than hull forms with more variation.

The simulation tools used for this study are Navy Ship Motion Program (SMP95) (Conrad, 2005; Meyers and Batis, 1985; Meyers et al., 1981) and Large Amplitude Motion Program (LAMP) (Lin et al., 1990, 1994). SMP95 is a linear strip-theory seakeeping code first developed in 1981 that uses the Salvensen-Tuck-Faltinsen strip-theory (Salvensen et al., 1970) with modified forward-speed terms. It uses Frank’s close-fit method (Frank, 1967) to calculate radiation forces. Roll damping is estimated from appendage geometry using Ikeda-Tanaka-Himeno (1978) and Kato (1958) empirical formulae. Non-linear roll damping is included by an iterative process to match the calculated response with roll angle associated with the roll damping estimate used to calculate the response. SMP95 calculates motions, velocities, and accelerations at center of gravity and defined points, as well as, relative motion between points on the hull and the incident wave.

LAMP is a time domain ship motion and wave loads simulation code that was developed by Science Applications International Corporation (SAIC) beginning in 1991 to complement linear frequency domain codes. LAMP calculates three dimensional wave-body hydrodynamics using a potential flow approach. The basic hydrodynamic calculations include non-linear Froude Krylov forces and non-linear hydrostatics as well as linear potential flow calculations. Roll damping, appendage lift and other viscous and vortical forces are estimated using empirical formulae and/or tuned coefficient models. LAMP can calculate combined seakeeping and maneuvering, and includes rigid and elastic beam models for computing hydrodynamic loads. LAMP calculates motions, velocities, and accelerations at center of gravity and defined points, as well as relative motion between points on the hull and the incident wave.

3. COMPARISON RESULTS

The results are non-dimensionalized by dividing by the value associated with the 3.25m

significant wave height. The non-dimensional wave height ranges from 1.0 to 3.69. If the motions scale linearly with wave height, they should follow the same range. Figures 2 to 8 show the comparison of non-linear (LAMP) and linear (SMP95) seakeeping predictions. In Figures 2 and 8, the roll data are not presented due to values being very small in head and following seas.

LAMP heave and pitch results are very close to the linear seakeeping line over the entire wave height range. The differences are most notable at head (0 deg), bow (30deg), and following (180 deg) seas above non-dimensional wave height 2.5 (1.25 times draft). Pitch behavior in beam seas is not linear as values are small. LAMP and SMP95 are very close in dimensional values as well.

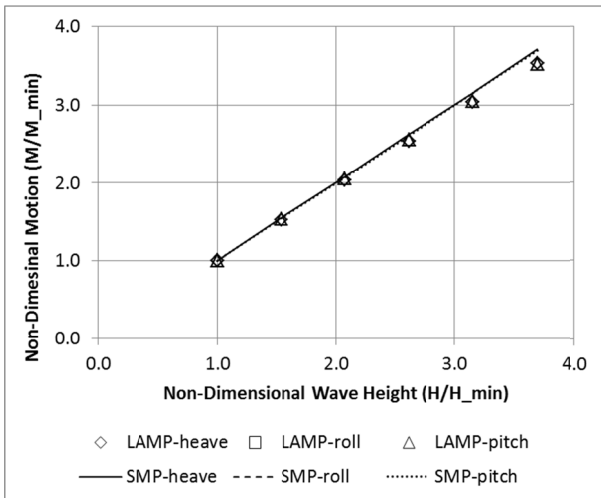


Figure 2: Comparison of non-linear and linear seakeeping at Fr=0.21 and head seas (0 deg).

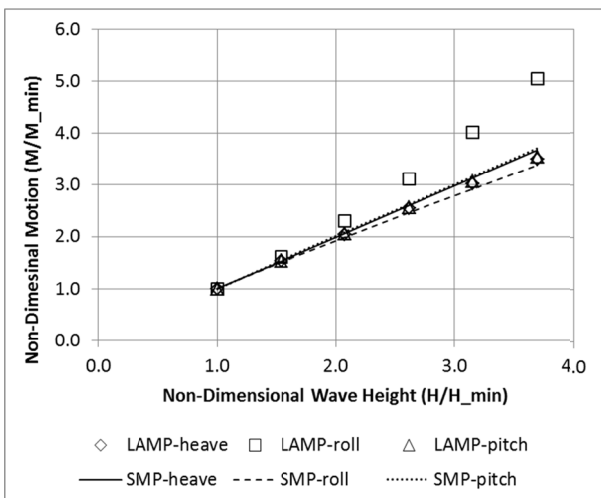


Figure 3: Comparison of non-linear and linear seakeeping at Fr=0.21 and bow seas (30 deg).

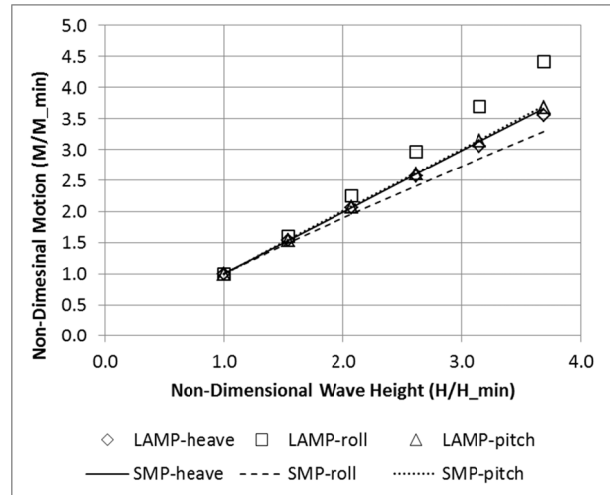


Figure 4: Comparison of non-linear and linear seakeeping at Fr=0.21 and bow seas (60 deg).

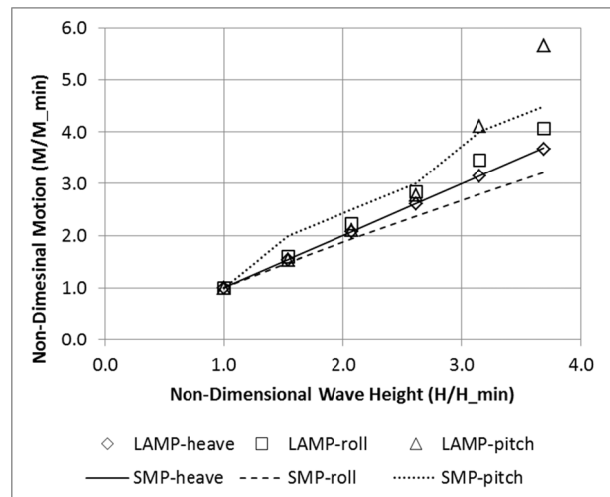


Figure 5: Comparison of non-linear and linear seakeeping at Fr=0.21 and beam seas (90 deg).

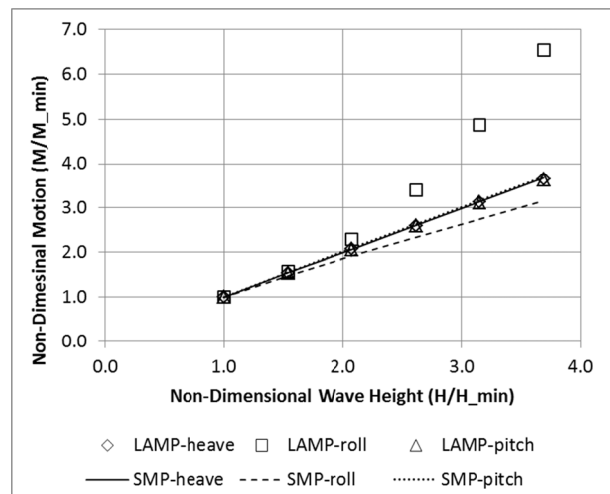


Figure 6: Comparison of non-linear and linear seakeeping at Fr=0.21 and quartering seas (120 deg).

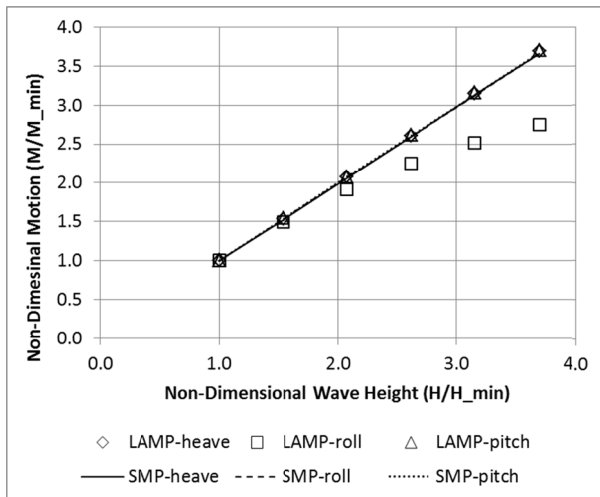


Figure 7: Comparison of non-linear and linear seakeeping at $Fr=0.21$ and quartering seas (150 deg).

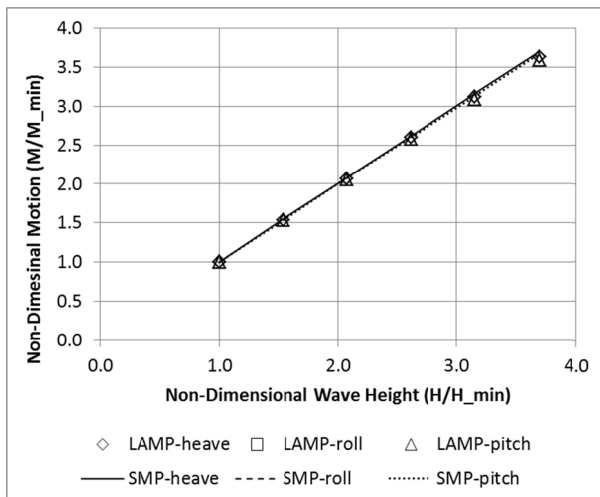


Figure 8: Comparison of non-linear and linear seakeeping at $Fr=0.21$ and following seas (180 deg).

Both LAMP and SMP95 roll results vary from linear behavior as expected. LAMP results have noticeable curvature as the wave height increases. SMP95 results are fairly linear with a different slope than 1:1 with wave height. LAMP roll results are almost twice the SMP95 roll values in dimensionl values. This is explained as difference in roll damping models and appendage suite.

4. APPLICABILITY METRIC

Grigoropoulos et al. (2003) indicates strip theory is appropriate for displacement monohulls under $Fn=0.3$. However, the RoPax ferry did not perform as well as expected. While the geometry is vertical above the waterline, the below waterline shape has significant taper. DTMB model 5415 has a relatively large bilge with nearly vertical sides at the waterline along most of the length. A typical oil tanker has vertical sides for most of it's length

and depth. Hull form considerations lead to a metric that quantifies the validity of linear seakeeping based on changes of waterplane area and relative motion.

An informal metric is that linear seakeeping is appropriate if the relative motion is less than half the draft; essentially to the top of the turn of the bilge. The rationale being this is the wall sided portion of the hull and the concern is motion relative to wave, not absolute motions. This metric is somewhat vague in terms of relative motion statistic, e.g., RMS, 1/10th highest, and point location.

Following Meyers et al. (1981) and applying the Rayleigh distribution, the probability of relative motion, σ , exceeding half the draft (critical distance D) can be found by

$$P = e^{-D^2/2\sigma^2} \quad (1)$$

The probability where the linear and non-linear results diverge becomes the limit of linear seakeeping applicability. Even so, this is somewhat subjective in terms of location of points at which to evaluate relative motion and selection of critical distance, e.g., half the draft.

This study proposes using points at 0.25LBP and 0.75LBP, centerline, and baseline to evaluate relative motion with respect to incident wave. The quarter length points bracket parallel middle body locations while representing some of the fore and aft geometry changes. The critical distance is the average of the distance from the mean waterline to where the station becomes decidedly non-vertical. This definition accommodates different hull geometries from RoPax ferry to oil tanker. For this case, the critical distance is half the draft (3.251m).

Also, note that the probability changes with speed and heading, so some minimum probability should be selected as the limit of applicability. Figures 9 to 12 show the probability of the SMP95 relative motion exceeding half the draft for cases that showed a difference between LAMP and SMP95. The forward point is the limiting point and as wave heading move aft of beam, the forward point line moves towards the aft point line and becomes coincident.

Looking at head seas, Figure 2 and Figure 9, LAMP heave and pitch are approximately 2% less than linear value near non-dimensional wave height

of 2 with a probability 0.14 for the forward point. The probabilities at bow seas are less for similar motion differences. Other headings have lower probabilities and less difference in motions for the same wave height. Roll shows more non-linearity, but within 10% difference at 2.0 non-dimensional wave height.

The threshold value to exceed, allowable motion difference, and relative motion point location are all inter-related and acceptability limits cannot be set independently. So taking the relative motion point location as the forward point and accepting 2% difference between linear and non-linear results sets the threshold probability at 0.14. So for other destroyer-like hull forms, if the probability of a forward relative motion point is less than 0.14, the difference between linear and non-linear response is less than 2%. Other relative motion points and acceptable differences would have other associated probabilities.

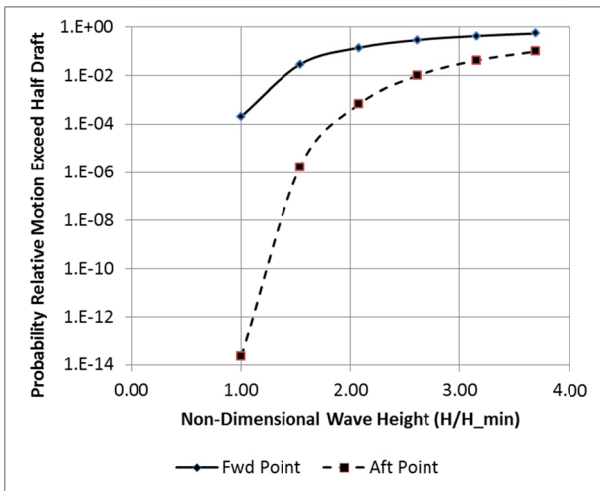


Figure 9: Probability of relative motion at bow and stern exceeding half the draft at Fr=0.21 and head seas (0 deg).

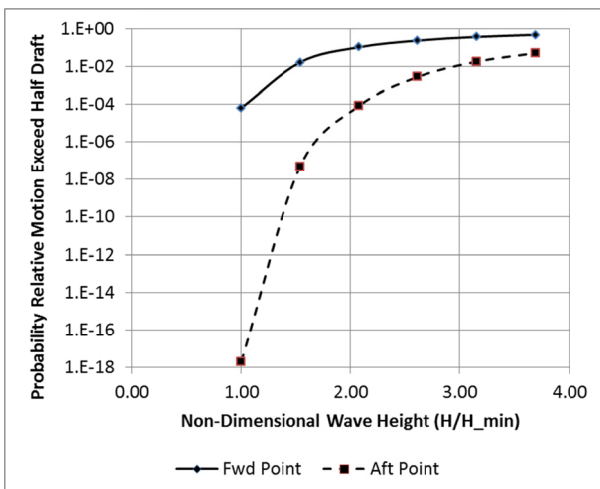


Figure 10: Probability of relative motion at bow and stern exceeding half the draft at Fr=0.21 and bow seas (30 deg).

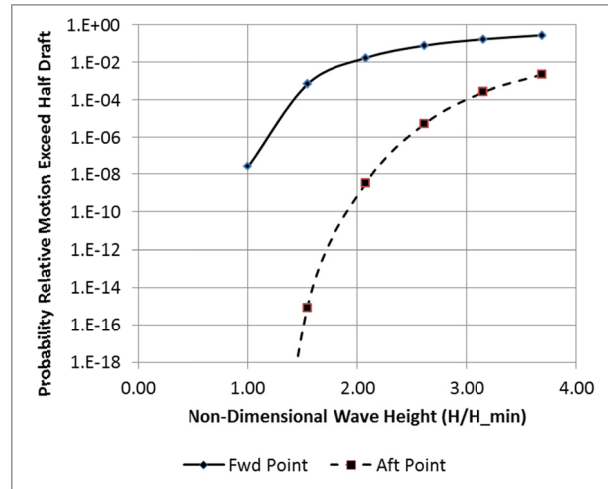


Figure 11: Probability of relative motion at bow and stern exceeding half the draft at Fr=0.21 and bow seas (60 deg).

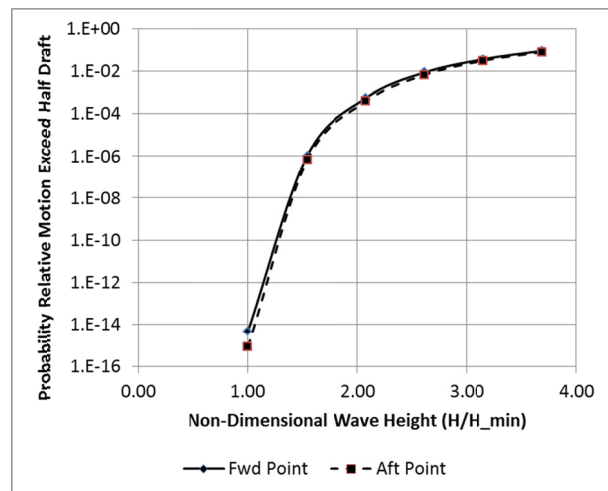


Figure 12: Probability of relative motion at bow and stern exceeding half the draft at Fr=0.21 and following seas (180 deg).

5. CONCLUSIONS

This study proposed a metric to quantify the applicability of linear strip-theory seakeeping. Motions were calculated for DTMB model 5415 using SMP95 and LAMP for a range of wave heights, a single speed, and multiple headings. The motions were compared to see where non-linear effects were apparent and important to the root mean square of the motions. A metric based on the probability of the relative motion exceeding a critical distance was proposed to define the range of applicability of linear strip-theory seakeeping predictions. This approach shows promise but needs to be expanded to other speeds and hull forms to determine general applicability. Other statistics such as average of 1/10th highest may provide more discrimination than root mean square

statistic. Additionally, there may be some complementary metric based on variation in waterplane area that would improve selection of critical distance.

6. ACKNOWLEDGEMENTS

The author would like to thank the many who discussed the idea and provided invaluable computational support. Mr. Robert “Tom” Waters provided a rough idea of the relative motion metric. Mr. Andrew Silver first used the probability of keel emergence in a systematic way in 2016. Mr. Kenneth Weems provided the description of LAMP and the input files for the LAMP calculations.

REFERENCES

- Conrad, R., 2005, SMP95: Standard Ship Motion Program User Manual,” NSWCCD-50-TR-2005/074.
- Frank W., 1967, “Oscillation of Cylinders in or Below the Free Surface of Deep Fluids” DTNSRDC, Rep. No. 2375, Washington, D.C.
- Grigoropoulos, G., Harries,S.,Damala, D., Birk, L. and Heimann, J., 2003, Seakeeping assessment for high-speed monohulls –A comparative study, 8thIntl. Marine Design Conf., Athens, 5-8 May.
- Ikeda, Y., Himeno, Y., and Tanaka, N., 1978, “Components of Roll Damping of Ship at Forward Speed,” Journal of Society of Naval Architects of Japan, Vol. 143.
- Kato, H., 1958, “On the Frictional Resistance to the Roll of Ships,” Journal of Society of Naval Architects of Japan, Vol. 102.
- Lin, W. M., and Yue, D. K. P., 1990, “Numerical Solutions for Large-Amplitude Ship Motions in the Time-Domain,” Proc. the 18th Symposium on Naval Hydrodynamics, The University of Michigan, Ann Arbor, Michigan.
- Lin, W. M., Meinhold, M. J., Salvesen, N. and Yue, D. K. P., 1994, “Large-Amplitude Motions and Waves Loads for Ship Design,” Proc. the 20th Symposium on Naval Hydrodynamics, University of California, Santa Barbara, California.
- Longo J., Stern F., 2005: “Uncertainty Assessment for Towing Tank Tests With Example for Surface Combatant DTMB Model 5415.”J. Ship Research. 49 (1) 55-68.
- Meyers W.G., Baitis A.E., 1985, “SMP84: improvements to capability and prediction accuracy of the standard ship motion program SMP81” DTNSRDC/SPD-0936-04.
- Meyers, W. G., Applebee, T. R., Baitis, A. E., 1981, “User’s Manual for the Standard Ship Motion Program, SMP,” DTNSRDC/SPD-0936-01.
- NATO Military Agency of Standardisation, 1983, STANAG 4194 Ed3, “Standardized Wave and Wind Environments and Shipboard Reporting of Sea Conditions”.
- O’Dea, J. F. and Walden, D. A., 1985, The Effect of Bow Shape and Nonlinearities on the Prediction of Large Amplitude Motions and Deck Wetness,” 15th Symposium on Naval Hydrodynamics, Hamburg, Germany, Sep 1984, pp. 163-176.
- Salvesen N., Tuck E.O., Faltinsen O., 1970,“Ship Motions and Sea Loads” Trans. SNAME 78: 250-287.

Including Diffraction and Radiation into Probabilistic Description of Capsizing

Kenneth Weems, *Naval Surface Warfare Center Carderock Division*

Vadim Belenky, *Naval Surface Warfare Center Carderock Division*

ABSTRACT

The paper reviews recent development on the assessment of the probability of capsizing in irregular waves using the split-time method with advanced numerical simulation codes. Particular attention is focused on including diffraction and radiation forces in motion perturbation simulations as well as generalizing the calculation scheme for 6 degrees of freedom. The implementation is based on the Large Amplitude Motion Program (LAMP), which is a hybrid code combining body-nonlinear formulation for hydrostatic and Froude-Krylov forces, a potential flow solution for diffraction and radiation and external coefficient-based models for viscous and vortical forces.

Keywords: *Probability of capsizing, numerical simulations, split-time method, motion perturbation.*

1. INTRODUCTION

This paper describes the implementation of the split-time method for the probabilistic assessment of capsizing in irregular waves using advanced numerical codes. It is a direct continuation of the paper presented at the previous workshop (Weems and Belenky, 2016). The motivation and general framework of this development was included in the cited paper and is not repeated in detail here. However, it should be noted that a key element of the split-time method is the use of motion perturbation simulations to compute a metric of the likelihood of capsizing when a particular event occurs in the course of normal random-wave time-domain simulations. In the present work, the event is the upcrossing of an intermediate threshold roll angle and the metric is based on the difference between the ship's roll rate at the upcrossing and a "critical" roll rate which would lead to capsizing. This critical roll rate is computed by performing a series of perturbed motion simulations starting at the upcrossing point with different roll rates. It is the implementation of these perturbed motion simulations which is the focus of the present paper.

2. LAMP

LAMP development began in the early 1990s in order to provide a nonlinear, time-domain prediction of ship motions and loads in waves (Lin

and Yue 1990) that would complement linear frequency domain analysis. The submerged portion of the body is represented with a general 3-D panel model, so there are very little limitations in terms of what kind of ship geometry can be handled by LAMP, see Figure 1.

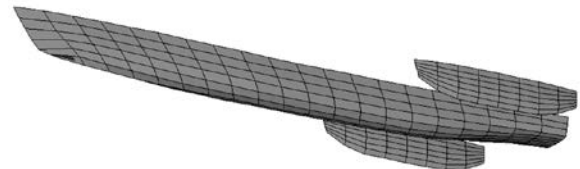


Figure 1: Example of trimaran geometry (Shin, et al 2003)

Hydrostatic and Froude-Krylov forces are generally computed by the integration of pressures over the instantaneous wetted portion of the panel model up to the incident waterline. There is an option to compute Froude-Krylov forces up to the mean waterline and hydrostatic restoring forces from waterplane quantities, but this option is used mostly only for comparison with linear frequency domain codes and the quantification of nonlinear effects (Smith and Silva, 2017).

Forces related to the disturbance of the wave surface by the ship, which includes radiation, diffraction and forward speed effects, are computed by distributing Rankine singularities over the body and free surface panels. The far-field influence is modeled with the damping beach or a set of transient Greens functions distributed over a

matching surface. Figure 2 shows an example of LAMP computational domain for a naval combatant.

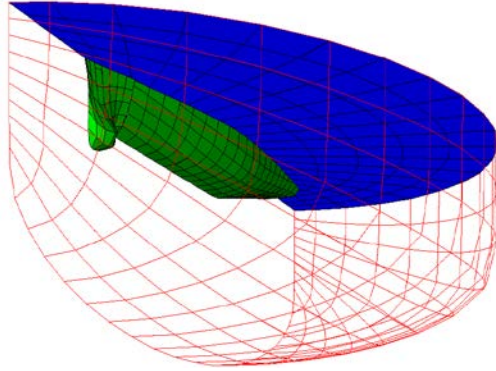


Figure 2: Example of LAMP computational domain

In the general case, the velocity potential of the wave-body disturbance is computed by applying combined body and linearized free surface boundary conditions, advancing the free surface in time, solving for the disturbance potential and computing the surface pressure distribution using Bernoulli's equation. This is known as the "direct" solution. The solution has been implemented in two coordinate systems. The basic solution is solved in a sliding system which moves with the constant forward speed, which provides robustness but cannot be used for cases with large lateral motion (large sway or yaw or significant change in speed). The extended solution allows large lateral motion but may require a smaller time step for stability.

An alternative is the Impulse Response Function (IRF) based solution, in which the perturbation velocity potential on each body panel is decomposed as:

$$\Phi_k(\vec{x}, t) = \sum_{k=1}^6 \Phi_k(\vec{x}, t) + \Phi_7(\vec{x}, t) + \Phi_8(\vec{x}, t) \quad (1)$$

where the Φ_k , $k=1..6$ are the radiation potentials for the six rigid-body motions, Φ_7 is the diffraction potential related to the incident wave potential Φ_0 , and Φ_8 is the steady state potential related to the constant forward speed U . To solve for the six radiation potentials Φ_k , six corresponding impulse response functions φ_k are introduced via the convolution integral:

$$\Phi_k(\vec{x}, t) = \int_0^t \varphi_k(\vec{x}, t - \tau) \dot{X}_k(\tau) d\tau \quad (2)$$

where X_k is the ship motion in mode k and the dot signifies the derivative with respect to time. The diffraction potential Φ_7 , the diffraction IRF φ_7 is introduced via the convolution integral

$$\Phi_7(\vec{x}, t) = \int_{-\infty}^{\infty} \varphi_7(\vec{x}, t - \tau) \zeta_0(\tau) d\tau \quad (3)$$

where ζ_0 is the incident wave elevation at the origin of the ship-fixed frame. In its present implementation, the IRF formulation is solved in the sliding system and cannot be used for cases with large lateral motion (large sway or yaw or significant change in speed). Further details on IRF formulation can be found in Weems, et al. (2000), while a summary description is available in Shin, et al. (2003).

There are two options for the principle frame of reference of the dynamic solver: ship-fixed and global. In either frame of reference, individual modes can be free, constrained or prescribed.

Different combinations of these options provide different "levels":

LAMP-1 Body-linear solution is used for both Froude-Krylov/hydrostatic and diffraction/radiation forces; limited to small lateral motions; IRF option is available. Not suitable for capsizing simulation due to linear restoring.

LAMP-2 Body-nonlinear solution for Froude-Krylov/hydrostatic forces and body-linear solution for diffraction and radiation; limited to small lateral motions; IRF option is available. Suitable for 3-DOF capsizing simulations where surge, sway and yaw are constrained to constant forward speed.

LAMP-3 Body-nonlinear solution for Froude-Krylov/hydrostatic forces and body-linear solution for diffraction and radiation; allows large lateral motion but is limited to ship-based motion constraints. Suitable for 6-DOF capsizing simulations.

LAMP-4 Body-nonlinear solution for both Froude-Krylov/hydrostatic forces, diffraction and radiation; allows large lateral motion. LAMP-4 is too slow to be practically used in perturbation simulations for all but exploratory studies and has not been fully integrated into the present rare problem solver. However, a set of exploratory studies for critical roll rate in calm water suggested that the body-nonlinear disturbance potential had little effect on the critical roll rate.

In addition to these levels, there is an option to suspend the potential flow solution of the wave-body disturbance and substitute user-defined coefficients for diffraction and radiation forces. This option is referred to as LAMP-0 and can be used with global or ship-based constraints.

3. LAMP_LITER

LAMP_Liter is a specialized implementation of the LAMP solver that performs motion perturbation simulation from the instants of upcrossing of the intermediate level by the roll motion, iterating to find the critical roll rate leading to capsizing. The general structure of the program is described in Weems and Belenky (2016), presented at the previous workshop; the present focus is on computational / modeling aspects of the problem.

LAMP_Liter can be configured with any of LAMP's hydrodynamic and dynamic options other than LAMP-4. The configuration and options of the perturbation simulation, which is part of the "rare" problem, does not need to exactly match the configuration for the original random wave simulation, which is the non-rare problem. As a result, it is possible to run the non-rare problem with LAMP-2 and then opt for LAMP-0 for the rare problem. Justification of these and other modeling choices must come from the context of the problem.

The ability to prescribe individual modes of motion has been used to allow a "mix-and-match" of degrees of freedom in the perturbation simulations. It is possible to simulate the perturbed motion in some mode(s) while using unperturbed solution for the rest. For example, 1-DOF roll only simulations can be performed for 3-DOF or 6-DOF non-rare data by allowing roll to be a free mode of motion while all other modes are prescribed using the results of the original non-rare simulation. Similarly, a 3-DOF (heave, roll, pitch) perturbation simulation could be used with a 6-DOF non-rare solution by prescribing surge, sway and yaw to match the unperturbed solution. This latter option preserves the ship's position in the wave from the original simulation.

Some care must be taken in selecting the dynamic system and motion constraints. For example, if a 3-DOF (heave, roll, pitch) set of constraints are applied in the ship-fixed system, the yaw constraint becomes un-physical as the roll angle nears 90 degrees. This is generally not a

problem when roll motions are moderate but can become so for perturbation simulations searching for very large roll motions or the transition to capsizing.

The biggest challenge with LAMP-based perturbation simulations is the potential flow based hydrodynamic disturbance inducing radiation and diffraction.

LAMP-0 3DOF

The most basic LAMP-based capsizing analysis is a 3-DOF (heave-pitch-roll) motion using the LAMP-0 model. It provides a verification of the implementation of the motion perturbation method in LAMP and can be directly compared to simpler models such as the SimpleCode that was used for statistical validation of the split-time method (Weems *et al.* 2016). Since the LAMP-0 model does not include the potential flow hydrodynamic disturbance model, it can provide directly continuous perturbation simulation from the crossing point (Weems and Belenky 2016).

LAMP-2 Direct Calculations

The first significant challenge introducing LAMP-2 hydrodynamics into the perturbation simulations is the transition of the hydrodynamic disturbance model. The most straight-forward approach is the "dead start" concept. In this approach, the hydrodynamic solution is being re-initialized at the start of each perturbation simulation, with the disturbance potential and elevations set to zero. The radiation and diffraction forces at the start will also be zero at the start of the perturbation, but are calculated as the simulation proceeds. Initial calculations in low to moderate speed (up to 15 knots) have shown this approach to be very effective, with only minor difference in motion for an "unperturbed" simulation, starting at the upcrossing point with the observed upcrossing rate as compared to the original non-rare simulation. While this may become more of an issue for higher speeds, the effects of inertia and restoring are still likely to dominate at larger initial roll rates.

A second potential issue with LAMP-2 hydrodynamics is the body-linear formulation of the potential flow problem, which is solved over the mean wetted surface. As the roll angle gets very large, this solution loses accuracy and may become numerically unstable. However, this instability has

only been observed when the roll angle exceeds 100~120 degrees, at which point the capsizing event already became a certainty and the critical roll rate evaluated. In order to enable simulation beyond those values, the calculations switch to the coefficient-based hydrodynamic forces model once the roll angle exceeds the prescribed value.

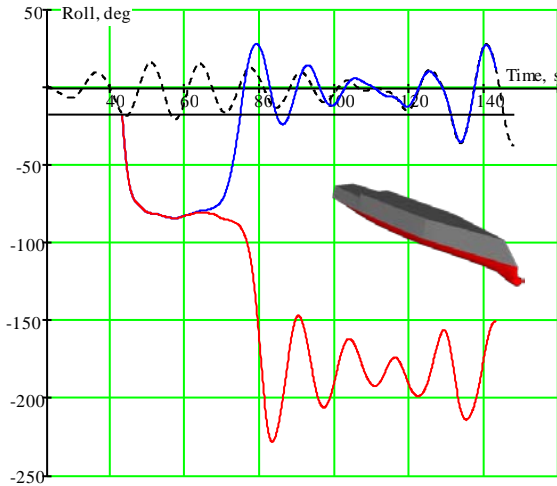


Figure 3: Perturbed and unperturbed roll motions calculated with LAMP-2

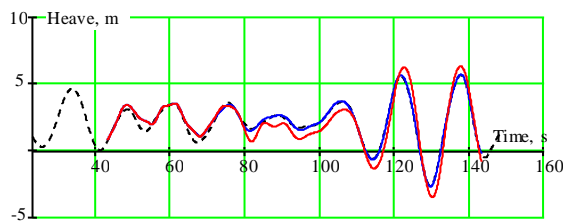


Figure 4: Perturbed and unperturbed heave motions calculated with LAMP-2.

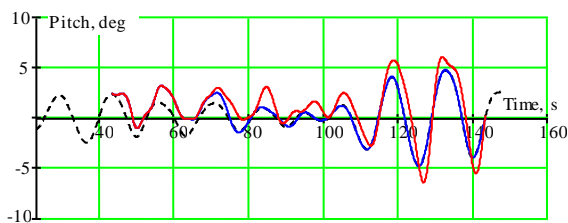


Figure 5: Perturbed and unperturbed pitch motions calculated with LAMP-2.

Figure 3 through 5 shows the results of a set of perturbation calculations using the direct LAMP-2 hydrodynamic calculations. The ship is the tumblehome variant of the ONR Toppides Series. The seaway is long-crested and is modeled by a Bretschneider spectrum with a significant wave height of 9.0m and modal period of 14.0 seconds. The ship speed is 10 knots and the heading is 45° (stern quartering waves). The dashed line indicates

the original “non-rare” simulation. Two perturbed solutions from the iteration for the critical roll rate are plotted. The first (blue) is just short of capsizing while the second (Red) is the smallest roll rate perturbation leading to capsizing. As expected, roll time history exhibits “hanging” around simultaneous position of unstable equilibrium before “deciding to capsize or not.” The duration of this hesitation depends on the tolerance required from the iterative process.

A second approach that has been explored for LAMP-2 motion perturbation simulations is the “re-start” concept. In this approach, the numerical solution– disturbance potential, free surface elevations, etc. – of the non-rare solution is stored at the moment of upcrossing and then used to initialize each perturbation calculation. This provides a full hydrodynamic solution from the start and a completely smooth transition when the perturbations are small, but the jump in velocity for larger perturbations can cause a larger problem than the dead start case. The complexity of identifying upcrossings and saving restarts during the non-rare run is a disadvantage to this approach.

Some of the disadvantages of both the deadstart and restart approaches could be mitigated by starting the perturbation simulation a short time before the upcrossing and prescribing all modes of motion up to the upcrossing point. This would mitigate the impulsive start of the deadstart approach and allow restart sets to simply be periodically saved without having to identify upcrossings in the non-rare problem. The perturbation could be feathered into the prescribed motion period. This approach has not been fully implemented but is being considered for future work.

LAMP-2 IRF Calculations

The IRF formulation was originally implemented to speed up simulations, as the cost of the convolutions with pre-computed IRF potentials is a fraction of the direct method, and a set of IRF potentials is dependent only on speed and heading and can be re-used for many wave conditions.

The same is true for the perturbation calculations, however there are additional benefits. The diffraction potential (3) does not include motions, only incident wave elevations. As the wave elevations are known exactly, the complete

diffraction potential can be used from the start of the perturbation. The steady forward speed potential, Φ_8 in (1), can also be used from the start. Only the radiation potential (2) needs to be re-started, and that could be mitigated by initializing the motion history with non-rare data, though this has not been done in the present simulations.

Figures 6 through 8 shows the original solution (dashed line) and two perturbations (solid lines: red – leading to capsizing and blue – short of capsizing). It is noticeable that the difference between the direct and IRF calculation is not that large actually. However, it is still too early to make any conclusions about the effect of diffraction and radiation forces on capsizing in the perturbation simulations.



Figure 6: Perturbed and unperturbed roll motions calculated with LAMP-2 / IRF option.

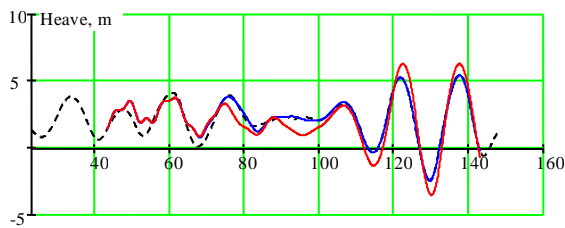


Figure 7: Perturbed and unperturbed heave motions calculated with LAMP-2 / IRF option.

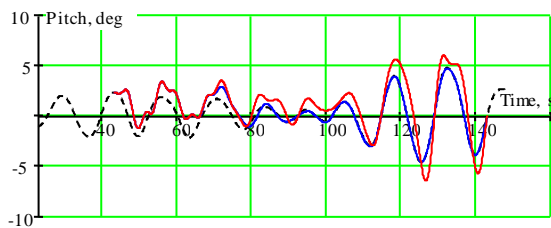


Figure 8: Perturbed and unperturbed pitch motions calculated with LAMP-2 / IRF option.

LAMP-0 6-DOF

The next complication in perturbation simulations is to include all 6 degrees of freedom. Including horizontal motion into a potential flow code is not trivial as the flow model does not implicitly capture maneuvering forces of a viscous or vortical nature. Modeling maneuvering forces with coefficients from a model test or CFD calculation is also not trivial as both experimental and CFD data do include wave forces that are also internally calculated within a potential flow code. To avoid potential double counting for wave forces, they have to be “subtracted” from the empirical coefficients, see Lin, *et al* 2006 for details.

A set of 6-DOF perturbation simulations are presented in Figure 9 through 14.

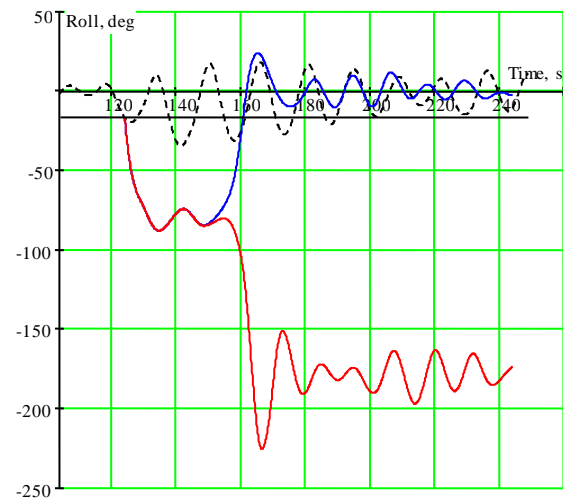


Figure 9: Perturbed and unperturbed roll motions calculated with LAMP-0 / 6-DOF

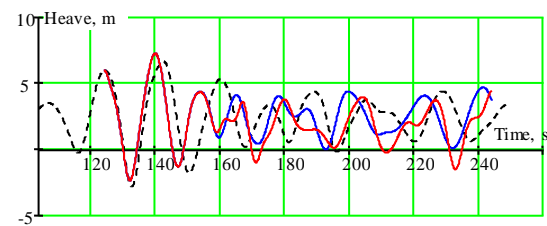


Figure 10: Perturbed and unperturbed heave motions calculated with LAMP-0 / 6-DOF.

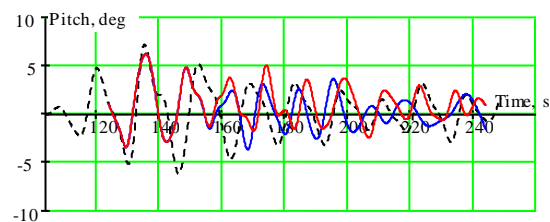


Figure 11: Perturbed and unperturbed pitch motions calculated with LAMP-0 / 6-DOF.

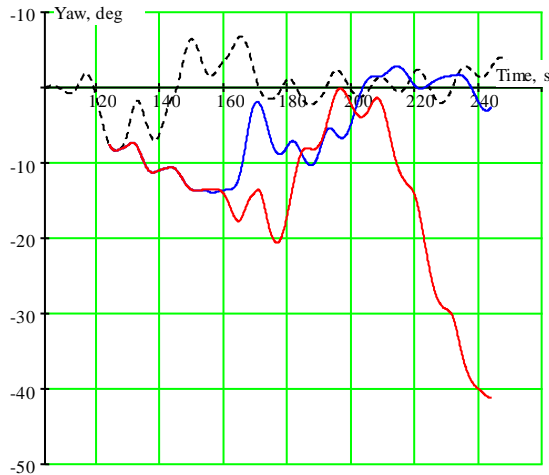


Figure 12: Perturbed and unperturbed yaw motions calculated with LAMP-0 / 6-DOF.

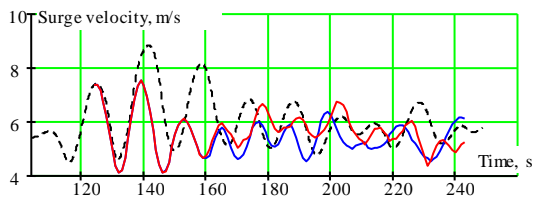


Figure 13: Perturbed and unperturbed surge velocity calculated with LAMP-0 / 6-DOF.

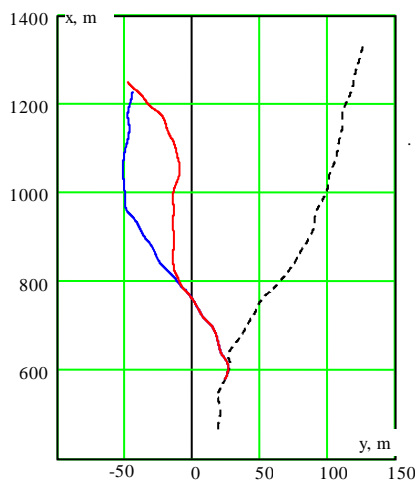


Figure 14: Perturbed and unperturbed trajectories calculated with LAMP-0 / 6-DOF

The results presented in Figure 9 through 14 are computed with LAMP-0, which is a natural starting point. While, in principle, the problem of double counting in the inclusion of horizontal motions has been solved, the full implementation of direct LAMP-3 hydrodynamic calculations for perturbations had not been completed at the time of writing this paper.

As expected in Weems and Belenky (2016), the 6-DOF perturbed solutions do not necessarily converge to the unperturbed time history as in the

3-DOF. The development of significant unsteady surge, sway motion and yaw angle (Figure 12) means that the ship in the perturbation simulations may encounter different waves in different places as it can be seen from trajectories in Figure 14. As a result, the convergence of the motion history can no longer be used as a criteria for truncating perturbation simulations. Aside from this, the 6-DOF rare problem is fundamentally identical to the 3-DOF problem.

As described above, the perturbation simulations for 6-DOF non-rare motions can alternatively be performed with 3-DOF (heave, roll pitch) or even 1-DOF (roll) free motions. The appropriateness of different DOFs, and of modeling options in general, will depend on the requirements of the perturbation-based analysis. For the present application of the split-time method to pure-loss-of-stability events, reduced DOF solutions appear to be adequate, but the full effects of DOF have yet to be evaluated.

4. SUMMARY AND CONCLUSIONS

The paper continues the discussion from the previous workshop regarding the implementation of motion perturbation analysis in a numerical seakeeping code. The focus is on the LAMP-based solution of the rare problem for critical roll rate in the split-time method for estimating a probability of capsizing in irregular waves.

Those motion perturbations are handled by a special implementation of the LAMP solver called LAMP_LITER. LAMP_LITER can be configured to use a number of computational models and up to 6-DOF, using direct calculations of diffraction and radiation, while an option to use pre-computed IRFs is available for select models.

The principal conclusion is that it is possible to implement motion perturbation simulations within the framework of potential flow hybrid codes originally intended for large amplitude motions and loads. However, the implementation is non-trivial and some effort is required in order to ensure that the code and selected options are appropriate to and consistent with the analysis being undertaken. In particular, it does appear that such codes can be incorporated within the split-time method for evaluating extreme events.

ACKNOWLEDGEMENTS

The work described in this paper has been funded by the Office of Naval Research through the NSWCCD Independent Applied Research (IAR) program under Dr. Jack Price.

Discussions with Dr. S. Zhang of NSWCCD have been very helpful.

REFERENCES

- Lin, W.M., and Yue, D.K.P., 1990 "Numerical Solutions for Large Amplitude Ship Motions in the Time-Domain," *Proc. 18th Symp. on Naval Hydrodynamics*, Ann Arbor, Michigan, USA, pp. 41-66
- Lin, W. M., Zhang, S., Weems, K. and D. Luit, 2006 "Numerical Simulations of Ship Maneuvering in Waves", *Proc. of 26th Symp. on Naval Hydrodynamics*, Rome, Italy.
- Shin, Y.S, Belenky, V.L., Lin, W.M., Weems, K.M. and A. H. Engle 2003 "Nonlinear time domain simulation technology for seakeeping and wave-load analysis for modern ship design" *SNAME Trans.* Vol. 111, pp. 557-578.
- Smith, T. and K. Silva, 2017 "Linear Seakeeping High Sea State Applicability," *Proc. 16th Intl. Ship Stability Workshop*, Belgrade, Serbia.
- Weems, K., Lin, W.M., Zhang, S, Treacle, T., 2000. "Time Domain Prediction for Motions and Loads of Ships and Marine Structures in Large Seas Using a Mixed-Singularity Formulation", *Proc. OC2000*, Osaka, Japan.
- Weems, K., and V. Belenky, 2016 "Split-time Algorithm Implementation in Advanced Hydrodynamic Codes" *Proc. 15th Intl. Ship Stability Workshop*, Stockholm, Sweden, pp. 83-88.
- Weems, K., Belenky, V., Campbell, B. 2016 "Validation of Split-time Method with Volume-Based Numerical Simulation", *Proc. 15th Intl Ship Stability Workshop*, Stockholm, Sweden. pp. 103-108.

This page is intentionally left blank

Modeling Broaching-to and Capsizing with Extreme Value Theory

Vadim Belenky, *Naval Surface Warfare Center Carderock Division*

Kenneth Weems, *Naval Surface Warfare Center Carderock Division*

Kostas Spyrou, *National Technical University of Athens*

Vladas Pipiras, *University of North Carolina, Chapel Hill*

Themistocles Sapsis, *Massachusetts Institute of Technology*

ABSTRACT

The paper reviews recent research on the application of extreme value theory for stability failures associated with qualitative physical change: capsizing in waves with account of stability change in waves and broaching-to. As these events are very rare, direct numerical simulation of these events with a code of reasonable fidelity is hardly practical. The assessment of probability must therefore be done without direct observation. This is done using the split-time framework, in which a metric of the likelihood of the failure is introduced. The metric is computed by perturbation of the dynamical system, in phase space, towards the failure state, therefore accounting for changing physics of extreme motions. Extreme value theory is applied to this metric to extrapolate a rate of failure.

Keywords: *Broaching-to, Capsizing in waves, Extreme values*

1. THEORY OF EXTREME VALUES

Any intact stability failure is an extreme event in the sense that its probability is very small, so the value of response associated with the failure, which might be a roll angle for capsizing or a yaw deviation for broaching-to, is quite far on the tail of its distribution. Extreme value theory is a part of mathematical statistics that studies those tails.

The essence of the extreme value theory is that the maxima of independent and identically distributed random variables have a limiting distribution, which is known as a Generalized Extreme Value (GEV) distribution. This is stated by the 1st extreme value or Fisher-Tippet-Gnedenko theorem. Another important distribution is the Generalized Pareto Distribution (GPD), which is derived from GEV as a conditional distribution above a “large-enough” threshold. The ability of GPD to approximate any tail above a certain threshold is stated by the 2nd extreme value or Pickands-Balkema-de Haan theorem.

These theorems present a possibility of modeling the behavior of the tail without modeling the entire distribution. This is, indeed, a very attractive way to solve many safety-related

engineering problems because the safety hazards are associated with large and rare excursions. Thus, the probabilistic assessment of ship stability does not require modeling of roll distribution over its full range – it is enough to know the tail. Both GEV and GPD have three parameters, counting location /threshold. It is therefore necessary only to find those parameters from simulated or measured data and the whole problem of probabilistic stability assessment is solved.

Unfortunately, the simplicity of this approach is quite superficial. Available procedures for finding those parameters simply find the values that fit the data best. However, a ship as a dynamical system is nonlinear and the nature of those nonlinearities manifest itself for the large roll angles. Both GEV and GPD are limit distributions so the applicability of extreme value theory is related to the context of the problem and specific physical mechanism of stability failure.

A review and principle logic of the derivation of both extreme value theorems is available from Coles (2001). The first application of extreme value theory to the stability problem is attributed to McTaggart (2000) and McTaggart and de Kat (2000).

2. NONLINEARITY AND STATISTICS

Peak-over-threshold (POT) is a form of application of the extreme value theory to data exceeding a certain threshold. Campbell, et al. (2016) reviewed the application of POT for roll peak data using the GPD. Smith and Zuzick (2015) described a statistical validation effort of roll data POT. The method seems to work well even for a target angle beyond the maximum of the roll restoring (GZ) curve; however, the confidence interval becomes rather large.

In principle, a decrease of the confidence interval may be achieved without increasing the sample size by introducing a deterministic relationship between the GPD parameters based on a physical consideration. If the shape parameter of GPD is negative, it has an upper limit with the probability equal to zero above that limit. Glotzer, et al. (2017) describe how the uncertainty of pitch extrapolation can be decreased by introducing a pitch angle limit of about 12 degrees. This limit was based on the idea that as the longitudinal GZ becomes flat, the ship can no longer receive significant energy from wave excitation.

Peaks of roll motions have a complex distribution tail structure. The possibility of capsizing implies an upper limit of roll peaks as a peak stipulates return. However, the statistics of roll peaks typically shows a positive shape parameter, suggesting that no limit exists. This problem was considered in Belenky, et al. (2016). It was found that the softening nonlinearity of the GZ curve around its maximum value leads to positive shape parameter through stretching in the phase plane.

Nonlinearity of the dynamical system may lead to a complex structure of the distribution tail; however, this structure can be revealed and included into the model.

3. CAPSIZING IN WAVES

Qualitative change of physics

Capsizing is a transition to the motions around another stable equilibrium that is dangerous from practical point of view, i.e. “mast down”. During this transition the dynamical system passes the unstable equilibrium at the point of vanishing stability, see Figure 1. The presence of the unstable equilibrium defines the topology of the phase plane in its vicinity and serves as a “separator” between

the domains of attraction to the motion around the upright and capsized equilibria. This influence in a statistical sense can be detected when the system is passing relatively close to the unstable equilibria (see considerations on “inflection point” in Belenky, et al. (2016a)). Indeed, this information is absent in the roll motion data set that does not contain a statistically significant number of capsizes or “near-misses”.

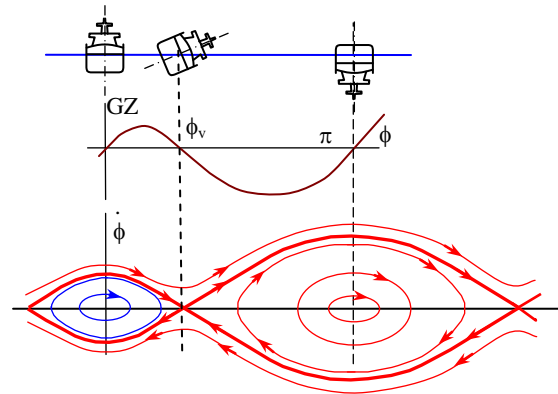


Figure 1: Phase plane of un-damped roll motion.

While the capsizing data is absent from the sample, it is still possible to compute a value reflecting how likely the capsizing is at any given instant of time using the motion perturbation method (MPM). In this method, the roll rate is perturbed until the capsizing is observed (see Figure 2) and the perturbed roll rate is recorded. The difference between the critical roll rate leading to capsizing and the observed roll rate provides a metric of the likelihood of capsizing at this instant of time.

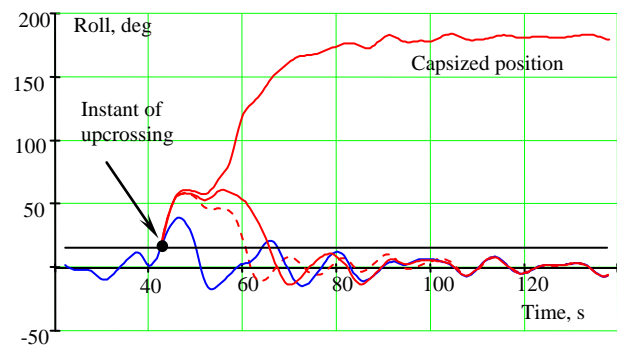


Figure 2: Calculation of critical roll rate (Belenky, et al. 2016b)

This metric is a random variable, as the phasing of the excitation and the stability in wave are random. The metric values can be considered independent if they are computed at the instances

that are far enough from each other – say, beyond the de-correlation duration. The independence of the data points in the sample allows extreme value theory to be applied straightforwardly to the metric values. With the motion perturbation method, the metric sample set reflects the change of physics as all of the effects of the transition are explicitly included in the calculation of the metric. Once the GPD is fitted to the metric data, the probability of capsizing can be found as the probability of the event that the observed roll rate reaches the critical roll rate.

In order to relate the probability of capsizing with time, the calculation of the metric can be carried out at the instant of upcrossing of an intermediate level by the roll angle. Capsizing is therefore defined as an upcrossing of an intermediate level in which the metric of capsizing exceeds its critical value (i.e. distance to failure falls below zero). This is how the probability of capsizing is treated under the split-time framework, whose development is described in Belenky, *et al.* (2016b).

Properties of tail of the metric

The application of the extreme value theory through the split-time method for capsizing has been successfully tested via statistical validation carried out for 14 combinations of sea state, heading and speed combination (Weems, *et al.* 2016). While the performance of the method was good, it could be improved by decreasing the uncertainty of the final estimate. To do this without additional data, the structure of the distribution tail of the metric has to be studied.

Does the distribution tail of the capsizing metric have a limit? Some general argument can be made on this matter. The metric, which is formulated in Belenky, *et al.* (2016b), has two random components:

$$y_i = 1 - \dot{\phi}_{Ui} + \dot{\phi}_{Cri}; \quad i = 1, \dots, N_U \quad (1)$$

$\dot{\phi}_{Cri}$ is the critical roll rate calculated for the i^{th} upcrossing, and $\dot{\phi}_{Ui}$ is the roll rate observed at the i^{th} upcrossing.

Both of these random variables are, in principle, limited. The minimum roll rate at upcrossing is a small positive number; a value of zero corresponds

to a “touch,” so for an upcrossing event to occur, the derivative must be positive.

The critical roll rate must be limited if the capsized equilibrium is stable. Since the capsizing condition always exists in terms of roll velocity, there should be maximum roll rate leading to capsizing from the least probable initial conditions. This idea is illustrated in Figure 3 for the case of damped calm-water roll motion. As the first guess, the limit of the critical roll rate can be taken as an intersection of the separatrix with the vertical axis of the phase plane.

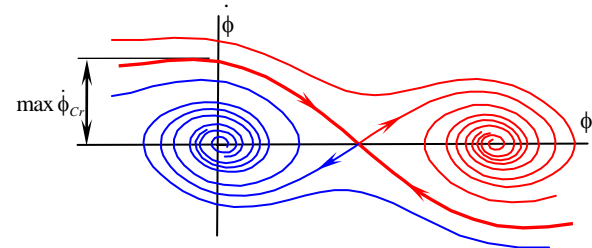


Figure 3: On the maximum critical roll rate

If this argument is correct, the fitting of the GPD is expected to yield a negative shape parameter; however, in many cases, the estimate of the shape parameter is positive (Weems, *et al.* 2016).

A similar picture has been observed for roll peaks and described in Belenky, *et al.* (2016). The value of the capsizing metric (1) below 1.0 corresponds to a large roll angle, thus it describes the same random event as the distribution of roll peaks. Does this mean that the tail of the metric (1) has a similar structure as the tail of roll peaks? Can the position of inflection point estimated for the roll peaks be extended for the metric (1)? These questions remain to be answered.

4. BROACHING IN IRREGULAR WAVES

Qualitative change of physics

Broaching-to is a violent uncontrolled turn occurring in following or stern-quartering waves despite full control effort applied on the opposite side. The most frequent mechanism of broaching includes surf-riding, after which the ship becomes directionally unstable. This directional instability leads to repelling in yaw direction.

Surf-riding in regular waves is driven by a dynamic equilibrium that appears when the surging component of the incident wave (Froude-Krylov)

force compensates for the difference between the available thrust and the ship’s resistance at a speed equal to wave celerity. A similar force balance can occur at instantaneous wave celerity in irregular waves, but such points are not strictly equilibria. The irregularity of the waves and wave forces make both celerity and force change with time so those balance points move unsteadily in the phase plane. The “acceleration” creates additional inertial forces that prevent the ship from staying at such balance points. Thus, those points are not a solution of the equation of motion. To reflect this fact, those points are further referred to as “pseudo-equilibria.”

These pseudo-equilibria define the topology of the phase space and create an attraction subset of initial conditions, known in literature as “Lagrangian Coherent Structure”, see Kontolefas and Spyrou (2016) for details. The appearance of the pseudo-equilibrium near the current position of a ship (within the coherent structure containing ship position) will accelerate the ship towards the instantaneous wave celerity. If this specific coherent structure makes the ship directionally unstable and if this directional instability lasts long enough, broaching must follow.

Thus, the development of broaching-to is related with the qualitative change of physics related to the appearance of the coherent structure capable of directional instability. If a time history or set of time histories from numerical simulations does not contain attraction events, attempts to fit GPD or GEV are futile as the sample does not contain relevant information on extreme behavior.

Metric of broaching likelihood

Broaching behavior may be included in extreme value consideration within the split-time framework using the motion perturbation method. The metric of broaching likelihood described in Belenky, *et al.* (2016) is based on a concept of “dangerous points” located inside those coherent structures. Not every point inside the structure leads to broaching as the structure may quickly disappear and a significant yaw angle may not have enough time to develop from the directional instability. As a result, the yaw angle deviation has been chosen as a criterion for the selection of dangerous points.

Figure 4 shows a perturbation from an observed position of a ship towards the dangerous point in the surging phase plane (Figure 4a), while the

dangerous points are defined as a set of initial conditions leading to large deviation of the yaw angle (25 degrees in Figure 4b).

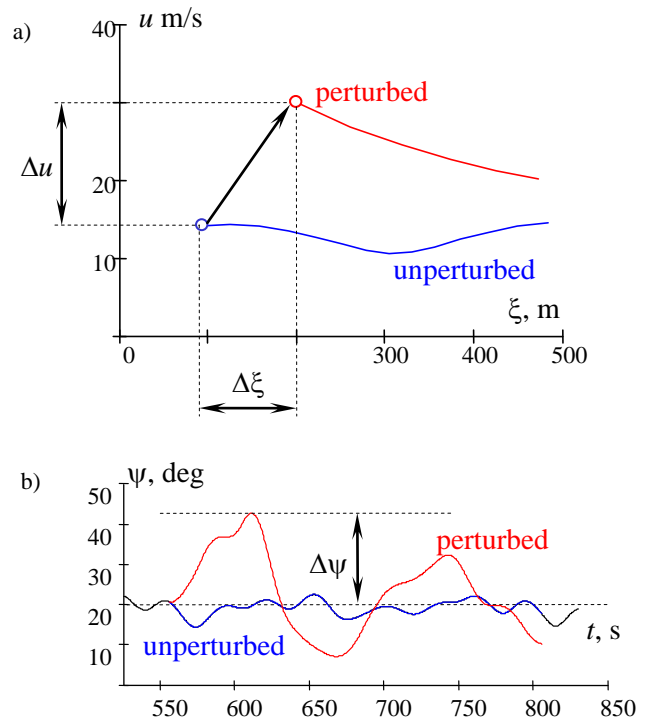


Figure 4: On the definition of the dangerous points: surging phase plane (a) and yaw time history (b)

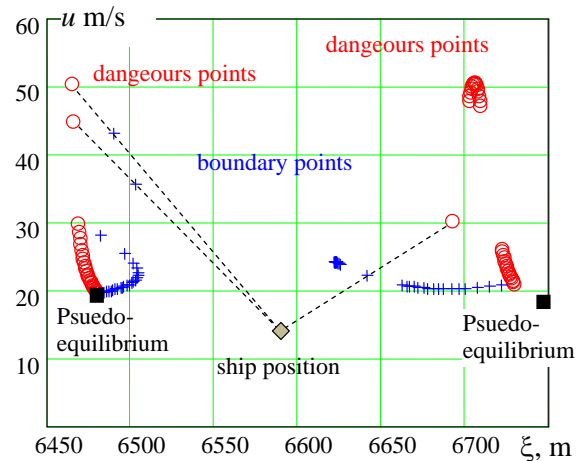


Figure 5: Dangerous and boundary points in the surging phase plane

Figure 5 shows a number of dangerous points found in the vicinity of two pseudo-equilibria closest to the ship position. The “boundary” points are defined as a set of initial conditions leading to exactly specified yaw deviation and are found along a line, in phase space, between the ship position and each dangerous point. The distance to the closest boundary point, referred further as a “critical distance”, is the basis of the metric value.

Distribution of the broaching metric

Further calculation procedure includes fitting of the GPD distribution as an approximation of the right tail. To facilitate this, the metric is formulated as

$$z_i = 100 - d_i; \quad i = 1, \dots, N_U \quad (2)$$

where d_i is the critical distance at the i^{th} up-crossing. When the critical distance equals zero, the yaw deviation is expected to be “dangerous” and the metric value equal to 100. Figure 6 shows the histogram of the metric before the dependent values of the metric. As the GPD requires independent points, a de-correlation time is used to eliminate dependent points prior to fitting the GPD.

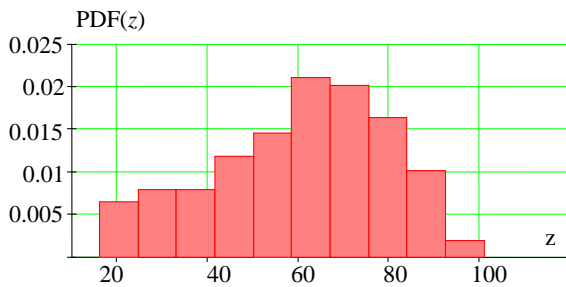


Figure 6: Histogram of the broaching metric before removing dependency

The shape of the distribution suggests a light tail; the initial fit indicates values of the shape parameters around -0.4 after the dependent points were removed.

SUMMARY AND CONCLUSIONS

Two problems were examined from the point of view of extreme value theory: the probability of capsizing and probability of broaching. Both problems are characterized by significant nonlinearity and a substantial change of physics during the transition to the state of failure.

If the information of those changes is not present in the available data, the direct application of extreme value theory will not be successful using only statistical methods. However, constructing an artificial value that does include the change of physics allows application of the extreme value theory to estimate the probability of failure. For the present problems, this is done by formulating metrics based on motion perturbation analysis.

The structure of the tail is a problem of special interest, as the appearance of the upper bound of Generalized Pareto Distribution may indicate the

existence of a physical limit. Some considerations have been given to this physical limit of the metric of capsizing in waves. Initial results of the broaching metric calculation indicate the existence of a limit as well.

Further understanding of a nature of those limits and the development of techniques for their estimation may be of significant practical and theoretical interest.

ACKNOWLEDGEMENTS

The work described in this paper has been funded by the Office of Naval Research (ONR) and ONR Global under Dr. Thomas Fu, Dr. Woei-Min Lin and Dr. Salahuddin Ahmed, and by NSWCCD Independent Applied Research (IAR) program. The participation of Prof. Pipiras and Prof. Sapsis was facilitated by the Summer Faculty Program supported by ONR and managed by NSWCCD under Dr. Jack Price, who also managed the IAR program.

REFERENCES

Belenky, V., Glotzer, D., Pipiras, V. and T. Sapsis 2016 “On the Tail of Nonlinear Roll Motions,” *Proc. 15th Intl. Ship Stability Workshop*, Stockholm, Sweden, pp. 109-114.

Belenky, V.L., Spyrou, K.J. Weems, K.M., 2016a “On Probabilistic Properties of Surf-Riding and Broaching-to in Irregular Waves,” *Proc. 31st Symp. Naval Hydrodynamics*, Monterey, California, USA.

Belenky, V., Weems, K. and W.M. Lin 2016b “Split-time Method for Estimation of Probability of Capsizing Caused by Pure Loss of Stability,” in *Ocean Engineering*, Vol. 122, pp.333-343.

Campbell, B., Belenky, V. and V. Pipiras 2016 “Application of the Envelope Peaks over Threshold (EPOT) Method for Probabilistic Assessment of Dynamic Stability,” in *Ocean Engineering*, Vol. 120, pp. 298-304.

Coles, S., 2001, *An Introduction to Statistical Modeling of Extreme Values*. London: Springer-Verlag.

Glotzer, D., Pipiras, V., Belenky, V., Campbell, B., T. Smith, 2017 “Confidence Interval for Exceedance Probabilities with Application to Extreme Ship Motions,” *REVSTAT Statistical J.* (Accepted)

Kontolefas, I., Spyrou, K.J. 2016 “Coherent structures in phase space, governing the nonlinear surge motions of ships in steep waves,” *Ocean Engineering*, Vol 120, 339-345.

McTaggart, K. A., 2000 “Ongoing Work Examining Capsize

Risk of Intact Frigates Using Time Domain Simulation,”
Contemporary Ideas of Ship Stability, D. Vassalos, *et al.*
(eds), Elsevier Science, pp. 587–595.

McTaggart, K. A., de Kat J.O., 2000 “Capsize Risk of Intact Frigates in Irregular Seas,” *Trans. SNAME*, Vol. 108, pp 147–177.

Smith, T. C., and Zuzick, A., 2015 “Validation of Statistical Extrapolation Methods for Large Motion Prediction,” *Proc. 12th Intl. Conf. on Stability of Ships and Ocean Vehicles (STAB 2015)*, Glasgow, UK.

Weems, K., Belenky, V. and B. Campbell 2016 “Validation of Split-time Method with Volume-Based Numerical Calculations,” *Proc. 15th Intl. Ship Stability Workshop*, Stockholm, Sweden, pp. 103-108.

Evaluation of the critical wave groups method for calculating the probability of extreme ship responses in beam seas

Panayiotis A. Anastopoulos, *Department of Naval Architecture and Marine Engineering, National Technical University of Athens, Greece, panasto@central.ntua.gr*

Kostas J. Spyrou, *Department of Naval Architecture and Marine Engineering, National Technical University of Athens, Greece, k.spyrou@central.ntua.gr*

ABSTRACT

The paper investigates the accuracy of the current formulation of the “critical wave groups” method for calculating the probability of extreme responses of vessels rolling in beam seas. The method employs short duration regular excitations to identify “critical” for ship stability wave events that cause slight exceedance of a given roll angle threshold. The probability of any exceedance of the roll angle threshold is then estimated by the probability of encountering any wave sequence higher than the determined critical, based on wave height and period distributions derived from spectral methods. In this study the “critical wave groups” method is extended by incorporating realistic wave group forms, characterized by high probability of occurrence. Both the regular and the irregular wave group schemes are applied to evaluate the probability of exceedance for several roll angle thresholds for two ship models. To increase the accuracy of the approach, wave group statistics are obtained from direct simulations of the wave field rather than from spectral methods. The results are tested against Monte Carlo simulations of ship roll motion.

Keywords: *wave group, probability, instability, roll, dynamics, resonance, rare events.*

1. INTRODUCTION

The study of large amplitude ship roll motions in stochastic beam seas is a non-trivial task expanding in both the fields of non-linear dynamics and probability. As known, roll statistics deviate from Gaussianity with increasing level of non-linearity, leading to probability distributions with heavy-tailed structure (Belenky et al., 2016b). However, calculating the probability of extreme roll events by employing “brute force” methods suffers from a number of deficiencies. First, the accuracy of a “direct counting” definition of probability becomes questionable when dealing with rare events. At the same time, the fact that ship response is not essentially an ergodic random process in the case of a non-linear system further increases the computational burden for tracing the complex shape of the tails (Belenky et al., 1998).

Several methods have been proposed to treat the so called “problem of rarity”, described in the above. Extrapolation methods employ statistics based on a limited number of realizations to predict the probability of an event that is too rare to be observed. The concept derives from Extreme Value

Theory which provides asymptotic expressions for the distribution of the maximum of a sample of independent and identically distributed random variables. Thus, the objective is the estimation of the parameters of an extreme value distribution by fitting the latter to a set of experimental or simulation data. The method has been demonstrated in several studies and much effort has been put into addressing practical issues regarding its application for ship stability assessment (e.g., Belenky et al., 2016a; Campbell et al., 2016).

On the other hand, wave group methods offer an alternative solution to the problem by focusing on specific time intervals when dangerous wave events occur. One of them is the “critical wave groups” method which quantifies instability tendency through the probability of encountering any wave group that could have provoked the instability (Themelis and Spyrou, 2007). In the deterministic part of the method, regular wave trains are employed to identify critical, in terms of ship stability, height thresholds. Then, in the probabilistic part, the probability of encountering any wave sequence higher than the specified thresholds is calculated using distributions of wave

heights and periods derived from spectral methods. A first attempt to validate the concept was presented by Shiginov et al. (2012) who selected a modern 8000 TEU containership to calculate the probability of exceedance for a 40degrees roll angle threshold. The results were tested against Monte Carlo simulations and fair coincidence was noted in the case of beam seas excitation.

As a next step, in this paper we employ the “critical wave groups” method to predict the probability of exceedance for a number of roll angle thresholds for two different ship models. At the same time, our recent work towards improving the deterministic part of the approach is continued, by incorporating more realistic wave group forms. The idea is to identify critical wave events in terms of the “most expected” wave groups of a given sea state using the method developed by Anastopoulos et al. (2016). To eliminate the impact of spectral methods on the accuracy of the probabilistic part, desired height and period distributions are obtained from direct simulations of the wave field. Finally, the conditions under which the “critical wave groups” method produces comparable results with those obtained from Monte Carlo simulations of roll motion are investigated and the focus is set on the region of extreme responses where the accuracy of the latter is disputable.

2. MATHEMATICAL FORMULATION

In the field of ocean and coastal engineering, wave groups are traditionally considered as sequences of waves with heights exceeding a certain preset level and slightly varying periods (Masson and Chandler, 1993; Ochi, 1998). Despite that several threshold-based definitions have been utilized in the past to study wave groupiness measures, one would argue that, from ship dynamics perspective, wave groups are sequences of waves which are sufficiently high to provoke instabilities.

Now, let us assume that we are interested in estimating the probability that a vessel exceeds a roll angle threshold φ_{crit} . The key idea of the “critical wave groups” method is to first identify the wave events that cause the exceedance and then, calculate the probability of encountering them. The essence of the approach is presented below:

$$p[\varphi > \varphi_{crit}] = \sum_k p \left[\varphi > \varphi_{crit} \middle| \underbrace{\left(\bigcup_i wg_{k,i}, ic_k \right)}_{=1} \right] \times p \left[\bigcup_i wg_{k,i}, ic_k \right] \quad (1)$$

where $wg_{k,i}$ is a wave group event with characteristics i , determined for the k^{th} set of initial conditions $\{\varphi_0, \dot{\varphi}_0\}$ of the vessel at the moment of the encounter. From a preliminary investigation, Themelis and Spyrou (2008) concluded that for sea states of moderate severity the influence of initial conditions may not be very significant and thus, examining only the upright position of the vessel $\{\varphi_0, \dot{\varphi}_0\} = \{0, 0\}$, denoted by $k=0$, can be somehow acceptable:

$$p[\varphi > \varphi_{crit}] = \sum_k p \left[\bigcup_i wg_{k,i} \middle| ic_k \right] \times p[ic_k] \approx p \left[\bigcup_i wg_{0,i} \middle| ic_0 \right] \quad (2)$$

Eventually, the method is implemented in two parts: a purely deterministic one, focused on the identification of the so called “critical” wave groups, i.e., those wave successions leading to only slight exceedance of φ_{crit} ; and a probabilistic part to calculate the probability of encountering any wave group higher than the determined critical. As realized, the accuracy of the method depends explicitly on the shape of the critical wave groups which are in fact height thresholds for the wave events that result in $\varphi > \varphi_{crit}$.

By assuming that individual wave group occurrences are independent events, eq. (2) is reformulated as (Themelis and Spyrou, 2007):

$$p[\varphi > \varphi_{crit}] = \sum_{i=1}^N p[wg_{0,i}] - \sum_{i=1}^{N-1} \sum_{r=i+1}^N p[wg_{0,i}, wg_{0,r}] + \dots + (-1)^{N-1} p[wg_{0,1}, wg_{0,2}, \dots, wg_{0,N}] \quad (3)$$

where $p[wg_{0,1}, wg_{0,2}, \dots, wg_{0,N}] = \prod_{i=1}^N p[wg_{0,i}]$.

A significant challenge in eq. (3) is to ensure that wave groups that provoke exceedance of φ_{crit} form

a set of mutually exclusive and collectively exhaustive events. To avoid possible overlaps in the calculations, it is convenient to identify wave groups with respect to their run length j , which is the number of consecutive heights exceeding a critical threshold:

$$p[\text{wg}_{0,i}] = p\left[\bigcup_m \{j=i, \mathbf{H}_i > \mathbf{h}_{cr,i}, \mathbf{T}_i \in \mathbf{T}_{cr,m}\}\right] \quad (4)$$

where $\mathbf{H}_i = \{H_1, \dots, H_i\}$ and $\mathbf{T}_i = \{T_1, \dots, T_i\}$ are vectors of random variables referring respectively to the heights H_n and periods T_n of an individual wave group event with run length i ($1 \leq n \leq i$), $\mathbf{h}_{cr,i} = \{h_{cr,1}, \dots, h_{cr,i}\}$ is a deterministic vector for the heights of a critical wave group with run length i and $\mathbf{T}_{cr,m}$ is the m^{th} range within which the critical periods are considered to vary. In the case of regular wave groups the width T_w of all critical ranges $\mathbf{T}_{cr,m}$ ($m=1, 2, \dots, M$) is fixed.

Modelling of wave successions as Markov chains has been one of the most successful approaches in wave group theory. Kimura (1980) was the first to elaborate on wave group statistics assuming that wave heights and related periods are Markov processes. Ever since the concept has been tested several times against numerical simulations and real wave field measurements with remarkable success (e.g., Stansell et al., 2002). In this context, the probability of encountering dangerous wave groups with certain specifications, as in eq. (4), is expressed as:

$$p[\text{wg}_{0,i}] = p_0 \times \prod_{n=2}^i \int_{h_{cr,n}}^{+\infty} \int_{\mathbf{T}_{cr,m}} \int f_{H_n, T_n | H_{n-1}, T_{n-1}}(h_n, t_n | h_{n-1}, t_{n-1}) dt_n dh_n \quad (5)$$

where $m=1, 2, \dots, M$ denotes different cases of critical period segments and:

$$p_0 = \int_{h_{cr,1}}^{+\infty} \int_{\mathbf{T}_{cr,m}} f_{H_1, T_1}(h_1, t_1) dt_1 dh_1 \quad (6)$$

In the above, $f_{H_n, T_n | H_{n-1}, T_{n-1}}$ is the conditional probability density function (PDF) of two

consecutive wave heights and related periods and f_{H_1, T_1} is the joint PDF of the height and period of a single wave.

Equation of roll motion

In this study ship motion is modelled under the Froude-Krylov assumption using the following simple uncoupled equation, written in terms of the relative roll angle ϕ :

$$(I_{44} + A_{44})\ddot{\phi} + D(\dot{\phi}) + g\Delta GZ(\phi) = M(t) \quad (7)$$

with I_{44} and A_{44} being the roll moment of inertia and the added moment of inertia, respectively, Δ is the ship displacement, g is the gravitational acceleration and D is the damping moment:

$$D(\dot{\phi}) = B_1\dot{\phi} + B_2\dot{\phi}|\dot{\phi}| \quad (8)$$

The restoring arm in still water is given as:

$$GZ(\phi) = \sum_k C_k \phi^k, \quad k=1, 3, 5, \dots \quad (9)$$

When information about the roll response amplitude operator (RAO) is available, the wave induced moment is estimated from:

$$S_{MM}(\omega) = |RAO(\omega)|^2 S_{\eta\eta}(\omega) \quad (10)$$

where $S_{\eta\eta}$ is the energy spectrum of the water surface elevation which is a stationary ergodic Gaussian process. Alternatively, in the presence of long incident waves, the concept of instantaneous wave slope at the middle of the ship α can be employed (Wright and Marshfield, 1980):

$$M(t) = -I_{44}\ddot{\alpha}(t) \quad (11)$$

Dividing eq. (7) by $I_{44} + A_{44}$ we finally obtain:

$$\ddot{\phi} + b_1\dot{\phi} + b_2\dot{\phi}|\dot{\phi}| + \sum_k c_k \phi^k = m(t) \quad (12)$$

Construction of realistic wave groups

Anastopoulos et al. (2016) extended the Markovian model of Kimura (1980) to develop a method for the systematic construction of irregular wave group profiles, characterized by high probability of occurrence. The key is to select the

height H_c and period T_c of the highest wave of the group to initiate the following iterative scheme:

$$\bar{h}_i = \int_0^{\infty} h_i f_{H_i|H_{i-1}, T_{i-1}}(h_i | h_{i-1}, t_{i-1}) dh_i \quad (13)$$

$$\bar{t}_i = \int_0^{\infty} t_i f_{T_i|H_i, H_{i-1}, T_{i-1}}(t_i | h_i, h_{i-1}, t_{i-1}) dt_i \quad (14)$$

Now, let us assume that we are interested in generating a sequence of j wave group heights and related periods with H_c and T_c occupying the i^{th} position ($1 \leq i \leq j$). Forward application of eqs. (13) and (14) will provide the heights and periods of the waves succeeding the initial (highest) one. Then, the “most expected” past outcomes are identified by applying the same procedure backwards in time. The calculation of the conditional expectation in eq. (13) precedes that of eq. (14) so as to take into account the correlation between the height and period of a predicted wave. The transition PDFs can be obtained either from spectral methods (Anastopoulos et al., 2016) or by analyzing data collected from Monte Carlo simulations of the wave field (Anastopoulos and Spyrou, 2016).

The next step is to construct the continuous-time counterparts of the generated sequences. To this end, we opt for a representation of water surface elevation η of the form:

$$\eta(x, t) = \sum_{n=0}^{(5j-3)/2} a_n f_n(x, t) \quad (15)$$

In our earlier studies the f_n basis functions were derived from the application of the Karhunen-Loève theorem (Sclavounos, 2012). Here, aiming at reducing the computational cost related to the solution of the Karhunen-Loève eigen-problem, we employ the widely used Fourier basis functions. The number of terms kept in eq. (15) is selected so as to satisfy a set of geometrical constraints which ensure that the shape of the produced waveform is compatible with the predictions of eqs. (13) and (14). More details can be found elsewhere (e.g., Anastopoulos and Spyrou, 2016). It is noted however that the truncation order in eq. (15) is lower than the originally recommended ($6j$) since

it was recently observed that fewer terms were enough to generate desired waveforms.

3. RESULTS AND DISCUSSION

In this section, the “critical wave groups method” is applied to two different ship models in order to predict the probability of exceedance for several roll angle thresholds. Both regular and irregular wave group excitations are employed and the results are tested against Monte Carlo simulations of roll motion. To improve the overall accuracy of the approach, the PDFs of successive wave heights and periods appearing in eqs. (5) and (6) are computed from direct simulations of the water surface displacement instead of spectral methods.

Regarding the construction of irregular wave group shapes, the transition probabilities in eqs. (13) and (14) were calculated according to the method described in Anastopoulos et al. (2016) with the only difference that the necessary correlation parameters were estimated from the generated wave data. In this way, the efficiency of the Markov model for determining the “most expected” wave height and period sequences is enhanced.

Ship model 1

An ocean surveillance ship, referred in the study of Su (2012), was selected as the first ship model. Main parameters of the vessel are given in Table 1.

Table 1: Main parameters of the ocean surveillance vessel.

Parameter	Dimensional value
$I_{44} + A_{44}$	$5.540 \times 10^7 \text{ kg} \cdot \text{m}^2$
Δ	$2.056 \times 10^6 \text{ kg}$
b_1	0.095 s^{-1}
b_2	0.052
c_1	1.153 s^{-2}
c_3	-0.915 s^{-2}

The ship is assumed to operate in a sea state described by the modified Pierson-Moskowitz (PM) spectrum with significant wave height $H_s = 4\text{m}$ and peak period $T_p = 6\text{s}$:

$$S_{\eta\eta}(\omega) = \frac{5.058 g^2 H_s^2}{\omega^5 T_p^4} \exp\left[-\frac{5}{4} \cdot \left(\frac{\omega_p}{\omega}\right)^4\right] \quad (16)$$

were ω_p is the peak frequency. The wave induced moment is modelled using eq. (10) and the roll response amplitude operator $|RAO(\omega)|$ of the vessel is presented in Figure 1.

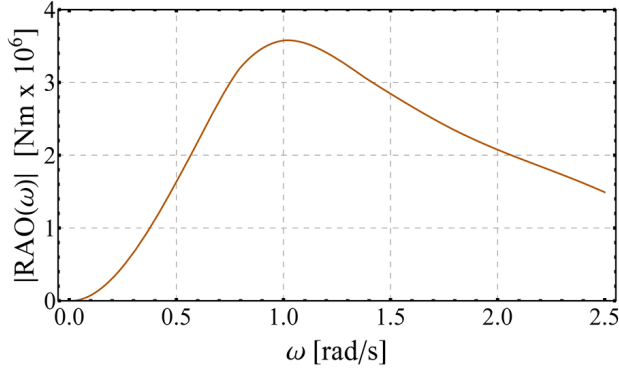


Figure 1: Roll response amplitude operator $|RAO(\omega)|$ for ship model 1.

For the simulations of the wave field, the model of Longuet-Higgins (1952) was adopted:

$$\eta(t) = \sum_n \sqrt{2S_{\eta\eta}(\omega_n)} d\omega_n \cos(\omega_n t + \varepsilon_n) \quad (17)$$

were ε_n are random variables uniformly distributed over $[0, 2\pi)$, ω_n are the frequencies of the wave components and $d\omega$ is the frequency resolution. In total, 18853 waves were analyzed from a set of 24 records of 1 hour. Finally, statistics of roll motion were estimated without assuming the ergodic property for the response (Belenky et al., 1998). As a corollary, the analysis was performed on a collection of approximately $15 \cdot 10^5$ short-duration realizations, sampled at a fixed time instant $t_s = 150s$.

In Figure 2 the iterative scheme of eqs. (13) and (14) is applied in order to predict the characteristics of the “most expected” wave groups of the examined sea state for various cases of $\{H_c, T_c\}$, values, here denoted by red nodes. The vertical axis shows the heights that derive from successive iterations and the horizontal axis shows the corresponding periods. The evolution of the procedure for a given set of $\{H_c, T_c\}$ parameters is indicated by black crosses along the dashed lines. The root of this tree-shaped diagram is the stationary state of the Markovian system and the structure of the “most expected” wave groups

depends on the distance of the highest wave from the root.

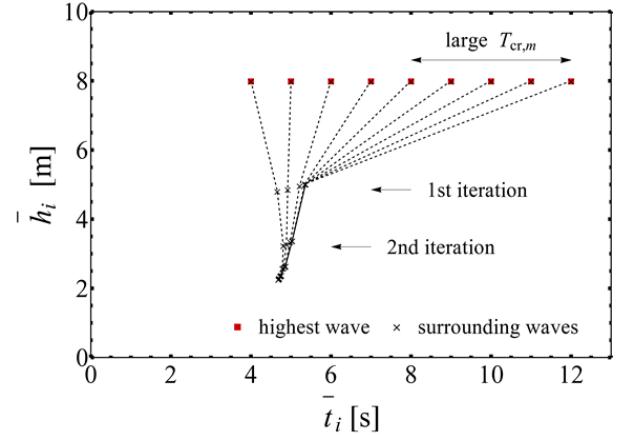


Figure 2: Characteristics of the most expected height and period sequences generated for the PM spectrum.

In Figure 3 the results of the Monte Carlo simulations (MC sim.) are presented in the same plot with the estimates of the “critical wave groups” method using regular wave groups with $j \leq 6$. For the latter two different cases of critical period range widths T_w were studied. As illustrated, for roll angles below 40degrees the method consistently underestimates the probability of exceedance. This demonstrates that for intermediate roll angle thresholds it is rather unlikely that the exceedance has been provoked by wave grouping phenomena. For larger angles, however, the accuracy of the method is improved but it is sensitive to the selection of T_w . The reason is that T_w is actually a measure of tolerance for the detection of resonant phenomena and as realized, the condition that $T_w = 1s$ is possibly too strict.

On the other hand, the method performs better for roll angle thresholds before the tail region in the case of irregular wave groups, as shown in Figure 3. In this implementation, however, the method is sensitive to the maximum period of the highest wave $T_{c,max}$. The reason is that, for irregular wave groups, the critical period ranges $T_{cr,m}$ are defined as the difference of the shortest from the longest period encountered within a generated sequence. As shown in Figure 2, for increasing T_c the highest wave progressively deviates from the mean period of the wave group and the critical period ranges $T_{cr,m}$ become larger. Therefore, the tolerance for the detection of resonant phenomena is relaxed and the method overestimates the probability of

exceedance. However, it is not clear at the moment if such cases should be included in the probability calculations since the period of the highest wave distorts the grouping character of the rest period sequence.

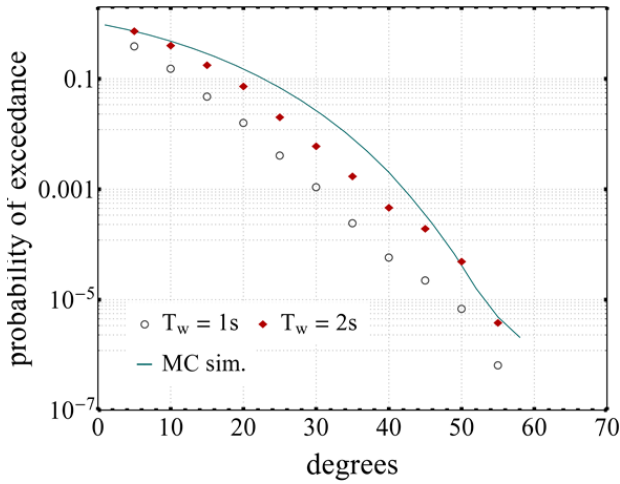


Figure 3: Probability of exceedance for ship model 1 using regular wave groups.

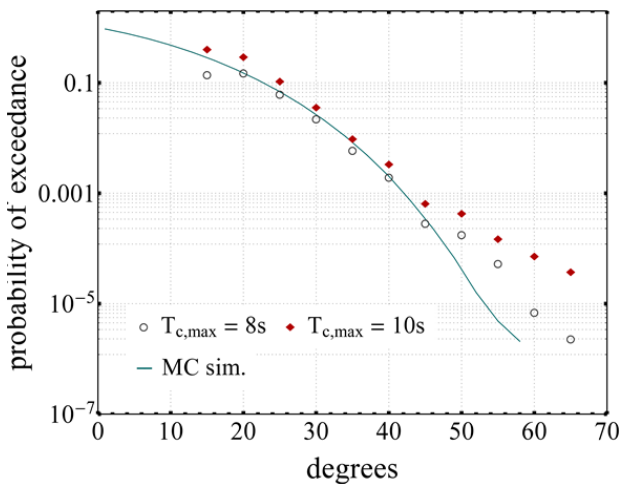


Figure 4: Probability of exceedance for ship model 1 using irregular wave groups.

In the deterministic part of the method, critical wave group parameters, identified for $\varphi_{crit} = 45^\circ$, are summarized in Figure 5 in the form Transient capsizes diagrams. These are plots of the wave steepness of a critical wave group against its period, here normalized with the natural period of the vessel $T_o = 5.9s$ (Rainey and Thompson, 1991). Regular wave groups are given by long dashed curves while irregular wave groups are represented both by their mean steepness (short dashed line) and by the steepness of the highest wave (solid line), always against the normalized period of the latter. As one obtains two boundary lines (depending on whether he employs the mean or the

maximum wave group steepness), for the case of irregular wave groups, shading has been applied between the two lines in order to enhance the contrast against the regular-wave-groups line. For $j = 2$, height thresholds defined by regular and irregular wave groups are, in the mean sense, relatively close. The shift of instability region towards the area of long waves has already been reported in Anastopoulos and Spyrou (2016). However, for $j = 3$ the dangerous zone is enlarged for the case of irregular wave groups.

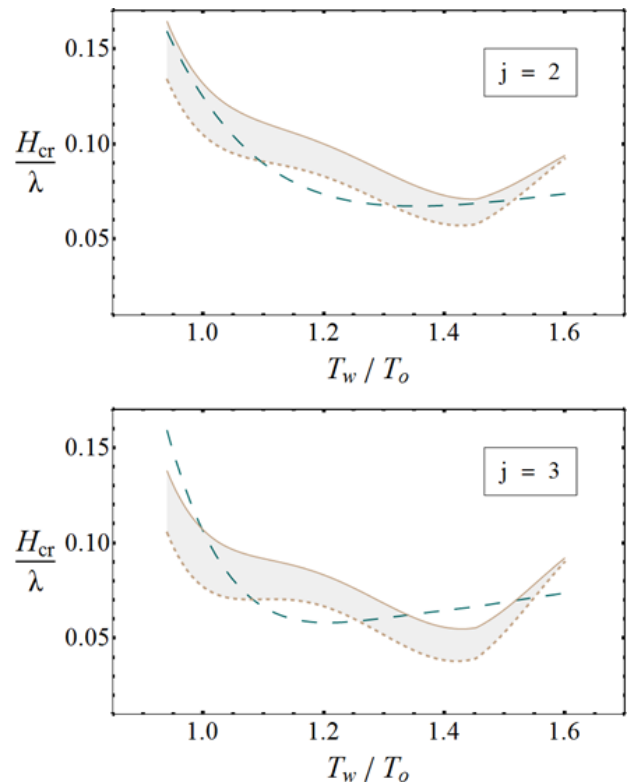


Figure 5: Transient capsizes diagrams for ship model 1 for different run lengths j and $\varphi_{crit} = 45^\circ$.

Ship model 2

A modern 4800 TEU Panamax containership with parameters listed in Table 2 and natural period $T_o = 15.2s$ is the second ship model that was studied. The restoring arm coefficients in eq. (9) were provided directly from the loading manual of the vessel. Since no information was available about the RAO function, wave excitation was approximated by eq. (11).

In this application the JONSWAP spectrum, given in eq. (18), with parameters $H_s = 10m$, $T_p = 14s$ and $\gamma = 1.932$ was selected to describe the sea state of operation. In the same spirit, 24 records of 1 hour length were generated according

to eq. (17), corresponding to a total population of 7875 waves. Monte Carlo simulations of roll motion were performed with the same setup as for ship model 1, however sampled at $t_s = 200s$.

$$S_{\eta\eta}(\omega) = \frac{0.01g^2}{\omega^5} \exp\left[-\frac{5}{4} \cdot \left(\frac{\omega_p}{\omega}\right)^4\right] \gamma \exp\left[\frac{1}{2} \left(\frac{\omega - \omega_p}{0.08\omega_p}\right)^2\right] \quad (18)$$

Table 2: Main parameters of the Panamax containership.

Parameter	Dimensional value
$I_{44} + A_{44}$	$1.122 \times 10^{10} \text{ kg} \cdot \text{m}^2$
Δ	$6.820 \times 10^7 \text{ kg}$
b_1	0.043 s^{-1}
b_2	0.056
c_1	1.667 s^{-2}
c_3	3.161 s^{-2}
c_5	-10.634 s^{-2}
c_7	8.349 s^{-2}
c_9	-2.150 s^{-2}

The results obtained from the implementation of the “critical wave groups” method when ship model 2 is excited by regular and irregular wave groups is shown in Figures 6 and 7, respectively. Again, for intermediate angle thresholds, better predictions are achieved by irregular waveforms. In the tail region, direct simulations of roll motion (MC sim.) fail to predict exceedances due to the problem of rarity while, in the same range, both schemes of the “critical wave groups” method yield reliable estimates.

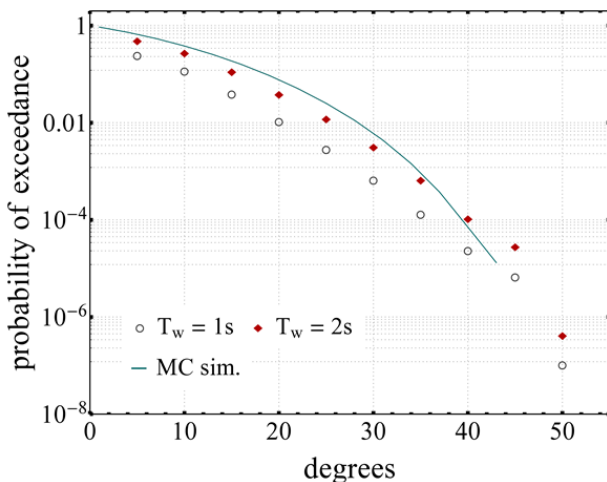


Figure 6: Probability of exceedance for ship model 2 using regular wave groups.

Finally, Figure 8 compares regular and irregular critical wave groups with run lengths $j=2$ and $j=3$ in terms of their individual probability of exceedance P_j . The calculations were made for the critical period parameters that provided the best agreement with the simulation results according to Figures 6 and 7. Thus, $T_w = 2s$ and $T_{c,max} = 15s$ were selected for the regular and the irregular case, respectively. The contribution of run lengths with $j > 6$ to the total probability of exceedance was found negligible.

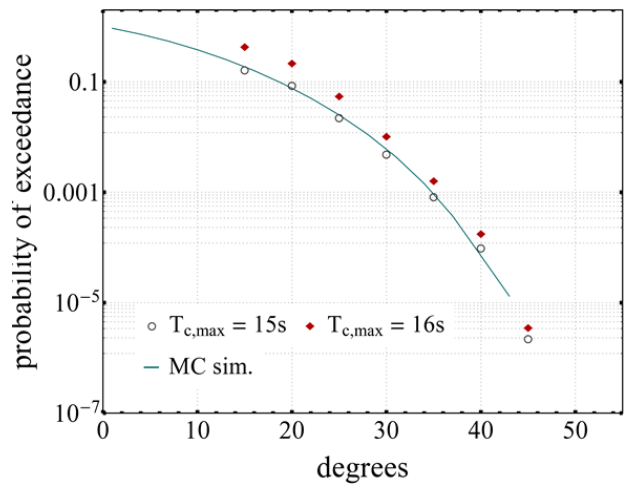


Figure 7: Probability of exceedance for ship model 2 using irregular wave groups.

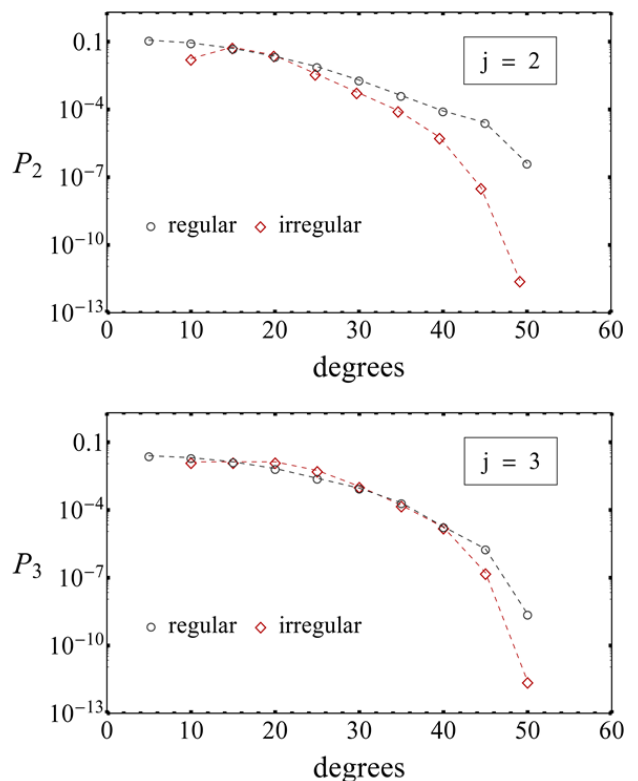


Figure 8: Contribution of individual run lengths j to the probability of exceedance for ship model 2.

4. CONCLUDING REMARKS

In this study the “critical wave groups” method was applied to predict the probability of large-amplitude ship motions in beam seas. The method was extended by incorporating realistic wave excitations representing the “most expected” wave groups of a sea state. Both the regular and the irregular wave group schemes were applied to two different ship models to estimate the probability of exceedance for several roll angle thresholds and comparisons with Monte Carlo simulations of roll motion were presented. The results indicate good coincidence in the tail region where the efficiency of direct simulations is generally low. For intermediate roll angle thresholds the “critical wave groups” method performs better when irregular wave groups are employed due to realistic modelling of wave period successions. However, the probability calculations are sensitive to the degree of variability that is allowed in the wave period groupings. The extent up to which wave group period variations are responsible for resonant phenomena is a topic of future research.

ACKNOWLEDGEMENTS

The final year thesis work of Mr. Georgios Papageorgiou, who graduated earlier this year from our School, has motivated partly the current study.

REFERENCES

- Anastopoulos P.A., Spyrou K.J., Bassler C.C. and Belenky V.L., 2016, “Towards an Improved Critical Wave Groups Method for the Probabilistic Assessment of Large Ship Motions in Irregular Seas”, *Probabilistic Engineering Mechanics* 44, pp. 18-27.
- Anastopoulos P.A. and Spyrou K.J., 2016, “Ship Dynamic Stability Assessment Based on Realistic Wave Group Excitations”, *Ocean Engineering* 120, pp. 256-263.
- Belenky V.L., Degtyarev A.B. and Boukhanovsky A.V., 1998, “Probabilistic Qualities of Nonlinear Stochastic Rolling”, *Ocean Engineering* 25(1), pp. 1-25.
- Belenky V.L., Weems K. and Lin W.M., 2016a, “Split-Time Method for Estimation of Probability of Capsizing Caused by Pure Loss of Stability”, *Ocean Engineering* 122, pp. 333-343.
- Belenky V.L., Glozter D., Pipiras V. and Sapsis T.P., 2016b, “On the Tail of Nonlinear Roll Motions”, *Proceedings of the 15th International Ship Stability Workshop*, Stockholm, Sweden, pp. 109-114.
- Campbell B., Belenky V.L. and Pipiras V., 2016, “Application of the Envelope Peaks Over Threshold (EPOT) Method for Probabilistic Assessment of Dynamic Stability”, *Ocean Engineering* 120, pp. 298-304.
- Kimura A., 1980, “Statistical Properties of Random Wave Groups”, *Proceedings of the 17th International Coastal Engineering Conference*, Sydney, Australia, pp. 2955-2973.
- Longuet-Higgins M.S., 1952, “On the Statistical Distribution of the Heights of Sea Waves”, *Journal of Marine Research* 11(3), pp. 245-66.
- Masson D. and Chandler P., 1993, “Wave Groups: A Closer Look at Spectral Methods”, *Coastal Engineering* 20, pp. 249-275.
- Ochi M., 1998, “Ocean Waves: The Stochastic Approach”, Cambridge University Press, Cambridge, England, ISBN: 978-0-521-01767-1.
- Rainey R.C.T. and Thompson J.M.T., 1991, “The Transient Capsize Diagram – A New Method of Quantifying Stability in Waves”, *Journal of Ship Research* 35(1), pp. 58-62.
- Sclavounos P.D., 2012, “Karhunen-Loève Representation of Stochastic Ocean Waves”, *Proceedings of the Royal Society A* 468(2145), pp. 2574-2594.
- Shigunov V., Themelis N. and Spyrou K.J., 2012, “Critical Wave Groups vs. Direct Monte-Carlo Simulations for Typical Stability Failure Modes of a Container Ship”, *Proceedings of the 11th International Conference on Stability of Ships and Ocean Vehicles*, Athens, Greece, pp. 11-20.
- Stansell P., Wolfram J. and Linfoot B., 2002, “Statistics of Wave Groups Measured in the Northern North Sea: Comparisons between Time Series and Spectral Predictions”, *Applied Ocean Research* 24, pp. 91-106.
- Su Z., 2012, “Nonlinear Response and Stability Analysis of Vessel Rolling Motion in Random Waves Using Stochastic Dynamical Systems”, Texas A&M University.
- Themelis N. and Spyrou K.J., 2007, “Probabilistic Assessment of Ship Stability”, *Transactions of SNAME* 115, pp. 181-206.
- Themelis N. and Spyrou K.J., 2008, “Probabilistic Assessment of Ship Stability Based on the Concept of Critical Wave Groups”, *Proceedings of the 10th International Ship Stability Workshop*, Daejeon, Korea, pp. 115-125.
- Wright J.H.G. and Marshfield W.B., 1980, “Ship Roll Response and Capsize Behavior in Beam Seas”, *RINA Transactions* 122, pp. 129-148.

Session 6

Stability and safety of inland and river-sea ships

Session Chairs

Gabriele Bulian

Igor Bačkalov

Practicalities of loading instruments for Inland Waterway Tankers

Herbert Koelman, *SARC*, H.J.Koelman@sarc.nl

Egbert van IJken, *SARC*, Egbert@sarc.nl

ABSTRACT

Intact and damage stability properties of Inland WaterWay (IWW) tankers are being considered to a much greater depth today than they used to be, because the 2015 edition of the applicable legislation not only requires an extensive (damage-) stability manual to be issued, but also an on-board loading computer to be installed. Although the formal framework is set by the rules, there are quite some issues left for interpretation or additional guidance, where also the classification societies play a role. Besides those practical issues, in this paper also data collection, specific loading instrument functions and loading software assessment are discussed.

Keywords: *ADN, IWW tanker stability, Loading instrument.*

1. INTRODUCTION

After the incident with MTS Waldhof, in 2011, many safety properties of Inland WaterWay (IWW) tankers transporting dangerous goods have been scrutinized. Notably, documents on paper, such as stability booklets and safety plans, but in particular also computer programs dedicated to the assessment of stability, freeboard and strength. As such, these aspects may be suspected to be quite conventional; after all, all required basic tools are standard and readily available. However, some specific properties of IWW ships and their world make loading instrument application less straightforward. In the following sections these aspects are discussed and commented, notably:

- Background of IWW tanker design and the application of loading instruments.
- The regulatory framework.
- Specific functions and features of the loading instrument software.
- Ship data collection and reliability.
- Application and acceptance of loading instruments by crew and management.
- Software assessment and appraisal.

The statements and opinions in this paper arise from intensive involvement of our company with this matter, either by providing services — making designs, preparing stability booklets — or by the

preparation and delivery of our ship loading and stability software, see SARC (2013).

2. BACKGROUND OF IWW TANKER DESIGN AND THE APPLICATION OF LOADING INSTRUMENTS

IWW tankers design are commonly governed by these requirements: high volume and dead-weight, low draft, low air draft and favorable hydrodynamic properties. As usual, these requirements are partially conflicting, and recent design methods are not always available. Fortunately, some things improve a bit over time, because in The Netherlands at this moment a four-year research project “Top Ships” is commenced, aimed at state-of-the-art prediction methods for resistance and propulsion of IWW vessels on shallow draft, see Rotteveel (2015, 2016).

From the regulatory point of view, ADN (2015), a classification is made into Gas tankers (type G), Chemical tankers (type C) and others (type N).

Loading instruments are quite common on sea-going vessels, however, until 2013 the application on IWW vessels was in general limited to container ships. After all, since 1986 container ships in the Rhine area have to comply with intact stability requirements, EU (2006), which could in principle be computed manually (e.g. with a table of maximum allowable VCG). However, with a

computer it is more convenient, notably if container weights are already available by Electronic Data Interchange.

In 2011 mv. Waldhof capsized in intact condition in the River Rhine, obstructing the river for some two weeks, which caused significant economical and logistical damage, see WSV (2013). To say that mv. Waldhof capsized by lack of stability is tautological, so, it is no surprise that authorities took the initiative to safeguard stability of IWW tankers.

3. THE REGULATORY FRAMEWORK

For safety issues of seagoing vessels IMO, a United Nations agency, plays the role of the international legislator. In Europe, for Inland Waterway Vessels a similar role is played by UNECE, which gather information from different parties, such as flag states, classification societies and the “Central Commission for Navigation on the Rhine” (CCNR). In 1971, the CCNR released the first set of regulations, called ADNR, covering the waterborne transport of dangerous goods, such as chemicals and gas. The letter R in ADNR stands for “Rhine”, which was indeed the original applicability of these rules. From 2000 these rules have been generalized to cover transport of dangerous goods on all European inland waterways, and are in force since 2008 under the name ADN. ADN is reviewed on a yearly basis, the latest version is ADN (2015).

Concerning stability, ADN poses criteria of a conventional nature, which require some minimum properties of the righting lever (GZ) curve. Tankers with cargo tanks with a breadth of less than 70% of the ship’s breadth are assumed to possess sufficient intact stability, which implies that this ship class is not subject to any regulatory intact stability check. For tankers with wider tanks these intact criteria apply:

- In the GZ curve up to immersion of the first non-watertight opening there shall be a GZ of not less than 0.10 m.
- The area under the positive GZ curve up to immersion of the first non-watertight opening and in any event up to an angle of heel $< 27^\circ$ shall not be less than 0.024 mrad.
- The metacentric height (GM) shall be not less than 0.10 m.

In practice these criteria are seldom critical, compared with damage stability requirements. Damage stability is evaluated deterministically, for side and bottom damage cases of fixed, prescribed dimensions, e.g. a damage length of 10% of ship’s length, and for side damages a penetration of 79 cm (type G and C) or 59 cm (type N). The survival criteria are related to the residual GZ-curve, as depicted in fig. 1, and read:

- At the stage of equilibrium (final stage of flooding), the angle of heel shall not exceed 12° .
- Non-watertight openings shall not be flooded before reaching the stage of equilibrium. If such openings are immersed before that stage, the corresponding spaces shall be considered as flooded for the purpose of the stability calculation.
- The positive range of the righting lever curve beyond the stage of equilibrium shall have a righting lever > 0.05 m in association with an area under the curve of > 0.0065 mrad. These values shall be satisfied up to immersion of the first non-watertight opening and in any event up to an angle of heel $< 27^\circ$.
- The lower edge of any opening that cannot be closed watertight shall, at the final stage of flooding, be not less than 0.10 m above the damage waterline.

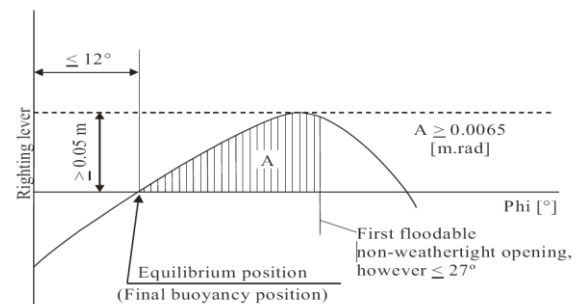


Figure 1: ADN (2013) damage stability requirements.

As such, these stability criteria are quite conventional, and it would be expected that they would not be subject to interpretation differences. However, it took multiple annual ADN meetings before some apparently minor issues have been regulated firmly. Those issues are:

- Watertightness of ventilation openings, such as gooseneck openings or tank vent check valves (as illustrated in fig. 2).

- Watertightness of the accommodation entrance, accommodation windows and the seal between accommodation and upper deck.
- Watertightness of the exhaust.



Figure 2: Examples of automatic closing tank vent device, with floating ball.

Although these “details” may look trivial at first glance, in many occasions they may be of prevailing importance for the economic feasibility of a ship design, see the example in fig. 3, where a damage to the aft cargo region is depicted, combined with a still intact engine room (ER). The damaged waterline is already situated above deck level in the ER region, threatening potentially critical points, such as windows, doors, ventilation openings and deckhouse seals. If one of these items cannot be considered watertight according to the applicable rules, and the ship’s subdivision cannot be redesigned anymore, the only remedy would be a sharp decrease of intact draft, leading to a significant loss of deadweight.

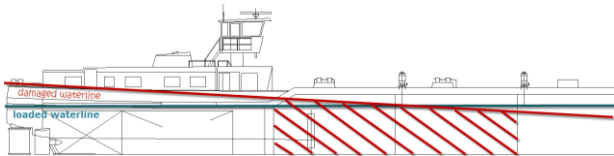


Figure 3: Damaged waterline in aft ship region.

Additionally, by ADN 2015, also longitudinal strength was required to be included in loading software. It is good that these aspects are also included in the safety assessment of an IWW tanker. After all, all required data are already available in the loading instrument, so the additional effort to compute shear forces and bending moments is not high.

By the way, as a side step, it should be noticed that double hull IWW tankers may show a remarkable amount of longitudinal strength. Take e.g. the ship of fig. 4, that sailed right through a weir in the river Meuse, on December 29, 2016. It

fell from the weir, some three meters down, and survived without major structural hull girder damage.



Figure 4: Tanker, just fallen from weir.

By ADN rules, tankers need to be equipped with a loading instrument from January 2015, and should comply with all other ADN 2015 requirements. In order to give the industry the opportunity to gradually process all vessels, a relaxation has been introduced, where this date is postponed until the first class certificate renewal. Because these certificates expire after five years, this implies that by the end of 2019 all tankers will comply, Lloyd’s Register (2016).

4. SPECIFIC FUNCTIONS AND FEATURES OF THE LOADING INSTRUMENT SOFTWARE

In general, a loading instrument for IWW application does not differ from instruments for other types of ships. In the course of the years, our loading software has been delivered for general cargo seagoing vessels, naval vessels, offshore platforms, submarines, etc. for which the basis is all the same. Obviously, there can be ship-type-specific enhancements, such as a stinger module for a pipe-laying vessel, a pipe loading module for offshore supply vessels or a periscope module and compression correction for submarines.

Similar specific module for IWW tankers are not required. However, there are five specific computational aspects that play a role in IWW (damage) stability calculation, these are elaborated below.

Automatic propagation of damage case

When evaluating the damage stability results, it might be concluded that a calculation does not comply with the damage stability criteria because an opening of an intact compartment is submerged.

One might wonder what the conclusion would be if the flooding would be extended through that opening. The evaluation of such *progressive flooding* requires flooding scenario assumptions, and is in general still uncharted territory. However, for IWW application, our software contains a provision — acceptable for at least one of the major classification societies — which may result in a larger loading. It is specifically targeted at the requirement that open openings should have a “freeboard” of 10 cm in the final flooding condition, and contains the following steps:

- If a particular damage case does not meet this criterion then the conclusion is drawn “It is yet undetermined whether this damage case complies”, and an additional damage case is created where the compartment connected to this opening will also be flooded.
- From these additional damage cases also the intermediate stages of flooding are computed, starting with a filling percentage of 1% for the newly added compartments. This reflects the fact that these are just about to be flooded, but also verifies whether the original damage case meets the other stability criteria.
- Since the flooding through such an opening may take a long time, it is not certain that in all cases assessment against the stability criteria for intermediate stages is allowed. Therefore, in this case the criteria for the final stage of flooding are applied.
- This mechanism reiterates, so, if such a newly generated damage case also does not comply because an other opening has a too small distance to the waterline, then a further additional damage case will be created, etc. etc. Until it is demonstrated that it will comply in this case of progressive flooding (in which case the original damage case complies), or until the ship no longer satisfies another stability criterion (in which case the damage case does not comply).

Computation to SB and PS combined, with integral stability requirements assessment

An elder version of our damage stability software initiated a computation with the determination of the “side with the worst stability” (PS or SB), which is determined with a very simple

metric, being the side of the heel. It has always been obvious that this is only an approximative criterion, but for sea-going vessels it was sufficient. However, IWW ships may have a rather asymmetric layout of openings, while openings play such an important role in stability assessment. So, it might very well be that an opening at the side opposite to the heel is critical. This effect can only be covered by a full computation to both sides, which is the standard today.

Maximum allowable VCG method vs. shift of liquid

Traditionally, the adverse effects of free surface moments are accounted in a virtual rise of VCG. This method has the disadvantage that the free surface effect is applied at all angles of heel, while in reality its effect may be limited to the smaller heeling angles. Notably with tanks which are almost empty or almost full. Taking into account the real shift of liquid — both transverse and longitudinal — is commonplace these days, and it is somewhat amazing to see how some people still make do with maximum allowable VCG tables based on the traditional virtual VCG.

Facility to compensate for ‘measured’ cargo tank volumes

Tank volumes of cargo (and fuel oil) tanks are available from two sources, either based on the “theoretical” (=design) volume of the hydrostatic model, Boolean intersected with the tank boundaries, or based on the “practical” tank shape, as measured from the as-built ship. The latter delivers the so-called “calibrated” tank tables, which are used by shippers and customs. Although in practice the difference between the two sets of tables may not be large, working with different tank volumes is confusing. For that reason the loading software contains a compensation facility, which smoothens out the volume differences, and consequently dampens the human mood.

Hydrostatic - elastic interaction

IWW vessels have a relatively low depth in common, and are consequently relatively flexible. So, their hogging or sagging situation may be rather deflected, which has an effect on deadweight and drafts. Because draft constraints are tight — bottom draft as well as air draft — taking such deflection into account in the hydrostatic analysis will lead to

a more accurate computation, which is beneficial to loading and for navigation in confined canals. Although such a feature would certainly be feasible, the interest from ship owners is limited. A factor in this respect is that the official tonnage determination is based on the UN (1966) Convention, which does not support deflection compensation.

5. SHIP DATA COLLECTION AND RELIABILITY

Loading instruments have to be installed on each and every chemical IWW type C and type G tanker, also the elder ones. For that purpose the static ship data have to be collected and defined in a computer-readable format. If drawings are available then this is (just) a matter of digitizing or measuring those drawings, such as:

- A lines plan or body plan, for the hull shape.
- Tank plan or general arrangement plan, for the shape of the internal geometry (tanks and spaces).
- Safety plan, for the locations of openings, and their types.
- Intact stability booklet, for the light weight and its Center of Gravity.

All quite standard, one would say. Unfortunately, more often than once, this data is not available, or not reliable. Notably for the elder vessels. Pitfalls and remedies are discussed in the sub-sections below.

Hull shape

In quite some cases loading instruments have to be retrofitted. If the vessel is of an elder make, obtaining the lines plan may be difficult. If the lines plan is lacking, the hull shape can be reconstructed on the basis of other shape information, such as a tank plan, a construction plan, or pictures. Anything with shape info can be of assistance. Anyway, an advanced hull form modeller is a prerequisite, because an IWW vessel may possess complex shape features, see the example in fig. 5. In the extreme case that no such info is available, shape measurement by laser scanning or photogrammetry, Koelman (2010), could be applied. However, the authors have not yet experienced a necessity to do so for IWW vessels.

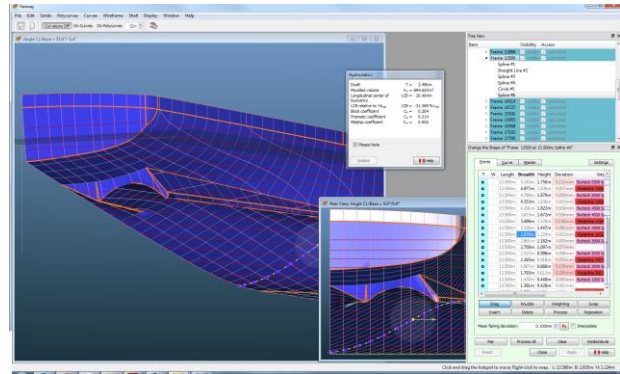


Figure 5: IWW vessel with integrated propeller tunnel.

Tank and compartment shape

Tank shape data, as laid down in a tank arrangement plan, appear to be quite reliable. Sometimes data for small consumable tanks are missing, or tank destinations are mixed up. In general such anomalies can be discovered and corrected quickly.

Openings

People often tend to emphasize on hull shape definition (“where is the lines plan?”). However, in practice other reliable ship data may be harder to find, for example non-watertight openings. A bit exaggerated, at SARC we sometimes say a correct list of openings is more important than the body plan. However, exaggerated? In section 3 it was illustrated that opening particulars can make or break the economic feasibility of a ship (design). Anyway, lists or drawings of openings are notoriously unreliable; the only reliable source is on-board measuring of type, location and connection of openings, an aspect which is also recognized by classification societies, who require independent verification of openings by a surveyor.

Measuring openings is essentially a simple task, which can easily be done with bloc note and measuring tape. However, in practice errors and confusions are easily made. At SARC a dedicated app was developed, from which the system diagram is depicted in fig. 6. This app provides a streamlined procedure, and makes the measurements to be more reliable and more traceable by illustrating them with pictures. The app also make the measurements more standard, and hence less sensitive to subjective considerations.

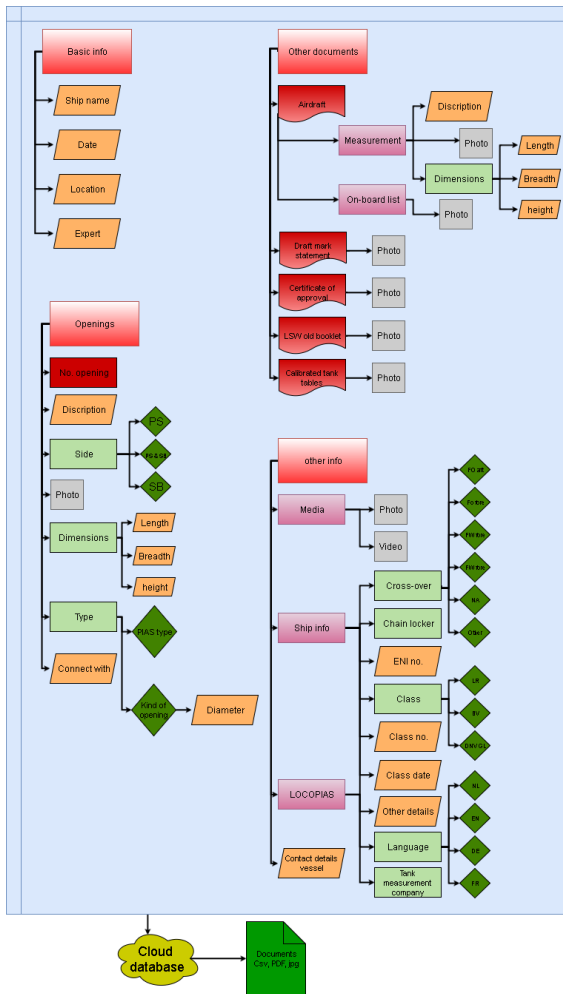


Figure 6: Flowchart of opening measurement tablet app.

Light ship weight, and its distribution

Being one of the most prominent weight items, the accuracy of light ship weight and Center of Gravity (CoG) is of paramount importance. As a rule, these data are readily available from design documents, or from tonnage measurement recordings. However, their reliability is not always guaranteed. Sources for inaccuracies may be:

- Light ship drafts taken for empty ship, without the deflection (hogging) taken into account.
- Light ship drafts taken while the ship is not completely ready to sail. Or the opposite, with non-empty consumable tanks.
- Increased light ship weight during the life time of the ship.

Light ship assumptions that differ from reality will be encountered by a difference in drafts as computed by the loading instrument, and the observed drafts. Such differences may lead to emotional responses by the crew, emailing “your software is faulty!”, while the cause can be brought

back to inadequate input data. In principle the remedy is easy: “just” enter the correct light ship weight and CoG. However, here is a small caveat. In the form of the classification society that may only accept observed draft measurements (for light ship!) and does not allow reverse engineering of light ship particulars based on drafts as measured for the fully loaded vessel.

As a workaround, at SARC we have developed a form and a procedure that can be used by the crew to a) track the real drafts for a number of voyages, b) convert those drafts into a deadweight constant, and c) add (or subtract) this constant to the pre-defined (and fixed) light ship and CoG of the loading instrument. So, through the backdoor of the deadweight constant — an established concept in sea shipping — the light ship can still be tuned to the observed drafts.

6. APPLICATION AND ACCEPTANCE OF LOADING INSTRUMENTS BY CREW AND MANAGEMENT

In general, management of major ship owners support the implementation of ADN requirements wholeheartedly, which is obvious, because it simply is the law. In one particular example the loading software is integrated with the ship owners’ logistic system, where the procedure is such that a ship is only allowed to depart if the loading for that particular journey has been computed and uploaded to that system, **and** if that computation indicates that it complies with all stability and strength criteria.

Crew acceptances are mixed. The majority accept the software and procedures as they are, which will also be assisted by the fact that operation of the software is quite obvious; the Graphical User Interface provides a “what you see is what you get” experience. Others debate the necessity of these practices, and find it to be only bureaucratic. Particularly annoying is the fact that the software can be produced on the basis of incorrect light ship data, which makes the computed drafts not to correspond with the observed drafts. This phenomenon may make a user to put the correctness of the loading instrument as such in question. Fortunately, with some explanation, the procedure as discussed in the previous section and the deadweight constant, this issue can be resolved.

7. ASSESSMENT AND APPRAISAL

Although all requirements are regulated by national laws and the ADN Convention, the authorities have sourced out the verification of certification to private companies, in the shape of the well-known classification societies. In general, they assess according to the same standards, and occasionally they don't, as illustrated in the next sub-sections.

Requirements for stability booklets and other documentation

Before loading software can be issued for appraisal at a classification society, the paper documentation needs to be ready and approved. This comprises:

- Intact and damage stability booklet. Depending on the software type (VCG vs. shift of liquid) including maximum allowable VCG tables.
- Computations of bending moments and shear forces, and verification against maximum allowable values.
- Damage control plan including all openings. The opening types and locations have to be witnessed by a class surveyor.

Software appraisal

Software appraisal procedures are at the discretion of the particular classification society. One society applies a type-approval process on loading software, which implies that on the basis of some generic test cases a five-year type approval certificate is issued. Additionally, a ship-specific software assessment is required where input data are verified. Other societies have only taken the ship-specific route, they don't offer or require a type approval. In any case the assessment is said to be supported by independent calculations.

Differences between classification societies

In section 3 the regulatory framework has been discussed. This is applicable to all ships, regardless of the classification society. The ADN committee decides annually on uniform interpretations, so that list is growing in time. Nevertheless some differences between classification societies remain to exist:

- A requirement is that the draft marks are not submerged. Differences are that some societies are satisfied by not submerging the average of

PS and SB marks, while other stipulate that not a single individual mark may be submerged.

- Similar differences are imposed between booklet and loading software. This may lead to a loading condition in the booklet that complies (and is accepted), while the same condition in the loading software does not comply.
- Watertightness of the exhaust pipe.
- Maximum allowable shear forces and bending moments. These are determined on the so-called Read-Out Points (ROP). Some societies provide maximum values only for midship, or on ROPs in the midship region, so no limits are imposed on the aft and forward extremes of the ship. Other societies linearly interpolate their maximum values between the parallel midbody value, and zero at the extremes. As illustrated in fig. 7, where the curved (red) line represents the actual bending moment. If the maximum allowable moment is simply assumed to be linear between points A and D, a small local exceedance of that maximum appears, leading to non-compliance. However, an analysis with a finer step size will show non-linearity, in a trend according to curve A-B-C-D, and hence lead to compliance. So, the conventional analysis can be a bit coarse and consequently somewhat unrealistic. As if the aft peak would break away from the vessel!



Figure 7: Actual and maximum bending moments.

Additional discomfort occurs sometimes when individual surveyors impose requirements that differ from their colleagues, or from the “company standard”. However, with some smooth talking, or reference to earlier projects such issues can often be resolved.

8. CONCLUSIONS AND RECOMMENDATIONS

An overview has been given of factors that exercise their effects on intact and damage stability assessment of IWW tankers, and on loading instruments for those ships. Although no specifically advanced theoretical concepts are required, the involvement of many actors — national authorities, the ADN Convention, ship owners, crew, shippers, classification societies, consultants, ship designers and software suppliers — made that it took some time to reach general consensus. Details thereof, and the standard from today have been sketched in this paper.

It will not be easy to change one of the bricks in this edifice. Having said that, the authors take the freedom to propose a few improvements:

- Relax a bit on the dogma that a class-witnessed inclining test or light ship survey results in the only truth of light ship particulars.
- Allow for taking into account the effect of hogging or sagging into hydrostatics. And consequently modernize the 1966 Tonnage Measurement Convention.
- Stimulate that more ship owners apply the good practices as touched in section 6.
- Increase awareness of the importance of keeping openings closed, such as doors and hatches. And enforcing these issues a bit more strict.
- Don't fall back on traditional computation methods where state-of-the art alternatives are available, as they have been discussed in section 4.

REFERENCES

- ADN 2015, "European Agreement concerning the International Carriage of Dangerous Goods by Inland Waterways". January.
- EU 2006, "Directive 82/714/EEC laying down technical requirements for inland waterway vessels", December 12.
- Koelman, H.J. (2010), "Application of a photogrammetry-based system to measure and re-engineer ship hulls and ship parts: An industrial practices-based report", *Computer-Aided Design, Volume 42, Issue 8, August*.
- Lloyd's Register EMEA. (2016), "Inland Waterways Computer Loading Instruments", July 6.

Rotteveel, E and Hekkenberg, R. (2015), "The influence of shallow water and hull form variations on inland ship resistance", Proc. IMDC 2015, Tokyo.

Rotteveel, E., Hekkenberg, R., v.d. Ploeg, A. (2016), "Optimization of ships in shallow water with viscous flow computations and surrogate modeling", Proc. PRADS 2016, Copenhagen.

SARC (2013), "LOCOPIAS online manual", www.sarc.nl/images/manuals/locopias/htmlEN/index.html.

UN 1966, "Convention on the measurement of inland navigation vessels", February 15.

WSV 2013, "TMS Waldhof accident investigation report - summary", www.ccr-zkr.org/files/actualitesfocus/focus-/Waldhof_Bericht_Zusammenfassung_en.pdf.

Stability and seakeeping of river-sea vessels: Classification rules

Jean-Michel CHATELIER, *Bureau Veritas, DNI*, jean-michel.chatelier@be.bureauveritas.com

Wa Nzengu NZENGU, *Bureau Veritas, DNI / RDT*, wa.nzengu@be.bureauveritas.com

Raffaele COCITO, *Bureau Veritas, DNI / APO*, raffaele.cocito@be.bureauveritas.com

ABSTRACT

River-sea vessels are vessels intended for inland navigation waterways and suitable for restricted navigation at sea. Suitability for restricted navigation at sea should be proven by the compliance with appropriate Rules of a recognized classification society as well as with applicable regulatory requirements. As statutory Regulations are not always available, classification Rules are expected to include those vessel design and equipment topics generally prescribed by administrations. This paper provides an overview of researches carried out by Bureau Veritas Inland Navigation Management aiming to support development of upgraded inland class Rules requirements related to vessel stability and seakeeping. For the sake of illustration of the requirements to be developed, the paper gives the proposed formulation together with the validation results of heave acceleration, vertical wave bending moment, roll amplitude and relative wave elevation, as well as basic considerations regarding the evaluation of the vessel intact stability.

Keywords: *class rules; river-sea navigation; hydrodynamics; seakeeping; stability.*

NOMENCLATURE

D_{ref}	Reference duration [s]
$G(\omega, \beta)$	Directional spreading
GM	Metacentric height [m]
H_s	Significant wave height [m]
k_{xx}	Gyration radius around the longitudinal axis [m]
L	Vessel length [m]
B	Vessel Breadth [m]
C_B	Block coefficient
T_z	Wave mean zero up-crossing period [s]
Δ	Vessel displacement [t]
σ	Relative measure of the width of the peak
γ	Peak enhancement factor
ω	Wave frequency [rad/s]
ω_p	Wave peak frequency [rad/s]
n	Navigation coefficient: $n = 0.85H_s$

1. INTRODUCTION

A solution to existing barriers in sea-inland connection is the development of a waterborne transport chain linking sea and inland waters, realised by vessels (sea-river or river-sea) that bypass seaport terminals and deliver cargo directly to inland destinations. Only river-sea vessels are considered in this paper, i.e. vessels intended for

inland navigation waterways and suitable for restricted navigation at sea. Suitability for restricted navigation at sea should be proven by the compliance with:

- applicable regulatory requirements prescribed by the competent authority,
- appropriate vessel design and equipment requirements of a recognized classification society.

An overview of existing applicable Rules and Regulations is given in Section 2. In these requirements, acceptability of the vessel is defined according to the following main approaches:

- probabilistic approach implemented in a risk assessment process defined by the competent authority,
- probabilistic approach implemented in a direct calculation process according to guidance of a recognized classification society,
- compliance with classification rule requirements developed on the basis of a deterministic approach.

In navigation areas not covered by regulatory requirements, classification Rules are expected to include those vessel design and equipment topics

generally prescribed by administrations. Today, most of classification prescriptive formulas and criteria dealing with seakeeping applicable to river-sea vessels are derived from seagoing vessels rules. Section 3 provides an overview of research activities carried out by Bureau Veritas Inland Navigation Management, aiming to support development of upgraded inland class Rules requirements related to vessel stability and seakeeping. Proposed requirements are derived from the results of direct simulations conducted on inland vessels operated in restricted sea water stretches characterised by a significant wave height $H_S \leq 2$ m. For the sake of illustration of the requirements to be developed, the paper gives the new formulation together with the validation results of heave acceleration, vertical wave bending moment, roll amplitude and relative wave elevation. Basic considerations regarding the evaluation of the vessel intact stability are given in Section 4.

2. RULES AND REGULATIONS

2.1 Statutory Rules

2.1.1 General

National Regulations are developed to address those vessels not covered by the international requirements, i.e., those vessels that only operate in their national waters [1]. A country may choose to develop entirely different standards or incorporate, where possible, the international Regulations. For inland navigation vessels intended for operation in territorial sea waters, the most significant topics covered by these Regulations are those regarding vessel sea worthiness, providing the requirements concerning vessel stability and seakeeping. Some examples of national Regulations thoroughly developed in [2] are given hereafter.

2.1.2 Belgian Regulations

In Belgium, a Royal Decree [3] governs cargo vessels operating along the Belgian coast at a maximum distance of 5 NM from the coast. To obtain the corresponding certificate, specific requirements are applicable covering fire safety, intact stability, lashing of containers, bilge arrangement, emergency power source, bulwark / handrails, anchors, life-saving appliances, radio communication and navigational equipment. Tank vessels must comply with MARPOL Annex I

requirements for double hulls, tank arrangements and damage stability. A hydrodynamic study must be carried out to assess seakeeping ability and the risk of slamming, shipping of water, excessive bending moment or lateral acceleration. The permissible occurrences are once a year for slamming and once in the vessel's lifetime for the other categories, where probability is based on 300 return voyages per year for a 20-year lifetime.

2.1.3 French Regulations

A French Regulation [4], similar to Belgian Royal Decree, applies to container vessels calling at Le Havre from the Seine. The vessels must comply with the Annexed Regulations of the A.D.N. [5], plus additional requirements. A hydrodynamic study must be carried out following the same principle as in Belgium taking the wave particulars of the area into account, although the assumptions regarding the number of voyages per year (100) and occurrences (once a year for all except bending moment and lateral acceleration, which are once in the vessel's lifetime) are different.

2.1.4 Indian Regulations

In India, so-called 'river-sea' vessels carrying dry cargo or oil products are allowed to operate along the Indian coast if they comply with national Regulations [6]. They are graded according to four types, depending on service and navigation conditions. Types 1 and 2 are designed for a maximum significant wave height of 2 m and may be considered as improved inland navigation vessels, while types 3 and 4 are regarded as seagoing ships.

2.1.5 Chinese Regulations

In China, there are Regulations for inland vessels [7] covering access to the maritime harbours of Shanghai and Hong Kong provided the route is not farther from the shore than 5 km. Inland navigation vessels are graded according to three categories of wave height, which can be up to 2 m (corresponding to probability of exceedance of 5%), while ships allowed to undertake longer voyages between ports within the territorial waters benefit from derogation to IMO conventions.

2.1.6 Russian Regulations

In Russia, there are comprehensive Regulations [8] covering all types of inland and river-sea vessels under which water basins are classed in four

categories depending on wind-and-wave conditions on the basis of the maximum normative wave height - up to 2 m (corresponding to probability of exceedance of 1%) and even 3 m (corresponding to probability of exceedance of 3%)

2.2 Class Rules

The national Regulations mentioned in Section 2.1 entail classification of the vessels according to the Rules of a recognized classification society. The classification Rules for inland navigation vessels can be used in part to ascertain a vessel’s suitability to operate in the maritime environment and to ensure the maintenance of proper levels of safety. The Rules of Bureau Veritas applicable to inland navigation vessels already include specific notations based on the maximum significant wave height, which may be up to 2.0 m. The classification Rules would have to be completed by requirements regarding topics not covered by classification such as navigational equipment, life-saving appliances and crew qualification, but also possibly with some other technical requirements for instance with regard to minimum bow height, freeboard, door sills, hatch coamings, etc. to take the actual local conditions into account.

3. SIMPLIFIED FORMULAS FOR LONG TERM RESPONSES PREDICTION

3.1 Introduction

Because of the complexity of sea waves and of the dynamic interaction between vessel and waves, the direct calculation of an appropriate design value of wave response for a given vessel is a very complex and time consuming task. Therefore, the main step of the research covered by this paper consists in developing simplified formulas allowing prediction of long term wave-induced responses to be used for the development of upgraded class Rules applicable to river-sea vessels. Simplified formulas are expressed in terms of the principal characteristics of the vessel. They are derived from results of direct simulations conducted on typical inland vessels according to the conditions and procedure described in this section and supported by the research reported in [9] and [10].

3.2 Vessels database

This study has been performed using a database made of 60 vessels with main characteristics lying within the ranges given in Tab. 1 and Fig. 1 to Fig.

3. Most of vessels are tankers with a few container vessels.

Table 1: Range of vessels parameters

Parameter	Range
Length (m)	$35 \leq L \leq 135$
Breadth (m)	$5.0 \leq B \leq 22.8$
Draught (m)	$2.2 \leq T \leq 5.2$
Displacement (t)	$405 \leq \Delta \leq 14428$
Block coefficient	$0.82 \leq C_B \leq 0.99$

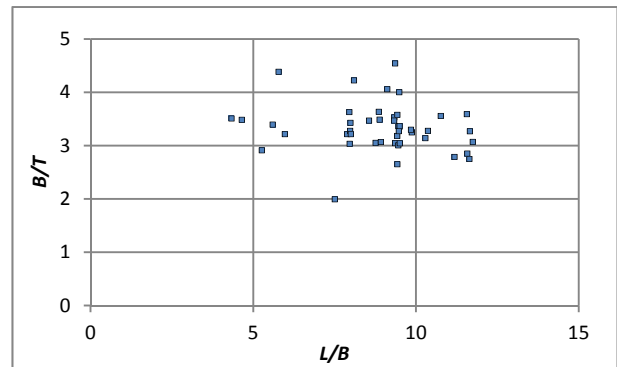


Figure 1: Range of B/T vs L/B

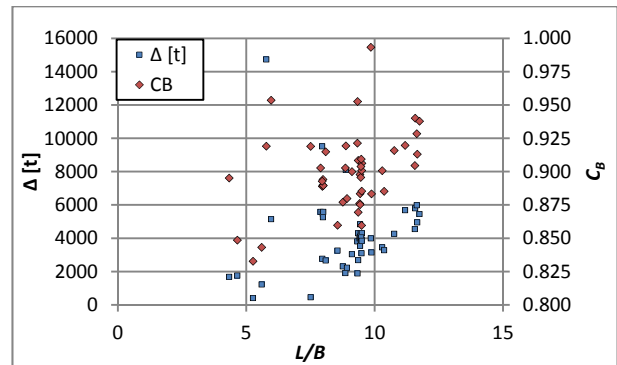


Figure 2: Ranges of Δ and C_B vs L/B

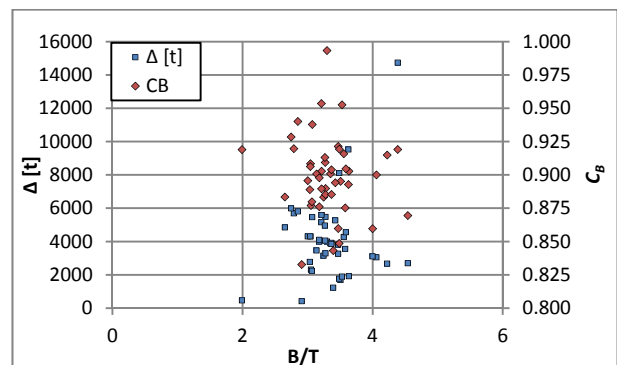


Figure 3: Ranges of Δ and C_B vs B/T

3.3 Operational parameters

3.3.1 Loading conditions

Simulations for each vessel are carried out in two loading conditions. The first loading condition

corresponds to the maximum allowable draught in which the vessel is fully loaded. The second loading condition is related to the minimum draught in which the vessel is ballasted. In these two loading conditions, the real weight distribution is taken into account.

3.1.2 Roll damping

As mentioned in [11], a typical ship without roll suppression devices such as bilge keels or the like will have a value of non-dimensional roll damping coefficient less than 5 percent. In this study, 5 percent is adopted when taking account of the fact that most of the river-sea vessels are equipped with bilge keels which increase considerably this non-dimensional damping coefficient. With respect to the non-dimensional damping coefficient of the vessels approved by BV, this value is quite conservative.

3.4 Environment and simulation parameters

Simulations are conducted for vessels operated in two navigation areas:

- the Belgian coastal water, according to the vessel course shown in Fig. 4
- the estuary of the river Seine to the harbour Port 2000 (Le Havre) in France, according to the vessel course shown in Fig. 5.

The water depth is taken to be 15 m, for both navigation zones. A constant velocity of 10 knots is adopted for all the vessels, corresponding to Froude number ranging between 0.14 and 0.28.

For the Belgian coast, one-year wave data collected in way of Bol Van Heist buoy, see location in Fig. 4, are used. A three-year wave data in the considered navigation area in France, collected in way of different buoys are considered for simulations. The comparison of wave scatter diagram envelope prevailing in both operating areas is shown in Fig. 6.

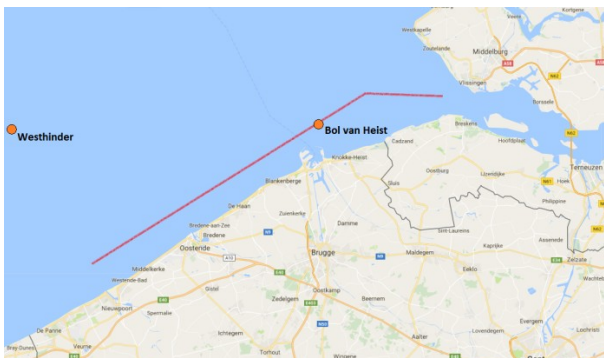


Figure 4: Scheldt – Nieuwpoort Route (BE)



Figure 5: La Seine - Port2000 Route (FR)

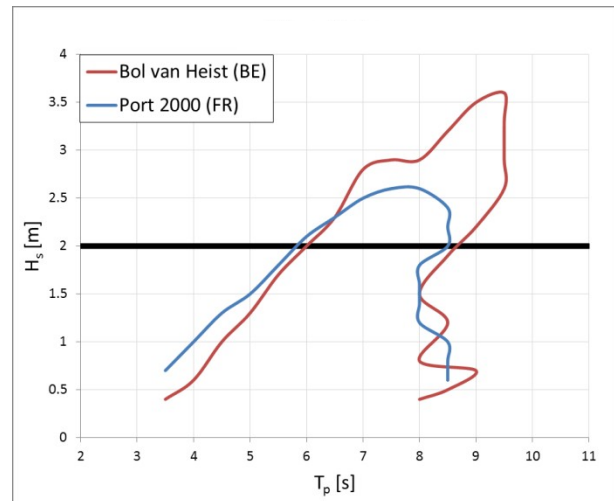


Figure 6: Wave scatter diagram envelope

3.5 Direct calculation of long term hydrodynamic responses

3.5.1 Calculation tool

The calculation of long term responses has been performed with the software HydroStar version 7.25. Based on the three-dimensional potential flow theory, HydroStar solves the problem of water wave diffraction and radiation around a ship or an offshore structure in deep water as well as in water of finite depth. The method of boundary integral equation (panel method) is used. It had benefited from continuous evolvement, the inspiration of most recent theoretical findings and efficient numerical algorithms. In particular, the advanced algorithms for the Green function - elementary solutions to the first order wave diffraction/radiation problems and application of newly-developed formulations to compute the second order wave loads in an efficient and accurate way. The most advanced features include multi-body hydrodynamics, wave-current-body interaction, coupling of seakeeping with effect of liquid motion in tanks, second-order low frequency and high-frequency QTF in multi-directional

waves, mixed panel-stick model and consistent interface of hydro and structure analysis.

3.5.2 Wave spectrum

Statistics of the sea states during one year at the buoy Bol van Heist such as significant wave height, peak period, wave direction and spectral energy are provided by the Belgian Authorities. By use of JONSWAP spectrum model (1) with $\gamma = 1$, it is seen that the modelled spectral energy fits very well the measured one.

$$S_w(\omega) = \frac{\alpha g^2}{\omega^5} \exp\left[-\frac{5}{4}\left(\frac{\omega_p}{\omega}\right)^4\right] \gamma \left[\exp\left(-\frac{(\omega-\omega_p)^2}{2\sigma^2\omega_p^2}\right)\right] \quad (1)$$

An example of the comparison between modelled wave spectrum energy and measured one for one sea state is shown in Fig. 7.

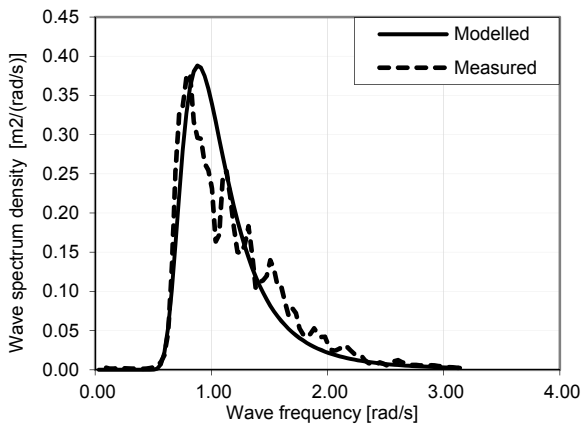


Figure 7: Comparison between modelled and measured wave spectrum energy

Sea states in the navigation zone toward/from Port 2000, in which JONSWAP spectrum model with $\gamma = 1.8$ is used are provided by the French Authorities then used as input data for the spectrum analysis in this study.

3.5.3 Long term statistics

A short term analysis is performed for each sea-state in a list of sea states observed during a reference duration D_{ref} . The long term distribution is obtained by cumulating the results from the short term analysis in order to obtain an extreme value at a probability of exceedance of 10^{-8} for vertical wave induced bending moment and at a probability of exceedance of 10^{-5} for local loads and motions. The method implemented consists in counting, over all sea-states up to $H_S = 2$ m, of all maxima of the

response (i. e. each response cycle). It can be written as:

$$n_{ex}(X) = \sum_{ss=1}^{ss=N_{SS}} n_{ss} (1 - P(X)) \quad (2)$$

where N_{SS} is total number of sea-states; $n_{ex}(X)$ is expected number of exceedance of a response level X , over a reference duration D_{ref} ; $P(X)$ is probability distribution for the sea-state ss :

$$P(X) = 1 - \exp\left(-\frac{X^2}{8m_0}\right).$$

n_{ss} is number of response cycles for a sea-state ss :

$$n_{ss} = \frac{D_{ref}}{T_z} Prob(ss),$$

where $Prob(ss)$ is the probability of occurrence of the sea-state ss .

X is range of response in double amplitude. The reference duration D_{ref} is calculated based on an assumption that the vessel of interest navigates during 85% of his 20-year lifetime.

3.5.4 Comparison of vessels responses between the two navigation areas considered

Due to similarity of the scatter diagram envelope up to $H_S = 2$ m (see Fig. 6), the values of vessels responses obtained for the 2 navigation areas covered by this study are very close as emphasized, for instance, in Fig. 8 and Fig. 9 for heave acceleration and roll amplitude respectively.

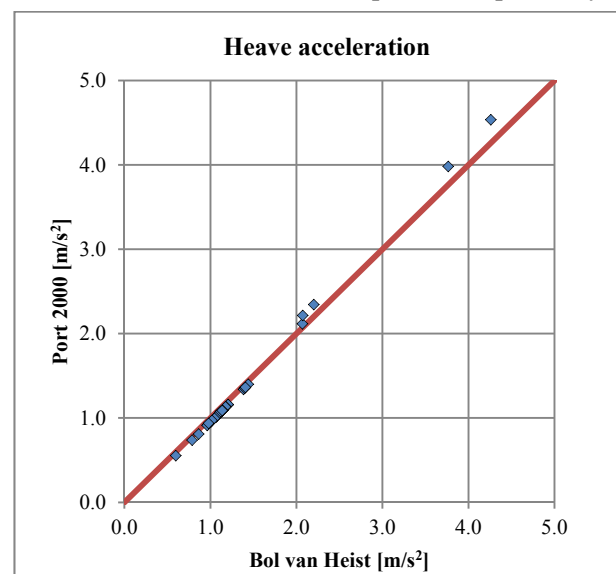


Figure 8: Comparison of responses – Heave acceleration ($H_S = 2$ m)

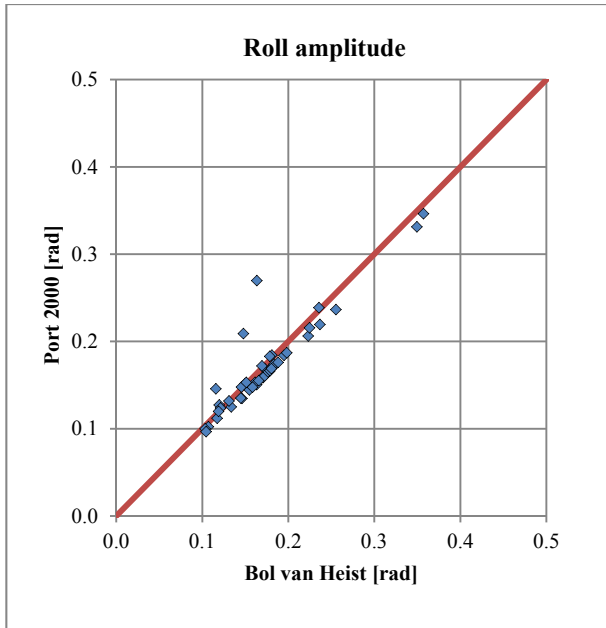


Figure 9: Comparison of responses – Roll amplitude ($H_S = 2$ m)

3.6 Development of simplified formulas

3.6.1 General

The long term response in the formulas to be developed is in single amplitude. Motions and accelerations are considered with regards to the centre of gravity.

3.6.2 Wave parameter

The study carried out by Hauteclocque and Derbanne [12] shows that in the existing BV Rules [13] and [14], the wave parameter H_W is used to figure out the influence of the vessel's length in its responses. Envelope formula for any given ship response X in single amplitude, can be written as follows:

$$X = H_W * L^{(k-1)} * \Gamma_S * f_{nl} * f_r, \quad (3)$$

where Γ_S is shape function, depending on the ship shape and mass properties; f_{nl} is non-linear factor; f_r is calibration factor; k is dimension number.

3.6.3 All motions, with the exception of roll

Using the procedure described in [12], the accelerations prediction formulas for sway, surge, heave pitch and yaw have been developed according to the following steps:

- The long term ship responses X obtained by the direct calculation are divided by $L^{(k-1)}$ (for k , see Table 2).

- The obtained values are scaled by γ which is a constant for each entity so that the maximum value of wave parameter H_W is equal to 1.
- The wave parameter is obtained in the following form:

$$H_W = \gamma \frac{X}{L^{(k-1)}} \quad (4)$$

- The wave parameter shape fitted to match the wave parameter values from direct calculation shown in Fig. 11 for each response, is given by formula (5):

$$H_W = \frac{n}{1.7} \left(\frac{L}{33.7} \right)^{-3} \quad (5)$$

- The non-linear factor $f_{nl} = 1$
- The calibration factor $f_r = 1$
- The dimension number k is given in Tab. 2.

Table 2: Dimension number

Entity	k
Linear acceleration	3
Angular acceleration	2

- Finally, the shape function Γ_S for each response is determined by the curve fitting on direct calculation.

$$F(P_L) = c_0 \prod_{p_i \in P_L} p_i^{c_i}$$

with $P_L = \{L/B, L/T, B/T, C_B \dots\}$

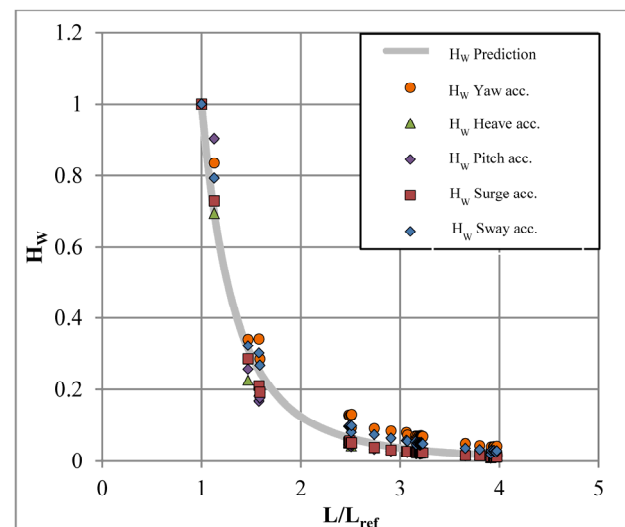


Figure 11: Wave parameters ($H_S = 2$ m) - Prediction vs direct calculation

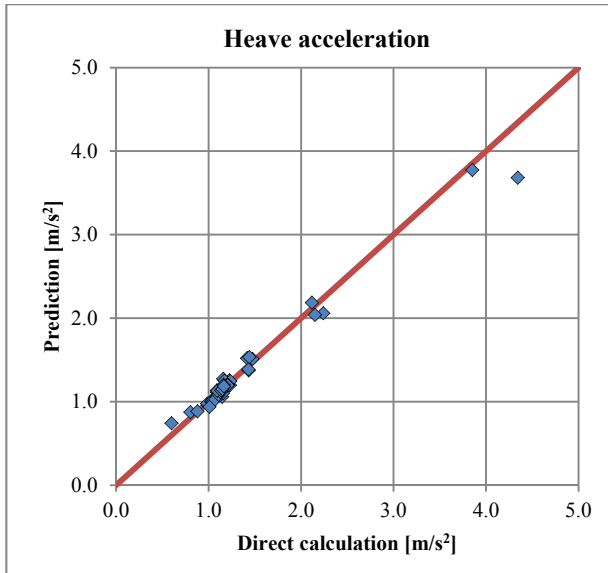
The accuracy of the developed prediction formulas is given in Tab. 3.

Table 3: Accuracy of proposed formulas

Response	Standard error	Mean error
a_{sway}	0.03	1.41 %
a_{surge}	0.01	-0.27 %
a_{heave}	0.12	-1.05 %
a_{pitch}	0.01	-1.53 %
a_{yaw}	0.00	3.44 %

Formula (6) shows an example of formula developed to predict heave acceleration. The predicted value is plotted versus direct calculation value for $H_S = 2$ m as shown in Fig. 12.

$$a_{\text{heave}} = 2.78 H_W L^2 \left(\frac{L}{B}\right)^{0.61} \left(\frac{T}{L}\right)^{0.38} C_B^{-1} 10^{-3} \quad (6)$$


Figure 12: Heave acceleration ($H_S = 2$ m) - Prediction vs direct calculation

3.6.4 Roll motion

The wave parameter H_W is given for roll motion as:

$$H_W = \frac{n}{1.7} \quad (7)$$

The extreme value of roll amplitude, in rad, is predicted by formula (8) and plotted against direct calculation value in Fig. 13 for $H_S = 2$ m.

$$A_R = H_W \left(\sqrt{\frac{GM}{k_{xx}}} + 2.15 \right) \frac{1}{\sqrt[3]{\Delta}} \quad (8)$$

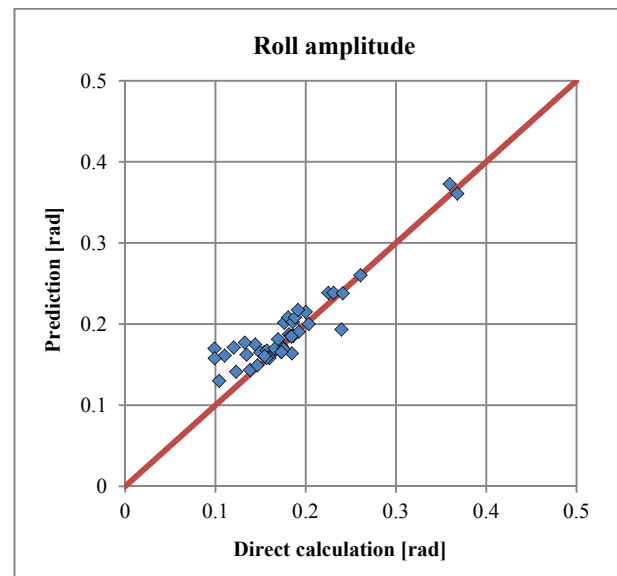
The roll acceleration may be calculated using formula (9)

$$a_R = A_R \left(\frac{2\pi}{T_R} \right)^2 \quad (9)$$

where T_R is roll period given by formula (10).

$$T_R = 2.3 \frac{k_{xx}}{\sqrt{GM}} \quad (10)$$

The accuracy of the developed prediction formulas is shown in Tab. 5 for roll amplitude and roll acceleration.


Figure 13: Roll amplitude ($H_S = 2$ m) - Prediction vs direct calculation

3.6.5 Vertical wave bending moment

The absolute value of the vertical wave bending moment, M_W is given by formula (11) and plotted against direct calculation value in Fig. 14 for $H_S = 2$ m.

$$M_W = 0.021 H_W L^2 B (C_B + 0.7) \quad (11)$$

Formula (11) has been derived from BV Inland Rules [13] by implementation of a unique formula (12) for the wave parameter H_W applicable to all vessels sizes.

$$H_W = n (10.5 - 0.023L) \quad (12)$$

The accuracy of the developed prediction formula is shown in Tab. 5.

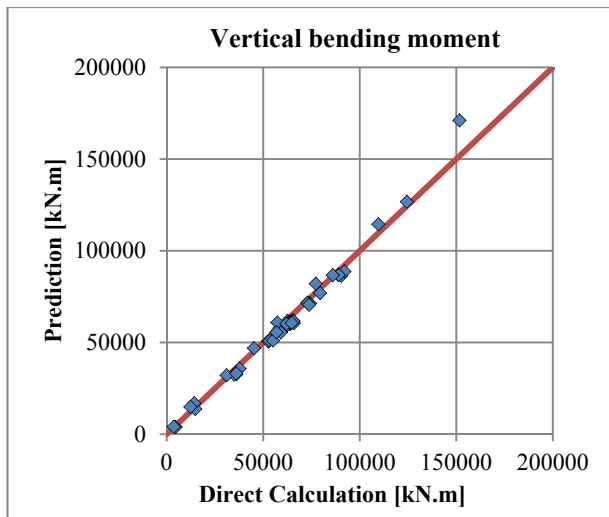


Figure 14: Vertical bending moment ($H_S = 2$ m) - Prediction vs direct calculation

3.6.6 Relative wave elevation

The wave parameter H_W is given for relative wave elevation as:

$$H_W = \frac{n}{1.7} \quad (13)$$

The extreme values of relative wave elevation, h_1 at different positions along the vessel are predicted by the formulas given in Tab. 4 and plotted against direct calculation values in Fig. 15 for $H_S = 2$ m.

The accuracy of the developed prediction formulas is given in Tab. 5 for relative wave elevation at location $x = 0.50$ L.

Table 4: Relative wave elevation

Location	h_1 [m]
$x = 0$ ($h_{1,AE}$)	$0.89 h_{1,M}$
$0 < x < 0.35 L$	$h_{1,AE} + \frac{h_{1,AC} - h_{1,AE}}{0.35} \frac{x}{L}$
$x = 0.35 L$ ($h_{1,AC}$)	$1.02 h_{1,M}$
$0.35 L < x < 0.50 L$	$h_{1,AC} + \frac{h_{1,M} - h_{1,AC}}{0.15} \left(\frac{x}{L} - 0.35 \right)$
$x = 0.50 L$ ($h_{1,M}$)	$4.7 H_W \frac{\Delta^{0.16}}{L^{0.4}}$
$0.50 L < x < 0.75 L$	$h_{1,M} + \frac{h_{1,FC} - h_{1,M}}{0.25} \left(\frac{x}{L} - 0.50 \right)$
$x = 0.75 L$ ($h_{1,FC}$)	$1.04 h_{1,M}$
$0.75 L < x < L$	$h_{1,FC} + \frac{h_{1,FE} - h_{1,FC}}{0.25} \left(\frac{x}{L} - 0.75 \right)$
$x = L$ ($h_{1,FE}$)	$17.5 H_W \frac{1}{\sqrt[3]{L}}$

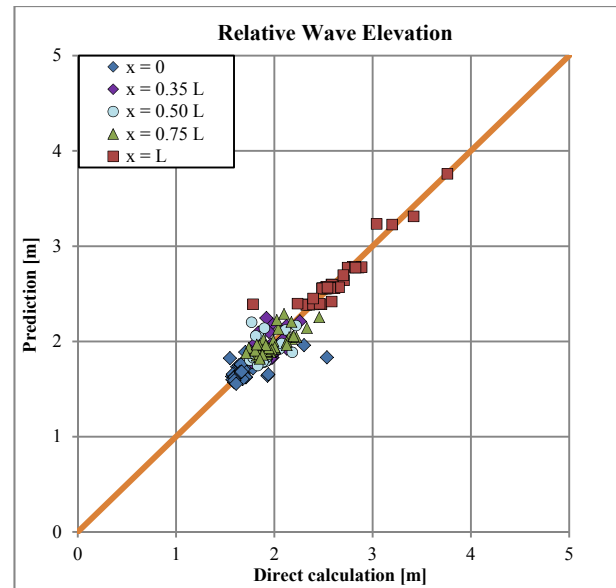


Figure 15: Relative wave elevation ($H_S = 2$ m) - Prediction vs direct calculation

Table 5: Accuracy of proposed formulas

Response	Standard error	Mean error
A_{roll} [rad]	0.03	4.89%
a_{roll} [rad/s ²]	0.03	8.94%
M_W [kN.m]	4102	-1.67%
$h_1(x = 0.5L)$ [m]	0.12	-0.18%

4. EVALUATION OF VESSEL STABILITY

4.1 Adequate intact stability

The vessel intact stability will be assessed according to the International Code on Intact Stability set out in the annex to the IMO Resolution MSC.267(85) [15], but using different parameters values as explained in Section 4.2.

4.2 Beam wind combined with rolling

4.2.1 Wind pressure

Wind data (maximum wind speed, V_{MAX} and mean wind speed, V) collected in way of Westhinder station on the Belgian coast (see location on Fig. 4) are plotted against significant wave height in Fig. 16. This figure also shows that the ratio V_{MAX}/V varies around 1.22. This ratio shows a good agreement with the increase of 50% in the heeling arm due to gust wind in comparison with steady wind as required in [15]. However, attention should be drawn to the fact that, depending on the geographical configuration of a considered operating area, the ratio of V_{MAX} to V may be higher.

In Fig. 17 are plotted against significant wave height the pressure induced by the mean wind speed calculated using formula (14) and the value of wind pressure prescribed by the European directive 2006/87/EC [16] for inland vessels stability assessment, $P = 250$ Pa. In the range of significant wave height considered, this pressure remains higher than the values derived from measured speed and, therefore, may be recommended as default value of steady wind pressure, where appropriate data are not available.

$$P = \frac{1}{2} \rho V^2 \tag{14}$$

where P is dynamic pressure, in Pa; ρ is air density, $\rho = 1.25 \text{ kg/m}^3$ at 10°C ; V is mean wind speed, in m/s at 10 m.

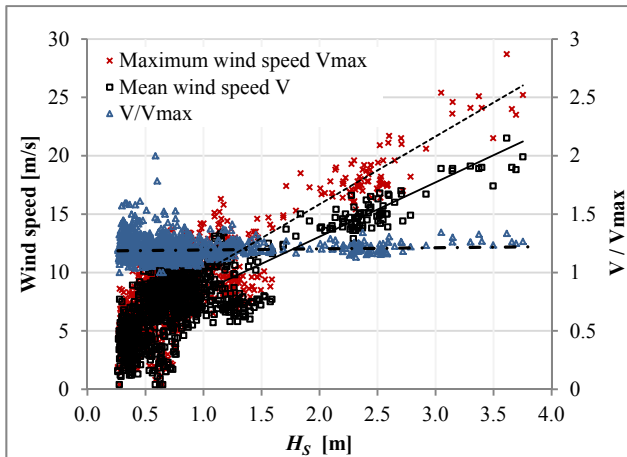


Figure 16: Wind speed – at station Westhinder

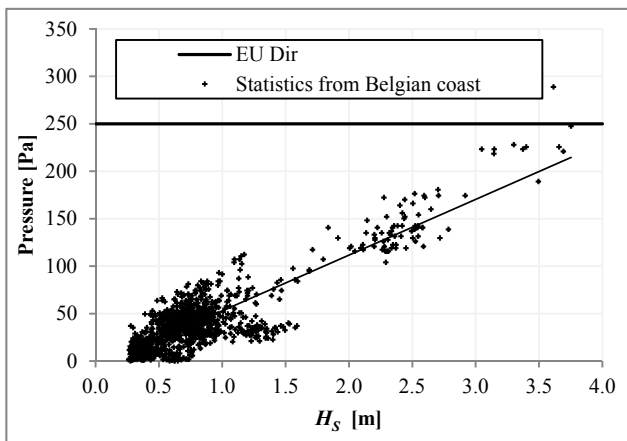


Figure 17: Wind pressure vs H_s at station Westhinder

4.2.2 Angle of roll to windward due to wave action

The angle of roll to windward due to wave action is calculated as follows:

$$\theta_1 = \theta_R + \theta_0 \tag{15}$$

where θ_R is roll angle:

$$\theta_R = \frac{180}{\pi} A_R \tag{16}$$

θ_0 is angle of heel under steady wind, A_R is roll amplitude determined according to paragraph 3.6.4.

4.3 Maximum allowable roll angle

The roll angle θ_R calculated according to (16) is to be limited as follows [3]:

$$\theta_R \leq \min (2\theta_f/3 ; 15^\circ),$$

where θ_f is the angle of heel in degree, at which openings in the hull, superstructures or deckhouses which cannot be closed weathertight immerse. In applying this criterion, small openings through which progressive flooding cannot take place need not be considered as open.

4.4 Safety clearance

The safety clearance is to be not less than the relative wave elevation determined according to paragraph 3.6.6. According to the Directive 2006/87/EC [16] the safety clearance is defined as the distance between the plane of maximum draught and the parallel plane passing through the lowest point above which the vessel is no longer deemed to be watertight.

5. CONCLUSIONS

Suitability for restricted navigation at sea of inland vessels should be proven by the compliance with appropriate Rules of a recognized classification society as well as with applicable regulatory requirements. In navigation areas not covered by regulatory requirements, classification Rules are expected to include those vessel design and equipment topics normally covered by statutory Regulations. This paper provides a short review of existing Rules and Regulations applicable to river-sea vessels as well as an overview of researches carried out by Bureau Veritas aiming to support development of upgraded inland class requirements related to vessel stability and sea-keeping. The main contribution of the works covered by this paper may be summarised by the following:

- systematic direct simulations conducted on inland vessels operated in restricted sea water stretches characterised by a significant wave height $H_S \leq 2$ m
- development of upgraded class prescriptive formulas allowing to predict vessel hydrodynamic responses
- proposal of basic considerations regarding the evaluation of the vessel intact stability.

Requirements to be proposed will be intended to be applicable to inland vessels complying with the database investigated for any restricted sea navigation where $H_S \leq 2$ m. Further investigation of vessel responses on other navigation areas remains to be performed for their validation.

REFERENCES

- [1] Ship Design and Construction VOL. I, Society of Naval Architects and Marine Engineers, New Jersey, 2003
- [2] J.M. Chatelier, Inland navigation, from waterways to restricted maritime areas, Congreso internacional de diseno e ingenieria naval, Cartagena de Indias, Colombia, March 2015
- [3] Belgisch Koninklijk besluit betreffende binnenschepen die ook voor niet-internationale zee-reizen worden gebruikt, March 2007
- [4] Arrêté du 15 décembre 2014 relatif à la navigation de bateaux porte-conteneurs fluviaux en mer pour la desserte de Port 2000 et des quais en Seine à Honfleur
- [5] United Nations Economic Commission for Europe, Annexed Regulations of the European Agreement concerning the International Carriage of Dangerous Goods by Inland Waterways (A.D.N), 2016
- [6] DG Shipping Order N° 18, Government of India, July 2013
- [7] Legal Inspection Rules for Ships and Maritime Equipment, Technical Regulation for Statutory Survey of Non-International Seagoing Vessels, Maritime Safety Administration of the People's Republic of China, 2011
- [8] Regulations on Classification of Inland and Combined (river-sea) Navigation Ships, Rules for the Classification and Construction of Inland Navigation Ships (RINS), Russian River Register, 2009
- [9] W. Nzengu, S. Rudaković, Investigation of vessels hydrodynamic responses within range of navigation IN(0,6 $\leq H_S \leq 2$ m), BV Internal Report, Antwerp, Belgium, October 2015
- [10] W. Nzengu, N. Todosijević, Development of empirical formulas allowing prediction of vessels hydrodynamic responses within range of navigation IN(0,6 $\leq H_S \leq 2$ m), BV Internal Report, Antwerp, Belgium, October 2016
- [11] Principles of Naval Architecture, Society of Naval Architects and Marine Engineers, Jersey City, 1989.
- [12] G. De Hauteclocque, Q. Derbanne, Generalized wave parameter for rules formulae, Proceedings of PRADS2016, Copenhagen, Denmark, September 2016
- [13] NR217, Bureau Veritas, Rules for the Classification of Inland Navigation Vessels, November 2014
- [14] NR467, Bureau Veritas, Rules for the Classification of Steel Ships, July 2016
- [15] International Maritime Organisation, Resolution MSC.267(85), International Code on Intact Stability, 2008
- [16] Technical Requirements for inland waterway vessels, Directive 2006/87/EC of the European Parliament and of the Council, December 2006

On application of standard methods for roll damping prediction to inland vessels

Stefan Rudaković,

University of Belgrade, Faculty of Mechanical Engineering, Department of Naval Architecture
srudakovic@mas.bg.ac.rs

Igor Bačkalov,

University of Belgrade, Faculty of Mechanical Engineering, Department of Naval Architecture
ibackalov@mas.bg.ac.rs

ABSTRACT

Proper estimation of roll damping moment is of paramount importance for adequate assessment of dynamic stability of ships. However, experimental data on roll damping of inland vessels are scarce and unreliable. Thus the applicability of classic Ikeda's method and its simplified version on typical European inland vessels is investigated, with specific focus on eddy making component. It is found that the simplified Ikeda's method, in comparison to the classic method, may considerably underestimate the eddy making component of damping of full hull forms, or even return negative values, although the block coefficient is within the limits of method applicability. Hence, the paper explores possibilities of adjusting the simplified Ikeda's method in order to improve the observed shortcoming, as well as to extend its application to stability analysis of inland ships.

Keywords: *Inland vessels, roll damping, Ikeda's method, simplified Ikeda's method, eddy damping.*

1. INTRODUCTION

Proper mathematical modeling of ship dynamics was indicated by Bačkalov et al (2016) as one of the most important tasks of future research on stability of inland vessels. In this respect, it is well-known that the outcome of the analysis of roll motion and, consequently, assessment of ship stability, considerably depend on roll damping. However, experimental data on roll damping of inland vessels are scarce and unreliable. In such case, a possible solution could be to use some of the existing semi-empirical methods in order to estimate roll damping coefficients.

Nevertheless, the viability of such approach is questionable knowing that the available methods are primarily intended for conventional seagoing ships. This concerns the well-established Ikeda's method (Himeno, 1981) and its "simplified" version (Kawahara et al, 2009) based on regression analysis of data generated by applying the classic method on a series of ships developed from the Taylor series. The question of applicability of the simplified method is particularly relevant as it was

recommended for use within the Second Generation Intact Stability Criteria framework (see, e.g. IMO, 2016), in absence of either experimental data or another, more suitable method.

In order to examine the relevance of the classic and simplified Ikeda's method for inland vessels, roll damping coefficients were calculated, using both methods, for several sample ships. The preliminary results were quite unexpected: for some ships, roll damping coefficients estimated by simplified method were found to be negative. Such results triggered further investigation with even more surprising findings that could concern safety assessment of seagoing ships as well. It is therefore believed that the outcome of the present study is not relevant for inland vessels only, but could have an impact on ship stability analysis in general.

2. APPLICATION OF THE METHODS TO SAMPLE INLAND VESSELS

Inland vessel hulls often have high breadth-to-draught ratios (i.e. $B/d > 4$), while geometry of some of the aft cross sections may yield as much as $B/d \approx 10$. In addition, hull form coefficients of these

vessels are typically $C_B = 0.82 \div 0.94$ and $C_M \geq 0.99$. The geometric properties of inland cargo ships used in the present investigation are given in Table 1.

Simplified Ikeda's method

Due to the aforementioned specific features, most of the vessels in Table 1 are clearly out of range of applicability of Ikeda's method. According to Kawahara et al (2009), the simplified method may be applied to ships having:

$$0.5 \leq C_B \leq 0.85, \quad 2.5 \leq B/d \leq 4.5, \quad \hat{\omega} \leq 1, \\ -1.5 \leq OG/d \leq 0.2, \quad 0.9 \leq C_M \leq 0.99.$$

Symbol $\hat{\omega}$ stands for non-dimensional frequency:

$$\hat{\omega} = \omega \cdot \sqrt{\frac{B}{2g}},$$

while the distance OG of the center of gravity from the calm water level from is downwards positive.

Table 1: Sample inland vessels.

Vessel	L [m]	B [m]	d [m]	C_B	B/d
T1	66.00	10.50	3.45	0.8212	3.043
T2	84.28	9.56	3.60	0.9226	2.656
T3	81.821	9.40	3.07	0.8497	3.062
T4	85.95	10.95	2.80	0.8535	3.911
T5	85.95	11.40	4.30	0.8514	2.651
T6	105.76	11.40	2.80	0.8806	4.071
C7	110.00	11.45	2.60	0.8783	4.634
C8	109.70	11.40	2.46	0.8664	4.404
C9	111.25	14.50	3.30	0.8336	4.390
T10	121.10	11.40	4.30	0.8976	2.651
T11	125.00	11.40	4.50	0.8992	2.533
C12	134.26	14.50	3.60	0.9031	4.028
C13	135.00	14.50	4.00	0.9123	3.625
C14	135.00	11.45	2.68	0.9088	4.272
C15	135.00	11.45	3.33	0.9101	3.438

Nevertheless, the roll damping coefficients were calculated for all sample ships, whereby the total roll damping was considered to consist of:

$$B_{44} = B_F + B_W + B_E, \quad (1)$$

where B_F is friction damping, B_W is wave damping and B_E is eddy damping. Bilge keel damping B_{BK} is omitted from the calculations, since inland vessels normally do not have bilge keels. Lift damping

component B_L is also excluded, since it is considered that the vessel speed is $v = 0$. It should be noted that whenever the limits of applicability range were exceeded, maximal values of B/d , C_B and C_M were used in the calculations. Consequently, since the use of the simplified method does not require knowledge of any details of hull geometry that would distinguish an inland vessel from a seagoing one, the calculated B_{44} coefficients could formally correspond to a Taylor standard series ship of the same characteristics.

Fig. 1 shows the non-dimensional equivalent linear total roll damping:

$$\hat{B}_{44} = \frac{B_{44}}{\rho \nabla B^2} \cdot \sqrt{\frac{B}{2g}}, \quad (2)$$

as a function of roll amplitude for all ships examined. It can be noticed that, except for the sample vessels T1 and C9, the total roll damping of the examined ships decreases with the increase of roll amplitude. Surprisingly, some ships (T2 and T10) may even reach negative roll damping at large enough rolling amplitudes.

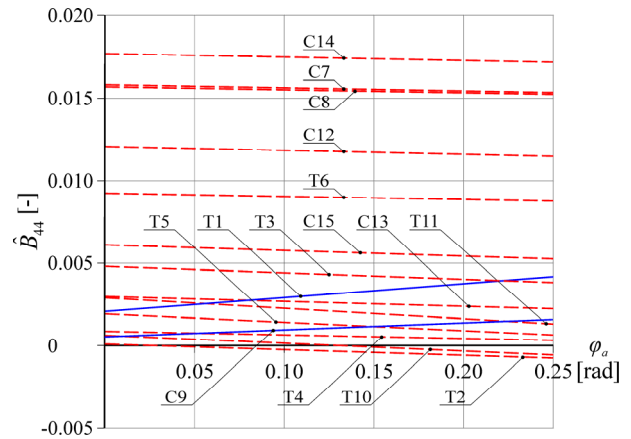


Figure 1: Total roll damping of examined ships as a function of roll amplitude φ_a , according to simplified Ikeda's method

A closer examination of components revealed that in all the cases analyzed (again, except for sample vessels T1 and C9), eddy making component was negative. The focus of investigation thus turned to the eddy damping.

Eddy damping is calculated as follows:

$$\hat{B}_E = \frac{4\hat{\omega} \cdot \varphi_a}{3\pi \cdot x_2 \cdot x_1^3} \cdot C_R, \quad (3)$$

where:

$$C_R = A_E \cdot \exp(B_{E1} + B_{E2} \cdot x_3^{B_{E3}}), \quad (4)$$

and

$$A_E = f(x_1, x_2), \quad B_{E1} = f(x_1, x_2, x_4),$$

$$B_{E2} = f(x_2, x_4), \quad B_{E3} = f(x_1, x_2),$$

while $x_1 = B/d$, $x_2 = C_B$, $x_3 = C_M$, $x_4 = OG/d$.

From formula (3) it may be concluded that eddy damping could be negative only if C_R becomes negative. Furthermore, C_R given by formula (4) could be negative only if A_E becomes negative. Therefore, it would be interesting to examine the structure of the formula for the computation of A_E :

$$\begin{aligned} A_E &= A_{E1} + A_{E2} = \\ &= \underbrace{(-0.0182 \cdot x_2 + 0.0155) \cdot (x_1 - 1.8)^3}_{A_{E1}} - \\ &\quad -79.414 \cdot x_2^4 + 215.695 \cdot x_2^3 - 215.883 \cdot x_2^2 + \\ &\quad + \underbrace{93.894 \cdot x_2 - 14.848}_{A_{E2}} \end{aligned} \quad (5)$$

If the geometric properties of an examined ship i.e. B/d and C_B remain within the boundaries of method applicability, A_{E1} cannot become negative. However, A_{E2} may become both negative and larger than A_{E1} in case $C_B > 0.84$, whereby the exact value of this “critical” block coefficient depends on B/d ratio. A_E as a function of B/d and C_B is given in Fig. 2. Now it is possible to explain the principal difference in eddy making component (and, consequently, the total roll damping) between ships T1 and C9 and the rest of the sample vessels: T1 and C9 are the only ships with $C_B < 0.84$.

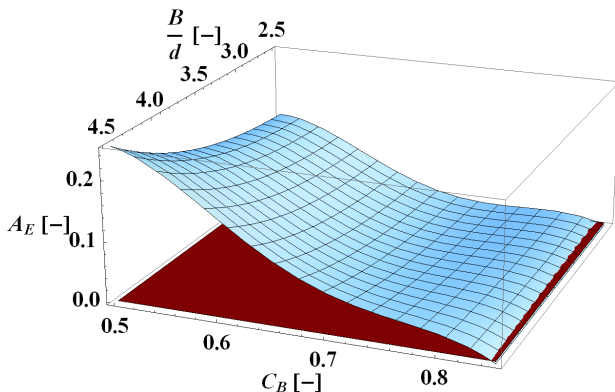


Figure 2: A_E as a function of B/d and C_B

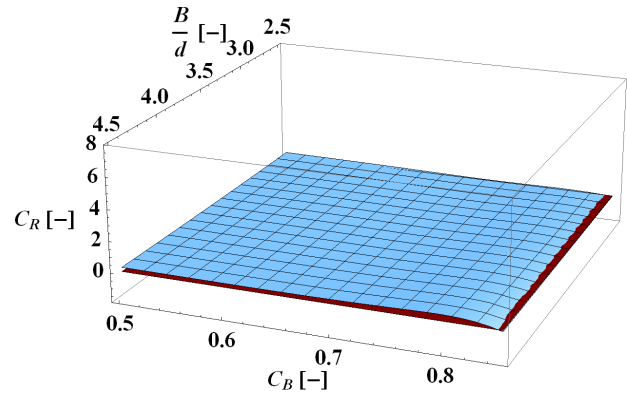


Figure 3: C_R computed over the applicability domain of simplified Ikeda's method, $OG/d = 0.2$, $C_M = 0.9$

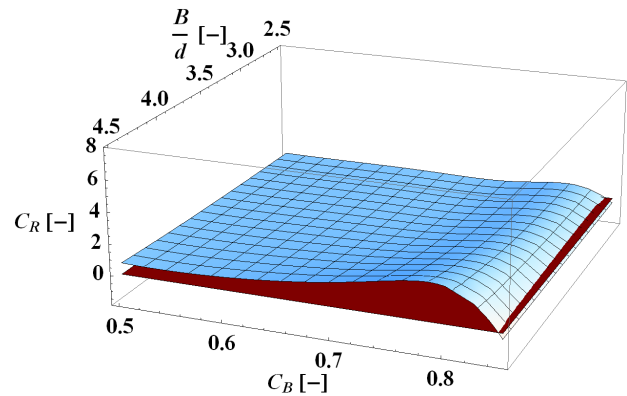


Figure 4: C_R computed over the applicability domain of simplified Ikeda's method, $OG/d = 0.2$, $C_M = 0.99$

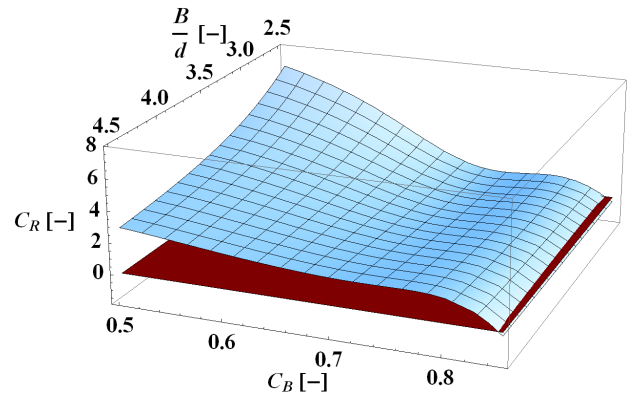


Figure 5: C_R computed over the applicability domain of simplified Ikeda's method, $OG/d = -1.5$, $C_M = 0.9$

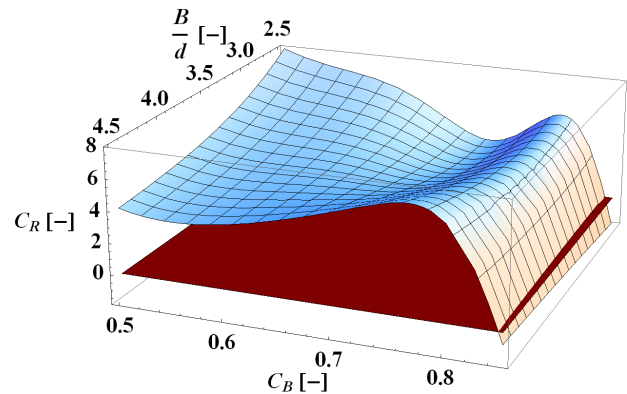


Figure 6: C_R computed over the applicability domain of simplified Ikeda's method, $OG/d = -1.5$, $C_M = 0.99$

The factor C_R computed over the complete domain of applicability of simplified Ikeda's method is given in Fig. 3 to Fig. 6. In line with the analysis of formulas (4) and (5), C_R is negative for high values of C_B regardless of B/d , OG/d and C_M . Another interesting feature is noticeable: the sign of the partial derivative of the function (4) with respect to C_B changes when block coefficient attains sufficiently high value. This happens at $C_B = 0.74 \div 0.81$ (depending on OG/d and C_M values) and becomes particularly evident for high mid-ship coefficients C_M .

Therefore, while the eddy making component of damping and, consequently, the total roll damping corresponding to $C_B > 0.84$ are obviously incorrect, it is also questionable whether B_{44} calculated with simplified Ikeda's method could be considered reliable in a much wider range of block coefficients, i.e. $0.74 < C_B < 0.84$. Thus, the issue of accuracy of the simplified method is not limited to inland vessels only, but may also concern seagoing ships with high block coefficients, otherwise believed to be covered by the method.

Classic Ikeda's method

It would be interesting to examine the possibility to amend the simplified Ikeda's method, so as to get more reliable prediction of eddy making component of damping for ships with high C_B , and ultimately for inland vessels.

A_{E2} as defined by equation (5) as well as some possible modifications are shown in Fig. 7. Obviously, there is an array of possibilities for adjustment of the function in the examined range of block coefficients.

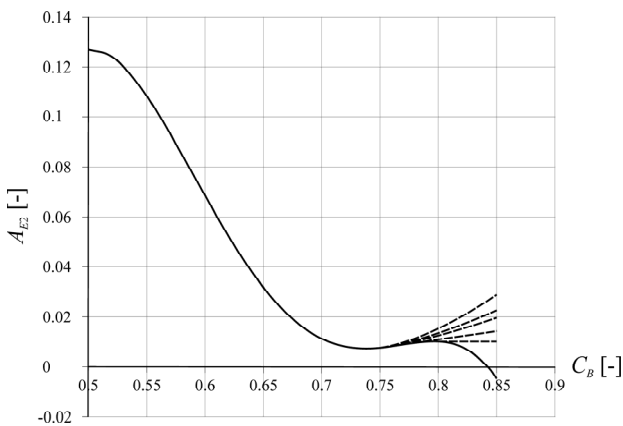


Figure 7: A_{E2} calculated by formula (5) (full line) and possible corrections (dashed lines)

In absence of experimental data, the appropriate modification of function A_{E2} could be sought by calculating eddy damping using the classic Ikeda's method and comparing it to the results obtained by a proposed amendment.

Unlike its simplified version, the classic Ikeda's method requires the knowledge of detailed hull geometry, that is, geometric particulars of cross-sections: sectional breadth B_s and draught d_s , sectional area coefficient σ , bilge radius r_b , and the local maximal distance between the roll axis and hull surface r_{max} . For this purpose, four vessels were selected from Table 1, whose body plans are given in Fig. 8. Two seagoing tankers with high block coefficients (Table 2) were considered as well. Eddy making component computations were performed using 51 equidistant cross sections. Block coefficients of the selected ships are in the range $C_B = 0.798 \div 0.851$.

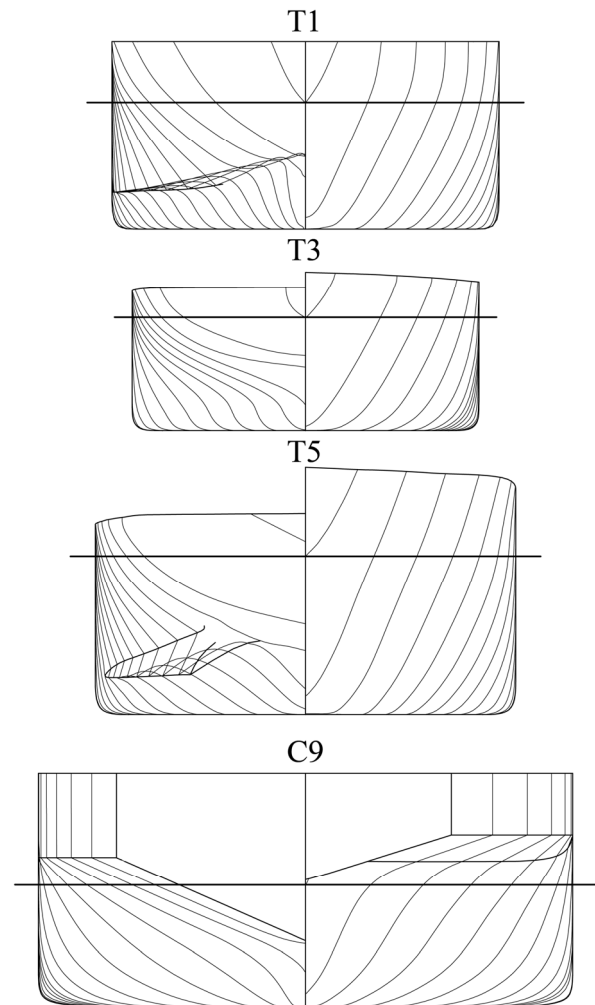


Figure 8: Inland vessels used in computation of eddy making component according to the classic Ikeda's method

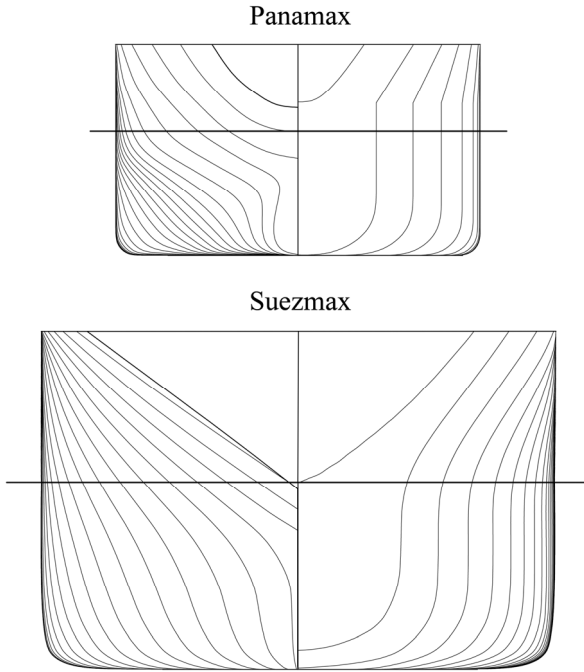


Figure 9: Seagoing tankers used in computation of eddy making component according to the classic Ikeda's method

Table 2: Sample seagoing tankers.

Vessel	L [m]	B [m]	d [m]	C_B	B/d
Panamax	287.78	32.20	11.00	0.8430	2.927
Suezmax	230.07	45.52	16.60	0.7982	2.742

It should be noted that in the classic method, the pressure distribution on the hull surface is obtained assuming the cross sections are approximated by Lewis forms. Clearly, this is not a proper approximation for a number of aft cross sections of examined inland vessels. Therefore, although the proposed procedure seems to be simple, it is not free from challenges.

With respect to that, it should be noted that for cross sections of certain geometric characteristics, (typically for combinations of high beam-to-draught ratios and relatively low area coefficients) sectional eddy damping calculated by the classic Ikeda's method could also be negative. This is often the case with forward- and aft-most cross sections of inland vessels. A trivial solution (and it seems, the usual remedy, see Kawahara et al, 2009) for this deficiency is to take the damping of a "problematic" cross section as zero. Having no possibility to estimate a correct value of eddy damping corresponding to such cross sections, the same approach was used in this paper.

3. A POSSIBLE ADJUSTMENT OF SIMPLIFIED FORMULA FOR EDDY MAKING COMPONENT OF DAMPING

In order to find an appropriate adjustment of formula (5), the following procedure is proposed. Assuming that, for each ship, it may be established:

$$B_{E(s)} \approx B_{E(c)}, \quad (6)$$

(where "s" stands for simplified and "c" stands for classic method) it would be possible to extract the "correct" value of A_{E2} corresponding to a given (high) block coefficient, provided that $B_{E(c)}$ is calculated beforehand.

$B_{E(c)}$ is obtained by numerical integration of sectional eddy damping over the ship length:

$$B_{E(c)} = \int_L B'_{E(c)} dx, \quad (7)$$

where

$$B'_{E(c)} = \frac{4 \cdot \omega \cdot \varphi_a}{3\pi} \cdot \rho d_s^4 \cdot C_{R(c)}. \quad (8)$$

The sectional $C_{R(c)}$ depends on B_s and d_s , σ , r_b , r_{max} , OG as well as pressure coefficient C_P . More precisely:

$$C_{R(c)} = \left(\frac{r_{max}}{d_s} \right)^2 \cdot f \left(\frac{r_b}{d_s}, \frac{B_s}{2d_s}, \sigma, \frac{OG}{d_s} \right) \cdot C_P. \quad (9)$$

Given the complexity of the procedure for the calculation of r_b , r_{max} and C_P , the respective expressions are omitted from the present paper, but may be found in e.g. Falzarano et al (2015), who presented the consolidated formulas of the classic method. On the other hand, eddy damping of a ship, according to the simplified method, is:

$$B_{E(s)} = \frac{4 \cdot \omega \cdot \varphi_a}{3\pi} \cdot \rho d^4 \cdot L \cdot C_{R(s)}, \quad (10)$$

where $C_{R(s)}$ is defined by equation (4). From equations (6) ÷ (8) and (10) it follows:

$$C_{R(s)} = \frac{1}{d^4 L} \int_L d_s^4 \cdot C_{R(c)} dx. \quad (11)$$

Then, using the formulas (4), (5) and (11), an estimate of A_{E2} may be obtained for a given ship.

Finally, using the described procedure, A_{E2} values were calculated for the selected inland vessels (see Fig. 10).

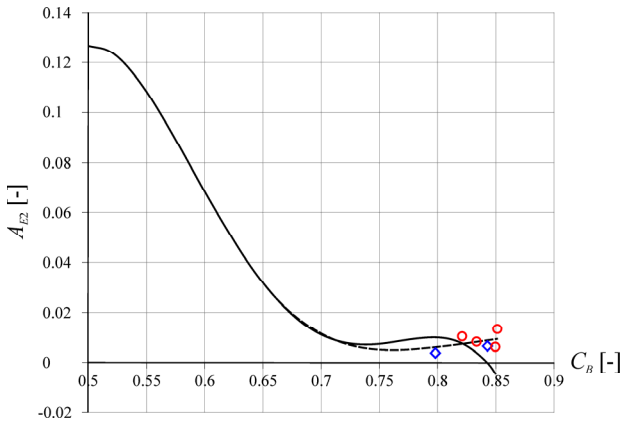


Figure 10: A_{E2} calculated by formula (5) (full line) and proposed correction given by formula (12) (dashed line). Circles represent the values calculated for inland vessels, while diamonds correspond to seagoing tankers.

Based on these results, a new expression for A_E , valid in the whole range of applicability of the simplified Ikeda's method, is proposed:

$$\begin{aligned}
 A_{E-new} &= A_{E1} + A_{E2-new} = \\
 &= \underbrace{(-0.0182 \cdot x_2 + 0.0155) \cdot (x_1 - 1.8)^3}_{A_{E1}} + \\
 &+ 151.48 \cdot x_2^5 - 567.603 \cdot x_2^4 + 840.297 \cdot x_2^3 - \\
 &\underbrace{-612.498 \cdot x_2^2 + 218.904 \cdot x_2 - 30.497}_{A_{E2-new}} \quad (12)
 \end{aligned}$$

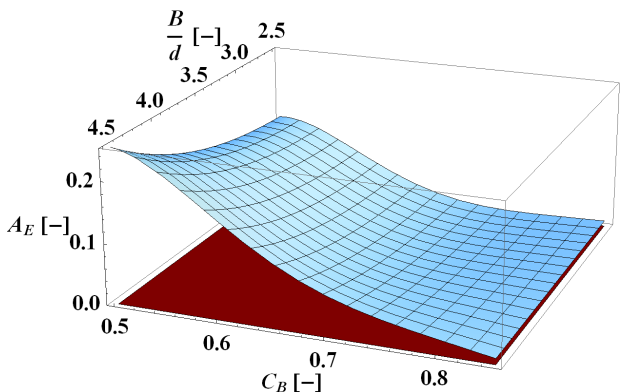


Figure 11: A_{E-new} as a function of B/d and C_B .

A_{E-new} as a function of B/d and C_B is given in Fig. 11. The factor C_R adjusted by formula (12) is computed within the range of applicability of the simplified Ikeda's method and given in Fig. 12 and Fig. 13. Finally, the non-dimensional equivalent

linear total roll damping of the sample ships given in Table 1 is computed using the adjusted simplified formula for eddy damping, see Fig. 14. Whenever the block coefficient exceeded the applicability range, the calculations were carried out with $C_B = 0.85$. As it can be seen in Fig. 14, the total roll damping attains an increasing trend with respect to roll amplitude, as it should be normally expected.

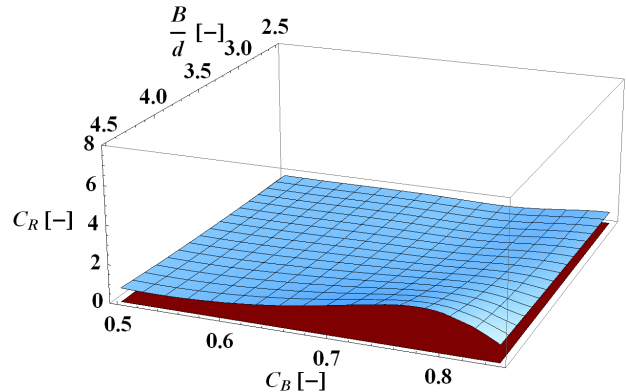


Figure 12: Factor C_R adjusted by formula (12) computed over the applicability domain of simplified Ikeda's method, $OG/d = 0.2$, $C_M = 0.99$.

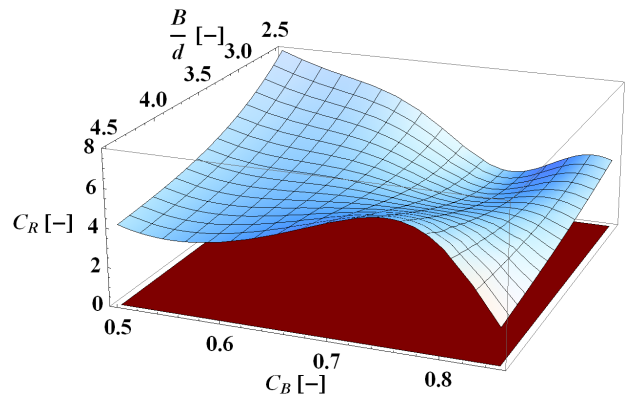


Figure 13: Factor C_R adjusted by formula (12) computed over the applicability domain of simplified Ikeda's method, $OG/d = -1.5$, $C_M = 0.99$.

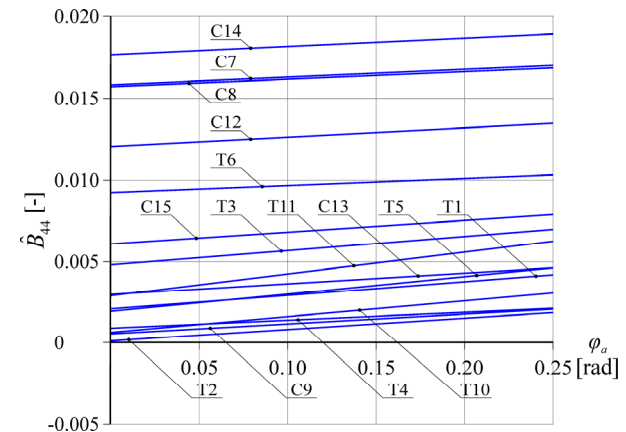


Figure 14: Total roll damping of examined ships as a function of roll amplitude ϕ_a , according to simplified Ikeda's method, taking into account proposed adjustment of eddy damping component

4. FURTHER EXTENSION OF SIMPLIFIED FORMULA FOR EDDY DAMPING TO INLAND VESSELS

It was already pointed out that most of the sample vessels given in Table 1, and most of inland vessels in general, fall out of the range of applicability of simplified Ikeda's method with respect to B/d and C_B . For instance, beam-to-draught ratios of typical European river cruisers are in the range of $5.5 \div 8.5$. Therefore, without model tests, it appears difficult to adjust the simplified Ikeda's method so as to extend its applicability to just any inland vessel.

For the sake of comparison, for some sample vessels having $C_B > 0.85$ (see Table 3), $C_{R(s)}$ was calculated by using formula (11), based on classic Ikeda's method, taking into account actual hull form geometry (corresponding to real C_B) in the computation of $C_{R(c)}$. These figures are subsequently compared to data obtained by applying the simplified formula (4) using both expression (5) for A_E and the proposed adjustment of A_E given by (12); in these two latter cases, $C_B = 0.85$ is always used, instead of actual block coefficients.

Table 3: Discrepancies in estimation of eddy making component using different formulas and limitations. All calculations were carried out for $OG = 0$ m.

Vessel	C_B	$C_{R(s)}$		
		(4) + (5)	(4) + (12)	(11)
T2	0.9226	-0.3773	0.7846	4.6228
T4	0.8535	-0.3876	0.8808	6.3669
C8	0.8664	-0.3744	0.9480	3.5575
C12	0.9031	-0.3862	0.8927	2.6430
C15	0.9101	-0.3884	0.8386	3.5152

Significant discrepancies between the values of C_R obtained using different approaches indicate that an accurate estimation of eddy making component of such full-bodied vessels remains a task for the future. For the time being, however, if the simplified Ikeda's method is employed, it is suggested to use the adjusted eddy damping formula (proposed in the paper and based on (12)) applying the method limitations whenever the geometric properties of the analyzed hull exceed the applicability range.

5. CONCLUDING REMARKS

In the course of investigation of applicability of the simplified Ikeda's method for roll damping prediction to European inland vessels, it was found that the eddy damping formula fails to properly predict the corresponding damping component if the block coefficient of the vessel is sufficiently large, i.e. $C_B > 0.8$. This deficiency is particularly striking for $C_B > 0.84$, when eddy making component of damping becomes negative.

Therefore, an adjustment of the simplified formula for eddy making component prediction is proposed, based on calculations performed using the classic Ikeda's method. The method was applied to several typical inland hulls with high block coefficients ($C_B = 0.82 \div 0.85$) and high mid-ship coefficients ($C_M \geq 0.99$), covering a complete range of applicability of the simplified method with respect to beam-to-draught ratios ($B/d = 2.6 \div 4.4$). Two typical seagoing tankers (having $C_B \approx 0.8$ and $C_B \approx 0.84$) were included in the calculations as well. It is expected that the derived expression could extend the applicability of the simplified Ikeda's method to inland ships, in absence of adequate experimental data.

Furthermore, it is believed that the adapted formula provides a better estimation of eddy damping component not only for inland vessels but also for seagoing ships with full hull forms.

6. ACKNOWLEDGMENTS

The paper is part of the project "Development of Next Generation of Safe, Efficient, Ecological (SE-ECO) Ships" executed by Department of Naval Architecture, Faculty of Mechanical Engineering University of Belgrade. The project is partly financed by Serbian Ministry of Education, Science and Technology Development, Contract No. TR35009.

The authors would like to thank Prof. Milan Hofman (University of Belgrade) and Dr. Gabriele Bulian (University of Trieste) for valuable suggestions and comments in course of study.

REFERENCES

- Bačkalov, I., Bulian, G., Cichowicz, J., Eliopoulou, E., Konovessis, D., Leguen, J.F., Rosén, A., Themelis, N., 2016, "Ship stability, dynamics and safety: Status and perspectives from a review of recent STAB conferences

and ISSW events”, *Ocean Engineering*, Vol. 116, pp 312-349

Falzarano, J., Somayajula, A., Seah, R., 2015, “An overview of the prediction methods for roll damping of ships”, *Ocean Systems Engineering* 5(2), pp. 55-76.

Himeno, Y., 1981, “Prediction of ship roll damping – State of the art”, Report No. 239, College of Engineering, University of Michigan.

IMO, 2016, ”SDC 4/5/1/Add.3-Annex 4: Draft Explanatory Notes on the vulnerability of ships to the dead ship stability failure mode”, Submitted by Japan, 11 November.

Kawahara, Y., Maekawa, K., Ikeda, Y., 2009, “A Simple Prediction Formula of Roll Damping of Conventional Cargo Ships on the Basis of Ikeda’s Method and Its Limitation”, Proceedings of the 10th International Conference on Stability of Ships and Ocean Vehicles, (STAB2009), St. Petersburg, Russia, pp. 387-398.

Session 7
Issues of stability modeling

Session Chair
Vladimir Shigunov

Verification and Validation Aspects of Development and Implementation of the Second Generation Intact Stability Criteria

Arthur M. Reed, *David Taylor Model Basin, Carderock Division, Naval Surface Warfare Center (NSWCCD)*, arthur.reed@navy.mil

ABSTRACT

The IMO Second Generation Intact Stability Criteria, and verification and validation (V&V) are introduced. Then the application of V&V to the Level 1, Level 2 and direct assessment stages of the Second Generation Intact Stability Criteria are discussed. From the perspective of Level 1 and Level 2 verification and validation, the user's only responsibility is to verify that the algorithms for assessing vulnerability to stability failure contained in IMO documentation are implemented correctly. For direct assessment using ship dynamics software for predicting motions in extreme seas, existing well established and documented V&V processes apply. The developers of the algorithms for the Level 1 and Level 2 vulnerability assessments need to validate that their algorithms are consistent across a large range of vessel types and sizes.

The one significant note is that even though, in general, the Level 1 vulnerability assessment can be performed "on the back of an envelope" using a hand calculator, those calculations need to be performed using a spreadsheet program on a personal computer or reliable and consistent verification will be virtually impossible.

Keywords *Verification & Validation, Second Generation Intact Stability Criteria.*

1. INTRODUCTION

For commercial vessels, the classical intact stability criteria is based on the work of Rahola (1939) and is incorporated in the International Code on Intact Stability, the 2008 IS Code (MSC 85/26/Add.1¹). Similar criteria for naval vessels is provided by Sarchin & Goldberg (1962) and codified in the NATO Naval Ship Code (NATO, 2007a,b) and by a US Navy Design Data Sheet (NAVSEA, 2016). These criteria are prescriptive—that is they are a set of criteria, defined based on empirical data, which are *assumed* to ensure that a vessel meeting the criteria will have adequate static stability. The history of development and the background of the IMO criteria are described by Kobylinski & Kastner (2003); a summary of the origin of these criteria is also available in chapter 3 of the Explanatory Notes to the International Code on Intact Stability (MSC.1/Circ.1281).

Beginning in the early 2000's efforts were initiated to develop performance based stability criteria for commercial vessels with the reestablishment of the intact-stability working group by IMO's Subcommittee on Stability and Load Lines and on Fishing Vessels Safety (SLF) (*cf.*, Francescutto, 2004, 2007). Over time, the terminology to describe the new intact stability criteria evolved from "performance based" to "next generation" to "2nd generation," the terminology in use today. This entire evolution is described in the introduction to Peters, *et al.* (2011).

The SLF Working Group decided that the second-generation intact stability criteria should be performance-based and address three modes of stability failure (SLF 48/21, paragraph 4.18):

- *Restoring arm variation* problems, such as parametric roll and pure loss of stability;
- *Stability under dead ship condition*, as defined by SOLAS regulation II-1/3-8; and
- *Maneuvering related problems in waves*, such as surf-riding and broaching-to.

Ultimately, a fourth mode of stability failure was added:

- *Excessive accelerations.*

The deliberations of the Working Group led to the formulation of the framework for the second-generation intact stability criteria, which is de-

¹ References to IMO documents such as "MSC 85/26/Add.1" appear in the list of references with an "IMO" prefix, *i.e.*, as: IMO MSC 85/26/Add.1. As there is no ambiguity in the names of the IMO citations, the year will be omitted from the citations.

scribed in SLF 50/4/4 and was discussed at the 50th session of SLF in May 2007. The key elements of this framework were the distinction between parametric criteria (the 2008 IS Code) and performance-based criteria, and between probabilistic and deterministic criteria.

As the second-generation intact stability criteria are more extensive (deal with multiple stability failure modes) and more complex than the older prescriptive approach to stability, it will be necessary to insure that the algorithms supporting the assessment are consistent and implemented correctly. It is the objective of this paper to provide some insights on these latter two issues.

The paper will begin with a description of the second-generation intact stability criteria process and a definition of Verification, and Validation (V&V). The paper will then discuss V&V for the various levels of the process from both the user's and the algorithm developer's perspective.

2. IMO SECOND GENERATION INTACT STABILITY CRITERIA

The second-generation intact-stability criteria are based on a multi-tiered assessment approach: for a given ship design, each stability-failure mode is evaluated using multiple levels of vulnerability assessment, as necessary. The first two tiers or levels of vulnerability assessment criteria are characterized by different levels of accuracy and computational effort, with the first level being simpler and more conservative than the second.

A ship, which fails to comply with the Level 1 criteria is assessed using the Level 2 criteria. In a case of unacceptable results at the second level, the vessel must then be examined by means of a *direct assessment* procedure based on tools and methodologies corresponding to the best state-of-the-art prediction methods in the field of ship-capsizing prediction. This third-level methodology should capture the physics of capsizing as practically possible.

The three levels of assessment are intended to be of increasing complexity with the Level 1 assessment being a simple "back of the envelope" calculation that should be simple enough that it can be completed for all stability failure modes in a day. The Level 2 assessment is more complex, and might require as much as a week's effort to assess

all stability failure modes, and require the use of computational algorithm implemented in a program such as Excel or MathCad—here after referred to as a *spreadsheet*. The third level direct assessment will require the use of serious computing resources and could take a month or more's effort.

The specific IMO rules and regulations are still under development, but the following publications document the current state of the envisioned process for Level 1 and Level 2 of each of the stability failure modes:

- Pure loss of stability: SDC 2WP.4, Annex 1; SDC 3WP.5, Annex 3; SDC 4/5/1/Add.5; SDC 4/5/6
- Parametric Roll: SDC 2WP.4, Annex 2; SDC 3WP.5, Annex 4; SDC 4/5/1/Add.1; SDC 4/5/1/Add.5, SDC 4/5/6
- Dead ship condition: SDC 3WP.5; SDC 3WP.5, Annex 6; SDC 4/5/1/Add.3; SDC 4/5/1/Add.5; SDC 4/5/6
- Surf riding/broaching: SDC 2WP.4, Annex 3; SDC 3WP.5, Annex 5; SDC 4/5/1/Add.2, SDC 4/5/1/Add.5, SDC 4/5/6
- Excessive Acceleration: SDC 3WP.5, Annex 2; SDC 3WP.5, Annex 7; SDC 4/5/1/Add.4; SDC 4/5/6

The procedure for performing direct assessment is described in: SDC 4/WP.4, Annex 1.

3. VERIFICATION AND VALIDATION

Software that is being used for engineering computations, upon which design decisions will be based needs to be correct. The processes by which software is assessed as to its correctness and being adequate for the job is called *verification* and *validation* (V&V)—verification assesses correctness and validation assesses the degree to which it is adequate for the task. Papers and reports by Beck, *et al.* (1996), AIAA (1998), DoD (1998, 2003, 2007, 2012), McCue, *et al.* (2008), ASME (2009), Reed (2009) and Reed & Zuzick (2015) provide different, although consistent, definitions of V&V. The U.S. DoD definitions for these terms are provided below, each followed by a practical commentary relevant to computational tools for predicting dynamic stability.

1. *Verification*—the process of determining that a model or simulation implementation accurately represents the developer's conceptual description and specification, *i.e.*, does the code accurately

implement the theory that is proposed to model the problem at hand?

2. *Validation*—the process of determining the degree to which a model or simulation is an accurate representation of the real world from the perspective of the intended uses of the model or simulation, *i.e.*, does the theory and the code that implements the theory accurately model the relevant physical problem of interest?

4. V&V FROM THE USER'S PERSPECTIVE

For the Second Generation Intact Stability Criteria, the question of V&V has to cover a broad range of computations/computational tools—from the “back of an envelope” assessment to sophisticated ship dynamics computational tools. As each of the levels of assessment has its own issues, they will be discussed separately, beginning with Direct Assessment, where the computational tools that are traditionally put through the V&V process would be employed.

Direct Assessment

As just stated, the hydrodynamic computational tools for predicting ship dynamics are the types of software for which the V&V processes have been developed. So while these are the most complex software tools that must be put through the V&V process, and the tools for which the most effort will have to be expended, they are the tools for which the process is the most mature. As stated previously, there is an abundance of literature on the subject of formal V&V of software (*cf.*, AIAA 1998; DoD 1998, 2003, 2007, 2012; ASME 2009). Reed & Zuzick (2015) provide a survey of the formal V&V process tailored for the ship stability community.

From the users perspective, it is unlikely that a user will be developing a computational tool for assessing dynamic stability performance in extreme seas; the user will most likely be employing software developed by a third party. Thus, the user will not be responsible for verification of the software, he will have to assume that the software vendor has performed that function, and the user will only be responsible for performing validation to assure that the software tool is adequate for predicting the stability failure mode(s) of concern. The Flag Administration, responsible for the vessel

being assessed, should have defined the process for *formal validation*.

Level 2 Criteria

For Level 2, the Second Generation Intact Stability Criteria will explicitly provide the user with the algorithm for use in assessing the vulnerability of a ship to each particular stability failure mode. Thus, there should be no requirement for the user to perform *validation* of a spreadsheet that is used to perform the vulnerability calculations. However, it will be necessary to perform *verification* to insure that the calculations are performed correctly.

The issue then becomes one of how best to perform this verification. It would appear that the ideal situation would be to have a series of benchmark cases for each stability failure mode. For each failure mode there would be pairs of cases, one of the pairs being a case that passes the vulnerability test for that mode and one that fails the vulnerability test. For Level 2 algorithms where there are binary decision points within the algorithm, there should be a pair of benchmark cases that will test each branch of the decision tree.

Under these conditions, the user would be required to enter each pair of benchmark data into his spreadsheet and show that the results of each case agree with the expected answer within a specified accuracy, say 2-percent. When a user has performed and passed this level of validation for all five stability failure modes, he could be “certified” by a Flag Administration to use his spreadsheet to assess the vulnerability of his design to stability failure.

Level 1 Criteria

In principle, the Level 1 V&V should be similar in complexity to the Level 2 problem, and have the same approach. However, there is one complication at Level 1. Level 1 vulnerability assessment has been characterized as an assessment that can be carried out on the “back of an envelope” using a hand calculator, but this opens the Level 1 assessment up to a lack of repeatability due to simple calculation errors.

Therefore, it is proposed that, even at Level 1, it be required that the vulnerability assessment for each mode of stability failure be implemented in a spreadsheet. This will vastly reduce the possibility of inadvertent errors due to “hitting the wrong key”

on a calculator, and will greatly facilitate verification using the same benchmarking process proposed for Level 2.

5. V&V FROM THE CRITERIA DEVELOPER'S PERSPECTIVE

The developers of the Level 1 and Level 2 intact stability vulnerability criteria are not developing software, so they do not have any responsibility for V&V in the traditional sense. However, they do have responsibility for ensuring that the algorithms that they are developing are consistent—this is a validation function.

What is meant by consistency of algorithms? If the Level 1 and Level 2 algorithms are developed from the same theoretical basis, then the validation can be performed largely at the theory/algorithm basis, but if *not*, then extensive computational testing is required. A *hypothetical* example of a theoretically consistent Level 1 and Level 2 vulnerability assessment would be where the Mathieu equation is used to evaluate the sensitivity to parametric roll, with the Level 1 algorithm using the Mathieu equation without the roll damping term and the Level 2 algorithm using the Mathieu equation with a roll damping term.

In the absence of such a consistent theoretical basis, the validation of the Level 1 and Level 2 algorithms consists of two steps. First, the algorithms must be rational, that is they should not be based on the use of logically inconsistent information and second they must undergo an extensive computational consistency check. To give a *ludicrous example* of a rationality check, a stability failure algorithm based, among other things, on the distance from the earth to the moon would be highly suspect. Someone other than the developer of the algorithm should conduct the *rationality* step of the validation.

The second step, the computational validation, will involve evaluating a large number of vessels of various types and sizes using both the Level 1 and Level 2 algorithms for each mode of stability failure. The metric here is two-fold, first that a vessel in a given loading condition that passes the Level 1 vulnerability test should not fail the Level 2 vulnerability check. And secondly, for those vessels that pass both the Level 1 and Level 2 vulnerability check, the margin at Level 2 should not be smaller than the margin at Level 1—if a vessel passes the

Level 1 check by a large margin, it should not pass the Level 2 check by only a small margin, this is admittedly somewhat subjective.

6. CONCLUSIONS

From the perspective of Level 1 and Level 2 verification and validation, the user's only responsibility is to verify that the algorithms for assessing vulnerability to stability failure contained in IMO documentation are implemented correctly. To facilitate this, there needs to be a comprehensive set of benchmark cases that both meet and fail to meet the vulnerability criteria, covering each of the stability failure modes. For direct assessment using ship dynamics software for predicting motions in extreme seas, the well established and documented V&V process of AIAA 1998; DoD 1998, 2003, 2007, 2012; and ASME 2009, *etc.* apply. The developer of the algorithms for the Level 1 and Level 2 vulnerability assessments need to validate that their algorithms are consistent across a large range of vessel types and sizes.

The one significant note is that even though, in general, the Level 1 vulnerability assessment can be performed “on the back of an envelope” using a hand calculator, those calculations need to be performed using a spreadsheet program on a personal computer or reliable and consistent verification will be virtually impossible.

REFERENCES

- AIAA (1998) Guide for the verification and validation of computational fluid dynamics simulations. AIAA G-077-1998 Guide, Reston, VA: American Institute of Aeronautics and Astronautics, viii+19 p.
- ASME (2009) V&V 20-2009, Standard for verification and validation in computational fluid dynamics and heat transfer. New York, NY: American Society of Mechanical Engineers, x+87 p.
- Beck, R. F., A. M. Reed & E. P. Rood (1996) Application of modern numerical methods in marine hydrodynamics. *Trans. SNAME*, 104:519--37, Jersey City, NJ.
- DoD (1998) DoD Modeling and simulation (M&S) glossary. DoD 5000.59-M, U. S. Department of Defense, 175 p.

- DoD (2003) DoD Modeling and simulation (M&S) verification, validation, and accreditation (VV&A). DoD Instruction 5000.61, U. S. Department of Defense, 10 p.
- DoD (2007) DoD Modeling and Simulation (M&S) Management. DoD Directive 5000.59, U. S. Department of Defense, 7 p.
- DoD (2012) Department of Defense, USD (AT&L) MIL-STD-3022 w/Change~1: Department of Defense Standard practice: Documentation of verification, validation, and accreditation (VV&A) for models and simulations, 55 p.
- Francescutto, A. (2004) Intact ship stability—The way ahead. *Marine Tech.*, 41:31–37.
- Francescutto, A. (2007) Intact stability of ships—Recent developments and trends. *Proc. 10th Int'l Symp. Practical Design of Ships and Other Floating Struct.* (PRADS '07). Houston, TX, Vol. 1, pp. 487–496.
- IMO MSC 85/26/Add.1 (2008) International code on intact stability, 2008 (2008 IS Code). London, 96 p
- IMO MSC.1/Circ.1281 (2008) Explanatory notes to the international code on intact stability, 2008. London, 30 p.
- IMO SDC 2-WP.4 (2015) Development of Second Generation Intact Stability Criteria, Development of amendments to Part B of the 2008 IS Code on towing, lifting and anchor handling operations, Report of the working group (Part 1). London, UK, 48 p.
- IMO SDC 3/WP.5 (2016) Finalization of Second Generation Intact Stability Criteria, Amendments To Part B of the 2008 IS Code on Towing, Lifting and Anchor Handling Operations Report of the working group (Part 1). London, UK, 141 p.
- IMO SDC 4/5/1/Add.1 (2016) Finalization of Second Generation Intact Stability Criteria, Report of the correspondence group (part 2). Submitted by Japan, London, UK, 39 p.
- IMO SDC 4/5/1/Add.2 (2016) Finalization of Second Generation Intact Stability Criteria, Report of the correspondence group (part 3). Submitted by Japan, London, UK, 18 p.
- IMO SDC 4/5/1/Add.3 (2016) Finalization of Second Generation Intact Stability Criteria, Report of the correspondence group (part 4). Submitted by Japan, London, UK, 24 p.
- IMO SDC 4/5/1/Add.4 (2016) Finalization of Second Generation Intact Stability Criteria, Report of the correspondence group (part 5). Submitted by Japan, London, UK, 17 p.
- IMO SDC 4/5/1/Add.5 (2016) Finalization of Second Generation Intact Stability Criteria, Report of the correspondence group (part 6). Submitted by Japan, London, UK, 51 p.
- IMO SDC 4/5/6 (2016) Finalization of Second Generation Intact Stability Criteria, Draft consolidated explanatory notes for the second generation intact stability criteria. Submitted by the United States, London, UK, 51 p.
- IMO SDC 4/WP.4 (2017) Report of the working group (Part 1). London, UK, 21 p.
- IMO SLF 48/21 (2005) Report to Maritime Safety Committee. London, UK, 65~p.
- IMO SLF 50/4/4 (2007) Framework for the development of New Generation Criteria for intact stability, submitted by Japan, the Netherlands and the United States. London, UK, 6 p.
- Kobylnski, L. K. & S. Kastner (2003) *Stability and safety of ships: regulation and operation*. Elsevier, Amsterdam, 454 p.
- McCue, L. S., W. R. Story & A. M. Reed (2008) Nonlinear dynamics applied to the validation of computational methods. *Proc. 27th Symp. on Naval Hydro*, Seoul, South Korea., 10 p.
- NATO (2007a) Buoyancy, stability and controllability. Chapter III of Naval Ship Code, NATO Naval Armaments Group, Maritime Capability Group 6, Specialist Team on Naval Ship Safety and Classification, Allied Naval Engineering Publication ANEP-77, vii+121 p.
- NATO (2007b) Guidance on NSC Chapter III Buoyancy and Stability, Part B: Application. Chapter 3, Guide to the Naval Ship Code, NATO Naval Armaments Group, Maritime Capability Group 6, Specialist Team on Naval Ship Safety and Classification, 91 p.
- NAVSEA (2016) Design practices and criteria for U.S. Navy surface ship stability and reserve buoyancy. NAVSEA Technical Publication T9070-AF-DPC-010/079-1. Naval Sea Systems Command. 175 pp.

- Peters, W., V. Belenky, C. Bassler, K. Spyrou, N. Umeda, G. Bulian, B. Altmayer (2011) The second generation intact stability criteria: An overview of development. *Trans. SNAME*, 119:225–264.
- Rahola, J. (1939) The judging of the stability of ships and the determination of the minimum amount of stability especially considering the vessel navigating Finnish waters. PhD Thesis, Technical University of Finland, Helsinki, viii+232 p.
- Reed, A. M. (2009) A Naval Perspective on Ship Stability. *Proc. 10th Int'l Conf. Stability of Ships & Ocean Vehicles (STAB '09)*, St. Petersburg, Russia, pp. 21–44.
- Reed, A. M. & A. V. Zuzick (2015). Direct assessment will require accreditation—What this means. *Proc. 12th International Conf. Stability of Ships & Ocean Vehicles (STAB'15)*. Ed. by S. Secretariat. Glasgow, UK, pp. 49–78.
- Sarchin, T. H. & L. L. Goldberg (1962) Stability and buoyancy criteria for U. S. Naval surface ships. *Trans. SNAME*, 72:418–58.

Study on Vulnerability Criteria for Surf-riding / Broaching with a Model Experiment

Min Gu, *China Ship Scientific Research Center, Wuxi, China, gumin702@163.com*

Jilong Chu, *China Ship Scientific Research Center, Wuxi, China, long8616767@163.com*

Yang Han, *China Ship Scientific Research Center, Wuxi, China, hanyang_2001@163.com*

Jiang Lu, *China Ship Scientific Research Center, Wuxi, China, lujiang1980@aliyun.com*

ABSTRACT

The vulnerability criteria for Surf-riding and broaching are currently under development at the International Maritime Organization (IMO) for the second generation intact stability criteria. Firstly, the vulnerability criteria for surf-riding and broaching are introduced, and the calculations of seven sample ships are conducted to analyze the applicability of the current vulnerability criteria. Secondly, a model experiment with a tumblehome vessel for surf-riding and broaching in following and stern-quartering waves is carried out. Four types of ship motions with periodic motion, stable surf-riding, broaching and capsizing due to broaching are observed in the model experiment while broaching is observed three times in one wave case. Finally, the results between the criteria calculations and the model experiment are compared to verify the feasibility of vulnerability criteria for the tumblehome vessel.

Keywords: *Second generation intact stability criteria, Surf-riding, Broaching, Model experiment*

1. INTRODUCTION

The second generation intact stability criteria for five stability failure modes including pure loss of stability, parametric roll, surf-riding and broaching, dead ship condition and excessive accelerations are under development at the International Maritime Organization (IMO) to guarantee sufficient safety of ships in waves (IMO SDC.4, 2017). The second generation intact stability criteria consist of two levels of vulnerability criteria based on simple physical models and direct stability assessment using advanced numerical simulation methods.

Surf-riding occurs when a ship is captured by a wave from the stern and forced to run with wave celerity. During surf-riding, the ship is often unstable and will turn uncontrollably despite keeping maximum rudder angle in the opposite direction, which is defined as broaching. Broaching is considered as one of the most dangerous phenomena in following and stern-quartering waves for high-speed ships, such as destroyers and fishing vessels.

Levels 1 and 2 vulnerability criteria for surf-riding and broaching have been determined at the

3rd session of Sub-committee on Ship Design and Construction (SDC) (IMO SDC.3, 2016a, 2016b). Because surf-riding is usually regarded as a precondition of broaching, the likelihood of surf-riding occurrence is used as vulnerability criteria instead of broaching. Level 1 criterion is simply checked by ship speed and length. The formula of level 2 criterion is obtained by using Melnikov method, the stochastic wave theory and the wave statistics, and the calculated value need to be compared with the safety level set as 0.005 currently.

It's important to estimate surf-riding thresholds in the level 2 criterion. Recently some approximate formulas based on Melnikov's method were proposed to predict surf-riding thresholds in following regular waves (Kan, 1990; Spyrou, 2006; Maki et al., 2010, 2014). Maki et al. (2010, 2014) also provided another analytical formula for calculating surf-riding thresholds using a continuous piecewise linear approximation, which is more transparent than Melnikov's method in obtaining the solution.

The prior task of IMO SDC 4 was drafting the guidelines for the specification of direct stability assessment procedures (IMO SDC.4, 2017). For the

numerical simulation of surf-riding and broaching, the numerical approach is required at least a 4 DOF mathematical model of surge-sway-roll-yaw motion, and hydrodynamic forces should consider hydrodynamic lift forces due to the coexistence of wave particle velocity and ship forward velocity.

Umeda and Hashimoto (2002) used a 4 DOF mathematical model of surge-sway-roll-yaw motion to qualitatively explain the capsizing phenomena associated with surf-riding and broaching in regular following and stern-quartering waves. In order to improve the calculation accuracy to realize quantitative prediction, Hashimoto et al. (2004, 2011) took into account several important nonlinear terms in the previous mathematical model.

For the numerical simulation in irregular waves, the issue is how to identify surf-riding and broaching in irregular waves. Belenky et al. (2012) proposed a method to detect surf-riding in irregular waves by the celerity of irregular waves, which is computed by finding the point of maximum wave steepness on the down slope of the wave nearest the ship (Spyrou et al., 2012). They also provided two novel metrics for likelihood of surf-riding and broaching used for evaluating the probability of surf-riding and broaching in irregular waves (Belenky et al., 2016a, 2016b).

In order to verify the applicability of vulnerability criteria for surf-riding and broaching, the calculations for seven sample ships including one unconventional ship are conducted. The free running experiment with the unconventional ship is carried out to provide validation data for criteria check.

2. ASSESSMENT ON VULNERABILITY CRITERIA FOR SURF-RIDING AND BROACHING

According to the updated drafts (IMO SDC.2, 2015; IMO SDC.3, 2016a, 2016b), vulnerability criteria for surf-riding and broaching are simply introduced as follows.

Level 1 criterion

A ship is judged to be vulnerable to the surf-riding and broaching failure mode if formula (1) is false:

$$L > 200\text{m or } Fn \leq 0.3 \quad (1)$$

where, $Fn = V_s/\sqrt{Lg}$ is the Froude number; V_s is service speed of the ship in calm water; L is the length of the ship; g is gravity acceleration. If the ship fails to pass level 1 criteria, a more detailed check of level 2 criteria should be applied.

Level 2 criterion

A ship is judged to be vulnerable to the surf-riding and broaching failure mode if the value C is larger than 0.005:

$$C = \sum_{HS} \sum_{TZ} \left(W2(H_s, T_z) \sum_{i=1}^{N_\lambda} \sum_{j=1}^{N_a} W_{ij} C2_{ij} \right) \quad (2)$$

where, $W2(H_s, T_z)$ is the weighting factor of short-term sea state according to wave statistics of the North Atlantic or other sources, H_s is the significant wave height, T_z is the average zero up-crossing wave period; W_{ij} is a statistical weight calculated with the joint distribution of local wave steepness and lengths; $C2_{ij}$ is calculated for each wave to judge whether surf-riding occurs, which is defined as follows:

$$C2_{ij} = \begin{cases} 1 & \text{if } Fn > Fn_{cr}(r_i, s_j) \\ 0 & \text{if } Fn \leq Fn_{cr}(r_i, s_j) \end{cases} \quad (3)$$

where, Fn_{cr} is the critical Froude number corresponding to the surf-riding threshold for the regular wave with steepness s_j and wavelength to ship length ratio r_i , and calculated by using the critical speed u_{cr} , which is determined by solving the following equation:

$$T_e(u_{cr}; n_{cr}) - R(u_{cr}) = 0 \quad (4)$$

where, T_e is the propulsor thrust in water; R is the calm water resistance of the ship; n_{cr} is the commanded number of propeller revolutions corresponding to the surf-riding threshold, which is estimated based on Melnikov method. The detailed estimation of n_{cr} is introduced in the draft explanatory notes for surf-riding and broaching (IMO SDC.3, 2016b).

Sample ships calculation

The check of level 2 criterion for a fishing vessel is conducted to compare with the example in the draft explanatory notes for surf-riding and broaching (IMO SDC.3, 2016b), and the comparison results of Fn_{cr} and the value C are shown in tables 1 and 2 respectively, which indicate that the software coded by the authors based on the updated vulnerability criteria for surf-riding and

broaching (IMO SDC.2, 2015; IMO SDC.3, 2016a, 2016b) has sufficient accuracy. As shown in table 3, the sample calculations for seven ships are conducted to analyze the applicability of the current vulnerability criteria for surf-riding and broaching.

Table 1 Comparison results of Fn_{cr}

λ/L	H/λ	Fn_{cr} in SDC 3	Fn_{cr} in this study	% difference
1.25	0.0504	0.3296	0.3292	-0.121%
1.50	0.0396	0.3563	0.3569	0.168%
1.50	0.0504	0.3428	0.3435	0.204%
1.50	0.0600	0.3325	0.3332	0.211%
1.75	0.0504	0.3577	0.3591	0.391%

Table 2 Comparison results of the value C

F_n	C in SDC 3	C in this study	% difference
0.30	0.000788	0.000810	2.792%
0.35	0.0231	0.0226	-2.165%
0.40	0.0591	0.0577	-2.369%
0.45	0.0877	0.0865	-1.368%
0.50	0.0919	0.0919	0.000%

Table 3 Summary of sample calculations

Ship Type	L_{PP} (m)	Maximum service F_n	Level 1	Level 2	
			Result	C	Result
Fishing ship 1	34.5	0.475	Fail	9.19E-2	Fail
Fishing ship 2 (Full load)	27.4	0.314	Fail	2.12E-3	Pass
Fishing ship 2 (Design load)	27.4	0.319	Fail	3.39E-3	Pass
Fishing ship 3	66.0	0.310	Fail	2.28E-3	Pass
DTMB 5415	142.0	0.413	Fail	2.77E-2	Fail
ONR tumble-home ship	154.0	0.397	Fail	2.17E-2	Fail
Container ship 1	262.0	0.254	Pass	3.50E-9	Pass
Container ship 2	150.0	<0.250	Pass	0.00E+0	Pass

The results of the sample calculations show that five ships fail to pass level 1 criterion, which need to check level 2 criterion, because their Froude numbers are larger than 0.3, while their lengths are less than 200m. Three ships with much higher speed still can't pass level 2 criterion, which need to be checked by the direct stability assessment.

There are no inconsistencies in the checks between two levels vulnerability criteria, which indicate that the mathematical model of the current level 2 criterion is reasonable.

In order to provide validation data for the calculation of vulnerability criteria, ONR tumblehome vessel as an unconventional ship with good performance of propulsion and seakeeping, which is one of standard models for the second generation intact stability criteria, is used as a subject ship in the following model experiment.

3. EXPERIMENTAL INVESTIGATION

Experiment

The free running experiment of the ONR tumblehome vessel was conducted to assess the surf-riding and broaching phenomena in regular following and stern-quartering waves at the maneuvering and seakeeping basin of China Ship Scientific Research Center (CSSRC). The basin is 69m length, 46m breadth and 4m depth, which is equipped with flap wave makers at the two adjacent sides of the basin. The ship model was equipped with double propellers and double rudders. Ship motions were measured by the MEMS (Micro Electro-Mechanical System)-based gyroscope placed on the ship model.

Table 4 Principal particulars of ONR tumblehome vessel

Items	Ship	Model
Length: L_{BP}	154.0m	3.8m
Breadth: B	18.8m	0.463m
Depth: d	5.494m	0.136m
Block coefficient: C_b	0.535	0.535
Displacement: W	8507ton	0.128ton
Design speed: V	15.43 m/s	2.424 m/s
Metacentric height: GM	2.068m	0.051m

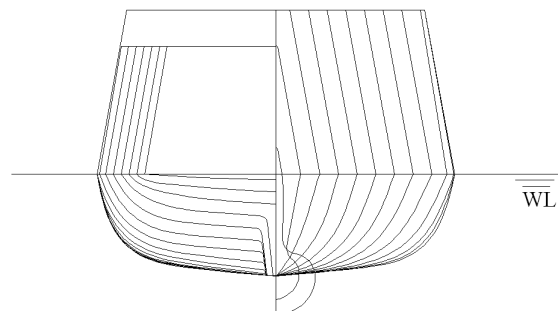


Figure 1: Body plan of ONR tumblehome vessel

The principal particulars and the body plan of the ONR tumblehome vessel are shown in Table 4 and Figure 1.

Results and discussions

As shown in Figures 2 and 3, the ship experiences surf-riding and broaching in two wave conditions respectively. Surf-riding and broaching often occur on the down slope of a wave, and broaching always accompanied with a large heel angle, may lead to stability failure, or even capsizing.

The experiment results in following waves are shown in Figures 4 and 5. The pitch motion of the ship appears periodic at the beginning, and then the amplitude of pitch motion is almost unchanged in later time. While yaw motion is generally small all the time. This reveals that stable surf-riding occurs.

With the wave steepness increasing and the heading changing to stern-quartering waves as shown in Figures 6 and 7, surf-riding occurs quickly. Then the ship can't keep its course even with maximum steering effort, and broaching occurs. At the same time roll angle increases rapidly. But with the action of rudders, the ship is stable at a new heading temporarily. And then the ship is captured again by a new wave and surf-

riding and broaching occur once more. At the third broaching event, the roll angle is so large that the ship capsizes at last.



Figure 2: A snapshot of surf-riding in the free running experiment



Figure 3: A snapshot of broaching in the free running experiment

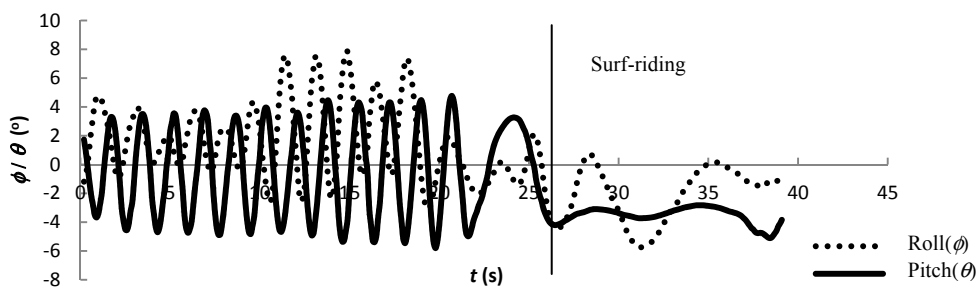


Figure 4: Time histories of roll and pitch ($F_n=0.4, \lambda/L=1.25, H/\lambda=0.05$, following waves $\chi=0^\circ$)

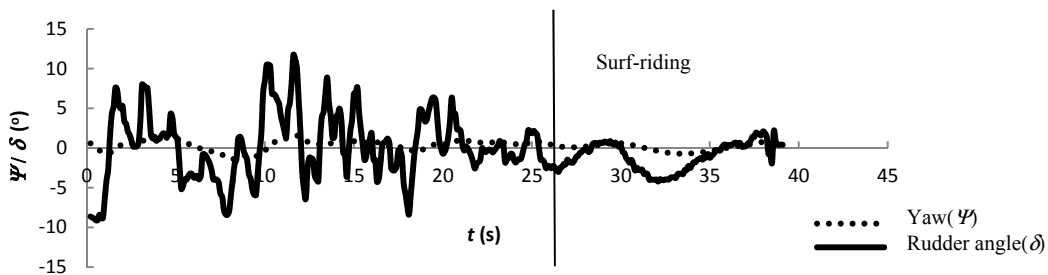


Figure 5: Time histories of yaw and rudder angle ($F_n=0.4, \lambda/L=1.25, H/\lambda=0.05$, following waves $\chi=0^\circ$)

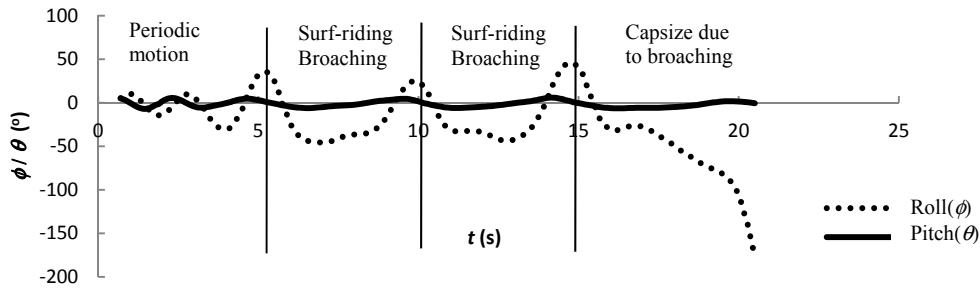


Figure 6: Time histories of roll and pitch ($F_n=0.4$, $\lambda/L=1.25$, $H/\lambda=0.06$, stern-quartering waves $\chi=30^\circ$)

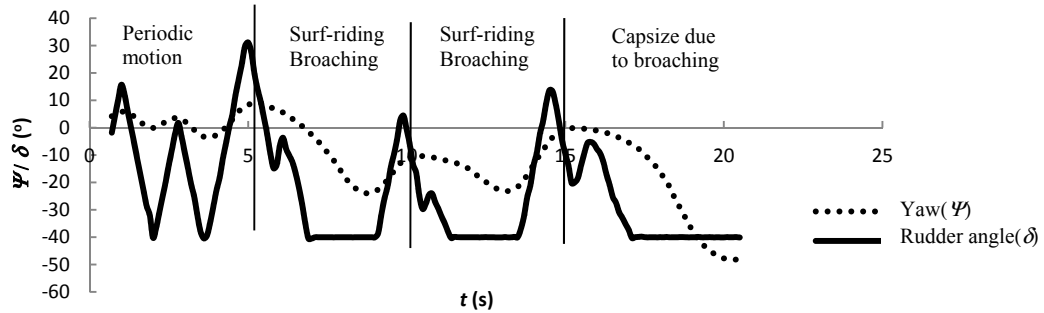


Figure 7: Time histories of yaw and rudder angle ($F_n=0.4$, $\lambda/L=1.25$, $H/\lambda=0.06$, stern-quartering waves $\chi=30^\circ$)

In the level 2 criterion for surf-riding and broaching, $C2_{ij}$ is used to judge whether surf-riding occurs in the regular following waves. The calculation results at different F_n are compared with the experiment results as shown in Figures 8 and 9. The comparison indicates that the calculation results are more conservative than experiment results.

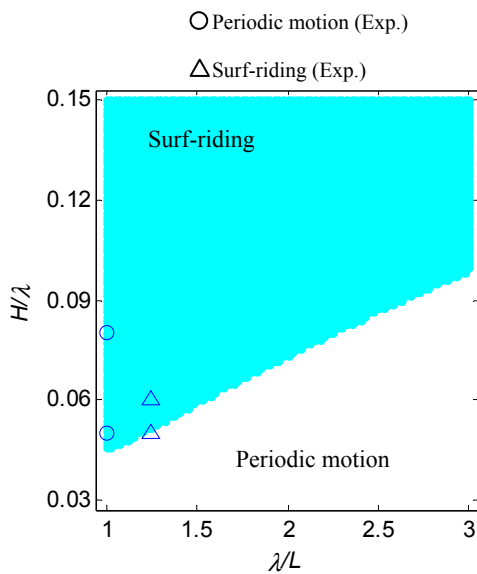


Figure 8: Comparison of the results between calculation and model experiment ($F_n=0.3$)

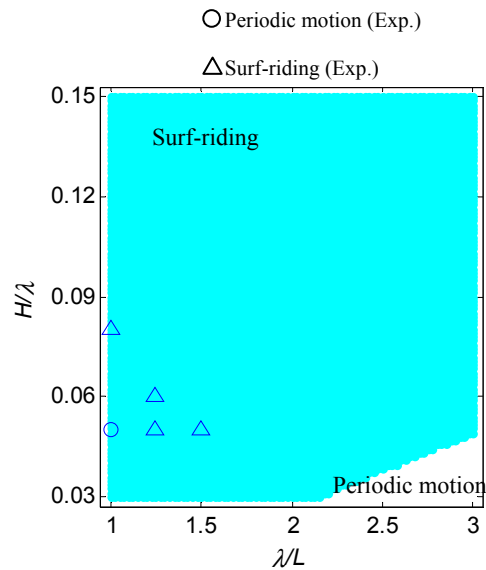


Figure 9: Comparison of the results between calculation and model experiment ($F_n=0.4$)

In the experiment, the ship doesn't experience surf-riding at the cases with small steepness and wavelength to ship length ratio ($F_n=0.3$, $\lambda/L=1.0$, $H/\lambda=0.05$ and 0.08 ; $F_n=0.4$, $\lambda/L=1.0$, $H/\lambda=0.08$), which are inconsistent with the calculation results. It's because that the mathematical model of level 2 criterion is based on a single degree of freedom surge equation with the linear Froude-Krylov force, and could conservatively predict surf-riding for the unconventional ship in waves with small steepness and wavelength to ship length ratio. However, level

2 criterion is practical for its simple and conservative. For the ONR tumblehome vessel, which fails to pass level 2 criterion, the direct stability assessment using the advanced state-of-the-art technology should be performed to avoid over conservative assessments.

4. CONCLUSION

Based on the sample calculation and the model experiment for surf-riding and broaching, the following conclusions can be summarized.

1) The mathematical model of the current level 2 criterion is reasonable by analyzing the applicability of vulnerability criteria with the sample calculations.

2) Four types of ship motions with periodic motion, stable surf-riding, broaching and capsizing due to broaching are observed in the experiment, while broaching is observed three times in one wave case.

3) With the comparison of results between calculations and model experiment, level 2 criterion for surf-riding and broaching is also applicable to ONR tumblehome vessel.

5. ACKNOWLEDGEMENT

The research is supported by Ministry of Industry and Information Technology of China (No. [2016] 26). The authors sincerely thank the above organization.

6. REFERENCES

Belenky V., Spyrou K., Weems K., 2012, "Evaluation of the Probability of Surf-riding in Irregular Waves with the Time-split Method", Proceedings of the 11th International Conference on the Stability of Ships and Ocean Vehicles, pp. 29-37.

Belenky V., Weems K., Spyrou K., 2016a, "On Probability of Surf-riding in Irregular Seas with a Split-time Formulation", Ocean Engineering, 120, pp. 264-273.

Belenky V., Spyrou K., Weems K., 2016b, "On Probability Properties of Surf-riding and Broaching-to in Irregular Seas", 31st Symposium on Naval Hydrodynamics, pp. 264-273.

Hashimoto H., Umeda N., Matsuda A., 2004, "Importance of Several Nonlinear Factors on

Broaching Prediction", Journal of Marine Science and Technology, 9, pp. 80-93.

Hashimoto H., Umeda N., Matsuda A., 2011, "Model Experiment on Heel-induced Hydrodynamic Forces in Waves for Realizing Quantitative Prediction of Broaching", Fluid Mechanics and Its Application, 96, pp. 379-398.

IMO 2015, Draft Amendments to Part B of the IS Code with Regard to Vulnerability Criteria of Levels 1 and 2 for the Surf-riding / Broaching Failure Mode, SDC 2/WP.4 Annex3.

IMO 2016a, Amendments to Part B of the 2008 IS Code on Towing, Lifting and Anchor Handling Operations, SDC 3/WP.5.

IMO 2016b, Draft Explanatory Notes on the Vulnerability of Ships to the Surf-riding/ Broaching Stability Failure Mode, SDC 3/WP.5 Annex 5.

IMO 2017, Draft Guidelines of Direct Stability Assessment Procedures for Use with the Second Generation Intact Stability Criteria, SDC 4/WP.4 Annex 1.

Kan M., 1990, "A Guideline to Avoid the Dangerous Surf-riding", Proceedings of the 4th International Conference on Stability of Ships and Ocean Vehicles, pp. 90-97.

Maki A., Umeda N., Renilson M., Ueta T., "Analytical Formulae for Predicting the Surf-riding Threshold for a Ship in Following Seas", Journal of Marine Science and Technology, 15, pp. 218-229.

Maki A., Umeda N., Renilson M., Ueta T., 2014, "Analytical Methods to Predict the Surf-riding Threshold and the Wave-blocking Threshold in Astern Seas", Journal of Marine Science and Technology, 19, pp. 415-424.

Spyrou K.J., 2006, "Asymmetric Surging of Ships in Following Seas and its Repercussion for Safety", Nonlinear Dynamics, 43, pp. 149-172.

Spyrou K., Belenky V., Themelis N., Weems K., 2012, "Conditions for Surf-riding in an Irregular Seaway", Proceedings of the 11th International Conference on the Stability of Ships and Ocean Vehicles, pp. 23-28.

Umeda N., Hashimoto H., 2002, "Qualitative Aspects of Nonlinear Ship Motions in Following and Quartering Seas with High Forward Velocity", Journal of Marine Science and Technology, 6(2), pp. 111-121.

Study on Standard Mathematical Model of Pure Loss of Stability in Stern-quartering Waves

Jiang Lu, *China Ship Scientific Research Center, Wuxi, China, lujiang1980@aliyun.com*

Min Gu, *China Ship Scientific Research Center, Wuxi, China, gumin702@163.com*

ABSTRACT

The guidelines for direct stability assessment of pure loss of stability are currently under development at the International Maritime Organization (IMO) for the second generation intact stability criteria. The present study intends to provide a standard mathematical model for predicting pure loss of stability, with sufficient accuracy and practically useful. Firstly, one Maneuvering Modeling Group (MMG) standard method for ship maneuvering predictions is referenced with the roll motion and heel-induced hydrodynamic forces taken into account. Secondly, existing mathematical models for broaching predictions are introduced into the standard mathematical model for predicting pure loss of stability. Finally, some crucial terms for predicting pure loss of stability in stern-quartering waves are numerically investigated with the ONR tumblehome vessel which is one of standard ship models for the second generation intact stability criteria, and some remarks are given for the standard mathematical model of pure loss of stability in stern-quartering waves.

Keywords: *Pure loss of stability, second generation intact stability criteria, MMG, broaching, ONR tumblehome.*

LIST OF SYMBOLS

a_H	Rudder force increase factor	K_r, N_r, Y_r	Derivative of roll moment, yaw moment and sway force with respect to yaw rate, their nondimensional K'_r, N'_r, Y'_r
AE, FE	After section and forward section	K_{rr}, N_{rr}, Y_{rr}	Derivative of roll moment, yaw moment and sway force with respect to cubic yaw rate, their nondimensional $K'_{rr}, N'_{rr}, Y'_{rr}$
A_R	Rudder area	$K_{r \phi}, N_{r \phi}, Y_{r \phi}$	Derivative of rollmoment, yaw moment and sway forcewith respect to yaw rate and heeling angle, their nondimensional $K'_{r \phi}, N'_{r \phi}, Y'_{r \phi}$
A_{sp}, A_{sb}	The port and starboard rudder area	K_{wr}, N_{wr}, Y_{wr}	Derivative of rollmoment, yaw moment and sway force with respect to squared yaw rate and sway velocity, their nondimensional $K'_{wr}, N'_{wr}, Y'_{wr}$
$B(x)$	Sectional breadth	K_{vr}, N_{vr}, Y_{vr}	Derivative of roll moment, yaw moment and sway force with respect to squared yaw rate and sway velocity, their nondimensional $K'_{vr}, N'_{vr}, Y'_{vr}$
C_T	Total resistance coefficient in calm water	K_v, N_v, Y_v	Derivative of roll moment, yaw moment and sway force with respect to swayvelocity, their nondimensional K'_v, N'_v, Y'_v
d	Ship draft	K_{vw}, N_{vw}, Y_{vw}	Derivative of roll moment, yaw moment and sway force with respect to cubic sway velocity, their nondimensional $K'_{vw}, N'_{vw}, Y'_{vw}$
$d(x)$	Sectional draught		
D_p	Propeller diameter		
$D(p)$	Roll damping moment		
F_N	Rudder normal force		
F_n	Froude number based on ship length		
f_α	Rudder lifting slope coefficient		
g	Gravitational acceleration		
GM	Metacentric height		
GZ_w	Righting arm in waves		
H_R	Rudder span length		
I_{xx}, J_{xx}	Moment and addd moment of inertia in roll		
I_{zz}, J_{zz}	Moment and addd momentof inertia in yaw		
J_p	Propeller advanced ratio		
k	Wave number		

$K_{\dot{v} \phi}, N_{\dot{v} \phi}, Y_{\dot{v} \phi}$	Derivative of roll moment, yaw moment and sway force with respect to sway velocity and heeling angle, their nondimensional $K'_{\dot{v} \phi}, N'_{\dot{v} \phi}, Y'_{\dot{v} \phi}$	X_R, Y_R, N_R, K_R	Surge force, lateral force, yaw moment and roll moment around center of ship gravity by steering
K_ϕ, N_ϕ, Y_ϕ	Derivative of roll moment, yaw moment and sway force with respect to roll angle, their nondimensional $K'_\phi, N'_\phi, Y'_\phi$	X_{rr}	Derivative of surge force with respect to squared yaw rate, its nondimensional X'_{rr}
K_p	Rudder gain	X_{vr}	Derivative of surge force with respect to toswayvelocity and yaw rate, its nondimensional X'_{vr}
K_T	Thrust coefficient of propeller	X_{vv}	Derivative of surge force with respect to squared sway velocity, its nondimensional X'_{vv}
L_{pp}	Ship length between perpendiculars	X_{vvvv}	Derivative of surge force with respect to 4th order sway velocity, its nondimensional X'_{vvvv}
ℓ_R'	Correction factor for flow-straightening due to yaw	X_w, Y_w, N_w, K_w	Surge force, lateral force, yaw moment and roll moment around center of ship gravity acting on ship hull induced by waves
m	Ship mass	Z_H	Vertical position of center of sway force due to lateral motion
m_x, m_y	Added mass in surge and sway	Z_{HR}	Vertical position of of additional lateral force due to rudder
n_p	Propeller revolution number	Z_R	Vertical position of center of rudder
OG	Vertical distance between center of gravity and waterline	α	Linear roll damping coefficient
P	Roll rate	α_R	Effective inflow angle to rudder
r	Yaw rate	β	Hull drift angle
R	Ship resistance	δ	Rudder angle
$S(x)$	Sectional area	η	Ratio of propeller diameter to rudder span
$S_y(x)$	Added mass of one section at sway direction	ε	Ratio of wake fraction at propeller and rudder position
$S_{y\eta}(x)$	Added moment of one section at roll direction	κ	Propeller-induced flow velocity factor
S_F	Wetted hull surface area	λ	Wave length
t_p	Thrust deduction factor	Λ	Ruder aspect ratio
t_R	Steering resistance deduction factor	φ	Roll angle
T	Propeller thrust	γ	Cubic nonlinear roll damping coefficient
T_E	Time constant for steering gear	γ_R	Flow-straightening effect coefficient
T_D	Time constant for differential control	θ	Pitch angle
T_ϕ	Natural roll period	χ	Yaw angle from wave direction
u, v	Surge and sway velocity	χ_c	Yaw angle of auto pilot course
u_R	Longitudinal inflow velocity component to rudder	ρ	Water density
U	Ship forward velocity	ω	Wave frequency
w_p	Wake fraction at propeller position	ω_e	Averaged encounter frequency
w_R	Wake fraction at rudder position	ξ_G	Longitudinal position of center of ship gravity from a wave trough
W	Ship weight	(ξ_G, η_G, ζ_G)	Position of center of ship gravity in the space-fixed coordinate system
x_{HR}	Longitudinal position of additional lateral force due to rudder	ζ_w	Wave amplitude
x_R	Longitudinal position of rudder		
X_H, Y_H, N_H, K_H	Surge force, lateral force, yaw moment and roll moment around center of ship gravity acting on ship hull		
X_p	Surge force due to propeller		

1. INTRODUCTION

The guidelines for direct stability assessment of five stability failure models including pure loss of stability are under development at the International Maritime Organization (IMO) for the second generation intact stability criteria (IMO SDC 4, 2017). Once the crest of the large wave passes the midship section of a ship with a slightly higher speed than ship speed, the state of stability loss at the crest may exist long enough to evolve a large heel angle, or even capsizing. It is urgently required to establish a standard mathematical model which is sufficient accuracy and practically useful for predicting pure loss of stability in stern-quartering waves.

Without external heel moment, once the wave crest passes the ship, the ship will finally return to the upright position with regained stability except for cases that the ship already heel too far or the metacentric height in the wave is negative. Roll moment excited by oblique waves and heel moments induced by a centrifugal force due to ship maneuvering motions are the relevant external moments. Several freely running experiments also prove that coupling with maneuvering motion is essential for explaining the forward speed effect on pure loss of stability in stern-quartering waves (IMO SDC 3, 2016).

Pure loss of stability in stern-quartering waves is a nonlinear phenomenon involving large amplitude roll motion and it is still difficult to be predicted quantitatively. Japan delegation (IMO SLF55, 2013) notes that predicting pure loss of stability with their newly 4 degrees of freedom (DOF) mathematical model is more accuracy than the 2 DOF mathematical model (Kubo et al., 2012). The delegations for the second generation intact stability criteria at IMO SDC4 gave top priority to discussing the guidelines for direct stability assessment and the 4 DOF for predicting pure loss of stability has been agreed at the current stage (IMO SDC 4, 2017).

Though the 4 DOF mathematical model for predicting pure loss of stability has not been investigated widely with simulations and experiments, a 4 DOF mathematical model for broaching prediction (Umeda, 1999) has been investigated for many years. For providing a accurate mathematical model for broaching

prediction, Umeda and Hashimoto had investigated essential terms in the 4 DOF mathematical model one by one by utilizing fishing vessels. Nonlinear maneuvering forces in calm water (Umeda & Hashimoto, 2002), wave effect on linear maneuvering forces, roll restoring and rudder force (Umeda et al., 2003), and several nonlinear factors were also investigated, such as nonlinear wave forces, nonlinear sway-yaw coupling, wave effect on propeller thrust, heel-induced hydrodynamic forces for large heel angle in calm water (Hashimoto et al., 2004), and wave effect on heel-induced hydrodynamic forces for large heel angle. A simplified mathematical model was proposed for more practically useful (Hashimoto et al., 2011a). Existing 4 DOF mathematical model was used for broaching prediction of the ONR tumblehome vessel, and a fair quantitative prediction was realized (Hashimoto et al., 2011b). Broaching is a nonlinear phenomena related to ship maneuvering in the wave, and above 4 DOF mathematical models are based on a Maneuvering Modeling Group (MMG) model, but simulation methods without standard expressions could not be used in general. Therefore a MMG standard method for ship maneuvering predictions was introduced (Yasukawa & Yoshimura, 2015). A 4 DOF mathematical model was refined for broaching prediction of the ONR flare topside vessel (Umeda et al., 2016).

For drafting guidelines for direct stability assessment, several crucial elements for predicting parametric roll were investigated with simulations and experiments by the authors (Lu et al., 2017), and some crucial terms in the 4 DOF mathematical for predicting pure loss of stability still require further experimental and numerical studies with more examples, though the above 4 DOF mathematical models for broaching prediction have a certain degree of reference. The physical mechanism of pure loss of stability is different from that of broaching and a 4 DOF standard mathematical model for predicting pure loss of stability has not been established widely. Therefore, systematic studies on the 4 DOF mathematical model for predicting pure loss of stability are hot tasks at this stage. Also IMO is calling for the validation of numerical methods or guidelines for the finalization of second generation intact stability with examples.

Based on the MMG standard method and existing mathematical model for broaching and pure loss of stability, the present study intends to provide a 4 DOF standard mathematical model with unified expressions for the prediction of pure loss of stability. Some crucial terms in the mathematical model were investigated using one standard ship. The experiment is also in progress as the next step.

2. MATHEMATICAL MODEL

2.1 Coordinate systems

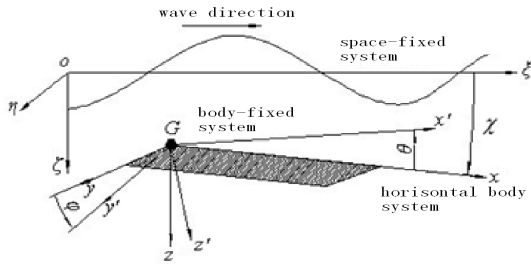


Figure 1: Coordinate systems

A space-fixed coordinate system $O-\xi\eta\zeta$ with the origin at a wave trough, a body-fixed system $G-x'y'z'$ with the origin at the center of gravity of the ship, and a horizontal body coordinate system (Hamamoto & Kim, 1993) $G-xyz$ which has the same origin with the body-fixed system but does not rotate around the x-axis and y-axis are adopted as shown in Fig. 1.

The relationships between the horizontal body coordinate system $G-xyz$, the body-fixed system $G-x'y'z'$ and the space-fixed system $O-\xi\eta\zeta$ are shown in Eq. (1) and Eq. (2), respectively.

$$\begin{bmatrix} x \\ y \\ z \end{bmatrix} = \begin{bmatrix} \cos\theta & \sin\theta\sin\phi & \cos\phi\sin\theta \\ 0 & \cos\phi & -\sin\phi \\ -\sin\theta & \sin\theta\cos\phi & \cos\theta\cos\phi \end{bmatrix} \begin{bmatrix} x' \\ y' \\ z' \end{bmatrix} \quad (1)$$

$$\begin{bmatrix} \xi-\xi_G \\ \eta-\eta_G \\ \zeta-\zeta_G \end{bmatrix} = \begin{bmatrix} \cos\theta\cos\chi & \sin\phi\sin\theta\cos\chi & \cos\phi\sin\theta\cos\chi \\ & -\cos\phi\sin\chi & +\sin\phi\sin\chi \\ \cos\theta\sin\chi & \sin\phi\sin\theta\sin\chi & \cos\phi\sin\theta\sin\chi \\ & +\cos\phi\cos\chi & -\sin\phi\cos\chi \\ -\sin\theta & \sin\theta\cos\theta & \cos\theta\cos\theta \end{bmatrix} \begin{bmatrix} x' \\ y' \\ z' \end{bmatrix} \quad (2)$$

2.2 Mathematical model

Heave and pitch response will be dynamic or static depending on the encounter frequency. In case of astern waves, the encounter frequency is much lower than the natural frequencies of heave and

pitch so that coupling with heave and pitch is almost static (Matsuda & Umeda, 1997). The 4 DOF mathematical model are expressed by surge, sway, yaw and roll motions as shown in Eq. (3) to Eq. (6), respectively. Control equation for keeping course by steering is added in the 4 DOF mathematical model as shown in Eq. (7).

$$(m+m_x)\dot{u}-(m+m_y)vr = X_H + X_R + X_P + X_W \quad (3)$$

$$(m+m_y)\dot{v}+(m+m_x)ur = Y_H + Y_R + Y_W \quad (4)$$

$$(I_{zz} + J_{zz})\dot{r} = N_H + N_R + N_W \quad (5)$$

$$(I_{xx} + J_{xx})\dot{p} - m_x z_H ur - m_y z_H \dot{v} = K_H + K_R + K_W \quad (6)$$

$$-D(\phi) - WGZ_W(\xi_G / \lambda, \chi, \phi)$$

$$\dot{\delta} = \{-\delta - K_P(\chi - \chi_C) - K_P T_D r\} / T_E \quad (7)$$

The subscripts H, R, P and W refer to hull, rudder, propeller and wave, respectively.

2.3 Hydrodynamic forces acting on ship hull

Hydrodynamic forces acting on a ship hull of a MMG standard method (Yasukawa & Yoshimura, 2015) is referenced with the roll motion and heel-induced hydrodynamic forces taken into account.

The hull forces in still water X_H, Y_H, N_H and K_H are expressed as follows:

$$X_H = -R(u) + \frac{1}{2} \rho L_{pp} d U^2 (X'_{vv} \cdot v'^2 + X'_{vr} \cdot v'r' + X'_{rr} \cdot r'^2 + X'_{vvv} \cdot v'^4) \quad (8)$$

$$Y_H = \frac{1}{2} \rho L_{pp} d U^2 (Y'_v \cdot v' + Y'_r \cdot r' + Y'_{vv} \cdot v'^3 + Y'_{vr} \cdot v'^2 r' + Y'_{vr} \cdot v' r'^2 + Y'_{rr} \cdot r'^3 + Y'_\phi \cdot \phi + Y'_{v|\phi} \cdot v' |\phi| + Y'_{r|\phi} \cdot r' |\phi|) \quad (9)$$

$$N_H = \frac{1}{2} \rho L_{pp}^2 d U^2 (N'_v \cdot v' + N'_r \cdot r' + N'_{vv} \cdot v'^3 + N'_{vr} \cdot v'^2 r' + N'_{vr} \cdot v' r'^2 + N'_{rr} \cdot r'^3 + N'_\phi \cdot \phi + N'_{v|\phi} \cdot v' |\phi| + N'_{r|\phi} \cdot r' |\phi|) \quad (10)$$

$$K_H = \frac{1}{2} \rho L_{pp} d^2 U^2 (K'_v \cdot v' + K'_r \cdot r' + K'_{vv} \cdot v'^3 + K'_{vr} \cdot v'^2 r' + K'_{vr} \cdot v' r'^2 + K'_{rr} \cdot r'^3 + K'_\phi \cdot \phi + K'_{v|\phi} \cdot v' |\phi| + K'_{r|\phi} \cdot r' |\phi|) \quad (11)$$

$$= Y_H \times Z_H$$

where v', r' denote nondimensional lateral velocity, and yaw rate, respectively and are expressed as follows:

$$\dot{v}' = \frac{v}{U}, \quad \dot{r}' = \frac{rL_{pp}}{U} \quad (12)$$

Each maneuvering coefficient can be determined by circular motion test, or oblique towing test (OTT). For providing unified expressions, the nondimensional maneuvering coefficients are rewritten as follows:

$$X'_{vv} = \frac{X_{vv}}{\frac{1}{2}\rho L_{pp}d}, \quad X'_{vr} = \frac{X_{vr}}{\frac{1}{2}\rho L_{pp}^2d} \quad (13)$$

$$X'_{rr} = \frac{X_{rr}}{\frac{1}{2}\rho L_{pp}^3d}, \quad X'_{vvvv} = \frac{X_{vvvv}}{\frac{1}{2}\rho L_{pp}d/U^2} \quad (14)$$

$$Y'_v = \frac{Y_v}{\frac{1}{2}\rho L_{pp}dU}, \quad Y'_r = \frac{Y_r}{\frac{1}{2}\rho L_{pp}^2dU}, \quad Y'_\varphi = \frac{Y_\varphi}{\frac{1}{2}\rho L_{pp}dU^2} \quad (15)$$

$$Y'_{vv} = \frac{Y_{vv}}{\frac{1}{2}\rho L_{pp}d/U}, \quad Y'_{vr} = \frac{Y_{vr}}{\frac{1}{2}\rho L_{pp}^2d/U}, \quad Y'_{rr} = \frac{Y_{rr}}{\frac{1}{2}\rho L_{pp}^3d/U} \quad (16)$$

$$Y'_{rrr} = \frac{Y_{rrr}}{\frac{1}{2}\rho L_{pp}^4d/U}, \quad Y'_{v|\varphi|} = \frac{Y_{v|\varphi|}}{\frac{1}{2}\rho L_{pp}dU}, \quad Y'_{r|\varphi|} = \frac{Y_{r|\varphi|}}{\frac{1}{2}\rho L_{pp}^2dU} \quad (17)$$

$$N'_v = \frac{N_v}{\frac{1}{2}\rho L_{pp}^2dU}, \quad N'_r = \frac{N_r}{\frac{1}{2}\rho L_{pp}^3dU}, \quad N'_\varphi = \frac{N_\varphi}{\frac{1}{2}\rho L_{pp}^2dU^2} \quad (18)$$

$$N'_{vv} = \frac{N_{vv}}{\frac{1}{2}\rho L_{pp}^2d/U}, \quad N'_{vr} = \frac{N_{vr}}{\frac{1}{2}\rho L_{pp}^3d/U}, \quad N'_{rr} = \frac{N_{rr}}{\frac{1}{2}\rho L_{pp}^4d/U} \quad (19)$$

$$N'_{rrr} = \frac{N_{rrr}}{\frac{1}{2}\rho L_{pp}^5d/U}, \quad N'_{v|\varphi|} = \frac{N_{v|\varphi|}}{\frac{1}{2}\rho L_{pp}^2dU}, \quad N'_{r|\varphi|} = \frac{N_{r|\varphi|}}{\frac{1}{2}\rho L_{pp}^3dU} \quad (20)$$

$$K'_v = \frac{K_v}{\frac{1}{2}\rho L_{pp}d^2U}, \quad K'_r = \frac{K_r}{\frac{1}{2}\rho L_{pp}^2d^2U}, \quad K'_\varphi = \frac{K_\varphi}{\frac{1}{2}\rho L_{pp}d^2U^2} \quad (21)$$

$$K'_{vv} = \frac{K_{vv}}{\frac{1}{2}\rho L_{pp}d^2/U}, \quad K'_{vr} = \frac{K_{vr}}{\frac{1}{2}\rho L_{pp}^2d^2/U}, \quad K'_{rr} = \frac{K_{rr}}{\frac{1}{2}\rho L_{pp}^4d^2/U} \quad (22)$$

2.4 Propeller thrust and the hull resistance in still water

The surge force due to propeller thrust X_P with twin propellers is expressed as follows:

$$X_P = 2 \times (1 - t_p) T \quad (23)$$

$$T = \rho n_p^2 D_p^4 K_T(J_p) \quad (24)$$

$$J_p = \frac{(1 - w_p)u}{n_p D_p} \quad (25)$$

The hull resistance in still water R in the surge motion is expressed as follows:

$$R = \frac{1}{2} \rho S_F u^2 C_T \left(\frac{u}{\sqrt{gL_{pp}}} \right) \quad (26)$$

2.5 Hydrodynamic force by steering

The steering rudder forces components X_R, Y_R, N_R and K_R are expressed as follows:

$$X_R = -(1 - t_R) F_N \sin \delta \quad (27)$$

$$Y_R = -(1 + a_H) F_N \cos \delta \quad (28)$$

$$N_R = -(x_R + a_H x_{HR}) F_N \cos \delta \quad (29)$$

$$K_R = (z_R + a_H z_{HR}) F_N \cos \delta \quad (30)$$

where

$$F_N = \frac{1}{2} \rho A_R u_R^2 f_\alpha \sin \alpha_R \quad (31)$$

$$= \frac{1}{2} \rho (A_{RP} + A_{RS}) u_R^2 f_\alpha \sin \alpha_R$$

$$u_R = \varepsilon (1 - w_p) u \sqrt{\eta \left\{ 1 + \kappa \left(\sqrt{1 + \frac{8K_T(J_p)}{\pi J_p^2}} - 1 \right) \right\}^2 + 1 - \eta} \quad (32)$$

$$\alpha_R = \delta - \gamma_R \frac{U}{u_R} (\beta - \ell'_R r') \quad (33)$$

$$f_\alpha = \frac{6.13\Lambda}{2.25 + \Lambda}, \quad \varepsilon = \frac{1 - w_R}{1 - w_p} \quad (34)$$

$$\eta = \frac{D_p}{H_R}, \quad \beta = \arctan\left(\frac{-v}{u}\right), \quad U = \sqrt{u^2 + v^2} \quad (35)$$

2.5 Excited wave force

The wave-induced forces as the sum of the Froude-Krylov force (W_{FK}) and the diffraction force (W_{Dif}) including hydrodynamic lift forces acting on the hull are rewritten as follows. The rudder forces due to wave particle velocity which are considered for broaching prediction (Umeda & Hashimoto, 2002) are not taken into account for predicting pure loss of stability. The Froude-Krylov roll moment is taken into account for calculating the roll restoring force variation, so that only the diffraction force is used in Eq. (39).

$$X_W(\xi_G / \lambda, u, \chi) = X_{W_FK}(\xi_G / \lambda, u, \chi) \quad (36)$$

$$= -\rho g \zeta_w k \cos \chi \int_{AE}^{FE} C_1(x) S(x) e^{-kd(x)/2} \sin k(\xi_G + x \cos \chi) dx$$

$$Y_W(\xi_G / \lambda, u, \chi) = Y_{W_FK}(\xi_G / \lambda, u, \chi) + Y_{W_Dif}(\xi_G / \lambda, u, \chi)$$

$$= \rho g \zeta_w k \sin \chi \int_{AE}^{FE} C_1(x) S(x) e^{-kd(x)/2} \sin k(\xi_G + x \cos \chi) dx \quad (37)$$

$$+ \zeta_w \omega \omega_e \sin \chi \int_{AE}^{FE} \rho S_y(x) e^{-kd(x)/2} \sin k(\xi_G + x \cos \chi) dx$$

$$- \zeta_w \omega \sin \chi \left[\rho S_y(x) e^{-kd(x)/2} \cos k(\xi_G + x \cos \chi) \right]_{AE}^{FE}$$

$$\begin{aligned}
 N_w(\xi_G / \lambda, \chi) &= N_{w_FK}(\xi_G / \lambda, u, \chi) + N_{w_Diff}(\xi_G / \lambda, u, \chi) \\
 &= \rho g \zeta_w k \sin \chi \int_{AE}^{FE} C_1(x) S(x) e^{-kd(x)/2} x \sin k(\xi_G + x \cos \chi) dx \\
 &+ \zeta_w \omega \omega_e \sin \chi \int_{AE}^{FE} \rho S_y(x) e^{-kd(x)/2} x \sin k(\xi_G + x \cos \chi) dx \\
 &+ \zeta_w \omega u \sin \chi \int_{AE}^{FE} \rho S_y(x) e^{-kd(x)/2} \cos k(\xi_G + x \cos \chi) dx \\
 &- \zeta_w \omega u \sin \chi \left[\rho S_y(x) e^{-kd(x)/2} x \cos k(\xi_G + x \cos \chi) \right]_{AE}^{FE}
 \end{aligned} \tag{38}$$

$$\begin{aligned}
 K_w(\xi_G / \lambda, u, \chi) &= K_{w_FK}(\xi_G / \lambda, u, \chi) + K_{w_Diff}(\xi_G / \lambda, u, \chi) \\
 &= -\rho g \zeta_w k \sin \chi \int_{AE}^{FE} C_1(x) \frac{B(x)}{2} \{d(x)\}^2 e^{-kd(x)/2} \sin k(\xi_G + x \cos \chi) dx \\
 &- \rho g \zeta_w k^2 \sin \chi \int_{AE}^{FE} C_4(x) \left\{ \frac{B(x)}{2} \right\}^3 d(x) e^{-kd(x)/2} \sin k(\xi_G + x \cos \chi) dx \\
 &- \zeta_w \omega \omega_e \sin \chi \int_{AE}^{FE} \rho S_y I_\eta(x) e^{-kd(x)/2} \sin k(\xi_G + x \cos \chi) dx \\
 &+ \zeta_w \omega u \sin \chi \left[\rho S_y I_\eta(x) e^{-kd(x)/2} \cos k(\xi_G + x \cos \chi) \right]_{AE}^{FE} \\
 &+ Y_w(\xi_G / \lambda, u, \chi) \cdot \overline{OG}
 \end{aligned} \tag{39}$$

$$C_1 = \frac{\sin(k \sin \chi \cdot B(x) / 2)}{k \sin \chi \cdot B(x) / 2} \tag{40}$$

$$C_4 = \{k \sin \chi \cdot B(x) / 2\}^{-3} \left[2 \sin \{k \sin \chi \cdot B(x) / 2\} - k \sin \chi \cdot B(x) \cos \{k \sin \chi \cdot B(x) / 2\} \right] \tag{41}$$

2.6 Roll restoring force variation

Pure loss of stability is one of the problems related to the roll restoring force variation. The restoring force variation in oblique waves can be calculated by integrating the pressure around the instantaneously wetted hull surface with static balance of heave and pitch as show in Eq.(42) which is based on Froude-Krylov assumption (Lu et al., 2017). The Froude-Krylov roll moment is taken into account in Eq. (42) in oblique waves, while the effect of wave heading is converted into the change of the effective wave height in longitudinal waves by using Grim's effective wave concept in the references (Umeda & Yamakoshi, 1994; Kubo et al., 2012). For avoiding double counting of the Froude-Krylov roll moment in case of oblique waves, only the diffraction force is used in Eq. (39).

$$\begin{aligned}
 W \cdot GZ_w &= \rho g \int_{AE}^{FE} y(x, \xi_G / \lambda) \cdot A(x, \xi_G / \lambda) dx + \rho g \sin \chi \cdot \\
 &\int_{AE}^{FE} z(x, \xi_G / \lambda) \cdot F(x) \cdot A(x, \xi_G / \lambda) \cdot \sin(\xi_G + x \cos \chi) dx
 \end{aligned} \tag{42}$$

$$F(x) = \zeta_w k \frac{\sin(k \frac{B(x)}{2} \sin \chi)}{k \frac{B(x)}{2} \sin \chi} e^{-k \cdot d(x)} \tag{43}$$

where, $A(x, \xi_G / \lambda)$ is the submerged area of local section of the ship. $y(x, \xi_G / \lambda)$ is the transverse position of buoyancy centre of local section.

$z(x, \xi_G / \lambda)$ is the vertical position of buoyancy centre of local section.

2.7 Roll damping force

Roll damping is one of essential terms for predicting roll motion, especially large amplitude roll motion. Linear and cubic nonlinear roll damping coefficients are used for predicting parametric roll and linear and squared nonlinear roll damping coefficients are used for predicting dead ship stability in the vulnerability criteria (IMO SDC 4, 2017). Linear and cubic nonlinear roll damping coefficients are adopted as shown in Eq.(44) for predicting pure loss of stability, which could lead to large amplitude roll motion, or even capsizing, in following and stern-quartering waves.

$$D(p) = (I_{xx} + J_{xx})(\alpha \cdot p + \gamma \cdot p^3) \tag{44}$$

3. SUBJECT SHIPS

The subject ship is the ONR Tumblehome vessel which is one of standard ships for the second generation intact stability criteria provided by the coordinator of corresponding group. The principal particulars and the lines of the ONR Tumblehome vessel are shown in Table 1 and Fig. 2, respectively.

Table 1 Principal particulars of the ONR tumblehome

Items	Ship	Model
Length:L	154.0m	3.800m
Draft:d	5.494m	0.136m
Breadth:B	18.8m	0.463m
Depth:D	14.5m	0.358m
Displ.:W	8507ton	127.8kg
C _B	0.535	0.535
GM	2.07m	0.044m
T _φ	12.38s	1.945s
κ _{yy}	0.25L	0.25L

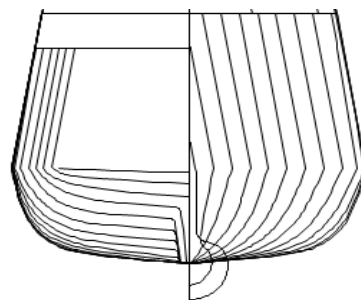


Fig.2 The ONR Tumblehome lines

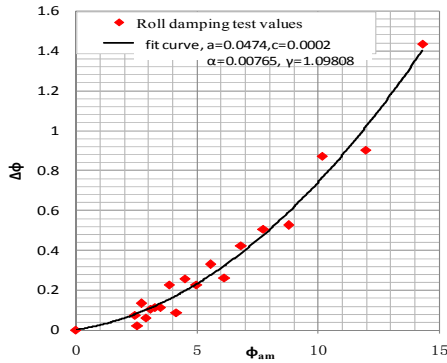


Fig.3 Extinction curve (a, c are linear and cubic extinction coefficients and α, γ are their nondimensional coefficients)

The nonlinear roll damping coefficients are obtained again from an existing model test (Gu et al., 2015) as shown in Fig.3.

4. SIMULATIONS AND DISCUSSIONS

The higher order maneuvering coefficients for hydrodynamic force acting on ship hull in the surge motion are taken into account in the MMG standard method for ship maneuvering prediction (Yasukawa & Yoshimura, 2015), and the higher order maneuvering coefficients without X_{vvv} are also recommended for predicting pure loss of stability by Japan (IMO SLF55, 2013; Kubo et al., 2012), while these higher order maneuvering coefficients are ignored for broaching prediction (Umeda et al., 2016). For investigating the effect of higher order maneuvering coefficients in the surge motion on predicting pure loss of stability, the following value $X'_{vv} = -0.040$, $X'_{vr} = -0.0622$, $X'_{rr} = 0.00841$, $X'_{vvv} = 0.771$ are used based on databases of ships.

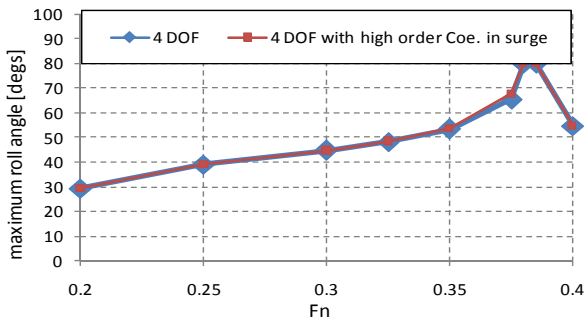


Figure 4 Comparison of maximum roll angle as function of the Froude number between the 4 DOF without and with higher order coefficients in the surge motion with $\lambda/Lpp=1.25$, $H/Lpp=0.05$, and $\chi=30^0$.

A comparison of maximum roll angle as function of the Froude number between the 4 DOF with and without higher order coefficients in the surge motion under the condition of $\lambda/Lpp=1.25$, $H/Lpp=0.05$, and $\chi=30^0$.

$Lpp=0.05$, and $\chi=30^0$ are carried out as shown in Fig.4. The results indicate that the effect of higher order maneuvering coefficients in the surge motion on predicting pure loss of stability is very small. The higher order maneuvering coefficients in the surge motion are ignored in following simulations.

The higher order maneuvering coefficients of heel-induced hydrodynamic forces are not considered in this study due to lack of referenced databases of ships. The other maneuvering coefficients mentioned in the references (Hashimoto et al., 2011b; Umeda et al., 2016) are used in this study.

For investigating the effect of different mathematical models on predicting pure loss of stability, a comparison of maximum roll angle as function of the Froude number between mathematical models with different DOF are conducted as shown in Fig.5.

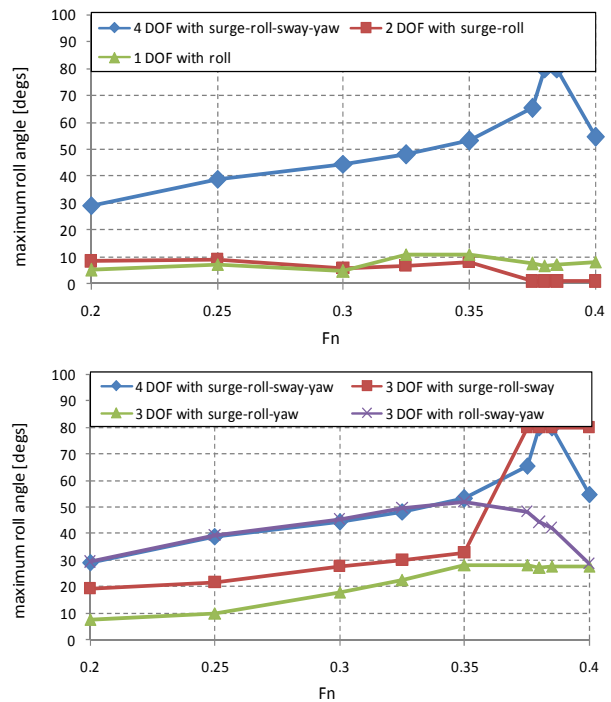


Figure 5 Comparison of maximum roll angle as function of the Froude number between mathematical models with different DOF with $\lambda/Lpp=1.25$, $H/Lpp=0.05$, and $\chi=30^0$.

The mathematical models with 1 DOF of roll motion and 2 DOF of surge-roll coupled motion could underestimate the roll angle and fail to predict capsizing due to pure loss of stability in stern-quartering waves. The mathematical model with 3 DOF of roll-sway-yaw coupled motion could predict the roll angle, but it also fails to predict capsizing at critical ship speeds due to pure loss of

stability. This means the surge motion is very important for predicting capsizing at critical ship speeds due to pure loss of stability. The surge motion cannot be ignored in the mathematical model for predicting pure loss of stability, that is to say, the forward speed effect on pure loss of stability in stern-quartering waves should be considered.

The roll angle predicted by the mathematical model with 3 DOF of surge-roll-yaw coupled motion is generally larger than that with 2 DOF of surge-roll coupled motion, but it also fails to predict capsizing at critical ship speeds due to pure loss of stability. The mathematical model with 3 DOF of surge-roll-sway coupled motion could also underestimate the roll angle, but it overestimates the capsizing range of critical ship speeds due to pure loss of stability. The mathematical model with 4 DOF of surge-roll-sway-yaw coupled motion could predict roll angle and appropriately estimate capsizing range of critical ship speeds due to pure loss of stability. This also supports the conclusion in the reference (Kubo et al., 2012) that the centrifugal force due to sway and yaw motions, other than the restoring reduction on a wave crest, are indispensable for explaining “pure” loss of stability on a wave crest. Therefore, both the sway and yaw motions should be considered in the mathematical model for predicting pure loss of stability.

The higher order maneuvering coefficients for hydrodynamic force acting on ship hull could affect predicting pure loss of stability, and a comparison of maximum roll angle between the 4 DOF with and without high order coefficients in roll, sway and yaw motions under the condition of $\lambda/Lpp=1.25$, $H/Lpp=0.05$, and $\chi=30^\circ$ are carried out as shown in Fig.6.

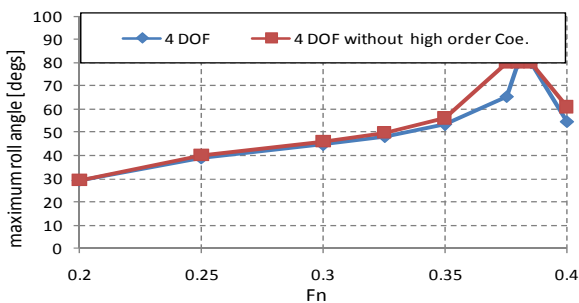


Figure 6 Comparison of maximum roll angle as function of the Froude number between the 4 DOF with and without higher order maneuvering coefficients in roll, sway and yaw motions with $\lambda/Lpp=1.25$, $H/Lpp=0.05$, and $\chi=30^\circ$.

The results indicate that the mathematical model of 4 DOF without higher order maneuvering

coefficients in sway, yaw and roll motions could predict roll angle, but it could overestimate the capsizing range of critical ship speeds due to pure loss of stability.

Diffraction forces are very important for predicting ship motions in waves, and for investigating the effect of diffraction forces on predicting pure loss of stability in stern-quartering waves, simulations with diffraction forces, without diffraction forces and only without diffraction forces in the roll motion are carried out as shown in Fig.7. The mathematical model of 4 DOF without diffraction forces could underestimate roll angle due to indirectly reducing the effect of maneuvering motions on the roll and it also fails to correctly predict capsizing range of critical ship speeds. The mathematical model of 4 DOF only without diffraction forces in the roll motion could estimate roll angle, but it completely fails to predict capsizing at critical ship speeds. This means diffraction forces should be taken into account for predicting pure loss of stability in stern-quartering waves.

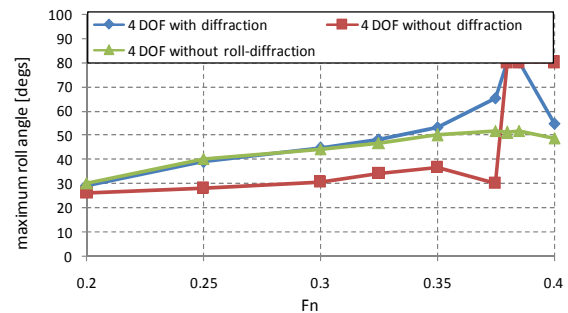


Figure 7 Comparison of maximum roll angle as function of the Froude number between with forces, without diffraction forces and only without diffraction forces in the roll motion with $\lambda/Lpp=1.25$, $H/Lpp=0.05$, and $\chi=30^\circ$.

Pure loss of stability is accompanied with large roll. The heel-induced hydrodynamic forces for large heel angle in calm water, which are hydrodynamic lift due to underwater non-symmetry induced by heel angle with forward velocity, could affect the prediction of pure loss of stability. The linear heel-induced hydrodynamic forces in calm water are investigated as shown in Fig.8. The 4 DOF mathematical model without linear heel-induced hydrodynamic forces, such as $Y'_\varphi \cdot \varphi$, $N'_\varphi \cdot \varphi$, $K'_\varphi \cdot \varphi$, could fail to predict capsizing at critical ship speeds due to pure loss of stability.

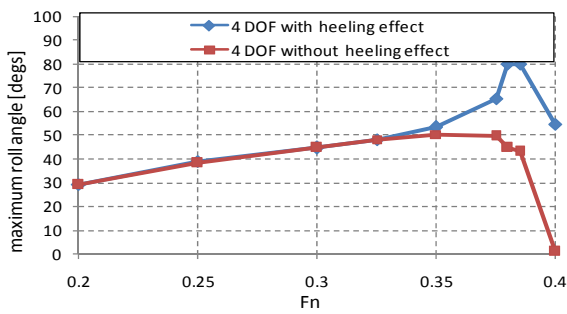


Figure 8: Comparison of maximum roll angle as function of the Froude number between the 4 DOF with and without linear heeling effect with $\lambda/Lpp=1.25$, $H/Lpp=0.05$, and $\chi=30^\circ$.

Roll damping is one of essential terms for predicting large amplitude roll motion, such as parametric roll, roll under dead ship condition and roll due to pure loss of stability. Linear and cubic nonlinear roll damping coefficients are adopted for predicting parametric roll (IMO SDC 4, 2017). The effects of nonlinear damping coefficient with linear and cubic nonlinear roll damping and equivalent linear roll damping coefficient on predicting pure loss of stability are investigated as shown Fig.9. Here the equivalent linear roll damping coefficient are derived by $a_e = a + c \cdot \phi_a = a + c \cdot 20$. It shows that the 4 DOF mathematical model with equivalent linear roll damping coefficient could overestimate the capsizing range of critical ship speeds.

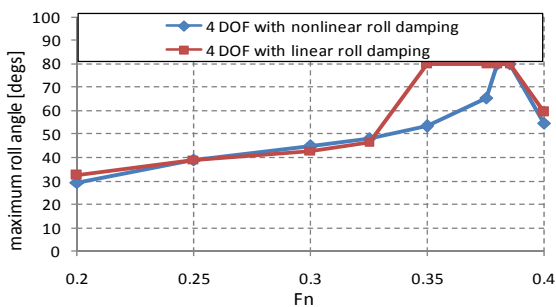


Figure 9: Comparison of maximum roll angle as function of the Froude number between the 4 DOF with nonlinear damping and linear damping with $\lambda/Lpp=1.25$, $H/Lpp=0.05$, and $\chi=30^\circ$.

5. CONCLUSIONS

On the basis of the numerical study on standard mathematical model of pure loss of stability in stern-quartering waves with the ONR tumblehome vessel, the following remarks can be made:

1) The effect of surge motion with varied forward speed effect on pure loss of stability in stern-quartering waves should be considered while the

higher order maneuvering coefficients in the surge motion can be ignored.

2) The centrifugal force due to sway and yaw motions and maneuvering motions with higher order maneuvering coefficients should be considered in the standard mathematical model of pure loss of stability.

3) The effect of linear heel-induced hydrodynamic forces in calm water on pure loss of stability in stern-quartering waves should be taken into account.

4) The nonlinear roll damping coefficient should be included for predicting pure loss of stability in stern-quartering waves.

The standard mathematical model with 4 DOF for predicting pure loss of stability should be further studied with experiments and more examples.

Acknowledgments

Some contents used in this research were once guided by Prof. Naoya Umeda during the first author’s Ph.D course at Osaka University supported by China Scholarship Council [No.2008606031]. The research is supported by Ministry of Industry and Information Technology of China (No. [2016] 26) and China research fund (No.B2420132001; No.51509124). These supports are gratefully acknowledged.

6. REFERENCES

Gu M., LuJ. and Wang T.H., 2015, “Stability of a Tumblehome Hull under Dead Ship Condition”, Journal of Hydrodynamics, Vol.27 (3), pp. 452-457.

Hamamoto M., Kim Y.S., 1993, “A New Coordinate System and the Equations Describing Manovering Motion of a Ship in Waves”, Journal of the Society of Naval Architects of Japan, Vol. 173, pp. 209-220.

Hashimoto H., Umeda N. and Matsuda A.,2004, “Importance of Several Nonlinear Factors on Broaching Prediction”, Journal of Marine Science and Technology, Vol. 9, pp. 80-93.

Hashimoto H., Umeda N. and Matsuda A.,2011a, “Model Experiment on Heel-Induced Hydrodynamics Force in Waves for Realising Quantitative Prediction of Broaching”, M.A.S. Neves et al. (eds.), Contemporary Ideas on Ship

Stability and Capsizing in Waves, Fluid Mechanics and Its Application 96, pp. 379-397.

Hashimoto H., Umeda N. and Matsuda A., 2011b, "Broaching Prediction of a Wave-piercing Tumblehome Vessel with Twin screws and Twin Rudders", Journal of Marine Science and Technology, Vol. 16, pp. 448-461.

IMO2013, Development of Second Generation Intact Stability Criteria, SLF55/INF.15.Annex 12

IMO2016, Finalization Second Generation Intact Stability Criteria, SDC 3/WP.5.Annex 3

IMO 2017, Finalization Second Generation Intact Stability Criteria, SDC 4/WP.4.

Kubo H., Umeda N., Yamane K., Matsuda A., 2012, "Pure Loss of Stability in Astern Seas -Is It Really Pure?", Proceedings of the 6th Asia-Pacific Workshop on Marine Hydrodynamics, pp. 307-312.

Lu J., Gu M. and Umeda N., 2017, "Experimental and Numerical Study on Several Crucial Elements for Predicting Parametric Roll in Regular Head Seas", Jour. of Marine Science and Technology, Vol. 22, pp. 25-37.

Matsuda A. and Umeda N., 1997, "Vertical Motions of a Ship Running in Following and Quartering Seas", Naval Architecture and Ocean Engineering, No.227, pp.47-55(in Japanese).

Umeda N., 1999, "Nonlinear Dynamics of Ship Capsizing due to Broaching in Following and Quartering Seas", Journal of Marine Science and Technology, Vol. 4, pp. 16-26.

Umeda N. and Hashimoto H., 2002, "Qualitative Aspects of Nonlinear Ship Motions in Following and Quartering Seas with High Forward Velocity", Journal of Marine Science and Technology, Vol. 6, pp. 111-121.

Umeda N., Usada S., Mizumoto K., and Matsuda A., 2016, "Broaching Probability for a Ship in Irregular Stern-quartering Waves: Theoretical Prediction and Experimental Validation", Journal of Marine Science and Technology, Vol. 21, pp. 23-37.

Yasukawa H. and Yoshimura Y., 2015, "Introduction of MMG Standard Method for Ship Maneuvering Predictions", Journal of Marine Science and Technology, Vol. 20, pp. 37-52.

Umeda N. and Yamakoshi Y., 1994, "Probability of Ship Capsizing due to Pure Loss of

Stability in Quartering Seas", Naval Architecture and Ocean Engineering, Vol.30, pp.73-85.

Session 8
Stability of fishing vessels

Session Chairs
Luis Pérez Rojas
Marcos Míguez González

A new era of fishing vessel safety emerges

Georgios Atzamos, *Maritime Safety Research Centre*, georgios.atzamos@strath.ac.uk

Dracos Vassalos, *Maritime Safety Research Centre*, d.vassalos@strath.ac.uk

Evangelos Boulougouris, *Maritime Safety Research Centre*, evangelos.boulougouris@strath.ac.uk

Donald Paterson, *Maritime Safety Research Centre*, d.paterson@strath.ac.uk

ABSTRACT

Commercial fishing is one of the least safe activities taking place within the EU and the worldwide community today. Several accidents and fatalities have been recorded over the past years stemming from various causes related to the operation, design of the vessels and severe weather conditions. This paper describes the background while attempting to elucidate and assess the impact of a new damage stability recovery system for new and existing fishing vessels, leading to high levels of survivability in the damaged condition. Highly expanded foam is injected in the most vulnerable compartments, rendering the whole ship a lifeboat. One case study is presented to provide the requisite evidence.

Keywords: *Fishing vessel; Safety; Damaged Stability, Risk, Survivability, DSRS*

1. INTRODUCTION

The safety problem of fishing vessels is a major issue across Europe and the rest of the world. Although, attempts to resolve the problem are taking place, the problem of damage stability is one that has yet to be solved as catastrophic accidents continue to happen, leading to societally unacceptable consequences.

The extent of the problem is further highlighted with the aid of the following statistics:

- Each year there is an average of 24,000 fatalities and 24 million non-fatal accidents.
- The fishing fatality rate is estimated at 80 deaths/100,000 individuals per annum, which is 79 times higher than the overall occupational fatality rate.
- In the period 2011-2015, almost 1,368 fishing vessels have been involved in 4,620 maritime accidents.
- It is estimated that there are 4 million fishing vessels operated globally, 1.3 million decked vessels and 2.7 million un-decked vessels; about 15 million people are employed aboard fishing vessels and about 98% of these people work on vessels less than 24m in length.

- In 2017, the total European fishing fleet has reached 183,104 vessels. (FAO, 2016)
- 5k and 10k fishing vessel newbuildings are expected in Europe and worldwide, respectively, within the next 8 years.
- The risk of a fishing-related accident in EU waters is 2.4 times greater than the average of all EU industry sectors.

Out of all the recorded accidents over 60% involve trawlers, whilst 15% dredgers (EMSA, 2015). The most critical location of the main casualties is the engine room as shown in Figure 1 .

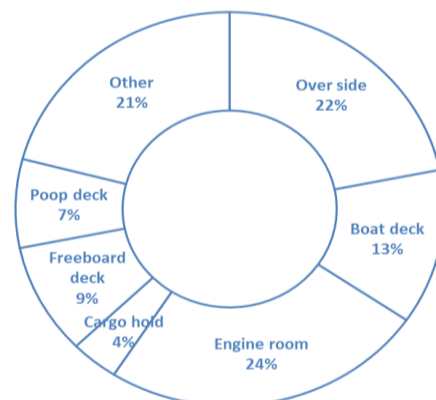


Figure 1: Main Casualty Areas in Fishing Vessel Accidents

Post-accident analyses have indicated that the main causes relate to ship stability and the influence of adverse weather conditions (Vassalos,

2006) . Particularly, the vessel is operated close to its stability limits in following / quartering to beam seas, where the waves adversely affect its dynamic stability. Also, fishing vessels are erroneously overloaded, in particular with heavy loads (fishing apparatus) in the ship superstructures; Doors or hatches left open, causing water ingress in case of green water on the stern deck and finally fishing gear suddenly becoming hooked on the sea bottom, etc. cause large scale water ingress.

Many attempts to develop warning systems and guidelines have repeatedly failed over the years. Traditionally, design/passive measures have been the only means to achieve damage stability enhancement in a measurable way (SOLAS 2009, Ch. II-1). However, limited choice for passive protection creates inertia and safety stagnation. Operational/active systems, instead, would enable the maritime industry to draw from a wealth of experiential or technological fund of knowledge to reduce the highly unacceptable loss of life. All the above points to the need for a foolproof approach to increase the resilience of the fishing vessels to capsize whether in intact or damaged condition. This paper paves the way in this direction by providing the background and rationale for such a framework and by introducing an alternative system for damage stability enhancement that involves injecting highly expandable foam in the compartment(s) undergoing flooding during the initial post-accident flooding phase. This leads to enhancing damage stability and survivability of fishing vessels well beyond the design levels in the most cost-effective way currently available.

2. DAMAGE STABILITY RECOVERY SYSTEM (DSRS)

System description

The Damage Stability Recovery System (DSRS) (Paterson, et al., 2016) focuses on compartments prone to high risk as a last line of defence against large scale flooding. The working principle of the proposed system is simple: when a vessel is subjected to a critical damage, stability is recovered through the reduction of floodable volume within the vessel's high risk compartment(s). This is achieved by rapidly distributing fast setting, high expansion foam to the protected compartment(s) resulting in a multitude of positive effects that enhance stability, floatability and watertight integrity. Lost buoyancy is minimised whilst free surface effects are eliminated, floodwater is contained and KG is reduced.

The system consists of a fixed supply of foam resin and hardener agents, each stored within a stainless steel container. Both containers are connected to a piping network for distribution to the protected compartment(s). A gauging and sampling pipe on each tank allows the tanks to be gauged and for periodical samples of each component to be extracted for testing. Tank ventilation is enabled through a ventilation line equipped with a non-return valve and vacuum relief is offered by a secondary ventilation line also equipped with a non-return valve.

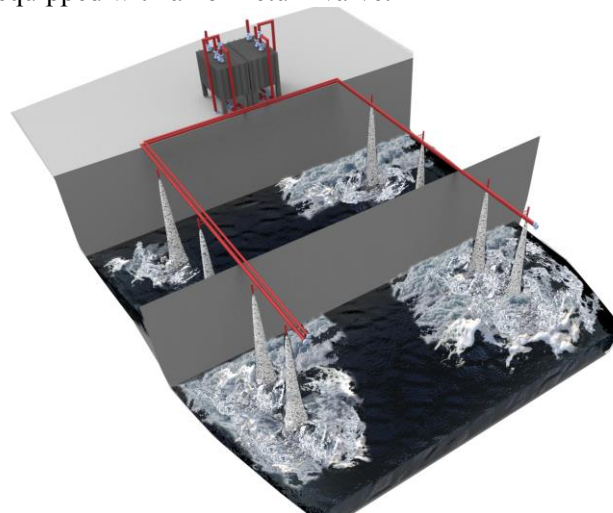


Figure 2: DSRS Graphical Representation

Two electrically driven internal gear pumps, located on the resin and hardener lines respectively, are used to deliver both foam components to a number of mixing nozzles located within the protected compartment. Each pump may be operated from the main or emergency electrical supply and must be started by manual means either remotely from the bridge control console or from their local switches. Both resin and hardener lines have re-circulation loops whereby the pumps can be used to circulate each component periodically. This enables faster foam deployment as it removes the requirement for pump-priming while also allowing the pumps to be tested when necessary.



Figure 3: DSRS Graphical Representation

Within the protected compartment(s) the resin and hardener lines divide into both port and starboard side branches for uniform filling of the space. Each branch contains a number of static mixing nozzles where resin and hardener components are mixed to form a homogeneous solution. The interaction of the two components produces a chemical reaction that enables the in situ production of foam.

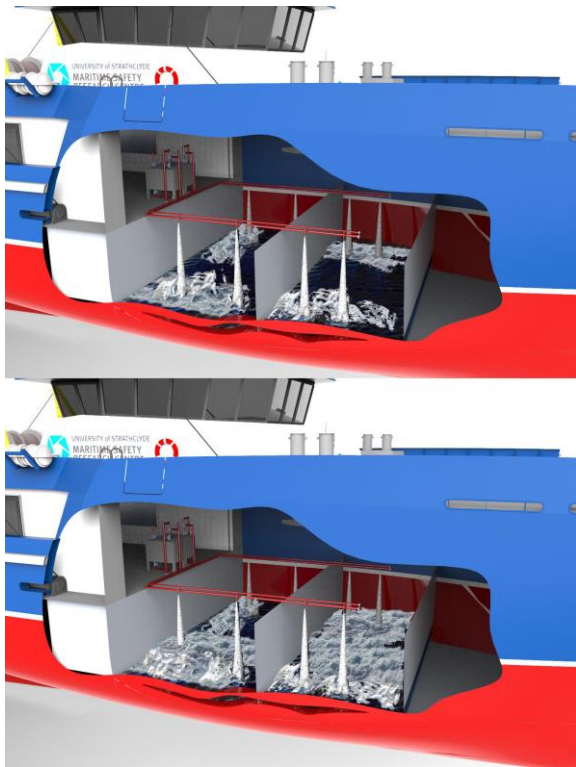


Figure 4: DSRS Graphical Representation

The system is interfaced and can be controlled from the Safety Management System (SMS) coupled with a Decision Support System (DSS), which in the event of a collision or grounding incident will provide the master with an advised course of action based on the extent of flooding, damage location and condition of the vessel. This is facilitated by a water ingress detection system with sensors located in the protected compartment and also within adjacent compartments both fore and aft of the protected space in order to cover damage lengths extending up to in most cases three compartment damage.

Finally, the foam compound meets all the environmental and health criteria, it is not harmful to humans, it is non-flammable and its release does not pose any danger to the crew on-board or the environment.

3. ADOPTED METHODOLOGY

Overview

One fishing vessel has been investigated with a view to assess the effectiveness of the proposed Damaged Stability Recovery System (DSRS) as a risk reduction technology. The study has been conducted with the aid of the probabilistic approach to damage stability (SOLAS 2009) as a means of establishing the initial level of flooding risk associated with the vessel. The effects of the DSRS have then been modelled in order to assess the risk reduction afforded by the system.

DSRS implementation & modelling

In order to ascertain the impact of the proposed system on vessel safety, the overall (collision) flooding risk level associated with the vessel had to first be identified, namely:

$$\text{Collision Flooding Risk}_{total} = 1 - A \quad (1)$$

This provides a benchmark from which to gauge any improvement on the vessel safety afforded by the DSRS. In order to ensure the system is applied in the most efficient manner, it was reasoned that the compartment(s) protected by the system should be those which contributed maximally to the risk. As such, a risk profile of the vessel was created in order to aid in the identification of design vulnerabilities. This then provided the foundation from which a risk-informed decision could be made with regards to the compartment(s) that should be protected by the system while also highlighting the circumstances under which this protection is necessary.

The results from the probabilistic damage stability assessment afforded a straightforward way of determining the vessel risk profile by firstly considering the local risk associated with each damage scenario, as provided by equation 2 below.

$$\text{Collision Risk}_{local} = p_i \cdot (1 - s_i) \quad (2)$$

These local risk values could then be mapped along the vessel according to damage centre in order to form the risk profile as depicted for an example in Figure 5.

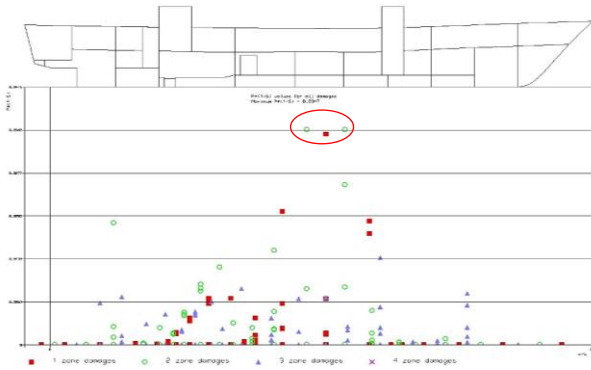


Figure 5: Example Case, Local Risk Profile

In the above risk profile, risk is plotted on the vertical axis and the damage position along the horizontal. Differing lengths of damage, as measured by multiples of adjacent zones, are distinguished by marker type and colour. This enables the identification of safety critical design areas, hence opportunities where safety could be improved most significantly and efficiently. Three cases in particular, circled in Figure 5 are identified as large risk contributors. As such, it can be reasoned that the DSRS would be best applied in the protection of one or both compartments, which give rise to this risk in the most efficient way.

The effects of the DSRS system were modelled through alterations to the permeability of the protected compartment(s) to account for the presence of the foam. The required volume of foam in each case was taken as the minimum volume required, ensuring the fishing vessel survived the most demanding high risk damage scenario (s).

4. CASE STUDY

Vessel overview

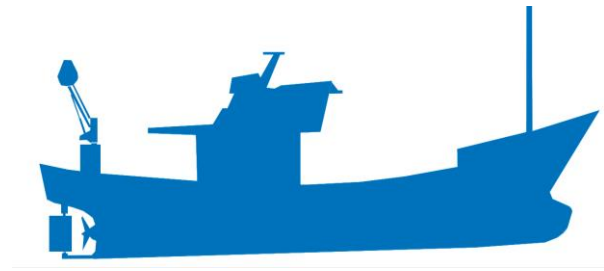


Figure 6: Vessel Profile

The vessel is an example of a typical fishing vessel operating within UK coastal waters. It is operated by 15 crew members with the provision of cabins for overnight sail. Also, it is subdivided into 8 watertight compartments and it is not equipped with life boats due to coastal operation. The principal particulars are provided in Table 1 below along with the vessel’s profile in Figure 6.

Table 1: Main particulars

Displacement (t)	392.6
Length overall (m)	30.80
Length B. P. (m)	29.58
Draught MLD (m)	3.230
Breadth (m)	6.840
Depth (m)	6.40
Crew number	15
Gross Tonnage	230

Stability Assessment

Even though SOLAS 2009 does not apply to this type of vessels, it is an instrument that facilitates a whole-vessel vulnerability to (collision) flooding. In addition, it leads to a risk level estimation that offers a reference and a means of comparison with other similar vessels. Stability assessment is conducted in an iterative manner; the first, to identify compartments susceptible to high risk, whilst the rest to evaluate progressively the effects of the DSRS.

A total of 320 damage case scenarios are generated and assessed utilising the main three loading conditions in accordance with the SOLAS 2009 framework, namely the light service, partial and deepest subdivision draughts, which combine to form a theoretical draught range/distribution for a given vessel.

Table 2: Loading conditions

	Draught (m)	GM (m)	Displ(t)
Light (DL)	2.280	0.308	233.3
Partial (DP)	2.740	0.215	306
Deepest (DS)	3.230	0.374	390

The damage stability assessment results can be found in Table 3 along with the vessel’s initial local risk profile in Figure 7.

Table 3: Initial damage stability results

Required Index	0.673
Adl	0.558
Adp	0.541
Ads	0.711
Attained Index	0.612
Risk (1-A)	0.388

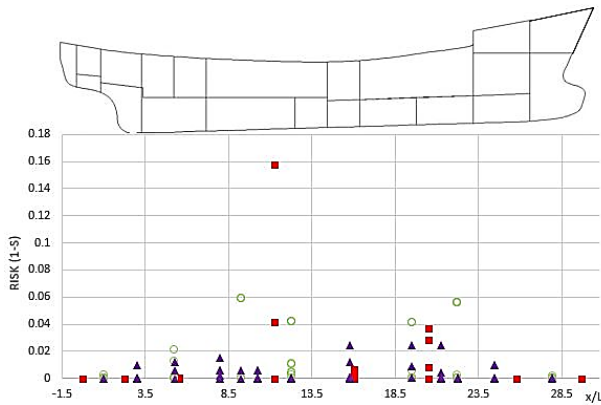


Figure 7: Initial local risk profile

It is apparent from the results that the vessel’s risk profile reveals several vulnerabilities. The maximum local risk recorded is $P \times (1 - S) = 0.16$ for damage cases centered close to the engine room. Two cases are identified as the largest risk contributors and therefore deemed appropriate for protection by the system. The first comprises the engine room, aft crew cabins and two centralised vivariums. In the second case, the fishing store compartment deteriorates safety and can instigate potential large scale flooding.

The total volume of foam required in these cases was identified as that required to mitigate the

risk stemming from three compartment damages equating to 170 m³ expanded volume. The expansion ratio of the foam is considered to be 50, thus the raw foam volume required is 3.4 m³. Yet, the total weight of the system consisting of the primary and auxiliary components is estimated to be 9.1 tonnes.

The damage stability performance was then reassessed following a permeability change to all the critical compartments to account for the effects of the foam. The new stability assessment results are provided in Table 4 below.

Table 4: Final damage stability results

Adl	0.92
Adp	0.97
Ads	0.98
Attained Index	0.96
Risk (1-A)	0.04
DA	36%
DR	90%

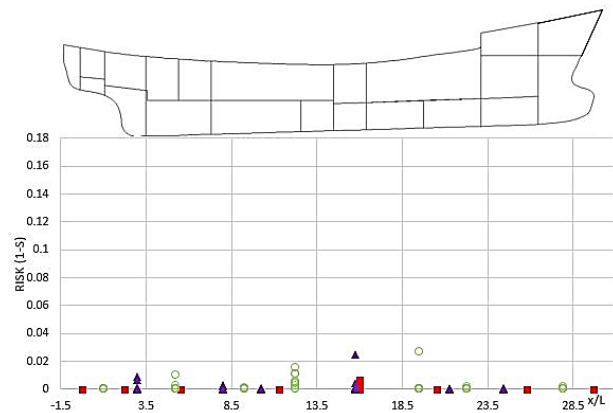


Figure 8: Final local risk profile

As presented in Figure 8, the maximum local risk has been significantly decreased to $P \times (1 - S) = 0.026$. The increase in the Attained index ensued from the implementation of the DSRs is 36%, whereas, the capsizing risk has been almost eradicated. In addition, the risk stemming from all three compartment damages has been eradicated for all potential damage case scenarios along the length of the vessel. This is an exceptional improvement in the damage stability of the vessel, accentuating the vital role of the DSRs.

Furthermore, the effect of the DSRs in decreasing the vessel’s required GM limit curve is

assessed, demonstrating further the improvements afforded. As it is displayed in Figure 9, in terms of damage stability alone, the new derived limiting GM curve compared to the original limiting GM curve yields a decrease of approximately 79% for the partial subdivision draught and around 55% for the deepest draught respectively. This can be translated into substantial contribution to the safety of the vessel.

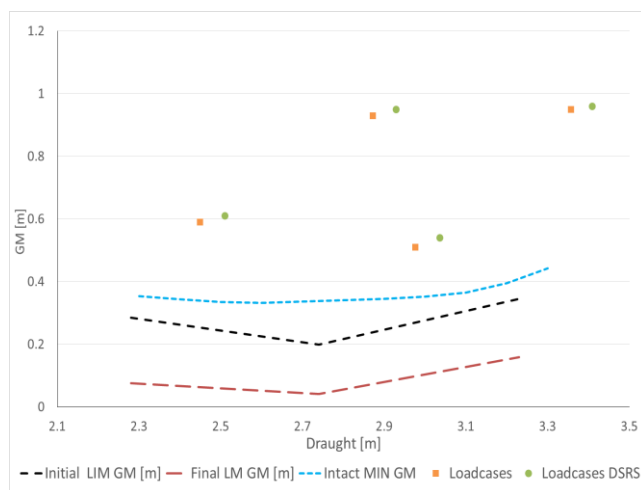


Figure 9: GM (m) for intact and damage stability

Intact stability is paramount for small vessels and therefore it is necessary to account for the change imposed by the additional weight of the system. As it is apparent from Figure 9, four different load cases have been assessed. The difference in the GM and draught can be justified purely by the increase in the weight. The effects of this change on the load case GM margin ranges from 2% to 17% reduction. Finally, the vessel complies with all fishing vessel intact stability criteria as outlined within IMO's resolution A749-4.2.

Importantly and expectedly, intact stability requirements for small vessels dominates over damage stability requirements with regards to limiting GM. This vulnerability of small fishing vessels is well known. Fishing vessels, in general, are susceptible to parametric roll and broaching but these are not covered by any legislation and criteria. Studies (Gonzales et al, 2014) have shown that vessels with Froude number higher than 0.3 have a high tendency to these effects.

5. CONCLUSIONS

The Potential influence of the DSRS is indeed manifold. It has been identified as a non-intrusive cost-effective and very flexible solution to the damage stability problem of fishing vessels that does not interfere with the existing characteristics of the vessel or its functionality altogether, enabling the vessel to remain competitive whilst being safe.

Such improvement in safety represents a significant step-change, one that holds great promise for both new buildings and existing fishing vessels and with the potential to raise international and domestic safety standards, saving thousands of lives.

The use of an active system marks an important paradigm shift in the damage stability standards. The significant enhancement of damage stability levels, ushers in a new era of 3-compartment standard vessels.

6. REFERENCES

- EMSA. (2015). *Annual overview of marine casualties and incidents 2015*. Prague.
- FAO. (2016). *Statistics on fishing vessel fleet*. London: Food and agriculture organisation.
- González, M. M., Casás, V. D., Rojas, L. P., Ocampo, F. J., & Pena, D. (2014). Application of second generation IMO intact stability criteria to medium-sized fishing vessels. *The 14th International Ship Stability Workshop (ISSW), Malaysia*.
- Paterson, D., Vassalos, D., Boulougouris, E., Liggat, J., Cullen, J., & Kanerva, M. (2016). An Alternative system for damage stability enhancement. *Design and operation of ferries & Ro-Pax vessels, London, UK*.
- Vassalos, D. (2006). Human lives for fish! Can we stop the rot? *UoS, Glasgow*.

The characteristics of capsizing phenomena of Japanese fishing vessels

Akihiko Matsuda, Fisheries Research and Education Agency amatsuda@fra.affrc.go.jp

Daisuke Terada, Fisheries Research and Education Agency dterada@fra.affrc.go.jp

Hirotsada Hashimoto, Kobe University hashimoto@port.kobe-u.ac.jp

ABSTRACT

The 2nd generation intact stability code is discussed at International Maritime Organization. The code shows 5 dangerous phenomena, pure loss of stability, broaching-to, dead ship condition, parametric roll, and acceleration. Authors carried out the free running capsizing model experiments in following and quartering heavy seas with more than 16 Japanese fishing vessels. The dangerous phenomena of the results were pure loss of stability, broaching-to and bow-diving. A parametric roll was not indicated.

Keywords: Japanese fishing vessels, broaching-to, bow-diving, pure loss of stability, model experiments

1. INTRODUCTION

In 2008, 135GT Japanese purse seiner was capsized at anchoring with parachute anchor. In 2009, 135GT Japanese purse seiner was capsized at quartering heavy seas. In 2010, Japanese trawler was capsized at head seas. More than 30 fishermen’s lives are lost in these accidents. So, authors are conducting the free running capsizing model experiments using more than 16 Japanese fishing vessels.

The second generation intact stability criteria to be developed by the IMO are requested to cover 5 stability failure modes due to dead ship condition, pure loss of stability, broaching-to, parametric rolling and exceeding roll. Level 1 Vulnerability criteria was developed for calculating by handy calculator. So, characteristics of dangerous phenomena vary depending on the types of ships.

In this paper, we conduct the results of free running model experiments using Japanese fishing vessels. Secondly, the dangerous phenomena of capsizing are discussed. Finally, we conduct the characteristics of capsizing phenomena of Japanese fishing vessels.

2. MODEL EXPERIMENTS

2.1 Experimental system

In this research, either the Tele-tele System of Osaka University produced by Hamamoto et.al (1996) before 2009 shown in Fig.1 or the Model Motion Tracking System of National Research Institute of Fisheries Engineering produced by Matsuda et.al (2016) after 2010, shown in Fig.2 are used. Both of them, models were controlled for course keeping with autopilot of rudder gain 1 and constant propeller revolution. All model experiments followed Recommended Procedure of ITTC(2008). These model experiments were conducted at Marine Dynamics Basin of National Research Institute of Fisheries Engineering shown in Fig. 3. During the past 20 years, we conducted free running model experiments with not only Japanese fishing vessels but also European fishing vessels or commercial vessels.

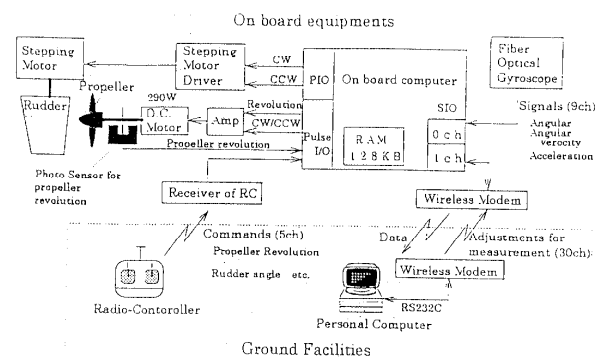


Figure 1: Tele-tele System

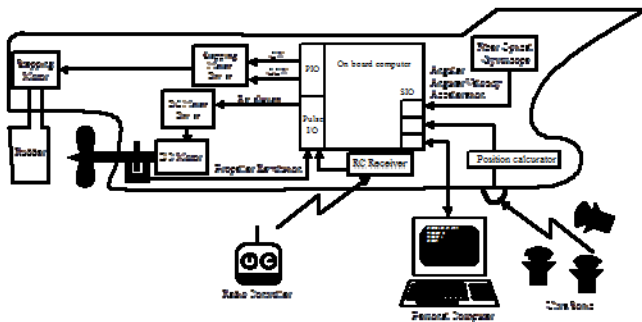


Figure 2: Model Motion Tracking System

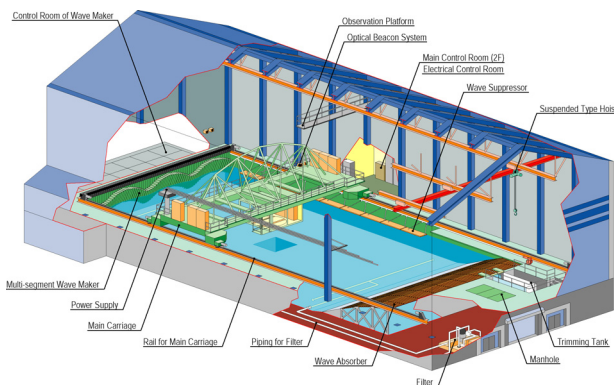


Figure 3: Marine Dynamics Basin

2.2 Subject ships

16 Japanese fishing vessels shown in Table.1 are used. Ship A to Ship H are purse seiner, Shi I to Ship L are trawler, Ship M is fishing vessel for set net, ship N to ship P are fishing vessel for Pacific saury and Ship Q is North European purse seiner. Some subject ships are shown in Figs.4-7. We conducted more than 2000 runs of capsizing free running model experiments.

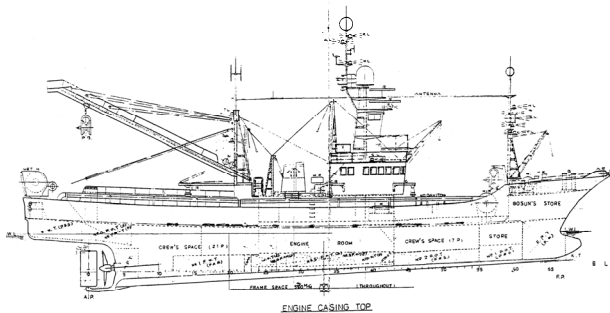


Figure 4: Ship A (135GT Purse seiner)

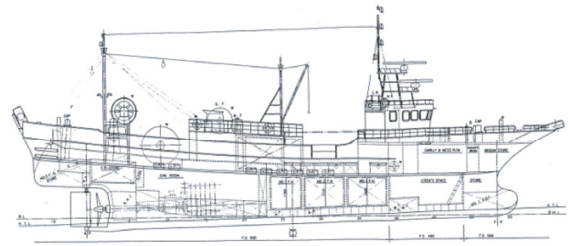


Figure 5: Ship I (Trawler)

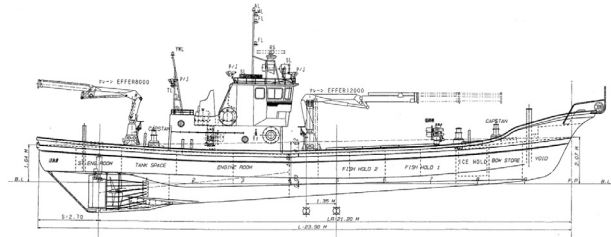


Figure 6: Ship M (Fishing Vessel for Set net)

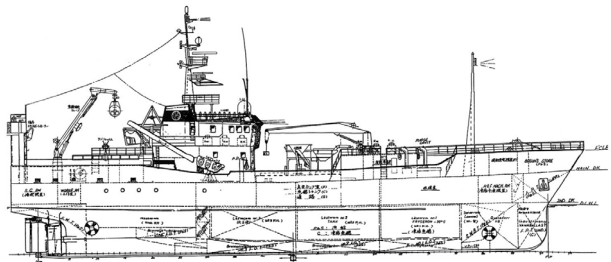


Figure 7 Ship Q (North European Purse Seiner)

Table 1: Subject ships

	Length (L _{pp})	Breadth (B)	Depth (D)	Max Speed(Fn)
Ship A	34.5m	7.6m	3.07m	0.43
Ship B	29.0m	6.8m	2.6m	0.46
Ship C	28.8m	7.5m	2.6m	0.4
Ship D	30.0m	7.9m	2.78m	0.33
Ship E	29.0m	6.9m	2.58m	0.38
Ship F	23.0m	5.9m	2.15m	0.43
Ship G	21.2m	6.35m	2.41m	0.46
Ship H	20.35m	5.83m	1.76m	0.43
Ship I	26.85m	5.9m	2.6m	0.44
Ship J	26.85m	6.6m	2.85m	0.38
Ship K	17.8m	3.24m	2.24m	0.39
Ship L	11.35m	5.1m	2.1m	0.49
Ship M	21.2m	4.82m	1.26m	0.43
Ship N	21.35m	5.21m	1.22m	0.5
Ship O	19.8m	4.80m	1.99m	0.41
Ship P	22.4m	4.58m	1.71m	0.41
Ship Q	55.0m	12.0m	7.6m	0.24

3. EXPERIMENTAL RESULTS

3.1 Experimental results

Experimental results are shown in Table 2 including Umeda et.al (2009). Japanese fishing vessels were occurred pure loss of stability, broaching-to and bow-diving. But there is not only parametric roll but also harmonic roll. On the other hands, Ship Q was occurred harmonic roll and there is no pure loss of stability, broaching-to and bow-diving on the grounds of low forward velocity.

Table 2 Experimental results

	Pure loss of Stability	Broaching -to	Bow-diving	Parametric roll (Harmonic Roll)
Ship A	✓	✓		
Ship B	✓	✓	✓	
Ship C	✓		✓	
Ship D	✓			
Ship E	✓		✓	
Ship F	✓	✓		
Ship G		✓		
Ship H				
Ship I	✓		✓	
Ship J				
Ship K	✓	✓		
Ship L		✓		
Ship M	✓	✓	✓	
Ship N		✓	✓	
Ship O		✓		
Ship P		✓		
Ship Q				✓

3.2 Pure loss of stability

The time series of capsizing phenomena by pure loss of stability is shown in Fig.8 and in Photo 1. In this case, the model was running in quartering seas with same speed of wave velocity and continued to a dangerous situation which is midship at wave crest. Thus, it is considered that the model ship was capsized due to pure loss of stability.

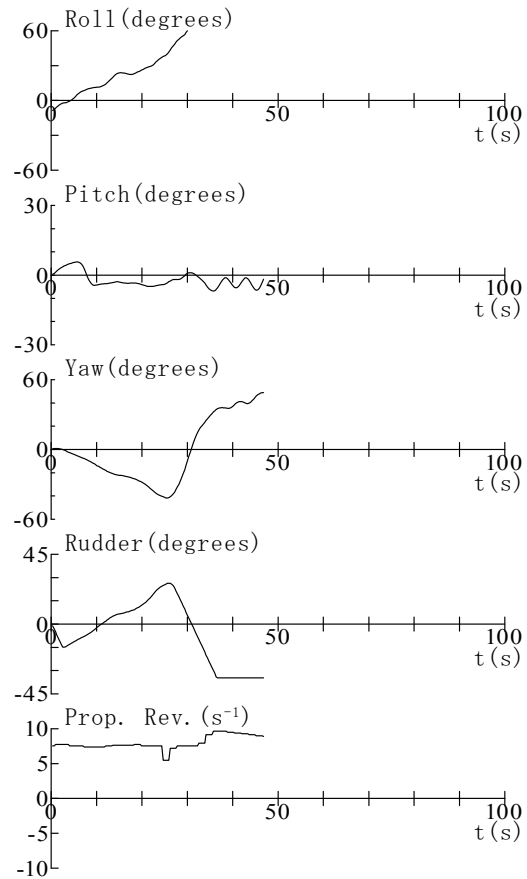


Figure 8 Pure loss of stability of Ship F (39GT purse seiner) ($F_n=0.43$, $\chi=-15$ degrees, $\lambda/L=1.25$, $h/\lambda=1/9$)

3.3 Broaching-to

The time series of broaching-to is shown in Fig. 9 and Photo 2. In this case, the model accelerated with following sea. After the surfriding, she could not keep the autopilot course and capsized.

3.4 Bow-diving

Typically, after the surfriding, extra power makes stable surfriding. But, if she has not enough height of bow, she dived into the front wave slope and had massive water on deck. Finally she capsized. The time series of bow-diving is shown in Fig. 10 and Photo 3. In this case, Ship N was occurred broaching-to without capsizing. There is no ship with capsizing of broaching-to and without capsizing of bow-diving. So, probably bow-diving is danger for Japanese fishing vessels than broaching-to.

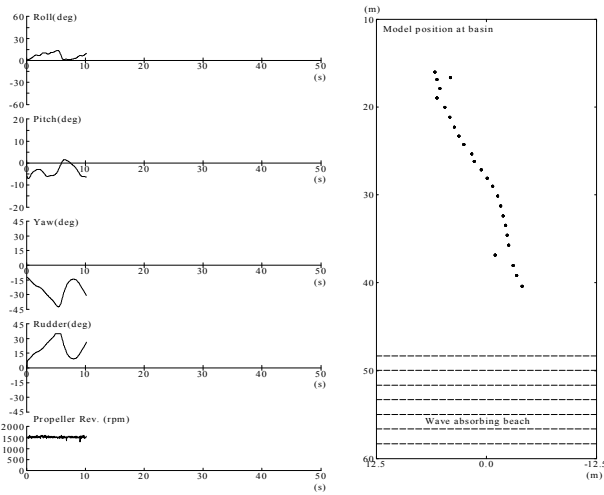


Figure 9 Broaching-to of Ship G (19GT purse seiner) ($F_n=0.43$, $\chi=-5$ degrees, $\lambda/L=1.5$, $h/\lambda=1/9$)

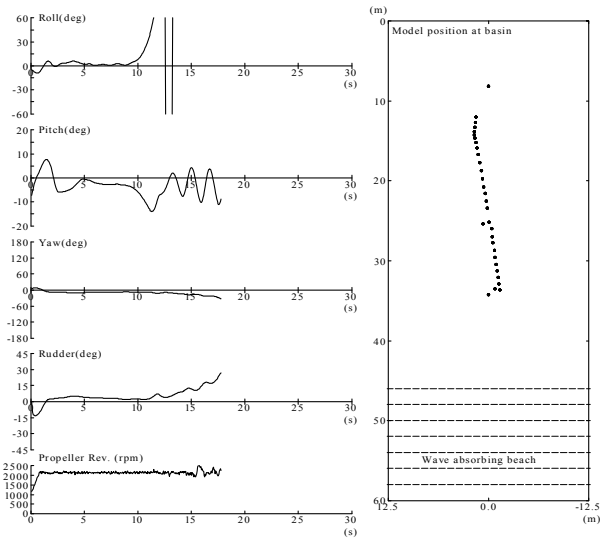


Figure 10 Bow-diving of Ship N (fishing vessel for Pacific saury) ($F_n=0.50$, $\chi=-5$ degrees, $\lambda/L=1.5$, $h/\lambda=1/9$)

4. CHARACTERISTICS OF HARMONIC ROLL

Japanese fishing vessels were occurred pure loss of stability, broaching-to and bow-diving. But there is not only parametric roll but also harmonic roll. On the other hands, European fishing vessel (Ship Q) was occurred harmonic roll. Hamamoto et.al (1995) studied that a ship with hard spring type GZ is occurred parametric roll. GZ curve of Ship Q is shown in Fig.11 and GZ curves of Japanese fishing vessels are shown in Fig.12. Fig.11 shows that GZ curve of Ship Q is a hard spring type. Fig.12 shows that all GZ curve of Japanese fishing vessels are soft spring type. So,

Japanese fishing vessels are not occurred parametric roll and harmonic roll.

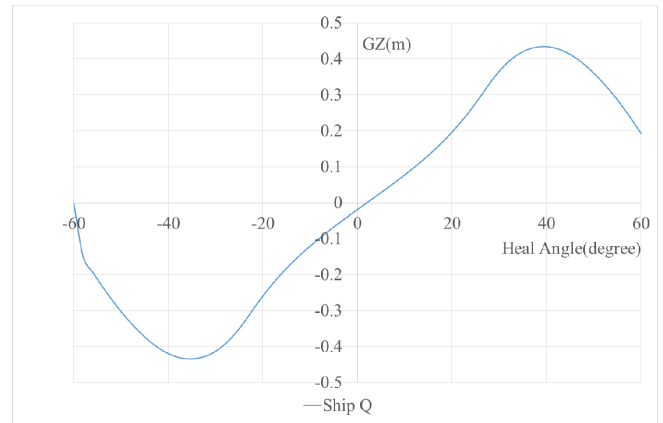


Figure 11 GZ curve of European Fishing Vessel

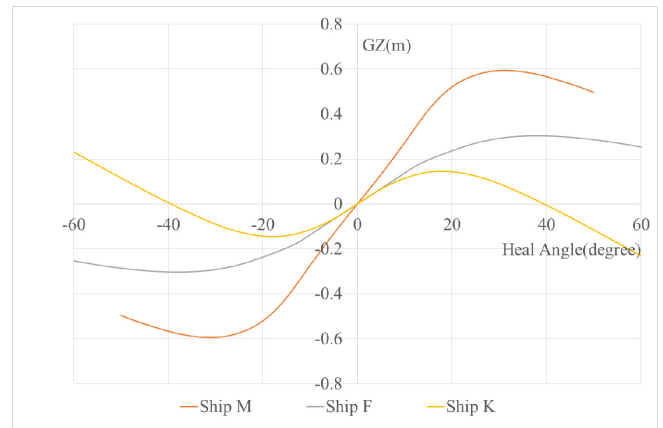


Figure 12 GZ curves of Japanese Fishing Vessels

5. CONCLUSIONS

In this study we conclude as follows.

1. Dangerous phenomena of Japanese fishing vessels are broaching-to, pure loss of stability and bow-diving.
2. Dangerous phenomena of a European fishing vessel of a hard spring type GZ is harmonic roll.
3. Japanese fishing vessels of soft spring type GZ were not occurred parametric and harmonic roll.

REFERENCES

M. Hamamoto, N. Umeda, A. Matsuda and W. Sera, Analyses on Low Cycle Resonance of Ship in Astern Seas, Journal of The Society of Naval Architects of Japan, pp.197-206, 1995

M. Hamamoto., T. Enomoto, W. Sera, J.P. Panjaitan, H. Ito, Y. Takaishi, M. Kan, T. Haraguchi and T. Fujiwara “Model Experiments of Ship Capsize in Astern Seas - Second Report -”, Journal of The Society of Naval Architects of Japan, pp.77-87, 1996

N. Umeda, A. Matsuda, M. Hamamoto and S. Suzuki, Stability Assessment for Intact Ships in the Light of Model Experiments, Naoya Umeda, Journal of Marine Science and Technology, Vol.4, No.2, pp.45-57, 1999.

Recommended Procedures, Model Tests on Intact Stability, 7.5-02-07-04.1", ITTC, 2008

A. Matsuda, H. Hashimoto, D. Terada and Y. Taniguchi “Validation of Free Running Model Experiments in Heavy Seas”, Proceedings of 3rd International Conference on Violent Flows, 2016, Osaka.

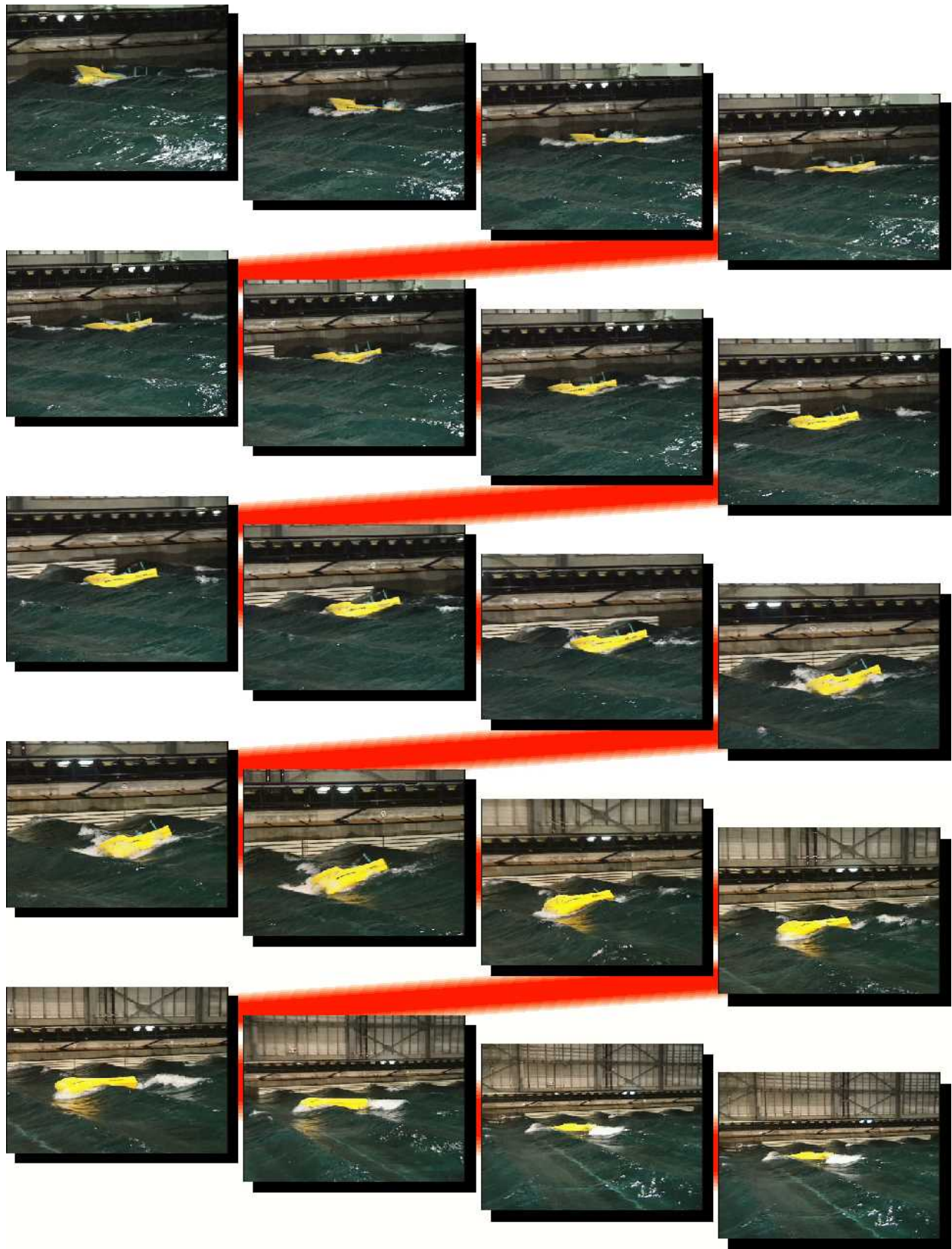


Photo.1 Pure loss of stability

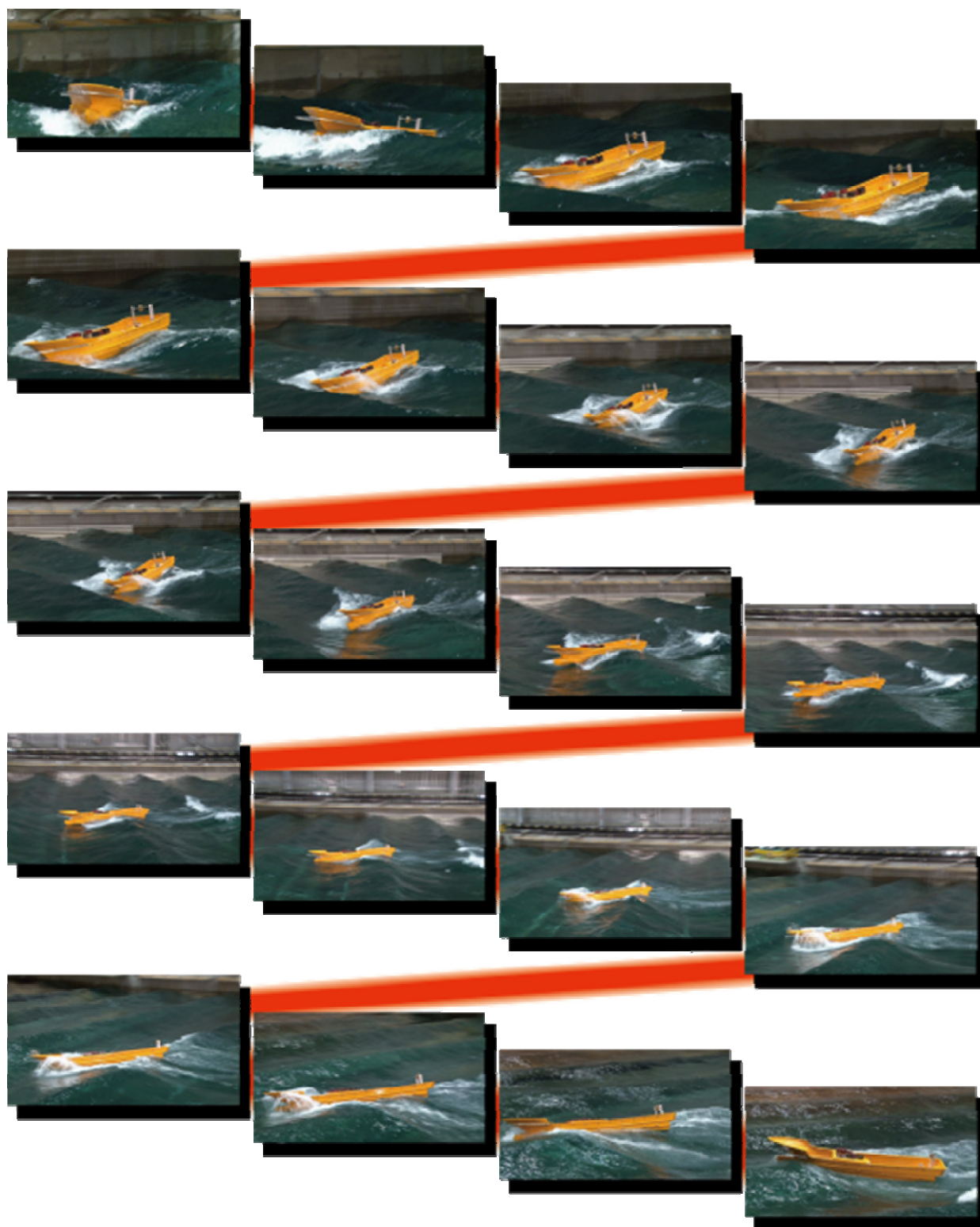


Photo 2. Broaching-to



Photo 3 Bow diving

Contributions on Roll Damping Coefficient for Fishing Vessels

Adriana Oliva-Remola, *Universidad Politécnica de Madrid*, adriana.oliva@upm.es

Luis Pérez-Rojas, *Universidad Politécnica de Madrid*, luis.perezrojas@upm.es

ABSTRACT

Roll damping coefficient is one of the main parameters that characterize the performance of a ship in a seaway and, consequently, it is the most influential factor in certain stability criteria failure modes. This article applies the approved Dead Ship Condition failure mode to a trawler fishing vessel using two different damping coefficients; one determined applying the Ikeda's Method and the other determined empirically by forced roll tests. Both results will be compared, analysed and discussed.

Keywords: *Roll damping, forced roll tests, Ikeda's method, ship stability, ship safety, fishing vessels.*

1. INTRODUCTION

Roll damping coefficient is one of the main parameters that characterize the performance of a ship in a seaway and the corresponding operability and safety.

It has been the great unknown for many years and possibly still is (Falzarano et al., 2015). Recently, and specially during the development of the Second Generation Intact Stability Criteria (SGISC), described in (Peters et al., 2011) and (Umeda et al., 2016), emphasis has been placed on it as it influences the majority of the failure modes considered. In fact, the damping coefficient is a determining parameter in three of the five established failure modes, namely parametric roll, dead ship condition and excessive acceleration. This parameter has been studied extensively for passenger and cargo vessels, however, fishing vessels have been left out of most of the studies, (Bačkalov et al., 2016). The main reason is that there are significant differences between hull forms depending on the country and the type of fishing gear.

In the present article, a trawler fishing vessel is used to evaluate if the accepted semi-empirical method by the IMO (IMO, 2016a), the so-called Simplified Ikeda's method (Kawahara et al., 2009), properly estimate the damping coefficient for this particular fishing vessel. Moreover, the dead ship condition (DSC) failure mode is applied to this vessel, considering both the semi-empirical damping coefficient and the one obtained by forced

roll test experiments. Evaluating, therefore, the influence of the roll damping coefficient on the DSC failure mode.

2. SHIP DESCRIPTION

A trawler fishing vessel of 41.7 LOA has been used. A profile view of the vessel is shown in Figure 1 and Table 1 shows the main characteristics of the ship. In Figure 2 the righting arm curve in calm water of the loading condition under analysis is shown.



Figure 1: Profile view of the trawler fishing vessel.

Table 1: Trawler fishing vessel characteristics.

Parameter	Value
Length overall, LOA (m)	41.700
Length at the waterline, LWL (m)	40.111
Moulded Breadth, B (m)	11.500
Draught, D (m)	4.072
Trim, t (m)	0.000
Displacement, Δ (t)	997.900
Block coefficient, C_B (-)	0.424
Midship coefficient, C_M (-)	0.736
Corrected metacentric height, GM_C (m)	0.774
Lateral windage area, A_L (m ²)	248.020
Vertical distance from the centre of A_L to D/2, Z (m)	5.300
Natural roll frequency, w_0 (rad/s)	0.592
Service velocity, V_S (kn)	12.000

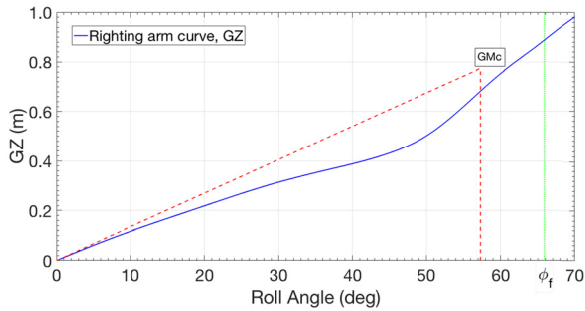


Figure 2: Righting arm curve of the trawler fishing vessel (ϕ_f represents the down-flooding angle)

This vessel was tested at the ETSIN towing tank, whose dimensions are 100m length, 3.8m breadth and 2.2m depth. The scale used for the ship model is 20.666.

3. DETERMINATION OF THE ROLL DAMPING COEFFICIENT

Simplified Ikeda's method

The Ikeda's method is based on the assumption that the damping coefficient can be split in different independent components, such as the frictional and eddy damping components (Himeno, 1982). The Simplified Ikeda's method is a set of regression formulas for each independent damping coefficient component obtained applying the Ikeda's method to a series of parametric hull shapes (Kawahara et al., 2009).

Each regression formula has applicable ranges which depend on the block coefficient, the midship coefficient, the breath to depth ratio and the vertical position of the centre of gravity to depth ratio. As these formulas were obtained considering cargo vessels, the trawler fishing vessel used in the present work is outside the applicable ranges, namely the block coefficient and the midship coefficient. However, as it is currently recommended in (IMO 2016b), if a vessel parameter exists outside the applicable range, the Simplified Ikeda's method may be applied only keeping as the parameter value the one corresponding to the limited value. Therefore, instead of using the coefficients shown in Table 1, the following coefficients have been considered for the Simplified Ikeda's method:

- $C_{B,ikeda} = 0.500$
- $C_{M,ikeda} = 0.900$

As a result of applying the Simplified Ikeda's method to a range of roll angle values from 0 to 25 deg, the following damping coefficients have been obtained:

- $\mu = 0.0020$ [1/s]
- $\beta = 0.1898$ [-]
- $\delta = 0.0000$ [s]

Forced roll tests

Apart from obtaining roll damping coefficients by semi-empirical or theoretical methods, it may be obtained experimentally.

One of the most relevant experimental technique is the forced roll test (Handschel et al., 2014). In these kind of experiments, the ship rolls due to an external moment or force. The most common way is to exert a roll moment to the model applying beam sinusoidal waves or by generating a sinusoidal moment using contra-rotating masses. From forced roll tests results, the roll response curves are obtained. Each roll response curve represents the mean roll amplitude that the ship experiences per each wave slope (or, not being the current case, each wave height) and per each wave frequency. Taking into account the peak amplitude and frequency values, the damping coefficient components may be obtained.

In the present work, the moment was generated using an internal moving mass which moves transversally through a linear rail.

The internal moving mass is placed at the centre of the linear guide and is allowed to move, from the centre, 90 mm on each side. This internal mass moves thanks to an electrical engine controlled by an encoder, as shown in Figure 3.

As the internal mass in motion not only produces a roll moment but also other forces and moments, to avoid these negative effects, as far as feasible, the linear guide is placed inside and near the centre of gravity of the ship model. The linear guide position in the trawler fishing vessel model is shown in Figure 4.

The roll motion and the other rotations and translations are measured using an optical trackable system, namely the OptiTrack. The trackable panel position is shown in Figure 4.

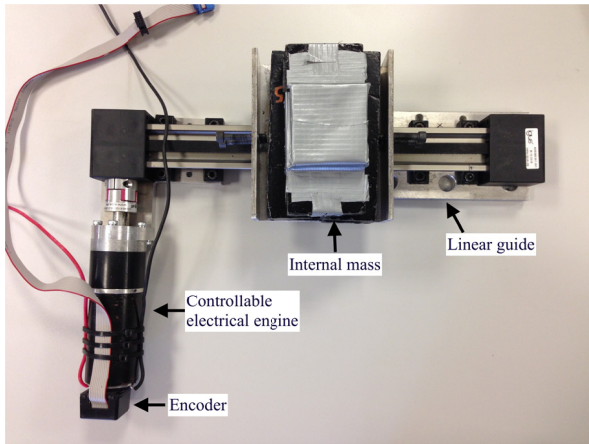


Figure 3: Linear rail components.

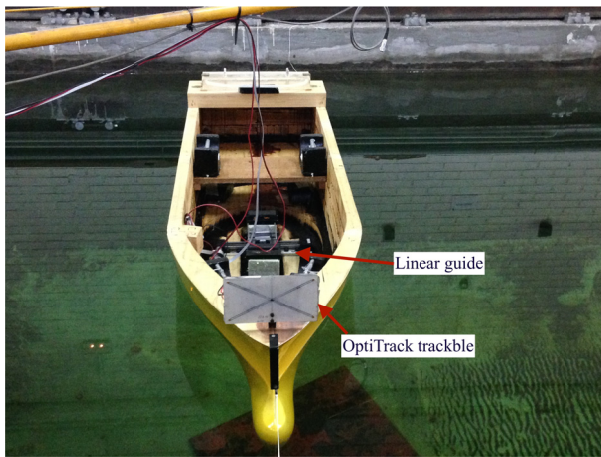


Figure 4: Linear guide and trackable panel position.

The internal moving mass weight is such that a specific wave slope is simulated. The moving weights values are deduced from the equilibrium between the static moment generated by the moving mass located at its maximum amplitude position and the ship righting moment, as Equation 1 shows:

$$m y_{m,max} \cos \phi = \Delta GZ(\phi) \quad (1)$$

Where:

- m , represents the moving mass weight.
- $y_{m,max}$, represents the maximum mass amplitude.
- ϕ , represents the roll angle.
- $GZ(\phi)$, represents the righting arm value for a specific roll angle.

Three wave slopes (α) were considered, namely 0.5, 1.0 and 1.5 deg, thus, three different roll

response curves were obtained. The experimental values are shown in Figure 5.

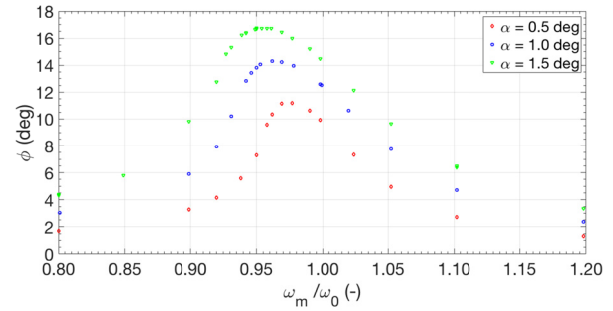


Figure 5: Experimental roll response curves

The peak amplitude and frequency values are shown in Table 2.

Table 2: Peak frequencies and amplitudes values per each wave slope

Wave slope, α (deg)	Peak frequency, ω_{peak} (rad/s)	Peak amplitude, A_{peak} (deg)
0.5	2.63	11.2
1.0	2.59	14.3
1.5	2.56	16.8

The damping coefficients are obtained fitting the equivalent linear damping coefficient, $\mu_{eq}(\omega_{peak}, A_{peak})$, to the following Equation (Bulian et al., 2009):

$$\begin{aligned} \mu_{eq}(\omega_{peak}, A_{peak}) &= \mu \\ &+ \frac{4}{3\pi} \beta(\omega_{peak}, A_{peak}) \\ &+ \frac{3}{8} \delta(\omega_{peak}, A_{peak})^2 \end{aligned} \quad (2)$$

Where $\mu_{eq}(\omega_{peak}, A_{peak})$ is obtained from Equation 3:

$$\begin{aligned} \mu_{eq}(\omega_{peak}, A_{peak}) &= \frac{m y_{m,max} \omega_0^2}{\Delta GM 2 A_{peak} \omega_{peak}} \end{aligned} \quad (3)$$

Equation 3 has been deduced from the one degree of freedom (1-DoF) roll equation, shown in Equation 4, assuming that the effect of the internal moving mass can be represented simply by an external forcing term and knowing that the actual mass motion is sinusoidal.

$$\begin{aligned} \phi'' + 2\mu_{eq}\phi' + \omega_0^2 \frac{GZ(\phi)}{GM} \\ = \omega_0^2 \frac{m y_{m,max} \sin \omega_m t}{\Delta GM} \end{aligned} \quad (4)$$

As the moving mass motion is sinusoidal, it is considered that the response of the ship is sinusoidal too. Thus, at resonance:

$$\begin{aligned} \phi &= A_{peak} \sin \omega_{peak} t \\ \phi' &= A_{peak} \omega_{peak} \cos \omega_{peak} t \end{aligned} \quad (5)$$

And knowing that at resonance the damping and the external moment components are in phase and opposed to each other, as stated in Equation 6. Therefore, Equation 3 is deducted from Equation 6.

$$2\mu_{eq}A_{peak} \omega_{peak} = \omega_0^2 \frac{m y_{m,max}}{\Delta GM} \quad (6)$$

From the fitting of the equivalent linear damping coefficient obtained in Equation 6 with Equation 2, the following damping coefficients for the trawler fishing vessel have been obtained:

- $\mu = 0.0038$ [1/s]
- $\beta = 0.0000$ [-]
- $\delta = 0.5951$ [s]

Comparison

In Table 3 the damping coefficients obtained using both Simplified Ikeda’s method and forced roll tests are shown.

Table 3: Roll damping coefficients obtained

Method used	μ [1/s]	β [-]	δ [s]
Simplified Ikeda’s Method	0.0020	0.1898	0.0000
Forced Roll Tests	0.0038	0.0000	0.5951

As can be seen in Table 3, the Simplified Ikeda’s method characterize the roll damping of the trawler fishing vessel as being linear-quadratic, while the

forced roll tests experiments characterize it as being linear-cubic. It is a considerable difference which will definitely influence the DSC evaluation.

4. EVALUATING THE DEAD SHIP CONDITION FAILURE MODE

The fishing vessel under analysis complies with the Level 1 criterion for the DSC failure mode but it does not complies with the Level 2.

The Level 2 criterion for the DSC failure mode has been evaluated for the trawler fishing vessel using a code developed by the authors.

The code has been verified analysing the robustness of the results but it has not been validated as no complete sample calculations have been available. For instance, in the example of application of the Level 2 DSC Criterion shown in the Explanatory Notes (IMO, 2016c) some input data is missing.

In Table 4, the results of the DSC Level 2 evaluation using both damping coefficients are shown considering the long-term probability index denoted as C:

Table 4: Dead Ship Condition Level 2 evaluation.

Method used	C
Simplified Ikeda’s method	0.124
Forced Roll Tests	0.174

As can be seen in Table 4, the trawler fishing vessel does not comply with the DSC Level 2 criterion as both C values are above 0.06 or 0.04, which are the two standard values under consideration.

Despite not complying with the criterion, it is worth mentioning that the C values obtained differ to each other by 40%, which is a considerably high difference. Also, even if the C value obtained using the forced roll tests damping coefficient is ship-specific, no scale effects have been considered. Therefore, the DSC Level 2 criterion has a large sensibility to the roll damping, as also emphasized in (Míguez et al., 2015).

5. CONCLUSIONS

The Level 2 criterion for the DSC failure mode has been applied to a trawler fishing vessel considering two different damping coefficients.

Each method has some drawbacks. The first method used to obtain the damping of the current

fishing vessel has been the Simplified Ikeda's method, which has the inconvenience of being determined considering cargo vessels, besides being the ship under consideration outside some applicable ranges. The second method used is forced roll tests, which has the advantage of being ship-specific although no scale effects are considered. However, the latest method is expensive and time consuming.

The results obtained either considering both damping coefficients show that the fishing vessel considered does not comply with the Level 2 criterion. The most relevant fact is that the long-term probability index obtained (C) differ by 46% between both methods, which is a considerable and non-insignificant difference.

Consequently, the difference of the C values between both cases needs to be further analysed. Despite of this, it is an indicator of the great influence that the damping coefficient has in the Dead Ship Condition Level 2 criterion.

6. QUESTIONS TO BE FORMULATED

During the development of the present work, some questions have emerged.

Referring to the damping coefficient determination:

- Although it is known that the Simplified Ikeda's method may be used for cargo vessels and that it is recommended to use it when inside all the application ranges, it is of common understanding that the use of this method outside the application ranges is conservative. However, from the results obtained it seems to be the opposite. Therefore, have the consequences of being outside the application ranges of the Simplified Ikeda's method been analysed?
- Otherwise, when using experimental tests, there are many points that can be raised due to the lack of standard. Moreover, depending on the experimental technique used, the damping coefficients may differ considerably as the hydrodynamic scenario is different. Is it necessary to develop standard procedures for decay tests and forced roll tests?
- Also, regarding experimental tests, there are still many uncertainties regarding the

damping scale effects. Do the scale effects have to be taken into account? If so, how?

Referring to the Level 2 Criterion for the Dead Ship Condition failure mode:

- It is not possible to validate the codes as there is not a complete sample calculation or example. Should it be a high priority issue for the finalization of the SGISC?
- As seen in the present work, depending on the damping coefficient used, considerable differences may be obtained in the C value. Therefore, it may be determinant when checking the compliance with the criteria. Has the influence of the damping coefficient on the DSC Level 2 criterion been studied?

REFERENCES

- Bačkalov, I., Bulian, G., Cichowicz, J., Eliopoulou, E., Konovessis, D., Leguen, J-F., Rosén, A., Themelis, N., 2016, "Ship stability, dynamics and safety: Status and perspectives from a review of recent STAB conferences and ISSW events", *Journal of Ocean Engineering*, Vol. 116, pp. 312-349, DOI: <http://dx.doi.org/10.1016/j.oceaneng.2016.02.016>.
- Bulian, G., Francescutto, A., Fucile, F., 2009, Project HYD-III-CEH-5: Determination of relevant parameters for the alternative assessment of Intact Stability Weather Criterion on experimental basis – Appendix 1", Technical Report, HYDROLAB PROGRAMS, pp. 95 – 102, November 2009.
- Falzarano, J., Somayajula, A., Seah, R., 2015, "An overview of the prediction methods for roll damping of ships", *Journal of Ocean Systems Engineering*, Vol. 5 (No. 2), pp. 55-76, DOI: <http://dx.doi.org/10.12989/ose.2015.5.2.055>.
- Handshcel, S., Abdel-Maksoud, M., Fröhlich, M. 2014, "Experimental and numerical investigation of ship roll damping by applying the harmonic forced roll motion technique", 30th Symposium of Naval Hydrodynamics, 2-7 November 2014, Hobart, Tasmania, Australia.
- Himeno, Y., 1981, "Prediction of ship roll damping: State of the art", Final report No.239, Department of Naval Architecture and Marine Engineering, College of Engineering, University of Michigan.
- IMO 2016a, "SDC3/WP.5/Annex1 – Finalization of the Second Generation Intact Stability Criteria. Report of the Working Group: Part 1", pp. 1-9, February 2017, London, United

Kingdom.

IMO 2016b, “SDC4/5/1/Add.1/Annex2 – Finalization of the Second Generation Intact Stability Criteria. Report of the Correspondance Group: Part 4”, pp. 28-33, 11 November 2016.

IMO 2016c, “SDC4/5/1/Add.3 – Finalization of the Second Generation Intact Stability Criteria. Report of the Correspondance Group: Part 4, Annex 4”, pp. 21-22, 11 November 2016.

Kawahara, Y., Maekawa, K., Ikeda, Y., 2009, “A Simple Prediction Formula of Roll Damping of Conventional Cargo Ships on the Basis of Ikeda’s Method and Its Limitation”, Proceedings of the 10th International Conference on Stability of Ships and Ocean Vehicles, (STAB2009), pp. 387-398, St. Petersburg, Russia.

Míguez-González, M., Díaz-Cásas, V., Pérez-Rojas, L., Pena-Agras, D., Junco-Ocampo, F., 2015, “Investigation of the applicability of the IMO Second Generation Intact Stability Criteria to Fishing Vessels”, Proceeding of the 12th International Conference on the Stability of Ships and Ocean Vehicles, 14-19 June 2015, Glasgow, United Kingdom.

Peters, W., Belenky, V., Bassler, C., Spyrou, K., Umeda, N., Bulian, G., Altmayer, B., 2011, “The Second Generation Intact Stability Crietria: An overview of development”, *Annual Meeting of the Society of Naval Architects and Naval Engineers*, Vol. 121, SNAME, Houston, Texas.

Umeda, N., Francescutto, A., 2016, “Current state of the Second Generation Intact Stability Criteria – Achievements and remaining issues”, Proceedings of the 15th International Ship Stability Workshop (ISSW2011), 13-15 June 2016, Stockholm, Sweden.

Use of the Wolfson stability guidance for appraising the operational stability of small fishing vessels

Matteo Scarponi, *Wolfson Unit MTIA, University of Southampton*, M.Scarponi@soton.ac.uk

ABSTRACT

This paper describes the use of the Wolfson guidance and other stability criteria in the context of two recent accident investigations on small fishing vessels: 11.4m scallop dredger JMT and 9.9m stern trawler Stella Maris. Both vessels capsized and sank whilst handling their catch in benign weather conditions. The Wolfson guidance, which is suitable for all types of fishing vessels including those with no stability information, enables estimation of the safe operational limits for both JMT and Stella Maris. Also, given the probable loss scenarios and residual stability characteristics, the Wolfson guidance predicted that both vessels were operating outside such limits at the time of each loss.

Keywords: *Stability, Safety, Wolfson Guidance, Stability Notice, Freeboard Mark.*

1. BACKGROUND

Statistics published by the Food and Agriculture Organisation show that ‘fishing holds the record as the most dangerous occupation pursued by man’ [1], which is underpinned by a fatality rate in excess of 24000/year worldwide [2]. Further statistics quoted in [3] show that the fatality rate in the UK fishing industry is ‘of the order of 100 times higher than that of the general workforce’.

Although there are many causes of accidents, most of the fatalities are caused by capsize or swamping because they occur without warning and with little prospect of survival. Statistics of fishing vessel accidents investigated by Canada’s Transportation Safety Board between 1990 and 2000 show that more than half the fatalities occurred in incidents where loss of stability was a known factor [4]. Data presented in [5] show that 10 fishing safety recommendations issued by the UK’s Marine Accident Investigation Branch (MAIB) between 1992 and 2006 are attributed to stability issues that caused the loss of 6 fishing vessels with a total of 13 fatalities.

Safety is dependent on the stability and seaworthiness of the vessel and its size in relation to the seastate. Small vessels, therefore, are particularly vulnerable, but they are the ones for which no stability calculations are required. Existing UK fishing vessels under 15m overall length are not

currently required to comply with statutory stability requirements. Whilst the proposed Small FV Code is re-introducing stability requirements for 12-15m fishing vessels joining the UK Register, the existing under 15m fleet and newly built craft under 12m registered length need not comply with any current or proposed stability standards. Should such vessels seek compliance on a voluntary basis, guidance is available and presented in MGN 427(F), which also states that ‘it is not acceptable to do nothing and assume the vessel’s stability is satisfactory’ [6].



Figure 1 – Salvaged wreck of F/V JMT (Credit: MAIB)

2. AVAILABLE METHODS

MGN 427(F) describes five methods that may be used, on a voluntary basis, for assessing the stability of small fishing vessels. These are summarized below:

2.1 Full Stability Information

Currently, this requirement applies to all vessels of 15m overall length and over. It involves conducting an inclining experiment to derive the lightship displacement and centre of gravity, and the calculation of loading conditions representative of a fishing voyage.

Standard loading conditions (ie gear stowed and catch on/below deck) must be assessed against the stability criteria and beam trawlers have a 20% uplift with the criteria. Operating conditions, however, may be more onerous than standard conditions due to raised gear and heavy lifts, but are not normally assessed.

2.2 Small Commercial Vessel Code Heel Test

This method prescribes a maximum heel angle and adequate freeboard with a 1t load applied on deck at the maximum outboard position. The method may only be used for fishing vessels carrying up to 1t of catch.

2.3 Small Passenger Vessel Heel Test

This is an alternative method to 2.2 and assumes a 2/3 : 1/3 catch distribution on each side of the vessel. It prescribes a maximum heel angle and a minimum freeboard requirement, and may be used for fishing vessel carrying in excess of 1t of catch.

2.4 Wolfson Guidance

This method was formulated by Barry Deakin and is based on the findings of extensive model tests conducted for MCA Research Project 509 [7] combined with evidence from UK casualty statistics. The development of the Wolfson guidance is described in [8, 9], whilst [10] is an independent commentary undertaken at the request of RINA.

The Wolfson Guidance suits fishing vessels of any size and enables owners and skippers to produce a single page Stability Notice showing an indication of their vessel's level of safety. The Guidance consists of two separate formulations and assessment routes, depending on the availability of a full stability analysis for the vessel.

For vessels with stability information (typically 15m overall length or more) the Wolfson Guidance is based on an assessment of the residual stability when loaded or lifting.

For vessels with no stability information such as JMT or Stella Maris, the Guidance is based on the

residual freeboard when loaded or lifting heavy loads, and the freeboards referred to in the Stability Notice should be marked on the side of the vessel using a standard Freeboard Guidance Mark ('Wolfson mark'). The mark should be positioned at the lowest freeboard, or where the freeboard becomes lowest when lifting.

The relevant formulae and example results are given in Annex 5 of MGN 427(F), which is intended for use by consultants tasked with the production of Stability Notices.

2.5 IMO Roll Period Approximation

This method enables skippers to monitor whether stability changes over time, on the basis of the vessel's measured roll period. It is an operational method rather than a stability criterion, so it was not taken into account in the accidents investigations discussed herein.

3. FV JMT INVESTIGATION

MAIB Report [11] describes an investigation into the capsizing and sinking of 11.4m scallop dredger JMT. The accident occurred on 9th July 2015 and resulted in two fatalities.



Figure 2 – Lady Patricia (Credit: trawlerpictures.net)



Figure 3 – JMT following 2013 conversion (Credit: trawlerpictures.net)

3.1 Construction and modifications

JMT (previously Lady Patricia) was built in 1988 as a conventional stern trawler and was fitted with a forward wheelhouse, amidships ‘scotch poles’ and a stern gantry (Figure 2). Between 2003 and 2013 the vessel’s stern gantry was raised and a port side shelterdeck was added. Subsequently, the vessel was converted for scallop dredging, which involved fitting winches and outriggers for handling the scallop gear, removing the shelter deck, raising the stern gantry further and replacing the scotch poles with a goalpost gantry. The latter vessel configuration (Figure 3) was approved by Seafish Marine Survey in 2013 and, subsequently, by the MCA.

The vessel had been fishing off Plymouth since May 2015 and usually operated in daylight. At the time of its loss, JMT carried two dredges weighing 750kg each, 0.5t of bagged catch on deck and very little fuel. An underwater survey identified that the starboard side dredges were empty and inverted, whilst the port side dredges were suspended from a goalpost block 5m above deck, unrestrained and full of 400kg of catch and debris.

3.2 Stability assessment

Initially the Wolfson Unit conducted a lines survey and an inclining experiment on the salvaged wreck. Then it prepared a stability model within Wolfson’s hydrostatics and stability software HST and performed a stability analysis against MGN 427(F). Four standard loading conditions and three operational conditions representing the vessel at the time of its loss were formulated and assessed against methods 2.1 and 2.4 above. Heel tests 2.2 and 2.3 were conducted numerically, at the appropriate loading conditions. Table 1 gives the calculated load conditions. Readers are referred to Annex A of MAIB report [11] for the full stability assessment.

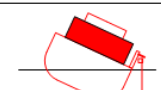
3.3 Results

The vessel failed the full stability assessment (method 2.1) required by larger fishing vessels, which indicates insufficient reserve stability. In particular, the six stability criteria are not met in any of the conditions. Also, the minimum freeboard of conditions 1 and 2 is below 300mm, which is the minimum recommended freeboard given in the Seafish Standard [12].

The vessel failed both numerical heel tests. It had no positive stability in the SCV heel test and failed the minimum freeboard requirement of the small passenger vessel heel test.

The vessel’s Wolfson Stability Notice and Freeboard Mark are given in Figure 4 and its calculated level of safety in the various load conditions is given in Table 2. The Wolfson guidance indicated that the vessel had:

- a. low residual freeboard due to loading in all the standard conditions and in two operational conditions, namely no.7 - tow lift, dredges just off seabed and no.8 - full dredges resting on bulwarks;
- b. low residual freeboard due to lifting in the operational condition that probably triggered the capsized: no.9 - starboard dredges emptied on deck and port dredges suspended from goalpost gantry;
- c. that the vessel was in danger of capsized in seastates exceeding 0.7m significant wave height (low end of Douglas seastate 3).

STABILITY NOTICE				
Name JMT No. 0 Owner 0 Length 11.42 metres Beam 4.38 metres	Loading & Lifting Guidance	Safety Zone	Minimum Freeboard	Maximum Recommended Seastate
	Good margin of residual freeboard	Good margin of safety	At least 52 cm	
	Loading or lifting reduces minimum freeboard to less than 52 cm	Low level of safety	26 to 52 cm	1.4 metres
	Excessive loading or lifting reduces minimum freeboard to less than 26 cm	Danger of capsized	Less than 26 cm	0.7 metres

Freeboard Guidance Mark - size and location

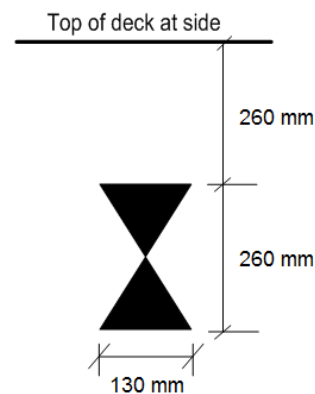


Figure 4 – Stability Notice and Freeboard Guidance Mark for FV JMT

Table 1: Loading conditions (S: standard, O: operational, H: heel test). No.9 is the probable loss condition.

Name	Displ. (t)	Minimum freeboard (mm)
1: S Departure Port	48.49	263
2: S Arrival Grounds	47.96	274
3: S Depart Grounds	44.88	322
4: S Arrival Port	44.29	331
5: H SCV Code Heel Test	49.49	submerged
6: H Small Pax Vessel Heel Test	49.04	14% of requirement
7: O Tow Block Lift & Full Dredges	43.75	261
8: O Full Dredges on Bwks	43.98	327
9: O SS Tipped, PS Full & Suspended	43.98	219

Table 2 – Vessel’s freeboard at Freeboard Guidance Mark, 25% LOA

Safety Zone	Minimum Freeboard cm	Freeboard at Load Conditions cm						
		STD				OP		
		1	2	3	4	7	8	9
Good margin of safety	At least 52							
Low level of safety	26 to 52	31	31	32	33	28	33	
Danger of capsize	Less than 26							22

3.4 Conclusions

The MAIB report concludes that the capsize was probably triggered by the sudden release of the contents of the starboard side dredges, while the unrestrained port side dredges and their contents remained suspended from the 5m high ‘goalpost’ gantry.

It was also highlighted that ‘of the alternative stability assessment methods detailed in MGN 427(F), only the Wolfson method would have provided an indication of the vessel’s operational limits, and when caution was required’ [11]. MAIB recommendation 2016/130 to the Maritime and Coastguard Agency emphasizes that ‘all existing vessels of under 15m should be marked using the Wolfson Method, or assessed by use of another acceptable method’.

4. FV STELLA MARIS INVESTIGATION

MAIB Report [13] describes an investigation into the capsize and foundering of 9.96m stern trawler Stella Maris, on 28th July 2014. The two crew abandoned to a liferaft and were later rescued.

The Wolfson Unit was not involved in the accident investigation, which included a stability assessment against the Wolfson guidance and other simplified methods. Such an assessment concluded that ‘the craft had a reasonable measure of stability’. It is the Author’s opinion, however, that the Wolfson guidance would have predicted that the vessel was endangered, had it been applied correctly. Sections 4.3 to 4.5 below offer the Author’s view on the application of the Wolfson guidance to Stella Maris.

4.1 Construction and modifications

Stella Maris was built in 1999 as a conventional stern trawler. Initially, it was equipped with a gilson derrick for performing cod end lifts over the side and releasing the catch on deck. In 2013 it underwent major modifications, see Figure 5, to enable lifting over the stern into a catch hopper, thus improving the quality of the catch. To that effect, the gilson derrick was removed and a stern gantry was fitted, which raised the lifting point by approximately 1m. Also, the cod end had to be raised by approximately 1.65m above the bulwark to clear the upper edge of the hopper, so it could be emptied in the hopper from an overhead position. The catch would then remain in the hopper and gradually feeding to the sorting area beneath the shelterdeck.

It is stated in [13] that ‘no post-modification inspection by the MCA was required, or carried out, following the modernisation’.



Figure 5 – Stella Maris following 2013 modification (Credit: Jon Irwin)

4.2 Loss scenario

The vessel capsized and sank whilst attempting to lift a heavy cod end of fish and debris. The estimated weight in air of the cod end was 1.8t and the stern lift was performed using a 2.8t (first layer pull) rated winch and a gilson block fitted near the top of the stern gantry ie about 6m above deck.

As successive layers of wire built up during the lift, the winch pull reduced until the cod end could not be lifted any higher and remained suspended from the gilson block. The skipper then veered the winch in an attempt to lower the cod end back into the sea, but the net snagged on a guide pole fitted at the starboard transom corner. This caused the starboard transom quarter to submerge and, ultimately, resulted in a capsize.

4.3 Longitudinal position of the Wolfson mark

Figure 16 of Ref. [13] identifies the size and position of the Wolfson mark temporarily applied to Stella Maris’ sister vessel. The estimated longitudinal position of the mark is 35% LOA forward of AP, assuming that the centreline of the mark coincides with that of the port side access door opening (see the GA presented in Annex B, page 13).

The vessel’s GA indicate that 35% LOA forward of the transom is the minimum freeboard position for the 100% Port Departure condition given in Annex B. The vessel has approximately 30mm stern trim in this condition.

With regard to positioning the Wolfson mark, MGN 427(F) states that ‘In selecting the location, the most likely reason for reduced freeboard should be borne in mind. If a large load is added well forward or aft, or is lifted from a point that is well forward or aft, the load might induce a large trim, resulting in the minimum freeboard being at a different longitudinal location compared with the upright case’ [6].

The calculations presented in Annex B of Ref. [13] show that performing a centreline, 1.8t lift over the stern from the gilson block induces a large trim by the stern, about 8 times the port departure trim. This causes the minimum freeboard position to shift further aft than at port departure, by a distance between 5 and 10% LOA. Thus the Wolfson mark should be positioned between 25 and 30% LOA forward of transom, not at 35% LOA to represent the true residual stability of the vessel when lifting.

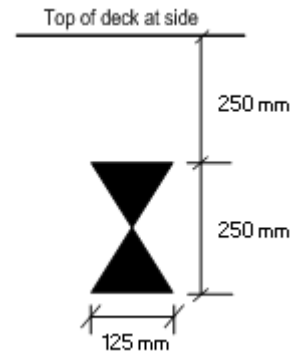


Figure 6 – Freeboard Guidance Mark for Stella Maris

4.4 Vertical position of the Wolfson Mark

The dimensions of the Wolfson mark may be calculated from the vessel’s beam and overall length as per Appendix A, and are shown in Figure 6.

Section 1.9 of Ref. [13] describes the temporary application of the Wolfson mark to Stella Maris’ sister vessel, during the post-accident stability assessment. Figure 16 of Ref. [13] shows the Wolfson mark affixed to the port side of the sister vessel in the as inclined condition, and Figure 7 below is MAIB’s Figure 16 with tentative dimensions edited in.

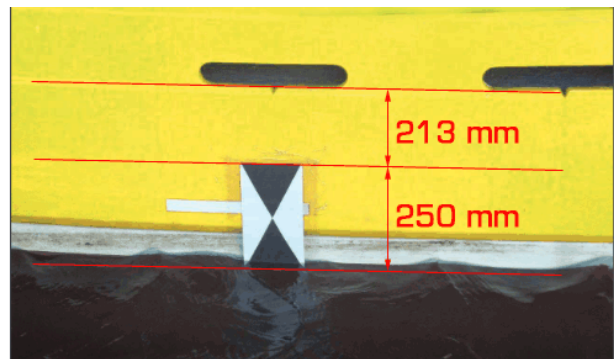


Figure 7 – Wolfson mark as applied in Ref. [12] with tentative dimensions added. As-inclined waterline.

As the sister vessel’s calculated port departure freeboard was 40mm higher than at inclining, a small clearance was expected between the lower edge of the mark as applied to the sister vessel and its port departure waterline, so the MAIB Report concluded that the sister vessel would have been ‘just in the Wolfson guidance mark green safety zone in the depart port condition’ [13].

However, Figure 7 indicates that perhaps the mark should have been lowered by about 40mm to achieve the calculated 250mm separation between the deck at side and the top edge of the mark. Such a vertical shift would position the lower edge of the Wolfson mark at the port departure waterline, as

shown in Figure 8. So the vessel in the port departure condition appears to be at the boundary of the green and amber safety zones.

4.5 Operational stability assessment

Figure 8 shows two waterlines derived from the vessel’s calculated draughts at FP and AP, as indicated in Annex B of Ref. [13]. The Wolfson mark is positioned as per MAIB report, but its correct position may be further aft and approximately 40mm lower than in the report, as discussed in Sections 4.3 and 4.4 above.

The red waterline of Figure 8 represents the 1.8t stern lift, zero heel condition described in Annex B, page 64. As the Wolfson mark is partially immersed, the Wolfson guidance indicates a ‘low level of safety’ for the vessel in that load condition.

The gilson winch is rated at 2.8t (first layer pull) so hoisting 1.8t should be regarded as a realistic operating condition that reduces the vessel’s freeboard to a level that, according to the Wolfson guidance, may endanger the vessel.

For the probable loss condition described in Annex B, page 69 the calculated equilibrium heel angle is 8.4 degrees to starboard. A simple calculation shows that a Wolfson mark affixed on the starboard side of the vessel would be submerged at that heel angle. Therefore, the Wolfson guidance predicts that the vessel’s residual stability is reduced to an unsafe level in such a condition, and the vessel is in danger of capsizing.

According to the deadweight tables of Annex B Ref. [13], the heeling moment resulting in deck flooding and capsize was approximately 1t.m, that is a 1.8t point load (cod end) applied 0.55m from the centreline. It is reasonable to assume that heeling moments of such a magnitude may be applied whilst the vessel is in operation (eg. cod end retrieval in beam seas), thus reducing the vessel’s freeboard to an unsafe level due to the combined effect of trim and heel. Similarly to heavy lifts over the stern, these scenarios are also realistic and therefore should be assessed against the Wolfson guidance.

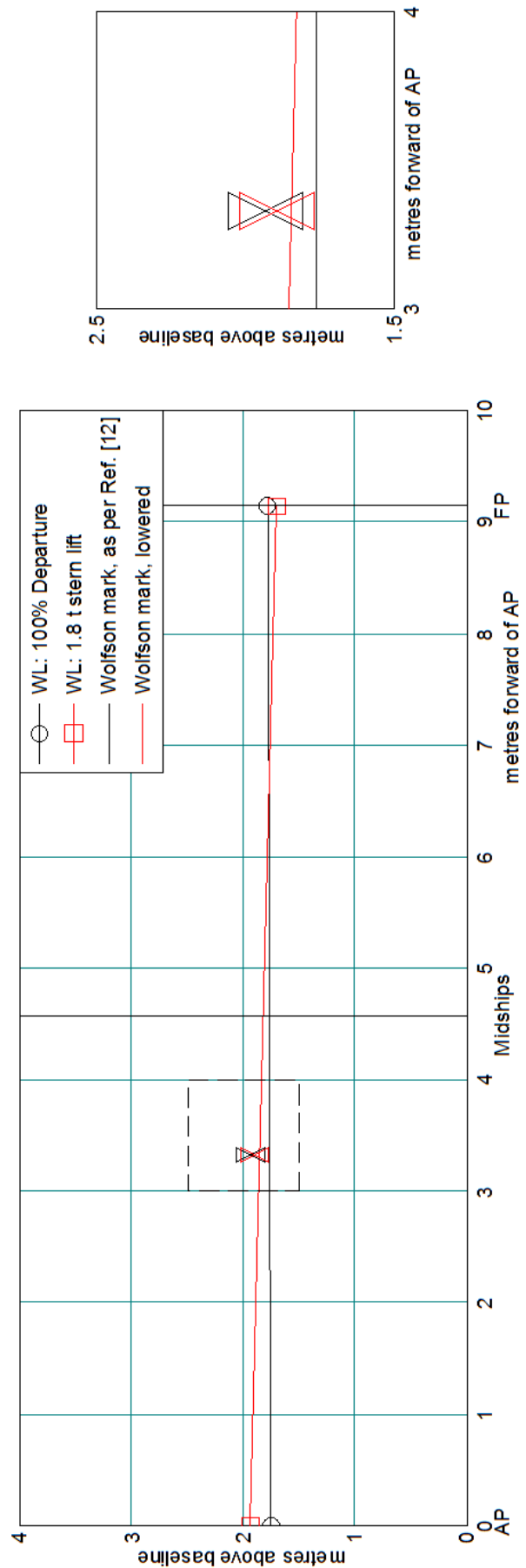


Figure 8 – 100% departure and 1.8t stern lift waterlines

4.6 Conclusions

Calculations based on the data presented in Ref. [13] suggest that the position of the freeboard mark applied to the sister vessel of FV Stella Maris was incorrect. In particular, the appropriate position of the mark appears to be approximately 40mm lower and further aft (at the minimum freeboard location when undertaking a heavy lift) than indicated in the report, resulting in a more onerous freeboard requirement for the vessel.

Section 2.3.3 of Ref. [13] states that ‘Assessment of Stella Maris’s sister vessel by Roll Test, Small Commercial Vessel Heel Test and Wolfson Guidance indicated that the craft had a reasonable measure of stability’. The Wolfson guidance, however, indicates that the vessel had a ‘low level of safety’ when lifting a 1.8 t cod end from the stern gantry and was probably ‘unsafe, and in danger of capsizing’ had such load shifted transversely by about 0.5 metres.

Section 2.3.2 of Ref. [13] states that ‘Any vessel can be capsized, and it is the duty of vessel’s operators to work within the vessel’s safe limits. However, this is not easily achieved when those limits are not known’. The Wolfson method is a simple guidance for identifying such limits and relate them to the vessel’s operation, thus raising awareness on how certain loading or lifting operations will reduce the safety of the vessel, and on the limit seastates in which such operations should be conducted.

5. DISCUSSION

Currently, UK fishing vessels under 12m registered length such as JMT and Stella Maris, are not required to comply with statutory stability criteria and there is presently no intention to introduce such requirements. However, the stability methods presented in MGN 427(F) are available and the MCA recommend that small vessels are assessed against such methods to ensure that they have a satisfactory measure of stability [6]. These methods include a full stability assessment, which is mandatory for fishing vessels over 15m LOA, heel tests and the Wolfson Guidance.

The Wolfson Guidance is intended to provide fishermen with some indication of their vessel’s level of safety. On a small fishing vessel such safe limits may not be exceeded in the port

departure/arrival and grounds arrival/departure conditions normally assessed in stability booklets but, crucially, may be exceeded whilst the vessel is in operation and its residual stability is reduced due to heavy loading or lifting. Such operating conditions are often more onerous than the standard conditions and should be appraised.

MGN 526(F) is expected to replace MGN 427(F) and its current draft version [14] continues to present the Wolfson Guidance as a suitable method for assessing and maintaining stability on small fishing vessels, whilst the other methods are no longer discussed.

The draft Small Fishing Vessel Code [15] recommends that vessels up to 12m registered length carry stability information but it is unclear what it should consist of and no reference to MGNs 427 or 526 is made.

The draft Small Fishing Vessel Code reintroduces mandatory stability compliance for vessels between 12m registered length and 15m overall length entering the UK Register. But are stability books alone going to make such vessels safer? Or should simple stability guidance also be available to fishermen and adhered to? It should be borne in mind that:

- a. Fishing vessels are not currently required to meet the standard stability criteria with the gear raised or deployed.
- b. Currently it is not mandatory to assess the stability of a fishing vessel in the most onerous load case eg heaviest lift, furthest outboard, highest position.
- c. The above is a stark contrast to other vessel types such as workboats, where vessels fitted with cranes must be assessed ‘in the worst anticipated service condition for lifting operations’ and against criteria prescribing the maximum heel angle, or minimum freeboard, whilst lifting [16].
- d. Upgrading lifting gear and winches enables more onerous lifts, resulting in larger heeling moments applied and/or higher vessel VCG whilst lifting. This is unlikely to invalidate the approved lightship, or affect compliance with standard criteria unless operational conditions are assessed.

e. The preparation and updating of formal stability information is expensive, and not perceived as an asset by owners and skippers.

f. If a stability booklet was mandatory and available onboard, the skipper would still have no idea how safe he is. All he knows is the vessel has met the criteria so he assumes that it must be safe.

REFERENCES

- Petursdottir, G., Hannibalsson, O., Turner, 2001, "Safety at sea as an integral part of fisheries management", FAO Fisheries Circular No. 966.
- International Labour Organisation, 1999, "Report on Safety and Health in the Fishing Industry".
- Maritime and Coastguard Agency, 2015, "Annex H – Fishing Vessel Codes Impact Assessment".
- MIL Systems, 2002, "Analysis of Canadian fishing vessel accidents 1990 to 2000", MIL Project 2127/01, Levis, Quebec.
- Marine Accident Investigation Branch, 2008, "Analysis of UK Fishing Vessel Safety 1992 to 2006".
- Maritime and Coastguard Agency, MGN 427(F) "Stability guidance for Fishing Vessels of Under 15m Overall Length".
- Deakin, B., 2005, "An Experimental Evaluation of the Stability Criteria of the HSC Code", Proceedings of the 8th International Conference on Fast Sea Transportation, (FAST 2005), St. Petersburg, Russia.
- Deakin, B., 2006, "Developing Simple Safety Guidance for Fishermen", 9th International Conference on Stability of Ships and Ocean Vehicles, Rio de Janeiro, Brasil.
- Deakin, B., 2010, "Collating Evidence for a Universal Method of Stability Assessment or Guidance", Trans RINA, Vol. 152, Part A2, International Journal of Maritime Engineering.
- Birmingham, R., 2014, "Commentary on the Wolfson Stability Guidance and Associated Discussion", publicly available on <http://www.rina.org.uk>
- Marine Accident Investigation Branch, 2016, "Report on the Investigation of the Capsize and Foundering of the Fishing Vessel JMT (M99)", No.15/2016.
- Sea Fish Industry Authority, 2012 "Less than 15m LOA Construction Standards".
- Marine Accident Investigation Branch, 2015, "Report on the Investigation of the Capsize and Foundering of FV

Stella Maris", No.29/2015.

- Maritime and Coastguard Agency, MGN 526(F) "Stability guidance for Fishing Vessels of Under 15m Overall Length", draft electronic copy available on <https://www.gov.uk/government/consultations>.
- Maritime and Coastguard Agency, 2014, "The Code of Practice for the safety of fishing vessels of less than 15 metres length overall", draft electronic copy available on <https://www.gov.uk/topic/working-sea/maritime-safety>.
- Maritime and Coastguard Agency, 2014, "The Safety of Small Workboats and Pilot Boats – a Code of Practice".

APPENDIX A

Wolfson Freeboard Mark calculations for FV Stella Maris (overall length 10.14m, beam 4.09m) as per Ref. [5]:

$$Hs, \text{amber} = \sqrt{1 + 0.4 * LOA} - 1 = 1.25 \text{ m} \quad (1)$$

$$Hs, \text{red} = \frac{Hs, \text{amber}}{2} = 0.62 \text{ m} \quad (2)$$

where Hs, amber and Hs, red are the significant wave heights at the green/amber boundary and amber/red boundary respectively.

$$\text{Freeboard, amber} = \frac{\text{Beam}}{LOA} * Hs, \text{amber} = 0.5 \text{ m} \quad (3)$$

$$\text{Freeboard, red} = \frac{\text{Freeboard, amber}}{2} = 0.25 \text{ m} \quad (3)$$

where Freeboard, amber and Freeboard, red are the minimum freeboards at the green/amber boundary and amber/red boundary respectively.

Towards real-time identification of initial stability from ship roll motion analysis

Marcos Míguez González, *Integrated Group for Engineering Research, University of A Coruña*
A Coruña, Spain, mmiguez@udc.es

Gabriele Bulian, *Department of Engineering and Architecture, University of Trieste, Trieste, Italy,*
gbulian@units.it

Lucía Santiago Caamaño, *Integrated Group for Engineering Research, University of A Coruña*
A Coruña, Spain, lucia.santiago.caamano@udc.es

Vicente Díaz Casás, *Integrated Group for Engineering Research, University of A Coruña*
A Coruña, Spain, vdiaz@udc.es

ABSTRACT

Stability related failures are known to represent an important cause of accidents involving fishing vessels, and are usually related to the crew lack of capability for assessing the stability level of their ships in an objective way. The use of simplified guidance systems could be adopted as a possible risk control option for trying to address this problematic situation. However, the need for manual interaction with the crew, is one of the major drawbacks of such systems. In this paper, a sample application of a methodology based on spectral analysis of roll motion for obtaining the natural roll frequency of the vessel is presented. The final intention is to have a tool which, from roll frequency estimation, could be used for the estimation of initial ship stability characteristics. The proposed methodology is tested by using roll motion results from a nonlinear one degree of freedom roll model, under the excitation of beam irregular waves and lateral gusty winds. The obtained results are promising, but some open aspects, relevant to the real application of such approach, require further discussion and investigation.

Keywords: *Fishing vessels, Intact stability, stability monitoring, Guidance systems.*

1. INTRODUCTION

Operational guidance systems are common and broadly used today among the commercial fleet, including within them loading and intact stability guidance systems, weather routing systems, damage stability analysis software and dynamic stability evaluation codes (Palmquist and Nygren, 2004). The use of these systems has helped crews to increase the safety of their vessels and their economic performance. Although their operation is usually non-straightforward and their working principles require a more-than-average knowledge of naval architecture, dedicate crew training programs can be put in place among shipping companies to familiarize crews with such systems (Huss, 2016). In fact, the importance of guidance to masters has been already highlighted by the IMO and the Classification Societies, as could be seen, for example in the IMO bad weather sailing guidelines

(IMO, 2007). In addition to this, the development of direct stability assessment regulations is also under consideration in the framework of the IMO second generation intact stability criteria (Umeda and Francescutto, 2016). In Bačkalov et al. (2016) and references therein, a discussion on the importance, potentialities and open issues related to operational guidance can be found.

The case of fishing vessels is largely different to that described above. Crews of fishing vessels are not usually trained in risk and stability analysis, especially in the smallest vessels. Guidance systems are not common at all onboard those vessels and most regulators have not tackled the problem of guidance in fishing vessels (Míguez González et al., 2012). This issue is particularly relevant if the number of casualties which occur within the fishing sector is taken into account (Gudmundsson, 2013). A relevant amount of these deaths is due to stability issues, being the crew lack of objective capability for

determining the risk level of the vessel one of their main causes (Jensen et al., 2014).

However, some national authorities and institutions proposed in the last years their own alternatives of simplified stability guidance systems, with different degrees of success and levels of implementation among the corresponding fleets (Wolfson Unit, 2004; Viggosson, 2009; Womack, 2002). The authors have also proposed a tool based on a naval architecture software that, together with an IMU module and a simplified user interface, analyzes the ship motions and the ship loading condition, and provides the master with real-time information of the safety level of the ship in the current sailing situation (Míguez González et al., 2012; Míguez González et al., 2016). Within the mentioned tool, this safety level is presently obtained by using the intact stability characteristics of the vessel and the maximum wave to capsize approach proposed by Deakin (2006).

Most of the nowadays available proposals fulfill a given set of basic requirements, including ease of use, simplicity of implementation and reduced cost of implementation and maintenance. However, all of them rely, up to some extent, on subjective interaction with the crew. Such interaction can occur, for instance, through the comparison of the current situation of the vessel to those provided by a suitable stability poster (Deakin, 2006; Womack, 2002), or through the inputting of information within a stability guidance software (Míguez González et al., 2012).

In this paper, a sample application of a methodology focused on the final intention of providing the crew with realistic stability data of their vessel in real time, minimizing the need for user interaction and the influence of subjective analysis, is presented. This approach is based on the estimation of the vessel natural roll frequency in real time from the analysis of its roll motion spectrum. The underlying idea is that this information can then be used for the estimation of the initial metacentric height of the vessel. This information is in fact fundamental for any guidance system relying on ship motions prediction, irrespective of whether such approach is based on short-term deterministic assessment (e.g. Míguez González et al., 2011), more classical linear-seakeeping-based weather forecasting (Nielsen et al., 2006), or more advanced approaches intended to address also potentially

dangerous dynamic stability phenomena in waves (Ovegård et al., 2012). In order to test the proposed methodology, a nonlinear model of a medium sized stern trawler, under the excitation of beam irregular waves and lateral gusty winds, has been applied.

2. REAL TIME ESTIMATION OF NATURAL ROLL FREQUENCY

As it has been already mentioned, the proposed methodology relies on the estimation of natural roll frequency in real time, as a basis for obtaining the vessel metacentric height (\overline{GM}), which would be of major importance if the stability condition of the ship wants to be monitored. From the well-known roll natural frequency formula, obtained under the simplifying assumption of 1-DOF uncoupled linear roll model,

$$\omega_0 = \sqrt{\frac{\Delta \cdot \overline{GM}}{I_{xx} + I_{add}}} \quad (1)$$

it can be observed that, apart from the natural roll frequency, the vessel displacement (Δ), the dry inertia (I_{xx}) and the hydrodynamic added inertia term (I_{add}) are unknown parameters that are also necessary for obtaining the vessel \overline{GM} . Although this work focuses on ω_0 , some comments regarding the other parameters can be found in (Míguez González et al., 2016).

The method proposed herein for the estimation of natural roll frequency is based on the analysis of the roll spectrum, obtained in real time from the analysis of the vessel roll motion time series. A different approach was proposed in the past by Terada et al. (2016), based on an autoregressive procedure and a general state space modelling.

Míguez González et al. (2016), reported some results applying an approach similar to that presented herein to a set of towing tank tests of a medium sized stern trawler in longitudinal regular waves, under parametric roll resonance conditions. In that work, *Fast Fourier Transform* (FFT) analysis was directly applied to a single chunk (180 seconds) of each of the analyzed roll motion time series, with the goal of obtaining the roll spectrum for that given chunk. The length of these chunks was defined considering that, under operational conditions, the stability characteristics of such a vessel could be assumed to be invariant within that time. Once the spectrum was obtained, the natural roll frequency of

the ship could be estimated from the location of the spectrum maximum value, taking as a basic assumption that most of the energy would be concentrated around the roll natural frequency.

In addition to this, the performance of the system if windowing was applied to the spectra computation was also investigated, concluding that no significant improvement was obtained with these techniques.

Although the obtained results were satisfactory, there were some points which remained open for discussion. On the one hand, the tested cases were limited to the head waves case. Under these conditions, roll excitation was just limited to that due to small misalignments of the model in the tank or, if the conditions were likely, to parametric excitation in roll (and so, approximately at the vessel roll natural frequency). Roll energy was then mainly concentrated around natural roll frequency, which lead to clear single – peaked spectra. On the other hand, the studied conditions, under regular waves, represented an idealized scenario. Both issues lead to the fact that the tested conditions were far from realistic operational situations.

Proposed methodology

In this paper, some of the aforementioned drawbacks are tackled, proposing a refined and improved methodology, and a more realistic test condition. This approach is, as the previously described one, based on the fundamental assumption that the peak frequency of the roll spectrum corresponds, at least approximately, to the roll natural frequency. Such assumption is herein made as a consequence of the peculiar dynamical characteristics of roll, which tends to cut the effect of those excitations which are not leading to roll oscillations close to the roll natural frequency. However, it is clear that this is an approximation and this assumption requires further analysis.

Although the proposed methodology also relies on the estimation of the vessel roll spectrum using FFT analysis, it is more onboard-implementation oriented and three main considerations have been taken into account, which have not been previously considered. Firstly, there is the FFT frequency resolution. Secondly, there is the consideration of the variation of the roll spectrum with time. And finally, there is the need for overlapped analysis in real time.

Regarding the FFT frequency resolution, it is well known that the frequency resolution which a

FFT analysis can provide and that determines the accuracy of the spectrum shape, is only related to the length of the time series under analysis (T (s)) (Oppenheim et al., 1999). This resolution can be obtained as:

$$\delta\omega = \frac{2 \cdot \pi}{T} = \frac{2 \cdot \pi \cdot f_s}{N} \text{ (rad / s)} \tag{2}$$

where $\delta\omega$ is the FFT frequency resolution (rad/s), f_s is the sampling frequency in Hz, T is the analysis time in seconds, and N is the number of samples analyzed by the FFT. As it can be appreciated, if the aforementioned 180 seconds analysis time is applied, it will result in a $\delta\omega = 0.035 \text{ (rad / s)}$. This is not a negligible magnitude and, for the fishing vessel described later in the paper, it amounts to more than a 6 % of the natural roll frequency. This fact makes it difficult to accurately estimate the natural roll frequency from the location of the peak of a roll spectrum which is so scarcely discretized.

Taking into account that roll motion data will be available in real time and that the roll spectrum shape of each analyzed time chunk could be different from each other, a strategy based on overlapped measures and averaging of spectra has been adopted. Based on this methodology, the analyzed spectrum will be, instead that of a given time chunk, the one obtained from averaging a number of spectra, obtained from a set of overlapped measures (of an “Analysis Time” length), sampled at a defined “Sample Time”. The resulting spectrum will be an average spectrum along a given “Averaging Time”, which will be representative of the roll spectrum of the vessel during that time. The proposed methodology is represented in Figure 1.

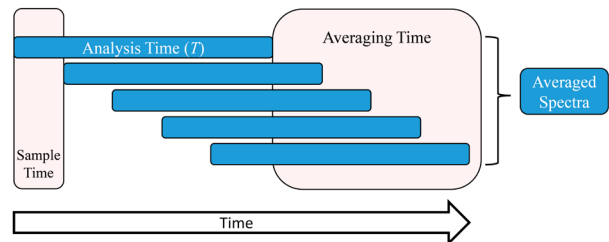


Figure 1. Proposed methodology.

However, the resulting averaged spectrum is still affected by the aforementioned lack of frequency resolution, which is of course independent of the averaging process. In order to try to increase the frequency resolution of the intended results, a fitting process of the averaged spectrum with a simple

parametric model based on the superposition of three Gaussian functions has been implemented. The parametric model has 9 parameters, which correspond to three for each of the three Gaussian functions. The number of functions has been selected as to allow the fitting of up to three superimposed spectra, which could correspond with the wind and wave excitation, and the natural roll motion of the vessel. The simplified parametric model takes the following form:

$$S_{roll}(\omega) = a_1 \cdot e^{-\left(\frac{\omega-b_1}{c_1}\right)^2} + a_2 \cdot e^{-\left(\frac{\omega-b_2}{c_2}\right)^2} + a_3 \cdot e^{-\left(\frac{\omega-b_3}{c_3}\right)^2} \quad (3)$$

It is important to note that the main purpose of the model is not to provide a very accurate fitting of the roll spectrum, but to be a robust model for the identification of the most prominent peak, which is assumed herein to be associated to the roll frequency.

The fitting process has been divided into two steps; the first one is done by a minimization process by applying a genetic algorithm, which provides a first set of fitting parameters. In the second step, this set of parameters is used as starting guess point for a Nonlinear Least Squares Fitting process, which is used to determine the final parameters of the fitting function. Once the fitting is completed, the analytical expression (3) is used for the identification of the maximum peak which is associated with the vessel natural roll frequency. This latter step is no longer bound by the frequency resolution associated from the Fourier analysis.

In order to improve the performance of this process, a previous smoothing of the average spectrum has been done by applying a 5-point moving average technique. Thus, the previously described fitting process is applied to this smoothed spectrum.

Regarding the selection of the Analysis, Sample and Averaging Times, the typical operational profile of the tested vessel (a medium sized stern trawler, which will be later described), has been taken into account. Regarding the Analysis Time, it has to fulfil two main requirements. On the one hand, it has to be sufficiently long as to provide a minimum basic frequency resolution. And on the other hand, it has to be short enough to allow the detection of changes on the vessel stability characteristics, which is in fact

the main objective of the proposed methodology. Under these premises, an analysis time of 180 seconds have been considered, taken the comments in (Míguez González et al., 2016) also into account.

Regarding Sample Time, its selection is only determined by the speed of the analysis algorithm and the possibility of being able to track any possible variation on ship natural frequency in real time. In this case, a 10 seconds Sample Time has been selected.

Finally, Averaging Time is the period in which the spectral information of the roll motion is averaged, and so “stored” by the system. Very long averaging time will lead to a hiding of possible changes in the vessel condition, while if it is too short, the results will be largely affected by the very short term estimations. In this case, Averaging Time has been taken as 120 seconds.

3. TEST ENVIRONMENT

Fishing vessel model

In order to test the proposed methodology under more realistic conditions, the ship roll motion in irregular beam seas has been simulated by applying a one degree of freedom nonlinear model, where the excitation due to waves, mean wind and wind gustiness, has been taken into account. The details of this model, which has been already applied to the case of a small fishing vessel, can be found in (Bulian and Francescutto, 2004). The structure of this model is the following,

$$\ddot{\phi} + 2 \cdot \nu \cdot \omega_0 \cdot \dot{\phi} + \beta \cdot \dot{\phi} \cdot |\dot{\phi}| + \omega_0^2 \cdot \frac{\overline{GZ}(\phi)}{GM} = \omega_0^2 \cdot (m_{wave}(t) + m_{wind}(t)) \quad (2)$$

where ν and β are, respectively, the linear and nonlinear quadratic damping coefficients, ω_0 is the natural roll frequency of the ship, \overline{GM} is the still water metacentric height and $\overline{GZ}(\phi)$ is the nonlinear righting lever as a function of the absolute roll angle. $m_{wave}(t)$ and $m_{wind}(t)$ represent the time dependant nondimensional moments due to the effect of beam waves and lateral wind.

Regarding wave excitation, it has been modelled through the “Absolute Angle Approach” (Bulian and Francescutto, 2006). The effective wave slope coefficient ($r(\omega)$) has been obtained from linear hydrodynamic analysis of the proposed vessel

(Bulian and Francescutto, 2009). Finally, a Bretschneider spectrum has been selected to model irregular waves (ITTC, 2002).

Wind speed excitation has been divided into a steady component (mean wind speed) and a fluctuating one (wind gustiness), which reflect in a time dependent, non-zero-mean heeling moment. In order to obtain the total wind moment, aerodynamic coefficients have been obtained using experimental data from Blendermann (1996). Mean wind speed is obtained as a function of significant wave height applying the relationship used in the Pierson – Moskowitz spectrum (ITTC, 2002). Finally, wind gustiness has been modeled by applying a Davenport spectrum (Davenport, 1961).

The selected test vessel is a medium sized stern trawler, which details are reported in Table 1, hull sections are shown in Figure 2, *GZ* curve in calm water in Figure 3 and effective wave slope coefficient in Figure 4.

Test condition

As a sample test case, the aforementioned model has been used to generate a 3600 seconds roll motion time series, to which the proposed methodology has been applied.

The tested wave conditions have been obtained from historical data (period 1997–2015) of a set of four SeaWave buoys placed in Galician coastal area (Spain) (FOM, 2017). From these data, an average scatter diagram was constructed. The conditional mean value of significant wave height for each characteristic period was then determined, leading to a limited set of sea scenarios (T_p, H_s).

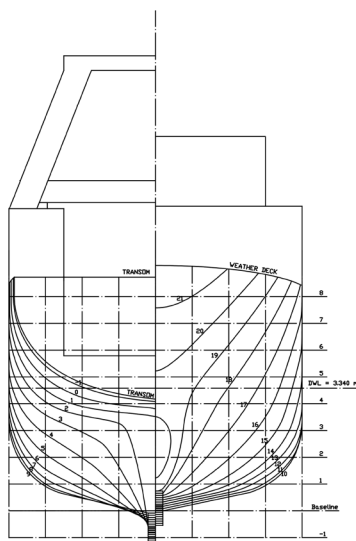


Figure 2. Test vessel: hull sections.

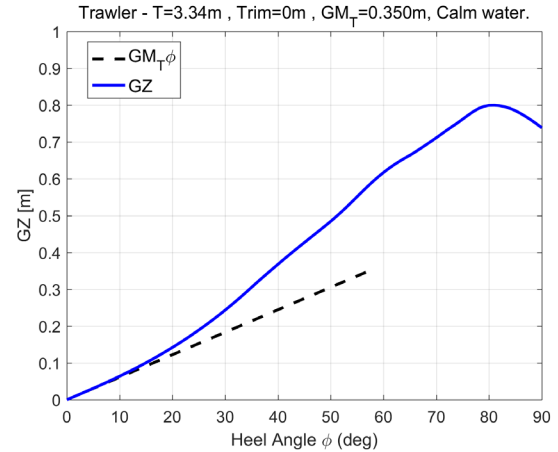


Figure 3. Test vessel: *GZ* curve in calm water.

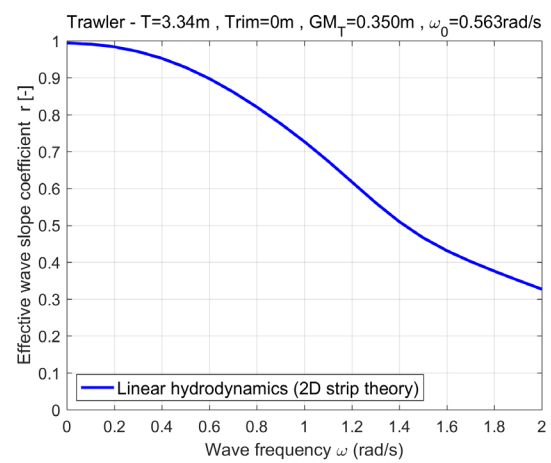


Figure 4. Test vessel: effective wave slope coefficient.

Table 1. Test vessel: main characteristics.

Overall Length	34.50 m
Beam	8.00 m
Depth	3.65 m
Draft	3.340 m
Hull Volume	448 m ³
Metacentric Height (<i>GM</i>)	0.350 m
Natural Roll Frequency (ω_0)	0.563 rad/s
Natural Roll Period (s)	11.16 s
Linear Roll Damping Coefficient (ν)	0.0187
Quadratic Roll Damping Coefficient (β)	0.393 1/rad
Lateral Area (A_{lat})	163.19 m ²
Vertical center of A_{lat} over waterline (H_{up})	2.670 m

Table 2. Tested wave and wind conditions.

Significant wave height (H_s)	1.971 m
Peak period (T_p)	10 s
Mean wind speed (\bar{V}_w)	9.375 m/s

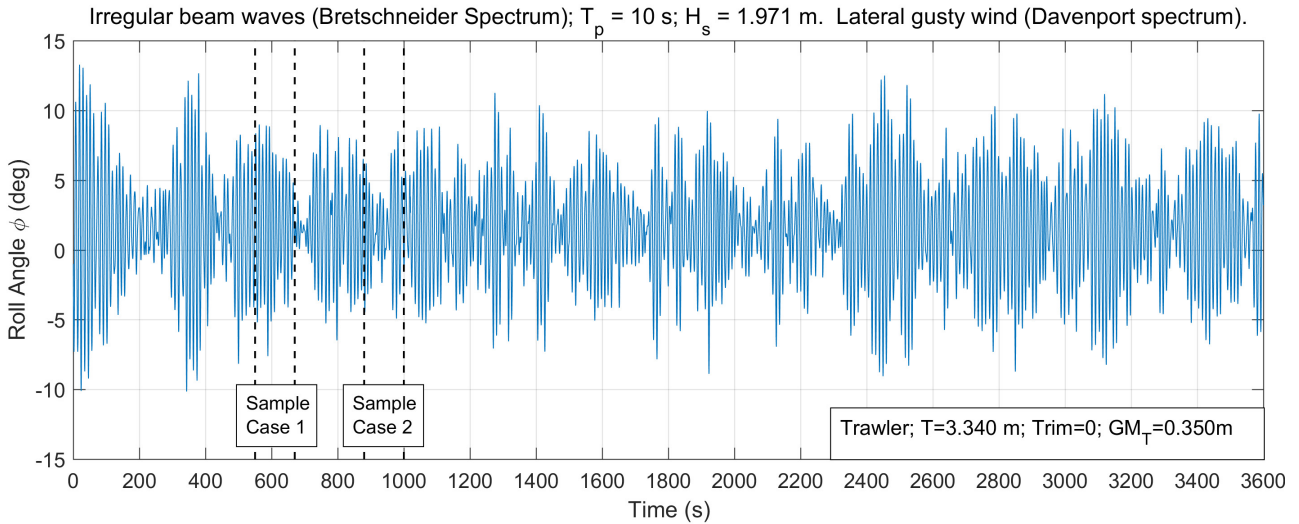


Figure 5. Analyzed roll motion time series. Irregular beam waves. Lateral gusty wind.

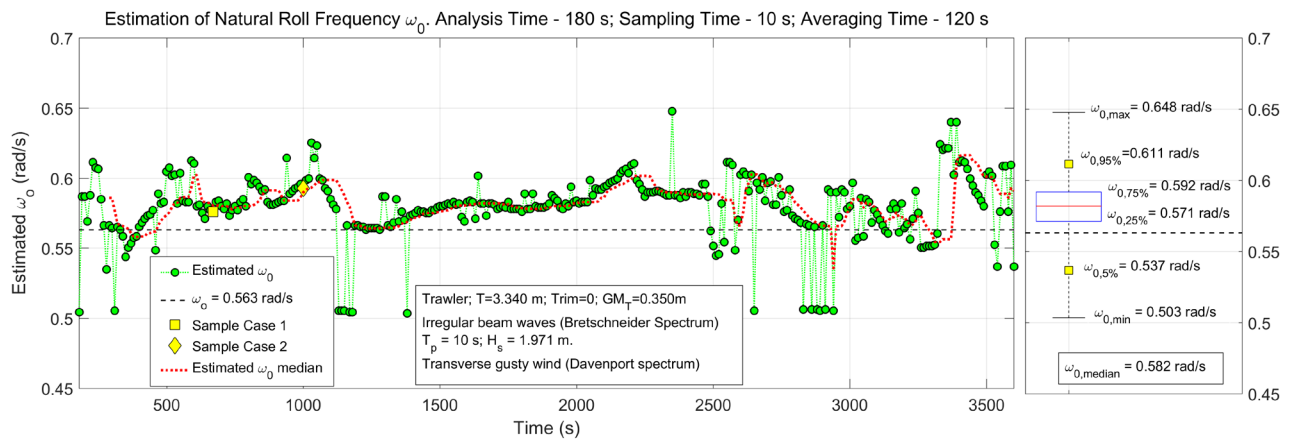


Figure 6. Left: Natural roll frequency estimation results. Right: representation of estimated natural roll frequency distribution through minimum observed value, 5%, 25%, 50%(median), 75% and 95% estimated percentiles, and maximum observed value.

From these, the one associated with the characteristic period with maximum marginal probability of occurrence, has been selected. Its parameters are shown in Table 2. 1000 components were used for generating irregular wave and wind moments, and a 20 Hz sampling rate has been selected.

The obtained roll time series is shown in Figure 5. As it can be appreciated, the ship roll motion presents an asymmetric behavior due to the effect of mean wind pressure. In addition, some low frequency motion, caused by wind gustiness, can also be observed. The wave spectrum peak period is relatively close the vessel natural roll period, thus some relatively large amplitude motions due to harmonic resonance were expected, and in fact, can be observed in the roll time series.

4. RESULTS

In order to test the performance of the described methodology, it has been applied to the test time series which has been already described. The spectrum analysis algorithms have been executed in a continuous way, following the same procedure as it would have been done in a real case. In Figure 6, the obtained results are presented. The green dots in this figure represent the estimated natural roll frequency, obtained every 10 seconds (Sample Time)

These values are obtained from the averaging of the previous spectra (120 seconds of Averaging Time), which were estimated from the analysis of 180 seconds time chunks (Analysis Time).

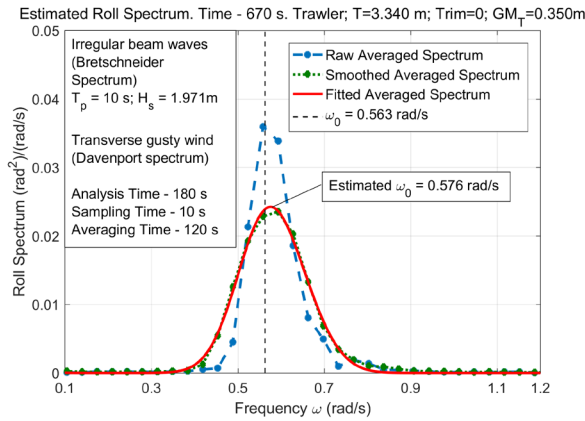


Figure 7. Sample Case 1. Estimated roll spectrum.

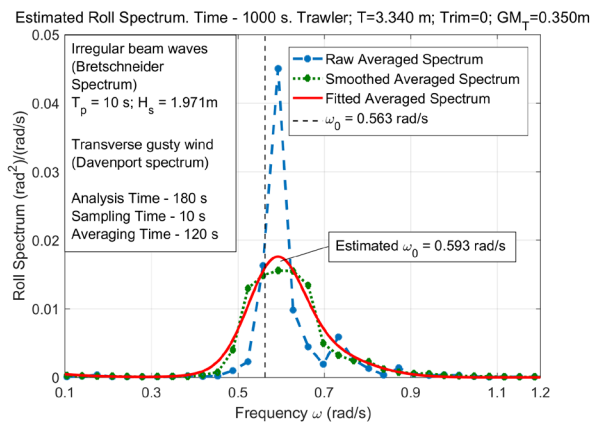


Figure 8. Sample Case 2. Estimated roll spectrum.

In addition to the above, and for a better understanding of the proposed strategy, two sample cases taken from the Figure 6 results are shown in Figure 7 and 8 (highlighted in yellow in Figure 6).

These two spectra correspond to the time instants 670 s and 1000 s respectively. In both figures, the dashed blue lines represent the raw averaged spectrum (for the time intervals shown in Figure 5 between the black dashed lines). As it can be appreciated, the frequency resolution, in the range of interest, is quite low. Dotted green lines represent the smoothed spectrum, aimed at reducing the secondary peaks that could appear in the raw spectra. And finally, the red continuous line represents the spectra obtained after the fitting process of the smoothed spectra using Gaussian functions.

Regarding the general results shown in Figure 6, it can be appreciated that, although the obtained estimations do not exactly match the real natural frequency, they remain continuously on the vicinity of the target value $\omega_0 = 0.563$ rad/s, with the exception of some outlier values, as those present around 1100 s and 2900 s. Even though these outliers

are taken into account, the 90% of the estimated roll frequency samples remains in the range $[0.537 - 0.611]$ rad/s (corresponding to estimated 5% and 95% percentiles). This range corresponds to a percentage difference with respect to the target value in the range $[-4.6\%, +8.5\%]$.

Regarding the aforementioned outliers, and as it can be appreciated from Figure 6, they are values which do not last in time, as the situation only lasts for a single Sample Time (10 seconds in this case). This fact makes it relatively easy to discard such points, always verifying that these values do not extend in time (which, otherwise, could instead represent a real change in the vessel state). One option for robustifying the approach is to use, at each Sample Time, a moving median, where the reference estimated frequency value is determined as the median of the estimated natural roll frequencies from a group of past local estimations. Such an approach, which is based on the assumption of slowly varying ship stability characteristics, allows to disregard the outliers of short duration. An example result from this approach is shown as the red dotted line in Figure 6, where the median is calculated from the group of past 12 local estimations.

The systematic average over prediction of ω_0 observed along the whole time series in Figure 6, could be partially explained by the fact that, under the relatively large roll motions present in the simulated condition, nonlinear effects in restoring (which is of the hardening type, see Figure 3) become more noticeable, and thus the observed dominant roll oscillation frequency tends to be slightly increased.

5. DISCUSSION

It is worth mentioning that, although the obtained estimation ranges in natural frequency could seem to be relatively accurate, the main final target of this methodology, which is to estimate the vessel metacentric height (\overline{GM}), has to be kept in mind. If only the possible error in the estimation of the natural roll frequency is taken into account (from all the needed parameters in Equation (1)), and the [5%-95%] percentiles range of estimated natural frequency are considered ($\omega_0 \cdot (1 + [-4.6\%, 8.5\%])$), this will lead to a range of error in the \overline{GM} estimation of $[-9.1\%, 17.8\%]$.

These errors in the estimation of \overline{GM} , combined with the unavoidable uncertainties in the estimation of the other relevant parameters (vessel displacement and dry and added inertias), could lead to overestimations of \overline{GM} . Such overestimations of the metacentric height are of course non-conservative from a safety perspective and, if too large, they could be not acceptable.

In addition to this, it is also important to remark that the performance of the proposed methodology is largely dependent on the selected Analysis and Averaging times. A detailed analysis of the real operation of these vessels would be needed to determine, in a more accurate way, which is the maximum length of time series chunk which could track loading condition changes.

Finally, further work regarding statistical analysis of the natural roll frequency estimation in different realistic seaways, exclusion of outlier points and error propagation, is therefore needed before a conclusion regarding the applicability of this methodology could be achieved.

6. CONCLUSIONS

In this paper, a methodology based on the spectral analysis of medium sized fishing vessels roll motion, for the estimation of the vessel roll natural frequency while in operation, has been described. This methodology represents one step towards the development of a technique for the on-board real-time identification of \overline{GM} .

A demonstration case of the aforementioned methodology has been presented, taking as a test case the roll motion of a mid-sized stern trawler under the effect of beam irregular waves and gusty lateral wind, applying a one degree of freedom nonlinear uncoupled roll mathematical model.

Although the obtained results seem to be promising, further work is needed to reduce the levels of error in the estimation of natural roll frequency, especially when such errors can potentially lead to unacceptable overestimations of metacentric height of the vessel.

Finally, some points remain open for discussion, including the level of error in the estimation of \overline{GM} which can be considered to be acceptable if such a system is installed onboard a ship, and the maximum analysis time which would be acceptable for accurately tracking the possible variations in the

vessel loading condition (and subsequently on its risk level).

ACKNOWLEDGEMENTS

Part of the present work was carried out during a research visit at University of Trieste, supported by the Spanish Ministry of Education, Culture and Sport (<http://www.mecd.gob.es>) under the “José Castillejo” program, grant CAS16/00013.

REFERENCES

- Bačkalov, I., Bulian, G., Rosén, A., Shigunov, V., Themelis, N., 2016, “Improvement of ship stability and safety in intact condition through operational measures: challenges and opportunities”, *Ocean Engineering* 120, pp. 353-361.
- Blendermann, W., 1996, *Wind Loading of Ships: Collected Data from Wind Tunnel Tests in Uniform Flow, IFS Bericht 574*. Institut für Schiffbau, Universität Hamburg, Hamburg, Germany.
- Bulian, G., Francescutto, A., 2004, “A simplified modular approach for the prediction of the roll motion due to the combined action of wind and waves”, *Proceedings of the Institution of Mechanical Engineers, Part M: Journal of Engineering for the Maritime Environment* 218, pp. 189-212.
- Bulian, G., Francescutto, A., 2006, “Safety and Operability of Fishing Vessels in Beam and Longitudinal Waves”, *The Transactions of The Royal Institution Of Naval Architects. Part B, International Journal of Small Craft Technology* 148, pp. 1-16.
- Bulian, G., Francescutto, A., 2009, "Experimental results and numerical simulations on strongly nonlinear rolling of multihulls in moderate beam seas", *Proceedings of the Institution of Mechanical Engineers - Part M - Journal of Engineering for the Maritime Environment* 223, pp. 189-210.
- Davenport, A.G., 1961, “The spectrum of horizontal gustiness near the ground in high winds”, *Quarterly Journal of the Royal Meteorological Society* 87, pp. 194–211.
- Deakin, B., 2006, “Developing Simple Safety Guidance for Fishermen”, Proc. 9th International Conference on Stability of Ships and Ocean Vehicles, (STAB 2006), Rio de Janeiro, Brazil.
- FOM, 2017, “Predicción de oleaje, nivel del mar ; Boyas y mareografos”, Ministerio de Fomento, Government of Spain, Madrid, Spain. Retrieved from www.puertos.es/es-es/oceanografia/Paginas/portus.aspx on the 1/03/17.
- Gudmundsson, A., 2013, “The FAO/ILO/IMO Safety

- Recommendations for Decked Fishing Vessels of Less than 12 metres in Length and Undecked Fishing Vessels – a major milestone to improve safety for small fishing vessels”, Proc. 13th International Ship Stability Workshop (ISSW 2013), Brest, France, pp. 112-120.
- Huss, M., 2016, “Operational stability beyond rule compliance”, 15th International Ship Stability Workshop, (ISSW 2016), Stockholm, Sweden, pp. 193-200.
- IMO, 2007, “MSC.1/Circ.1228 – Revised Guidance to the Master for Avoiding Dangerous Situations in Adverse Weather and Sea Conditions”, 11 January, London, UK.
- ITTC, 2002, “The Specialist Committee on Waves. Final Report and Recommendations to the 23rd ITTC”, Proc. of the 23rd International Towing Tank Conference, (ITTC 2002), Venice, Italy, pp. 505-736.
- Jensen, O.C., Petursdottir, G., Holmen, I.M., Abrahamsen, A., Lincoln, J., 2014, “A review of fatal accident incidence rate trends in fishing”, *International Maritime Health* 65 (2), pp. 47-52.
- Míguez González, M., López Peña, F., Díaz Casás, V., Neves, M.A.S., 2011, “Large Amplitude Roll Motion Forecasting through an Artificial Neural Network System”, Proc. 12th International Ship Stability Workshop, (ISSW 2011), Washington D.C., U.S., pp. 219-224.
- Míguez González, M., Caamaño Sobrino, P., Tedín Álvarez, R., Díaz Casás, V., Martínez López, A., López Peña, F., 2012, “Fishing vessel stability assessment system”, *Ocean Engineering* 41, pp. 67-78.
- Míguez González, M., Díaz Casás, V., Santiago Caamaño, L., 2016, “Real-time stability assessment in mid-sized fishing vessels”, Proc. 15th International Ship Stability Workshop, (ISSW 2016), Stockholm, Sweden, pp. 201-208.
- Nielsen, J. K., Pedersen, N. H., Michelsen, J., Nielsen, U. D., Baatrup, J., Jensen J. J., Petersen, E. S., 2006, “SeaSense - real-time onboard decision support”, Proc. World Maritime Technology Conference, London, UK.
- Oppenheim A.B., Schafer R.W., Buck J.R., 1999, *Discrete Time-Signal Processing*, Prentice-Hall, Inc, New Jersey, U.S.
- Ovegård, E., Rosén, A., Palmquist, M., Huss, M., 2012, “Operational guidance with respect to pure loss of stability and parametric rolling”, Proc. 11th International Conference on the Stability of Ships and Ocean Vehicles, (STAB2012), Athens, Greece.
- Palmquist, M., Nygren, C., 2004, “Recordings of head-sea parametric rolling on a PCTC”, Annex to IMO Document SLF47/INF.5 (see also SFL47/6/6) submitted by Sweden, 10 June.
- Terada, D., Tamashima, M., Nakao, I., Matsuda, A., 2016, “Estimation of the metacentric height by using onboard monitoring roll data based on time series analysis”, Proc. 15th International Ship Stability Workshop, (ISSW 2016), Stockholm, Sweden, pp. 209-215.
- Umeda, N., Francescutto, A., 2016, “Current state of the second generation intact stability criteria-achievements and remaining issues”, Proc. 15th International Ship Stability Workshop, (ISSW 2016), Stockholm, Sweden, pp. 13-15.
- Viggosson, G., 2009, “The Icelandic Information System on Weather and Sea State”, Seminar on Fishing Vessels’ Crews and Stability, World Fishing Exhibition, Vigo, Spain.
- Wolfson Unit, 2004, “MCA Research Project 530. Simplified presentation of fishing vessels stability information. Phase 1. Final Report”, Wolfson Unit, University of Southampton, U.K.
- Womack, J., 2002, “Small commercial fishing vessel stability analysis. Where are we now? Where are we going?”, Proc. 6th International Ship Stability Workshop, (ISSW 2002), Webb Institute, U.S.

This page is intentionally left blank

Session 9
Stability of high-speed craft

Session Chairs
Frans van Walree
Anders Rosén
Toru Katayama

A Motion Estimation Method of High Speed Craft in Irregular Sea by using Onboard Monitoring Motion Time Series Data for Motion Control

Daisuke Terada, *National Defense Academy*, dterada@nda.ac.jp

Ryosuke Amano, *Osaka Prefecture University*

Toru Katayama, *Osaka Prefecture University*, katayama@marine.osakafu-u.ac.jp

ABSTRACT

In order to establish a control method for automatic dangerous situations avoidance using an onboard monitoring ship motions data, a time series model for model predictive control is investigated. A radial basis function-based state-dependent autoregressive (RBF-AR) model is selected, since it is confirmed that the model is effective to predict nonlinear phenomena. As to the parameter estimation of RBF-AR coefficients and so on, the structured parameter optimization method is focused on, moreover it is improved that their method to an algorithm to realize on-line analysis. In order to verify the effectiveness of the proposed modeling procedure, off-line analysis using model experiment data is carried out. As the results, it is confirmed the effectiveness of the proposed procedure, although several future tasks exists.

Keywords: *RBF-AR model, AIC, Simplified structured parameter optimization method.*

1. INTRODUCTION

Planing crafts in irregular seas are subject to excessive acceleration due to the waves they encounter. In the worst case, marine accidents such as injuries of passengers and crew and hull damage occur (e.g. Japan Marine Accident Tribunal 2017). In order to prevent such the situation, it is necessary for ship's crews to understand the characteristics of encounter waves. This is called "sharp lookout" in maritime terms.

As to a way of the sharp lookout, there are visual observation and RADAR and so on. If a captain, officers and crews, namely, ship operators can handle the situation well, then basically it can prevent marine accidents caused by waves by the sharp lookout with these ways. If such a premise does not satisfy, then marine accidents occur as described above. Therefore, in order to prevent marine accidents under wave conditions beyond the capacity of ship operators, it is necessary to develop a system that supports decision making of ship operators and an automatic control system to avoid dangerous situations. To realize this purpose simply, it is necessary only to monitor the ship motions appropriately according to the knowledge of statistical science. In recent years, many inexpensive

and highly reliable measuring devices have been developed, so the monitoring of ship motions has become relatively easy (Sasa et al., 2015). Thus, the idea as the mentioned here is feasible.

As to a general displacement type ship, a decision making support system using ship motions data had been already proposed by Iseki and Terada (2001). However, there are no studies on decision making support systems in planing crafts. With regard to the automatic dangerous situation avoidance system, neither research on displacement type nor research on planing crafts has been conducted. The reason for this is that because the motion of the planing craft is highly nonlinear, it is difficult to construct a mathematical model or a time series model.

In this research, a time series model for model predictive control is investigated for the purpose of establishing a control method for automatic dangerous situations avoidance using an onboard monitoring ship motions data. A radial basis function-based state-dependent autoregressive (RBF-AR) model (Vesin, 1993) as a time series model to predict nonlinear phenomena is focused on. As to the modeling procedure of it, the parameter estimation procedure proposed by Peng et al. (2002)

is focused on, because it can realize the stable computation for the parameter estimation. In order to verify the effectiveness of the model, off-line analysis using model experiment data is carried out. Obtained findings are reported in detail.

2. RADIAL BASIS FUNCTION-BASED STATE-DEPEND AUTOREGRESSIVE MODELING PROCEDURE

The RBF-AR model is expressed as

$$y_n = \phi_0(\mathbf{x}_{n-1}) + \sum_{i=1}^L \phi_i(\mathbf{x}_{n-1})y_{n-i} + \varepsilon_n \quad (1)$$

where y_n is the measured time series and ε_n is the normally distributed white noise in the observed noise with mean 0 and variance σ^2 , and

$$\mathbf{x}_{n-1} = [y_{n-1}, y_{n-2}, \dots, y_{n-n_x}]^T \quad (2)$$

$$\mathbf{z}_k = [z_{k,1}, z_{k,2}, \dots, z_{k,n_x}]^T \quad (k = 1, \dots, M) \quad (3)$$

$$\phi_0(x_{n-1}) = c_0 + \sum_{k=1}^M c_k \exp\left(-\lambda_k \|x_{n-1} - z_k\|_2^2\right) \quad (4)$$

$$\begin{aligned} \phi_i(x_{n-1}) &= c_{i,0} \\ &+ \sum_{k=1}^M c_{i,k} \exp\left(-\lambda_k \|x_{n-1} - z_k\|_2^2\right) \end{aligned} \quad (5)$$

where z_k denotes the center of the RBF network, and λ_k is the scaling parameter. c_k ($k = 0, \dots, M$) and $c_{i,k}$ ($k = 0, \dots, M$) are the weighting coefficients, L and M are the orders of regression, n_x is the dimension of vector \mathbf{x}_{n-1} , and $\|\cdot\|_2$ is the L2 norm, respectively.

The unknown parameters in equation (1) are estimated using a method introduced by Peng et al. (2002). In this method, by assigning suitably assumed values for z_k and λ_k , the problem changes into that of the least squares estimation of the linear parameters c_k and $c_{i,k}$. Subsequently, the estimated values to the linear parameters are assigned and z_k and λ_k are estimated by the Levenberg–Marquardt method, which is a nonlinear optimization method. Iterative calculations are then performed until the convergence condition is satisfied and the final estimates of each parameter are obtained. The best model is determined by using the Akaike

information criterion (AIC) (Akaike, 1974) shown in equation (6).

$$\begin{aligned} \text{AIC} &= N \log \hat{\sigma}^2 + 2(s + 1) \\ &\text{for } N \gg \max(L, M) \end{aligned} \quad (6)$$

where N is the data number for the fitting of the RBF-AR model, and $\hat{\sigma}^2$ is the variance of the residual of the fitting, and s is the total number of the parameters.

In order to evolve a process suitable for online analysis, the method adopted in the present study skips the iterative calculation of cases where the fitting in the initial calculation is poor. Thus, we were able to neglect the unnecessary calculations for model selection.

3. TECHNIQUE FOR FAST COMPUTATION OF PARAMETERS

In this study, as mentioned before, the planing craft which is high speed as the target ship is focused on. Thus, in order to perform the on-line analysis, it is needed to calculate at high speed for the parameter estimation. Then, in order to evolve a process suitable for on-line analysis, the method adopted in the present study skips the iterative calculation of cases where the fitting in the initial calculation is poor. That is, it is able to neglect the unnecessary calculations for model selection. By this processing, high speed calculation for the modeling is realized.

4. OFF-LINE ANALYSIS USING MODEL EXPERIMENT DATA

4.1 Outline of model experiments

To verify the effectiveness of the proposed procedure, an off-line analysis using model experiment data is conducted. In the model experiment, the object ship is toward at the constant speed in irregular waves, and the vertical acceleration of the bow is measured by an acceleration sensor made by Kyowa Electronic Instruments Co., Ltd. That is, the object ship is towed at 25 knots in actual scale, and the acceleration measurement is done at the sampling interval 200 Hz. Fig. 1 shows the experimental set up and the definition of coordinate system. As shown this figure, the acceleration upward is positive. Table 1 and Fig. 2 show principal particulars in the actual

scale and the body plan of the object ship, respectively. Table 2 shows the wave condition in the actual scale. In this case, the mean period of waves is calculated by the Equation (7). Equation (8) shows the shape of spectrum proposed by the International Ship and Offshore Structures Congress (ISSC, 1964), and irregular waves are reproduced based on this equation.

$$T_1 = 3.86\sqrt{H_{1/3}} \quad (7)$$

$$S(\omega) = \frac{0.11}{2\pi} H_{1/3}^2 T_1 \left(\frac{\omega T_1}{2\pi}\right)^{-5} \times \exp\left\{-0.44\left(\frac{T_1}{2\pi}\omega\right)^{-4}\right\} \quad (8)$$

where, ω is an angular frequency of waves.

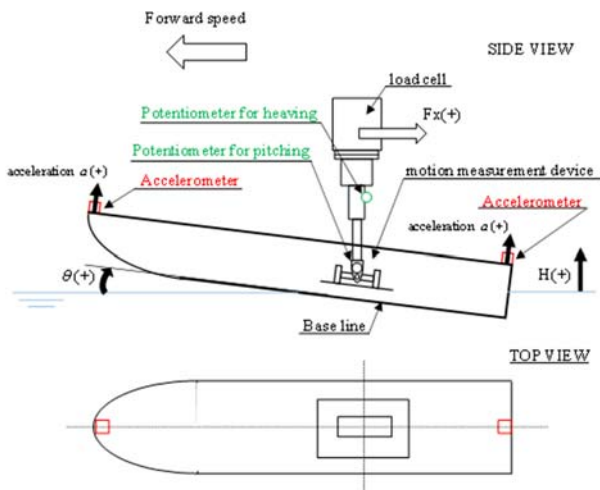


Figure 1: Schematic view of experimental set up and the definition of coordinate system.

Table 1: Principal particulars of the object ships in actual scale.

Scale of model: 1/s	1/23.4
Water line length: L_{WL} [m]	21.46
Breadth: B [m]	4.0
Deadrise angle at s.s. 5: β [deg]	16.0
Draft: d [m]	0.76
Displacement [ton]	37.0

Table 2 Wave condition in actual scale.

Significant wave height $H_{1/3}$ [m]	2.0
Mean wave period T_1 [s]	5.5

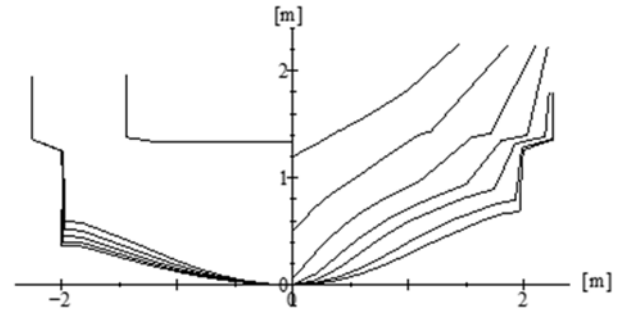


Figure 2: Body plan of the target ship.

4.2 Example of prediction results

In this subsection, the one example of prediction results is shown. As to the prediction based on the RBF-AR modeling, from the view point of computational time, it is decided that the maximum of model order L is 10, the maximum value of the number of center of the RBF network M is 3 and the maximum value of the dimension n_x of state vector is 3, respectively. Here, Fig. 3 shows the result of the 30th step ahead prediction, namely the prediction for 1.5 seconds, in which the number of data N for the fitting of the RBF-AR model, which is called "Batch data", is 300. In this figure, the horizontal axis indicates the time, and the vertical axis indicates the vertical acceleration. Moreover, the black line indicates the measured data in the experiment, and the dotted red line indicates the predicted one. As you can see, the predicted data captures the tendency of the measured one. Thus, it is considered that the proposed procedure has the possibility to predict the vertical acceleration such that the strong nonlinearity.

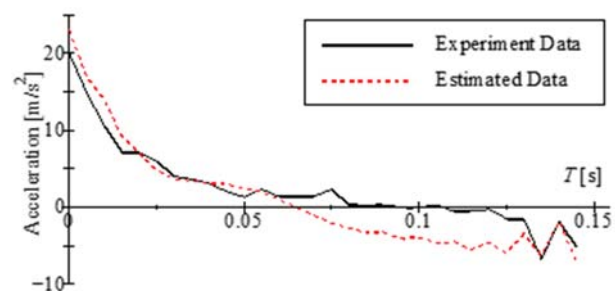


Figure 3: Comparison with the measured time history and predicted vertical acceleration. Note that this figure does not include the data set of the analysis.

4.3 Verification of accuracy

In the previous subsection, the usefulness of the proposed procedure is confirmed.

In this subsection, as to the recursive fitting of the RBF-AR model, the accuracy of the proposed procedure in detail more is verified. That is, the several off-line analysis in which the number of prediction step and the number of data N for the fitting of the RBF-AR model are changed is carried out. The conditions for the verification is summarized in Table 3. Here the measured data as a notation A_{Exp} , and the predicted one as a notation A_{Pre} are defined respectively. Firstly, the dispersion relationship between the A_{Exp} and the A_{Pre} based on a root mean squares (RMS) of them, which expresses the following equation, is investigated.

$$\text{RMS} = \sqrt{\frac{1}{n_{(Pre)}} \sum_{i=1}^{n_{(Pre)}} (A_{Exp}(i) - A_{Pre}(i))^2} \quad (9)$$

In this case, it is evaluated that “RMS > 500 (m/s²)” is a failed prediction. Fig. 4 shows one of the example for the time series of RMS and measured vertical acceleration. In this figure, the horizontal axis indicates the time, the left side vertical axis indicates the measured vertical acceleration and the right side vertical axis indicates the RMS. Moreover, the upper figure shows the result of the condition in which $N=400$ and $n_{(pre)}=30$, and the lower figure shows the result of the condition in which $N=500$ and $n_{(pre)}=5$. From these figures, it can be seen that when an impact acceleration occurs, the value of RMS exceeds the threshold value 500 and the evaluation of the result is the failed prediction. This tendency regarding other cases is also confirmed, although the ratio of divergence varies depending on the combination of the N and $n_{(pre)}$. This result is caused by calculating RMS using all values in the prediction period $n_{(pre)}$. Basically, the phenomena dealt with here is strongly nonlinear. Therefore, even if the prediction of several steps ahead can be achieved successfully, there are many events in which the prediction result diverges in the subsequent prediction period. The results shown here express this fact well and it is necessary to decide the prediction period after making sufficient consideration. It should be noted that as to one ahead prediction the result can predict the measured one well.

Table 3: Conditions for the verification.

Number of the Batch Data for the model fitting: N	50, 100, 200, 300, 400, 500
Number of the prediction period: $n_{(Pre)}$	5, 10, 20, 30

It is certain that there are cases where it can be predicted well, although there are the failed prediction in the several conditions. Thus, the all combinations of the N and the $n_{(pre)}$ as shown in Fig. 5 are investigated secondly. In this figure, the horizontal axis indicates the N , and the vertical axis indicates the rate in which RMS diverges, respectively. As to each symbol, as shown in the figure, the circle indicates the results of $n_{(pre)}=5$, the square indicates the results of $n_{(pre)}=10$, the diamond indicates the results of $n_{(pre)}=20$, and the triangle indicates the $n_{(pre)}=30$, respectively. This figure shows the following.

- (1) The more N and the less $n_{(pre)}$, the rate in which RMS diverges is smaller.
- (2) When the N exceeds 400 samples, the ratio of divergence is almost the same.

Therefore, it is considered that as to the data number N for the model fitting, it is desirable to use more than 400 samples, although the problem of the computational time for the model fitting exists.

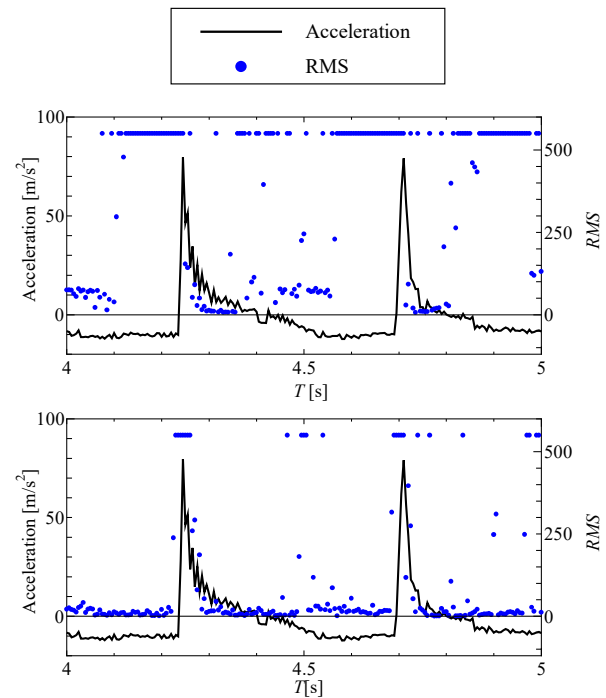


Figure 4: Time series of RMS and measured vertical acceleration; Upper figure: $N=400$, $n_{(pre)}=30$, Lower figure: $N=500$, $n_{(pre)}=5$.

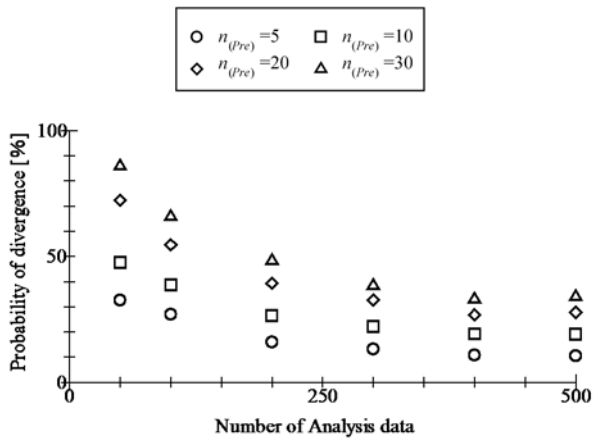


Figure 5: The ratio of divergence of RMS for each conditions for verification.

5. CONCLUSIONS

In this research, a time series model for model predictive control in order to establish a control method for automatic dangerous situations avoidance using an onboard monitoring ship motions data is investigated. Concretely, a radial basis function-based state-dependent autoregressive (RBF-AR) model as a time series model to predict nonlinear phenomena is focused on. As to the modeling procedure of it, the structured parameter optimization method as the parameter estimation procedure is focused on, their method to an algorithm for realizing on-line analysis is improved. In order to verify the effectiveness of the model, off-line analysis using model experiment data is carried out. Obtained findings are summarized as follows:

- (1) As to the prediction used the Batch Data, it can be seen that the predicted results are good agreement with the measured data as shown in the subsection 4.2. Therefore, the proposed procedure is useful for the prediction of the vertical acceleration in the batch data analysis.
- (2) As to the recursive fitting of the RBF-AR model, the predicted results diverge sometimes in meaning of the root mean square (RMS). This cause is the calculation of the RMS using all values in the prediction period.
- (3) However, the more data for the model fitting and the less prediction period, the rate in which RMS diverges is smaller. Moreover, if the data for the model fitting exceeds 400 samples, then the ratio of divergence is almost the same.

As a future task, it is needed to investigate to improve the accuracy of prediction.

6. ACKNOWLEDGEMENT

A part of the present study is supported by This work was supported by JSPS KAKENHI Grant Number 17K06978 and Fundamental Research Developing Association for Shipbuilding and Offshore (REDAS). We are grateful for the support.

REFERENCES

- Akaike, H., 1974, "A new look at the statistical model identification", *IEEE Trans. Autom. Control* vol. 19, pp. 716–723.
- Iseki, T. Terada, D., 2002, "Bayesian estimation of directional wave spectra for ship guidance system", *International Journal of Offshore and Polar Engineering*, Vol. 12, No. 1, pp.25–30.
- ISSC, 1964, "Report of the Committee 1. Environmental Conditions", *Proceedings of 2nd ISSC*.
- Japan Marine Accident Tribunal, 2017/04/11(accessed), "<http://www.mlit.go.jp/jmat/saiketsu/saiketsu.htm>" (In Japanese).
- Peng, H., Ozaki, T., Haggan-Ozaki, V. and Toyoda, Y., 2002, "Structured parameter optimization method for the radial basis function-based state-dependent autoregressive model", *Int. J. Systems Science*, vol. 33(13), pp. 1087–1087.
- Sasa, K., Terada, D., Shiotani, S., Wakabayashi, N., Ikebuchi, T., Chen, C., Takayama, A, Uchida, M, 2015, "Evaluation of ship performance in international transportation using an onboard measurement system – in case of a bulk carrier in international voyages", *Ocean Engineering*, Vol. 104, pp.294–309.
- Vesin, J., 1993, "An amplitude-dependent autoregressive signal model based on a radial basis function expansion", in *Proc. ICASSP*, vol. 3, pp. 129–132.

This page is intentionally left blank

High-speed craft dynamics in waves: challenges and opportunities related to the current safety philosophy

Anders Rosén, *KTH Royal Institute of Technology, Stockholm, Sweden*, aro@kth.se

Ermina Begovic, *University of Naples “Federico II”, Naples, Italy*, begovic@unina.it

Mikael Razola, *SSPA, Stockholm, Sweden*, mikael.razola@sspa.se

Karl Garne, *KTH Royal Institute of Technology, Stockholm, Sweden*, garne@kth.se

ABSTRACT

This paper considers the assessment of vertical accelerations of high speed planing craft in waves as the principal element for the risk management approach, i.e. formulation and application of operational limitations and operational guidance. Semi-empirical methods used by classification societies for vertical acceleration assessment are scrutinized. Insights from model experiments performed at the University of Naples “Federico II” (UNINA) and simulations performed at the Royal Institute of Technology (KTH) are presented. Deficiencies of the prevailing semi-empirical methods, and challenges and opportunities with a combined experimental-numerical approach, are discussed in perspective of the IMO high-speed craft safety philosophy.

Keywords: *high-speed craft, impact accelerations, experiments, simulations, safety philosophy, IMO HSC Code, class rules*

1. INTRODUCTION

High-speed craft operating in planing modes are subject to numerous stability related hazards, e.g.: reduction of transverse stability with increasing speed; chine tripping; chine walking; porpoising; bow diving; and directional instabilities such as surf-riding/broaching. The major limiting factor for high-speed planing craft in waves is however generally the hydrodynamic slamming loads and the related vertical impact accelerations occurring at violent wave encounters (Savitsky & Koelbel 1993). These vertical accelerations might impair the ability of the crew to carry out their duties and have adverse effects on their health and safety (e.g. Begovic et al 2015, de Alwis & Garne 2017). If not considered properly these impact loads might also impair the functioning of machinery and other on-board systems and the integrity of the hull structure (IMO 2008).

The safety philosophy of the IMO HSC Code is that an appropriate safety level can be achieved based on active management and reduction of risk in combination with the traditional philosophy of passive in-built safety (IMO 2008). Some of the key elements in this risk management approach are the formulation and application of *operational limitations* in terms of service area restrictions

(typically maximum distance to safe port) and speed reductions in heavy weather, and *operational guidance* to the crew typically in terms of signboards in the wheelhouse stipulating the maximum allowable speed as function of significant wave height (IMO 2008, DNVGL 2015).

As described for example in Savitsky & Koelbel (1993), a number of different aspects can be seen as limiting the speed in waves. If all these aspects are combined, the allowable speed-wave height envelope can be formulated as illustrated for a hypothetical high-speed planing craft in Figure 1.

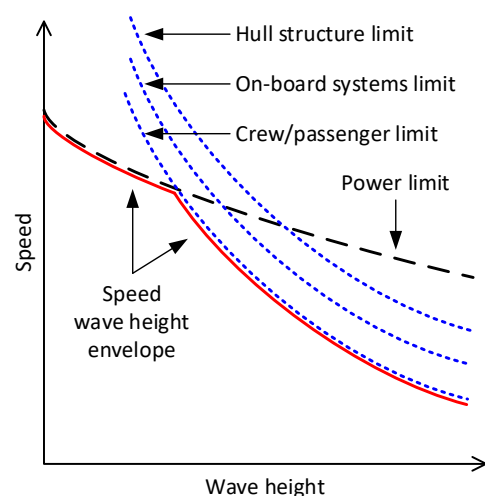


Figure 1: Different aspects limiting the speed in waves and definition of the speed-wave height envelope.

For the hypothetical craft in Figure 1, the added resistance in waves in relation to the installed power would, as seen, result in involuntary speed reduction up to a certain wave height. In higher waves the vertical accelerations would be intolerable to the crew, and to enable their continued on-board duties and to protect their health and safety, the crew would voluntarily reduce the speed. The installed power and crew tolerance related speed reductions would in this case, as seen in Figure 1, give safety margins for the on-board systems and the hull structure. Some safety margins might be good. However, if the structure is designed to withstand loads that are much larger than the crew/passengers can tolerate or the installed power can generate, that would imply an over-dimensioned and unnecessarily heavy structure, which in turn would imply a less efficient craft.

It is in the hands of the designer to create good balance between safety and performance for the craft in its intended operation, by balancing the installed power, the crew/passenger and systems situation and tolerances, and the structure load carrying capacity. The speed-wave height envelope could be formulated either as a target for, or as a consequence of, the design decisions. It is then in the hands of the crew to operate the craft with active consideration of the stipulated speed-wave height envelope, to achieve as high performance as possible without endangering safety and functionality.

The IMO high-speed craft safety philosophy and related classification rules (e.g. DNVGL 2015, RINA 2009) certainly opens up for design optimization. A craft could for example be optimized for its “normal” operating conditions taking into account well informed speed reductions in more rarely occurring rougher conditions. In practice, however, designers’ abilities to create such balanced and optimized designs, and crews’ abilities to judge the operational conditions and operate the craft within detailed speed-wave height limits, are still rather limited. There is also a large knowledge gap regarding the effects on health and work ability for high-speed craft crew in rough conditions (e.g. de Alwis & Garne 2017).

An obvious limitation is in the prevailing methods for assessing slamming loads and vertical accelerations in waves. Here state-of-the-art is still the semi-empirical formulas developed by Savitsky & Brown (1976) and Allen & Jones (1978) as

implemented in classification rules such as DNVGL (2015), RINA (2009), and ISO (2008). These formulas are good in that they are well established and that they, with very limited effort and resources, enable determination of design pressures and speed-wave height limit curves that can be provided as operational guidance to the crew. However, the limitations of these methods are obvious and their accuracy has been extensively questioned (e.g. Koelbel 1995, Rosén et al 2007, Grimsley et al 2010, McCue 2012, Bowles & Soja 2014, Razola et al 2014, Razola et al 2016, Begovic et al 2016).

An obvious potential for improvement would be to use direct assessment methods, either experimental or numerical or a combination. Due to the high speed, the high level of non-linearity, the transient nature of the loads and responses, and the randomness of the waves and responses, the situation of a high-speed planing craft in waves is however very challenging to model, experimentally as well as numerically.

This paper presents lessons learned from extensive model experiments performed at the University of Naples “Federico II” (UNINA) and simulations performed at the Royal Institute of Technology (KTH). The prevailing semi-empirical methods for assessing high-speed craft dynamics in waves are scrutinized and challenges and opportunities related to establishing alternative direct assessment methods are discussed. Finally the presented findings are discussed in perspective of the IMO high-speed craft safety philosophy and the Second Generation Intact Stability Criteria.

2. EXPERIMENTS

The experimental campaign, basis of this work, has been presented extensively in Begovic et al (2012, 2014, 2016). Here some important information is recalled. The tested model has a mathematical monohedral hull with parabolic bow and a constant deadrise angle of 16.7 deg. The deadrise is chosen as representative for modern planing hull design trends for the aft part. The parabolic bow section makes the model comparable with the Fridsma (1971) models having 10, 20 and 30 degrees. Many previous experiments have been performed in sea states which could be considered to be too severe for small high-speed planing craft, typically $H_{1/3}/B_C = 0.222, 0.444$ and 0.666 . This

experiment is hereby filling a gap by focusing on $H_{1/3}/B_C$ lower than 0.2.

Seakeeping tests were performed at the University of Naples “Federico II” Towing Tank (135m x 9m x 4.2m). Before performing seakeeping tests, the model centre of gravity location and relevant radii of gyration were measured by an inertial balance and are reported in the Table 1. The model was towed at constant speed in head seas, free to heave and pitch and restrained for all other motions and connected to the towing carriage through a mechanical arm apt to measure heave and pitch, as shown in Figure 2. Two Cross Bow CXL04GP3-R-AL accelerometers were installed: one at the CG position and one at the bow. Encountered waves were measured by two BAUMER UNDK 301U6103/SI4 ultrasonic gauges, the former located on the side at LCG, the latter at centreline, 3.48 m ahead from CG. Four different speeds have been tested: 3.40, 4.60, 5.75 and 6.30 m/s, corresponding to volumetric Froude numbers: 1.92, 2.60, 3.25 and 3.57. All experiments were performed in irregular waves representing a JONSWAP sea spectra with target significant wave height 0.055 m, spectral peak period 1.17 s, and peak factor 3.3. All data were sampled at 500 Hz.

Table 1: UNINA model principal characteristics.

Length (over all)	L	m	1.900
Width (chine)	B	m	0.424
Deadrise	β	deg	16.7
Displacement	Δ	kg	32.56
Draught (aft perp.)	T	m	0.096
Static trim	τ	deg	1.66
Long. centre of gravity	LCG	m	0.697
Vert. centre of gravity	VCG	m	0.143
Pitch gyradius	k_{55-air}/L	-	0.307



Figure 2: UNINA model experimental set up (photo at model speed $V = 5.75\text{m/s}$).

3. SIMULATIONS

Simulations are here performed on the same craft using a non-linear time-domain strip method developed at the KTH Royal Institute of Technology (Garme 2005, Garme & Rosén 2003). The simulation approach is in the tradition of Zarnick (1978). The 2-d hydrodynamic coefficients are initially determined by a panel method for a set of different draughts, here 121. The coefficients in the equations of motions are up-dated at every time step during a predictor-corrector time-stepping procedure and the solution describes the non-linear situation of the planing hull in head waves. During the simulation, pre-calculated hydrostatic and hydrodynamic coefficients are collected with reference to the momentary sectional draught. The hydrostatic coefficients are defined relative to the wave surface level and the dynamic coefficients relative to the piled-up surface level. The hydrodynamic section loads are determined as the momentary time rate of change of fluid momentum both for chines-wet and chines-dry parts of the hull. The decrease of pressure close to the transom stern, not caught by the 2-dimensional theory, is treated by a semi-empirical correction of the load distribution. The simulation model has been successfully validated for speeds corresponding to Froude number based on ship width, C_v , larger than 2. Simulations are here performed with a time step 0.0016 s in the same speeds and wave conditions as the experiments. Self repetition is avoided in the realization of the irregular waves.

The code is not optimized for speed and the cpu-time, for modelling HSC in irregular waves by running the code on a standard computer, is in the order of 10 times real-time. Nevertheless, it is considered absolutely feasible to lessen this to a one-to-one relation, simply by efficient programming in a faster language.

4. SOME OBSERVATIONS FROM THE EXPERIMENTS AND SIMULATIONS

The purpose here is to highlight some important observations from the performed experiments and simulations and discuss the capabilities of these two modelling approaches.

According to ITTC (1999) a minimum of 100 wave encounters is recommended for testing high-speed craft in irregular head seas. Due to the high speed and the time needed for accelerating and

decelerating the model, even in a long towing tank a large number of repeated test runs are required to achieve appropriate number of wave encounters. In the here presented experiments repeated tests resulted in 280 wave encounters at constant speed of 3.40 and 4.60 m/s, 230 for a speed of 5.75 m/s, and 160 for a speed of 6.30 m/s. When evaluating the results the constant speed parts of the different runs have been spliced together for each speed. The here used simulation model has been developed with concern regarding the trade-off between accuracy and computational effort to allow for long simulations in irregular waves. In the here presented study the simulation time in irregular waves is 1000 s giving more than 700 wave encounters in each speed.

In Table 2 and Table 3 the standard deviation and the mean values of the peak-to-peak zero-crossing amplitudes of the heave and pitch responses are presented. As seen the agreement between the experiments and the simulations is very good for pitch and reasonably good for heave, particularly for the peak-to-peak amplitudes. For the heave at 4.60 m/s the simulated mean peak-to-peak amplitude is however distinctly larger than the experimental.

Table 2: The heave standard deviation, $\eta_{\beta\sigma}$, and the mean peak-to-peak amplitudes, $\eta_{\beta m}$, from experiments and simulations. Relative errors are also presented.

v [m/s]	$\eta_{\beta\sigma,exp}$ [m]	$\eta_{\beta\sigma,sim}$ [m]	E_{σ} [%]	$\eta_{\beta m,exp}$ [m]	$\eta_{\beta m,sim}$ [m]	E_m [%]
3.40	0.0040	0.0040	0.0	0.0096	0.0096	0.0
4.60	0.0042	0.0050	19.0	0.0099	0.0115	16.2
5.75	0.0044	0.0052	18.2	0.0108	0.0115	6.5
6.30	0.0046	0.0053	15.2	0.0111	0.0116	4.5

Table 3: The pitch standard deviation, $\eta_{\gamma\sigma}$, and the mean peak-to-peak amplitudes, $\eta_{\gamma m}$, from experiments and simulations. Relative errors are also presented.

v [m/s]	$\eta_{\gamma\sigma,exp}$ [m]	$\eta_{\gamma\sigma,sim}$ [m]	E_{σ} [%]	$\eta_{\gamma m,exp}$ [m]	$\eta_{\gamma m,sim}$ [m]	E_m [%]
3.40	0.499	0.464	-7.0	1.120	1.180	5.4
4.60	0.478	0.462	-3.3	1.157	1.139	-1.6
5.75	0.427	0.429	0.5	0.977	1.003	2.7
6.30	0.430	0.424	-1.4	0.999	0.973	-2.6

The characteristic transient nature of the slamming related vertical accelerations for high-speed craft in waves is seen in Figure 3 and Figure 4 which show examples from experiments and simulations for a model speed of 5.75 m/s. It should be noted that the experiments and simulations are performed in different realizations of the same sea state. Direct comparison between the measured and

simulated signals in the time domain is therefore not relevant. Instead statistical analysis is required for detailed comparison between experiments and simulations.

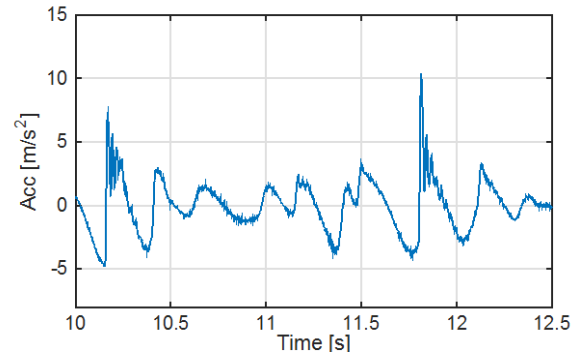


Figure 3: Example of vertical acceleration data from experimental measurements at $v=5.75$ m/s.

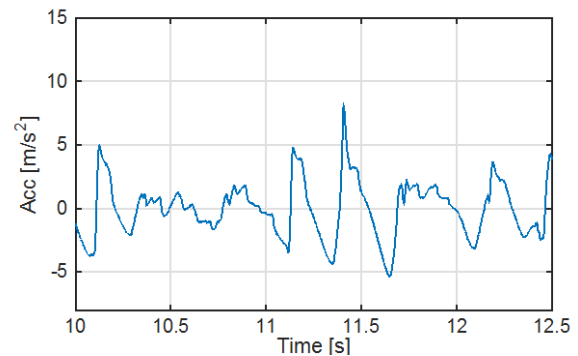


Figure 4: Example of simulated vertical acceleration data at $v=5.75$ m/s.

The vertical acceleration process for high-speed craft in irregular waves is generally characterized in terms of statistical peak fraction averages, such as the average of the largest 1/10th or 1/100th of the peak acceleration values. Defining and identifying peaks related to rigid body acceleration in signals as the ones in Figure 3 and Figure 4 is far from trivial. In this study the peak values are here identified according to Razola et al (2016) which in turn principally follows the Standard-G approach by Riley et al (2010). The vertical threshold value is set to the standard deviation of the acceleration process, and the horizontal threshold is set based on the encounter frequency.

The convergence of various statistical measures are exemplified in Figure 5 for simulations at $v=5.75$ m/s. The experimental results show a similar pattern. As seen the average of the largest 1/100th peak values would require 500 or more peaks for convergence. This is far more than what is generally achieved in experiments. The lower level averages (1/3rd and 1/10th) can however be considered to reach

reasonable convergence with the number of wave encounters realized in the here presented experiments, maybe with exception from the average of the largest 1/10th peak values at the highest speed where only 160 wave encounters are measured. More on statistical analysis of high-speed craft vertical impact accelerations can for example be found in Razola et al (2016), Begovic et al (2016), and Katayama & Amano (2015).

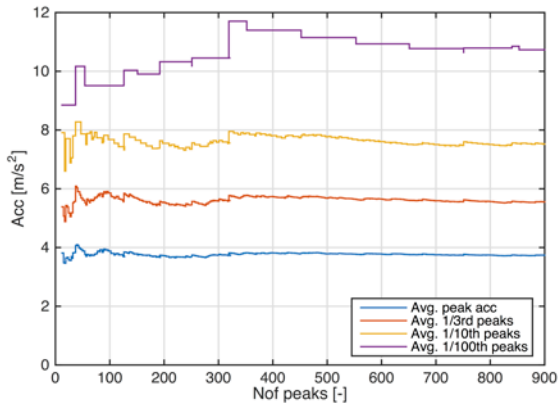


Figure 5: Convergence of the statistical measures of the peak acceleration process for the simulated data for $v=5.75$ m/s.

Another challenge is the non-rigid body vibrations which are very difficult to completely eliminate in experiments due to flexibilities in the model structure and vibrations in the towing carriage. Such vibrations are for example seen in Figure 3. According to the frequency spectra in Figure 6 these vibrations are mainly found in the frequency range $\sim 30-40$ Hz. Unfortunately this is in the same time scale as the slamming process and typical rise times of the vertical acceleration signal at impact. This affects the experimental data where the peak values to some extent will be amplified by the vibrations.

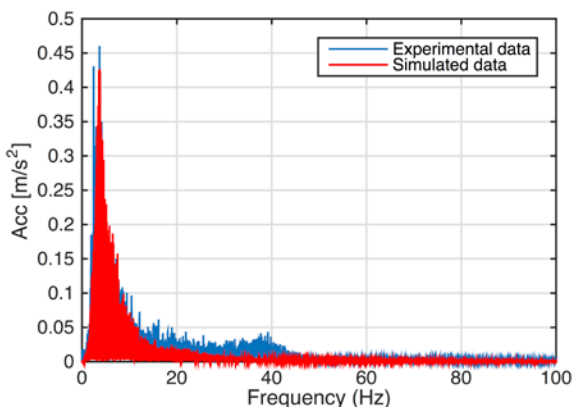


Figure 6: Single-sided frequency spectrum for the experimental and simulated acceleration data for a speed of $v=5.75$ m/s.

However, by considering the fact that the numerical model only simulates the rigid body motions, the simulated and experimental data can be combined to determine an appropriate frequency level for low-pass filtering of the experimental data. In Figure 7 peak acceleration statistics for a model speed of 5.75 m/s is displayed as function of low-pass filtering cut-off frequency using a 4th order Butterworth filter. As seen, for the simulated signals the statistics are principally unaffected for cut-off levels down to 25-30 Hz. The largest peaks might be affected by filtering on that level, however only to a degree that is not captured by the here studied statistics. On the other hand the experimental statistics is clearly affected at cut-off levels below 60 Hz. Based on such analysis a low-pass cut-off level of 30 Hz can be concluded to be appropriate for these experiments. An approach for eliminating towing carriage vibrations could be to use a free-running model as demonstrated in Savitsky (2016).

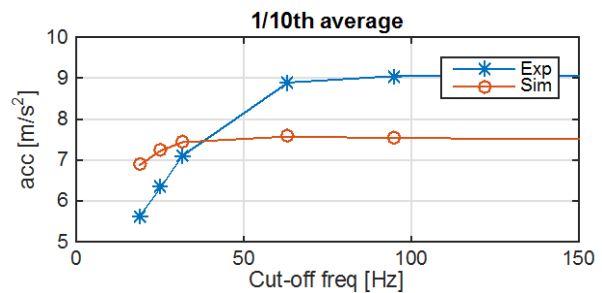


Figure 7: Effect of the low-pass filtering frequency on the acceleration peak statistics for a speed of $v=5.75$ m/s.

In Figure 8 the peak fraction average statistics is compared between experimental data low-pass filtered at 30 Hz and unfiltered simulated data. As seen the agreement is good for the higher speeds where the differences are in the order of a few percent. The lower speed $v=3.60$ m/s corresponds to a Froude beam number $C_v=1.77$ which is smaller than the validated speed regime for the simulation model, $C_v>2.0$. This could explain the difference between the experiments and simulations at this speed.

The results from this limited study are encouraging and indicates promising capabilities of the presented experimental setup and the numerical approach in capturing the slamming related vertical acceleration process for high-speed planing craft in waves. More thorough evaluations will come in a later paper.

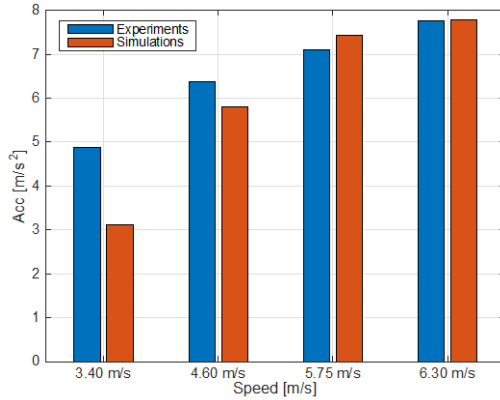


Figure 8: Comparison of the average of the 1/10th highest acceleration peaks from experiments low-pass filtered at 30 Hz and unfiltered simulations.

5. SPEED-WAVE HEIGHT LIMITS

The state-of-the-art approach for deriving speed-wave height limit curves as in Figure 1, is to use formulas relating craft vertical acceleration, speed and wave height, provided by classification societies. These formulas can all be derived back to the semi-empirical formula presented in Savitsky & Brown (1976), which in turn was derived based on the model experiments by Fridsma (1971). According to Savitsky & Brown the average of all acceleration peak values, when a high-speed planing craft is operating in V knots in irregular head seas with a significant wave height $H_{1/3}$, is given by

$$a_{1/1} = 0.0104 \left(\frac{H_{1/3}}{B} + 0.084 \right) \frac{\tau}{4} \left(\frac{5 - \beta}{3 - 30} \right) \left(\frac{V}{\sqrt{L}} \right)^2 \frac{L/B}{C_A} \quad (1)$$

where L , B , τ , β , and C_A are craft length, beam, trim, deadrise and load coefficient. Savitsky & Brown assumed that the acceleration peak process is exponentially distributed and hereby expressed the statistical average of the $1/N^{\text{th}}$ highest peak values as

$$a_{1/N} = a_{1/1} (1 + \log_e N) \quad (2)$$

As an illustration of the similarities between today's classification rule formulas and the Savitsky & Brown source work, for example the formula by DNVGL (2015) is expressed as

$$a_{cg} = \frac{k_h g_0}{1650} \left(\frac{H_{1/3}}{B} + 0.084 \right) (50 - \beta) \left(\frac{V}{\sqrt{L}} \right)^2 \frac{LB^2}{\Delta} \quad (3)$$

A comparison between different formulas is made in Figure 9 for the craft studied in the experiments and simulations in the previous sections, here however in full-scale where a scale factor 1:10 gives a craft length 19 m, significant wave height 0.55 m, and speeds 21, 28, 35, 39 kn.

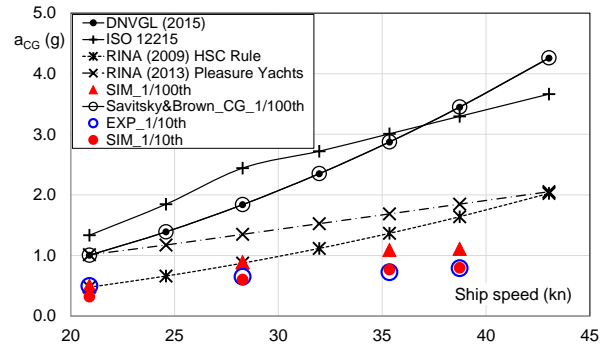


Figure 9: Vertical acceleration at CG in head seas as function of speed according to Savitsky & Brown, various scantling codes, and from the presented experiments and simulations.

The Savitsky & Brown results are here presented on the 1/100th average level. The DNVGL (2015) High-Speed and Light Craft Rules do not specify what statistical level their formula is corresponding to. Figure 9, however, makes it obvious that the DNVGL formula is corresponding exactly to Savitsky & Brown on the 1/100th level. The RINA (2009) HSC Rules on the other hand explicitly defines a design vertical acceleration on the 1/100th average level. However, in Figure 9 it can be observed that the RINA (2009) results are far below the Savitsky & Brown results on the 1/100th level. It can be shown that the RINA (2009) results instead correspond to Savitsky & Brown on a 1/5th average level. Also the RINA (2013) Rules for Pleasure Yachts are claimed to be on the 1/100th average level. As seen however these results are between the Savitsky & Brown 1/100th and RINA (2009) results. The ISO (2008) formula is similar to the Savitsky & Brown formula up to $a_{cg}=3$ g, however with the significant wave height fixed to $H_{1/3}=L/10$ which is much larger than the 0.55 m here used in the other formulas.

Let's consider that the hull structure of a certain high-speed craft (for some reason) should be designed with respect to an overall design acceleration/load factor $a_{cg}=2g$. The corresponding speed-wave height limit curve can then easily be derived by using class formulas, such as equation (3), simply by substituting the constant limiting acceleration $a_{cg}=2g$ and extracting V as function of $H_{1/3}$ from the formula. From Figure 9 and the discussion above it is however obvious that the same design acceleration/load factor would result in very different speed-wave height limits from the different classification rule sets.

As mentioned in the introduction, several previous studies have questioned the Savitsky & Brown method, in particular the assumption that the acceleration peak values would be exponentially distributed. For example in Razola et al (2016) it is shown that calculation of the average of the 1/100th highest acceleration peaks, $a_{1/100}$, by scaling the average of all peaks, $a_{1/1}$, according to equation (2), would give much higher values than if calculated directly from the 1/100th highest acceleration peaks. In the DNVGL (2015) rules this “error” is however fortunate, whether conscious or not, since the Allen & Jones (1978) design slamming pressure as implemented in the DNVGL (2015) rules otherwise would have been significantly under-predicted if the average of the 1/100th highest acceleration peaks would have been correctly calculated. Whether the observed down-scaling of the RINA (2009) accelerations, compared to the Savitsky & Brown 1/100th average, is a conscious consideration of the error in the Savitsky & Brown exponential distribution assumption is not obvious. However, comparing the Allen & Jones (1978) design slamming pressure implementation in DNVGL (2015) and RINA (2009) and the difference in their respective implementations of the Savitsky & Brown accelerations, again makes it obvious that the design acceleration and the related design pressures have different meanings between different classification societies. As long as these different formulas are only used within each rule set it might be ok. However, what actual safety level that is achieved is far from explicit and might be debated.

The previous section demonstrated promising capabilities of the presented experimental and numerical approaches in modelling the characteristics of high-speed planing craft in waves. This might indicate an opportunity to replace the prevailing semi-empirical methods, partly or completely, with direct assessment methods. Applying simulations or experiments in the design of high-speed planing craft however still involves a number of challenges.

As seen, Figure 9 also includes the results from the here presented experiments and simulations on a 1/10th average level from Figure 8 and also simulated values on a 1/100th level. As seen these values, even the simulated values on the 1/100th level, are significantly lower than the corresponding outcomes from the semi-empirical rule formulas, except from

the RINA (2009) results which are in parity with the experimental and numerical results at lower speeds. One obvious explanation for these differences is that the experiments and simulations have only been performed in one sea state where the match between wave mean period and craft speed might not correspond to the worst regarding response resonance. It should also be noted that the here studied wave height is rather low. Another reason for the differences between simulation/experiments and the semi-empirical methods is the above described “error” in the way Savitsky & Brown and the rule formulas calculate the statistical fraction averages resulting in over-prediction. All these aspects must be very carefully considered if the prevailing Savitsky & Brown based semi-empirical approach should be replaced or complemented by experiments or simulations.

Another challenge is the extensive effort involved in applying direct assessment methods compared to semi-empirical methods. Deriving just one point on a speed-wave height limit curve, would require a substantial amount of iterative simulations or experiments to find the speed for each wave height that corresponds to a certain limiting acceleration, e.g. the average of the highest 1/100th acceleration peaks equal to 2g. Additional simulations or experiments would be needed to also take different wave mean periods into consideration, either finding the one resulting in the largest responses or deriving a two-dimensional speed/wave height/wave period limit curve/surface.

Considering that more than 500 wave encounters are required for convergence of the 1/100th average, as observed in the previous section, it can be concluded that a purely experimental approach would be prohibitively expensive. However, as mentioned, the here used simulation model is a rather simple non-linear strip method that has been developed with concern regarding the trade-off between accuracy and computational effort to allow for long simulations in irregular waves. With some further improvements of the code efficiency it should therefore be realistic to actually go through with the number of simulations needed for deriving speed-wave height limits.

An interesting option might be to use a combined approach. The first step could here be to use simulations to derive a speed/wave height/wave period limit curve/surface for an acceleration limit

expressed in terms of the 1/10th average. The second step could be to perform experiments corresponding to a few points on the simulation based limit curve/surface. The outcome from the experiments could then either be used to confirm the simulations or to tune the simulation based limit curve/surface if the experiments are considered to be more accurate than the simulations. Finally the simulations could be used to further scale the limit curve/surface to represent an acceleration limitation in terms of another statistical measure such as the 1/100th average or an extreme value.

6. CONCLUDING REMARKS & OUTLOOK

The paper has presented some lessons learnt and results from an extensive experimental campaign and simulations performed on a high-speed planing craft in waves. Though rather limited, the study is encouraging and indicates promising capabilities of the presented experimental setup and the numerical approach in capturing the vertical impact acceleration processes for high-speed planing craft in waves. The prevailing semi-empirical approach and related classification rule formulas for assessing high-speed craft vertical accelerations, have been reviewed and scrutinized and a number of questions regarding the validity of these methods and the resulting safety levels have been raised. Challenges related to establishing direct assessment methods are highlighted and opportunities with a combined experimental-numerical approach are discussed.

The IMO high-speed craft safety philosophy has high and modern ambitions, opening up for complementing the traditional philosophy of passive in-built safety with active management of risk. By applying *operational limitations* and *operational guidance* there is a potential to achieve optimized designs with appropriate safety levels. Still, as demonstrated in the paper, the prevailing semi-empirical methods for assessing high-speed craft dynamics in waves, and providing guidance to crew, are rather primitive and their validity could be questioned. Based on these observations, and the findings and discussions in the paper, a number of questions could be raised for further consideration:

- a) Is high-speed planing craft design, based on the prevailing semi-empirical methods, nothing but qualified guess work?
- b) How well do we actually know the current safety levels for high-speed craft in waves?

- c) What would be an appropriate safety level?
- d) Are the currently available direct assessment methods mature for being practically applied in high-speed planing craft design? If so, would a combined experimental-numerical approach be feasible?
- e) How should the safety levels be assessed and related to the current safety levels if/when direct assessment methods are established?
- f) Despite the highlighted limitations and deficiencies in the prevailing semi-empirical methods, the IMO high-speed craft safety philosophy is actually in place and applied both by designers and crews. Could something be learnt from this when establishing the *Second Generation Intact Stability Criteria*, for example regarding risk management, the concepts *operational limitations* and *operational guidance*, and regarding the choice of methods and approaches for direct assessment and formulation of operational guidance?

The authors are looking forward to discussing these issues and other aspects of the paper with the participants at the 16th International Ship Stability Workshop.

ACKNOWLEDGEMENTS

This work has been supported by the Swedish Mercantile Marine Foundation and the Swedish Maritime Administration which are both gratefully acknowledged.

REFERENCES

- Allen R G, Jones R R, 1978, "A Simplified Method for Determining Structural Design Limit Pressures on High Performance Marine Vehicles", Proceedings of the AIAA/SNAME Advanced Marine Vehicle Conference.
- Begovic E, Bertorello C, 2012, "Resistance Assessment of Warped Hull Forms", Ocean Engineering Vol. 56, pp. 28-42.
- Begovic E, Bertorello C, Pennino S, 2014, "Experimental Seakeeping Assessment of Warped Planing Hull", Ocean Engineering Vol. 83, pp. 1-15.
- Begovic E, Bertorello C, Pennino S, Piscopo V, Scamardella A, 2015, "Experimental Assessment of Comfort on Board Planing Hulls", Towards Green Marine Technology and Transport, pp. 493-500.
- Begovic E, Bertorell C, Pennino S, Piscopo V, Scamardella A,

- 2016, "Statistical Analysis of Planing Hull Motions and Accelerations in Irregular Head Sea", *Ocean Engineering*, Vol. 112, pp. 253-264.
- Bowles J, Soja J, 2014, "Comparative Analysis of Common Methods for Predicting Vertical Acceleration of Hard Chine Planing Monohulls including Correlation to Hydrodynamic Model Test Data", 4th Chesapeake Powerboat Symp., US.
- de Alwis M P, Garme K, 2017, "Adverse Health Effects and Reduced Work Ability due to Vertical Accelerations in High-Performance Marine Craft Personnel", 16th Int. Ship Stability Workshop (ISSW2017), Belgrade, Serbia.
- DNVGL, 2015, "Rules for Classification, High speed and light craft", Part 3.
- Fridsma G, 1971, "A Systematic Study of the Rough Water Performance of Planing Boats. Irregular Waves – Part II", Stevens Institute of Technology, March 1971, report SIT-DL-71-1495
- Garme K, Rosén A, 2003, "Time-Domain Simulations and Full-Scale Trials on Planing Craft in Waves", *International Shipbuilding Progress*, Vol.50, No.3.
- Garme K, 2005, "Improved Time-Domain Simulation of Planing Hulls in Waves by Correction of the Near-Transom Lift", *International Shipbuilding Progress*, Vol.52, No.3.
- Grimsley J, Liu Y, Hou G, 2010, "An Examination of the Statistical Behavior of Planing Craft Peak Vertical Accelerations in Irregular Waves", 29th American Towing Tank Conference: pp. 31-39, US.
- IMO, 2008, "International Code of Safety for High-Speed Craft".
- ISO, 2008, "Small craft – Hull construction and scantlings – Part 5: Design pressures for monohulls, design stresses, scantlings determination", ISO 12215-5.
- ITTC, 1999, "Recommended Procedures and Guidelines, Testing and Extrapolation Methods, High Speed Marine Vehicles Seakeeping Tests", ITTC 7.5-02-05-04.
- Katayama T, Amano R, 2015, "An Experimental Study on the Characteristics of Vertical Acceleration on Small High Speed Craft in Head Waves", 12th Int. Conf. Stability of Ships and Ocean Vehicles (STAB2015), pp. 587-597, UK.
- Koelbel J G, 1995, "Comments on the Structural Design of High Speed Craft" *Marine Technology* 32(2), pp. 77–100.
- McCue L, 2012, "Statistics and Design Implications of Extreme Peak Vertical Accelerations from Slamming of Small Craft", *Journal of Ship Production and Design* 28(3), pp.112–127.
- Razola M, Rosén A, Garme K, 2014, "Allen and Jones Revisited", *Ocean Engineering*, Vol.89, pp.119–133.
- Razola M, Olausson K, Garme K, Rosén A, 2016, "On High-Speed Craft Acceleration Statistics", *Ocean Engineering*, Vol.114, pp.115–133.
- Riley R M, Haupt K, Jacobson D, 2010, "A generalized approach and interim criteria for computing A1/n accelerations using full-scale high-speed craft trials data", Technical report: NSWCCD-23-TM-2010/13.
- RINA, 2009, "RINA Rules for the Classification of High-Speed Craft".
- RINA, 2013, "RINA Rules for the Classification of Pleasure Yachts, Part B Hull and Stability".
- Rosén A, Garme K, Kutenkeuler J, 2007, "Full-Scale Design Evaluation of the Visby Class Corvette", 9th Int. Conf. on Fast Sea Transportation (FAST'07), China.
- Savitsky D, Brown P W, 1976, "Procedures for Hydrodynamic Evaluation of Planing Hulls in Smooth and Rough Water", *Marine Technology*, Vol.13, No.4.
- Savitsky D, Koelbel J G, 1993, "Seakeeping of Hard Chine Planing Hulls", *Society of Naval Architects and Marine Engineers (SNAME)*, Technical Research Bulletin No. 42.
- Savitsky D, 2016, "Direct Measure of Rigid Body Accelerations for Wave Impact of a Planing Hull", *Journal of Ship Production and Design*, Vol. 32, No. 4, pp. 235–244.
- Zarnick E E, 1978, "A Nonlinear Mathematical Model of Motions of a Planing Boat in Regular Waves", David W. Taylor Naval Ship R&D Center, USA.

This page is intentionally left blank

Validation of Simulation Tools for a RHIB Operating in Heavy Seas

Frans van Walree, *MARIN*, F.v.Walree@marin.nl

William L. Thomas, *USCG Surface Forces Logistics Center*, William.L.Thomas@uscg.mil¹

ABSTRACT

The paper describes model test experiments representing a Rigid Hulled Inflatable Boat (RHIB) in heavy seas. A numerical simulation tool is briefly described. Simulation and experimental results are compared in a deterministic way. The cases that are compared include regular and irregular waves from various directions.

Keywords: *Small boat, Heavy seas, Numerical Simulation, Validation.*

1. INTRODUCTION

The US Coast Guard has undertaken a project to develop a standard process to define operability limits for small boats supporting naval missions. Coast Guard boats are often operated in challenging sea conditions, requiring considerable operator skill to avoid swamping, capsizing, and broaching.

Analytical tools for small boat seakeeping predictions must be developed and validated for use in the definition of operating limits. Scale model testing was chosen as one means to provide validation data and identify nonlinear behaviors for a model representing a cutter boat.

2. MODEL AND TEST PROGRAM

Considerable efforts have been made in seakeeping model tests of conventional ships during the past century. Up to now, only limited research has been performed on small boat seakeeping.

Seakeeping test facilities throughout the world are typically designed to test ship models at scale factors between 1/36 and 1/22. As a result, the wave makers in the test facility have been designed to generate moderate to large seaways at these scale ratios.

Unfortunately, small boat model testing at the aforementioned range of scale factors would require small models which are too small for instrumentation and are subject to scale effects.

The approach taken for this model test was to build a 1 meter light-weight model with full

instrumentation and conduct tests in moderate and steep seaways. Concerns regarding scale effects in roll damping were dealt with by comparing model scale roll damping with roll decay tests performed full-scale. Trim as a function of speed was also verified by comparing model scale data with full scale.

A carbon fiber RHIB model was constructed with main dimensions given in Table 1. Propulsion and steering is by means of a single centerline water jet unit with steerable nozzle.

Table 1 Main particulars

Item	Magnitude	
	Design Load	Full Load
Lpp (m)	6.00	6.00
B-wl (m)	2.144	2.144
Tf (m)	0.446	0.547
Ta (m)	0.646	0.689
Vol (m ³)	3.762	4.559
GMt (m)	0.720	0.551
Tφ (s)	2.04	2.46

The model scale was dictated by maximum wave height that can be generated in the SMB of MARIN. The required significant wave height was 3.00 m yielding scale 6.7 model with a length of 1 m.

Due to high speed and large motions in the horizontal plane the carriage cannot always follow the model. The model needs therefore to be fully

¹ The views expressed herein are those of the author and are not to be construed as official or reflecting the views of the Commandant or of the US Coast Guard.

free running with on-board position measurement system, autopilot computer, power supply, measurement instrumentation and data storage.

The instrumentation consisted of:

- Optical motion tracking system;
- XSENS inertia and rate gyros in 6 DoF at CoG;
- Accelerometers forward and aft;
- Propulsion motor RPM;
- Steering nozzle angle;
- Cockpit and collar water level sensors;
- Incident wave sensors at three locations around the model;
- Pressure transducers to record green water impacts against steering console;
- On-board mini camera;
- miniature PC with autopilot software and hard disk for data storage;
- system for transmission of measurement data to carriage via WiFi.

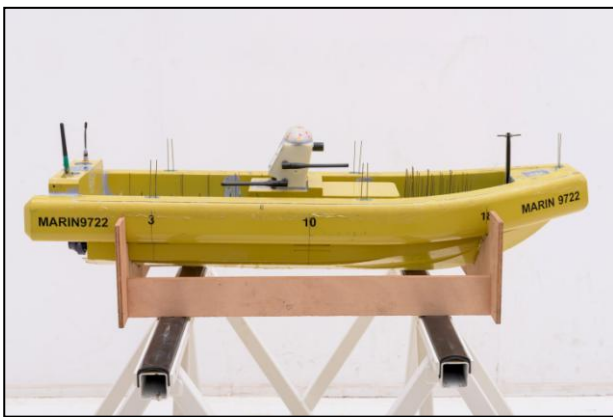


Figure 1 Model photo

The tests were performed in the Seakeeping and Manoeuvring Basin of MARIN. The basin measures 170 x 40 x 5 m in length, width and depth. It is equipped with wave makers along one long and one short side. The wave maker consists of 331 flaps that are all individually driven by an electronic engine. This facilitates generation of regular and long and short crested irregular waves from any direction. A main carriage (x-direction) and a sub-carriage (y-direction) attempt to follow the free-sailing model. The optical motion tracking system functions when the model is in the measurement window of the carriage. It sends position information to the on-board autopilot. When not in the measurement window the on-board inertia navigation system takes over.

Test conditions consisted of:

- Nominal speeds of 6 and 12 knots (Froude numbers 0.35 and 0.70) complemented with free drifting tests;
- Steep regular waves with steepness $H/\lambda=1/15$ and varying wave length, height and directions between and including head and following seas;
- Moderate irregular waves with $H_{1/3}=1.7$ m and $T_p=6.9$ s with directions between and including head and following seas;
- Steep (breaking) irregular waves with $H_{1/3}=2.5$ to 3.0 m and $T_p=5.2$ s with directions between and including head and following seas;

3. MODEL TEST RESULTS

The regular wave tests show that:

- Motion responses are typical for planing craft hull forms operating in the sub-planing speed ranges;
- High vertical accelerations and pitch angles are recorded in head waves, especially for the higher speeds. Transverse accelerations are substantial in beam seas;
- Some ingress of water occurred for the lower speeds in head waves;
- Impact pressures at the steering console occurred for a few head wave conditions only.

In irregular waves safe operation limits are reached occasionally in NATO Sea State 4 and more frequently in a steep Sea State 5:

- Excess horizontal and vertical accelerations occur for operation in head and bow quartering seas at 12 knots;
- Excess pitch angles are recorded prior to wave jumping, i.e. when the boat jumps out of a wave crest;
- Water ingress over the bow occurs in head and bow quartering seas, especially for the lower speed conditions;
- Surf riding occurs in Sea States 4 and 5 at 12 knots speed in stern quartering and following seas. Broaching after surf riding with accompanying high heel angles does not occur;
- Loss of course control is seen in Sea States 4 and 5 stern quartering seas;
- In stern quartering sea state 5 conditions at a 6 knots speed the boat is swamped due to breaking wave crests overtaking the boat. In

these conditions capsizing may also occur due to loss of course control resulting in beam-on breaking waves. One capsize has been observed for the design load condition and two for the full load condition for a half hour test duration for each loading condition. Figure 2 shows a swamping event.



Figure 2 Swamping event

4. SIMULATION TOOLS

The PanShip(NL) time domain panel methods are characterized by:

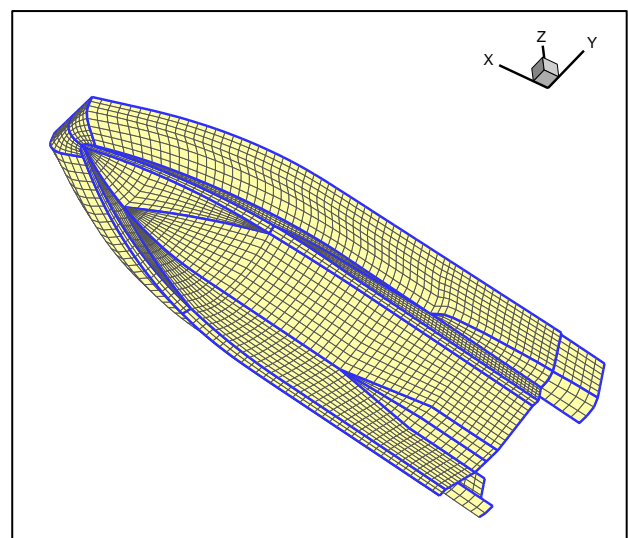
- 3D transient Green function to account for linearized free surface effects, exact forward speed effects on radiation and diffraction forces and a Kutta condition at ventilated transom sterns;
- 3D panel method to account for Froude-Krylov forces on the instantaneous submerged body;
- Cross flow drag method for viscosity effects;
- Resistance (in waves) is obtained from pressure integration each time step;
- Propulsion and steering using propeller open water characteristics, semi-empirical lifting-surface characteristics and propeller-rudder interaction coefficients. Also a semi-empirical water jet propulsion and steering method is incorporated;
- Empirical viscous roll damping by either the FDS or Ikeda methods;
- Autopilot steering.

There are two versions of the simulation tool: a semi-linear (PanShip v2.4) and a semi-nonlinear one (PanShipNL v1.2). In PanShip, it is assumed that the motions of the craft are small, i.e. the submerged geometry does not change in time. Furthermore, the

speed and heading are assumed to be constant so that the Green functions can be computed a priori for use at each time step in the simulation. In effect, the radiation and diffraction problems are then solved in a linearized manner while the wave excitation and restoring forces are treated in a nonlinear way by using the actual submerged hull geometry under the disturbed incident wave.

In PanShipNL the motions may be large while the speed and heading are not necessarily constant. The discretisation of the submerged geometry and the computation of the Green function convolution integrals are performed each time step. This approach is still not fully nonlinear due to the use of the Green functions which satisfy the linearized free surface condition. By discretising the actual submerged hull form and using the submergence relative to the undisturbed incident wave surface rather than the calm water surface, a semi-nonlinear approach is obtained. More detailed information can be found in De Jong (2011) and Van Walree and Turner (2013).

The hull form of MARIN model 9722 was discretized into a surface mesh consisting of some 1900 below water and 2100 above water panels. Figure 3 shows this mesh with segment boundaries in blue. The flow streaks on the hull bottom and transom flaps were not included in the mesh. The effects of these were included empirically in PanShip(NL).



During the simulations the ship was free running and self-propelled and kept on course

through an autopilot. The impeller RPM was set such that the mean speed in waves was approximately equal to that of the model tests. The autopilot gains were the same as used for the model tests.

For all PanShip simulations the effect of forward speed on sinkage and trim was taken into account by determining the calm water equilibrium position a priori and adapting the hull mesh accordingly. For the PanShipNL simulations this was automatically achieved during the simulation since the mesh was adapted to the instantaneous motions and incident wave profile each time step.

Viscous roll damping is included by means of the FDS method, see Blok and Aalbers (1991). No tuning of the roll damping on basis of model test data has been applied.

5. VALIDATION RESULTS

Validation is based on direct time trace comparison, whereby the input wave train was reconstructed in the simulations. For regular waves this is a simple procedure. For irregular wave the procedure is more elaborate as explained in Van Walree et al (2016).

5.1 Regular waves

In the steep regular waves considered here acceleration responses may be non-sinusoidal. It is noteworthy to mention that for the higher 12 knots speed the linear PanShip code could not deal with head sea conditions. In the simulation, the boat jumps out of the steep waves to reach pitch angles over 90 degrees. The non-linear PanShipNL code however can deal with these conditions. Figures 4 through 8 show comparisons between experimental and simulated time traces for a steep regular head wave with a frequency of 1.88 rad/s and an amplitude of 0.58 m, i.e. $H/\lambda=1/15$. The waterjet RPM was set for a calm water speed of 15 knots. Figure 4 shows that in waves the speed (X0d) varied between about 7 and 10 knots which is well predicted by PanShipNL.

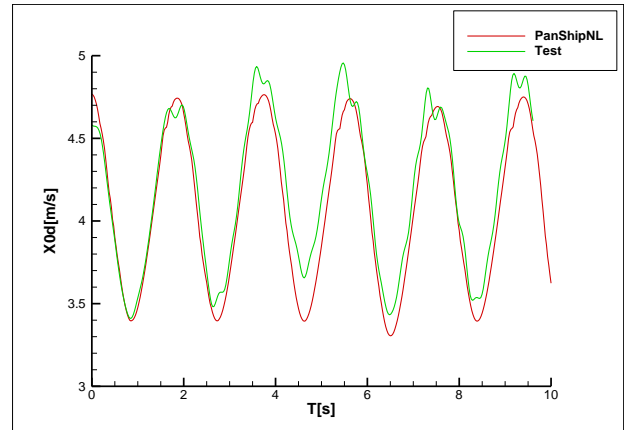


Figure 4 Comparison of forward speed

The heave (Z0) and pitch (Theta) time traces shown in Figures 5 and 6 show adequate predictions as well. Note the slight trochoidal character of the pitch motion.

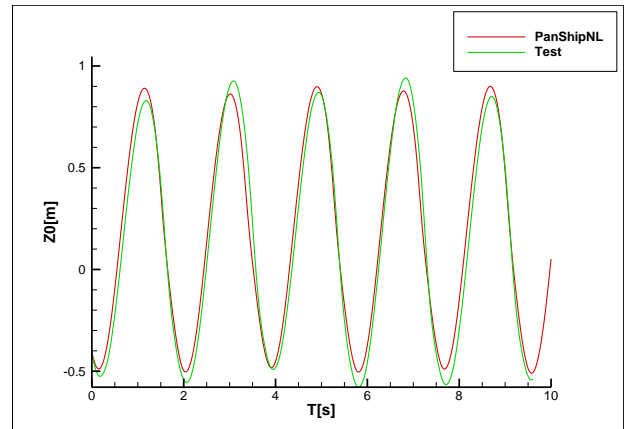


Figure 5 Comparison of heave

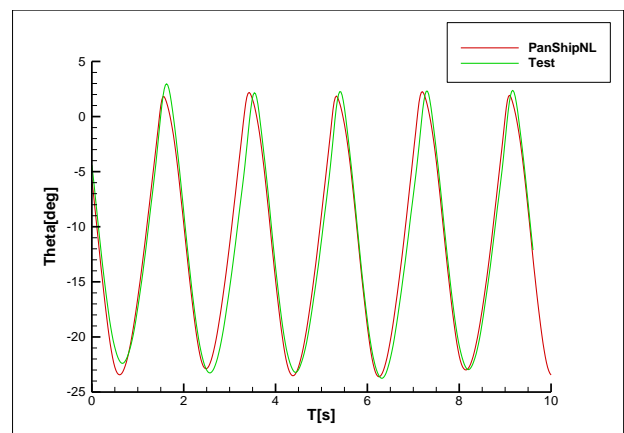


Figure 6 Comparison of pitch

The longitudinal (Acc-x04) and vertical (Acc-z04) acceleration components at the bow shown in Figures 7 and 8 show slamming peaks which are

reasonably well predicted. The experimental time traces show the effect of a slight variation in wave amplitude which is due to non-linear wave propagation effects in the basin.

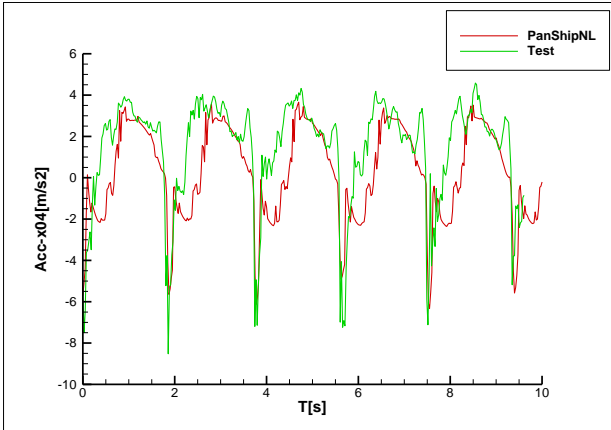


Figure 7 Comparison of x-acceleration

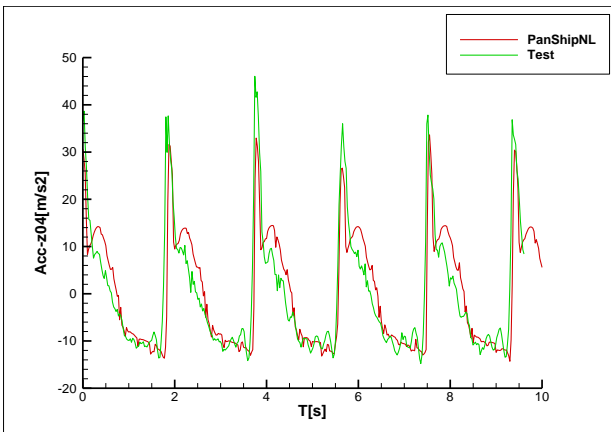


Figure 8 Comparison of z-acceleration

Figures 9 through 16 show a comparison of time traces for a near following seas condition with a wave direction of 15 degrees off the stern. The wave frequency is 1.88 rad/s and the wave amplitude is 0.45 m with $H/\lambda=1/20$. The waterjet RPM was set for a 6 knots calm water speed, yet the speed in waves varies between about 14 and 19 knots, when the model is captured and released by the wave crest, see Figure 9. This speed variation is well predicted by the linear PanShip code.

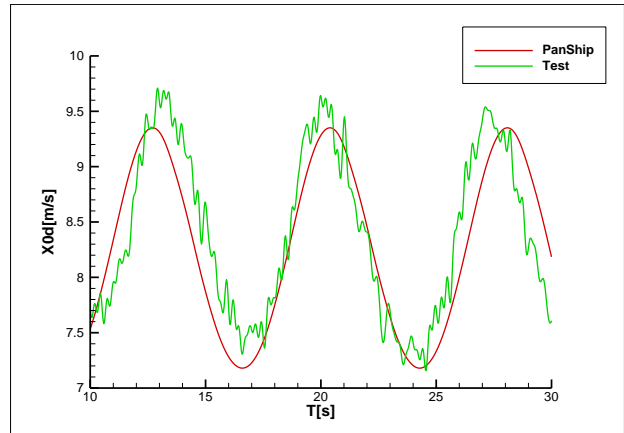


Figure 9 Comparison of forward speed

Figures 10 through 13 show that the motions are reasonably well predicted although the experimental roll and yaw motions are somewhat affected by wave reflections from the basin beaches.

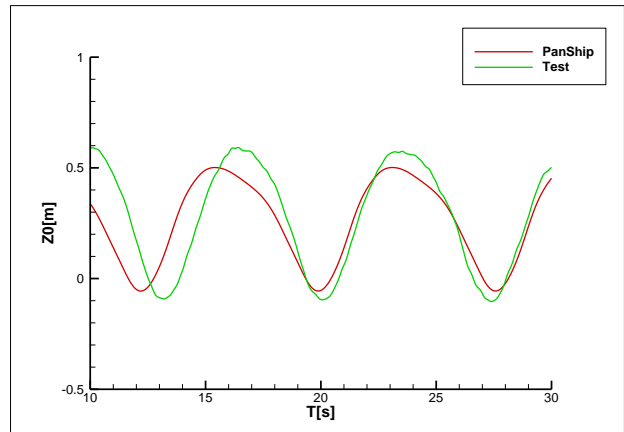


Figure 10 Comparison of heave

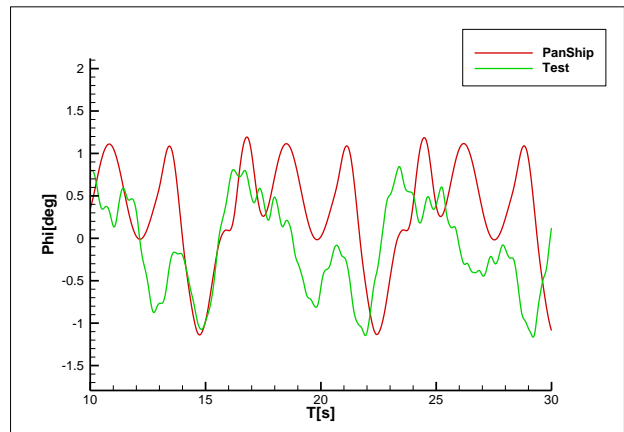


Figure 11 Comparison of roll

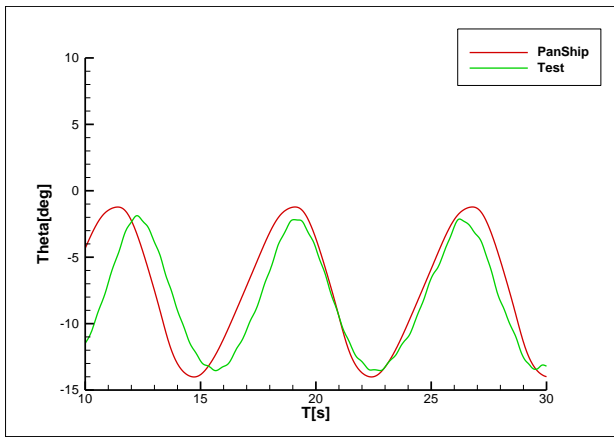


Figure 12 Comparison of pitch

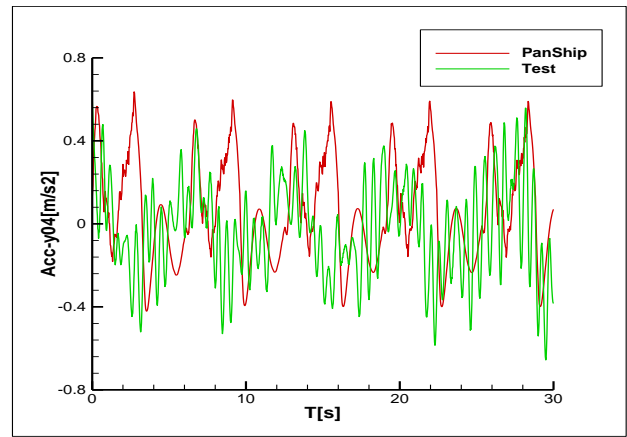


Figure 15 Comparison of y-acceleration

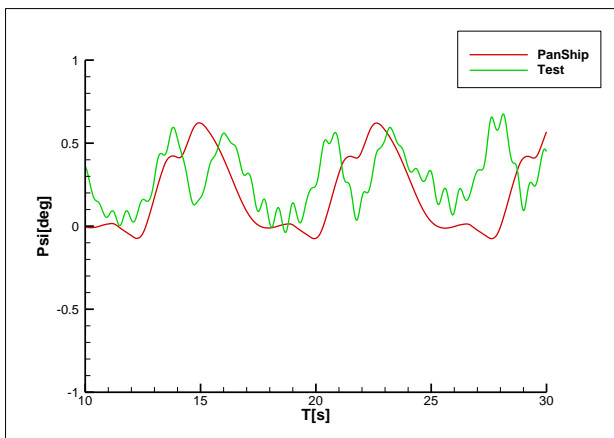


Figure 13 Comparison of yaw

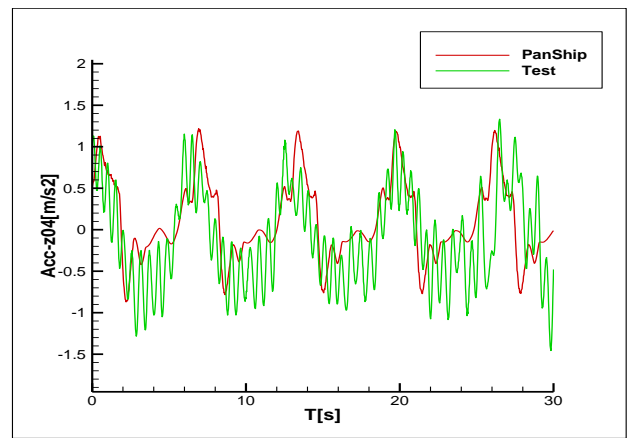


Figure 16 Comparison of z-acceleration

The acceleration components are relatively low and the experimental signals show the noise due to the propulsion system, see Figures 14 , 15 and 16.

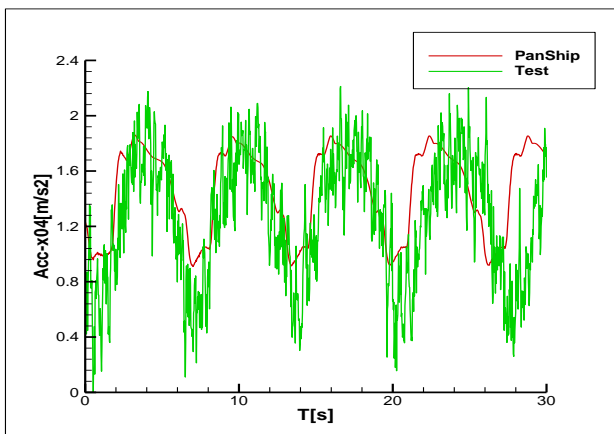


Figure 14 Comparison of x-acceleration

5.2 Irregular waves

The first case concerns a PanShipNL simulation for a steep irregular head sea with $H_{1/3} = 2.5$ m and $T_p = 5.2$ s. The nominal forward speed is 12 knots ($F_n=0.70$). Figures 17 through 21 show a comparison of time traces for forward speed, heave, pitch, and acceleration components. It is seen that the comparison is not perfect, especially for the highest wave amplitudes. One reason for this is that wave reconstruction method cannot deal with breaking waves. This is illustrated in Figure 22 showing a comparison between the measured and reconstructed wave time traces for the time frame with the highest wave amplitudes. Figure 23 shows a detail of the pitch time traces for that time frame. The bow-up pitch amplitude is rather high: some 35 degrees causing the model to fly above water for a short while, see Figure 24. This event is reasonably well captured by PanShipNL. Even if the waves were perfectly reconstructed there would be differences because PanShipNL cannot deal with breaking waves and waterjet intake ventilation.

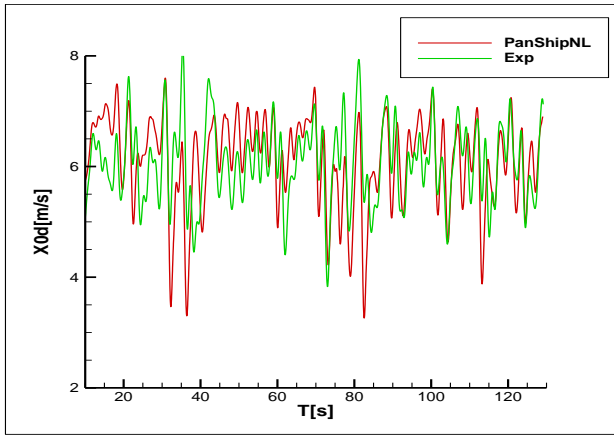


Figure 17 Comparison of velocity

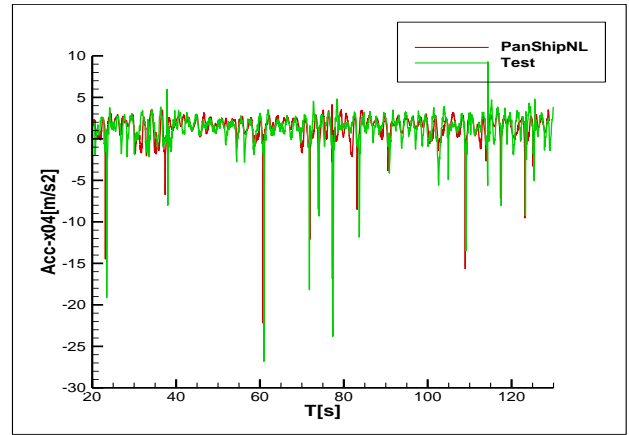


Figure 20 Comparison of x-acceleration

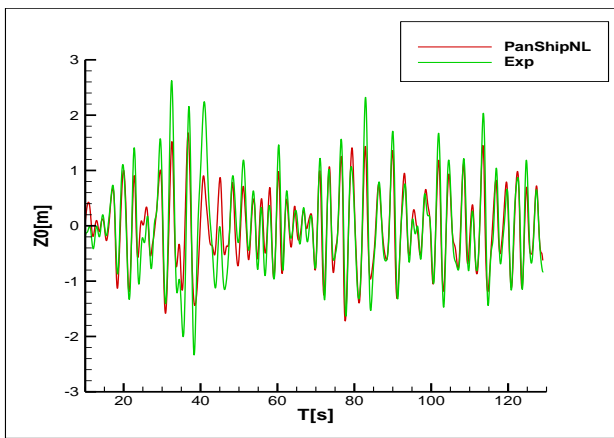


Figure 18 Comparison of heave

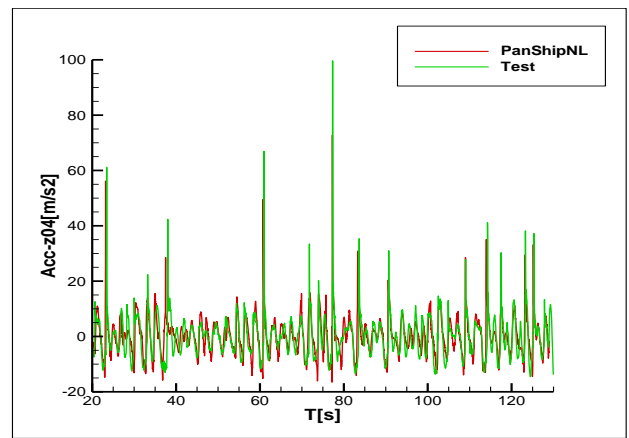


Figure 21 Comparison of z-acceleration

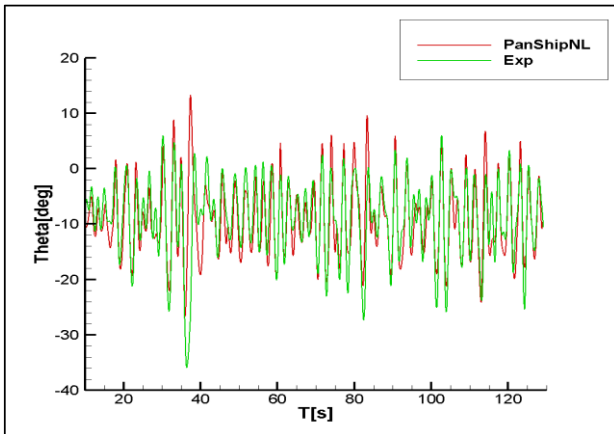


Figure 19 Comparison of pitch

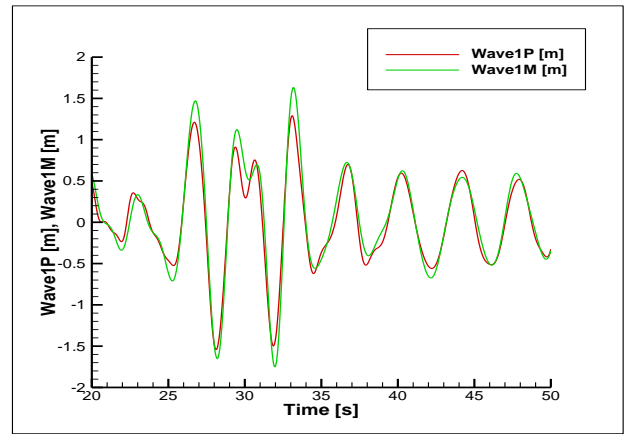


Figure 22 Comparison of reconstructed (Wave1P) and experimental (Wave1M) wave time trace

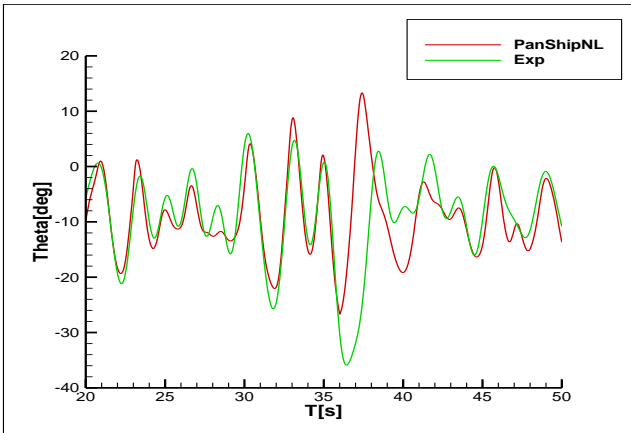


Figure 23 Comparison of pitch time trace detail

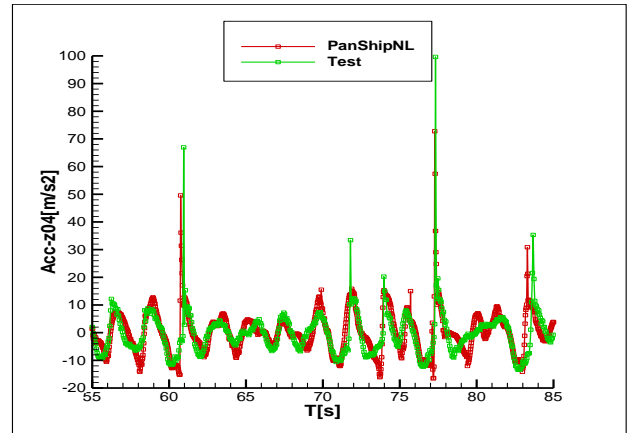


Figure 25 Comparison of z-acceleration (detail)

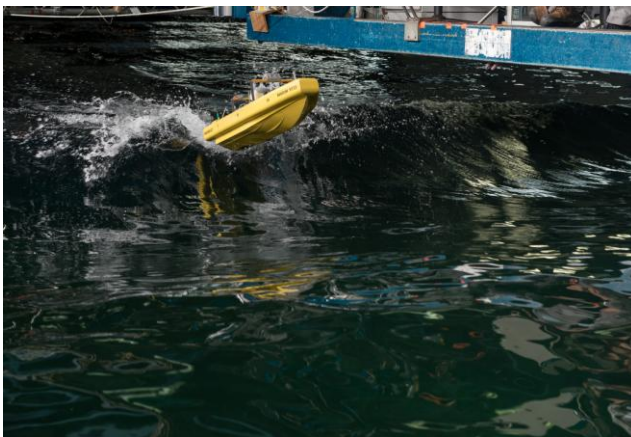


Figure 24 Flying model

The second comparison the same sea state ($H_{1/3}=2.5$ m, $T_p=5.2$ s) but now as a beam sea. The speed is 12 knots. Figures 26 through 31 show comparisons between experimental and simulated time traces. It is seen that the predicted yaw time traces deviate from the experimental result. This has an effect on the sway and pitch motions and forward speed as well. Heave and roll are reasonably well predicted. It is believed that the difficulty in predicting yaw is again partially due to the presence of breaking waves. Other reasons may be the use of a semi-empirical method for water jet steering in PanShipNL and the occurrence of waterjet intake ventilation.

Interestingly, the highest vertical accelerations do not occur during the event described above. Figures 25 and 26 show a detail of the acceleration time traces. The high peak values are reasonably well captured by PanShipNL.

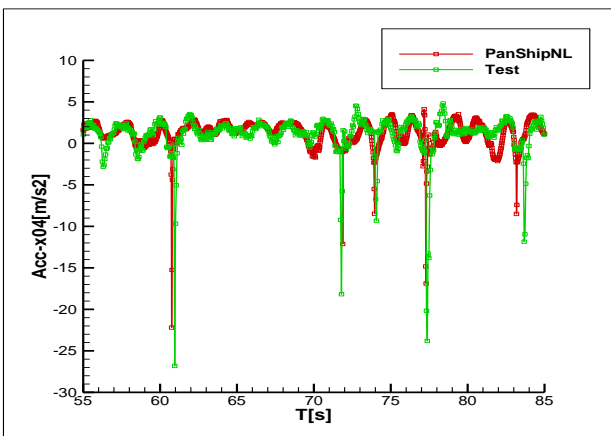


Figure 25 Comparison of x-acceleration (detail)

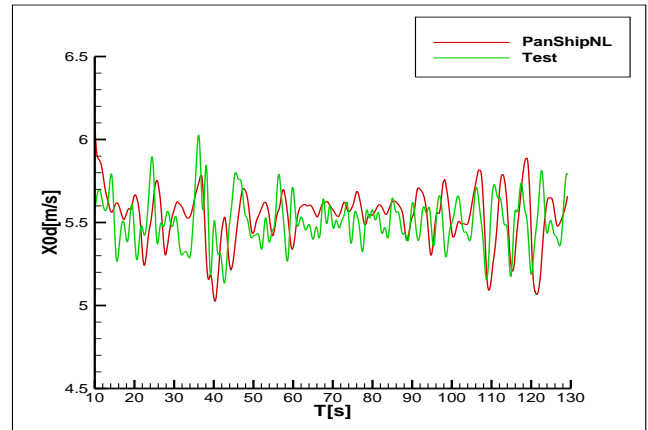


Figure 26 Comparison of velocity

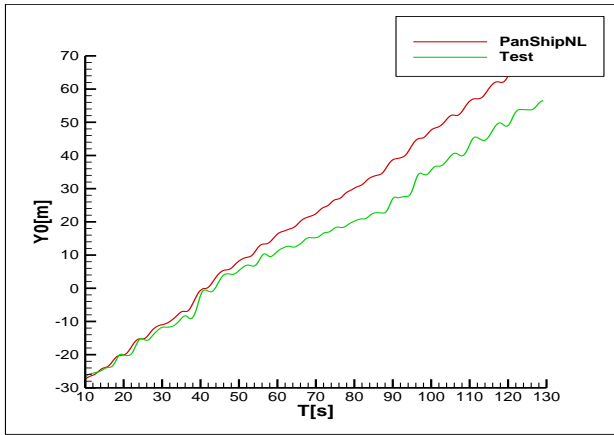


Figure 27 Comparison of sway

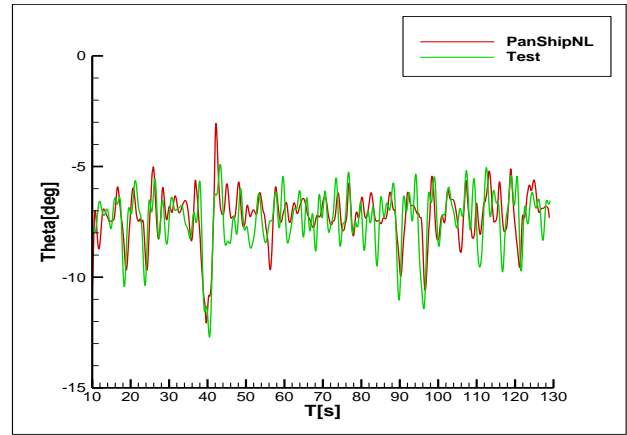


Figure 30 Comparison of pitch

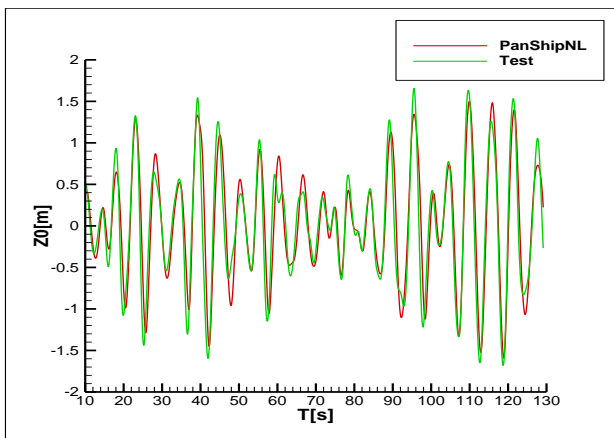


Figure 28 Comparison of heave

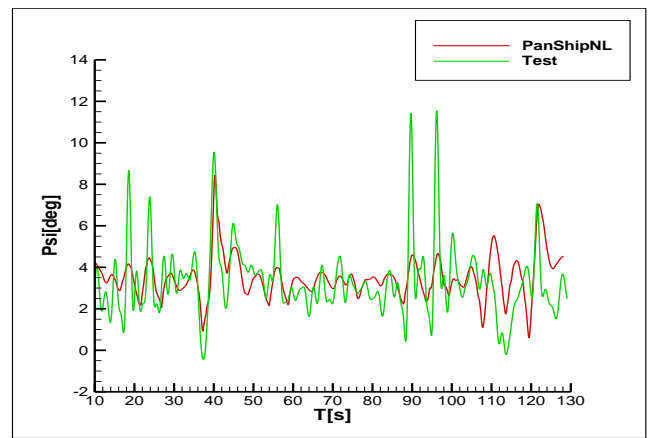


Figure 31 Comparison of yaw

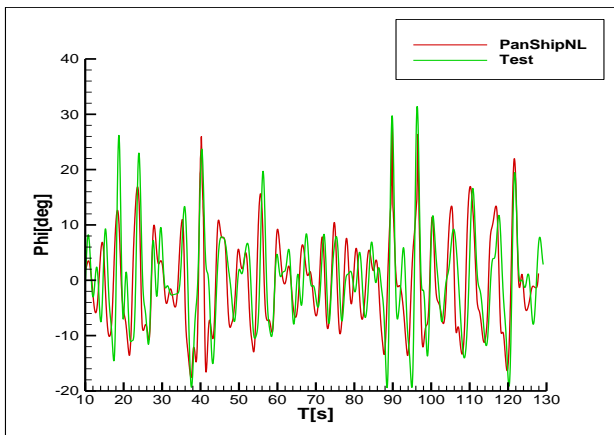


Figure 29 Comparison of roll

6. CONCLUDING REMARKS

The comparisons between experimental and simulated time traces shows that PanShip provides adequate predictions for low amplitude yet steep regular waves.

Predictions for steep and heavy irregular seas show that non-linear events in head seas such as jumping out of wave crests and acceleration peaks are reasonably well predicted. In beam seas heave, roll and pitch are reasonably well predicted as well, however yaw and sway deviate. This is believed to be at least partially due to the effects of breaking waves and water jet intake ventilation. Such phenomena are not included in the simulation tools.

The tests in the steep irregular waves from a stern quartering direction showed the occurrence of swamping and capsizing in breaking waves. Such events occur about two to four times per hour. It would have been of interest to show deterministic validation results for such events. This has not been attempted because the simulation methods used cannot deal with breaking waves and the resulting water ingress leading to a capsize. This remains a challenge, even for CFD based tools.

REFERENCES

- De Jong P., 2011, "Seakeeping Behavior of High Speed Ships, an Experimental and Numerical Study", Ph. D. Thesis, Delft University of Technology.
- Van Walree F. and Turner T.G., 2013, "Development and validation of a time domain panel code for prediction of hydrodynamic loads on high speed craft", International Conference of High Speed Sea Transportation, FAST'2013, Amsterdam.
- Van Walree F., Sgarioto D. and Turner T.G., "Validation of a Time Domain Panel Code for Prediction of Impulsive Loads on High Speed Ships", 31th Symposium on Naval Hydrodynamics, Monterey, California, 11-16 September, 2016.
- Blok, J.J., Aalbers, A.B., 1991, "Roll Damping Due to Lift Effects on High Speed Monohulls", Proceedings from the First International Conference on Fast Sea Transportation: FAST'91, Trondheim, June 1991.

Proceedings of the 16th International Ship Stability Workshop (ISSW 2017)
Belgrade, Serbia, 5-7 June, 2017

Editor
Igor Bačkalov

Published in 2017 by
Faculty of Mechanical Engineering, University of Belgrade
Kraljice Marije 16, 11120 Beograd, Serbia

Printed by
Planeta Print, Beograd

Cover photo
Özen Güney

Printing
110 copies

CIP - Каталогизација у публикацији
Народна библиотека Србије, Београд

629.5.015.1(082)
532.583.4(082)

INTERNATIONAL Ship Stability Workshop
(16 ; 2017 ; Beograd)

Proceedings of The 16th International Ship Stability Workshop,
Belgrade, 5-7 June 2017 / [editor Igor Bačkalov ; organizer
Department of Naval Architecture, Faculty of Mechanical
Engineering University of Belgrade]. - Beograd
: University, Faculty of Mechanical Engineering,
2017 (Beograd : Planeta Print). - 258 str. : ilustr.
; 30 cm

Tiraž 110. - Abstracts. - Bibliografija uz svaki rad.

ISBN 978-86-7083-935-9

1. Mašinski fakultet (Beograd). Katedra za brodogradnju
a) Бродови - Стабилитет - Зборници

COBISS.SR-ID 234631180